NEWCASTLE UNIVERSITY LIBRARY

087 11814 4

Thesis L3310

REINFORCED CONCRETE DEEP BEAMS : BEHAVIOUR, ANALYSIS AND DESIGN

by

Chi Wai John TANG, B.Sc. (Hons.)

A thesis presented for the Degree of Doctor of Philosophy
in the University of Newcastle upon Tyne

Department of Civil Engineering

University of Newcastle upon Tyne

October 1987

ACKNOWLEDGEMENTS

The Author would like to acknowledge his indebtedness to his supervisor, Professor F. K. Kong, whose professional expertise and careful guidance were responsible for the motivation of this research.

The Author wishes to express his appreciation and gratitude to Professor M. B. Pescod, Head of Department, for his encouragement and for extending the facilities of the Heavy Structures Laboratory for this research.

Special thanks go to the staff of Civil Engineering Department whose enthusiasm and close cooperation contributed not only to the quality of the research but to making the task of its preparation a pleasant one. Particular thanks are owed to M. Armstrong, A. Jefferson, J. Allen, G. Stacey, G. Hall, K. Scholefield, J. Bennett, C. Hastie and E. Edmond.

The Author is grateful to the Committee of Vice-Chancellors and Principals of the Universities of the United Kingdom for providing the ORS Awards for this study.

Finally, the Author thanks his colleagues H. H. A. Wong and M. Chemrouk with whom the Series E tests on the slender deep beams without web-openings were carried out as a joint pilot project.

SYNOPSIS

The work described in this thesis is concerned with the behaviour, analysis and design of reinforced concrete beams. A brief historical review of the methods of analysis on deep beams is given. The current major codes of practice and design manuals associated with reinforced concrete deep beams are reviewed. This study has been useful in identifying the limitations of the current design documents on the subject of deep beams. Because of the acute shortage of information regarding buckling, web-opening and combined loading, three test programmes are performed to provide experimental evidence on these topics. Their behaviour is examined in terms crack developments, crack patterns, modes of failure, in-plane and lateral displacements, ultimate loads, strains and stresses.

The ultimate buckling strength of the slender deep beams without web-openings are analysed using the methods described in the CIRIA Guide [1977]. Adopting the same methods in the guide, an attempt has been made to analyse the buckling strength of deep beams with web-openings. Based on the structural idealization of Kong et al [1973a], a modified approach is proposed for the ultimate shear strength of deep beams with web-openings. In addition, the CIRIA ultimate shear interaction equation for deep beams under combined top and bottom loadings is studied and an equation is proposed for the uniformly distributed loading cases. Finally, based upon these findings, some design recommendations are given.

CONTENTS

Acknowledgements ii

Synopsis iii

1 INTRODUCTION 1

1.1 Nature of the Problem 1

1.2 Object and Scope 3

1.3 Organisation of the Thesis 4

2 DEEP BEAM ANALYSIS - A REVIEW WITH COMMENTARY 5

2.1 Introduction 5

2.2 Mathematical Analysis 5

2.3 Experimental Analysis 9

2.3.1 Elastic Experimental Analysis 9

2.3.2 Experiment on Reinforced Concrete Deep Beams 11

3 CODES AND MANUALS - A CRITICAL REVIEW 22

3.1 Introduction 22

3.2 Current Design Methods 22

3.2.1 Preliminary Remarks 22

3.2.2 Deep Beams without Web-Openings 23

3.2.3 Deep Beams with Web-Openings 45

3.2.4 Deep Beams with Combined Top and Bottom Loadings . . . 52

3.3 Comments 54

4 MATERIALS, SPECIMENS AND INSTRUMENTATION 57

4.1 Geometry and Details of Specimens 57

4.1.1 Slender Deep Beams without Web-Openings 57

4.1.2 Slender Deep Beams with Web-Openings 58

4.1.3 Deep Beams under Combined Top and Bottom Loadings . . 59

4.2 Materials 60

4.2.1 Cements 60

4.2.2 Aggregates 60

4.2.3 Chemical Admixture 60

4.2.4 Steel 61

4.2.5 Concrete 61

4.3 Manufacture of Specimens 62

4.3.1 Slender Deep Beams without Web-Openings 62

4.3.2 Slender Deep Beams with Web-Openings 62

4.3.3 Deep Beams under Combined Top and Bottom Loadings . . 63

4.3.4 Casting and Curing 63

4.3.5 Control Specimen 64

4.4 Instrumentation 65

4.4.1 The Test Rig 65

4.4.2 Servo-hydraulic Jacking System 66

4.4.3 Combined Top and Bottom Loading System 66

4.4.4 LVDT Displacement Transducers 67

4.4.5 Mechanical Dial Gauges 68

4.4.6 Electrical Demountable Strain Transducers 68

4.4.7 Mechanical Demec Gauge 71

4.4.8 Data Logging System 71

4.4.9 Bottom Bearings 71

4.4.10 Top Bearings 72

5 EXPERIMENTAL PROGRAMMES 73

5.1 Introduction 73

5.1.1 Slender Deep Beams without Web-Openings 73

5.1.2 Slender Deep Beams with Web-Openings 74

5.1.3 Deep Beams under Combined Top and Bottom Loading . . . 75

5.2 Test Programmes 76

5.2.1 Slender Deep Beams without Web-Openings 76

5.2.2 Slender Deep Beams with Web-Openings 77

5.2.3 Deep Beams under Combined Top and Bottom Loadings . . 77

5.3 Beam Notation 78

5.3.1 Slender Deep Beams without Web-Openings 78

5.3.2 Slender Deep Beams with Web-Openings 78

5.3.3 Deep Beams under Combined Top and Bottom Loadings . . 79

5.4 Test Procedures 79

5.5 Buckling Failure Predictions 83

5.6 Summary 83

6 EXPERIMENTAL RESULTS 85

6.1 Introduction 85

6.2 Crack Patterns and Modes of Failure 85

6.2.1 Slender Deep Beams without Web-Openings 85

6.2.2 Slender Deep Beams with Web-Openings 89

6.2.3 Deep Beams under Combined Top and Bottom Loadings . . 92

6.3 Lateral Deformations 95
6.3.1 Slender Deep Beams without Web-Openings 96
6.3.2 Slender Deep Beams with Web-Openings 97
6.3.3 Deep Beams under Combined Top and Bottom Loadings . . 99
6.4 Vertical Deformations 99
6.4.1 Slender Deep Beams without Web-Openings 99
6.4.2 Slender Deep Beams with Web-Openings 99
6.4.3 Deep Beams under Combined Top and Bottom Loadings . 100
6.5 Ultimate Loads 100
6.5.1 Slender Deep Beams without Web-Openings 100
6.5.2 Slender Deep Beams with Web-Openings 102
6.5.3 Deep Beams under Combined Top and Bottom Loadings . 105
6.6 Direct Strains 108
6.6.1 Slender Deep Beams without Web-Openings 109
6.6.2 Slender Deep Beams with Web-Openings 110
6.6.3 Deep Beams under Combined Top and Bottom Loadings . 111
6.7 Principal Strains 113
6.7.1 Slender Deep Beams without Web-Openings 114
6.7.2 Slender Deep Beams with Web-Openings 116
6.7.3 Deep Beams under Combined Top and Bottom Loadings . 117
6.8 Principal Stresses 118
6.8.1 Slender Deep Beams without Web-Openings 120
6.8.2 Slender Deep Beams with Web-Openings 121
6.8.3 Deep Beams under Combined Top and Bottom Loadings . 122
6.9 Summary 123

7 ANALYSIS OF TEST RESULTS 125

7.1 Introduction 125

7.2 Ultimate Buckling Strength 126

7.2.1 Slender Deep Beams without Web-Openings 126

7.2.2 Slender Deep Beams with Web-Openings 128

7.3 Ultimate Shear Strength 131

7.3.1 Slender Deep Beams without Web-Openings 131

7.3.2 Slender Deep Beams with Web-Openings 133

7.3.3 Deep Beams under Combined Top and Bottom Loadings . 142

7.4 Summary 147

8 CONCLUDING REMARKS AND DESIGN RECOMMENDATIONS 148

8.1 Concluding Remarks 148

8.1.1 Slender Deep Beams without Web-Openings 148

8.1.2 Slender Deep Beams with Web-Openings 150

8.1.3 Deep Beams under Combined Top and Bottom Loadings . 152

8.2 Design Recommendations 153

8.2.1 Slender Deep Beams without Web-Openings 153

8.2.2 Slender Deep Beams with Web-Openings 154

8.2.3 Deep Beams under Combined Top and Bottom Loadings . 156

References 157

Appendix A : WORKED EXAMPLES FOR DEEP BEAMS WITHOUT WEB-OPENINGS . 164

Appendix B : WORKED EXAMPLES FOR DEEP BEAMS WITH WEB-OPENINGS . . . 181

Tables 199

Figures 213

CHAPTER ONE

INTRODUCTION

1.1 NATURE OF THE PROBLEM

At a seminar given recently to a group of about 70 engineers at Ove Arup and Partners in London [Kong, 1986], it became clear that reinforced concrete deep beams had many useful applications in tall buildings, offshore structures and foundations, and hence the behaviour, analysis and design of reinforced concrete deep beams was of great interest to many practising engineers.

The efficient analysis and design of reinforced concrete deep beams require a sound understanding of their structural behaviour. The simple bending theory, based on the Navier-Bernoulli hypothesis of a straight-line stress distribution, is not applicable. Equally the use of the biharmonic equation with the appropriate Airy stress function will only produce moderately satisfactory solutions even before cracking occurs. Attempts have been made to apply the upper and lower bound theorems of plastic theory to deep beams, but they seemed to raise as many questions as they answered [Kong and Charlton, 1983; Kubik, 1978]; besides, these theorems are largely irrelevant to the important question of crack widths.

Solutions produced by photoelastic studies can be useful qualitatively [Garcia, 1981]. Unfortunately, they still suffer from the limitations imposed by the simplifying assumptions regarding elasticity, isotropy and homogeneity.

It is only comparatively recently that research on reinforced concrete deep beams was carried out in a realistic manner and on a practical scale [Albritton, 1965; C&CA, 1969], and even more recently that design recommendations could be given in official documents. Indeed, deep beam design was not covered by CP 110 : 1972 nor is it covered by the new BS 8110 : 1985, which explicitly states that "for the design of deep beams, reference should be made to specialist literature". The first official document that included provisions for deep beams was the International Recommendations published by the Comité Européen du Bèton and the Fédèration Internationale de la Prècontrainte (CEB-FIP) in 1970. In 1971, the American Code for the first time included recommendations for deep beams [ACI 318-71, 1971]. In the United Kingdom, recognizing industry's need for data and guidance, the Construction Industry Research and Information Association issued "CIRIA Guide 2 : The Design of Deep Beams in Reinforced Concrete" in 1977.

Currently, the major documents covering deep beam design are :

(a) CIRIA Guide 2 [1977] - reprinted with corrections in 1984,

(b) CEB-FIP Model Code [1978],

(c) Reinforced Concrete Designer's Handbook [Reynolds and Steedman, 1981],

(d) ACI Building Code 318-83 [1983, revised 1986], and

(e) Canadian Code CAN3-A23.3-M84 [1984].

It should be pointed out that the deep beam provisions in ACI 318-83 are very similar to those in the 1971 Code; likewise, the deep beam provisions in the 1978 CEB-FIP Model Code remain similar to those in the 1970 CEB-FIP International Recommendations. Indeed, to this day,

the CIRIA Guide remains not only the most comprehensive deep beam guide available, but also in fact the most technically advanced. An examination of the official documents cited above reveal that their main recommendations were concerned with ultimate strength in flexure and shear and with bearing capacity. Because of the acute shortage of information regarding buckling, web-opening and combined loading, the official documents tend to give only very limited guidance on these topics. Knowledge gained from practice is essentially limited to the service condition. Therefore, a comprehensive review and evaluation of the guidelines in the official documents is necessary.

1.2 OBJECT AND SCOPE

The objectives of this study are as follows :

1. To give a brief historical review of the subject.
2. To investigate the effects of slenderness, web-openings and combined top and bottom loadings on the behaviour of reinforced concrete deep beams.
3. To investigate the limitations of the design recommendations in current design manuals and codes of practice on reinforced concrete deep beams.
4. To search for safe and convenient design procedures for reinforced concrete deep beams.
5. To develop design guidelines and simple rules on deep beam design.

1.3 ORGANISATION OF THE THESIS

This thesis has been arranged into eight chapters. Chapter 2 is a brief historical review on the methods of analysis on deep beams. It shows that the basic approaches can be broadly classified into two main categories; namely, the mathematical analysis and the experimental analysis. Comments are provided as appropriate. Chapter 3 discusses the major documents covering deep beam design and together with Chapter 2 constitute the bulk of the technical knowledge and their limitations available on deep beam analysis and design.

The materials used, the details of the specimens as well as the instrumentation for three systematic series of deep beam tests regarding buckling, web-openings and combined loadings are described in Chapter 4. Chapter 5 gives the additional information to these three tests. In Chapter 6, the results of the three tests are presented and discussed. Chapter 7 analyses the test results obtained. Modified design concept and new design equations are given and checked with the existing data and the results of the present tests. Chapter 8 summarizes the principal conclusions of this study. Some recommendations based upon these findings are also suggested for practical design.

CHAPTER TWO

DEEP BEAM ANALYSIS - A REVIEW WITH COMMENTARY

2.1 INTRODUCTION

This chapter gives a brief historical review of the analysis of reinforced concrete deep beams. Comments are provided as appropriate.

2.2 MATHEMATICAL ANALYSIS

Before the days of limit state design, elastic theory was usually employed in deep beam design, in spite of its inadequacy [e.g. CP 114 : 1957]. The literature on this topic frequently considered reinforced concrete as isotropic, homogeneous and linear elastic. Many of the methods of analysis were valid only for uncracked sections. These limitations severely restricted what practising engineers could do.

Dischinger [1932] was probably the first to make a serious attempt to analyse the stresses in continuous deep beams. Using the theory of elasticity and the biharmonic equation, he determined an Airy stress function which satisfied the boundary conditions. The applied loads were represented by Fourier series. Later, based on Dischinger's work, the Portland Cement Association in the U.S.A. issued a guidance document [PCA, 1946], which included solutions for both continuous and single-span deep beams. Looking back, there are several obvious objections to the Portland Cement Association's design recommendations :

(a) Dischinger's analysis was based totally on the theory of elasticity and hence does not apply to practical reinforced concrete deep beams, which are cracked even under service loading.

(b) Dischinger's Airy stress function implied particular distributions of normal and shear stresses at the ends of the beams. Since these stress distributions are normally very different from those in the real beams, Dischinger's stresses might be quite unreliable, particularly as the span-to-depth ratios of deep beams tend to be small.

Subsequently, numerous variations had been introduced, including those of Conway, Chow and Morgan [1951], which dealt with the boundary conditions of single-span deep beams. They obtained a solution by superimposing two stress functions. The first function was in the form of a trigonometric series which satisfied all boundary conditions except the non-zero normal stresses on the vertical edges. Then, with the principle of least work, these residual boundary stresses were settled by the second stress function. The results were compared with the solutions obtained by finite difference method. In addition, Chow, Conway and Winter [1952] later provided a comprehensive treatment of single-span deep beams with the aid of the finite difference method. Graphical representation of bending and shear stresses for five loading cases together with three span-to-depth ratios was included. They emphasised the effects of the normal stresses along the loaded edges and concluded that stress distribution would depend upon the elevation of the applied load. Furthermore, owing to the arrangement

of reinforcement and cracks in deep beams, they claimed that the behaviour of deep beams designed in accordance with the rules of the Portland Cement Association would not conform to the assumption of homogeneity. Therefore, they recommended that engineers should distribute the horizontal reinforcement uniformly throughout the tension zone. In a later closing discussion [Chow et al, 1953], Guzman and Luisoni ascribed the numerical inaccuracy of Chow's finite difference solution to the coarse density of the network.

In Uhlmann's [1952] contribution, simultaneous with that of Chow, Conway and Winter [1952], much effort was devoted to the stress analysis of deep beams with span-to-depth ratio equal to unity. He drew the designer's attention to the need to consider the effects of web-openings and the possibility of buckling. To determine the amount of reinforcement required, Uhlmann placed the emphasis on determining the correct lever arm; hence his method is different from that of the Portland Cement Association. In the case of top uniformly distributed loading, Uhlmann considered that the placement of the vertical reinforcement was unnecessary.

Cheng and Pei [1954] elaborated the findings of Dischinger on continuous deep beams with equal span and fixed support. They studied beams which included their self-weight and were subjected to concentrated, partial or full uniform loads at the top and bottom edges. The authors have some interesting results : for deep beams with roller supports, when a uniformly distributed load was applied over the whole span, the bending and shear stresses at the top and bottom edges would be identical; however, this was not so in the case

of fixed supports. Also, regardless of the support conditions, these stresses would be identical when the same load was applied to the bottom edge.

Based upon the strain energy method, Archer and Kitchen [1956, 1957, 1960] eliminated the drawback of Conway's solution. They described a method which was not dependent on the solution of continuous beams. Their results showed reasonable agreement with those obtained by Conway et al. They suggested that the maximum extreme stress did not necessarily occur at the section of maximum moment.

Geer [1960] vindicated the solution of finite difference method by using a finer computational grid than those used by Conway et al. For deep beams with clear-span-to-depth ratio less than 2, he found that the effect of the gravitational stresses due to the self-weight of the beam were practically the same as if the identical loading was applied at the top edge. Geer confirmed the findings of Archer and Kitchen, and proposed that the maximum extreme stress depended on the spread of the localised forces near the vicinity adjoining the loads.

Coull [1966] circumvented the problem of unsymmetric loading by the principle of least work and the Fourier series. He demonstrated that any applied load system could be superimposed by symmetric and unsymmetric components. This method gave a more accurate solution of stresses than those obtained from the finite difference method.

Recently, Barry and Ainso [1983] described a multiple Fourier technique for single-span deep beams under uniform top and bottom

loadings. They proceeded to deal with the boundary conditions by three stress functions. The first one satisfied the boundaries of the upper and lower edges while the other two satisfied the residual odd and even stresses on the free vertical edges of the beam. This method is more accurate than the finite difference method for stresses predicted at regions with abrupt changes of stress and boundary condition. Moreover, it could be extended to continuous deep beams with different load configurations. However, a major impediment to this method stems from the heavy use of the correction factors in Schleel's paper [1964] whereby solutions are not unique.

2.3 EXPERIMENTAL ANALYSIS

2.3.1 Elastic Experimental Analysis

Although some of the foregoing mathematical treatments contain some valuable details of interest to designers of deep beam, the sources of more immediately usable information are those obtained from the experimental tests on homogeneous materials.

Using the photoelastic technique, Caswell [1954] studied two series of annealed Bakelite deep beams with span-to-depth ratios varying from 1.05 to 5.32. The beams in the first series were subjected to pure bending moment which was created by loads applied beyond their supports. In the second series, identical beams were subjected to the same bending moment produced by a central top load. The maximum stresses were compared with the calculated values. Close agreement was found in the beams of the first series. However, the results in the second series were found to be safe but unsatisfactory when the span-to-depth ratios were reduced.

Kaar [1957] reported two series of experiments on centrally loaded single-span deep beams. A series of six aluminium beams with span-to-depth ratios varying from 0.3 to 1.0, and a series of five steel beams with span-to-depth ratio of 0.5 to 1.0 were tested. The strains were measured by electrical extensometers on both faces of the beam. He concluded that the stresses obtained from the simple bending theory would be in error when the span-to-depth ratio of the beam is lower than 1.5.

Three steel single-span deep beams having a span-to-depth ratio of 1.0, 1.5 and 2.0 were tested by Archer and Kitchen [1960]. Electrical resistance strain gauges were mounted at six points on the bottom edge of the beam. Except for the beam with span-to-depth ratio equal to 1.0, they found that the experimental stresses were bound between their analytical results and those given by the simple bending theory.

Saad and Hendry [1961a] carried out photoelastic tests on three simply supported Catalin deep beams under central top load with span-to-depth ratio of 0.63, 1.0 and 1.5. Observations showed that the horizontal stresses differed from those obtained by the simple bending theory when the span-to-depth ratio of the beam was less than 0.67. Their experimental results confirmed the theoretical solutions obtained by Durant and Garwood [1947] and Chow, Conway and Winter [1951]. Later, Saad and Hendry [1961b] presented another series of tests on beams having span-to-depth ratio of 0.45, 0.67, 0.89 and 1.85. Gravitational loading was studied using a centrifuge in conjunction with the frozen stress method of photo-elasticity. They

concluded that the finite difference method would produce accurate analysis of the gravitational stresses in deep beams. When a deep beam has a span-to-depth ratio less than 1.0, they deduced that the top portion of the beam above the depth equal to its span would hardly contribute any resistance to the bending moment caused by its self-weight. They emphasized that when the load was unsymmetric or there were holes in the beam, theoretical solutions would be very complicated.

2.3.2 Experiment on Reinforced Concrete Deep Beams

Klingroth [1942] recognised the importance of local reinforcement in the bearing zones of deep beams. From his experiment on three series of deep beams under top load with span equal to depth, he found that all beams failed by bearing crushing while their flexural reinforcement was still below their yield strengths.

Thereafter, Graf, Brenner and Bay [1943] tested a deep beam under bottom loading with side strips at the supports. It had a span-to-depth ratio equal to 0.5. Load was applied through the brackets on the bottom edges. Only fine horizontal cracks were observed even at about 30 percent of the failure load. They recognised the formation of a tied-arch as the load further increased. Horizontal cracks were formed gradually away from the bottom edge and sloped towards the side strips. Their beam failed at the horizontal connection between the bottom edge and the brackets.

Nylander and Holst [1946] assessed several series of tests on single-span and continuous deep beams under top loading. The

objective of their tests was to investigate the effects of cracking on the behaviour of deep beams. The prime concern of these tests was the principal tensile stress. Two series of continuous reinforced concrete deep beams were reinforced with special arrangement of web reinforcement according to the principal stresses distribution derived from their photoelastic tests for the stages before and after cracking. Besides, four series of concrete slabs with different amount of transverse steel were tested with concentric loading to study the effect of local reinforcement against local bearing crushing. Their results suggested that the position and the amounts of the transverse reinforcement would have little effect on the behaviour and capacity of the concrete slabs.

The results of the above tests drew Schütt's [1956] attention to the arrangement of reinforcement for the bearing zone of deep beams. He investigated two series of reinforced concrete deep beams subjected to top and bottom loading, respectively, with side strips. In general, for a beam under top loading, failure was suddenly brought about by the formation of a vertical crack at the junction between the side strips and the beam. Without the presence of horizontal web reinforcement, bent-up main reinforcement would not prevent such failure. For the bottom loaded beams, Schütt found that horizontal cracks would form on those beams reinforced with short suspension reinforcement as used by Graf and others. These cracks would occur above the ends of these bars. He found that a proper tied-arch would form when these reinforcements were carried up to the top edge. Substantially the failure load could be about 15 percent higher than those reinforced with short suspension reinforcement.

The effect of the bent-up reinforcement was not significant in such cases.

In an endeavour to assess the behaviour of beams from the transition range of shallow beam to deep beam, nineteen single-span reinforced concrete deep beams were tested under two-point top load by de Paiva and Siess [1965]. Their span-to-depth ratios were 1.8, 2.7 and 3.4. The concrete strength and the amount of tension reinforcement were their main parameters of interest. It was noted that their beams were reinforced vertically or inclined as those normally provided for conventional shallow beams. Therefore, other than reducing the mid-span deflection and the visible damage, these had little effect on the formation of inclined cracks and the failure loads regardless of the modes of failure. Beyond the inclined cracking, all their beams behaved essentially as tied-arches. Their modes of failure, which depending on the amount of main reinforcement, were flexural, shear and flexural-shear. They concluded that the formation of the inclined cracks would cause high stresses in the main reinforcement at the support and hence sufficient anchorage of these bars must be provided. The concrete strength appeared to have negligible effect on those beams which failed in flexure.

Leonhardt and Walther [1966] carried out 18 tests on single-span, continuous and indirectly supported deep beams. Of these, nine single-span deep beams were tested with span equal to depth. Five were tested under uniform top-loading while the other four were tested under uniform bottom load. Bent-up and inclined

reinforcements between 45 and 67 degrees to the horizontal were studied. Orthogonal mesh was provided as the nominal web reinforcement and vertical or horizontal hooks were used as the anchorage. Side strips, brackets and additional vertical web bars were introduced for the application of bottom load. The modes of failure of these beams were flexural failure, bearing crushing, failure of the notional concrete struts, and shear failure of the side strips or the bottom brackets. They recommended that vertical hooks should be avoided for the anchorage of the main reinforcement as they appeared to cause early bearing failure. They observed that beams with bottom loading would have multi-layers of cracking arches superimposed on each other. These cracks would extend at least to a height equal to its span and hence those vertical suspension bars should be extended beyond that level preferably with detailed hooks. Here, higher tied-arch stresses were found for the bottom loaded beams. Surprisingly, for the bottom loaded beams, compressive stresses were found immediately above the brackets. They summarized that bent-up bars were not effective for top loaded beams. However, under bottom loading, these bars would participate at the regions of the vertical hanger bars. Owing to the high compressive stresses induced by an adequately reinforced beam, the design criteria would be those of the ultimate stresses of the bearing zones or the compressive arches.

Two continuous two-span deep beams subjected to top load were also investigated. The first beam was reinforced with four bent-up main reinforcements at the supports. The second beam had its straight main reinforcement crossing the supports with horizontal

hooks. Additional bars were inserted above the intermediate supports. The first beam was subjected to uniformly distributed top load up to 82 percent of its failure load, then it was tested under two concentrated loads on each span to their failure. The second beam was tested under the same arrangement of concentrated loads. While a wider intermediate support bearing length was used for the first beam, additional side strips were cast in the second beam at the intermediate support to prevent premature bearing failure. Inclined cracks were found to be initiated near the bottom edge and propagated toward the upper edge of the beam. They found that under uniformly distributed load, the computed moment distribution of their tested beam using the method of Bay [1931] or Schleeh [1964] was within 10 percent of the measured values. They attributed the existence of a second neutral axis at the top edge of the first beam to the fault of support settlement. For the same moment, the flexural stress of the second beam was found to be 2.75 times that of the first beam when it was under uniformly distributed load. Better control of crack widths was due to the first beam which had adopted the inclined reinforcement pattern. Both beams failed by shear from the edge of the intermediate supports to the top edge.

Additional data on two indirectly loaded and supported single-span deep beams were also reported. The central load and the two end supports were applied through three transverse panels. These two beams were identical other than their arrangement of reinforcement. In particular, the main reinforcement of the first beam were bent-up at 60 degrees and fanned out from the centre to both ends. The transverse panels were reinforced to the same extent

as the main beams. Top loads were applied to the ends of the central transverse panel and the main beam was rested on two simply supported transverse panels on its ends. They observed that the crack patterns of the end transverse panels were similar to those bottom-loaded single-span deep beams but with a flatter arching of cracks. At about 90 percent of the failure load, the first test was interrupted because of the necessity to reinforce the premature damage at the junction of a bent-up bar of the central transverse panel. Both beams failed by crushing of the inclined notional concrete strut. Even under indirect loading, tied-arch action prevailed, whereby the individual struts supported themselves directly on the bottom corners of the main beam. The inclined bars would act as shear and suspension reinforcement at the same time. They also had a better control on crack widths than the orthogonal reinforcement of the main beam and the end transverse panels. However, this was the opposite for the central transverse panel. The arrangement of the reinforcement would have an insignificant effect on deflections and failure loads. From their experience, recommendations were given at the end of their report for the design of deep beams with span-to-depth ratio less than 2. Cases such as single-span or continuous deep beam and indirect loads or supports were accounted for.

An important contribution on tests of large-scale specimens was due to Crist [1971] on the formulation of a design equation for shear capacity of deep beams. He conducted a series of static and dynamic tests on reinforced concrete deep beams. Nine single-span deep beams were tested under uniformly static load with span-to-depth ratios of

1.6, 2.7 and 3.8. Five beams were reinforced with orthogonal web reinforcement and four were reinforced without web reinforcement. It was found that the former beams failed essentially in flexure while the latters were in shear. Furthermore, three more beams with span-to-depth ratio of 1.6 were tested under dynamic loads. They had different amounts of web reinforcement. None of these beams was tested to destruction. Their crack patterns were similar to those in the static tests.

Great experimental effort on single-span reinforced concrete deep beams was made by a team of researchers under the general direction of Kong [kong et al, 1970-1972d]. Based on 135 destruction tests on two-point top-loaded reinforced concrete deep beams, a semi-empirical equation was developed to cover a range of single-span deep beams with span-to-depth ratio between 1 and 3. This equation was well justified with different arrangements of web reinforcement. A sequence development of their research extended the equation to encounter deep beams with web-openings. They concluded that the clear-shear-span-to-depth ratio was a more important parameter than the span-to-depth ratio. The major mode of failure of their beams was diagonal cracking. Bearing failure and failure of the notional concrete strut were only the secondary effects. In view of the scarcity of experimental evidence on deep beams with web-openings, two-point and four-point loadings were adopted for a wide range of deep beams with rectangular web-openings and different reinforcement arrangements. In addition, 8 large-scale tests on 4.0 m x 1.8 m deep beams, including normal weight and light weight concrete, were tested to destruction. From these, a general structural idealization of

upper and lower load paths transmission theory was introduced. The proposed equation was modified accordingly for the design of shear capacity of deep beams with rectangular web-openings [Kong and Sharp, 1973a,b; 1977]. More recently, the research attention was drawn towards the buckling and instability of slender deep beams [Kong et al, 1986a,b]. 38 tests were reported on slender reinforced concrete deep beams having height-to-thickness ratios in the range of 25 to 67. Details of these tests would be discussed in Chapter 6 of this thesis.

In order to investigate more thoroughly the actual behaviour of reinforced concrete deep beams before cracking, Garcia [1981] used a photoelastic coating to observe the behaviour of small top loaded reinforced concrete deep beams with span-to-depth ratio equal to 0.22. From the overall photoelastic stress patterns, he observed that flexural cracks would develop at the mid-span during the initial stage of loading. At high load, diagonal cracks would initiate near the supports and would propagate downward and upward. He confirmed the analogy of split cylinder action to the diagonal cracking of deep beams.

Besser [1983] performed a systematic experimental study on 24 single-span reinforced concrete deep beams examining a combination of top and bottom loadings and very deep beams. 17 single-span deep beams with bottom loading brackets were investigated under various combinations of uniformly distributed top and bottom loadings. They were 72 mm thick and 1000 mm deep with a simple span of 1000 mm. Five layers of 10 mm diameter plain bars were used in pairs as the

main reinforcement. The web reinforcement was provided by 6 mm diameter plain bars in an orthogonal pattern on both faces of the beam. The percentage of vertical web reinforcement used was varied from 0 to 2 percent. Five different combinations of top and bottom loads in the form of top load only, bottom load only, equal top and bottom loads or top and bottom loads in the ratios of 2 to 1 and 1 to 2 were investigated. For beams under top load only, it was noticed that the crack patterns were almost unaffected by the amount of vertical web reinforcement. Flexural cracks were the first to appear and were then followed by diagonal cracks. Bearing failure was the characteristic mode of failure among these beams. When the beam was loaded on the bottom only, the increase of the amount of vertical web reinforcement would reduce the crack widths of the specimen. The first crack to form was always a long horizontal crack at the middle third of the span at about 200 mm from the soffit. A series of arch-shaped cracks would form as the load increased. Generally, the angles of inclination of the diagonal cracks were flatter than on a top loaded beam. With different proportions of top and bottom loads acting simultaneously, the behaviour of the beam was intermediate between that of a purely top loaded beam and a purely bottom loaded beam. The degree of resemblance of this former behaviour with the latter varied with the relative magnitude of the top and bottom loads.

Though most of these tests were terminated before the destruction of the specimens, it should be noted that as the amount of vertical reinforcement increased, bearing crushing was the most common mode of failure. With a high percentage of vertical reinforcement, cracks

would be more serious and extensive toward the upper portion of the beam. From his analysis, Besser concluded that beams designed according to CIRIA [1977] and ACI Code [1983] were conservative for top loading. Nevertheless, the serviceability limit on crack widths set by these documents was satisfactory for bottom loading cases [Cusens and Besser, 1985].

In addition, seven slender single-span deep beams with depth-to-thickness ratio ranging from 10 to 40 were tested under two-point top loads [Besser and Cusens, 1984]. Constant thicknesses of 72 mm and 720 mm simple span were used. The span-to-depth ratio varied from 0.25 to 1.0. The main reinforcement was provided by four plain bars in 2 layers and they were well anchored to the end steel blocks. Orthogonal plain bar mesh was placed on each face as web reinforcement. Five of these beams failed at their bearing zone. Buckling was the failure mode of the deepest beams.

Rogowsky, MacGregor and Ong [1983; 1986a,b] tested 23 reinforced concrete deep beams. Six single-span and 17 two-span continuous deep beams were tested under central top loading with shear-span-to-depth ratios varying from 1 to 2.5. Minimum and maximum web reinforcement as specified in the ACI Code [1983] together with beams without web reinforcement were studied. Fixed spans of two metres were used for all tests. Various shear spans were obtained by varying the depth and the size of the column stubs which were cast integrally with the beams. The same type of straight deformed reinforcement was maintained and detailed with vertical hooks throughout. After the first failure, each beam was reinforced externally on the failed span

with a yoke and retested. For beams with or without light web reinforcement, major inclined cracks appeared at about 25 percent of the failure load. Then, these beams behaved essentially like that of a tied-arch. Failure was suddenly brought about by the crushing of the compression strut. In the case of heavy reinforced deep beams, the compression struts tended to be less well defined and failures were more ductile. Also, their failure loads were not affected by their shear-span-to-depth ratios. Rogowsky et al [1986b] reported that the horizontal web reinforcement had little effect on the behaviour of all their beams. With their more realistic load and support columns, it is interesting to note that no bearing failure was observed. They suggested that the transition range of shallow beam and deep beam behaviour occurred when the shear-span-to-depth ratio was about 2.

CHAPTER THREE

CODES AND MANUALS - A CRITICAL REVIEW

3.1 INTRODUCTION

This chapter discusses the design of the following types of reinforced concrete deep beams :

(1) Deep beams without web openings.

(2) Deep beams with web openings.

(3) Deep beams subjected to combined top and bottom loadings.

As stated in Chapter 1, the major documents covering deep beam design are :

(a) CIRIA Guide 2 [1977] - reprinted with corrections in 1984,

(b) CEB-FIP Model Code [1978],

(c) Reinforced Concrete Designer's Handbook [Reynolds and Steedman, 1981],

(d) ACI Building Code 318-83 [1983, revised 1986], and

(e) Canadian Code CAN3-A23.3-M84 [1984].

Each of these documents will be discussed, where appropriate, for the design of the above-mentioned three types of deep beams.

3.2 CURRENT DESIGN METHODS

3.2.1 Preliminary Remarks

The ACI Code [1983, revised 1986], listed in Section 3.1 above, refers to the PCA Concrete Information ST66 [1946]. Hence, Section 3.2.2 below will begin by explaining how to use the PCA bulletin to obtain the data for subsequent use with the ACI Code.

3.2.2 Deep Beams without Web-Openings

Portland Cement Association (PCA)

The PCA Concrete Information ST66 [1946] is based on Dischinger's elastic analysis [1932] and not on the results of ultimate load tests. It applies to simply supported beams of span/depth ratios up to 1.5 and to continuous beams of span/depth ratios up to 2.5.

The bending moment, the tensile force T and the lever arm z are to be obtained from design charts, using two characteristic ratios ϵ and β, which are defined as follows. For a continuous beam, ϵ is taken as equal to c/L and β as equal to h/L, where

c is the width of a support (e.g. the dimension of a column in the directions of a column in the direction of the span),

L is the beam span, and

h is the overall height of deep beam.

For a simply supported beam, ϵ and β need careful interpretation [PCA, 1946] :

When under uniformly distributed load,

$$\epsilon = \frac{l}{2} \quad \text{and} \quad \beta = \frac{h}{2L}$$

When under a single point load applied at mid-span,

$$\epsilon = \frac{c}{2L} \quad \text{and} \quad \beta = \frac{h}{2L}$$

The PCA documents does not cover two-point loading, but for two-point

loads applied at the third-span points, Kong et al [1975] have recommended that the quantity L in the above equations should be replaced by 2L/3.

The tensile force T to be resisted can be read from a chart in the PCA, as reproduced here in Fig.3.1. The required area of the flexural steel A_s can then be obtained from the appropriate allowable working stress of steel f_s. That is,

$$A_s = T / f_s$$

The shear capacity V should satisfy the following expression :

$$\frac{8\ V}{7\ bd} = \frac{v}{3}\left(1 + \frac{5H}{L}\right)$$

where v is the allowable shear stress for shallow beams;

H is the overall height;

L is the simple span;

b is the width of the beam;

d is the effective depth of the tensile steel.

Subsequent refinements were made to extend this design method even into the ultimate limit states. Chow, Conway and Winter [1952] proposed that the amount of the tensile steel should be increased by 50 percent to secure homogeneous action and reduce cracking. Park and Paulay [1975] proposed that the moment arm should be derived from the CEB-FIP Recommendations [1970]. To avoid cracking at service load, the PCA "Note on ACI 318-83" [PCA, 1984] limited the tensile stresses to the modulus of rupture of concrete. In the design

examples of this document, factored moment and shear were included to comply with the strength design method of the ACI Code [1983, revised 1986]. By using the working stress design criteria, the attainable reserve strength of deep beams after cracking could not be furnished.

The Comité Européen du Béton - the Fédération Internationale de la Précontrainte (CEB-FIP)

Adopting most of the findings from the experimental evidence given by Leonhardt and Walther [1966], the Comité Européen du Béton - the Fédération Internationale de la Précontrainte (CEB-FIP) published the "International Recommendations for the Design and Construction of Deep Beams, Appendix 3" [CEB-FIP, 1970]. To date, the CEB-FIP Modal Code [1978] still recommends engineers to consult the deep beam design provisions given by this earlier document. It applies to single-span deep beams having span-to-depth ratio up to 2.

The effective span L of a simply supported beam is taken as the lesser of

1. the distance between the centres of supports,
2. 1.15 times the clear distance between the column faces.

The lever arm z for the ultimate moment is defined as a function of the span/depth ratio L/h :

For a single-span deep beam,

$$z = 0.2\ (L + 2h) \quad \text{(when } L/h \text{ is between 1 and 2)}$$

$$\text{or } z = 0.6\ L \quad \text{(when } L/h \text{ is less than 1)}$$

When the span-to-depth ratio is greater than 2, the lever arm will be

the same as for normal shallow beams.

The bending moment M is calculated from the effective span L determined above. The amount of flexural reinforcement required is then adjusted by the ultimate bending moment M with its lever arm, that is,

$$A_s = M/(0.87f_y\, z)$$

where f_y is the yield stress of steel.

These flexural bars should be spread uniformly over a height equal to (0.25h - 0.05L) from the soffit. They should be anchored beyond the supports without curtailment. It is recommended that small diameter bars should be used, to reduce crack widths and to facilitate anchorage fixing. Vertical type anchorage hooks are not recommended, as cracking is likely to be promoted. It explicitly excludes the problem of concrete crushing in the compression zone. The problem of instability or lateral buckling is recognised; however, only very crude suggestions, such as providing lateral supports or increasing the width of the beam, are given to avoid buckling.

The effective height h_a of a deep beam is taken as the lesser of :

1. the actual height h,
2. the effective span L.

The ultimate shear capacity of the deep beam section is then taken as $0.1bh_a[f_c'/\gamma_m]$, where b is the beam thickness, f_c' is

the concrete cylinder strength and γ_m is the partial safety factor taken as 1.5 here. The amount of web reinforcement is generally regarded as nominal and depends on the configuration of the loading. For a top-loaded beam, the minimum area of the web reinforcement should be at least $0.0025bS_v$ for plain round bars and $0.0020bS_v$ for deformed bars, where S_v is the spacing of the web bars. When the load is small, an orthogonal arrangement is preferred. Smaller spacing of bars should be used near the support regions. Additional horizontal reinforcement is recommended at each support, to spread over the length $0.3h_a$ of the span, while additional vertical reinforcement is required to cover the lower half of the beam within $0.2h_a$ from each support face. For bottom loading, to activate the upper portion of the beam, additional stirrups should be introduced to supplement the former arrangement. These stirrups should enclose the flexural bars without interruption and extend the full effective height h_a. Regardless of the dimensions of the deep beam, the maximum spacing of the vertical bars is restricted to 150 mm.

Deep beams with vertical connections or cruciform columns are considered as being indirectly loaded. Suspension reinforcement should be provided in the form of vertical stirrups or bent-up bars (when loading is large). Only 60 percent of the total load is allowed to be carried by the bent-up bars with a minimum radius of curvature equals to 20 times its diameter. Deep beams which rested over massive supports are defined as indirectly supported.

Orthogonal mesh could be used at their design stress :

the vertical and horizontal bars should be designed to take the total

shear force and 80 percent of the total shear force, respectively. The horizontal bars should spread to a height equal to half of its effective height ($0.5h_a$) and the vertical bars should spread to 0.4H or 0.3L, whichever is the lesser.

Alternatively, especially when the shear load exceeds 75 percent of the ultimate shear capacity of the section, inclined bars are recommended to take 80 percent of the total shear. These bars should spread horizontally over the length $0.4h_a$ of the span from each support face, and also vertically to a height equals to $0.6h_a$ from the soffit.

The CEB-FIP Recommendations have detailed provisions for calculating bearing capacities. For the simple case of a deep beam of rectangular cross section, the bearing capacity is taken as $0.8f'_cbc$ at a simple support and as $1.2f'_cbc$ at an intermediate support, where b, c and f'_c are as defined earlier.

American Building Code (ACI)

Prompt action followed after the CEB-FIP recommendations [1970]; in the following year, the American Building Code ACI-71 [1971], for the first time, stipulated shear design provision for deep beams with clear-shear-span-to-depth ratios greater than 2.5 (1.25 for continuous beams). However, no recommendations are provided for deep beams in flexure, even in the latest edition [1983, revised 1986]. Designers are merely urged with a reminder to take strain nonlinearity and lateral buckling into account, and to refer to the PCA bulletin [1946] for the required flexural steel area A_s - see

previous section above. The provisions for the shear strength are based on those obtained from the experimental findings of de Pavia and Siess [1965], and Crist [1971]. They are applicable to deep beams having clear-span-to-depth ratios of less than 5, and loaded at the top and supported on the bottom so that compression struts can develop between the load and support points. Generally, the factored shear capacity of a section is expressed as follows : that is, the factored shear contribution from the concrete plus the factored shear contribution from the steel. The critical section for shear, measured from the face of support is :

1. Uniform loading : $0.15L_n$ or d, whichever is the less, where L_n is the clear span and d is the effective depth,
2. Concentrated loading : $0.5a_v$ or d, whichever is the less, where a_v is the shear span between the load and the face of the support.

Firstly, the overall depth and thickness of the beam are checked against the following shear provisions [ACI-318M, 1985] :

When the ratio is between 2 and 5, the shear strength is given by,

$$V_n = 2/3\ (10 + L_n/d)\sqrt{f'_c}\ b_w\ d$$

where b_w is the width of the web in mm

When the ratio is less than 2, the term $(10 + L_n/d)$ is equal to 1.

Then, the nominal concrete strength of the section can be determined as follows :

$$V_c = (2\sqrt{f'_c}/6)\ b_w\ d$$

Besides, the effects of flexural steel and M_u/V_u d factor can be taken into account by the expression stated below :

$$V_c = (3.5 - 2.5\ M_u/V_u\ d)[(\sqrt{f'_c} + 120\ \rho_w\ M_u/V_u\ d)/7]\ b_w\ d$$

where the term (3.5 - 2.5 M_u/V_u d) should be less than 2.5,

V_c must be less than $(\sqrt{f'_c}/2)\ b_w\ d$,

ρ_w is the main steel area to the area of the concrete section bd ratio, and

M_u and V_u are the factored moment and shear

As mandatory, an orthogonal web mesh of at least 0.15 percent of the horizontal concrete sectional area bL, and 0.25 percent of the vertical concrete sectional area bd should be provided.

Additional shear strength can be provided throughout the span by increasing the web reinforcement with the following expression :

$$V_s = \left[\frac{A_v}{S} \left(\frac{1 + L_n/d}{12} \right) + \frac{A_{vh}}{S_2} \left(\frac{11 - L_n/d}{12} \right) \right] f_y\ d$$

where A_v is the shear reinforcement perpendicular to the flexural bars within a distance S (S < d/5 or 500 mm);

and A_{vh} is the shear reinforcement parallel to the flexural bars within a distance S_2 (S_2 < d/3 or 500 mm)

When loads are applied at the bottom or sides of the beam, no special shear provision is provided and normal shear design rules should be used.

The Construction Industry Research and Information Association (CIRIA)

In the United Kingdom, the latest Code of practice for structural concrete members, the BS 8110 [1985], has followed its predecessor CP 110 [1972], in that deep beam design is excluded. In BS 8110 : Part 1 : Clause 3.4.1.1, deep beam designers are told to consult specialist literature. To date, it can be said that the most comprehensive specialist literature on deep beam design in the United Kingdom, and indeed in Europe, is "CIRIA Guide 2 : The Design of Deep Beams in Reinforced Concrete", which was issued by the Construction Industry Research and Information Association [CIRIA, 1977] in 1977. The Guide is intended to be used for single-span deep beams with span-to-depth ratio less than 2 and for multi-span deep beams with span-to-depth ratio less than 2.5.

The CIRIA Guide quotes extensively from the works of Leonhardt et al [1966] and Kong et al [1970-73b], and from the CEB-FIP recommendations [1970]. It gives two design rules for deep beams; namely, the Simple Rules and the Supplementary Rules both of which are to be used in conjunction with the old code CP 110. The Simple Rules cater for the simple types of deep beams whereas more complex cases such as those involving concentrated loading, buckling and

web-openings, are dealt with by the Supplementary Rules. The CIRIA Guide defines the effective span L of a deep beam as :

$$L = L_o + \frac{c_1}{2} + \frac{c_2}{2}$$

where

L_o is the clear span, and

c_1 (or c_2) is the support width which is to be taken as $0.2L_o$ if it exceeds $0.2L_o$.

The active height h_a of a deep beam is defined as equal to the actual height h or the effective span L_o, whichever is less. The amount of flexural reinforcement required is (as given in the Appendix 3 of the CEB-FIP recommendation [1970]) :

$$A_s = M/(0.87f_y\ z)$$

where f_y is the yield stress of steel.

The minimum proportion of this steel, related to the local area of concrete in which it embedded, should not be less than $0.52\sqrt{f_{cu}}/0.87f_y$ as tabulated in Table 1 of the Guide. These bars should spread over a depth $0.2h_a$ from the soffit of the beam.

The ultimate moment capacity M of the concrete section should not exceed $0.12f_{cu}\ b\ h_a^2$. Different provisions are given to design the shear capacity of deep beams with bottom-loading and top-loading.

For a bottom-loaded beam, the shear capacity V is

$$V < 0.75\ b\ h_a\ v_u$$

where v_u is the shear stress value as given in Table 6 of CP 110 (for normal weight concrete) or in Table 26 (for lightweight concrete) of CP 110 [1972].

These hanger bars should be designed for a stress capacity equal to $0.87f_y$ and should also be anchored to comply with Clause 2.4.2 of the Guide.

Nominal horizontal web reinforcement is required over a length $0.4h_a$ from each support. The minimum amount of web steel should comply with Clause 3.11 and 5.5 of CP 110 [1972].

For top-loaded beams, the concept of effective-clear-span x_e, as introduced by Kong et al [1972d, 1975], is adopted. It is defined as the least of the following :

1. the clear-shear-span of the load which takes more than half of the total shear force at the support;
2. L/4 for uniformly distributed load;
3. the weighed average of clear-shear-span of all the individual load.

The shear capacity of the concrete section should satisfy all the conditions listed below :

For h_a/b less than 4,

$$V < 2.0\ b\ h_a\ v_c/x_e$$

For h_a/b greater than or equal to 4,

$$V < 1.2\ b\ h_a\ v_c/x_e$$

$$V < b\ h_a\ v_u$$

where v_c is taken from Table 5 of CP 110 (for normal concrete) and from Table 25 of CP 110 (for lightweight concrete).

Where the actual beam height h exceeds the active height h_a, the CIRIA Guide recommends that the contribution of the web steel which lies within the active height h_a can be taken into account by using a modified equation developed by Kong et al [1972d, 1975] :

$$\frac{V}{b\ h_a} = \lambda_1 \left[1 - 0.35 \frac{x_e}{h_a} \right] \sqrt{f_{cu}} + \lambda_2 \frac{\sum 100\ A_r y_r \sin^2\theta_r}{b\ h_a^2} \qquad (3.1)$$

where

$\lambda_1 = 0.44$ for normal concrete,

$= 0.32$ for lightweight concrete;

$\lambda_2 = 1.95\ N/mm^2$ for deformed bars,

$= 0.85\ N/mm^2$ for plain round bars;

b = the beam thickness;

h_a = the beam height h or beam span L_o whichever is less;

f_{cu} = the concrete cube strength;

A_r = the area of a typical web bar intersecting the critical angle θ_r (Fig.3.2).

For a beam with orthogonal web reinforcement pattern, the above equation can be simplified as :

$$\frac{V}{b\ h_a} = \lambda_1 v_x + \beta_1 v_{ms} + \beta_2 v_{wh} + \beta_3 v_{wv} \qquad (3.2)$$

where

λ_1 is defined as above;

β_1, β_2 and β_3 are equal to 1.0, 0.4 and 0.7 for deformed bars, plain round bars and wire weld mesh, respectively;

v_x is the concrete shear stress parameter.

It is equals to $(1 - 0.35\ x_e/h_a)\sqrt{f_{cu}}$ as defined in the first term of the above equation (3.1);

v_{ms}, v_{wh} and v_{wv} are the steel shear stress parameters of the main steel, the horizontal and the vertical web steel, respectively. These values depend on the x_e/h_a ratio and the percentage of steel and are tabulated in Table 6, 7 and 8 of the Guide.

In using equation (3.1) or (3.2) the steel contribution should not be less than 20 percent of the total shear V. The overall ultimate shear capacity should also not exceed an upper limit as given below,

$$\frac{V}{b\ h_a} = 1.3\ \lambda_1\sqrt{f_{cu}}$$

The maximum crack width is controlled by the spacing of steel given in Table 2 and Table 3 of the Guide for crack width of 0.3 mm and 0.1 mm respectively. The minimum amount of nominal web reinforcement should comply with the requirements for walls in Clauses 3.11 and 5.5 of CP 110 in both vertical and horizontal directions.

The limiting bearing stress is taken as $0.4f_{cu}$. If the concrete area is confined with additional steels according to Clause 3.4.3 in the Guide, this limit can be increased up to $0.6f_{cu}$ at the end supports and to $0.8f_{cu}$ under concentrated loading.

As the depth-to-thickness ratio of a deep beam is greater than, say 25, the risk of buckling failure will cause real concern and has to be dealt with. Among all the main design documents, the CIRIA Guide is the only one that explicitly includes recommendations for the design of buckling strength of slender deep beams. Buckling failures are catastrophic and difficult to predict. However, experimental evidence on buckling failure is very scarce [Kong et al, 1986b]. Therefore, the emphasis of design rules in the CIRIA Guide is not on the acquisition of the physical insight into the buckling behaviour, but on the provision of a tool that can be used to achieve a safe design. An elastic approach is adopted in the CIRIA Guide. The elastic stress distribution of the beam is assumed to be known. Typical elastic stress distribution of the beam can be obtained in Appendix A of the Guide or from other specific elastic analysis such as finite element analysis.

In the Simple Rules (Clause 2.2.3), it is stated that the capacity of a deep beam need not be reduced if its effective-height-to-thickness ratio is less than 12 (the definition of short braced wall in Clause 3.8.1.1 of CP 110), and also if adequate bracing is provided against lateral instability. When such conditions cannot be met, the slenderness effects have to be dealt with; the Guide gives three methods with increasing refinement :

a. the Supplementary Rules - CIRIA Guide Clause 3.2.2

b. the Single-Panel Method - CIRIA Guide Appendix C

c. the Two-Panel Method - CIRIA Guide Appendix C

The aim of these methods is to find an effective height or length for each panel to achieve a safe lower bound solution.

In the Supplementary Rules, the following conditions have to be satisfied :

1. the beam must be adequately braced and rectangular in shape.
2. at least two opposite edges of the beam are laterally restrained.
3. the average shear stress ($V/b\ h_a$) of the beam must not be greater than 50 percent of the average vertical or horizontal axial compressive stress, whichever is the greater.

The effective height or length h_e of the panel concerned is determined as follows :

1. when all four edges of the beam are restrained, h_e is equal to 1.1 x the shortest distance between the centres of the parallel lateral restraints;
2. when one or two opposite edges of the beam are free, h_e is equal to 1.5 x the distance between centres of parallel lateral restraint;
3. when both rotational and lateral movements of the beam are restrained, h_e is equal to the clear distance between the restraints.

A vertical or horizontal strip of unit width is then chosen to check for its sectional strength as described in Clause 3.8.1 of CP 110 for slender wall. The choice of the strip depends on the direction of the maximum stress : a vertical strip should be used when the maximum vertical axial stress is greater than the maximum horizontal axial stress, or vice verse. The total ultimate moment of

the section M_t is presented as the sum of two moments, that is,

$$M_t = M_i + M_{add}$$

where

M_i is the initial moment due to an initial eccentricity e_i, say 0.05b, with an axial load N_v per unit width;

M_{add} is the additional moment caused by the slenderness effect, $M_{add} = N_v\, e_{add}$,

From equation (33) of CP 110, e_{add} is taken as

$$\frac{b}{1750} [h_e/b]^2 [1 - 0.0035\, h_e/b]$$

h_e is the effective height or length of the column strip.

In order to determine the buckling load N_v, a load-moment interaction diagram is required either by using the standard column charts in CP 110 : Part 2 or by constructing it in accordance with the 'Notes on the derivation of design charts' given in Appendix A of CP110 : Part 2. A straight line, with a slope given by the reciprocal of the sum of the initial and additional eccentricities, can be drawn to intersect the interaction curve. Hence, the ultimate axial load of the section can be read off.

The Single-Panel and the Two-Panel Methods require a more rigorous analysis to determinate the effective height and length of the panel. Notional safe equivalent panels are chosen first to carry

the equivalent applied load (see Fig.123 in the CIRIA Guide). In the Single-Panel Method, the overall dimensions of a rectangular equivalent panel are taken at the positions where the actual applied stresses are at a maximum. Mean shear stresses are applied at the edges. The equivalent vertical, horizontal and shear applied stresses (N_v, N_h and τ) are those corresponding to the safe equivalent applied load as described on p.106 of the Guide. The theoretical critical stresses of the panel are determined as below :

Critical Vertical Stress :

$$N'_{vcr} = \frac{K \pi^2 \, EI'}{a^2}$$

Critical Horizontal Stress :

$$N'_{hcr} = \frac{K \pi^2 \, EI'}{a^2}$$

Critical Shear Stress :

$$\tau'_{cr} = \frac{4.7 \pi^2 \, EI'}{b^2}$$

where a and b are the overall dimensions as defined in Fig.124 and Fig.128 of the Guide;

K is the reduction coefficient;

EI' is the flexural rigidity of the panel per unit width.

The ratios of the above stresses are then calculated as follows :

Vertical Stress Ratio, $R'_v = N_v / N'_{vcr}$

Horizontal Stress Ratio, $R'_h = N_h / N'_{hcr}$

Shear Stress Ratio, $R'_s = \tau / \tau'_{cr}$

The CIRIA Guide also introduces new stress ratios :

$$R_1' = R_h'$$

$$R_2' = R_v'$$

$$R_2'' = R_2'/M_2'$$

where M_2' is a modification factor which depends upon the shear moment M_s and the ratio of R_2'/R_s' as given in Fig.129 of the Guide.

With these modification factors, another two modification factors M_1 and M_2 are found by using Fig.130 of the Guide.
The modified critical stresses are then given as follows :

$$N_{vcr} = M_2 \times N_{vcr}'$$

$$N_{hcr} = M_1 \times N_{hcr}'$$

The effective height, h_e, and the effective length, l_e, are determined from their theoretical critical stresses expressed below :

$$h_e = \sqrt{\pi^2 EI' / N_{vcr}}$$

$$l_e = \sqrt{\pi^2 EI' / N_{hcr}}$$

Hence, the vertical and horizontal strips of unit width are checked for their sectional strength as mentioned before.

In the Two-Panel Method, similar procedures are adopted for two panels. The effective height will be determined from the first panel by employing an upper-bound equivalent horizontal load together with a lower-bound equivalent vertical load. The second panel will give

the effective length by adopting a lower-bound equivalent horizontal load and an upper-bound equivalent vertical load.

Canadian Concrete Code (CAN3-A23.3-M84)

Most recently, a rational approach to shear design was introduced by the 1984 Canadian Concrete Code (CAN3-A23.3-M84) [1984]. Based on the compression field theory, plasticity concepts and truss models, a direct design procedure - the General Method - was developed which enable engineers to approximate a top-loaded deep beam by a strut and tie truss model. Following the flow of internal forces developed by the applied loads and support reactions, an equilibrium truss model, which consists of compressive struts, tension tie and nodal points, is used to simplify the complex mechanism :

1. Concrete struts are used to model the region with uni-directional compressive stress,
2. Tension ties are used to represent the main longitudinal reinforcement,
3. At the nodes where the struts and ties meet, the concrete is subjected to multi-directional stresses. These nodes are regarded as the nodal zones.

In general (see Fig.3.3), for a single-span deep beam with two-point loading, two compressive struts can be obtained. Each of them transfers an applied load P directly from the loading nodal zone to the support nodal zone. Both struts are inclined at an angle α_s to a horizontal tension tie. At the loading nodal zone, the applied load P is balanced by a horizontal force C of the concrete

compressive strut at the top edge of the beam and the forces induced by the inclined compressive strut. At the bottom of the inclined strut, the strut emerges to the support nodal zone and its compressive force is balanced by the applied reaction P together with the tension tie force T. The top part of the inclined strut is directed to the loading nodal point which is connected to another horizontal compressive strut that rests on the top edge of the beam between the two loading zones.

First, the bearing stresses at the load and support zones are checked against the allowable bearing stress, that is,

$$\text{Allowable bearing stress} = \lambda \phi_c f_c'$$

where λ is the reduction factor for concrete,

to be taken as 0.6 here;

ϕ_c = 0.85 in nodal zone with no tension tie,

= 0.75 in nodal zone anchoring a tension tie,

= 0.60 in nodal zone anchoring more than one tension tie;

f_c' = concrete cylinder compressive strength.

Next, the area of the tension tie required is determined by using the equilibrium conditions of the tension tie force T, the compressive force C and the applied moment M as follows :

Equilibrium of forces :

$$T = C$$

where $T = \lambda \phi_c f_c' a' b$

$C = \lambda \phi_c f_c' a b$

a = the depth of the upper nodal zone

a' = the depth of the lower nodal zone

The primary depth of the lower nodal zone can be easily estimated as,

say, $a' = (0.85/0.75)a = 1.13a$

Equilibrium of moments :

Applied moment = $P a_t$

$= C (h - a/2 - 1.13a/2)$

where a_t is the total shear span

From this equation, the depth of the upper nodal zone and hence the depth of the lower nodal zone are found. A suitable amount of steel can be chosen to distribute over the depth of the lower nodal zone. The effective area of concrete should have the same centroid as the tension reinforcement. In addition, sufficient anchorage should be provided for the tension force T to develop.

The compressive strength of the horizontal strut should be checked against the allowable strength, that is,

$$C = \lambda \phi_c f_c' a b$$

Next the compressive stresses of the inclined strut F ($= P/\sin\alpha_s$) is checked to ensure that it is not exceeded by the

allowable compressive stress $f_{2\ max}$.

As no tension tie is crossing the top region of the inclined strut, the allowable compressive stress $f_{2\ max}$ is normally taken as $\phi_c f'_c$. However, the bottom region of the inclined strut is crossed by the tension tie and hence the $f_{2\ max}$ value has to be reduced. An average strain value, e_s, say 0.001 (or f_y/E_s, where E_s is the elastic modulus of steel) has to be assumed in the tension tie to determine the principal tensile strain e_1 in the strut. From strain compatibility,

$$e_1 = e_s + (e_s + 0.002) / \tan^2\alpha_s$$

then the limiting stress is calculated as

$$f_{2\ max} = \lambda \phi_c f'_c / (0.8 + 170\ e_1)$$

To maintain the crack control and ductility of the beam, additional uniform distributed pairs of web bars should be provided in both vertical and horizontal directions of the beam. The maximum spacing S of the vertical and horizontal bars are restricted to one-fifth and one-third of the effective depth of the tension steel, respectively. In no case should S be greater than 300 mm. The minimum amount of steel should not be less than 0.002bS in each direction.

3.2.3 Deep Beams with Web-Openings

In practice, openings might have to be included in deep beams to provide access and services. Experimental evidence on the strength and behaviour of deep beams with web-openings became available only very recently (e.g. Kong et al [1973a,b; 1977; 1978]). All the major concrete structure design codes such as the BS 8110 [1985], ACI-318 [1983], CEB-FIP [1978] and CAN3-A23.3-M84 [1984]) had excluded the subject of web-openings for deep beams in their design provisions.

Earliest design methods on this aspect, and even recent ones, were mainly based upon the theory of elasticity and the results obtained from photoelastic tests [Rasheeduzzafar and Al-Tayyib, 1986]. In essence, these methods dealt with localized stresses around the holes. The presence of holes was assumed to have little influence on the elastic stress distribution in a deep beam. Uhlmann [1952] assumed that the internal forces of a deep beam which intercepted a hole could be redirected around such a hole. This would increase the stresses along the edges of the hole in the direction tangential to those original stress lines without the hole. Opposite stresses were also induced along the other edges which were perpendicular to these stress lines. This design approach, however, offered no guidance on the size and location of the opening in a deep beam.

Later, in Figures 17 to 21 of the CIRIA Guide [1977], approximate stress patterns of different loading configurations and geometries were provided to assess the admissibility of holes. The location and size of holes were compared with the appropriate force band pattern. There was insufficient experimental evidence available at the time of

its publication to confirm its validity; it now seems, however, that this method is excessively conservative. The dimensions of holes were restricted to 0.2 times the width of the notional force band. By using the concept of 'equivalent' hole, two pairs of simply-supported square deep beams were assumed to envelope the real hole. They were oriented orthogonally to the principal stress axis. Equal amount of bending reinforcement was recommended to be placed parallel to the faces of the real holes and the equivalent hole.

Though the aforementioned methods are interesting, their application to reinforced concrete deep beams is not satisfactory, partly because of their excessive conservatism and partly due to their incompatibility with the behaviour of the beam after cracking. To date, valuable information on reinforced concrete deep beams with web-opening is provided by the experimental evidence given by Sharp [1977]; Kubik [1978]; Singh, Ray and Reddy [1979, 1980]; and, Swaddiwudhipong and Shanmugam [1985]. Of these cited works, the most systematic investigations had been those undertaken by Sharp and Kubik.

Sharp conducted 79 tests on simply-supported reinforced concrete deep beams with rectangular web-openings. The overall dimensions of his specimens were 1500 mm span by 750 mm overall depth by 100 mm width. Eight different arrangements of web reinforcement, various sizes and location of web-openings were investigated. From his results, Sharp observed that the failure modes of deep beams would depend upon the extent of interruption to which a hole intersected with the notional load path that joining the load and support points

(see Fig.3.4). Inclined web reinforcement was found to be effective for crack width control and would marginally increase the ultimate shear strength of a deep beam. In contrast, trimming the opening has little beneficial effect on its ultimate capacity. In addition, Sharp proposed a structural idealization (the truss model) for deep beams with web-openings. He suggested that the applied load was transmitted to the support mainly by a lower path and partly by an upper path around the opening. When the opening was kept clear from the load path, the ultimate shear strength could be calculated from an equation by Kong, Robins, Singh and Sharp [1972d] regardless of the opening.

$$\frac{V}{b\ h_a} = C_1 \left[\ 1 - 0.35\ \frac{x_e}{h_a}\ \right]\sqrt{f_{cu}} + C_2\ \frac{\sum 100\ A_r y_r\ \sin^2\theta_r}{b\ h_a^{\,2}} \qquad (3.3)$$

When the opening intersected the load path, then a modified equation should be used to reduce its ultimate shear strength [Kong et al, 1975] :

$$\frac{V}{b\ h_a} = C_1\ \left[1 - 0.35\ \frac{k_1 x_e}{k_2 h_a}\right]\ k_2\sqrt{f_{cu}} + \lambda C_2\ \frac{\sum 100\ A_r y_r\ \sin^2\theta_r}{b\ h_a^{\,2}} \qquad (3.4)$$

where C_1 = 1.4 for normal weight concrete,

= 1.0 for lightweight concrete;

C_2 = 3.0 N/mm^2 for deformed bars,

= 1.3 N/mm^2 for plain round bars;

λ = 1.0 for main longitudinal reinforcement,

= 1.5 for web reinforcement;

k_1, k_2 = coefficients defining the position of an opening;

b = the beam thickness;

h_a = the beam height h or beam span L_o, whichever is less;

f_{cu} = the concrete cube strength;

A_r = the area of a typical web bar intersecting the diagonal crack at a depth y_r and an angle θ_r (Fig.3.5).

It should be noted that the constants, C_1 and C_2, in equations (3.3) and (3.4) are different from those constants, λ_1 and λ_2, adopted in the CIRIA Guide (Section 3.2.2, equation (3.1)). The CIRIA equation only accepts 75 percent of the total computed value from equation (3.3) and has incorporated the partial factors of safety 1.5 for concrete and 1.15 for steel.

Kubik [1978] (Fig.3.6) assumed that the equilibrium of forces among blocks A to D is maintained only at the hinges 1 to 4. The applied load is divided into two components, in which the portion above the opening is Q_T, and the portion below the opening is Q_B. Each hinge is acted upon by a vertical force Q and a horizontal force H together with a moment M.

The ultimate strength of the beam can be determined if all hinges are under-reinforced in flexure so that all their moments (M_1, M_2, M_3 and M_4 are at their ultimate values M_y, where

$$M_y = \sum \frac{(A)(f_y)(y^2)(\sin^2\alpha)}{h \sin \theta}$$

where

A = cross-sectional area of a reinforcing bar

f_y = yield stress of of a reinforcing bar

h = overall beam depth

M_y = ultimate moment in a deep beam corresponding to reinforcement yielding

y = depth at which a reinforcing bar intersects a defined plane

θ = inclination of a flexural hinge in a deep beam to the direction of beam span

α = acute angle between a critical plane and a reinforcing bar

Therefore, from the equilibrium of forces, we have

$$(Q_T)_F = \frac{M_1 (h_o + h_L) + M_2 h + M_3 h_u}{a_u (h_o + h_L) - h_u (a_L - x_o)}$$

$$(Q_B)_F = \frac{M_3 + M_4}{a_L} - \frac{h_L}{a_L} \frac{M_1 (a_L - x_o) + M_2 a + M_3 a_u}{a_u (h_o + h_L) - h_u (a_L - x_o)}$$

$$(H)_F = \frac{M_1 (a_L - x_o) + M_2 a + M_3 a_u}{a_u (h_o + h_L) - h_u (a_L - x_o)}$$

where

a is the shear span

a_L is the shear span below a web opening

a_u is the shear span above a web opening

h_L is the depth of beam web below an opening

h_o is the depth of a web opening

h_u is the depth of beam web above an opening

$(H)_F$ is the horizontal force induced around a web opening which is corresponding to rotational failure

M_i is the hinge moment (i = 1 to 4)

x_o is the length of a web opening

$(Q_B)_F$ is the value of Q_B corresponding to rotational failure of the load path below the web opening, and

$(Q_T)_F$ is the value of Q_T corresponding to rotational failure of the load path above the web opening

Based upon the experimental evidence conducted by Sharp and himself, Kubik has concluded that flexure failure due to concrete crushing does not exist. The only possible mode of failure is premature shear failure which may occur in the region above and below the web opening or in between the end of the beam and the opening. Applying the equation of Kong et al [1972d], the ultimate shear strength of these regions are as follows (see Fig.3.7) :

When $Q_T > (Q_T)_{S1}$, failure occurs along the plane above the opening,

$$(Q_T)_{S1} = C_1 \left[1 - 0.35 \frac{x_u}{h_u}\right] b\, h_u \sqrt{f_{cu}} + C_2 \frac{\sum 100\, A_u\, Y_u \sin^2\alpha_u}{h_u^2}$$

$$(H)_S = C_1 \left[1 - 0.35 \frac{h_o}{t}\right] b\, t \sqrt{f_{cu}} + C_2 \frac{\sum 100\, A_t\, Y_t \sin^2\alpha_t}{t^2}$$

$$(Q_T)_{S2} = (Q_T)_F \frac{(H)_S}{(H)_F}$$

$$(Q_B)_S = C_1 \left[1 - 0.35 \frac{x_L}{h_L}\right] b\, h_L \sqrt{f_{cu}} + C_2 \frac{\sum 100\, A_L\, Y_L \sin^2 \alpha_L}{h_L^2}$$

where

A = cross-sectional area of a reinforcing bar;

b = thickness of beam;

C_1 = 1.4 for normal weight concrete,

= 1.0 for lightweight concrete;

C_2 = 3.0 N/mm^2 for the deformed bar,

= 1.3 N/mm^2 for the plain round bar;

f_y = yield stress of a reinforcing bar;

$(H)_S$ = value of H corresponding to shear failure in the region between the beam end and the web opening;

$(Q_B)_S$ is the value of Q_B corresponding to shear failure of the load path below the web opening;

$(Q_T)_{S1}$ is the value of Q_T corresponding to shear failure of the beam in the region above the web opening;

$(Q_T)_{S2}$ is the value of Q_T corresponding to shear failure of the beam in the region between the beam end and the web opening;

t = distance between a web opening and beam end;

x_L = clear shear span below a web opening;

Y_L = depth at which a reinforcing bar intersects a defined plane below an opening;

Y_t = horizontal distance measured from the web opening at which a reinforcing bar intersects a defined plane between the beam end and the web opening;

Y_u = depth at which a reinforcing bar intersects a defined plane above an opening;

$\alpha_u, \alpha_t, \alpha_L$ = acute angle between a critical plane and a reinforcing bar (see Fig.3.7 (a), (b) and (c)).

Above all, based on the findings of Kong and his co-workers, the two empirical equations (3.3) and (3.4) were adopted in "Reinforced Concrete Designer's Handbook" [Reynolds and Steedman, 1981] to allow practising engineers to design deep beams with and without web-openings.

3.2.4 Deep Beams with Combined Top and Bottom Loadings

When loading is applied along the bottom edges of a deep beam, the foregoing recommendation on reinforced concrete deep beam design can no longer be employed. Until recently, the only document that provided guidelines on deep beams with bottom loading was the CIRIA Guide [1977].

The allowable bottom shear capacity of concrete is defined as before in Section 3.2.2, that is,

$$V < 0.75\ b\ h_u\ v_u$$

A design stress of $0.87f_y$ should be adopted for the steel reinforcement discussed below. In the case of uniformly bottom loaded deep beams, only the vertical web reinforcement contribution is considered. For a deep beam with bottom concentrated loading, additional vertical hanger bars should be provided to take the design load and should spread 0.15L both ways from the load width. When the proportion of the bottom load is comparatively large, a combination of inclined and vertical bars should be used. The vertical components of the inclined bars should not be more than 60 % of the maximum shear force, Q, at such a location. The inclined bar should be bent at 40° to the horizontal and should have a minimum radius of 20 diameters at the loading point. The vertical bars should carry the rest of the concentrated load Q.

Thus, for a bottom loaded deep beam, the maximum bottom shear capacity of the beam, V_{cb}, is the lesser of the concrete shear strength, V, and the shear strength of the vertical reinforcement which is designed for such a loading.

For deep beams with combined top and bottom loadings, the CIRIA Guide has given an non-dimensional interaction equation defining the shear capacity :

$$\frac{V_{at}}{V_{ct}} + \frac{V_{ab}}{V_{cb}} < 1 \qquad (3.5)$$

where V_{ct} is the shear capacity assuming top loads only (as defined in Section 3.2.2, Eqn.(3.1));

V_{cb} is the shear capacity assuming bottom loads

or indirect loads on an indirect support only;

V_{at} is the applied shear from top loads;

V_{ab} is the applied shear from bottom or indirect loads or with indirect supports.

3.3 COMMENTS

In this chapter, the current major codes of practice and design manuals associated with reinforced concrete deep beams have been reviewed. This study has been useful in identifying the limitations of the current design documents on the subject of deep beams.

Most of the available literature concentrates on deriving empirical equations and semi-empirical relations or providing design rules based upon past experience on the results of deep beam tests. Indeed, for instance, the CEB-FIP Model Code [1978] and the CIRIA Guide [1977] adopted most of the experimental findings by Leonhardt and Walther [1966] and those by Kong et al [1970-1986b]. However, they should be used with caution and their range of validity should not be exceeded.

An examination of the associated assumptions of these design provisions shows that the most commonly adopted theories are the shear friction theory and the diagonal compression strut analogy. Examples of such approaches are the American Code ACI-318-83 [1983], which is based on the former and the Canadian Code CAN3-A23.3-M84 [1984], based on the latter. In the classical elastic theory approach, the stress design criteria has limited the applicability of

the PCA bulletin [1946].

The empiricism of most of the design rules arises from the fact that the actual behaviour of deep beams is often very complex and that there are always several possible modes of failure. This explains why no known method of design to date has been based on a full implementation of all the possible modes of failure.

Although there is a sufficient library of work on stocky deep beams regarding shear, a rational and unified approach to the design of slender deep beams is not yet available. It is evident that such a rational approach can only be obtained by having a clear understanding of the physical behaviour of deep beams. Moreover, the problems of the design of deep beams with web-openings and the design of deep beams under combined top and bottom loadings have left several questions unanswered.

It is worth pointing out that the work by Kong et al [1973a, 1977] on the deep beams with web-openings has ignored buckling consideration. In addition, the validity of the CIRIA combined top and bottom loadings interaction equation is doubtful because of the lack of experimental evidence [Besser, 1983]. There are further unknowns in applying such an equation to uniformly distributed loads and direct concentrated loads cases. Furthermore, there is a need to justify the compression field theory [Vecchio and Collins, 1986], which has now been incorporated into the Canadian Code [CAN3-23.3-M84, 1984], by experimental data.

Therefore, in the next three chapters, three test programmes will be described with an aim to develop and modify the existing design methods on deep beams in the light of the new experimental evidence as it became available.

CHAPTER FOUR

MATERIALS, SPECIMENS AND INSTRUMENTATION

4.1 GEOMETRY AND DETAILS OF SPECIMENS

In the earlier chapters of this thesis, the important work and findings on deep beam design were highlighted. These studies suggest the need for further tests on deep beams. In this chapter, the details of forty four tests are described. Three different types of specimens were tested to investigate the behaviour of deep beams :

(a) slender deep beams without web-openings (Section 4.1.1),

(b) slender deep beams with web-openings (Section 4.1.2), and

(c) deep beams under combined top and bottom loadings (Section 4.1.3).

4.1.1 Slender Deep Beams without Web-Openings

The test specimens consisted of 12 rectangular deep beams (Series E beams in Table 4.1 and loading scheme 1 in Fig.4.1), with a simple span L of 1400 mm, giving a span-to-height ratio L/h of 1.4. Each beam was 1700 mm long by 1000 mm deep. Their thickness varied between 40 mm and 15 mm, giving a height-to-thickness ratio h/b between 67 and 25. Both the total-shear-span x_t and the clear-shear-span x were kept constant at 400 mm and 170 mm, respectively. All load and support regions were locally strengthened in order to avoid premature local failure before buckling occurred at these positions. The thickness of these regions was increased locally as shown in Fig.4.2.

The beams had a rectangular-mesh web reinforcement (Fig.4.3). Plain round web bars, of size 6 mm and average yield stress 410 N/mm^2, were used, except for the thinner beams where size 2 mm wires of 410 N/mm^2 were used. The main tension reinforcement consisted of three deformed bars placed near the bottom of the beam. End plates were used to improve the strength of the anchorages. Depending on the beam thickness, the following bar sizes were used : 6 mm (310 N/mm^2), 8 mm (500 N/mm^2), 12 mm (480 N/mm^2), and 16 mm (480 N/mm^2).

4.1.2 Slender Deep Beams with Web-Openings

The test specimens in this group consisted of 16 W-Series rectangular deep beams (Table 4.2). These were each 1700 mm long by 1000 mm deep, i.e. these dimensions were the same as those in Section 4.1.1. A constant thickness b of 35 mm was used throughout giving a height-to-thickness ratio h/b of 29. Unlike the specimens in Section 4.1.1, the specimens here were not strengthened locally as this was not considered necessary. Of the 16 specimens :

(a) seven were cast with 170 mm wide by 200 mm deep rectangular web-openings,

(b) seven were cast with 203 mm diameter circular web-openings,

(c) two were cast as control specimens, i.e. without web-openings.

Six of the seven beams in each of the (a) and (b) groups above were tested with a standard span of 1400 mm; one from each of these two groups was tested with a simple span of 1230 mm, to investigate the effect of the clear-shear-span as a variable. The standard 1400 mm

simple span was used for the control specimens.

A rectangular-mesh web reinforcement of hard drawn plain bars of size 5 mm and yield stress 485 N/mm^2, was used. The main tension reinforcement consisted of three deformed bars of size 16 mm diameter and yield stress 480 N/mm^2. No anchorage end plates were used.

4.1.3 Deep Beams under Combined Top and Bottom Loadings

There were 16 CB-Series rectangular deep beams in this group (Table 4.3). Each beam had a pair of hangers to allow the bottom loading to be applied. The following dimensions were kept constant for all these specimens (Fig.4.4) :

(a) length (1700 mm) and depth (1000 mm) were the same as those beams in Section 4.1.1 and 4.1.2

(b) thickness (50 mm)

(c) top clear-shear-span (235 mm)

(d) bottom clear-shear-span (210 mm)

(e) top bearing length (100 mm)

(f) bottom bearing length (230 mm)

(g) the centres of the vertical hangers to the centreline of the beam (300 mm)

The main longitudinal reinforcement consisted of 3 (Type 2) deformed bars of size 12 mm. They were spaced at 30 mm vertically. There were eight (Type 2) deformed bars of size 10 mm on each hanger. Similarly six of this type of bar were provided as the inclined steel for each of the beams with inclined steel arrangement. On each face of the beam, nominal web reinforcement was provided by a fabricated

200 mm by 200 mm square mesh of size 5 hard drawn plain bars. Additional shear reinforcement was provided by size 5 mm hard drawn bars. For each beam, two bottom hangers were cast with their reinforcement projected about 300 mm outside the soffit. Each hanger consisted of 4 pairs of size 10 (Type 2) deformed bars spaced at 50 mm along the beam axis. The lateral centre to centre distance of each pair of these bars was 30 mm. No anchorage end plate was used for the main flexural bars. Anchorages of all the other reinforcement were provided by 180-degree hooks, to fulfill the requirement stated in Section 2.4.2 and Section 3.4.2 of the CIRIA Guide [1977]. The yield stress of all the reinforcement was about 485 N/mm^2.

4.2 MATERIALS

4.2.1 Cements

Ferrocrete rapid hardening Portland cement conforming to BS 12 [1978] was used throughout. All cement was supplied by the Blue Circle Group in 50 kg bags.

4.2.2 Aggregates

The aggregate used was zone M sand from the local Caistron Quarry. The grading of the sand was determined by sieve analysis in accordance with BS 882 [1983].

4.2.3 Chemical Admixture

Melment L10 Category A (sulphonated melamine-formaldehyde condensates) superplasticizer supplied by the Hoechst (U.K.) Limited

was used for beams with high strength concrete. The plasticizer was used to achieve the required workability and flowing characteristics.

4.2.4 Steel

The material properties of all reinforcing bars (which conformed to BS 4449 [1984]) were obtained in accordance with BS 18 : Part 2 [1971] and their typical tensile properties are as shown in Table 4.4.

4.2.5 Concrete

Two concrete mixes were used : Mix L (lower strength) and Mix H (higher strength) :

Details of Mix L :

1. a water/cement ratio of 0.65;
2. an aggregate/cement ratio of 4.5;
3. no superplasticizer was used.

The finished concrete had a minimum 7-day cube strength of 28 N/mm^2.

Details of Mix H :

1. a water/cement ratio of 0.35;
2. an aggregate/cement ratio of 2.3;
3. a dosage of 25 ml superplasticizer per kg of cement (except for the 15 mm thick beams, 30 ml of superplasticizer per kg of cement were used).

The finished concrete had a minimum 7-day cube strength of

65 N/mm^2.

4.3 MANUFACTURE OF SPECIMENS

4.3.1 Slender Deep Beams without Web-Openings

Before the day of casting, web reinforcement was set up in the Heavy Structures Laboratory. The 6 mm bars or meshes were cut into the required length and tied together by steel wires. Light wire meshes (size 2 mm) were placed near the top and bottom of the whole span. The lifting loop was bent and fixed to the top mid-span of the web. Plastic spacers were used to hold the reinforcement in place. The formwork and the moulds of the control specimens were cleaned and coated with mould oil. The side and bottom closers were greased with petroleum jelly to reduce leakage of concrete through the joints.

After the main flexural reinforcement bars had been cleaned with acetone, they were placed on the bottom of the formwork with the side closers. The web reinforcement was fixed in position and the formwork was assembled. The two uprights were bolted together by tightening all the tie bolts and studs. The required thickness was checked by means of a pair of callipers and six M12 tie studs on the top of the uprights of the formwork which were adjusted to the required thickness of the beam. All bolts of the formwork were checked and re-tightened to ensure that effective vibration transmission was achieved.

4.3.2 Slender Deep Beams with Web-Openings

In order to save time and effort in preparing the beams with web-openings, one sheet of plywood was used on each face of the

formwork (see Section 4.3.1 for a description of the formwork). Such an arrangement is necessary because no recess should be cast into the beam. A pair of circular (or rectangular) wooden blocks, made up of small components that facilitate demoulding, were fixed to the plywoods to provide the necessary web-openings. These blocks were fixed by screws onto the plywood at the required position. After fixing the main flexural reinforcement (i.e. three size 16 mm bars), a 5 mm welded mesh was placed into the formwork and the length of the bars which intercepted the openings were cut off. Extra wire meshes were placed near the top and bottom of the whole span. The formwork was then assembled in the same manner as explained earlier in Section 4.3.1.

4.3.3 Deep Beams under Combined Top and Bottom Loadings

Owing to the projected vertical hangers on the soffit of the beams in this group, all specimens were cast upside down, vertically. One sheet of plywood was used on each face of the formwork to eliminate the recesses as in Section 4.3.1. The procedure was similar to that explained in Section 4.3.1 (and Section 4.3.2).

4.3.4 Casting and Curing

The sand was first mixed thoroughly; samples were then taken for moisture content determination by the use of a SPEEDY Moisture Tester. The quantities of materials required for the casting were calculated and weighed. The sand and cement were dry mixed for two minutes in a two-cubic-feet horizontal pan mixer, after which water was added.

The fresh concrete was immediately transferred to the Heavy Structures Laboratory in buckets and placed in the formwork and moulds of the control specimens. The beam was compacted by continuous vibration and the control specimens were compacted by a hand-operated vibrator. The formwork and moulds were then moist cured with damp hessian and polythene sheets after casting. After 24 hours, the beam and the control specimens were stripped from the moulds. The beam was lifted out by the overhead electrical crane and laid horizontally on three carefully spaced timber joists on the laboratory floor. The control specimens were placed on the top of the beam above the joist position in order to reduce the risk of warping. All the specimens were moist cured for another six days and were left to cure in the air thereafter.

It should be mentioned that, for Mix H (Section 4.2.5), a superplasticizer was added two minutes after the mixing water had been added. Slump and Vebe tests were carried out at intervals (BS 1881 : Part 102 [1983a] and Part 104 [1983b]) to check the workability of the fresh concrete. The typical slump was within the range of 125 mm to 160 mm, and a Vebe time of 2 to 3 seconds was common. Placing of the concrete was completed within 30 minutes of adding the superplasticizer.

4.3.5 Control Specimen

The control specimens for each mix consisted of nine 100 mm x 100 mm cubes, one 100 mm diameter cylinder and one 152 mm diameter cylinder. The 7-day cube strength was obtained by testing three cubes in compression in accordance with BS 1881 : Part 116 [1983d].

At the day of the beam test, three other cubes were tested in compression and the remaining three cubes were tested for tensile splitting strength in accordance with BS 1881 : Part 117 [1983e]. The concrete cylinders were used to determine the stress-strain relationship of the concrete mix in uniaxial compression and hence the modulus of elasticity (BS 1881 : Part 110 [1983c]).

4.4 INSTRUMENTATION

4.4.1 The Test Rig

The purpose-built test rig used in these tests was self-straining and its design capacity was 6000 kN. It provided simple rigidity for all the tests. The general arrangement of the test rig is shown in Fig.4.5. The test rig provided the necessary lifting and jack mounting facilities. Two heavy Universal Columns were connected to the vertical ties by cross-beams at the top and bottom as the reference beams. Two single-acting jacks were used and the whole frame was supported on four corner columns which had welded steel end-plates that were bolted to the floor (grouted with CONBEXTRA HF non-shrink cementitious grout to the floor). Each cross-beam to vertical tie connection was made with 12 pairs of M24 General Grade High Strength Friction Grip Bolts to BS C395 : Part 1 [1969]. The bolts were tightened against load indication washers to ensure that a correct shank tension was achieved with a hand-operated torque multiplier.

4.4.2 Servo-hydraulic Jacking System

The loading devices were supplied by the DARTEC Limited (Fig.4.6). The whole system consisted of two single acting hydraulic jacks, a hydraulic power pack and a system control console. The two EPZ single hydraulic jacks were of 600 kN capacity each. Each jack was mounted vertically so that lateral forces were not transmitted to the piston. The jacks had a maximum stroke of 150 mm. Both jacks were connected by hydraulic pressure lines to a common manifold on the flow control unit. Oil was supplied from the oil tank of a hydraulic power pack through a smaller hydraulic hose at the top of the jack. The piston was induction hardened and ran in a plain bore with no seals. Any cross piston leakage which occurred during operation was passed through a fast return line from the larger hose of the jack back to the oil tank of the hydraulic power pack. A safety by-pass valve was mounted beside each jack which opened automatically at full-stroke to prevent over-stroke of the piston and oil was returned through this by-pass to the fast return line to prevent the piston from being pushed completely out of the cylinder. The piston would return under the tension of several coil springs back inside to the cylinder. A micro-switch was mounted beside each jack and controlled by a purpose-made lever arm to shut down the pump of the hydraulic power pack when full stroke occurred.

4.4.3 Combined Top and Bottom Loading System

For the combined top and bottom loading tests (CB-Series), two specially built load-transferring steel frames were made to transmit the top loading from the hydraulic jacks to the bottom hangers (Fig.4.7). Each steel frame was designed to substain a loading of

600 kN. The top loading was applied at the top yoke of each frame by the hydraulic jack. This was transmitted through the two side columns to the bottom yoke where a mechanism of roller and steel block was attached (Fig.4.8). The applied load was then transferred to another steel block through two high strength tie-rods. With this steel block, the applied load was evenly distributed to another system of rollers and four smaller steel blocks which were in turn connected to eight hanger bars of the test beam, each with a split collet grip.

In addition, two proving rings (of 2000 lb. and 1250 lb. capacity, respectively) were used to maintain and to check the vertical position of the beam during testing. Each proving ring was mounted perpendicular to the beam faces near the central top edge of the beam (see Fig.4.9). On loading, the test beam would be subjected solely to bottom loading which applied at the hanger bars. The top loading would commence after the bottom hangers reached their yield strength. Then, the total applied load would be shared between the bottom hanger bars and the top portion of the beam up to failure.

4.4.4 LVDT Displacement Transducers

The lateral displacement profiles of the test beams were obtained by three vertical groups of Linear Variable Differential Transformer (LVDT) displacement transducers (Fig.4.10). Each group consisted of five transducers located on the vertical lines passing through the two supports and mid-span of the test beams. They were spaced at 700 mm from each other with the outer groups 150 mm from the vertical edges. All displacement transducers were spaced at 200 mm apart with

100 mm from the top and bottom vertical edges of the test beams. This arrangement allowed the measurement of displacements on the compression face of the beams. All displacement transducers were fixed with a purpose-made aluminium block and clamped to a rigid steel frame which was erected alongside the test rig. The transducers could be removed shortly before the collapse of the beam in the test.

4.4.5 Mechanical Dial Gauges

The mechanical dial gauges used in all tests were of 25 mm travel, and the dials were graduated in 0.01 mm divisions. For the buckling and instability tests, two dial gauges were fitted to magnetic stands attached to the independent steel frame that carried the displacement transducers; they were placed at the mid-height of each end of the test beams. They were used to serve as a device to check the performance of the LVDT displacement transducers so as to give a visual warning of the impending failure of the test beams. In addition, in all tests, two pairs of dial gauges were mounted on two magnetic stands and placed horizontally at each end of the bottom bearings at 100 mm from their centre lines. They were used to detect the out-of-plane translation and in-plane rotation movements of the support bearings.

4.4.6 Electrical Demountable Strain Transducers

Electrical demountable strain transducers were used to monitor the surface strains at specified locations of the beams. They were used both individually and as 45 degree rosettes. These transducers

were originally designed by Cook [1980] of the Design Research Department of the Cement Concrete Association. They were manufactured in the Civil Engineering Department at the University of Newcastle upon Tyne.

The general arrangement and dimensions of the strain transducers are shown in Fig.4.11. All strain transducers used were identically designed with a gauge length of 100 mm. Each strain transducer consisted essentially of an aluminium strip, with an aluminium block cemented to its bottom face at each end. Each of these blocks had a conical pin attached to it; these pins provided the means of fixture to the Demec studs that were cemented on to the concrete beam surface.

Four small aluminium blocks were bonded on the top surface of the strip. The outer blocks were mounted over the pins to provide sufficient height to extend the fixing springs, which would hold the transducer in place. The inner pair of blocks were mounted in line with the inner end of the lower blocks, and their purpose was to prevent the cemented joint between the strip and the lower block from peeling apart when the transducer was extended. An instant cyanoacrylate adhesive was used to cement all the components. An advantage of using this adhesive is to provide a series of 'weak links' for all component parts. A sharp knock or impact would break the adhesive joints, and the transducer would then be reduced to its component parts of a strip and several blocks. Hence minimum damage would be suffered and the component parts could be reassembled easily with the aid of a simple purpose-made aluminium dummy Tee-section.

Each transducer had four electrical resistance strain gauges Type N11-FA-5-120-23 with a gauge length of 5 mm, supplied by the SHOWA Measuring Instruments Co., Limited. All gauges were selected to have a temperature compensation matched to aluminium. Each had a gauge resistance of 120 ohm $\pm$ 0.4 % and gauge factor of 2.10 $\pm$ 1.0 %. The gauges were bonded in pairs on each side of the flexible strip by using the cyanoacrylate adhesive. The four gauges were wired up to provide a full bridge, which was sensitive to the bending strain induced in the strip, and insensitive to any axial strain. The strain gauges were protected by a clear varnish coating, which was cured to produce a thin tough coating over the gauges and the wires. The connecting cable of the transducer was secured by the cyanoacrylate adhesive on the side edge of the aluminium strip.

The transducer was held in contact with the specimen by using a S.W.G.-16 wire which was bent into a loop at each end, with tension springs hooked into each loop. The wire was hooked over the transducer as shown in Fig.4.11. The other ends of the tension springs were bonded to the surface of the specimen on either side of the Demec stud. A small hole drilled in the upright arm of the angle allowed the spring to be hooked in. A thin layer of ARALDITE epoxy resin quick-setting adhesive was applied to the concrete surface and the reference Demec studs were pressed on in the required position; the exact location being ensured by use of a dummy gauge bar. Springs were then used to maintain the gauge in position.

4.4.7 Mechanical Demec Gauge

Additional strain measurements on the test beams were facilitated by the use of mechanical Demec gauges. Each Demec gauge had a gauge length of 102 mm (4 in.), and a gauge factor of 0.00002 (i.e. strain = change in reading x 0.00002).

4.4.8 Data Logging System

The data logging system consisted of an adjustable direct current voltage supply, a Solartron Integrated Measurement System and an Apple II micro-computer. The Solartron Instrumentation Group supplied a Solartron Merlin data logging program diskette to control the data recording process.

4.4.9 Bottom Bearings

For all the 44 beams, out-of-plane rotation, in-plane rotation and horizontal translation were allowed for by the bottom bearings (Fig.4.11). Polytetrafluoroethylene sheet bearings were placed between cylindrical segment contact surfaces to provide the nominally frictionless surfaces. They were sandwiched between two machined cylindrical segment mild steel plates. The lower bearing plate was machined to form the rocker bearing which allowed for in-plane rotation. Horizontal translation was provided by needle roller bearings and a raceway of hardened steel plate. The test beam was clamped to the bearing by means of steel angles bolted through the slotted holes to accommodate different thicknesses of test beams and ease the task of eccentricity alignments. The bearing was bedded to the concrete beam with a quick setting polyester paste to give a rigid and even bearing surface. A 50 mm thick mild steel block was

used to divert the loading from the rocker bearing onto the raceway.

4.4.10 Top Bearings

For the 12 E-Series beams and the 16 W-Series beams, two top bearings were designed to allow for the vertical displacement and out-of-plane rotation (Fig.4.11). The top part of the bearings were mounted to the piston of the DARTEC hydraulic jacks. The lower section of the bearing was a steel block. This was fixed to the test beam with steel angle plates bedded on polyester paste. The differences in the thickness of the beams were accommodated by the slotted holes in the angle plates. A cylindrical segment was bolted to the top of the steel block and eccentricity was set with the slotted holes on the segment. Polytetrafluoroethylene sheet bearings were sandwiched between the lower and upper cylindrical segment bearings to provide the necessary frictionless surface.

CHAPTER FIVE

EXPERIMENTAL PROGRAMMES

5.1 INTRODUCTION

A total of 44 beams were tested :

(a) 12 E-Series slender deep beams without web-openings (see Section 4.1.1)

(b) 16 W-Series slender deep beams with web-openings (see Section 4.1.2)

(c) 16 CB-Series deep beams under combined top and bottom loadings (see Section 4.1.3)

Of these, the 12 E-Series beams in (a) were pilot tests carried out jointly with others (Kong et al, [1986b]). The remaining 32 beams were tested solely by the Author. Section 5.1 to 5.3 of this chapter gives additional information to that in Section 4.1.

5.1.1 Slender Deep Beams without Web-Openings

The first type of tests concerns the buckling and instability of slender reinforced concrete deep beams. Because of the lack of knowledge of the buckling behaviour of deep beams, current design procedures usually use elastic stress distributions for the ultimate limit state design [e.g. CIRIA, 1977]. Indeed, at the end of the CIRIA Guide's Appendix C ('buckling strength of deep beams') it is explicitly pointed out that 'there is no experimental evidence to substantiate these procedures'. Information on the buckling of deep beams is difficult to find [PCA, 1984]. In 1984, Besser and Cusens [1984] reported tests on seven deep beams, four of which had

comparatively high height/thickness ratios h/b of 25, 30, 35, and 40, respectively. Laboratory test results which have been obtained to date suggest that the current design methods on buckling and instability of slender reinforced concrete deep beams are grossly inadequate.

The first tests on the buckling of reinforced concrete deep beams were carried out by Garica [1981] (see Table 4.1, Series A and B, 18 beams, Fig.5.1) at Cambridge University; these investigations were followed up by Paine [1984] (Table 4.1, Series C and D, 8 beams) at the University of Newcastle upon Tyne. These early investigations left important questions unanswered, and hence another twelve beams (Table 4.1, Series E, 12 beams) were tested to destruction. The results have been published as a joint paper [Kong et al, 1986b]. It is believed that the 38 tests reported in the joint paper, and the four reported by Besser and Cusens, represent most of the experimental data available to date on slender concrete deep beams.

5.1.2 Slender Deep Beams with Web-Openings

Compared with slender deep beams without openings, experimental data on slender deep beams with openings is even more difficult to find. It would appear that the Author's tests, as described in this thesis, are the first to be carried out anywhere. Looking back, the main reason for the scarcity of buckling experiments on slender concrete deep beams must have been that such tests are comparatively difficult to carry out as they require close attention to detail to prevent injury to personnel or damage to equipment.

Web openings in deep beams, whether stocky or slender, are not yet covered by any of the major codes of practice, such as the ACI 318-83 [1983], BS 8110 [1985], Canadian Code [1984], CEB-FIP Model Code [1978] and the (draft) Euro-Code No.2 [1984]. The CIRIA Guide [1977] does give some recommendations on web openings. However, because of the lack of information on deep beam behaviour, these recommendations are very restrictive. In particular :

(a) the CIRIA recommendations apply only to stocky deep beams, and exclude buckling considerations.

(b) the CIRIA recommendations only cover :

1. where to locate the openings if such openings are required,
2. how to trim the openings with reinforcement

There is no guidance on how to estimate the ultimate strength of deep beams with web-openings. Several ultimate load investigations on openings in deep beams have been reported in the literature (Sharp, [1977]; Kubik, [1978]; Singh, Ray and Reddy [1979, 1980]; and, Swaddiwudhipong and Shanmugam [1985]). However, these were all concerned with stocky deep beams and the openings were essentially rectangular. In the present investigation, the Author has extended the investigation to slender deep beams and to cover also circular openings (Fig.5.2).

5.1.3 Deep Beams under Combined Top and Bottom Loading

The problem of large concentrated forces crossing reinforced concrete deep beam members is one of the frequent occurrences in

structural engineering construction. Secondary beams crossing wall panels or uneven ground settlement and the like are two examples of bottom loading problems of deep beams. However, because of the few reported experiments in this context, very little guidance is given in codes of practice.

In the 1977 Construction Industry Research and Information Association (CIRIA) Guide 2, some design rules were included for reinforced concrete deep beam design which should be used in conjunction with the old code CP 110. In particular, for the first time, an interaction expression was propounded to control the ultimate combined top and soffit shear capacity of a deep beam. This is, however, neither based on any consistently rational treatment nor does it appear to lead to economical designs. Previous tests [Cusens and Besser, 1985] provide insufficient experimental evidence to enable the design rules to be applied with confidence. Therefore, as part of the on-going research, a group of 16 reinforced concrete deep beams under the combination of top and bottom loadings were tested to destruction. High strength and low strength concretes were used for identical pairs of beams in two series. The study of the effect of the orthogonal and inclined steel patterns on the behaviour of deep beams was the main theme of the present work (Fig.5.3).

5.2 TEST PROGRAMMES

5.2.1 Slender Deep Beams without Web-Openings

In the E-Series tests, 12 rectangular deep beams were tested in two groups with eccentricities (Table 4.1, E Series, see also Section 4.1.1). All beams were tested under two-point top loading. High

strength concrete was used for all beams. Eccentric loads and reactions were provided by off-setting the bearings, to produce a single curvature buckling profile for the test beams. In the first group, six beams were tested with eccentricities of 0.1b (where b is the beam thickness) at the load and support points. In the second group, the eccentricities were doubled to 0.2b.

5.2.2 Slender Deep Beams with Web-Openings

Details of this group of beams were given earlier in Section 4.1.2. Two-point top loading was used throughout. All beams were tested with a constant eccentricity of 3.5 mm at their load and support points (i.e. with a single curvature buckling profile). All the specimens were of high strength concrete (see Section 4.2.5). Five different web-opening positions were investigated (position A to E, Fig.5.4). The parameters studied are as follows :

1. the slenderness effect,
2. the position of the web-openings,
3. the shape effect of the rectangular (R) holes or the circular (C) holes, and
4. the effect of shear span

Control tests were provided by two comparable beams without web-openings, which were denoted as Beams W-29-0.1-R1 and W-29-0.1-R2.

5.2.3 Deep Beams under Combined Top and Bottom Loadings

A total of 16 beams were tested in this group - beams CB-H1 to CB-H6 and CB-L1 to CB-L9. As explained in the beam notation in

Section 5.3.3, beams CB-H1 to CB-H6 were made with high strength concrete (Section 4.2.5) and beams CB-L1 to CB-L9 with low strength concrete (Section 4.2.5). The reinforcement arrangements 1 to 8 are shown in Fig.5.5. Beam CB-L9 was a control specimen for Beam CB-L5; in reinforcement arrangement Type 9 (not shown in Fig.5.5), the orthogonal mesh was identical to that in Type 5 (Fig.5.5) but the amount of inclined reinforcement was halved.

5.3 BEAM NOTATION

5.3.1 Slender Deep Beams without Web-Openings

In Table 4.1, the series letter is given before the hyphen; this is followed by the height-to-thickness ratio h/b and then by the top-eccentricity-to-thickness ratio e_2/b. For example, E-29-0.2 refers to a beam in series E having a h/b ratio of 29 and a e_2/b ratio of 0.2.

5.3.2 Slender Deep Beams with Web-Openings

In Table 4.2, the two control specimens without web-openings are defined similarly as in Section 5.3.1 with R1 (or R2) followed after a hyphen. For beams with web-openings, the letter W indicates beam series with web opening; after the hyphen, the first letter (A to E) which defines the position of the opening (see Fig.5.4), while the second letter (R or C) indicates the shape of the opening (R for rectangular and C for circular). A letter R following the hyphen, if any, indicates a repeated test; similarly, a letter S indicates a special test in which the clear-shear-span is 85 mm (and not 140 mm as in the other beams, see Table 4.2). For example, W-AC-R refers to

a W-Series beam which has circular web-openings in position A and the test is repeated.

5.3.3 Deep Beams under Combined Top and Bottom Loadings

In Table 4.3, the first letter CB is used to distinguish the beam for the combined loading tests; the second letter H (or L) stands for high strength concrete (or low strength concrete); and then follows a number which represents the steel arrangement. For example, Beam CB-H1 denotes a beam in the combined loading tests made with high strength concrete (Section 4.2.5) and a reinforcement arrangement Type 1 (Fig.5.5); Beam CB-L3 is made with low strength concrete (Section 4.2.5) and has a reinforcement arrangement Type 3 (Fig.5.5).

5.4 TEST PROCEDURES

The test beam was lifted to a suitable place and a straight-edge was used to detect warping of the beam. Demec studs and restraining springs for the demountable strain transducers were stuck on special locations of interest with rapid-hardening ARALDITE epoxy resin. The beam was coated with white emulsion paint to facilitate the detection of cracks. A 100 mm square grid was marked on both faces of the beam, so that cracks could be easily located and accurately recorded.

For the buckling and instability tests, offset lines and centrelines at the required load eccentricity were drawn on the top and bottom faces of the load and support bearings. Each lower section of the top bearings was fixed on the load points and aligned with the centreline (Fig.4.12). It was then fixed in position by the slotted angle plates. The cylindrical segment was then bolted in

line with the offset. The support bearing blocks were aligned to the reference lines marked on the steel plates of the concrete blocks. Next, the bolts of the restraining clips were tightened. For the combined loading tests, the two specially built load-transferring frames would be set up at the hanger positions of the test beam and assembled. Only the bottom bearings needed to be fixed in such a case.

The beam was lifted into the test rig with the electric overhead travelling crane and lowered onto the support bearings. The top of the beam was restrained by a tie stud through the middle lifting loop, and the crane was released and removed. Two other lifting loops on each end of the beam were each hooked by slings to prevent the beam from falling out of the test rig at failure. In the case of combined loading tests, two steel angles were fixed to the front and back columns of the test rig (see Fig.4.9). These angles would prevent injury to persons and equipment during testing. One proving ring was to be mounted on each angle to maintain and to check the vertical position of the beam.

A small hand-operated ENERPAC jack was used to lift the beam slightly when setting the offset line; the bottom of the beam was aligned to the marked centreline of the bottom bearing. Polyester paste was applied and the steel angles of the bottom bearings were bolted. Misalignment was adjusted by means of a plastic hammer.

The data logging system was switched on and the Solartron Merlin Program was fed to the Apple computer. The operation parameters for scanning the transducers were set up and necessary information was

input to the program. The control console of the DARTEC testing machine was checked and the servo-hydraulic jacks were brought onto the top bearings of the beam at very small initial loading of 3 to 4 kN. The jacks held the beam in position and the top tie stud and the clamping bolts and restraining clips of the bottom bearings were released. Instructions were keyed into the computer to scan the initial readings of all the transducers. The initial readings of all dial gauges and Demec studs were also taken. The twin-limit detector was set to monitor the mid-span deflection with a LVDT displacement transducer placed vertically on the top of the test beam. Experience had shown that the vertical mid-span deflection of test beams hardly exceeded 3 mm before failure.

Incremental load was added by operating the mean level potentiometer on the meter control panel under load-control mode. Load was increased by 10 to 25 kN depending on the expected failure load of the individual beam. After each load increment, the applied load was kept steady and data recording begun. 15 to 20 minutes were spent on marking the cracks and taking the dial gauge readings. For the combined loading cases, after the bottom hangers yielded, the flat bottom part of the top loading yokes would rest on the top edge of the test beam, and so top loading would commence. At each load increment the following readings were taken :

1. The applied load to the beam was taken from the digital load indicator on the DARTEC meter control unit.
2. The mid-span vertical deflection of the LVDT displacement transducer placed on the top or bottom of the test beam was noted from the displacement indicator on the DARTEC control unit.

3. Except the transducers mentioned above, all other transducers were scanned with the Solartron and their output voltages were recorded on a printer.
4. Dial gauge readings on the rear of the beam and supports were recorded. In the case of combined loading, the readings of the load cells at the top edge of the beam and the four dial gauges of the supports were recorded.
5. Additional strain readings were taken by the use of Demec gauges until the beam was on the verge of failure.
6. Cracks were detected and marked on the beam with the help of a torch. The crack pattern was sketched and the maximum diagonal crack width was measured with the aid of a hand microscope (magnification of 40) and a torch.
7. Photographs of the development of cracks were taken. Special observations were marked. The total time normally required was 2 to 4 hours for the buckling and instability tests. In the case of combined loading tests, a failure test lasted for five hours or more depending on the concrete strength and the steel arrangement of the beam.

After the test, further marking of the crack pattern was done. Photographs were taken on the front and side views. Then the beam was lifted away from the test rig. The bearings, springs and Demec studs were removed from the beam for future use. The hardened polyester was cleaned from all bearing plates.

Control specimens were tested on the same day as the test of the beam was performed.

5.5 BUCKLING FAILURE PREDICTIONS

Buckling failure was sudden and without warning. Up to the instant of buckling, the beams would appear to the naked eye to remain perfectly flat. Nevertheless, the experience gained in the tests has made it possible to describe two signs of impending collapse. The first sign is this. At each load increment after diagonal cracking, one would expect the diagonal cracks to extend and widen. However, after a certain load increment, the major diagonal cracks might cease extending; this was an indication that the beam was likely to fail by buckling.

Another sign was provided by the lateral displacement measurements. If, at a constant load, the lateral displacements continued to increase, buckling was imminent. The rate of increase, which could be as low as 0.1 mm/min even at mid-height level, was imperceptible to the naked eye but clearly measurable. Of these two signs, the former gave the earlier warning. However, it was not always available.

5.6 SUMMARY

Experimental investigations have played, and undoubtedly will continue to play, an important role in elucidating significant aspects of the actual behaviour of deep beams. The W-Series and the E-Series tests are intended to study the slenderness effect on the behaviour of deep beams with and without-openings, respectively. To date, the effect of combined top and bottom loadings interaction on the behaviour of deep beams is not well explored. Little is known

theoretically and relatively little experimental work has been done [Besser, 1983]. The objective of the CB-Series beams is, therefore, to achieve this goal.

CHAPTER SIX

EXPERIMENTAL RESULTS

6.1 INTRODUCTION

In this chapter, the results of the experimental tests concerning crack developments, crack patterns, modes of failure, vertical and lateral displacements, ultimate loads, direct strains, principal strains and principle stresses will be presented and discussed.

6.2 CRACK PATTERNS AND MODES OF FAILURE

The crack patterns at failure of all the test beams are given in Figs.6.1, 6.2 and 6.3. The loads in kN at which each crack was first observed are shown close to the lines which indicates the extent of such cracks. The bold lines indicate the cracks which participate failure of the beam while cross hatching identifies areas where spalling of concrete was observed.

6.2.1 Slender Deep Beams without Web-Openings

The general behaviour of the present 12 slender deep beams together with the other 26 beams tested by others are reported in a joint paper (Kong et al, [1986b]). To date, very little test data is available on slender deep beams, though much is known about the behaviour of stocky deep beams. Hence, it would be helpful to describe the behaviour of slender deep beams, as observed in the present tests and others, with reference to that of stocky deep beams as explained in Section 6.4 of the CIRIA Guide [1977] and elsewhere (Kong et al, [1970-1978]). The general behaviour can be broadly

summarized as follows :

(a) On loading, the first cracks to form were the flexural cracks in the midspan region (Fig.6.4 : Crack 1). The flexural cracking load was typically 20-40 % of the ultimate and was somewhat lower than for a stocky deep beam of comparable span-to-depth ratio.

(b) On further loading, diagonal cracks (Fig.6.4 : Crack 2) would form, usually with a fairly loud noise, which could be easily heard within a 5 m radius. Typically, these diagonal cracks initiated not at the soffit but within the depth of the beam. These cracks were usually fairly long, even when first observed. In all these respects, the diagonal cracks in slender and stocky deep beams are similar. A comparison of the observed behaviour of slender concrete deep beams with that of stocky deep beams has revealed a significant difference; namely, the major diagonal cracks in slender deep beams make a smaller angle of inclination with the horizontal than one would expect of the diagonal cracks in the stocky deep beams (Kong et al, [1986a]). With reference to Fig.6.5, the critical diagonal crack in a stocky deep beam can be represented by the dotted line joining the inside edge of the bearing block at the support to the outside edge of that at the loading point (CIRIA, [1977], Kong et al, [1975]). By comparison, the diagonal cracks in the slender deep beams generally made a smaller angle of inclination with the horizontal and were more accurately represented by the full line in Fig.6.5. This observation has important implications in deep beam design and in the application of the shear-strength equation in Cl.3.4.2 of the CIRIA Guide [1977], as will be discussed later in Chapter

7, Section 7.3.1.

(c) As the load was further increased, the failure mode depended mainly on the load-eccentricity-to-thickness ratio e/b. As shown in Fig.6.1, the following six beams all failed in shear :

A-50-0.05; A-40-0.05; A-33-0.05;
B-50-0.05; B-40-0.05; B-33-0.05;

Of the other 32 beams, 30 failed by buckling. The two exceptions (Fig.6.1) were Beam E-67-0.2, which was damaged accidentally, and Beam E-67-0.1 which failed by an unusual vertical splitting mode, as shown in Fig.6.1. Before further discussion of the failure modes it is helpful to refer to Table 4.1, which shows the e_1/b and e_2/b ratios for all the beams. In each beam in Series C to E, the e_1/b and e_2/b ratios were equal. The beams in Series A and B, however, were tested with $e_1/b = 0$ (loading scheme 1 in Fig.4.1(b)). In further discussion, reference will be made to an 'effective' load-eccentricity ratio e/b, calculated from eqn.(6.1) :

$$\frac{e}{b} = 0.4 \frac{e_1}{b} + 0.6 \frac{e_2}{b} \qquad (6.1)$$

Eqn.(6.1) follows the concept of the equation $M_i = 0.4\ M_1 + 0.6\ M_2$, given by CP 110: Cl.3.5.7.1 (BS 8110 : Cl.3.8.3.2) for the design of slender columns. Using eqn.(6.1), the e/b ratios of the above six beams worked out to be 0.03, which is 60% of the value of 0.05 specified by CP 110: Cl.3.5.7.1 (BS 8110: Cl.3.8.3.2) as the minimum eccentricity ratio for the design of slender columns. Again, using eqn.(6.1) it is seen that the e/b ratios for all the other beams were more than twice the CP 110/

BS 8110 minimum value. In other words, whether a beam would fail by shear or by buckling depended strongly on the e/b ratio, even for the very slender beams with h/b ratios of 50. Where the e/b ratio was half the CP 110/BS 8110 minimum, failure was by shear; where the e/b ratio was twice the CP 110/BS 8110 minimum, failure was by buckling.

In practical design, it is difficult to ensure that loads are truly centrally applied. For a slender deep beam, a slight eccentricity (which may be unintentional and not allowed for in the design) could change the failure mode and hence render the design calculation invalid.

(d) For those beams that failed in shear (Fig.6.1) the crack patterns and failure modes were broadly similar to those of stocky deep beams as described, for example, in Section 4.6 of the CIRIA Guide [1977] (see Fig.6.6).

(e) Thirty beams failed by buckling; each failure was sudden and without warning. Typically, a beam would appear stable even after the final load increment had been applied; then, after substaining this load for several minutes, it might suddenly buckle and collapse. The buckling mode is characterised by prominent horizontal cracking, usually across the length of the beam (Fig.6.4 : Cracks 3). Fig.6.1 shows clearly all the beams failed by buckling. Note that horizontal cracking could not be used as warning before failure, because these cracks formed at buckling and, in the tests, were observable only after the beams had collapsed.

6.2.2 Slender Deep Beams with Web-Openings

For similar reasons as explained in Section 6.2.1, experimental data on slender deep beams with web-openings is very scarce. It would be helpful to describe the behaviour of slender deep beams with web-openings, as observed in the present tests, with reference to those stocky deep beams reported earlier by Sharp [1977] and Kubik [1978] (see Fig.6.7(a)). In general, the behaviour of stocky deep beams with openings depended mainly on the extent to which the opening intercepted the 'load path' between the bearing blocks at the support and loading points (Fig.3.4) When the opening is reasonably clear of the 'load path', the beam will behave essentially as if it has no opening. Failure is always brought about by shear. However, for a slender deep beam, buckling failure is possible. Indeed, six of the present W-Series beams with web-openings at the mid-height failed by prominent horizontal cracking which is similar to those of the deep beams without web-openings as described in Section 6.2.1.

When an opening intercepted the load path, the behaviour of the slender deep beams can be broadly summarized with the aid of the diagrams illustrated in Figs. 6.7(a) and 6.7(b). The crack patterns of the beams with rectangular openings were essentially similar to those with circular openings :

(a) The first cracks to form were those at the corners of the rectangular openings (or the edges of the circular openings) which directly followed the load path (Fig.6.7 : Crack 1 and 2). The cracking load was typically 10-30 % of the ultimate and was higher than for a stocky deep beam (15-20 % of the ultimate load) of comparable size and location of openings as well as comparable

span-to-depth ratio (Kubik [1978]).

(b) In most cases, flexural cracks (Fig.6.7 : Crack 3) would appear at the same loading with the cracks mentioned in (a).

(c) On further loading (about 30-40 % of the ultimate load), horizontal cracks (Fig.6.7 : Crack 4a) would form on the vertical edges of the beam, and inclined cracks (Fig.6.7 : Crack 4b) would sometimes appear on the top edge of the beam.

(d) On further increase in loading (about 40-70 % of the ultimate load), the diagonal crack (Fig.6.7 : Crack 5 and 6) would appear, usually accompanied by a fairly loud noise, which could be easily heard within 5 m radius. However, unlike the stocky deep beams, these diagonal cracks were not always the dangerous cracks that caused the immediate collapse of the beam or led to its ultimate failure. In addition, the upper portion of the diagonal crack on the lower load path (Fig.6.7 : Crack 7 [Kubik, 1978]) was not found in any of the present slender beams. Likewise, the lower portion of the diagonal crack on the upper load path (Fig.6.7 : Cracks 8 and 9 [Kubik, 1978], or Crack 10 here) was only found in those beams with inclined hanger arrangements.

(e) Of the 14 slender deep beams with openings, six failed by buckling. For 8 beams with openings located at the mid-height, the major failure mode was buckling. This is characterised by prominent horizontal cracking, usually joined the bottom edges of the two openings (Fig.6.7 : Crack 11). For example, the following 4 beams with x/h = 0.17 buckled with prominent horizontal cracking :

W-AC; W-CR
W-BR; W-CC

The two exceptions were Beam W-AR-R and Beam W-AC-R which both failed in shear.

For beams with web-openings located near the bottom support, their failure modes would be shear :

W-DR; W-DC

For beams with openings located just above or below the load and support points, the failure mode would be shear. For example,

W-BC; W-ER; W-EC

Therefore, the location of the opening would profoundly affect the mode of failure of a slender deep beam.

(f) When the clear-shear-span/depth ratio x/h was reduced, the failure mode of beams with web-openings at the mid-height would change from shear to buckling :

Standard x/h - shear failure

W-AR	$x_t/h = 0.40$	x/h = 0.17
W-AC	$x_t/h = 0.40$	x/h = 0.17

Special x/h - buckling failure

W-AR-S	$x_t/h = 0.315$	x/h = 0.085
W-AC-S	$x_t/h = 0.315$	x/h = 0.085

6.2.3 Deep Beams under Combined Top and Bottom Loadings

The crack patterns for the 16 test beams are shown in Fig.6.3. The load figures include the self-weight of the two loading frames each of which is 4 kN. Fig.6.8 shows the typical sequence of the crack development in a deep beam under combined loading and it will be used to aid the following discussion. The order in which the cracks appeared depended largely on the steel arrangement of the beam :

(a) Although it is not immediately clear, beams with inclined steel arrangement would have a wider spread of cracking zone towards both edges of the beam. This is because of the higher load-carrying capacity of such beams when compared to those with orthogonal steel arrangement.

(b) Under low load, the behaviour of the high and low strength beams was essentially similar (Fig.6.8). Inclined cracks were first visible, at between 4 and 15 percent of the ultimate load, around the soffit region of the hangers (Fig.6.8 : Crack 1). They were sometimes accompanied by long vertical cracks. More inclined cracks would form and extend to higher levels beside the hangers as the load increased (Fig.6.8 : Crack 2).

(c) At about 10 to 20 percent of the ultimate load, horizontal cracks were also observed at about 60 percent of the overall height (Fig.6.8 : Crack 3). These cracks were wide and long, when they first appeared, and were frequently accompanied by a cracking noise.

(d) As the load was further increased to 20-50 percent of the ultimate load, these cracks lengthened and extended towards the supports and the soffit of the central span. Frequently, another

horizontal crack appeared at about 80 percent of the overall height (Fig.6.8 : Crack 4). More parallel inclined cracks appeared at the higher level (Fig.6.8 : Crack 5) and spalling in the bottom hanger zone increased in severity. Occasionally, a third horizontal crack formed at about 35 percent of the overall height (Fig.6.8 : Crack 6).

(e) The final failure occurred with local concrete crushing and excessive in-plane deformation. The modes of failure observed in the present tests fall into three categories : vertical shear, diagonal shear and bearing crushing.

(f) Vertical shear failure was found in the high strength concrete beams with orthogonal steel arrangement (see Fig.6.3, Beams CB-H2 and CB-H3). It is characterized by a violent bursting and spalling of the concrete strut immediately at the position of the hanger bars. With no shear and nominal web reinforcement, the low strength concrete Beam CB-L7 exhibited a vertical splitting.

(g) Diagonal shear failure also occurred in beam CB-H1-R due to inadequate shear reinforcement. The orthogonal meshes could not furnish the necessary resistance against such diagonal shear action.

(h) Irrespective of the concrete strength and steel arrangement, there was no radical difference between the first crack of the test beams (see Fig.6.9). A 0.02 to 0.08 mm crack width was common among the inclined cracks. They were not critical and their maximum width prior to failure was 0.4 mm.

Previous research has shown that inclined steel arrangement will give better control against diagonal or inclined cracks than the

orthogonal steel arrangement. To limit crack widths, the CIRIA Guide [1977] recommended that the inclined bar pattern for the shear reinforcement should be adopted when the design shear force is greater than one-third of the concrete shear capacity of the cross-section of the beam. Indeed, in the present study, for those beams with inclined web steel, the diagonal cracks were effectively controlled and a maximum crack width of about 0.4 mm was inevitably lower than those with orthogonal steel arrangement beams (maximum crack width was 1.7 mm). At this stage, it should be noticed that the alternative inclined steel arrangement adopted in the CIRIA Guide permitted 60 percent of the hanger bars stopping in the middle of the beam, and the other 40 percent extending to the top of the beams. However, it was believed that such a steel arrangement would be too conservative and unnecessary. Because of this, a modified version with all the hanger bars stopped at 600 mm from the soffit was chosen. This arrangement will reduce the percentage of reinforcement to a comparable level to those beams with an orthogonal steel arrangement. In the present investigation, the level where these hangers stopped always allows a long and wide horizontal crack to form. The maximum crack width of these horizontal cracks could be 0.16 mm wide at their first appearance and widen to 1.4 mm before failure.

In general, with the orthogonal steel arrangement, a crack width of 0.2 mm was not uncommon for the first appearance of the diagonal cracks. For a given load, the crack widths of the low strength beams were wider than those of high strength.

At high load, after the top load had commenced, the width of the horizontal cracks of most specimens decreased. It was observed that the widest crack on the beams with orthogonal steel were the diagonal cracks and not the horizontal ones. For example, for beam CB-H1-R, the diagonal crack width was 1.36 mm and its horizontal crack was 0.38 mm prior to failure.

It is generally accepted that cracking is affected both by cover and by the arrangement of the steel. The risk of corrosion is greatest for bars which lie parallel to these cracks. In both steel arrangements, the detrimental effects of those cracks which lie parallel to the steel bars are of great concern.

6.3 LATERAL DEFORMATIONS

The measured displacement profiles of all the 44 beams are given in Fig.6.10 to Fig.6.12. These recorded lateral (out-of-plane) displacements were measured at 15 points on the surface of the specimens tested relative to their original positions at the first increment of loading. These points were distributed along the lines coinciding with the two supports (Position LL and RR) and the mid-span (Position MM) of the test beam. The objectives of measuring the lateral displacement were to detect bending or buckling of the beams in the vertical axis, and to detect any substantial horizontal translation of the specimens under test.

6.3.1 Slender Deep Beams without Web-Openings

Understandably, from among twelve lateral displacement graphs (Fig.6.10(a) to Fig.6.10(1)), the shape of the profiles along the specified vertical lines of each beam were different. In general, deformations of the beams were insignificant before failure became imminent. Owing to the eccentricities and restraints of the load and support points, maximum lateral displacements were always found approximately at or just below the mid-height of the web above any support. The displacements increased rapidly as failure of the beam was imminent. The identification or recording of the maximum displacements was sometimes very difficult because its occurrence was unpredictable at this stage. In some cases, no records could be made because of the sudden failure of the beam.

It should be noted that failure of beams was always initiated on the side where maximum lateral displacements were recorded probably because of unavoidable experimental errors of the eccentricities set on the bearings. This kind of error was more pronounced in the thinner beams. In addition, the accuracy of placing the web reinforcement to the prescribed casting positions was difficult to achieve because of the slender nature of the test beams.

Substantial horizontal translation of the bottom bearings was found in all cases, especially on the side where failure was found. It was apparent that the maximum lateral displacement recorded was 7.7 mm in Beam E-33-0.2 over the right hand support at failure. Also near the soffit of Beam E-25-0.2, the unrestrainted mid-span maximum lateral displacement was 4.4 mm, whilst the top edge of the beam moved slightly backwards 1.0 mm away from the front tension face

because of the restraining effect of the top bearings. A similar observation was recorded by Paine [1984] in his tests.

It should be emphasized, however, that these recorded lateral displacements took no account of the translation or rotations of the bottom rocker bearings and, strictly speaking, these values should be adjusted accordingly with the bearing movements.

6.3.2 Slender Deep Beams with Web-Openings

The lateral displacement profiles of the 16 test beams in this W-Series are shown in Fig.6.11(a) to Fig.6.11(o). All these beams are loaded with eccentricities of 0.1b at their load and support points to produce single curvature buckling profiles. The displacement profiles of these beams were essentially the same as of those deep beams without web-openings reported in Section 6.3.1. The following observations can be made :

(a) There are no displacement profiles recorded for the control specimen Beam W-29-0.1-R1. Fig.6.11(a) shows the lateral displacement profiles of the repeated test Beam W-29-0.1-R2. As this beam failed in shear, the displacement profiles show that the lateral deformations of this beam are small when compared with the other beams in this Series. It is noted that, though their reinforcements are different, the displacement profiles of Beam E-29-0.1 (buckling failure) in the E-Series are similar to this beam (see Fig.6.10(e)).

(b) For those deep beams which had the prominent horizontal cracks, their displacement profiles show that two buckling stages existed. Firstly, at low load, the rate of increase of the

maximum lateral displacements per load increment of these beams is small, say less than 0.01 mm per 25 kN. This rate would be maintained for the first few load increments. These deformations were almost instantly observed as the load was applied. However, as the load was increased further, the second buckling stage would begin. Deformations at the mid-height of the beam would increase dramatically, say 0.5 mm per 25 kN, as compared to the values in the first stage. The rate would increase to, say 2.0 mm per 25 kN, on the verge of collapse of the beam. However, unlike the first stage, it would take, say 2 minutes, to deform from the previous deformations to their final deformations shape.

(c) Fig.6.11 also shows the displacement profiles of those beams which failed in shear. The crack patterns of these beams (Fig.6.2) did not have the characteristic horizontal cracks as in those beams with the web-openings at the mid-height (see (b)). However, the displacement profiles show that these beams also had large lateral deformations near their mid-height before they failed in shear. For example,

W-BC;	W-DR;	W-ER
W-AR-R;	W-DC;	W-EC

Though these beams failed in shear mode, they inevitably deformed laterally as the load was applied.

(d) In view of the displacement profiles of these beams, beams with web-openings are more prone to lateral buckling than those beams without the openings. It is apparent that the web-openings, in particular those located at the mid-height where maximum lateral deformations occur, would reduce the buckling resistance capacity

of the beam. This would in turn deform more seriously than a comparable beam without web-openings.

6.3.3 Deep Beams under Combined Top and Bottom Loadings

The lateral displacement profiles of the 16 test beams in this CB Series are shown in Fig.6.12(a) to Fig.6.12(o). These 16 beams were loaded concentrically at their load and support points. As the depth/thickness ratio h/b of these beams are equal to 20, they fall into the category of slender beam.

6.4 VERTICAL DEFORMATIONS

6.4.1 Slender Deep Beams without Web-Openings

Fig.6.13 shows the central in-plane deflection curves of the 12 beams in the E-Series. The maximum mid-span deflections of all beams are normally below 3 to 4 mm. It is noted that the central deflections of those beams with smaller 0.1b eccentricities on the load and support points are larger than those with 0.2b eccentricities at the same load. This is probably because beams with 0.1b eccentricities are comparatively more prone to vertical deformation while beams with 0.2b eccentricities are comparatively more prone to lateral deformation.

6.4.2 Slender Deep Beams with Web-Openings

The vertical mid-span deformations of the beams with web-openings are similar to those beams without the openings. Fig.6.14 shows the central in-plane deflection curves of the 16 beams in the W-Series. The maximum central deflections are always below 3 to 4 mm. It is

noted that, in general, those beams with circular web-openings have slightly smaller maximum central deflection values than those comparable beams with rectangular web-openings.

6.4.3 Deep Beams under Combined Top and Bottom Loadings

Fig.6.15 shows the load-deflection curves of the 16 CB-Series beams under combined loading. It is noted that, in all cases, specimens with an inclined steel arrangement have a better control of central in-plane deflection than those beams with orthogonal steel arrangement. Concrete strength appeared to have no effect on deflection. The maximum mid-span deflection for any tested beam exceeded 4 mm before the collapse load was reached.

6.5 ULTIMATE LOADS

6.5.1 Slender Deep Beams without Web-Openings

The ultimate loads of all the present test beams together with others are given in Table 6.1. The table shows that six beams failed in shear and 30 beams failed by buckling. The following observations can be made :

(a) Six beams in Series A and B failed in shear. The failure loads of these beams were distinctly higher than the corresponding beams that failed by buckling as shown, for example, in the comparisons below :

B-33-0.05 (shear 692 kN)	B-33-0.2 (buckling 560 kN)
B-40-0.05 (shear 550 kN)	B-40-0.2 (buckling 340 kN)
B-50-0.05 (shear 460 kN)	B-50-0.2 (buckling 146 kN)

The failure mode of slender deep beams was sensitive to the load-eccentricity/thickness ratio e/b. According to the

calculations given earlier, the six beams failing in shear had an e/b ratio of 0.03. Table 6.1 shows that, when e/b = 0.1, the beams failed by buckling. Thus the transition from the shear mode to the buckling mode occurred somewhere between e/b = 0.03 and e/b = 0.1.

In practice, it is almost impossible to ensure that the e/b ratio is truly zero. The experimental results obtained from the tests demonstrate that a significant reduction in the ultimate load will result when the beam changes from the shear mode to buckling mode. Therefore, it is desirable in design to adopt a minimum eccentricity ratio.

(b) Table 6.1 shows that, within the test range of 25 to 67, a low h/b ratio did not guarantee that the beam would not buckle. Indeed, the four beams with h/b ratio of 25 all failed by buckling :

A-25-0.2; B-25-0.2; E-25-0.1; E-25-0.2

Similarly, the six beams with h/b of 29 all buckled. For those buckled beams, their failure loads reduced rapidly as h/b ratio became higher than 40 (E-40-0.1 was an only exception).

(c) In Table 6.1, the Series A and B beams had the following total-shear-span/height x_t/h and clear-shear-span/height x/h ratios :

Series A	$x_t/h = 0.40$	$x/h = 0.14$
Series B	$x_t/h = 0.22$	$x/h = 0.0$

Table 6.1 shows that, for shear failure, the failure loads in Series A were lower than those of the corresponding Series B beams. From previous observations on stocky deep beams [CIRIA,

1977; Kong et al, 1972a], this was expected as Series B beams had lower shear-span/height ratios than Series A beams. However, for buckling failures, there was no clear relation between the failure loads and the x_t/h and the x/h ratios.

(d) The Series C beams and the first five beams in Series E were designed to be identical except for the concrete strengths f_{cu} and f_t. Comparison of the buckling loads shows no consistent variation. Buckling loads are, by nature, more variable than, say, failure loads in shear or flexure.

6.5.2 Slender Deep Beams with Web-Openings

The ultimate loads of all the W-Series beams are given in Table 6.2. Fig.6.2 shows that six beams failed by buckling and 10 beams failed in shear. The following observations can be made :

(a) Table 6.2 shows clearly that, regardless of their failure modes, all the failure load of the beams with circular web-openings are 15 to 28 percent higher than those comparable beams with rectangular web-openings (Beam W-AR is the only exception because of its distorted openings). Therefore, in practice, the designer should consider their web-openings to be as close to the circular-shape as possible. At least, they should consider having the problem of stress concentration developed at the abrupt corners. It should be noted that trimming of the openings with additional reinforcement cannot increase the load-carrying capacity of a deep beam [Sharp, 1977].

(b) Load-eccentricities of 0.1b were included in all the 16 beams. As expected, the two control specimens without web-openings (Beam

W-29-0.1-R1 and Beam W-29-0.1-R2) had higher failure loads than the other 14 beams with web-openings. Beam W-29-0.1-R1 failed by bearing crushing and therefore had a lower failure load than Beam W-29-0.1-R2 :

W-29-0.1-R1 (bearing 700 kN)
W-29-0.1-R2 (shear 950 kN)

(c) Table 6.2 shows that beams which failed in shear or buckling did not have distinct differences in their failure load as compared with deep beams without web-openings in Table 6.1. For example, in the comparison below, both Beam W-AC and Beam W-AC-R failed at a comparable load :

W-AC (buckling 540 kN) W-AC-R (shear 560 kN)

(d) In Fig.6.2, Beam W-BR and Beam W-BC had web-openings just below their applied loading points. They were used as a check for the validity of Kong et al's equation (Eqn.3.4) for deep beams with web-openings. Table 4.2 and Table 6.2 show that when the web-openings were very near to the applied load (e.g. Beams W-BR and W-BC), the limiting conditions set by Kong et al [1975] for the lower load path, namely the 30° minimum inclination, do not necessarily apply to the upper load path. In fact, Sharp [1977] states that when the inclination Ø' is over 75°, the upper load path would be more effective than the lower load path.

(e) Four beams served as a special study on the limiting conditions set by Sharp [1977], in particular the 30° minimum inclination of the lower load path, on deep beams with web-openings. These four beams are :

W-DR; W-DC; W-ER; W-EC

It is noted that the deep beams tested by Sharp [1977] and Kubik [1978] were stocky (with h/b between 7.2 and 7.5) and none of their beams had the web-openings as close to the support as Beam W-ER and Beam W-EC with inclination Ø of 90° and 86.8°, respectively. Fig.6.2 shows that Beam W-ER and Beam W-EC failed in shear.

(f) Previous range of clear-shear-span/depth ratios x/h covered by the Sharp and Kubik tests was between 0.2 and 0.4. In the present tests, the range of the x/h ratios was extended between 0.085 and 0.14 (Table 4.2). Therefore, for deep beams failing in shear, it is reasonable to suggest that Kong et al's equations [1975] or the Author's equations should be applicable over the extended range 0.085 to 0.4 for x/h.

(g) As mentioned earlier in Section 6.2.2(f), the total-shear-span/depth ratio x_t/h and the clear-shear-span/depth ratio x/h of Beam W-AR-S and Beam W-AC-S were smaller than the standard values. Fig.6.2 shows that, for beams with web-openings at mid-height, the failure mode for those beams with the standard x/h is mainly shear while those with the reduced special x/h is by buckling. Despite this difference in their failure modes, Table 6.2 shows that the failure loads of the two beams with the reduced x/h were higher than the corresponding beams with the standard x/h. This agrees with the findings reported earlier in Section 6.5.1(c) for slender beams without web-openings and also with those stocky beams tested by Sharp [1977] and Kubik [1978].

6.5.3 Deep Beams under Combined Top and Bottom Loadings

The ultimate loads of all the CB-Series beams are presented in Fig.6.16. It was found that 11 beams failed by bearing crushing. This is probably due to the high percentage of web reinforcement used, which makes the possibility of a shear failure very remote. The shear reinforcements adopted in this series are as those recommended in the CIRIA Guide [1977] C1.3.4.2 (Fig.26 and Fig.27 of the Guide) for indirect and bottom loads. The diagonal shear and hanger reinforcements are modified from Fig.28 and Fig.29 of the Guide. Based on the 16 tests, the following observations can be made :

(a) Fig.6.16 shows the comparison of ultimate load capacity of the 16 CB-Series beams. The relevant concrete strengths are as listed in Table 4.3. In general, an increase in concrete strength causes an increase in the ultimate load capacity of the comparable beam with the same steel arrangement and failure mode. For example, Beam CB-H4 has an ultimate load capacity of 1130 kN whereas Beam CB-L4 only attained 800 kN ultimate load, even though both beams are similar in terms of the steel arrangement and mode of failure (see Table 4.3). The same is true for Beam CB-H6 and Beam CB-L6, and all other comparable beams as presented in Fig.6.16.

(b) Fig.6.16 shows that, in general, the performances of those low strength beams with inclined steel arrangement, in particular the control specimen CB-L8, are comparable to the high strength beams. The implication of this is that the steel arrangement is more important than the strength of the concrete when considering the ultimate load of a deep beam under combined loading.

(c) CIRIA Guide [1977] Fig.26 and Fig.27 recommended that shear reinforcement should be included in a deep beam under direct concentrated top and bottom loads (reproduced here as Fig.6.17 and Fig.6.18, respectively). Referring to Fig.5.5, beams with Type 1 to 6 steel arrangements were designed to study the effect of such a recommendation. It is found that, in most cases, there is little significant effect on the ultimate load capacity on the beams with shear reinforcement as compared with those beams without such reinforcement. For example, for beams which failed in shear, the ultimate load capacity of Beam CB-H1-R (850 kN) is comparable to Beams CB-H2 (930 kN) and CB-H3 (900 kN). The likelihood is that the shear reinforcement has little influence on the ultimate capacity of the beam.

(d) In addition to the observations in item (c), it is found that the advantages of using the orthogonal bottom hangers arrangement and the inclined hanger arrangement as given in Fig.28 and Fig.29 of the CIRIA Guide (reproduced here as Fig.6.19 and Fig.6.20, respectively) are apparent. For beams made with low concrete strength (see Section 4.2.5), the ultimate load capacity of the beams with the orthogonal hanger arrangement (eg. Beam CB-L2, 650 kN) are smaller than that of those with the inclined hanger arrangement (eg. Beam CB-L5, 1000 kN). However, the distinction of these two bottom hanger arrangements in those beams made with high strength concrete is not immediately clear. For instance, the ultimate loads of Beam CB-H2 (930 kN) is comparable to Beam CB-H5 (1000 kN).

(e) As mentioned earlier in Section 6.2.3(h), it was believed that

the inclined hanger arrangement in Fig.29 of the Guide (see Fig.6.20) was too conservative compared with the orthogonal hanger arrangement in Fig.28 (see Fig.6.19). With the intention of saving the additional vertical suspension steel (which is recommended to design for 40 % of the applied load) and to limit the percentage of steel used in both arrangements to a comparable amount, the present tests allowed the vertical hanger bars of the inclined hanger arrangement to stop at 600 mm height (see Fig.5.5). Indeed, regardless of the modes of failure, the ultimate loads of the beams with inclined hanger arrangement are comparable with those with the CIRIA orthogonal hanger arrangement.

(f) Fig.6.3 shows that most of the beams failed by bearing crushing. This is probably due to the use of a high percentage of web reinforcement as recommended in the CIRIA Guide. For the control test beams without orthogonal meshes and shear reinforcement (eg. beams with Type 7 and Type 8 arrangements in Fig.5.5), their ultimate loads are only slightly lower than those beams with the meshes (eg. beams with Type 1 and 4 arrangements in Fig.5.5).

(g) Beam CB-L9 was tested with a view to reducing the percentage of steel for the inclined hanger arrangement. Beam CB-L9, which has halved the steel ratio of the inclined steel in Beam CB-L5, failed at a lower load than Beam CB-L5 (Fig.6.15). It is also noted that the maximum crack widths of Beam CB-L9 are larger than Beam CB-L5 (Fig.6.9). Therefore, in reducing the number of inclined bars in the inclined bottom hanger reinforcement arrangement for a more economical design case should not be taken

in view of the reduced strength capacity and the poor performance in crack control.

(h) As experienced by the present test specimens, the most common type of failure was bearing failure at the supports. This type of failure was always sudden and difficult to predict. Table 6.3 summarizes the bearing stresses of the test beams at failure. The last two columns in the table show that the bearing stress limit (0.4 f_{cu}) adopted in the CIRIA Guide [1977] is realistic.

6.6 DIRECT STRAINS

As stated earlier in Sections 4.4.6 and 4.4.7, electrical demountable strain transducers and mechanical Demec gauges were used to determine the surface strains of the present test beams. The measured strains were obtained by interpolating the scanned voltages of the individual transducer from the calibration graphs prepared before or after the tests (for example, see Fig.6.21). Most of the strain transducers and mechanical Demec gauges were arranged in rectangular rosettes so that the magnitudes and directions of the principal strains could be determined. Typical results are presented in Figs.6.22, 6.23 and 6.24. The sign convention adopted for tensile strain is positive and for compressive strain is negative. For the buckling test beams, the face which is expected to deform in concave shape is denoted as the 'Back' face while the opposite convex face is denoted as 'Front'. The number at the end of each curve is the gauge reference number.

6.6.1 Slender Deep Beams without Web-Openings

Three types of strain gauge arrangement were used for the 12 E-Series beams :

Type 1 in Fig.6.25 : Beam E-33-0.1

Type 2 in Fig.6.25 : Beam E-40-0.1

Type 3 in Fig.6.25 : all other E-Series beams

Fig.6.22 shows the typical results of the measured strains on the notional load path that gave the maximum strain. When cracking appeared at the position of the strain transducer, a sudden change of sign or order of magnitude of the strain readings was found. It is evident from Fig.6.22 that the maximum direct compressive strains always appeared on the notional load paths that joined the load and support points, while the maximum direct tensile strain often appeared normal to such paths. In general, the measured strains on the notional load paths were higher than strains measured at other locations. The tensile cracks were normally found to be about 23 % of the ultimate load near the mid-height of the middle span.

At low loads, say 20 percent of the utlimate load, the direct strains measured at the comparable positions of all the tested beams are of similar order of magnitudes. The maximum strains were always found on the side with the maximum lateral deformation. In the case of predominant bending, the compressive strains obtained on the compression face (which was expected to be concave when loaded, 'Back') were higher than those on the tension face (which was expected to be convex when loaded, 'Front'). Moreover, with only a few exceptions, high compressive strains on one compressive face

would normally be accompanied by high tensile strains on the opposite tension face.

It was noticed that experimental errors in setting up the eccentricity of the load and support points of these slender beams, in particular Beams E-67-0.1, E-50-0.1 and E-67-0.2, are almost unavoidable. The lateral deformation profiles of the aforementioned beams were found to be different from their expected form, and hence the compressive strains on the expected tension face were higher than those on the expected compression face. Furthermore, because of their slenderness, the behaviour of the beams was very unstable during the first few load increments. They might change their lateral deformation from convex to concave, and then back again to convex on further loading. Thus the sign sequences of the strain records were altered.

6.6.2 Slender Deep Beams with Web-Openings

The strain measurements in the W-Series beams with web-openings were more problematic than beams without web-openings. The arrangements of the strain gauges were different in each individual test. This is because the notional load paths of these W-Series beams are not as readily defined as in those beams without the openings. Moreover, there is a lack of knowledge of the behaviour of beams with web-openings and eccentric loading at the same time. Therefore, the main feature of the gauge arrangement is to follow, as closely as possible, the line joining the load and support points (see Fig.6.26). Additional gauges were used to measure the strains on the theoretical upper and lower load paths (see Fig.3.5, [Sharp,

1977]). In some cases, Demec gauges were also used to obtain additional readings on the front face of the beams.

Despite the variations on the shape and location of the web-openings among these W-Series beams, the measured strains plotted in Fig.6.23 do show certain characteristic trends. It is evident that, on loading, the measured strains on the theoretical load paths [Sharp, 1977] were usually higher than those on the other positions. In general, on the load paths, the measured strains near the top bearings were smaller than those measured near the supports, whereas the largest strains very often occurred at the mid-height. As revealed from the measured strains, the theoretical upper and lower load paths, as suggested by Sharp [1977], seem to reasonably represent the most critical diagonal cracks that would affect the ultimate load of a beam. The significance of these paths to the ultimate shear strength of a deep beam depends mainly on the position of the web-openings.

6.6.3 Deep Beams under Combined Top and Bottom Loadings

Owing to the concentric loadings configuration of the CB-Series beams, only one single type of strain gauge arrangement was used throughtout these tests (for example, see Fig.6.27). Direct access to the beam proved to be very difficult and dangerous not only because of the congested loading environment but also because of the rather uncertain behaviour of these beams. Therefore, all the strain measurements were taken solely by the strain transducers.

The typical results of the measured strains on these beams are presented in Fig.6.24. It is obvious that the maximum measured compressive strains are always found near the support areas whereas the maximum tensile strains are often found at the bottom hanger areas. It is evident that the amount of steel in a beam does produce significant improvement in reducing the maximum strains. Indeed, at comparable loading, the maximum measured strains in a heavily reinforced beam are lower than in one which is lightly reinforced. For instance, for two beams with similar orthogonal web steel patterns, the maximum compressive strain in the one with larger steel ratio (e.g. Beam CB-H3, Fig.6.24, Gauge 17) is higher than the maximum compressive strain in the one with smaller steel ratio (e.g. Beam CB-H1-R, Fig.6.24, Gauge 17).

It is found that the increase of concrete strength has little significant effect on the measured strains. In fact, for example, the maximum compressive strain in Beam CB-H1-R, which is made of high strength concrete (see Fig.6.24, Gauge 17), is comparable to that of Beam CB-L1, which is made of low strength concrete (see Fig.6.24, Gauge 17). This is probably due to the fact that the thickness and the overall dimensions of all the present CB-Series beams are similar, and therefore the strains within these beams would be relatively similar.

The measured strains at the top edges as well as those near the supports are found to be always in compression. This supports the tied-arch analogy which is commonly used to model the top loaded deep beams (e.g. the Canadian Code [CAN3-A23.3-M84, 1984]). It should be

noticed that the tied-arch action in the bottom loaded beams is observed in the tests reported earlier by others (e.g. Besser [1983], Leonhardt and Walther [1966]) and now in the present CB-Series beams reported herein.

6.7 PRINCIPAL STRAINS

The principal strains and the principal directions of the direct strains (Section 6.6) can be obtained from the 45°-rectangular rosettes formed by the electrical demountable strain transducers and the mechnical Demec gauges as described earlier in Section 4.4. Each rosette consisted of three strain transducers or three pairs of Demec points at 50 mm from their common points of interest. The magnitudes and the directions of their principal axes are evaluated by using the Mohr's Circle [Hendry, 1977] :

$$e_{p,q} = \frac{1}{2}(e_1 + e_3) \pm \frac{1}{2}[2 (e_1 - e_2)^2 + (e_2 - e_3)^2]^{0.5}$$

$$\theta_{p,q} = \frac{1}{2} \tan^{-1}\left(\frac{2 e_2 - (e_1 + e_3)}{e_1 - e_3} \right)$$

where $e_{p,q}$ = the maximum and minimum principal strains

$\theta_{p,q}$ = the maximum and minimum principal directions

e_i = the measured direct strain (i = 1, 2 and 3)

The computed principal strains and their corresponding directions were all based on the convention that tensile strains are positive

and the compressive strains are negative (as in Section 6.6). Since the results of each individual test are numerous, only the results of the first and the last load increments are presented.

6.7.1 Slender Deep Beams without Web-Openings

The typical results of the principal strains of the E-Series beams after the first load increments are given in Fig.6.28 while those of the last load increments are presented in Fig.6.29.

Apart from certain slight discrepancies, it is obvious that, in general, the minimum principal strains on the notional load paths were always pointed towards the top bearings whereas the maximum principal strains were perpendicular to that direction. The maximum principal strains were, for most of the time, in tension while the minimum principal strains were always in compression.

Neglecting all the misleading results due to concrete cracking or the malfunction of the damaged strain transducers, the maximum compressive principal strains was found to be about 2000 micro-strain (Fig.6.25, Type 3 arrangement, Rosette No.1) in Beam E-29-0.1 (with 0.1b eccentricities at the load and support points) at the ultimate load (700 kN). The maximum tensile principal strain was about 300 micro-strain at 80 percent of the ultimate load (Fig.6.25, Type 3 arrangement, Rosette No.6) in the same beam. For beams with larger eccentricities (0.2b), the highest compressive principal strain at the ultimate load was about 1600 micro-strain (Fig.6.25, Type 3 arrangement, Rosette No.1) recorded in Beam E-25-0.2 with the corresponding maximum tensile strain about 400 micro-strain

(Fig.6.25, Type 3 arrangement, Rosette No.5).

It is observed that, in the vicinity of the top bearings, the directions of the principal compressive strains were generally inclined with steeper angles to the horizontal than those on the lower positions of the load paths. These principal compressive strains always pointed towards the centre top of the beams. Furthermore, at the same specified positions and comparable loadings, the maximum principal tensile and compressive strains on the compression faces of the load paths were normally higher than those on the tension faces.

Although the computed directions of the compressive principal strains were scattered, at comparable loadings and positions, the angles of the diversion from the lines joining the load paths in regard to the top bearings were usually larger in those beams with small eccentricities (0.1b, where b is the thickness) than in those with larger eccentricities (0.2b). In addition, the values of these angles were larger on the tension face than those on the corresponding compression face.

It is worth noting that, generally, at comparable loadings and rosette positions, larger tensile and compressive principal strains were found on both faces of those beams with 0.1b eccentricities than those with 0.2b. This is reasonable because those beams with small eccentricities were more prone to shear failure than buckling. They could attain relatively high shear ultimate loads and hence their relatively high strain values. Conversely, beams with large eccentricities were more prone to attain low buckling load and hence

their relatively low strain values.

6.7.2 Slender Deep Beams with Web-Openings

The typical results of the principal strains of the W-Series beams after the first load increments are given in Fig.6.30 while those of the last load increments are presented in Fig.6.31. Fig.6.30 shows clearly that there is always a general trend in the principal strains. The minimum principal strains were always in compression while the maximum principal strains were often in tension. Clearly, the flow of the internal strains is also shown in the directions of the minimum principal strains. For beams without web-openings, the shape of the strain flow would be that similar to that of a tied-arch (e.g. see Fig.6.30, Beam W-29-0.1-R1). For those beams with web-openings, the strain flow would diverge around the openings (e.g. see Fig.6.30, Beam W-CR).

For those beams which failed by buckling (see Fig.6.2), the magnitude of the principal compressive strains in the tension face (Front) is always lower than those found in the compression face (Back) (e.g. Beam W-AR-R). However, the trend of the principal tensile strains is difficult to follow. In addition, the maximum principal compressive strain would always be found in the compression face (Back) while the maximum tensile strain normally appeared in the tension face (Front).

At comparable loading, the magnitude of the principal compressive strains of a beam with rectangular web-openings is normally higher than for one with circular openings (Figs.6.30 and 6.31). For

example, at 50 kN, the maximum principal compressive strain in Beam W-AR-R is 70 micro-strain and is slightly higher than 63 micro-strain as found in Beam W-AC-R at similar position.

6.7.3 Deep Beams under Combined Top and Bottom Loadings

The typical results of the principal strains of the CB-Series beams after the first load increments are given in Fig.6.32, while those of the last load increments are presented in Fig.6.33. Before the ultimate strength of the bottom hangers was reached, all the beams were subjected to bottom loading only (Section 4.4.3). After the hangers reached their ultimate strength, the yoke of the steel frame would rest on the top edge of the beam and the total applied load would then be shared between the bottom hangers and the top portion of the beam.

It is possible to deduce the general trend of the strain distribution on these beams by referring to Figs.6.32 and Fig.6.33. In broad outline it can be inferred from these tests that, before the commencement of the top load, the flow of strain is essentially akin to that of a tied-arch. The compressive strain flow would arch from the supports to the upper portion of the beam which forms the crown of the tied-arch. This indicated that appreciable tied-arch action was occurring well before major diagonal web cracking, whereas normally this effect is only noticeable after cracking in ordinary beams. Large compressive strains are always found near the support regions. Likewise, large tensile strains always appeared in the regions near the bottom hangers.

6.8 PRINCIPAL STRESSES

The results of the measured strains in Section 6.6 can be used to compute the principal stresses. However, current analytical procedures for reinforced concrete problems under short-term loading are essentially one-dimensional. It is well known that for isotropic and linear-elastic materials, the principal stresses and strains relationships based on Mohr's stress circle can be expressed as follows [Hendry, 1977] :

$$f_p = E (e_p + v e_q) / (1 - v^2)$$

$$f_q = E (e_q + v e_p) / (1 - v^2)$$

where e_p, e_q are the principal strains in the p and q principal directions, respectively;

f_p, f_q are the corresponding principal stresses in the p and q principal directions, respectively;

E is the constant modulus of elasticity in tension and compression; that is

$E = 2 f_c' / e_c'$, and

$f_c' = -0.75 f_{cu}$;

v is the constant Poisson's ratio (say, 0.23).

An important implication of these equations is that the principal direction of the stresses and strains coincide. This assumption holds before initial cracking. After initial cracking, the principal strain inclination would rotate more rapidly than the principal stress inclination. However, in spite of its shortcomings, the linear-elastic theory is the most widely used relationship for concrete structures in their before cracking and after cracking stages.

Before cracking, it is useful to check the elastic stresses to see if the beam is overstressed, as this may cause undesirable cracks, creep or fatigue effects (Figs.6.34, 6.36 and 6.38) However, after cracking, the considerable variability of the measured strains meant that sensible comparisons between individual beams could not be made. It is deemed desirable, therefore, to use a more appropiate method of stress analysis, which could take cracking into account, to show the state of stress in the beam. The compression field theory which makes use of the average strain and the average stress conditions is adopted (Collins and Mitchell, [1986]; Vecchio and Collins, [1986]; CAN3-A23.3-M84 [1984]). Figs.6.35, 6.37 and 6.39 show the typical results of the principal stresses using such theory. Before cracking (when the principal tensile strain e_1 is less than or equal to the cracking strain of concrete e_{cr}), the principal tensile stress f_{c1} is given by :

$$f_{c1} = E_c\, e_1$$

where

E_c = the modulus of elasticity of concrete, $2\, f'_c/e'_c$,

$f_{cr} = 0.33/f'_c$,

$e_{cr} = f_{cr}/E_c$

When the principal tensile strain e_1 is greater than the cracking strain of concrete e_{cr}, the average principal stresses and the average principal strains relationship for the cracked concrete are as follows :

$$f_{c1} = f_{cr} \,/\, (1 + \sqrt{200\, e_1})$$

$$f_{c2} = f_{c2max} \left[2\,(e_2/e'_c) - (e_2/e'_c) \right]$$

where

$f_{c1,c2}$ = the principal stresses

f_{c2max} = $f_c' / (0.8 - 0.34\ e_1/e_c')$,

f_{c2max} should be less or equals to f_c' ;

e_c' = -0.002 (compressive)

As a further simplification, the directions of the principal stresses are assumed to coincide with the directions of the principal strains.

6.8.1 Slender Deep Beams without Web-Openings

Fig.6.34 shows the results of the principal stresses after the commencement of the first load increment using the theory of elasticity. It shows that the maximum principal stresses were, most of the time, in tension while the minimum principal stresses were always in compression.

Fig.6.35 shows the results of the principal stresses at the last stage of loading. As expected, both the principal tensile and compressive stresses produced by the theory of elasticity show an increase in their magnitudes with the increased loads. The magnitudes of the maximum principal tensile stresses were found to be of the order of 3 to 4 N/mm^2. This is just below their splitting tensile strengths. It is, however, recognized that the maximum principal compressive stresses were invariably low, and hardly exceeded 50 N/mm^2, which is about 60 percent of the cube strength. Higher principal compressive stresses always appeared on the compression faces (Back) but seldom on the tension faces (Front).

The principal compressive stresses produced by the theory of elasticity are normally lower than the ones computed by using the compression field theory (Fig.6.40). However, for those stresses computed by the compression field theory, the maximum principal tensile stresses are always about 2 N/mm^2.

It is observed that the eccentricities affect the magnitude of the principal stresses. On the compression faces (Back), the principal compressive stresses were higher in beams with high eccentricities (0.2b) than in ones with low eccentricities (0.1b). However, on the tension faces (Front), the opposite behaviour was found.

6.8.2 Slender Deep Beams with Web-Openings

After the first load increment, the principal stresses associated with the theory of elasticity are shown in Fig.6.36. Despite the difference in the amount of web steel, the stress distributions on Beams W-29-0.1-R1 and W-29-0.1-R2 without any web-opening are comparable to that on Beam E-29-0.1 of the E-Series tests (beams without web-openings). This supports the argument that, before cracking, these beams may behave akin to ones made of homogenous material, and hence proves the validity of the theory of elasticity for working load design.

A closer look at the principal compressive stresses values in Fig.6.36 shows that the flow of stress diverges around the web-openings. Their magnitudes on the compression faces (Back) are normally higher than those on the opposite faces (Front). It is

clear that their magnitudes are higher on the side edges of the holes than those above or below the web-openings.

For the last load increments, the prinicpal stresses computed by the theory of elasticity are presented in Fig.6.37 and those computed by the compression field theory are given in Fig.6.41. In Fig.6.37, it can be seen that the trend of the computed principal stresses is difficult to distinguish. For the results computed by the compression field theory (Fig.6.41), the magnitudes of the principal tensile stresses are always limited to about 2 N/mm^2. The general trend of the corresponding principal compressive stresses is difficult to isolate. There is not a general trend in the magnitudes of the stresses that one can compare with the two theories.

6.8.3 Deep Beams under Combined Top and Bottom Loadings

Fig.6.38 shows the principal stresses of the CB-Series beams after their first load increment. The directions of the principal stresses, in particular the principal compressive stresses clearly indicate that tied-arch action has occurred. The maximum compressive stress among these beams was found at the support of Beam CB-H3, as 6 N/mm^2. The maximum tensile stress was, however, difficult to find as early tension cracks appeared even at this stage of loading.

In an attempt to try to distinguish between the principal stresses computed by the theory of elasticity and the compression field theory, the computed principal stresses after the last load increment using both theories are shown in Fig.6.39 and Fig.6.42, respectively. It should be noted that, in all cases, top loading has

already commenced. The stresses computed by the two theories are different; a stress found in a particular location using one theory does not neccessary have the same sign as that using the other theory.

A careful examination of the principal tensile stresses in Figs.6.39 and 6.42 immediately shows that the maximum tensile stresses computed by the compression field theory are always very much lower than the ones computed using the theory of elasticity. The former theory always produces a maximum tensile stress around 2 N/mm^2 while the latter can be as high as 600 N/mm^2 (e.g. in Beam CB-H2). Conversely, the principal compressive stresses produced by the compression field theory are normally higher than the ones produced by the theory of elasticity.

It is believed that the principal stresses produced by the compression field theory are more appropriate to represent the stress distribution of the test beams, in particular at the last stage of loading. It is, however, difficult to recognize the tied-arch action from the results obtained at this stage.

6.9 SUMMARY

This chapter has summarized and discussed the experimental results of the 44 deep beam tests with regard to buckling, web-openings and combined top and bottom loadings. From the results of the E-Series tests, it can be concluded that the behaviour of the slender deep beams is more difficult to predict than that of the stocky deep beams. While shear failure is the major mode of failure

in the stocky deep beams, the slender deep beams are more prone to buckling failure. Therefore, in beams with slenderness ratio (height/depth ratio) of, say, more than 25, it is necessary to take buckling into design consideration. More information on the E-Series tests is given elsewhere [Tang, 1985].

The results of the W-Series beams, with the web-openings together with the ecccentric loadings, clearly indicated that any openings within the web of a deep beam would diverge the load paths and would change the modes of failure of the beams. The importance of the theoretical upper or lower load paths, as proposed by Kong et al [1975], is very much dependent on the shape, size and position of the openings within the beam, and certainly not solely on the lower load path as propounded by Kong et al [1975]. The ultimate buckling and shear strengths of the E-Series and the W-Series beams will be further investigated in Chapter 7.

Deep beams under direct combined top and bottom loadings are explored in the CB-Series tests. The CIRIA provisions [1977] have been studied and checked with the experimental results. It is found that concrete strength is not the major parameter of the ultimate strength. Moreover, there is little difference between the ultimate strength of beams using the inclined shear reinforement and the orthogonal shear arrangement. The stress or strain distribution show that the tied-arch action is occurring even before the cracking stage is reached. The interaction of the top and bottom shear loadings will be studied more thoroughly in Chapter 7.

CHAPTER SEVEN

ANALYSIS OF TEST RESULTS

7.1 INTRODUCTION

In this chapter, the experimental results obtained from the deep beam tests undertaken by the Author together with the previous tests done by others are analysed and discussed. The test results were described earlier in Chapter 6. The ultimate buckling strength of the slender deep beams without web-openings are analysed using the methods described in the CIRIA Guide [1977]. Adopting the same methods in the guide, an attempt has been made to analyse the buckling strength of slender deep beams with rectangular and circular web-openings.

The ultimate shear strength of the aforementioned slender deep beams was also studied. For deep beams with web-openings, the appropriateness of the equations proposed by Kong et al [1975] and Kubik [1978] were investigated and a modified approach is suggested. Furthermore, the structural idealization of deep beams with rectangular web-openings based upon Kong et al's model and Kubik's model are generalised to the Author's deep beams with circular web-openings.

For deep beams under combined top and bottom loadings, the ultimate shear interaction equation provided by the CIRIA Guide is also checked with the experimental data reported earlier by Besser [1983] and with the 16 beams tested by the Author. Based on this two experimental evidence, a modified interaction equation is proposed.

7.2 ULTIMATE BUCKLING STRENGTH

7.2.1 Slender Deep Beams without Web-Openings

Table 6.1 shows the measured buckling loads, together with the computed buckling loads by the CIRIA Guide [1977]. Worked examples for Beam A-25-0.2 are given in Appendix A of this thesis. It should be noted that Appendix A should supersede the Worked Examples given earlier in the research reports [Kong et al, 1985a,b] as well as those results reported in the joint paper [Kong et al, 1986b]. This is because of the inadvertent use of the equivalent applied stress of the Supplement Rules in these two articles. As mentioned in Section 3.2, the Guide gives three methods, of increasing refinement :

(1) the Supplementary Rules - CIRIA Guide Clause 3.2.2,

(2) the Single-Panel Method - CIRIA Guide Appendix C, and

(3) the Two-Panel Method - CIRIA Guide Appendix C.

In Table 6.1, the factors of safety calculated by these three methods [Kong et al, 1986b] are indicated by R_{SR}, R_{SP} and R_{TP}, where

$$R = \frac{\text{Measured Buckling Load}}{\text{Computed Buckling Load}}$$

The computed buckling loads here include the material safety factors of 1.5 for concrete and 1.15 for steel. The particular CIRIA method used for the computed load is indicated by the subscripts to R :

R_{SR} - Supplementary Rules

R_{SP} - Single-Panel Method

R_{TP} - Two-Panel Method

The CIRIA Guide specifies that all three methods are to be used in

conjunction with CP 110. Table 6.1 also shows the R_{SR}, R_{SP} and R_{TP} values that would have been obtained if BS 8110 were used instead of CP 110. The following comments can be made :

When used in conjunction with CP 110, the mean factors of safety are : R_{SR} = 31.27, R_{SP} = 12.42, and R_{TP} = 6.39. A closer scrutiny of Table 6.1 shows that, for beams having height/thickness ratios h/b of 25 and 29, the R_{TP} values range from about 3 to 7, with many values in the region of 5. Since buckling failures of slender deep beams are sudden and catastrophic, a safety factor of 5, say, is not unduly high; indeed, a safety factor of less than 3 might be considered too low. Where the h/b ratio was 33 or more, Table 6.1 shows that the R_{TP} values tend to be higher than 7 and occasionally higher than 10. The CIRIA Guide is therefore too conservative for the very slender beams. However, two points should be borne in mind :

(a) the relatively unpredictable nature of buckling failures (two similar beams could buckle at quite different loads);

(b) the relatively rare occurrence, in practice, of very slender deep beams.

Hence the main requirement of a design method is that it should be safe. The fact that such a method might be too conservative for some very slender beams should not rule out its use, though, of course, the search should continue for methods that are both safe and accurate. In this connection, it is appropriate to mention that the method, given in CP 110 Cl.3.5.7 for the design of slender columns, can also be too conservative for very slender columns [Cranston, 1972]. However, as Cranston [1972] pointed out, provided a method is

safe, its accuracy becomes progressively less important as the slenderness increases.

Of the three methods given by the CIRIA Guide, the Supplementary Rules are the easiest to use, the Single-Panel Method is more difficult to use, and the Two-Panel Method even more so [Kong et al, 1986b]. Table 6.1 shows that, the Two-Panel Method gave the most realistic results, while the Supplementary Rules gave the least realistic results; note, in particular, that the Single-Panel Method gave results almost as good as those given by the Two-Panel Method. In practical design, therefore, if the deep beam is such that the easier-to-use Supplementary Rules are considered as too conservative, it is worthwhile moving straight to the Single-Panel Method. If the Single-Panel Method is still considered as conservative, a more economic design may be obtained by using the Two-Panel Method.

The CIRIA Guide, used in conjunction with BS 8110, generally gave slightly higher factors of safety than when used with CP 110. Table 6.1 shows, for example, that the mean values of R_{TP} are 6.39 (CP 110) and 7.05 (BS 8110). The overall pattern, however, was little changed.

7.2.2 Slender Deep Beams with Web-Openings

None of the current major codes of practice include guidelines for the design of deep beams with web-openings. Though the buckling strength of deep beams without web-openings can be obtained using the CIRIA Guide [1977], there are no such rules for deep beams with web-openings. In the absence of any analytical methods, the

following tentative approach is introduced to analyse the 14 W-Series beams with web-openings.

Following the methods as described in the CIRIA Guide [1977], namely the Supplementary Rules, Single-Panel Method and Two-Panel Method which are used in conjunction with CP 110 and BS 8110, it is argued that the width of the column strip should be reduced in addition to the 'effective height' concept given in Cl.3.2.2 and Appendix C of the Guide (see Section 3.2.2). It is clear that openings have an adverse effect on the buckling strength of a deep beam [Sharp, 1977]. The portion of column strip which intersects the opening can be thought of as completely ineffective in resisting the applied load directly acting on that column strip. Thus, this applied load is assumed to be distributed uniformly over those portions of the panel not intercepted by the opening. The ultimate load-carrying capacity of the panel is therefore equal to the sum of its original applied load plus the additional load from the column strip intersected by the opening. When considering the vertical column strip, the modified effective length L_m of the equivalent panel (Step 2 of Appendix B) can be evaluated as below (see Fig.7.1),

$$L_m = L_e - L_s$$

where L_m is the modified effective length of the panel

L_e is the effective length of the panel (CIRIA)

L_s is the total length of column strip intersected by the web-openings

Similarly, when considering the horizontal column strip, the modified effective height h_m of the equivalent panel can be evaluated as

below,

$$h_m = h_e - h_s$$

where h_m is the modified effective height of the panel

h_e is the effective height of the panel (CIRIA)

h_s is the total depth of column strip intersected by the web-openings

It should be borne in mind that the modified effective length or height concept apply only to the analysis of the section and not to the size of the equivalent panel. Worked examples for Beam W-AC are given in Appendix B of this thesis. Table 6.2 shows the results of analysis on the buckling strength of the 16 beams using the present modified CIRIA methods. The particular CIRIA method used for the factors of safety provided by the three methods are as defined before (see Section 7.2.1). The following observations can be made :

(a) When the three methods are used in conjunction with CP 110, the mean factors of safety, excluding the two control specimens (W-29-0.1-R1 and W-29-0.1-R2), are : R_{SR} = 19.03, R_{SP} = 5.60, and R_{TP} = 4.61. These values are comparable to the factors of safety of the two control specimens despite the difference in the modes of failure. A close examination of Table 6.2 shows that, for the six beams which failed by buckling the R values using the Supplementary Rules range from about 18 to 22. For the other two methods, the R values range from about 5 to 6 and 4 to 5, respectively. Therefore, it is fair to say that the results using the present approach are consistent. Slender deep beams occur relatively rarely in practice, and their behaviour is relatively unpredictable, hence for these reasons buckling design

for deep beams with web-openings can afford to proceed cautiously and conservatively.

(b) Table 6.2 shows that the R values tend to be lower as the web-openings are located near the supports. The R_{TP} could be as low as 3 (CP 110) (for example, Beam W-DR). Since buckling failures are sudden and catastrophic, an R ratio which is less than, say 3, might be considered low. When the openings are located near the applied load, for example Beam W-BR and Beam W-BC, the R values are comparable to those beams with their openings at mid-height which range from about 4 to 7.

(c) Table 6.2 shows that the R values of the beams with rectangular web-openings tend to be lower than those comparable beams with circular web-openings. Therefore, in practice, a designer would expect a higher factor of safety for a beam with circular web-openings than for a beam with rectangular web-openings.

(d) As expected from the results of the previous beams without web-openings in Section 7.2.1, the present analysis using the CIRIA Guide, in conjunction with BS 8110, generally gave slightly higher factors of safety than when used with CP 110. For example, the mean values of R_{TP} are 4.61 (CP 110) and 4.69 (BS 8110).

7.3 ULTIMATE SHEAR STRENGTH

7.3.1 Slender Deep Beams without Web-Openings

Section 3.4.2 of the CIRIA Guide [1977] states that the ultimate shear load P of a deep beam loaded at the top (Fig.7.2(a)) is given earlier by equation (3.1) (P = 2 V). The CIRIA equation is based

upon tests on stocky deep beams [Kong et al, 1975] and assumes that the critical diagonal crack may be represented by the dotted line in Fig.7.2(b). From the total 12 slender deep tests done by the Author and his co-workers and the 32 other slender deep beams tests [Kong et al, 1986b], the results of a further study of the actual critical diagonal cracks are shown in Table 7.1, where

ϕ = angle of inclination as measured from the crack records,

ϕ_1 = angle adopted by the CIRIA Guide (Eqn.3.1, Section 3.2), and

ϕ_2, ϕ_3 = angle of inclination of the full line (chain-dot line) in Fig.7.2(b).

Table 7.2 shows that the measured failure loads P_m of the beams, together with the P_1, P_2 and P_3 values obtained are as follows :

P_1 = 2V, where V is calculated from the CIRIA equation (Eqn.3.1) without modification, i.e. the critical diagonal cracks is taken as the dotted line in Fig.7.2(b).

P_2, (P_3) = 2V, where V is calculated from Eqn.3.1 modified by taking the critical diagonal crack as the full line (chain-dot line) in Fig.7.2(b), with consequent implications on x_e, y_r and ϕ_r.

Thus x_e and P_2 is the total shear span between the load and the reaction, and y_r and ϕ_r are measured from the full line

in Fig.7.2(b).

Six beams in Table 7.2 failed in shear and the corresponding numerical values are printed in bold. These bold numbers show that the CIRIA equation gives a mean factor of safety P_m/P_1 of 1.63, and that the modified equations give P_m/P_2 of 1.78 and P_m/P_3 of 2.03. The CIRIA equation is intended for stocky deep beams which should give a factor of safety of about 2. The CIRIA equation as it stands will over-estimate the shear capacity and hence reduce the design factor of safety to below that intended by CIRIA Guide. In view of the P values in Table 7.2, it is tempting to adopt P_3 as the critical diagonal crack for design (the chain-dot line in Fig.7.2(b)). However, the evidence in Table 7.2 is such that the full line in Fig.7.2(b) should be used, at least until further evidence is available.

The numbers printed in light type in Table 7.2 refer to those beams that failed by buckling for which the factors of safety are low (e.g. mean for $P_m/P_1 = 0.99$) and the standard deviations are high (e.g. mean for $P_m/P_1 = 0.32$). Thus the CIRIA Guide equation, modified or not, should not be used for slender deep beams failing in the buckling mode.

7.3.2 Slender Deep Beams with Web-Openings

The ultimate shear strength of a stocky deep beam with web-openings could be calculated using the equation proposed by Kong et al [1973a,b] (i.e. Eqn.3.4). This equation is based on the structural idealization as shown in Fig.7.3. The applied load is

transmitted to the support mainly by a lower path ABC and partly by an upper path ADC. When the opening is reasonably small or is so located as not to interfere significantly with the load path, the ultimate shear strength would be predicted as the value given by equation (3.3) in Section 3.2.3. However, when these are not met, the ultimate strength would be calculated using the modified equation which takes the form of equation (3.4) in Section 3.2.3. The first term on the right-hand side of this equation is a semi-empirical expression for the capacity of the lower path CB; the ultimate capacity of the strut CB is reached and failure in a splitting mode results in the formation of a so-called critical diagonal crack along CB. To use this equation, designers should limit their design parameter k_2 to be greater than 0.2 and the angle $\emptyset$ to be greater than 30°.

However, it is noted that as the opening is located very near to the applied load, the predicted ultimate shear load of a deep beam will be over-estimated. For example, the measured to predicted ultimate shear load of Beam O-0.3/13 in Sharp's tests [1977] is 0.62 (Table 7.3). After including the partial safety factors 1.15 for steel and 1.5 for concrete together with a reduction factor 0.75, the factor of safety rose to 1.08. Practically speaking, this is still unsafe.

On the contrary, when the opening is located too near to the side edge and the support, the predicted load using such an equation would be extremely conservative. For example, the measured to predicted

ultimate shear load of Sharp's Beam O-0.2/16 and Beam O-0.3/16 are 3.7 and 4.0, respectively (Table 7.3). This is because the equation ignores the contribution of the concrete strength in the upper load path to the ultimate shear strength of the beams.

The measured ultimate load to the predicted ultimate load ratios of those beams which had an angle of inclination of their critical diagonal cracks either Ø' on the upper load path or Ø on the lower load path which was less than the limit 30° set by Kong et al [1977] are compared as follows (Table 7.3) :

Beam	Load Ratio (Kong et al)	Ø' (degree)	Ø (degree)
M-0.4/1	0.98	0.00	63.13
O-0.4/2	1.05	0.00	63.13
O-0.4/7	0.99	26.26	71.34
O-0.3/13	0.62	24.07	65.75
O-0.3/16	4.06	65.75	24.07

For the first three listed beams here, their measured ultimate loads are almost equal to their predicted ultimate loads by using the Kong et al's equation (3.4). However, for Beam O-0.3/13, its lower path angle Ø is 65.75° which is higher than the 30° limit. Its low load ratio of 0.62 revealed that the limiting condition set by the Kong et al's equation is not adequate. Indeed, a close examination of the angle of inclination of the critical diagonal cracks of these 80 beams revealed that only one of them, Beam O-0.3/16, had an angle of inclination of 24° on the lower path. Therefore, the 30° limit on the lower load path is doubtful and a further examination should be made.

It is fair to say that the ultimate shear strength of a stocky deep beam with web-openings does not solely depend on the lower load path or the upper load path. Previous available crack patterns of deep beam tests with web-openings show that the upper and lower load paths are equally important in transmitting the applied load to the support. Of course, this also depends on the size and location of the opening.

It is apparent that the above shortcomings can be circumvented by introducing a more logical approach. Adopting the structural idealization propounded earlier by Kong et al [1973a], it is possible to show that the upper path can also be the major load path of transmission (see Fig.7.3). It is clear that failure of such a beam would occur only if the major load path collapses (the upper load path in this case). As one of the load paths (upper or lower, whichever is weaker) failed, the second load path would become the major load path to transmit the applied load to the support. The release of load from the first load path to the remaining load path does not necessarily imply immediate collapse of the beam. Thus, further increase of the applied load is possible until the ultimate capacity of the remaining load path is reached. One possible way to account for this case is to express the concrete contribution of a deep beam with web-openings as the larger value of the following :

(1) Lower load path (Kong et al [1973a])

$$V_c = C_1 \left(1 - 0.35 \frac{k_1 x_e}{k_2 h_a}\right) f_t \, b \, k_2 \, h$$

(2) Upper load path

$$V_c = C_1 \left(1 - 0.35 \frac{k_1' x_e}{k_2' h_a}\right) f_t \, b \, k_2' \, h$$

It is assumed that the remaining load path can carry the additional load after the capacity of the weaker load path is reached. Hence, the ultimate shear load of the beam with web-openings would be given by one of the following expressions :

1. When the load path is not intersected by the opening, then the CIRIA equation is used (Eqn.(3.3)) :

$$\frac{V}{b \, h_a} = C_1 \left[1 - 0.35 \frac{x_e}{h_a}\right] \sqrt{f_{cu}} + C_2 \frac{\sum 100 \, A_r y_r \sin^2\theta_r}{b \, h_a^2} \qquad (7.1)$$

2. When the opening intersected the load path, then the larger V obtained from the two modified equations below should be used :

(a) Kong et al [1973a], Eqn.(3.4) in Section 3.2.3, -

$$\frac{V}{b \, h_a} = C_1 \left[1 - 0.35 \frac{k_1 x_e}{k_2 h_a}\right] k_2 \sqrt{f_{cu}} + \lambda C_2 \frac{\sum 100 \, A_r y_r \sin^2\theta_r}{b \, h_a^2} \qquad (7.2)$$

(b) Author's proposed equation -

$$\frac{V}{b \, h_a} = C_1 \left[1 - 0.35 \frac{k_1' x_e}{k_2' h_a}\right] k_2' \sqrt{f_{cu}} + \lambda C_2 \frac{\sum 100 \, A_r y_r \sin^2\theta_r}{b \, h_a^2} \qquad (7.3)$$

where C_1 = 1.4 for normal concrete,

= 1.0 for lightweight concrete;

C_2 = 3.0 N/mm^2 for deformed bars,

= 1.3 N/mm^2 for plain round bars;

λ = 1.0 for main longitudinal reinforcement,

= 1.5 for web reinforcement;

k_1, k_2 = coefficients defining the position of an opening (see Fig.3.5);

k_1', k_2' = coefficients defining the position of an opening (see Fig.3.5);

b = the beam thickness (mm);

h_a = the beam height h or beam span L_o, whichever is less (mm);

f_{cu} = the concrete cube strength (N/mm^2);

A_r = the area of a typical web bar intersecting the diagonal crack at a depth y_r and an angle θ_r (Fig.3.5).

These equations have assumed that local areas, in particular the regions just below the applied load, the regions just above the support or the side edges besides the openings, are well protected against local failure such as buckling or bearing failure.

In any application of Kong et al's [1973a] equations to deep beams with web-openings, its conservatism must be kept in view. The equations were based on tests on 20 beams made with normal weight concrete and another 60 beams made with lightweight concrete carried out by Sharp [1977] and Kubik [1978]. Their attempt was understandably cursory because there was not enough experimental evidence on deep beams with web-openings at the time while, in spite

of this, there was an urgent need to provide practising engineers with a design tool. In addition, very few measurements and observations were taken from the tests of Sharp [1977]. As a minor part of the Ph.D. programme, Kubik only performed 8 large-scale deep beam tests with web-openings. Although more measurements were taken by Kubik, there are still insufficient data to justify the validity of the approach, which is based on the concrete contribution of the lower path.

Kong et al's equations are simple and comparatively quick to apply but involve under-estimates (or over-estimates) of shear strength as the openings are near the support (or load) points. A better solution could be produced by using the Author's approach. Here, the stronger load path would be more appropriate than using the lower path as the capacity of the concrete contribution of the beam.

On the basis of the lower load path and upper load path, 80 previously available tests carried out by Sharp and Kubik were analysed by using equations (7.1), (7.2) and (7.3) (see Fig.7.4). A summary of the mean of the measured ultimate load to the predicted ultimate load ratios and of their standard deviations are given in Table 7.3. Use of the larger concrete contribution, based on the present proposed approach, resulted in mean of ratios considerably better than the other methods. In particular, the standard deviation and the relative error of the Author's approach are 0.05 and 17.83 %, respectively. Though the mean and standard deviation of the method which only use the upper load path concrete contribution are comparatively good, it has the same shortcomings as the Kong et al

method [1973a] and therefore should be discarded.

When comparing those beams with openings very near to the side edge and support, the present proposed method would be less conservative or have the same value as that predicted using Kong et al's equation. For example, considering the measured/predicted ratios of the ultimate shear load of Sharp's beams with openings near the supports, the following comparison could be made :

	M-0.4/6	2.65 (Kong et al) 0.87 (Author)
	O-0.4/6	2.57 (Kong et al) 0.71 (Author)
	O-0.25/6	2.24 (Kong et al) 0.86 (Author)
	O-0.3/15	1.42 (Kong et al) 0.68 (Author)
+	O-0.3/16	4.06 (Kong et al) 0.67 (Author)
	O-0.2/16	3.70 (Kong et al) 1.09 (Author)
	NW6A-0.3/15	2.04 (Kong et al) 1.05 (Author)
	M-0.4/1	0.98 (Kong et al) 0.98 (Author)
	O-0.4/2	1.05 (Kong et al) 1.05 (Author)
	O-0.4/7	0.99 (Kong et al) 0.99 (Author)
*	O-0.3/13	0.62 (Kong et al) 0.62 (Author)
	O-0.2/13	0.99 (kong et al) 0.99 (Author)

* The use of Kong et al's [1973a] equation is not recommended for this beam since the angle of inclination of the critical diagonal crack on the lower path Ø is less than 30°

+ This beam has an angle of inclination of the critical diagonal crack on the upper path Ø' of less than 30°

It should be noted that the Author's approach assumed that the critical diagonal cracks occurred either on the line AD or BC as in Fig.7.4. This assumption is only true in one of the several possible modes of deep beam failure. It would be extremely difficult to cater for all the possible cases in one single equation with such a complex problem of this nature. Therefore, as long as the equation gives a reasonably safe lower bound solution by introducing a reduction

factor, say 0.75, to its calculated value, the accuracy of the prediction is less important. For design purpose, the partial safety factors of concrete (1.5) and of steel (1.15) should also be included to achieve the necessary factor of safety (say 1.77).

It is tempting to apply the present proposed approach to the 16 W-Series slender beams tested by the Author. Table 7.4 shows the results of the measured ultimate load to the predicted ultimate load ratios of these beams using the three approaches proposed by Kong et al [1973a], Kubik [1978] and the Author. It should be borne in mind that the present 16 W-Series beams were all slender (h/b = 29) and six of them failed in buckling mode. Moreover, strictly speaking, the equations proposed by Kong et al and Kubik are only applicable to deep beams with rectangular web-openings. Therefore, the Author has generalised their methods to include circular web-openings by following similar structural idealization of the present deep beams (see Fig.7.5 and Table 7.4). The last column of Table 7.4 shows the results of the mean and standard deviation of the measured/predicted ratios of the ultimate loads using the Author's approach. Indeed, the mean value is the best among these three approaches. However, it is also noticeable that the relative error is the worst. A close scrutiny of Table 7.4 shows that for beams which have openings very near to the supports, the predicted values using the Author's approach would be too high. Thus the measured/predicted ultimate shear load ratios of the four beams with openings near to the supports were poor in comparison to those values predicted using Kong et al's [1973a] equation :

W-DR : 1.13 (Kong et al) 0.68 (Author)

W-DC	1.18	(Kong et al)	0.75	(Author)
W-ER	0.71	(Kong et al)	0.56	(Author)
W-EC	0.79	(Kong et al)	0.64	(Author)

However, it should be noticed that these four beams had their web-openings very close to the supports and therefore should not be recommended in practice.

7.3.3 Deep Beams under Combined Top and Bottom Loadings

The behaviour of deep beams with this loading condition makes it very difficult to design the ultimate shear load capacity with a single formula. Concerning the interaction between top and bottom loads on the overall shear capacity, a standard interaction equation is given on page 17 of the CIRIA guide [1977] as follows (Eqn.3.5) :

$$\frac{V_{at}}{V_{ct}} + \frac{V_{ab}}{V_{cb}} < 1$$

where

V_{at} is the applied top shear load;

V_{ab} is the applied bottom shear load;

V_{ct} is the shear capacity with top load only;

V_{cb} is the shear capacity with bottom load only;

Also, for the design shear load, $V < V_{cb}$.

Therefore, the limit of V is restricted to 0.75 b h_a v_u, the tensile capacity of the vertical hangers or the shear capacity of the shear reinforcement. Here v_u is defined in Table 6 of CP 110 [1972], b is the beam thickness, h_a is the active height of beam or the beam span L_o, whichever is the less. It is noted that CP 110 has been superseded by BS 8110 [1985]. However, the maximum allowable shear stress in BS 8110 is only slightly increased to 5

N/mm^2 instead of 4.75 N/mm^2 as in CP 110. Therefore, this 4.75 N/mm^2 value was used throughout the present analysis. For the top shear load capacity, the empirical equation given in Cl.3.4.2 of the CIRIA Guide [1977] was used (Eqn.(3.1)).

The actual failure mechanisms of the CB-Series beams fell into one of the following four cases, namely :

Case 1 : failure of the bottom shear reinforcement;

Case 2 : failure of the bottom shear capacity of the beam;

Case 3 : yielding of the bottom hangers; and

Case 4 : collapse of the bottom hangers.

These four cases are examined in Table 7.5. Generally speaking, failure of the bottom shear reinforcement (Case 1), as stipulated in the guide seems too stringent and certainly not the direct concern of the tested specimens. Therefore, the choice of a factor of safety rests on the discretion of the designer and his engineering judgement. As discussed in Section 6.5.3(d), the orthogonal and inclined shear arrangements would have little effect on the ultimate capacity of a deep beam. Moreover, the common bearing failures and the comparatively high ultimate load capacity of those beams without the web meshes, suggest that the CIRIA orthogonal and inclined hanger arrangements may be too conservative in practice.

It is clear that the CIRIA's equation for the combined top and bottom shear loadings, as applied, does not distinguish between a concentrated or uniformly distributed load situation. In reviewing Table 7.5, the question arises as to whether the configuration of the applied loadings would affect the application of the CIRIA combined

shear equation or not. In general, beams with concentrated loadings are more prone to cracking and will reach earlier failure load than beams with uniformly distributed loads. This is probably due to the higher localised stresses that would be attained in the former. Therefore, an attempt has been made in this study to correlate the top and bottom shear loadings data as reported by Besser [1983] on uniformly distributed load tests and those concentrated direct load tests of the present investigation.

For deep beams under uniformly distributed combined top and bottom loadings, the ultimate shear interaction diagrams of 16 Besser's beams are given in Figs.7.6 and 7.7 based on the amount of their bottom shear reinforcement. For the sake of interest, Besser's beam with 1.93 % of vertical shear reinforcement is included. The bottom shear capacity of this beam, based on its percentage of vertical shear reinforcement, is larger than the bottom ultimate shear limit set in the CIRIA Guide, and therefore is not recommended in practice. The thick full straight lines in these figures represent the CIRIA interaction equation. Fig.7.6 show that the CIRIA equation, when in use, seriously under-estimated the ultimate shear capacity of deep beams.

The need for a simple, reasonably accurate method of calculating the ultimate combined shear load, to be expected for such a given top and bottom loadings condition, led to an attempt being made to provide a simple equation based on the CIRIA approach. A better quantitative agreement eventually has been reached between the theoretical predictions and the experimental data. The theoretical

equation takes the following form (the dotted curve lines in Figs.7.6 and 7.7) :

$$\left(\frac{V_{at}}{V_{ct}}\right)^2 + \left(\frac{V_{ab}}{V_{cb}}\right)^2 < 1$$

where V_{at}, V_{ct}, V_{ab} and V_{cb} are as defined earlier [CIRIA, 1977].

The experimental curves (dotted lines in Figs.7.6 and 7.7) are drawn by joining both the ultimate load of beams tested with top load only and the ultimate load of those corresponding beams tested solely with bottom load using this modified equation. These curves are certainly of the shape predicted by the above equation and reasonably accurate values can be approached. Excluding the beam with 1.93 % vertical shear reinforcement, the bottom load capacity can be closely estimated. The accuracy of this modified equation is, therefore, largely dependent on the accuracy of the prediction of the top shear capacity of the beam. Fig.7.6 shows that the CIRIA ultimate top shear equation (full straight lines) has under-estimated the load-carrying capacity of Besser's top loaded beams, and thus the predictions (full curve lines) are generally under-estimated. Fig.7.7 shows the comparison of the safety margins of Besser's beams, when both the CIRIA and the present modified equations are used in practice. The partial factors of safety of concrete (1.5) and steel (1.15) are included in the computation.

For deep beams under concentrated combined top and bottom loadings, the interaction diagrams of the 16 CB-Series beams are drawn separately in Fig.7.8. As opposed to the findings on uniformly

distributed loaded beams, the CIRIA combined shear loading equation always gives better predictions (dotted straight lines in Fig.7.8) than those predictions (dotted curve lines in Fig.7.8) using the modified equation. The modified equation tends to over-estimate the predictions. This is expected because of the localised stresses problem as explained earlier.

Fig.7.8 also shows the computed lines of both the CIRIA equation (full straight lines) and the modified equation (full curve lines) including the partial factors of safety of material, 1.5 for concrete and 1.15 for steel. Fig.7.8 shows that, with direct concentrated loadings, deep beam design using the modified equation (full curve lines) is certainly safe. It would be, however, very difficult to be sure unless further experimental evidence is available to confirm fully or invalidate the findings observed in this study.

Therefore, it can be concluded that, in general, the use of the CIRIA shear interaction equation for deep beams under combined top and bottom loadings can be safely recommended for design purposes at this stage as it always produces conservative results. For a more economical solution, it is recommended that the modified equation can be used for the design of deep beam under uniformly distributed combined top and bottom loadings. However, for deep beams under concentrated combined top and bottom loadings, the CIRIA combined shear loading equation should be used.

7.4 SUMMARY

In this chapter, the CIRIA [1977] buckling strength design of deep beams without web-openings has been studied. In the light of such an approach, a modified effective length concept is used to extend the CIRIA buckling strength design methods to deep beams with web-openings. The Kong et al [1973a] top shear design equation on deep beams with web-openings is also studied and the design concept is modified. Furthermore, the CIRIA interaction equation on combined top and bottom shear loadings is reviewed and checked with the existing data [Besser, 1983] and the present new test results. A new shear interaction equation is then proposed for the design of deep beams under uniformly distributed combined top and bottom loadings.

CHAPTER EIGHT

CONCLUDING REMARKS AND DESIGN RECOMMENDATIONS

8.1 CONCLUDING REMARKS

The behaviour, design and analysis on reinforced concrete deep beams have been studied in the previous chapters. In this Chapter, the major concluding remarks which can be drawn from the present and other relevant tests are summarized.

8.1.1 Slender Deep Beams without Web-Openings

(1) The failure mode of slender concrete deep beams without web-openings is strongly dependent on the eccentricity of the load. When the effective eccentricity-to-thickness ratio e/b was 0.1 or more, even test beams of height-to-thickness ratio h/b down to 25 failed by buckling.

(2) The transition from the shear failure mode to the buckling failure mode is accompanied by a significant reduction in the failure load. In practical design, it is difficult to be sure that structural members are truly centrally loaded, even when the drawing shows that they are. Depending on the slenderness of a deep beam, even a comparatively small eccentricity of the loading could mean that the eccentricity-to-thickness ratio e/b is sufficiently high to change the failure mode from shear, say, to buckling. In practice, the load-carrying capacities of slender deep beams should therefore be based on the buckling mode rather than on shear or flexure. In the design of slender columns, both

CP 110 and the new BS 8110 specify a minimum design eccentricity ratio e/b of 0.05. For slender deep beams of h/b ratio higher than 20, say, it would seem that a minimum e/b ratio should be similarly specified. Further investigations are desirable on the effect of the e/b ratio on the strength and stability of slender deep beams; in the mean time it is suggested that this minimum e/b ratio should be taken conservatively as 0.1.

(3) The buckling recommendations in the CIRIA guide were found to be safe for all the beams tested. For those beams of height-to-thickness ratio h/b of 25 and 29, the factors of safety were mostly of the order of 5 which, for buckling failures, should not be considered too high. For the very slender beams of h/b ratio of 33 or more, the CIRIA procedures were generally too conservative. Nevertheless, designers should bear in mind several points. First, buckling failures are catastrophic and difficult to predict; hence a comparatively high factor of safety is called for. Secondly, very slender deep beams occur only infrequently in practice; hence, provided a method is safe, its accuracy becomes progressively less important as the slenderness increases. Thirdly, the tests reported here represent the first attempt to check the CIRIA guide predictions against experimental results. In view of these three points, it is prudent not to propose a change in the CIRIA buckling design procedures until, say, further evidence is available from other independent investigators.

(4) The CIRIA guide specifies that its buckling design procedures are to be used in conjunction with CP 110. If CP 110 is superseded

by BS 8110, the factor of safety against buckling failure will usually become slightly higher.

(5) Insofar as buckling is concerned, the analytical methods that can be readily used by the practising engineers appear to be the relatively crude procedures as given in the CIRIA Guide [1977]. Although the computed buckling loads using such procedures are safe, the perplexing problem of the lack of agreement between the CIRIA theoretical model and the actual behaviour of the slender deep beams, as observed in the tests, still remains unsolved. The need at this time is to extend the understanding of the buckling behaviour of reinforced concrete deep beams to a greater number of beam geometries, boundaries and loading conditions.

8.1.2 Slender Deep Beams with Web-Openings

(1) The location of web-openings profoundly affected the failure mode of the slender deep beams with web-openings. When the openings are located very near to the load or support points, shear failure is predominate. However, when the openings are located near to the mid-height of the beam, buckling is possible.

(2) Reducing the clear-shear-span/depth ratio x/h of a deep beam with web-openings would change its failure mode, say from shear to buckling. This is possible because when the clear-shear-span is reduced, the in-plane bending moment on the beam is also reduced. In other words, the beam-action of the beam is becoming less important as compared to the column-action. Therefore, a beam with reduced x/h is more prone to buckling than shear failure.

(3) Slender deep beams with web-openings are more prone to buckling than ones without web-openings. This would be expected because the inclusion of the web-openings reduces the cross-sectional stiffness of a beam, and hence weakens its resistance to lateral buckling.

(4) Regardless of the failure modes, the ultimate strength of deep beams with circular web-openings are always 15 to 28 percent higher than those comparable beams with rectangular web-openings. In practice, designers should consider positioning their web-openings as close to the circular-shape as possible.

(5) From the 80 tests done by Sharp [1977] and Kubik [1978], it is clear that the usefulness of the lower path 30° limit of the Kong et al's [1973a] equation for deep beams with web-openings is doubtful. It is obvious that some limitations should be set for the position of web-openings in order to provide a safe and reliable design.

(6) Section 7.3.2 shows that the predicted ultimate shear loads using Kong et al's [1973a] equation for deep beams with web-openings can seriously under-estimate the ultimate shear strength when the openings are located too near to the applied load. Likewise, it can over-estimate the ultimate shear strength when the openings are located too near to the supports.

(7) For deep beams with web-openings located just above or below the load or support points, the Kong et al [1973a] equations should be used with great care. At this stage, it is difficult to quantify what restrictions should be imposed on the shape, size and location of the openings. Nevertheless, practising engineers

should avoid placing web-openings too near to the beam supports.

8.1.3 Deep Beams under Combined Top and Bottom Loadings

(1) The ultimate bearing stress, as quoted in the CIRIA Guide [1977], 0.4 f_{cu}, is not unrealistic. In the CB-Series tests, most of the beams failed by bearing crushing. This is probably due to the relatively high percentage of web reinforcement being used.

(2) Properly proportioned and positioned reinforcement can increase the ultimate load capacity. For example, the ultimate strength of beams with the proper amount of inclined web reinforcement is higher than one with a comparable amount of orthogonal web reinforcement.

(3) Because of the relatively higher ultimate load that an inclined reinforced deep beam can attain compared with one reinforced with orthogonal steel, wider spread of the cracking zone is found on those deep beams with inclined steel arrangement than on those ones with orthogonal steel arrangement.

(4) As far as serviceability limit state is concerned, the crack control of a deep beam with the inclined steel arrangement is not better than one with the orthogonal steel arrangement. The paramount aim of such a design is, therefore, to provide an adequate amount of reinforcement to evenly distribute the hanging load from the bottom portion of a beam to its upper portion. It is apparent that the inclined steel arrangement is not satisfactory in controlling the growth of cracks in this context.

(5) Different modes of failure may result for comparable beams with

different concrete strength.

(6) Increase of concrete strength can increase the ultimate load capacity of a deep beam under combined loading. However, such an increase is only marginal in some cases.

(7) The orthogonal and inclined shear arrangement patterns proposed by the CIRIA Guide [1977] probably has little influence on the ultimate capacity of a beam. It should be noticed that, for deep beams under bottom loading, the amount of web reinforcement used is usually high. Therefore, the effectiveness of the shear reinforcement is relatively insignificant.

(8) The CIRIA interaction expression for combined shear loading will lead to a safe but conservative lower bound solution. While the bottom shear capacity can be accurately predicted by the CIRIA bottom shear provision, the conservatism of the interaction equation is mainly due to the relatively poor prediction of the CIRIA top shear equation.

8.2 DESIGN RECOMMENDATIONS

The significance of the present investigations has led to certain tentative recommendations that should be considered in the practical design of deep beams :

8.2.1 Slender Deep Beams without Web-Openings

(1) The CIRIA guide states that Eqn.(3.1), for estimating the shear capacity of top-loaded deep beams, is intended to apply over the range of effective clear-shear-span/depth ratio x_e/h_a of 0.23 to 0.7. The test results have shown that the CIRIA equation can be applied to an extended range of 0 to 0.7 x_e/h_a ratio.

However, this equation was based on tests on stocky deep beams and gives a reduced factor of safety for slender deep beams. Therefore, for deep beams with h/b ratio greater than, say 25, the CIRIA shear equation should not be used.

(2) The CIRIA guide gives three methods for buckling design of deep beams : the supplementary rules, the single-panel method, and the two-panel method. The supplementary rules should be used wherever applicable; if the supplementary rules are not applicable, it is advisable to move to the single-panel method for an economical solution. A more economical solution can be obtained by using the the two-panel method.

(3) Where the possibility of buckling exists, consideration should be given; it is suggested that the minimum effective eccentricity -to-thickness ratio e/b should be taken conservatively as 0.1.

8.2.2 Slender Deep Beams with Web-Openings

(1) Since the significance of the web-openings to the ultimate buckling strength of a deep beam is difficult to quantify, the prudent approach must be one of conservatism. While knowledge of this subject is very limited, conservative estimates of the buckling strength can be made by applying appropriate reduction in their strength to account for the geometric imperfections and the non-linear material behaviour. The simplest method is to modify the CIRIA buckling design procedures; namely, the supplementary rules, the single-panel method and the two-panel method. By introducing the modified effective length or height

concept as described in Section 7.2.2, it is possible to produce a safe design solution. In practice, the minimum effective-eccentricity/thickness ratio e/b, should be set to, say 0.1, whenever the height-to-thickness ratio h/b is greater than, say 20. Since slender deep beams occur relatively rarely in practice, and their behaviour is relatively unpredictable, buckling design for deep beams with web-openings can afford to proceed cautiously and conservatively.

(2) The Kong et al's [1973a] shear equations for the top-loaded deep beams with web-openings could lead to a too conservative solution and sometimes an unsafe design. For the openings located near the supports, the concrete shear contribution would be too conservative to rely solely on the lower load path below the openings. Therefore, for the time being, it is proposed that a more economical and rational design can be achieved by using the concept as described in Section 7.3.2, whereby the larger concrete contribution of the lower and upper load path should be used in addition to the steel contribution.

(3) The Kong et al's [1973a] equations, for designing the shear strength of top-loaded deep beams with web-openings, are intended to apply over the range of 0.2 to 0.4 clear-shear-span/depth ratio x/h. The present test results indicated that these equations should be applicable over the extended range of 0.085 to 0.4 for x/h.

(4) In practice, designers should consider their web-openings to be as close to the circular-shape as possible. At least, the problem of stress concentration developed at the abrupt corners

should be dealt with properly. However, it should be noted that trimming of the openings with additional reinforcement cannot increase the load-carrying capacity of a deep beam [Sharp, 1977].

8.2.3 Deep Beams under Combined Top and Bottom Loadings

(1) The serviceability limit state is one of the criteria on which design has to be based. For deep beams under combined top and bottom loadings, a complete design method which produces a safe, serviceable and economical solution is not yet available. The perference of using an inclined bottom hanger arrangement to that of an orthogonal bottom hanger arrangement is not immediately clear. In practice, the use of the CIRIA orthogonal steel arrangement seems to be the best approach to achieve most of the above objectives.

(2) The CIRIA shear interaction equation for deep beams under combined top and bottom loadings can, if used safely, be recommended for design purposes at this stage, as it always produces conservative solutions. For a more economical solution, it is recommended that the modified equation, as given in Section 7.3.3, can be used for the design of deep beams under uniformly distributed combined top and bottom loadings. However, for deep beams under combined top and bottom concentrated loadings, the CIRIA combined shear equation should be used.

REFERENCES

ACI COMMITTEE 318 [1971], " Commentary on Building Code Requirements for Reinforced Concrete (ACI 318-71) ", American Concrete Institute, Detroit, 1971, 72pp.

ACI COMMITTEE 318 [1983], " Building Code Requirements for Reinforced Concrete (ACI 318-83) ", American Concrete Institute, Detroit, Nov. 1983 , (revised 1986), pp.111.

ACI COMMITTEE 318 [1985], " Building Code Requirements for Reinforced Concrete (ACI 318M-83) ", American Concrete Institute, Detroit, 1985, pp.111.

ALBRITTON, G.E. [1965], " Review of Literature Pertaining to the Analysis of Deep Beams ", Technical Report No.1-701, U.S. Army Engineer Waterways Experiment Station, Vicksburg, Miss., Nov. 1965, 80pp.

ARCHER, F.E. and KITCHEN, E.M. [1956], " Stresses in Single Span Deep Beams ", Australian Journal of Applied Science, Vol.7, No.4, Dec. 1956, pp.314-326.

ARCHER, F.E. and KITCHEN, E.M. [1957], " Strain Energy Methods for the Solution of Deep Beams ", Civil Engineering and Public Works Review, Vol.52, No.618, Dec. 1957, pp.1375-1378.

ARCHER, F.E. and KITCHEN, E.M. [1960], " Stress Distribution in Deep Beams ", Civil Engineering and Public Works Review, Vol.55, No.643, February 1960, pp.230-234.

BARRY, J.E. and AINSO, H. [1983], " Single-Span Deep Beams ", Proceedings, ASCE, Vol.109, No.ST3, March 1983, pp.646-663.

BAY, H. [1931], " Uber den Spannungszestand in hohen tragern und die bewchrung von eiscabetontragwanden ", Stuttgart, Germany, 1931, 64 pp.

BESSER, I.I. [1983], " Strength of Slender Reinforced Concrete Walls ", PhD Thesis at University of Leeds, Apirl, 1983.

BESSER, I.I. and CUSENS, A.R. [1984], " Reinforced Concrete Deep Beam Panels with High Depth/Span Ratios ", Proc. Instn Civ. Engrs., Part 2, Vol. 77, June 1984, pp.265-278.

BS 12 [1978], " Specification for Ordinary and Rapid-hardening Portland Cement Composition Manufacture and Chemical and Physical Properties ", British Standards Intitute, London, amended 1983, 4pp.

BS 18 [1971], " Part 2 : Methods for Tensile Testing of Metals. Steel (General) ", British Standards Intitute, London, 1971, 28pp.

BS 882 [1983], " Specification for Aggregates from Natural Sources for Concrete ", British Standards Intitute, London, amended 1986, 12pp.

BS 1881 [1983a], " Part 102 : Method for Determination of Slump ", British Standards Intitute, London, 1983, 4pp.

BS 1881 [1983b], " Part 104 : Method for Determination of Vebe Time ", British Standards Intitute, London, 1983, 8pp.

BS 1881 [1983c], " Part 110 : Method for Making Test Cylinders from Fresh Concrete ", British Standards Intitute, London, 1983, 8pp.

BS 1881 [1983d], " Part 116 : Method for Determination of Compressive Strength of Concrete Cubes ", British Standards Intitute, London, 1983, 8pp.

BS 1881 [1983e], " Part 117 : Method for Determination of Tensile Splitting Strength ", British Standards Intitute, London, 1983, 8pp.

BS 4395 [1969], " Part 1 : Specification for High Strength Friction Grip Botls and Associated Nuts and Washers for Structural Engineering ", British Standards Intitute, London, amended 1977, 36pp.

BS 4449 [1984], " Specification for Hot Rolled Steel Bars for the Reinforcement of Concrete ", British Standards Intitute, London, 1984, 16pp.

BS 8110 [1985], " Code of Practice of the Structural Use of Concrete ", British Standards Intitution, London, 1985.

CAN3-A23.3-M84 [1984], " Design of Concrete Structures for Buildings ", Canadian Standards Association, CSA Committee A23.3, Rexdale, Dec. 1984, 281pp.

CASWELL, J.S. [1954], " Stresses in Short Beams ", Engineering, 12 and 19, Vol.178, Nos.4633-4634, Nov.1954, pp.625-628 and pp.655-658.

CEB-FIP [1970], " International Recommendations for the Design and Construction of Concrete Structures - Appendix 3 : Deep Beams ", Prague, (English Edition, Cement and Concrete Association, London), June 1970, p.19.

CEB-FIP [1978], " Model Code for Concrete Structures ", International Recommendations, Comite Euro-International du Beton - Federation Internationale de la Precontrainte, Paris, 3rd. Edition, 1978, 348pp.

C&CA [1969], " Bibliography on Deep Beams ", Library Bibliography, No.Ch.71(3/69), Cement and Concrete Association, London, 1969, 8pp.

CHENG, D.H. and PEI, M.L. [1954], " Continuous Deep Beams ", Proceeding of the American Society of Civil Engineers, Structural Division, Vol.80, No.450, June, pp.1-17, 1954.

CHOW, L., CONWAY, H.D. and WINTER, G. [1952], " Stresses in Deep Beams ", Pro. ASCE, Vol.78, Separate No.127, May 1952, pp.686-708.

CHOW, L., CONWAY, H.D. and WINTER, G. [1953], " Discussion of "Stresses in Deep Beams" by Guzmán, A.M. and Luisoni, G.J.; Conwell, W.A.; Conway, H.D. and Winter G. ", Proceeding of the American Society of Civil Engineers, Vol.79, Separate No. D-127, February 1953, 6 pp.

COLLINS, M.P. and MITCHELL, D. [1986], " A Rational Approach to Shear Design - The 1984 Canadian Code Provisions ", ACI JOURNAL, Nov.-Dec. 1986, pp.925-933.

CONWAY, H.D., CHOW, L. and MORGAN, G.W. [1951], " Analysis of Deep Beams ", JOURNAL of Applied Mechanics, Amercian Society of Mechanical Engineering, Vol.18, No.2, June 1951, pp.163-172.

COOK, C.F. [1980], " An Electrical Demountable Strain Transducer ", Journal of the British Society for Strain Measurement, Vol.16, No.3, July 1980, pp.113-119.

COULL, A. [1966], " Stress Analysis of Deep Beams and Walls ", The Engineer, February 1966, Vol.22, No.5744, pp.310-312.

CP 110 [1972], " Code of Practice for the Structural Use of Reinforced Concrete in Buildings ", British Standards Institute, London, 1972.

CP 114 [1957], " Code of Practice for the Structural Use of Reinforced Concrete in Buildings ", British Standards Institute, London, 1957.

CRANSTON, W.B. [1972], " Analysis and Design of Reinforced Concrete Columns ", Research Report 20, Cement and Concrete Association, 1972, 54pp.

CRIST, R.A. [1971], " Static and Dynamic Shear Behaviour of Uniformly Reinforced Concrete Deep Beams ", PhD Thesis, University of New Mexico, 1971.

CUSENS, A.R. and BESSER, I.I. [1985], " Shear Strength of Reinforced Concrete Wall-Beams under Combined Top and Bottom Loads ", The Structural Engineer, Vol.63B, No.3, September 1985, pp.50-56.

DE PAIVA, H.A.R. and SIESS, C.P. [1965], " Strength and Behaviour of Deep Beams in Shear ", Proceedings, ASCE, Vol.91, ST5, Oct. 1965, pp.19-41.

DISCHINGER, F. [1932], " Contribution to the Theory of Wall-Like Girders ", Publications, International Association for Bridge and Structural Engineering, Vol.1, 69, 1932, p.69-93.

DURANT, N.J. and GARWOOD, F. [1947], " Ministry of Works, Tech. Note No.78 ", Oct., 1947.

EUROCODE NO.2. (DRAFT) [1984], " Common Unified Rules for Concrete Structures ", International Processes Building and Civil Engineering, Commission of the European Communities, Luxembourg, 1984.

GARCIA, R.C. [1981], " Strength and Stability of Concrete Deep Beams ", PhD Thesis, University of Cambridge, August 1981.

GEER, E. [1960], " Stresses in Deep Beams ", Proc. ACI, Vol.56, Jan. 1960, pp.651-661.

GRAF, O., BRENNER, E. and BAY, H. [1943], " Versuche mit einem wandartigen trager aus stahlbeton ", Deutschuss Fur Stahlbeton, Heft 99, Berlin, 1943.

HENDRY, A.W. [1977], " Elements of Experimental Stress Analysis ", Pergamon Press, SI Edition, 1977, 193pp.

KAAR, P.H. [1957], " Stresses in Centrally Loaded Deep Beams ", Proceedings of the Society for Experimental Stress Analysis, Vol.15, No.1, 1957, pp.77-84.

KLINGROTH, H. [1942], " Versuche an stahlbetontrag wanden und daren answertung ", Beton und Eisen, No.9, 1942.

KONG, F.K. [1985], Letter from Mr. A. Stevens of Ove Arup and Partners, London, to F.K. Kong of University of Newcastle upon Tyne, dated 4 February 1985 (Ove Arup ref. AS/ML).

KONG, F.K. [1986], " The Design of Reinforced Concrete Deep Beams ", Lecture delivered at Ove Arup & Partners, London, 3 October, 1986.

KONG, F.K., ROBINS, P.J. and COLE, D.F. [1970], " Web Reinforcement Effects on Deep Beams ", American Concrete Institute JOURNAL, Proceedings, Vol.67, No.12, December 1970, pp.1010-1017.

KONG, F.K. and ROBINS, P.J. [1971], " Web Reinforcement Effects on Lightweight Concrete Deep Beams ", American Concrete Institute JOURNAL, Proceedings, Vol.68, No.7, July 1971, pp.514-520.

KONG, F.K. and ROBINS, P.J. [1972a], " Shear Strength of Reinforced Concrete Deep Beams ", Concrete, Vol.6, No.3, March 1972, pp.34-36.

KONG, F.K., ROBINS, P.J., KIRBY, D.P. and SHORT, D.R. [1972b], " Deep Beams with Inclined Web Reinforcement ", American Concrete Institute JOURNAL, Proceedings, Vol.69, No.3, March 1972, pp.172-176.

KONG, F.K. and SINGH, A. [1972c], " Diagonal Cracking and Ultimate Loads of Lightweight Concrete Deep Beams ", American Concrete Institute JOURNAL, Proceedings, Vol.69, No.8, August 1972, pp.513-521.

KONG, F.K., ROBINS, P.J. SINGH, A. and SHARP, G.R. [1972d], " Shear Analysis and Design of Reinforced Concrete Deep Beams ", The Structural Engineer, Vol.50, No.10, October 1972, pp.405-408.

KONG, F.K. and SHARP, G.R. [1973a], " Shear Strength of Lightweight Reinforced Concrete Deep Beams with Web Openings ", The Structural Engineer, Vol.51, No.8, August 1973, pp.267-275.

KONG, F.K. and SHARP, G.R. [1973b], " The Design of Reinforced Concrete Deep Beams with Web Openings ", Cambridge University Mechanics Colloquium, 8 November, 1973.

KONG, F.K., ROBINS, P.J. and SHARP, G.R. [1975], " The Design of Reinforced Concrete Deep Beams in Current Practice " The Structural Engineer, Vol.53, No.4, April 1975, pp.173-180.

KONG, F.K. and SHARP, G.R. [1977], " Structural Idealization for Deep Beams with Web Openings ", Magazine of Concrete Research, Vol.29, No.99, June 1977, pp.81-91.

KONG, F.K., SHARP, G.R., APPLETON, S.C., BEAUMONT, C.J., and KUBIK, L.A. [1978], " Structural Idealization for Deep Beams with Web Openings : Further Evidence ", Magazine of Concrete Research, Vol.30, No.103, June 1978, pp.89-95.

KONG, F.K. and CHARLTON, T.M. [1983], " The Fundamental Theorem of the Plastic Theory of Structures ", Proc. M.R. Horne Conference on Instability and Plastic Collapse of Steel Structures, Manchester, Editor J.L. Morris, Granada Publishing, London, 1983, pp.9-15.

KONG, F.K., PAINE, J.M., CHEMROUK, M., TANG, C.W.J. and WONG, H.H.A. [1985a], " Worked Examples on the use of CIRIA Guide No.2 (in conjunction with CP 110:1972) to calculate the buckling strengths of slender concrete deep beams ", Technical Report STRUCT 5/9A, Department of Civil Engineering, University of Newcaslte upon Tyne, England, 1985, pp.15.

KONG, F.K., PAINE, J.M., WONG, H.H.A., TANG, C.W.J. and CHEMROUK, M. [1985b], " Worked Examples on the use of CIRIA Guide No.2 (in conjunction with BS 8110:1985) to calculate the buckling strengths of slender concrete deep beams ", Technical Report STRUCT 5/9B, Department of Civil Engineering, University of Newcaslte upon Tyne, England, 1985, pp.15.

KONG, F.K., TANG, C.W.J., WONG, H.H.A. and CHEMROUK, M. [1986a], " Diagonal Cracking of Slender Concrete Deep Beams ", Research Seminar - The Behaviour of Concrete Structures, Cement and Concrete Assoication, 30 June - 2 July, 1986, pp.213-217.

KONG, F.K., GARCIA, R.C., PAINE, J.M., WONG, H.H.A., TANG, C.W.J. and CHEMROUK, M. [1986b], " Strength and Instability of Slender Concrete Deep Beams ", The Structural Engineer, Vol.64B, No.3, Sept. 1986, pp.49-56.

KUBIK, L.A. [1978], " Strength and Serviceability of Reinforced Concrete Deep Beams ", PhD Thesis, University of Cambridge, 1978.

LEONHARDT, F. and WALTHER, R. [1966], " Deep Beams (Wandartige Trager) ", Bulletin 178, Deutscher Ausschuss fur Stahlbeton, Berlin, 1966, 159pp. (English Translation : C&CA, London, 1970)

NYLANDER, H. and HOLST, H. [1946], " Reinforced Concrete Deep Beams and Slabs ", Royal Technical University , Stockholm (1946), (In Swedish : English translation by courtesy of Ove Arup and Partners, London).

OVE ARUP and PARTNERS [1977], " CIRIA Guide 2 - The Design of Deep Beams in Reinforced Concrete ", London, Construction Industry Research and Information Association, January 1977 (reprinted 1984), 131 pp.

PAINE, J.M. [1984], " Strength and Buckling of Reinforced Concrete Deep Beams ", MSc. Thesis, University of Newcastle upon Tyne, May 1984.

PARK, P. and PAULAY, T. [1975], " Reinforced Concrete Structures ", Wiley-Inter-Science, New York, 1975, 769pp.

PCA [1946], " Design of Deep Girders ", Concrete Information No.ST66, Portland Cement Assoication, Chicago, 1946, 10pp.

PCA [1984], " Notes on ACI (318-83) Building Code Requirements with Design Applications ", Portland Cement Association, Chicago, 1984.

RASHEEDUZZAFAR, M.H. and AL-TAYYIB, A.H.J. [1986]," Stress Distirbution in Deep Beams with Web Openings ", Proceedings, ASCE, Vol.112, No.ST5, May 1986, pp.1147-1165.

RAY, S.P. and REDDY, C.S. [1979], " Strength of Reinforced Concrete Deep Beams With and Without Opening in the Web ", Indian Concrete JOURNAL, Sept. 1979, pp.242-246.

REYNOLDS, C.F. and STEEDMAN, J.C. [1981], " Reinforced Concrete Designer's Handbook ", Ninth Edition, Viewpoint Publication, 1981, pp.402-403.

ROGOWSKY, D.M. and MACGREGOR, J.G. [1983], " Shear Strength of Deep Reinforced Concrete Continuous Beams ", Structural Engineering Report No.110, Department of Civil Engineering, University of Alberta, Edmonton, Nov. 1983, 178pp.

ROGOWSKY, D.M. and MACGREGOR, J.G. [1986a], " Design of Reinforced Concrete Deep Beams ", Concrete International, August 1986, pp.49-58.

ROGOWSKY, D.M., MACGREGOR, J.G. and ONG, S.Y. [1986b], " Tests of Reinforced Concrete Deep Beams ", ACI JOURNAL, Proceedings, Vol.83, No.4, July-August 1986, pp.614-623.

SAAD, S. and HENDRY, A.W. [1961a], " Stresses in a Deep Beam with a Central Concentrated Load ", Proceedings of Society for Experimental Stress Analysis, Vol.38, No.1, June 1961, pp.192-198.

SAAD, S. and HENDRY, A.W. [1961b], " Gravitational Stresses in Deep Beams ", The Structural Engineer, Vol.39, No.6, June 1961, pp.185-194.

SCHLEEH, W. [1964], " Die statisch unbestimmt gestützte durchlaufende Scheibe ", Beton und Stahlbetonbau, Vol.59, 1964, No.3, pp.49-56; No.4, pp.91-94; No.5, pp.111-119.

SCHÜTT, H. [1956], " Uber das travermogen wandertiger stahlbetongrager ", Beton und stahlbetonbau, Vol.51, No.10, 1956, pp.220-224.

SHARP, G.R. [1977], " Reinforced Concrete Deep Beams with Openings ", PhD Thesis, University of Nottingham, 1977, 121pp.

SINGH, R., RAY, S.P. and REDDY, C.S. [1980], " Some Tests on Reinforced Concrete Deep Beams With and Without Opening in the Web ", Indian Concrete JOURNAL, Vol.54, July 1980, pp.189-194.

SWADDIWUDHIPONG, S. and SHANMUGAM, N.E. [1985], " Fiber-Reinforced Concrete Deep Beams with Openings ", Proceedings, ASCE, Vol.111, No.ST8, August 1985, pp.1679-1690.

TANG, C.W.J. [1985], " Reinforced Concrete Deep Beams : Behaviour, Analysis and Design ", Research Report, Department of Civil Engineering, University of Newcastle upon Tyne, England, 1985, 472pp.

UHLMANN, H.L.B. [1952], " The Theory of Girder Walls with Special References to Reinforced Concrete Design ", The Structural Engineer, Vol.30, August 1952, pp.172-181.

VECCHIO, F. and COLLINS, M.P. [1986], " The Modified Compression-Field Theory for Reinforced Concrete Elements Subjected to Shear ", ACI JOURNAL, March-April 1986, pp.219-231.

Appendix A

WORKED EXAMPLES FOR DEEP BEAMS WITHOUT WEB-OPENINGS

WORKED EXAMPLES on the use of CIRIA GUIDE No.2

to calculate the Buckling Strengths of Slender

Concrete Deep Beams without Web-Openings

WORKED EXAMPLES on the use of CIRIA GUIDE No.2 to calculate the Buckling Strengths of Slender Concrete Deep Beams without Web-Openings

SUMMARY

Reinforced Concrete deep beams are not yet covered by CP 110 : 1972, nor the new BS 8110. Currently the main documents for deep-beam designers are the American Code ACI 318-83 [1983], the CEB-FIP Model Code [1978] and the CIRIA Guide No.2 [1977]. Of these, the CIRIA Guide is the only one that gives recommendations on the buckling strength of slender deep beams.

The CIRIA buckling provisions deal with a complex subject of which relatively little information is available in the literature. First-time users of the CIRIA provisions tend to find them difficult to follow. This Appendix gives three worked examples to illustrate the calculation of buckling loads using the three methods* of the Guide :

(a) The Supplementary Rules

(b) The Single Panel method

(c) The Two Panel method

Comments are given at the end of each Example.

---

* The CIRIA Guide specifies that all the three methods are to be used in conjunction with CP 110:1972. In addition, the use of the CIRIA Guide in conjunction with BS 8110:1985 is also illustrated.

EXAMPLE A.1 Using the Supplementary Rules in Cl.3.2.2 of the CIRIA Guide [1977], calculate the buckling load of *Beam A-25-0.2 of Table 6.1

+ SOLUTION

Step 1 : Calculate effective height h_e

From CIRIA Guide, Cl.3.2.2,

$h_e = 1.5\ h = 1.5 \times 1000 = 1500$ mm (Fig.4.1)

Step 2 : The equivalent applied stresses

From p.106 of the CIRIA Guide, the equivalent applied vertical stress (see Comment (a) below) is :

$$N_v = \frac{\text{Support Reaction } (= P/2)}{\text{Length of Support Bearing } (=0.23 \text{ m})}$$

$$= 2.17\ P \quad (kN/m)$$

where P is the buckling load (kN).

Step 3 : Calculate additional and total moments

From CP 110, Cl.3.5.7.1,

$$M_t = M_i + \frac{N_v\ b}{1750} \left[\frac{h_e}{b} \right]^2 \left[1 - 0.0035 \frac{h_e}{b} \right]$$

(BS 8110, Cl.3.8.3.2, $M_t = M_i + \frac{N_v\ b}{2000} \left[\frac{h_e}{b} \right]^2$)

---

* The Beam Notation in this Worked Example is identical to that in Kong et al [1986b], and is explained in the footnote to Table 4.1.

+ Notation as in CIRIA Guide, unless otherwise defined.

where

M_t (M_i) is the total (initial) moment per unit width

N_v is the load per unit width

From Eqn.(34) of CP 110 : Cl.3.5.7.1 (BS 8110, Cl.3.8.3.2) :

$$M_i = 0.4\ N_v\ e_1 + 0.6\ N_v\ e_2$$

Substituting

e_1 = 0 (Table 4.1); e_2 = 0.2 x 40 = 8 mm (Table 4.1)

h_e = 1500 mm (Step 1); b = 40 mm (Table 4.1), we obtain

$$M_t = 32.72\ N_v$$

(BS 8110, $M_t = 32.92\ N_v$)

Step 4 : Determination of failure load

The equation $M_t = 32.72\ N_v$ can be expressed in the equivalent form

$$\frac{N_v}{b} = 1.22\ \frac{M_t}{b^2} \quad \text{(where thickness b = 40 mm)}$$

$$\text{(BS 8110, } \frac{N_v}{b} = 1.21\ \frac{M_t}{b^2}\text{)}$$

This equation is now drawn as the straight line OA in Fig.A.1, to intersect the interaction diagram at point A' (see Comments below for the construction of the interaction diagram).

From Fig.A.1,

$$\left[\frac{N_v}{b}\right] \text{ of point A' = 1.74 (BS 8110, 1.72, Fig.A.2);}$$

$$N_v = 1.74 \times 40 \times 10^{-3} = 0.0696\ \text{kN/mm} = 69.6\ \text{kN/m}$$

(BS 8110, N_v = 68.6 kN/m)

Therefore the CIRIA buckling load is :

$$P = N_v / 2.17 = 69.6 / 2.17$$

$$= \underline{32} \text{ kN} \quad \text{(BS 8110, 31.6 kN)}$$

From Table 6.1, experimental buckling load = 620 kN

Factor of Safety,

$$R_{SR} = \frac{620}{32} = 19.37 \quad \text{(BS 8110, 19.61)}$$

as in Table 6.1

Comments on Example A.1

The interaction diagrams in Fig.A.1 (Fig.A.2) has been specially constructed in accordance with the "Notes on the derivation of design charts" given in Appendix A of CP 110 : Part 2 (BS 8110 : Part 3 : Appendix 3), using the actual properties of Beam A-25-0.2 (see Table 4.1) and the GHOST80 graphical package at the Computing Laboratory of the University of Newcastle upon Tyne. In practical design, it is usually possible to use the standard column charts in CP 110 : Part 2 (BS 8110 : Part 3).

EXAMPLE A.2 Using the Single Panel method in Appendix C of the CIRIA Guide [1977], calculate the buckling load of *Beam A-25-0.2.

+ SOLUTION

Step 1 : The equivalent panel

The notional safe equivalent panel (see Fig.123 of the CIRIA Guide) is in this case simply a rectangle of length and height equal to the actual values (Fig.4.1(a): length = 1700 mm, height = 1000 mm).

Step 2 : The equivalent applied stresses

From p.106 of the CIRIA Guide, the equivalent applied vertical stress (see Comment (a) below) is :

$$N_v = \frac{\text{Support Reaction (= P/2)}}{\text{Length of Support Bearing (= 0.23 m)}}$$

$$= 2.17\ P \quad (kN/m)$$

where P is the buckling load (kN).

The equivalent applied horizontal stress is taken from Fig.51 of the CIRIA Guide (see Comment (b) below) :

$$N_h = \frac{0.36\ P}{1.4 \text{ (Fig.4.1(a): } L_o = 1.4)} = 0.26\ P \quad (kN/m)$$

The shear stress applied at the ends of the equivalent panel may be taken as zero (see Comment (c) below). That is $\tau = 0$

---

* The Beam Notation as in Example A.1 (see footnote on p.166)
+ Notation as in CIRIA Guide, unless otherwise defined.

Step 3 : The critical stresses

From Fig.127 of the CIRIA Guide,

$$\text{vertical critical stress} \quad N'_{vcr} = \frac{1.0\ \pi^2\ EI'}{(1.0)^2} = 9.86\ EI'$$

From Fig.126 of the CIRIA Guide, $\emptyset = 0.588$,

$$\text{horizontal critical stress} \quad N'_{hcr} = \frac{0.96\ \pi^2\ EI'}{(1.0)^2} = 9.47\ EI'$$

Step 4 : The stress ratios R'_v, R'_h, R'_s

$$R'_v = \frac{N_v \text{ (see Step 2)}}{N'_{vcr} \text{ (see Step 3)}} = \frac{2.17\ P}{9.86\ EI'} = 0.22\ \frac{P}{EI'}$$

$$R'_h = \frac{N_h \text{ (see Step 2)}}{N'_{hcr} \text{ (see Step 3)}} = \frac{0.26\ P}{9.47\ EI'} = 0.027\ \frac{P}{EI'}$$

$R'_s = 0$ since $\tau = 0$ (see Step 2)

Step 5 : The stress ratios R'_1, R'_2, R''_2

In this example, the shorter edges of the equivalent panel are the vertical edges; the CIRIA Guide introduces new stress ratios as follows :

R'_1 = R'_h of Step 4 (= 0.027 P/EI')

R'_2 = R'_v of Step 4 (= 0.22 P/EI')

R''_2 = R'_2/M'_2 (see Comment (d) below)

From Fig.129 of the CIRIA Guide, for $R'_s = 0$ (see Step 2),

$M'_2 = 1.0$

Therefore

$$R''_2 = R'_2/1.0 = R'_2\ (= R'_v \text{ of Step 4}) = 0.22\ P/EI'$$

$$\frac{R''_2}{R'_1} = \frac{0.22\ P/EI'}{0.027\ P/EI'} = 8.11$$

Step 6 : The modification factors M_1 and M_2

$R''_2/R'_1 = 8.11$ from Step 5

Referring to Fig.130 of the CIRIA Guide, the ratio $\emptyset = 1.7$, so that the modification factors are :

$M_1 = 0.11$ and $M_2 = 0.92$

Check : $\dfrac{M_2}{M_1} \cdot = \dfrac{R''_2}{R'_1} \cdot = 8$

The modified critical stresses are then :

$N_{vcr} = M_2 \times N'_{vcr}$ of Step 3

$= 0.92 \times 9.86\ EI' = 9.08\ EI'$

$N_{hcr} = M_1 \times N'_{hcr}$ of Step 3

$= 0.11 \times 9.47\ EI' = 1.04\ EI'$

Step 7 : The effective height h_e

$$h_e = \sqrt{\pi^2 EI'/N_{vcr}}$$

$= 1.04$ m (where $N_{vcr} = 9.08\ EI'$ from Step 6)

Step 8 : The additional and total moments

From CP 110, Cl.3.5.7.1 :

$$M_t = M_i + \frac{N_v\, b}{1750}\left[\frac{h_e}{b}\right]^2\left[1 - 0.0035\,\frac{h_e}{b}\right]$$

(BS 8110, Cl.3.8.3.2 : $M_t = M_i + \dfrac{N_v\, b}{2000}\left[\dfrac{h_e}{b}\right]^2$)

where

M_t (M_i) is the total (initial) moment per unit width

N_v is the load per unit width

From Eqn.(34) of CP 110 : Cl.3.5.7.1 (BS 8110, Cl.3.8.3.2) :

$M_i = 0.4\ N_v\ e_1 + 0.6\ N_v\ e_2$

Substituting

e_1 = 0 (Table 4.1); e_2 = 0.2 x 40 = 8 mm (Table 4.1)

h_e = 1040 mm (Step 7); b = 40 mm (Table 4.1)

$$M_t = [\ 0 + 0.6 \times 8\ N_v\ ] + \frac{40\ N_v}{1750}\left[\frac{1040}{40}\right]^2\left[\ 1 - 0.0035\ \frac{1040}{40}\ \right]$$

$$= 18.85\ N_v \quad (\text{BS 8110, } M_t = 18.32\ N_v)$$

Step 9 : The failure load

The relation $M_t = 18.85\ N_v$ can be expressed in the equivalent form :

$$\frac{N_v}{b} = 2.12\ \frac{M_t}{b^2} \qquad \text{(where b = 40 mm)}$$

$$\left(\text{BS 8110, } \frac{N_v}{b} = 2.18\ \frac{M_t}{b^2}\right)$$

This equation is now drawn as the straight line OB in Fig.A.1, to intersect the interaction diagram at point B' (see Comment (e) below). From Fig.A.1 :

$\left[\ \frac{N_v}{b}\ \right]$ of point B' = 6.28 (BS 8110, 6.63, Fig.A.2)

N_v = 6.28 b (where thickness b = 40 mm)

= $6.28 \times 40 \times 10^{-3}$ = 0.251 kN/mm

= 251 kN/m (BS 8110, 265 kN/m)

N_v is the load per metre width at which the notional column strip of the equivalent panel will collapse; N_v is therefore the 'equivalent applied compressive stress' as defined on p.106 of the CIRIA Guide.

Referring to Step 2,

N_v = 2.17 P, where P is the CIRIA buckling load (kN), i.e.

$P = N_v / 2.17 = 251 / 2.17$

$= \underline{115.8}$ kN (BS 8110, $\underline{122}$ kN)

Experimental buckling load (Table 2) = 620 kN

$$\text{Factor of Safety, } R_{SP} = \frac{620}{115.8} = 5.35 \quad \text{(BS 8110, 5.08)}$$

as in Table 6.1

Comments on Example A.2

(a) Note that Appendix C of the CIRIA Guide defines stresses as force per unit width (kN/m).

(b) The use of an upper-bound horizontal stress is to ensure a suitably low restraint of the conceptual "vertical strip" by the conceptual "horizontal strip". In the three worked examples here, which is concerned with Beam A-25-0.2 [Kong et al, 1986b], the stiffness of the "horizontal strip" at mid-height is the most relevant. Hence in Step 2 of Example A.2, the upper-bound horizontal stress at mid-height has been taken. In practical design, the engineer could either use his judgement in choosing where to take the upper-bound stress or he could take the absolute maximum value from Fig.51 of the CIRIA Guide, which is 1.15 in this example. If he chooses 1.15, he will err on the safe side and the resulting factor of safety will increase to 7.38 (BS 8110, 6.99).

(c) According to p.89 of the CIRIA Guide, the boundary shear stress may be taken as :

$$= \frac{\text{Support reaction } (= P/2)}{\text{Panel height } (= 1.0 \text{ m})} = 0.5\ P \text{ kN/m}$$

From Fig.125 of the Guide,

$$\text{Critical shear stress } \tau'_{cr} = \frac{4.7\,\pi^2 EI'}{1.0^2} = 46.39\ EI'$$

Therefore, applied shear stress ratio

$$R'_s = \frac{\tau}{\tau'_{cr}} = \frac{0.01\ P}{EI'}$$

To eliminate the effect of shear stress, the modification factor M'_2 and the modified stress ratio R''_2 are determined as follows :

$$\frac{R'_2 \text{ (see Step 5)}}{R'_s \text{ (see above)}} = 22.0$$

From Fig.129 of the CIRIA Guide, $\phi = 1.7$

and hence $M'_2 = 0.99$.

Therefore, $N''_{vcr} = M'_2 \times N'_{vcr}$ of Step 3

$$= 0.99 \times 9.86\ EI' = 9.76\ EI'$$

Hence

$$R''_2 = \frac{N_v \text{ (see Step 1)}}{N''_{vcr} \text{ (see above)}} = \frac{2.17\ P}{9.76\ EI'}$$

$$= 0.22\ \frac{P}{EI'} = R''_2 \text{ of Step 5}$$

Therefore the modification due to shear is negligible.

(The shear modification was also shown to be negligible in the design example on p.89 of the CIRIA Guide).

(d) The relation in Step 5, namely,

$$R''_2 = R'_2/M'_2$$

is misprinted in the CIRIA Guide as

$$R'_2 = R'_2 = R'_2/M'_2 \quad \text{[Kong, 1985])}$$

(e) See Comments at the end of Example A.1.

EXAMPLE A.3 Using the Two Panel method in Appendix C of the CIRIA Guide [1977], calculate the buckling load of *Beam A-25-0.2.

+ SOLUTION

Step 1 : The equivalent panel

As in Step 1 of Example A.2; length = 1700 mm, height = 1000 mm.

Step 2 : The equivalent applied stresses

PANEL No.1

For Panel No.1, the effective height is calculated using an upper-bound horizontal stress and a lower-bound vertical stress. According to p.109 of the CIRIA Guide, the lower-bound vertical stress is taken at mid-height of the panel. From Fig.51 of the Guide (see Comment (a) below),

$$N_v = \frac{0.36\ P}{1.4} = 0.26\ P \quad kN/m$$

where 1.4 is the simple span (Fig.4.1(a): L_o = 1400 mm) and

P (kN) is the buckling load.

The upper-bound horizontal stress is also taken at mid-height of the panel (see Comment (b) below). From Fig.51 of the CIRIA Guide,

$$N_h = \frac{0.36\ P}{1.4} = 0.26\ P \quad kN/m$$

---

* The Beam Notation as in Example A.1 (see footnote on p.166)
+ Notation as in CIRIA Guide, unless otherwise defined.

PANEL No.2

For Panel No.2, the effective height is calculated using an upper-bound vertical stress and a lower-bound horizontal stress. According to p.108 of the CIRIA Guide, the upper-bound vertical stress may be taken at one quarter of the panel height above the support level. From Fig.51 of the Guide,

$$N_v = \frac{3.49\ P}{1.4} = 2.49\ P \quad kN/m$$

Following the reasoning in Comment (b) of Example A.2, the lower-bound horizontal stress is taken at mid-height. Page 109 of the Guide states that this stress may be taken as two-third of the maximum value. From Fig.51 of the CIRIA Guide the stress coefficient at midpoint is 0.36.

$$N_h = \frac{2/3 \times 0.36\ P}{1.4} = 0.17\ P$$

Step 3 : The critical stresses

As in Step 3 of Example A.2 : $N'_{vcr} = 9.86\ EI'$;

$N'_{hcr} = 9.47\ EI'$

Step 4 : the stress ratios R'_v, R'_h, R'_s

PANEL No.1

$$R'_v = \frac{N_v \text{ (see Step 1)}}{N'_{vcr} \text{ (see Step 3)}} = \frac{0.26\ P}{9.86\ EI'} = 0.026\ \frac{P}{EI'}$$

$$R'_h = \frac{N_h \text{ (see Step 1)}}{N'_{hcr} \text{ (see Step 3)}} = \frac{0.26\ P}{9.47\ EI'} = 0.027\ \frac{P}{EI'}$$

$R'_s = 0$ (As in Step 4 of Example A.2)

PANEL No.2

$$R'_v = \frac{N_v \text{ (see Step 1)}}{N'_{vcr} \text{ (see Step 3)}} = \frac{2.49\ P}{9.86\ EI'} = 0.25\ \frac{P}{EI'}$$

$$R'_h = \frac{N_h \text{ (see Step 1)}}{N'_{hcr} \text{ (see Step 3)}} = \frac{0.17\ P}{9.47\ EI'} = 0.018\ \frac{P}{EI'}$$

$R'_s = 0$ (As in Step 4 of Example A.2)

Step 5 : The stress ratios R'_1, R'_2, R''_2

As in Step 5 of Example A.2, for both Panel No.1 and Panel No.2 :

R'_1 = corresponding R'_h of Step 4

$R''_2 = R'_2$ = corresponding R'_v of Step 4

PANEL No.1

$$\frac{R''_2}{R'_1} = \frac{R'_v}{R'_h} = \frac{0.026\ P/EI'}{0.027\ P/EI'} = 0.96$$

PANEL No.2

$$\frac{R''_2}{R'_1} = \frac{R'_v}{R'_h} = \frac{0.25\ \ P/EI'}{0.018\ P/EI'} = 13.9$$

Step 6 : The modification factors M_1 and M_2

PANEL No.1

$R''_2/R'_1 = 0.96$ (see Step 5)

With reference to Fig.130 of the CIRIA Guide, the ratio $\emptyset = 1.7$, so that the modification factors are :

$M_1 = 0.59$; $M_2 = 0.57$

Check : $\frac{M_2}{M_1} = \frac{R''_2}{R'_1} = 0.96$

Therefore, the modified critical stresses are then :

$N_{vcr} = M_2 \times N'_{vcr}$ of Step 3

$= 0.57 \times 9.86\ EI' = 5.62\ EI'$

$N_{hcr} = M_1 \times N'_{hcr}$ of Step 3

$= 0.59 \times 9.47\ EI' = 5.58\ EI'$

PANEL No.2

$R''_2/R'_1 = 13.9$ (see Step 5)

Hence from Fig.130 of the CIRIA Guide, modification factors are :

$M_1 = 0.067$ and $M_2 = 0.94$

Check : $\dfrac{M_2}{M_1} \cdot \dfrac{R''_2}{R'_1} = 14$

Then, the modified critical stresses are :

$N_{vcr} = M_2 \times N'_{vcr} = 9.27\ EI'$

$N_{hcr} = M_1 \times N'_{hcr} = 0.63\ EI'$

Step 7 : The effective height h_e

PANEL No.1

$$h_e = \sqrt{\pi^2 EI'/N_{vcr}}$$

$= 1.33$ m (where $N_{vcr} = 5.62\ EI'$ from Step 6)

PANEL No.2

$$h_e = \sqrt{\pi^2 EI'/N_{vcr}}$$

$= 1.03$ m (where $N_{vcr} = 9.27\ EI'$ from Step 6)

The effective height to be used is the larger of the above two h_e values. That is, $h_e = 1.33$ m.

Step 8 : The additional and total moments :

From CP 110, Cl.3:5.7.1 :

$$M_t = M_i + \frac{N_v\, b}{1750} \left[\frac{h_e}{b}\right]^2 \left[1 - 0.0035\, \frac{h_e}{b}\right]$$

(BS 8110, Cl.3.8.3.1, $M_t = M_i + \frac{N_v\, b}{2000} \left[\frac{h_e}{b} \right]^2$)

where M_t, M_i and N_v are defined for unit widths, as in Step 8 of Example A.2.

Substituting

$e_1 = 0$ (Table 4.1); $e_2 = 0.2 \times 40 = 8$ mm (Table 4.1)

$h_e = 1330$ mm (Step 7); $b = 40$ mm (Table 4.1)

$$M_t = [\, 0 + 0.6 \times 8\, N_v \,] + \frac{40\, N_v}{1750} \left[\frac{1330}{40} \right]^2 \left[1 - 0.0035 \frac{1330}{40} \right]$$

$$= 27.13\, N_v \quad (\text{BS 8110 } M_t = 26.91\, N_v)$$

Step 9 : The failure load

The equation $M_t = 27.13\, N_v$ can be expressed in the equivalent form :

$$\frac{N_v}{b} = 1.47 \frac{M_t}{b^2} \qquad \text{(where } b = 40 \text{ mm)}$$

$$\left(\text{BS 8110, } \frac{N_v}{b} = 1.49 \frac{M_t}{b^2}\right)$$

This equation is now drawn as the straight line OC in Fig.A.1, to intersect the interaction diagram at point C' (see Comment (c) below). From Fig.A.1 :

$\left[\frac{N_v}{b} \right]$ of point C' = 2.60 (BS 8110, 2.63, Fig.A.2);

$N_v = 2.60\, b$ (where thickness $b = 40$ mm)

$= 2.60 \times 40 \times 10^{-3}$ kN/mm = 103.9 kN/m

(BS 8110, $N_v = 105.2$ kN/m)

N_v is the vertical load per unit length of the beam at which buckling failure is considered to occur. Hence, for an overall

span length L of 1.7 m, the CIRIA buckling load is

$$P = N_v \times 1.7 = 103.9 \times 1.7 = 176.6 \text{ kN} \quad (\text{BS } 8110,\ 179 \text{ kN})$$

From Table 2, the experimental buckling load is 620 kN

$$\text{Factor of Safety, } R_{TP} = \frac{620}{176.6} = 3.51 \quad (\text{BS } 8110,\ 3.46)$$

as in Table 6.1

Comments on Example A.3

(a) Fig.51 of the CIRIA Guide gives the principal stress coefficients at the following positions : edge; 1/6th span; 1/3rd span; midspan.

Using Mohr-circle analyses, the vertical stress coefficients are : 1.95 (edge); 1.14 (1/6th span); 0.66 (1/3rd span); 0.36 (midspan). Hence, in Step 2 of this Example, the lower-bound vertical stress coefficient has been taken as 0.36.

(b) See Comment (b) at the end of Example A.2.

(c) For construction of the interaction diagram, see Comments at the end of Example A.1.

Appendix B

WORKED EXAMPLES FOR DEEP BEAMS WITH WEB-OPENINGS

WORKED EXAMPLES on the use of CIRIA GUIDE No.2

to calculate the Buckling Strengths of Slender

Concrete Deep Beams with Web-Openings

WORKED EXAMPLES on the use of CIRIA GUIDE No.2 to calculate the Buckling Strengths of Slender Concrete Deep Beams with Web-Openings

SUMMARY

Reinforced Concrete deep beams are not yet covered by CP 110 : 1972, nor the BS 8110. Currently the main documents for deep-beam designers are the American Code ACI 318-83 [1983], the CEB-FIP Model Code [1978] and the CIRIA Guide No.2 [1977]. Of these, the buckling strength of deep beams without web-openings can only be obtained using the CIRIA Guide. However, there are no such rules for deep beams with web-openings. In the absence of any analytical methods, a tentative approach is introduced to analyse the buckling strength of deep beams with web-openings provisionally using the CIRIA buckling strength guidelines for deep beams without web-openings.

This Appendix gives three worked examples to illustrate the calculation of buckling loads using the three methods* of the Guide :

(a) The Supplementary Rules

(b) The Single Panel method

(c) The Two Panel method

Comments are given at the end of each Example.

---

* The CIRIA Guide specifies that all the three methods are to be used in conjunction with CP 110:1972. In addition, the use of the CIRIA Guide in conjunction with BS 8110:1985 is also illustrated.

EXAMPLE B.1 Using the Supplementary Rules in Cl.3.2.2 of the CIRIA Guide [1977], calculate the buckling load of *Beam W-AC of Table 6.2

+ SOLUTION

Step 1 : Calculate effective height h_e

From CIRIA Guide, Cl.3.2.2,

$h_e = 1.5\ h = 1.5 \times 1000 = 1500$ mm (Fig.4.1)

Step 2 : Calculate modified effective length L_m

From Section 7.2.2, Fig.7.1,

$$L_m = L_e - L_s$$
$$= 1700 - 2 \times 203 \text{ mm}$$
$$= 1294 \text{ mm}$$

Step 3 : The equivalent applied stresses

From p.106 of the CIRIA Guide, the equivalent applied vertical stress (see Comment (a) below) is :

$$N_v = \frac{\text{Support Reaction } (= P/2)}{\text{Length of Support Bearing } (=0.23 \text{ m})}$$

$$= 2.17\ P \quad (\text{kN/m})$$

where P is the buckling load (kN).

---

* The Beam Notation in this Worked Example is given as in Section 5.3.2, and is explained in the footnote to Table 4.2.
+ Notation as in CIRIA Guide, unless otherwise defined.

Step 4 : Calculate additional and total moments

From CP 110, Cl.3.5.7.1,

$$M_t = M_i + \frac{N_v\, b}{1750}\left[\frac{h_e}{b}\right]^2\left[1 - 0.0035\,\frac{h_e}{b}\right]$$

(BS 8110, Cl.3.8.3.2, $M_t = M_i + \frac{N_v\, b}{2000}\left[\frac{h_e}{b}\right]^2$)

where

M_t (M_i) is the total (initial) moment per unit width

N_v is the load per unit width

From Eqn.(34) of CP 110 : Cl.3.5.7.1 (BS 8110, Cl.3.8.3.2),

$M_i = 0.4\, N_v\, e_1 + 0.6\, N_v\, e_2$

Substituting

$e_1 = e_2 = 0.1 \times 35 = 3.5$ mm (Section 5.2.2)

$h_e = 1500$ mm (Step 1); $b = 35$ mm (Section 4.1.2), we obtain

$M_t = 34.72\, N_v$

(BS 8110, $M_t = 35.64\, N_v$)

Step 5 : Determination of failure load

The equation $M_t = 34.72\, N_v$ can be expressed in the equivalent form

$$\frac{N_v}{b} = 1.01\,\frac{M_t}{b^2}$$ (where thickness $b = 35$ mm)

(BS 8110, $\frac{N_v}{b} = 0.98\,\frac{M_t}{b^2}$)

This equation is now drawn as the straight line OA in Fig.B.1, to intersect the interaction diagram at point A' (see Comments below for the construction of the interaction diagram).

From Fig.B.1,

$$\left[\frac{N_v}{b} \right] \text{ of point A' } = 1.63 \text{ (BS 8110, 1.56, Fig.B.2);}$$

$N_v = 1.63 \times 35 \times 10^{-3} = 0.0571$ kN/mm = 57.1 kN/m

(BS 8110, N_v = 54.6 kN/m)

Therefore the CIRIA buckling load is :

$P = N_v / 2.17 = 57.1 / 2.17$

= 26.3 kN (BS 8110, 25.16 kN)

From Table 6.2, experimental buckling load = 540 kN

Factor of Safety,

$$R_{SR} = \frac{540}{26.3} = 20.53 \quad \text{(BS 8110, 21.47)}$$

as in Table 6.2

Comments on Example B.1

The interaction diagrams in Fig.B.1 (Fig.B.2) has been specially constructed in accordance with the "Notes on the derivation of design charts" given in Appendix A of CP 110 : Part 2 (BS 8110 : Part 3 : Appendix A), using the actual properties of Beam W-AC (see Table 4.2) and the GHOST80 graphical package at the Computing Laboratory of the University of Newcastle upon Tyne. In practical design, it is usually possible to use the standard column charts in CP 110 : Part 2 (BS 8110 : Part 3).

EXAMPLE B.2 Using the Single Panel method in Appendix C of the CIRIA Guide [1977], calculate the buckling load of *Beam W-AC.

+ SOLUTION

Step 1 : The equivalent panel

The notional safe equivalent panel (see Fig.123 of the CIRIA Guide) is in this case simply a rectangle of length and height equal to the actual values (Fig.4.1(a): length = 1700 mm, height = 1000 mm).

Step 2 : Calculate modified effective length L_m

For the analysis of the section, the modified effective length L_m is used (Section 7.2.2, Fig.7.1) :

$$L_m = L_e - L_s$$
$$= 1700 - 2 \times 203 \text{ mm}$$
$$= 1294 \text{ mm}$$

Step 3 : The equivalent applied stresses

From p.106 of the CIRIA Guide, the equivalent applied vertical stress (see Comment (a) below) is :

$$N_v = \frac{\text{Support Reaction (= P/2)}}{\text{Length of Support Bearing (= 0.23 m)}}$$
$$= 2.17 \text{ P (kN/m)}$$

where P is the buckling load (kN).

---

* The Beam Notation as in Example B.1 (see footnote on p.183)
+ Notation as in CIRIA Guide, unless otherwise defined.

The equivalent applied horizontal stress is taken from Fig.51 of the CIRIA Guide (see Comment (b) below) :

$$N_h = \frac{0.36\ P}{1.4\ (\text{Fig.4.1(a): } L_o = 1.4)} = 0.26\ P \quad (kN/m)$$

The shear stress applied at the ends of the equivalent panel may be taken as zero (see Comment (c) below). That is $\tau = 0$

Step 4 : The critical stresses

From Fig.127 of the CIRIA Guide,

vertical critical stress $N'_{vcr} = \frac{1.0\ \pi^2\ EI'}{(1.0)^2} = 9.86\ EI'$

From Fig.126 of the CIRIA Guide, $\emptyset = 0.588$,

horizontal critical stress $N'_{hcr} = \frac{0.96\ \pi^2\ EI'}{(1.0)^2} = 9.47\ EI'$

Step 5 : The stress ratios R'_v, R'_h, R'_s

$$R'_v = \frac{N_v \text{ (see Step 2)}}{N'_{vcr} \text{ (see Step 3)}} = \frac{2.17\ P}{9.86\ EI'} = 0.22\ \frac{P}{EI'}$$

$$R'_h = \frac{N_h \text{ (see Step 2)}}{N'_{hcr} \text{ (see Step 3)}} = \frac{0.26\ P}{9.47\ EI'} = 0.027\ \frac{P}{EI'}$$

$R'_s = 0$ since $\tau = 0$ (see Step 3)

Step 6 : The stress ratios R'_1, R'_2, R''_2

In this example, the shorter edges of the equivalent panel are the vertical edges; the CIRIA Guide introduces new stress ratios as follows :

R'_1 = R'_h of Step 5 (= 0.027 P/EI')

R'_2 = R'_v of Step 5 (= 0.22 P/EI')

R''_2 = R'_2/M'_2 (see Comment (d) below)

From Fig.129 of the CIRIA Guide, for $R'_s = 0$ (see Step 3),

$M'_2 = 1.0$

Therefore

$$R''_2 = R'_2/1.0 = R'_2 \ (= R'_v \text{ of Step 5}) = 0.22\ P/EI'$$

$$\frac{R''_2}{R'_1} = \frac{0.22\ P/EI'}{0.027\ P/EI'} = 8.11$$

Step 7 : The modification factors M_1 and M_2

$R''_2/R'_1 = 8.46$ from Step 6

Referring to Fig.130 of the CIRIA Guide, the ratio $\emptyset = 1.7$,

so that the modification factors are :

$M_1 = 0.11$ and $M_2 = 0.92$

Check : $\frac{M_2}{M_1} = \frac{R''_2}{R'_1} = 8$

The modified critical stresses are then :

$N_{vcr} = M_2 \times N'_{vcr}$ of Step 4

$= 0.92 \times 9.86\ EI' = 9.08\ EI'$

$N_{hcr} = M_1 \times N'_{hcr}$ of Step 4

$= 0.11 \times 9.47\ EI' = 1.04\ EI'$

Step 8 : The effective height h_e

$$h_e = \sqrt{\pi^2 EI'/N_{vcr}}$$

$= 1.04$ m (where $N_{vcr} = 9.08\ EI'$ from Step 7)

Step 9 : The additional and total moments

From CP 110, Cl.3.5.7.1 :

$$M_t = M_i + \frac{N_v\, b}{1750}\left[\frac{h_e}{b}\right]^2\left[1 - 0.0035\,\frac{h_e}{b}\right]$$

where

M_t (M_i) is the total (initial) moment per unit width

N_v is the load per unit width

From Eqn.(34) of CP 110 : Cl.3.5.7.1 (BS 8110, Cl.3.8.3.2),

$$M_i = 0.4\ N_v\ e_1 + 0.6\ N_v\ e_2$$

Substituting

$e_1 = e_2 = 0.1 \times 35 = 3.5$ mm (Section 5.2.2)

$h_e = 1040$ mm (Step 7); $b = 35$ mm (Section 4.1.2)

$$M_t = 3.5\ N_v + \frac{35\ N_v}{1750}\left[\frac{1040}{35}\right]^2\left[1 - 0.0035\ \frac{1040}{35}\right]$$

$$= 19.32\ N_v$$

(BS 8110, $M_t = 18.95\ N_v$)

Step 10 : The failure load

The relation $M_t = 19.32\ N_v$ can be expressed in the equivalent form :

$$\frac{N_v}{b} = 1.81\ \frac{M_t}{b^2} \quad \text{(where b = 35 mm)}$$

(BS 8110, $\frac{N_v}{b} = 1.85\ \frac{M_t}{b^2}$)

This equation is now drawn as the straight line OB in Fig.B.1, to intersect the interaction diagram at point B' (see Comment (e) below). From Fig.B.1 :

$\left[\frac{N_v}{b}\right]$ of point B' = 5.50 (BS 8110, 5.75, Fig.B.2)

$N_v = 5.50\ b$ (where thickness b = 35 mm)

$= 5.50 \times 35 \times 10^{-3} = 0.1923$ kN/mm

$= 192.3$ kN/m (BS 8110, 201.3 kN/m)

N_v is the load per metre width at which the notional column strip of the equivalent panel will collapse; N_v is therefore the 'equivalent applied compressive stress' as defined on p.106 of the CIRIA Guide.

Referring to Step 3,

N_v = 2.17 P, where P is the CIRIA buckling load (kN), i.e.

P = N_v / 2.17 = 192.3 / 2.17

= 88.6 kN (BS 8110, 92.8 kN)

Experimental buckling load (Table 6.2) = 540 kN

$$\text{Factor of Safety, } R_{SP} = \frac{540}{88.6} = 6.09 \quad \text{(BS 8110, 5.82)}$$

as in Table 6.2

Comments on Example B.2

(a) Note that Appendix C of the CIRIA Guide defines stresses as force per unit width (kN/m).

(b) The use of an upper-bound horizontal stress is to ensure a suitably low restraint of the conceptual "vertical strip" by the conceptual "horizontal strip". In the three worked examples here, which is concerned with Beam W-AC (Table 6.2), the stiffness of the "horizontal strip" at mid-height is the most relevant. Hence in Step 2 of Example B.2, the upper-bound horizontal stress at mid-height has been taken. In practical design, the engineer could either use his judgement in choosing where to take the upper-bound stress or he could take the absolute maximum value from Fig.51 of the CIRIA Guide, which is 1.15 in this example. If he chooses 1.15, he will err on the safe side and the resulting factor of safety will increase to 8.50 (BS 8110, 8.30).

(c) According to p.89 of the CIRIA Guide, the boundary shear stress may be taken as :

$$= \frac{\text{Support reaction } (= P/2)}{\text{Panel height } (= 1.0 \text{ m})} = 0.5\ P \quad \text{kN/m}$$

From Fig.125 of the Guide,

$$\text{Critical shear stress } \tau'_{cr} = \frac{4.7\,\pi^2 EI'}{1.0^2} = 46.39\ EI'$$

Therefore, applied shear stress ratio

$$R'_s = \frac{\tau}{\tau'_{cr}} = \frac{0.01\ P}{EI'}$$

To eliminate the effect of shear stress, the modification factor M'_2 and the modified stress ratio R''_2 are determined as follows :

$$\frac{R'_2 \text{ (see Step 6)}}{R'_s \text{ (see above)}} = 22.0$$

From Fig.129 of the CIRIA Guide, $\emptyset = 1.7$

and hence $M'_2 = 0.99$.

Therefore, $N''_{vcr} = M'_2 \times N'_{vcr}$ of Step 4

$$= 0.99 \times 9.86\ EI' = 9.76\ EI'$$

Hence

$$R''_2 = \frac{N_v \text{ (see Step 1)}}{N''_{vcr} \text{ (see above)}} = \frac{2.17\ P}{9.76\ EI'}$$

$$= 0.22\ \frac{P}{EI'} = R''_2 \text{ of Step 6}$$

Therefore the modification due to shear is negligible.

(The shear modification was also shown to be negligible in the design example on p.89 of the CIRIA Guide).

(d) The relation in Step 6, namely,

$$R''_2 = R'_2/M'_2$$

is misprinted in the CIRIA Guide as

$$R'_2 = R'_2 = R'_2/M'_2 \quad \text{[Kong, 1985]}$$

(e) See Comments at the end of Example B.1.

EXAMPLE B.3 Using the Two Panel method in Appendix C of the CIRIA Guide [1977], calculate the buckling load of *Beam W-AC.

+ SOLUTION

Step 1 : The equivalent panel

As in Step 1 and 2 of Example B.2;

length = 1700 mm, height = 1000 mm;

modified effective length = 1294 mm.

Step 2 : The equivalent applied stresses

PANEL No.1

For Panel No.1, the effective height is calculated using an upper-bound horizontal stress and a lower-bound vertical stress. According to p.109 of the CIRIA Guide, the lower-bound vertical stress is taken at mid-height of the panel. From Fig.51 of the Guide (see Comment (a) below),

$$N_v = \frac{0.36\ P}{1.4} = 0.26\ P \quad kN/m$$

where 1.4 is the simple span (Fig.4.1(a): L_o = 1400 mm) and

P (kN) is the buckling load.

The upper-bound horizontal stress is also taken at mid-height of the panel (see Comment (b) below). From Fig.51 of the CIRIA Guide,

$$N_h = \frac{0.36\ P}{1.4} = 0.26\ P \quad kN/m$$

---

* The Beam Notation as in Example B.1 (see footnote on p.183)
+ Notation as in CIRIA Guide, unless otherwise defined.

PANEL No.2

For Panel No.2, the effective height is calculated using an upper-bound vertical stress and a lower-bound horizontal stress. According to p.108 of the CIRIA Guide, the upper-bound vertical stress may be taken at one quarter of the panel height above the support level. From Fig.51 of the Guide,

$$N_v = \frac{3.49\ P}{1.4} = 2.49\ P \text{ kN/m}$$

Following the reasoning in Comment (b) of Example B.2, the lower-bound horizontal stress is taken at mid-height. Page 109 of the Guide states that this stress may be taken as two-third of the maximum value. From Fig.51 of the CIRIA Guide the stress coefficient at midpoint is 0.36.

$$N_h = \frac{2/3 \times 0.36\ P}{1.4} = 0.17\ P$$

Step 3 : The critical stresses

As in Step 4 of Example B.2 : $N'_{vcr} = 9.86\ EI'$;

$N'_{hcr} = 9.47\ EI'$

Step 4 : the stress ratios R'_v, R'_h, R'_s

PANEL No.1

$$R'_v = \frac{N_v \text{ (see Step 1)}}{N'_{vcr} \text{ (see Step 3)}} = \frac{0.26\ P}{9.86\ EI'} = 0.026\ \frac{P}{EI'}$$

$$R'_h = \frac{N_h \text{ (see Step 1)}}{N'_{hcr} \text{ (see Step 3)}} = \frac{0.26\ P}{9.47\ EI'} = 0.027\ \frac{P}{EI'}$$

$R'_s = 0$ (As in Step 5 of Example B.2)

PANEL No.2

$$R'_v = \frac{N_v \text{ (see Step 1)}}{N'_{vcr} \text{ (see Step 3)}} = \frac{2.49\ P}{9.86\ EI'} = 0.25\ \frac{P}{EI'}$$

$$R'_h = \frac{N_h \text{ (see Step 1)}}{N'_{hcr} \text{ (see Step 3)}} = \frac{0.17\ P}{9.47\ EI'} = 0.018\ \frac{P}{EI'}$$

$R'_s = 0$ (As in Step 5 of Example B.2)

Step 5 : The stress ratios R'_1, R'_2, R''_2

As in Step 6 of Example B.2, for both Panel No.1 and Panel No.2 :

R'_1 = corresponding R'_h of Step 4

$R''_2 = R'_2$ = corresponding R'_v of Step 4

PANEL No.1

$$\frac{R''_2}{R'_1} = \frac{R'_v}{R'_h} = \frac{0.026\ P/EI'}{0.027\ P/EI'} = 0.96$$

PANEL No.2

$$\frac{R''_2}{R'_1} = \frac{R'_v}{R'_h} = \frac{0.25\ P/EI'}{0.018\ P/EI'} = 13.9$$

Step 6 : The modification factors M_1 and M_2

PANEL No.1

$R''_2/R'_1 = 0.96$ (see Step 5)

With reference to Fig.130 of the CIRIA Guide, the ratio $\emptyset = 1.7$, so that the modification factors are :

$M_1 = 0.59$; $M_2 = 0.57$

Check : $\frac{M_2}{M_1} = \frac{R''_2}{R'_1} = 0.96$

Therefore, the modified critical stresses are then :

$N_{vcr} = N_{hcr} = M_2 \times N'_{vcr}$ of Step 3

$= 0.57 \times 9.86\ EI' = 5.62\ EI'$

PANEL No.2

$R''_2/R'_1 = 13.9$ (see Step 5)

Hence from Fig.130 of the CIRIA Guide, modification factors are :

$M_1 = 0.067$ and $M_2 = 0.94$

Check : $\dfrac{M_2}{M_1} = \dfrac{R''_2}{R'_1} = 14$

Then, the modified critical stresses are :

$N_{vcr} = M_2 \times N'_{vcr} = 9.27\ EI'$

$N_{hcr} = M_1 \times N'_{hcr} = 0.63\ EI'$

Step 7 : The effective height h_e

PANEL No.1

$$h_e = \sqrt{\pi^2 EI'/N_{vcr}}$$

$= 1.33$ m (where $N_{vcr} = 5.62\ EI'$ from Step 6)

PANEL No.2

$$h_e = \sqrt{\pi^2 EI'/N_{vcr}}$$

$= 1.03$ m (where $N_{vcr} = 9.27\ EI'$ from Step 6)

The effective height to be used is the larger of the above two h_e values. That is, $h_e = 1.33$ m.

Step 8 : The additional and total moments :

From CP 110, Cl.3.5.7.1 :

$$M_t = M_i + \frac{N_v\, b}{1750} \left[\frac{h_e}{b}\right]^2 \left[1 - 0.0035\, \frac{h_e}{b}\right]$$

where M_t, M_i and N_v are defined for unit widths, as in Step 9 of Example B.2.

Substituting

$$e_1 = e_2 = 0.1 \times 35 = 3.5 \text{ mm (Section 5.2.2)}$$

h_e = 1330 mm (Step 7); b = 35 mm (Section 4.1.2)

$$M_t = 3.5\,N_v + \frac{35\,N_v}{1750}\left[\frac{1330}{35}\right]^2\left[1 - 0.0035\,\frac{1330}{35}\right]$$

$$= 28.54\,N_v \quad \text{(BS 8110, } M_t = 28.77\,N_v\text{)}$$

Step 9 : The failure load

The equation $M_t = 28.54\,N_v$ can be expressed in the equivalent form :

$$\frac{N_v}{b} = 1.23\,\frac{M_t}{b^2} \quad \text{(where b = 35 mm)}$$

$$\text{(BS 8110, } \frac{N_v}{b} = 1.22\,\frac{M_t}{b^2}\text{)}$$

This equation is now drawn as the straight line OC in Fig.B.1, to intersect the interaction diagram at point C' (see Comment (c) below). From Fig.B.1 :

$\left[\frac{N_v}{b}\right]$ of point C' = 2.34 (BS 8110, 2.30, Fig.B.2)

$N_v = 2.34\,b$ (where thickness b = 35 mm)

$= 2.34 \times 35 \times 10^{-3}$ kN/mm = 81.9 kN/m

N_v is the vertical load per unit length of the beam at which buckling failure is considered to occur. Hence, for a modified effective length L_m of 1.294 m, the CIRIA buckling load is

$P = N_v \times 1.294 = 81.9 \times 1.294 = 106$ kN

From Table 6.2, the experimental buckling load is 540 kN

$$\text{Factor of Safety, } R_{TP} = \frac{540}{106} = 5.10 \quad \text{(BS 8110, 5.18)}$$

as in Table 6.2

Comments on Example B.3

(a) Fig.51 of the CIRIA Guide gives the principal stress coefficients at the following positions : edge; 1/6th span; 1/3rd span; midspan.

Using Mohr-circle analyses, the vertical stress coefficients are : 1.95 (edge); 1.14 (1/6th span); 0.66 (1/3rd span); 0.36 (midspan). Hence, in Step 2 of this Example, the lower-bound vertical stress coefficient has been taken as 0.36.

(b) See Comment (b) at the end of Example B.2.

(c) For construction of the interaction diagram, see Comments at the end of Example B.1.

*Beam	Thickness	Eccentricity/Thickness		Total Shear-Span/Height	Clear-Shear-Span/Ht.	Cube Strength	Splitting Strength	Web Steel				Main Steel	
		Bottom	Top					Vertical		Horizontal			
	b	e_1/b	e_2/b	x_t/h	x/h	f_{cu}	f_t	Dia.	A_v/bs_v	Dia.	A_h/bs_h	Dia.	A_s/bh
	(mm)					(N/mm^2)	(N/mm^2)	(mm)	(%)	(mm)	(%)	(mm)	(%)
A-67-0.2	15	0	0.2	0.40	0.14	73	3.3	2	0.84	2	0.75	6	0.57
A-50-0.2	20	0	0.2	0.40	0.14	72	3.3	6	0.66	6	1.27	12	1.70
A-40-0.2	25	0	0.2	0.40	0.14	74	3.0	6	0.53	6	1.02	12	1.36
A-33-0.2	30	0	0.2	0.40	0.14	89	3.5	6	0.44	6	0.85	12	1.13
A-29-0.2	35	0	0.2	0.40	0.14	88	4.1	6	0.38	6	0.73	16	1.72
A-25-0.2	40	0	0.2	0.40	0.14	73	3.2	6	0.33	6	0.64	16	1.51
A-50-0.05	20	0	0.05	0.40	0.14	72	3.1	6	0.66	6	1.27	12	1.70
A-40-0.05#	25	0	0.06	0.40	0.14	74	3.4	6	0.53	6	1.02	12	1.36
A-33-0.05	30	0	0.05	0.40	0.14	89	3.3	6	0.44	6	0.85	12	1.13
B-67-0.2	15	0	0.2	0.22	0	74	3.4	2	0.84	2	0.75	6	0.57
B-50-0.2#	20	0	0.5	0.22	0	77	3.8	6	0.66	6	1.27	12	1.70
B-40-0.2	25	0	0.2	0.22	0	76	3.9	6	0.53	6	1.02	12	1.36
B-33-0.2	30	0	0.2	0.22	0	84	3.2	6	0.44	6	0.85	12	1.13
B-29-0.2#	35	0	0.3	0.22	0	87	3.7	6	0.38	6	0.73	16	1.72
B-25-0.2	40	0	0.2	0.22	0	86	4.1	6	0.33	6	0.64	16	1.51
B-50-0.05	20	0	0.05	0.22	0	79	3.7	6	0.66	6	1.27	12	1.70
B-40-0.05#	25	0	0.06	0.22	0	76	3.6	6	0.53	6	1.02	12	1.36
B-33-0.05	30	0	0.05	0.22	0	83	3.4	6	0.44	6	0.85	12	1.13
C-67-0.1	15	0.1	0.1	0.40	0.17	80	4.2	6	0.89	2	0.19	8	1.01
C-50-0.1	20	0.1	0.1	0.40	0.17	92	4.8	6	0.66	6	1.27	12	1.70
C-40-0.1	25	0.1	0.1	0.40	0.17	95	4.4	6	0.53	6	1.02	12	1.36
C-33-0.1	30	0.1	0.1	0.40	0.17	84	4.5	6	0.44	6	0.85	12	1.13
C-29-0.1	35	0.1	0.1	0.40	0.17	85	3.1	6	0.38	6	0.73	16	1.72
D-40-0.1	25	0.1	0.1	0.40	0.17	80	4.6	2	1.01	2&6	1.47	12	1.36
D-33-0.1	30	0.1	0.1	0.40	0.17	71	4.3	2&6	1.11	2&6	1.32	12	1.13
D-29-0.1	35	0.1	0.1	0.40	0.17	69	4.1	2&6	0.96	2&6	1.13	16	1.72
E-67-0.1	15	0.1	0.1	0.40	0.17	94	4.4	6	0.89	2	0.19	8	1.01
E-50-0.1	20	0.1	0.1	0.40	0.17	81	4.1	6	0.66	6	1.27	12	1.70
E-40-0.1	25	0.1	0.1	0.40	0.17	84	3.6	6	0.53	6	1.02	12	1.36
E-33-0.1	30	0.1	0.1	0.40	0.17	69	3.2	6	0.44	6	0.85	12	1.13
E-29-0.1	35	0.1	0.1	0.40	0.17	88	3.4	6	0.38	6	0.73	16	1.72
E-25-0.1	40	0.1	0.1	0.40	0.17	84	4.0	6	0.33	6	0.64	16	1.51
E-67-0.2	15	0.2	0.2	0.40	0.17	87	5.4	2	0.84	2	0.75	8	1.01
E-50-0.2	20	0.2	0.2	0.40	0.17	93	4.9	2	0.63	2	0.57	12	1.70
E-40-0.2	25	0.2	0.2	0.40	0.17	89	4.2	6	0.53	6	1.02	12	1.36
E-33-0.2	30	0.2	0.2	0.40	0.17	91	5.0	6	0.44	6	0.85	12	1.13
E-29-0.2	35	0.2	0.2	0.40	0.17	88	5.2	6	0.38	6	0.73	16	1.72
E-25-0.2	40	0.2	0.2	0.40	0.17	89	4.8	6	0.33	6	0.64	16	1.51

* BEAM NOTATION : The Series letter is given before the hyphen; this is followed by the h/b ratio and then by the e_2/b ratio. For example, A-67-0.2 refers to a beam in Series A having a h/b ratio of 67 and a e_2/b ratio of 0.2.

On re-checking after commencement of testing, the actual e_2/b ratios of these four beams were found to be as recorded in Column 4 of this table.

Table 4.1 : Properties of test beams

*Beam	Web-opening Shape	Parameters as defined in Fig.7.5 k_1x (mm)	k_2h (mm)	Clear-shear-span x (mm)	Cube Strength f_{cu} (N/mm^2)	Splitting Strength f_t (N/mm^2)
W-AR	Rectangular	170.0	400.0	140.0	85.7	5.0
W-AC	Circular	179.6	463.3	140.0	88.7	5.7
W-AR-R	Rectangular	170.0	400.0	140.0	91.0	4.2
W-AC-R	Circular	179.6	463.3	140.0	83.3	5.9
W-BR	Rectangular	340.0	600.0	140.0	93.5	5.9
W-BC	Circular	344.7	652.6	140.0	89.0	3.9
W-CR	Rectangular	340.0	400.0	140.0	95.8	5.4
W-CC	Circular	335.6	438.3	140.0	92.0	5.3
W-DR	Rectangular	170.0	200.0	140.0	90.7	7.0
W-DC	Circular	168.3	242.0	140.0	83.0	5.3
W-ER	Rectangular	0.0	200.0	140.0	83.5	6.5
W-EC	Circular	16.3	294.3	140.0	86.7	6.2
W-AR-S	Rectangular	127.5	400.0	85.0	93.0	7.1
W-AC-S	Circular	139.8	471.1	85.0	88.4	6.6
W-29-0.1-R1	No Openings	-	-	140.0	97.2	6.4
W-29-0.1-R2	No Openings	-	-	140.0	94.0	6.4

*BEAM NOTATION :

The letter W indicates beam series with web opening; after the hyphen, the first letter (A to E) defines the position of the opening (see Fig.5.4), while the second letter (R or C) indicates the shape of the opening (R for rectangular and C for circular). A letter R following the hyphen, if any, indicates a repeated test; similarly, a letter S indicates a special test in which the clear-shear-span is 85 mm (and not 140 mm as in the other beams on this Table). Beam W-29-0.1-R1 and Beam W-29-0.1-R2 are two comparable beams without web-openings which are defined similarly as in Section 5.3.1 with extra R1 (or R2) in the end.

Table 4.2 : Properties of test beams with web-openings

*Beam	Cube Strength f_{cu} (N/mm^2)	Splitting Strength f_t (N/mm^2)	Web Steel				Flexural Steel		Hanger Steel				Orthogonal Shear Steel				Inclined Shear Steel	
			Vertical		Horizontal				Vertical		Inclined		Vertical		Horizontal			
			Dia. (mm)	#A_v/bs_v (%)	Dia. (mm)	#A_h/bs_h (%)	Dia. (mm)	#A_s/bs (%)	Dia. (mm)	#A_s/bs (%)	Dia. (mm)	#A_s/bs (%)	Dia. (mm)	#A_s/bs (%)	Dia. (mm)	#A_s/bs (%)	Dia. (mm)	#A_s/bs (%)
CB-H1	93.6	4.8	5	0.42	5	0.39	12	0.23	10	1.45	-	0.0	-	0.0	-	0.0	-	0.0
*CB-H1-R	93.0	5.7	5	0.42	5	0.39	12	0.23	10	1.45	-	0.0	-	0.0	-	0.0	-	0
CB-H2	96.8	4.3	5	0.42	5	0.39	12	0.23	10	1.45	-	0.0	5	0.18	5	0.11	-	0.0
CB-H3	93.0	4.5	5	0.42	5	0.39	12	0.23	10	1.45	-	0.0	-	0.0	-	0.0	5	0.21
CB-H4	97.5	4.9	5	0.42	5	0.39	12	0.23	10	0.89	10	1.13	-	0.0	-	0.0	-	0.0
CB-H5	98.0	6.2	5	0.42	5	0.39	12	0.23	10	0.89	10	1.13	5	0.18	5	0.11	-	0.0
CB-H6	98.1	5.6	5	0.42	5	0.39	12	0.23	10	0.89	10	1.13	-	0.0	-	0.0	5	0.21
CB-L1	51.9	3.8	5	0.42	5	0.39	12	0.23	10	1.45	-	0.0	-	0.0	-	0.0	-	0.0
CB-L2	47.2	3.8	5	0.42	5	0.39	12	0.23	10	1.45	-	0.0	5	0.18	5	0.11	-	0.0
CB-L3	49.7	4.2	5	0.42	5	0.39	12	0.23	10	1.45	-	0.0	-	0.0	-	0.0	5	0.21
CB-L4	44.4	3.3	5	0.42	5	0.39	12	0.23	10	0.89	10	1.13	-	0.0	-	0.0	-	0.0
CB-L5	45.2	3.9	5	0.42	5	0.39	12	0.23	10	0.89	10	1.13	5	0.18	5	0.11	-	0.0
CB-L6	42.1	3.5	5	0.42	5	0.39	12	0.23	10	0.89	10	1.13	-	0.0	-	0.0	5	0.21
CB-L7	50.3	3.7	-	0.0	-	0.0	12	0.23	10	1.45	-	0.0	-	0.0	-	0.0	-	0.0
CB-L8	42.5	3.6	-	0.0	-	0.0	12	0.23	10	0.89	10	1.13	-	0.0	-	0.0	-	0.0
CB-L9	43.9	3.6	5	0.42	5	0.39	12	0.23	10	0.89	10	0.57	5	0.18	5	0.11	-	0.0

*BEAM NOTATION : The Series letter CB indicates combined-loading tests; the second letter H (or L) stands for high strength concrete (or low strength concrete); then follows a number which represents the steel arrangement (see Fig.5.5). Thus CB-H1 denotes a beam under combined loadings with high strength concrete and a Type 1 reinforcement arrangement.

* repeated test for CB-H1

percentage of (Total volume of steel) per (Total volume of concrete)

Table 4.3 : Properties of test beams under combined loadings

Bar Size (mm)	Details	Yield Stress (N/mm^2)	Ultimate Stress (N/mm^2)	Description
Series E : Slender Deep Beams without Web-Openings				
2	Plain round wire	-	412	Web reinforcement for Beam E-67-0.1
2	Plain round wire-mesh	-	366	Additional top and bottom steel meshes; web reinforcement for Beams E-67-0.2 and E-50-0.2.
6	Plain round bar	389	442	Vertical and horizontal web reinforcement
8	High yield deformed bar	497	677	Main flexural steel
12	High yield deformed bar	495	575	Main flexural steel
16	High yield deformed bar	572	612	Main flexural steel
Series W : Slender Deep Beams with Web-Openings				
2	Plain round wire-mesh	-	366	Additional top and bottom steel meshes
5	Plain round wire-mesh	485	670	Vertical and horizontal web reinforcement
16	High yield deformed bar	572	612	Main flexural steel
Series CB : Deep Beams under Combined Loading				
5	Plain round wire-mesh	485	670	Additional top and bottom steel meshes
10	Plain round wire-mesh	485	670	Vertical and horizontal web reinforcement
12	High yield deformed bar	485	670	Main flexural steel

Table 4.4 : Properties of Reinforcement

*Beam	Failure Load	CIRIA Guide used with CP 110			CIRIA Guide used with BS 8110		
	kN	$^{+}R_{SR}$	$^{+}R_{SP}$	$^{+}R_{TP}$	$^{+}R_{SR}$	$^{+}R_{SP}$	$^{+}R_{TP}$
A-67-0.2	148	46.69	24.57	10.39	64.14	28.94	13.45
A-50-0.2	360	55.56	26.28	11.95	67.33	28.58	13.91
A-40-0.2	420	42.61	17.94	8.87	48.21	18.57	9.73
A-33-0.2	560	37.51	13.32	7.49	40.61	13.22	7.88
A-29-0.2	682	30.88	9.13	5.86	32.27	8.71	5.96
A-25-0.2	620	19.37	5.35	3.51	19.61	5.02	3.45
A-50-0.05	440						
A-40-0.05	534		Specimens failed in shear				
A-33-0.05	640						
B-67-0.2	120	38.21	20.09	8.50	52.50	23.67	11.01
B-50-0.2	146	24.32	12.46	5.34	29.08	13.40	6.13
B-40-0.2	340	34.40	14.45	7.16	38.94	14.95	7.85
B-33-0.2	560	37.72	13.52	7.54	40.82	13.43	7.94
B-29-0.2	420	21.01	7.23	4.14	21.87	6.94	4.19
B-25-0.2	700	21.27	5.42	3.79	21.53	5.06	3.72
B-50-0.05	460						
B-40-0.05	550		Specimens failed in shear				
B-33-0.05	692						
C-67-0.1	60	19.53	10.22	4.34	26.87	12.06	5.63
C-50-0.1	120	22.51	10.39	4.82	27.38	11.35	5.63
C-40-0.1	270	31.37	12.61	6.47	35.63	13.09	7.12
C-33-0.1	450	34.02	11.65	6.74	36.88	11.56	7.11
C-29-0.1	550	27.00	7.47	5.06	28.26	7.11	5.14
D-40-0.1	300	22.02	9.32	4.60	24.88	9.64	5.04
D-33-0.1	340	13.18	5.18	2.69	14.19	5.15	2.82
D-29-0.1	538	14.37	5.41	2.88	14.93	5.15	2.92
E-67-0.1			Specimen failed by vertical splitting				
E-50-0.1	200	41.91	19.36	8.97	50.96	21.14	10.48
E-40-0.1	502	65.13	26.20	13.44	73.95	27.20	14.79
E-33-0.1	440	37.47	13.03	7.45	40.60	12.93	7.84
E-29-0.1	700	37.63	9.90	6.99	39.42	9.38	7.11
E-25-0.1	560	19.43	4.33	3.34	19.69	3.98	3.27
E-67-0.2			Specimen damaged (accident)				
E-50-0.2	170	37.05	17.93	8.02	44.71	19.44	9.30
E-40-0.2	210	29.21	12.90	6.16	32.89	13.32	6.72
E-33-0.2	300	27.76	10.97	5.69	29.88	10.90	5.96
E-29-0.2	400	25.39	8.82	5.03	26.42	8.46	5.10
E-25-0.2	540	23.68	7.10	4.49	23.94	6.61	4.42
Mean		31.27	12.42	6.39	35.61	12.97	7.05
Standard Deviation		11.82	6.16	2.60	15.05	7.13	3.20

*Beam notation as in Table 4.1

^{+}R = Ratio of the Measured Buckling Load to the Computed Buckling Load
Subscripts : SR - CIRIA's Supplementary Rules
SP - CIRIA's Single Panel method
TP - CIRIA's Two Panel method

Table 6.1 : CIRIA Buckling Loads for beams without web-openings

*Beam	Failure Load	CIRIA Guide used with CP 110			CIRIA Guide used with BS 8110		
	kN	$^{+}R_{SR}$	$^{+}R_{SP}$	$^{+}R_{TP}$	$^{+}R_{SR}$	$^{+}R_{SP}$	$^{+}R_{TP}$
W-AR	600	23.92	7.06	5.65	25.01	6.74	5.74
W-AC	540	20.53	6.09	5.10	21.47	5.82	5.18
W-AR-R	480	18.98	5.48	4.47	19.85	5.23	4.54
W-AC-R	560	21.49	6.52	5.36	22.46	6.24	5.46
W-BR	500	19.70	5.64	4.63	20.61	5.37	4.71
W-BC	640	24.32	7.21	6.04	25.43	6.89	6.14
W-CR	470	18.46	5.24	4.33	19.31	4.99	4.40
W-CC	540	20.43	5.98	5.07	21.36	5.71	5.15
W-DR	328	12.97	3.75	3.06	13.57	3.58	3.10
W-DC	400	15.36	4.66	3.83	16.05	4.46	3.89
W-ER	330	13.20	3.93	3.13	13.81	3.76	3.17
W-EC	400	15.26	4.56	3.80	15.95	4.36	3.86
W-AR-S	500	19.71	5.65	4.64	20.62	5.39	4.71
W-AC-S	580	22.06	6.55	5.49	23.07	6.26	5.57
W-29-0.1-R1	700	33.41	8.71	6.19	35.00	8.25	6.30
W-29-0.1-R2	950	45.50	12.00	8.45	47.66	11.38	8.59
$^{\#}$Mean		19.03	5.60	4.61	19.90	5.34	4.69
$^{\#}$Standard Deviation		3.63	1.08	0.92	3.79	1.03	0.93

*Beam notation as in Table 4.2

$^{+}$R = Ratio of the Measured Buckling Load to the Predicted Buckling Load
Subscripts : SR - CIRIA's Supplementary Rules
SP - CIRIA's Single Panel method
TP - CIRIA's Two Panel method

$^{\#}$Beams W-29-0.1-R1 and W-29-0.1-R2 are excluded

Table 6.2 : CIRIA Buckling Loads for beams with web-openings

Table 6.3 : Bearing Stress and Modes of Failure

*Title of Beam	Cube Strength (f_{cu})	Bearing Stress at Failure (f_c)	Mode of Failure	Limiting Bearing Stress (0.4 f_{cu})	$\frac{f_c}{f_{cu}}$	$\frac{f_c}{0.4\ f_{cu}}$
#CB-H1	93.6	22.6	Local Buckling	37.4	0.24	0.6
#CB-H1-R	93.0	37.0	Diagonal Shear	37.2	0.40	1.0
CB-H2	96.8	40.4	Vertical Shear	38.7	0.41	1.0
CB-H3	93.0	39.1	Vertical Shear	37.2	0.42	1.1
CB-H4	97.5	49.1	Bearing	39.0	0.50	1.3
CB-H5	98.0	43.5	Bearing	39.2	0.44	1.1
CB-H6	98.1	52.2	Bearing	39.2	0.53	1.3
CB-L1	51.9	32.6	Bearing	20.8	0.63	1.6
CB-L2	47.2	28.3	Bearing	18.9	0.60	1.5
CB-L3	49.7	37.0	Bearing	19.9	0.74	1.9
CB-L4	44.4	34.7	Bearing	17.8	0.78	2.0
CB-L5	45.2	43.5	Bearing	18.1	0.96	2.4
CB-L6	42.1	39.1	Bearing	16.8	0.93	2.3
CB-L7	50.3	27.0	Vertical Shear	20.1	0.54	1.4
CB-L8	42.5	34.8	Bearing	17.0	0.82	2.1
CB-L9	43.9	28.3	Bearing	17.6	0.64	1.6

*Beam Notation as in Table 4.3

#CB-H1 failed by local buckling near the support due to tilting of the test beam. Remedy measures were taken for all the other specimens. The same specimen was re-tested (CB-H1-R).

All stresses are in Newton per square mm.

Table 7.1 : Angles of inclination of the critical diagonal cracks

*Beam	Measured Angle Ø (degrees)	#CIRIA Angle $Ø_1$ (degrees)	#Angle $Ø_2$ (degrees)	#Angle $Ø_3$ (degrees)
A-67-0.2	63	82.0	68.2	56.6
A-50-0.2	66.5	"	"	"
A-40-0.2	75.5	"	"	"
A-33-0.2	65	"	"	"
A-29-0.2	68	"	"	"
A-25-0.2	60	"	"	"
A-50-0.05	65	"	"	"
A-40-0.05	46	"	"	"
A-33-0.05	69.5	"	"	"
B-67-0.2	-	90.0	77.6	65.8
B-50-0.2	-	"	"	"
B-40-0.2	71	"	"	"
B-33-0.2	84	"	"	"
B-29-0.2	60	"	"	"
B-25-0.2	80	"	"	"
B-50-0.05	60	"	"	"
B-40-0.05	67	"	"	"
B-33-0.05	73	"	"	"
C-67-0.1	-	80.4	68.2	57.8
C-50-0.1	-	"	"	"
C-40-0.1	76	"	"	"
C-33-0.1	67	"	"	"
C-29-0.1	64	"	"	"
D-40-0.1	64.5	80.4	"	"
D-33-0.1	63	"	"	"
D-29-0.1	62.5	"	"	"
E-67-0.1	66	80.4	68.2	57.8
E-50-0.1	-	"	"	"
E-40-0.1	67	"	"	"
E-33-0.1	55.5	"	"	"
E-29-0.1	63	"	"	"
E-25-0.1	61	"	"	"
E-67-0.2	59	"	"	"
E-50-0.2	64	"	"	"
E-40-0.2	68	"	"	"
E-33-0.2	65	"	"	"
E-29-0.2	62	"	"	"
E-25-0.2	67	"	"	"

*BEAM NOTATION : The Series letter is given before the hyphen; this is followed by the height/thickness ratio (h/b) and then by the load-eccentricity/thickness ratio (e/b). For example, A-67-0.2 refers to a beam in Series A having a h/b ratio of 67 and an e/b ratio of 0.2

#$Ø_1$, $Ø_2$ and $Ø_3$ as in Fig.7.2

Table 7.2 : Measured and calculated ultimate loads

*Beam	Ultimate Loads (kN)						
	Measured Shear Buckling	#CIRIA Equation					
	P_m	P_1	P_m/P_1	P_2	P_m/P_2	P_3	P_m/P_3
A-67-0.2		148	145	1.02	130	1.14	114	1.29
A-50-0.2		360	286	1.26	247	1.46	220	1.64
A-40-0.2		420	324	1.30	290	1.45	250	1.68
A-33-0.2		560	381	1.47	342	1.64	296	1.89
A-29-0.2		682	514	1.33	460	1.48	394	1.73
A-25-0.2		620	525	1.18	470	1.32	404	1.54
A-50-0.05	440		286	1.54	256	1.72	220	2.00
A-40-0.05	534		324	1.65	290	1.84	250	2.13
A-33-0.05	640		381	1.68	342	1.87	296	2.16
B-67-0.2		120	152	0.79	141	0.85	128	0.94
B-50-0.2		146	301	0.48	283	0.52	253	0.58
B-40-0.2		340	339	1.00	317	1.07	285	1.19
B-33-0.2		560	389	1.44	364	1.54	327	1.71
B-29-0.2		420	531	0.79	498	0.84	446	0.94
B-25-0.2		700	570	1.23	534	1.31	479	1.46
B-50-0.05	460		303	1.52	285	1.62	255	1.80
B-40-0.05	550		339	1.62	317	1.73	285	1.94
B-33-0.05	692		388	1.79	362	1.91	326	2.12
C-67-0.1		60	171	0.35	156	0.38	139	0.43
C-50-0.1		120	302	0.40	273	0.44	239	0.50
C-40-0.1		270	345	0.78	312	0.86	275	0.98
C-33-0.1		450	370	1.21	336	1.34	296	1.52
C-29-0.1		550	504	1.09	455	1.21	398	1.38
D-40-0.1		300	325	0.92	294	1.02	260	1.15
D-33-0.1		340	351	0.97	318	1.07	284	1.20
D-29-0.1		538	477	1.13	431	1.25	379	1.42
E-67-0.1		290	Specimen failed by vertical splitting					
E-50-0.1		200	292	0.69	264	0.76	231	0.87
E-40-0.1		502	333	1.51	301	1.67	265	1.90
E-33-0.1		440	349	1.26	316	1.39	278	1.58
E-29-0.1		700	509	1.38	460	1.52	402	1.74
E-25-0.1		560	540	1.04	488	1.15	428	1.31
E-67-0.2		300	Specimen damaged (accident)					
E-50-0.2		170	290	0.59	262	0.65	231	0.74
E-40-0.2		210	338	0.62	306	0.69	270	0.78
E-33-0.2		300	380	0.79	345	0.87	304	0.99
E-29-0.2		400	509	0.79	460	0.87	402	0.99
E-25-0.2		540	550	0.98	497	1.09	436	1.24
Mean	Shear			1.63		1.78		2.03
	Buckling			0.99		1.10		1.27
Standard Deviation	Shear			0.10		0.11		0.14
	Buckling			0.32		0.36		0.44

*Beam Notation as in Table 7.1

#P_1 values are calculated using $\emptyset_1$ of Fig.7.2(b)
P_2 values are calculated using $\emptyset_2$ of Fig.7.2(b)
P_3 values are calculated using $\emptyset_3$ of Fig.7.2(b)

*Beam	Failure Load (kN)	Mesured Ultimate Load / Computed Ultimate Load				Inclination of Load Path		@Remarks
		$^{+}R_L$	$^{+}R_U$	$^{+}R_S$	$^{+}R_H$	Ø' (Upper)	Ø (Lower)	
Sharp [1977] - Lightweight concrete deep beams with mesh reinforcement								
M-0.4/0#	595	0.91	0.91	0.91	0.91	0.0	67.94	
M-0.4/1	580	0.98	0.98	0.98	0.98	0.00	63.13	ULL
M-0.4/2	360	0.89	1.27	1.27	0.89	44.62	55.96	
M-0.4/3	445	1.93	1.75	1.93	1.75	63.13	44.62	
M-0.4/4	450	1.67	1.67	1.67	1.67	52.77	52.77	
M-0.4/5#	600	1.00	1.00	1.00	1.00	0.0	67.94	
M-0.4/6	270	2.65	0.87	2.65	0.87	59.20	30.63	
M-0.4/8	340	1.76	1.44	1.76	1.44	71.34	36.51	
M-0.4/9	240	0.90	0.90	0.90	0.90	47.99	47.99	
M-0.4/10	300	1.24	1.24	1.24	1.24	50.05	49.60	
M-0.4/11#	600	0.91	0.91	0.91	0.91	0.0	67.94	
M-0.4/12#	520	0.80	0.80	0.80	0.80	0.0	67.94	
M-0.4/13	130	0.80	0.80	0.80	0.80	36.51	36.51	
Sharp [1977] - Lightweight concrete deep beams without web steel								
O-0.4/0#	660	1.12	1.12	1.12	1.12	0.0	67.94	
O-0.4/2	370	1.05	1.05	1.05	1.05	0.00	63.13	ULL
O-0.4/4	340	1.23	1.23	1.23	1.23	52.77	52.77	
O-0.4/5#	540	0.98	0.98	0.98	0.98	0.0	67.94	
O-0.4/6	190	2.57	0.71	2.57	0.71	59.20	30.63	
O-0.4/7	420	0.99	1.69	1.69	0.99	26.26	71.34	ULL
O-0.25/0	660	1.00	1.00	1.00	1.00	0.0	67.94	
O-0.25/2	360	0.82	1.24	1.24	0.82	57.93	67.33	
O-0.25/4	460	1.36	1.36	1.36	1.36	64.83	64.83	
O-0.25/5#	560	0.81	0.81	0.81	0.81	0.0	75.93	
O-0.25/6	280	2.24	0.86	2.24	0.86	69.76	43.75	
O-0.3/2R	260	0.92	0.85	0.92	0.85	69.44	53.13	
O-0.3/3R	400	1.50	1.44	1.50	1.44	62.30	53.13	
O-0.3/4R	215	0.73	0.73	0.73	0.73	53.13	53.13	
O-0.3/5R	330	1.12	1.16	1.16	1.12	48.01	53.13	
O-0.3/0#	595	0.91	0.91	0.91	0.91	0.0	73.30	
O-0.3/1#	460	0.72	0.72	0.72	0.72	0.0	73.30	
O-0.3/2	390	1.32	1.22	1.32	1.22	69.44	53.13	
O-0.3/3	280	1.02	0.97	1.02	0.97	62.30	53.13	
O-0.3/4	260	0.95	0.95	0.95	0.95	53.13	53.13	
O-0.3/5	200	0.72	0.74	0.74	0.72	48.01	53.13	
O-0.3/6	250	0.87	0.95	0.95	0.87	41.63	53.13	
O-0.3/7	420	1.06	1.16	1.16	1.06	53.13	77.32	
O-0.3/8	380	1.11	1.19	1.19	1.11	53.13	69.44	
O-0.3/9	280	0.86	0.90	0.90	0.86	53.13	62.30	

(to be continue)

Table 7.3 : Ultimate Shear Loads for Beams without Web-openings

*Beam	Failure Load (kN)	Mesured Ultimate Load / Computed Ultimate Load $^{+}R_L$	$^{+}R_U$	$^{+}R_S$	$^{+}R_H$	Inclination of Load Path (Upper) Ø'	(Lower) Ø	@Remarks
Sharp [1977] - Lightweight concrete deep beams without web steel (cont'd)								
O-0.3/10	210	0.86	0.82	0.86	0.82	53.13	45.73	
O-0.3/11	360	0.77	1.31	1.31	0.77	56.11	65.75	
O-0.3/12#	560	0.79	0.79	0.79	0.79	0.0	73.30	
O-0.3/13	300	0.62	1.20	1.20	0.62	24.07	65.75	ULL
O-0.3/14#	560	0.84	0.84	0.84	0.84	0.0	73.30	
O-0.3/15	260	1.42	0.68	1.42	0.68	65.75	56.11	
O-0.3/16	195	4.06	0.67	4.06	0.67	65.75	24.07	BLL
O-0.2/0#	655	0.91	0.91	0.91	0.91	0.0	78.69	
O-0.2/4	360	1.01	1.01	1.01	1.01	63.43	63.43	
O-0.2/13	500	0.99	1.79	1.79	0.99	33.82	73.28	
O-0.2/16	340	3.70	1.09	3.70	1.09	73.28	33.82	
Sharp [1977] - Lightweight concrete deep beams with web steel								
WM-0.4/0#	660	0.99	0.99	0.99	0.99	0.0	67.94	
WM-0.4/18	500	1.40	1.41	1.41	1.40	55.83	56.09	
WM'-0.4/18	500	1.40	1.41	1.41	1.40	55.83	56.09	
W3-0.3/4	560	1.01	1.01	1.01	1.01	53.13	53.13	
W4-0.3/4	660	0.83	0.83	0.83	0.83	53.13	53.13	
W6-0.3/4	825	1.03	1.03	1.03	1.03	53.13	53.13	
W7-0.3/4	630	1.18	1.18	1.18	1.18	53.13	53.13	
W3(A)	500	1.18	1.18	1.18	1.18	53.13	53.13	
W4(A)	650	0.82	0.82	0.82	0.82	53.13	53.13	
W7(A)	670	1.24	1.24	1.24	1.24	53.13	53.13	
Sharp [1977] - Normal weight concrete deep beams without web steel								
NO-0.3/0#	680	0.79	0.79	0.79	0.79	0.0	73.30	
NO-0.3/4	240	0.65	0.65	0.65	0.65	53.13	53.13	
Sharp [1977] - Normal weight concrete deep beams with web steel								
NW3-0.3/4	620	0.95	0.95	0.95	0.95	53.13	53.13	
NW4-0.3/4	780	0.90	0.90	0.90	0.90	53.13	53.13	
NW6-0.3/4	1060	1.17	1.17	1.17	1.17	53.13	53.13	
NW7-0.3/4	720	1.22	1.22	1.22	1.22	53.13	53.13	
NW6A-0.3/0#	1215	1.22	1.22	1.22	1.22	0.0	73.30	
NW6A-0.3/1#	1015	1.07	1.07	1.07	1.07	0.0	73.30	
NW6A-0.3/4	620	1.14	1.14	1.14	1.14	53.13	53.13	
NW6A-0.3/7	930	1.40	1.53	1.53	1.40	53.13	77.32	

(to be continue)

Table 7.3 : Ultimate Shear Loads for Beams without Web-openings (cont'd)

*Beam	Failure Load (kN)	Mesured Ultimate Load / Computed Ultimate Load				Inclination of Load Path		@Remarks
		+R_L	+R_U	+R_S	+R_H	Ø' (Upper)	Ø (Lower)	
Sharp [1977] - Normal weight concrete deep beams with web steel (cont'd)								
NW6A-0.3/11	880	1.04	1.83	1.83	1.04	56.11	65.75	
NW6A-0.3/15	820	2.04	1.05	2.04	1.05	65.75	56.11	
NW6A-0.3/17	840	1.40	1.40	1.40	1.40	64.01	64.01	
Kubik [1978] - Normal weight concrete deep beams								
N1-A	3040	1.07	1.25	1.25	1.07	47.49	55.22	
N2-A	4160	1.14	1.28	1.28	1.14	47.49	55.22	
N3-A	4840	1.12	1.25	1.25	1.12	47.49	55.22	
N4-B	3240	1.85	1.03	1.85	1.03	61.19	35.75	
Kubik [1978] - Lightweight concrete deep beams								
L1-A	2650	1.25	1.35	1.35	1.25	47.49	55.22	
L2-A	3430	1.17	1.25	1.25	1.17	47.49	55.22	
L3-A	3630	1.06	1.11	1.11	1.06	47.49	55.22	
L4-B	2624	1.82	1.36	1.82	1.36	61.19	35.75	
Mean		1.21	1.09	1.28	1.03			
Standard Deviation		0.34	0.07	0.34	0.05			
Relative Error (%)		21.56	19.48	23.21	17.83			

*Beam notation as described [Sharp, 1977]

+R = Ratio of Measured Ultimate Load to Computed Ultimate Shear Load
Subscripts : (1) L - Shear with lower load path concrete contribution
(2) U - Shear with upper load path concrete contribution
(3) S - Smaller value of (1) and (2)
(4) H - Larger value of (1) and (2)

#Web-openings is assumed to have no effect on the shear capacity of the beam

@Remarks :

ULL - The inclination of upper load path Ø' is less than 30 degree

BLL - Beam is not recommended by Kong et al [1973a] as the inclination of the lower path Ø is less than 30 degree

Table 7.3 : Ultimate Shear Loads for Beams without Web-openings (cont'd)

*Beam	Measured Ultimate Load (kN)	Predicted Shear Strength (kN)			Measured Shear Strength / Predicted Shear Strength		
		Sharp	Kubik	Author	Sharp	Kubik	Author
		$^{+}P_S$	$^{+}P_K$	$^{+}P_A$	$^{+}R_S$	$^{+}R_K$	$^{+}R_A$
W-AR	600	480	504	480	1.25	1.19	1.25
W-AC	540	520	569	520	1.04	0.95	1.04
W-AR-R	480	485	510	485	0.99	0.94	0.99
W-AC-R	560	514	562	514	1.09	1.00	1.09
W-BR	500	527	439	527	0.95	1.14	0.95
W-BC	640	554	214	554	1.16	3.00	1.16
W-CR	470	370	370	370	1.27	1.27	1.27
W-CC	540	404	404	404	1.34	1.34	1.34
W-DR	328	290	338	484	1.13	0.97	0.68
W-DC	400	339	309	537	1.18	1.30	0.75
W-ER	330	463	246	594	0.71	1.34	0.56
W-EC	400	509	466	625	0.79	0.86	0.64
W-AR-S	500	517	540	517	0.97	0.93	0.97
W-AC-S	580	548	593	548	1.06	0.98	1.06
W-29-0.1-R1	700	653	653	653	1.07	1.07	1.07
W-29-0.1-R2	950	642	642	642	1.48	1.48	1.48
Mean					1.09	1.23	1.02
Standard Deviation					0.04	0.25	0.07

*Beam notation as in Table 4.2

^{+}R = Ratio of the Measured Ultimate Load to the Computed Ultimate Shear Load

Subscripts : S - Sharp's method [1977]
K - Kubik's method [1978]
A - Author's method

Table 7.4 : Ultimate Shear Loads for Beams with Web-openings

Table 7.5 : CIRIA Combined Loading

*Title of Beam	Failure Shear Load (kN)	$^{+}V_{ct}$ (kN)	$^{+}V_{cb}$ Case 1 (kN)	Applied Top Loading $^{+}V_{at}$ (kN) Case 1	2	3	4	Factor of Safety Case 1	2	3	4
CB-H1	260	261	50	203	42	0	0	1.93	1.39	0.0	0.0
CB-H1-R	425	260	50	368	207	120	4	2.56	2.02	1.61	1.02
CB-H2	465	271	116	332	247	160	44	2.37	2.14	1.74	1.16
CB-H3	450	266	83	355	232	145	29	2.48	2.10	1.70	1.11
CB-H4	565	307	50	508	347	260	144	2.80	2.35	2.00	1.47
CB-H5	500	314	116	367	282	195	79	2.32	2.12	1.77	1.25
CB-H6	600	313	83	505	382	295	179	2.76	2.44	2.09	1.57
CB-L1	375	211	50	318	157	70	0	2.66	1.97	1.48	0.0
CB-L2	325	211	116	192	107	20	0	2.06	1.73	1.25	0.0
CB-L3	425	213	83	330	207	120	4	2.70	2.19	1.71	1.02
CB-L4	400	242	50	343	182	95	0	2.57	1.98	1.54	0.0
CB-L5	500	250	116	367	282	195	79	2.62	2.35	1.93	1.32
CB-L6	450	244	83	355	232	145	29	2.60	2.17	1.74	1.12
#CB-L7	310	202	0	310	92	5	0	1.53	1.68	1.18	0.0
#CB-L8	400	233	0	400	182	95	0	1.72	2.01	1.56	0.0
CB-L9	325	227	116	192	107	20	0	1.99	1.70	1.24	0.0

Beam Notation as in Table 4.3

$^{+}V_{at}$, V_{ct} and V_{cb} as in Clause 3.4.2 of CIRIA Guide [1977].

#Beams CB-L7 and CB-L8 have no nominal web reinforcement or shear reinforcement.

Case 1 : failure of bottom shear reinforcement (as tabulated above);

Case 2 : failure of bottom shear capacity of beam (V_{cb} = 178 kN);

Case 3 : failure of bottom hangers (design ultimate strength V_{cb} = 265 kN); and

Case 4 : failure of bottom hangers (ultimate failure strength V_{cb} = 421 kN).

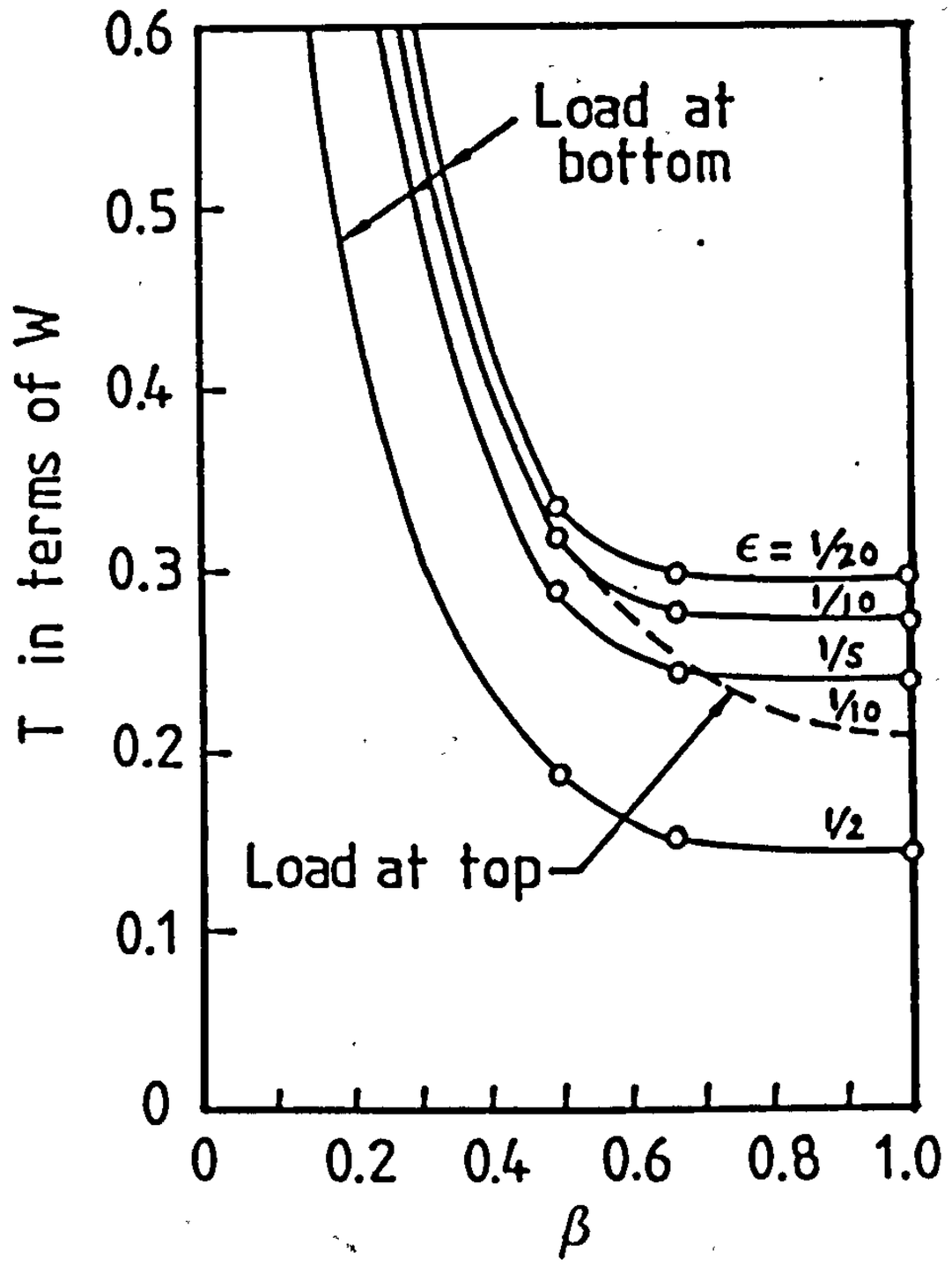

Figure 3.1 : PCA's Design Chart

Structural idealization

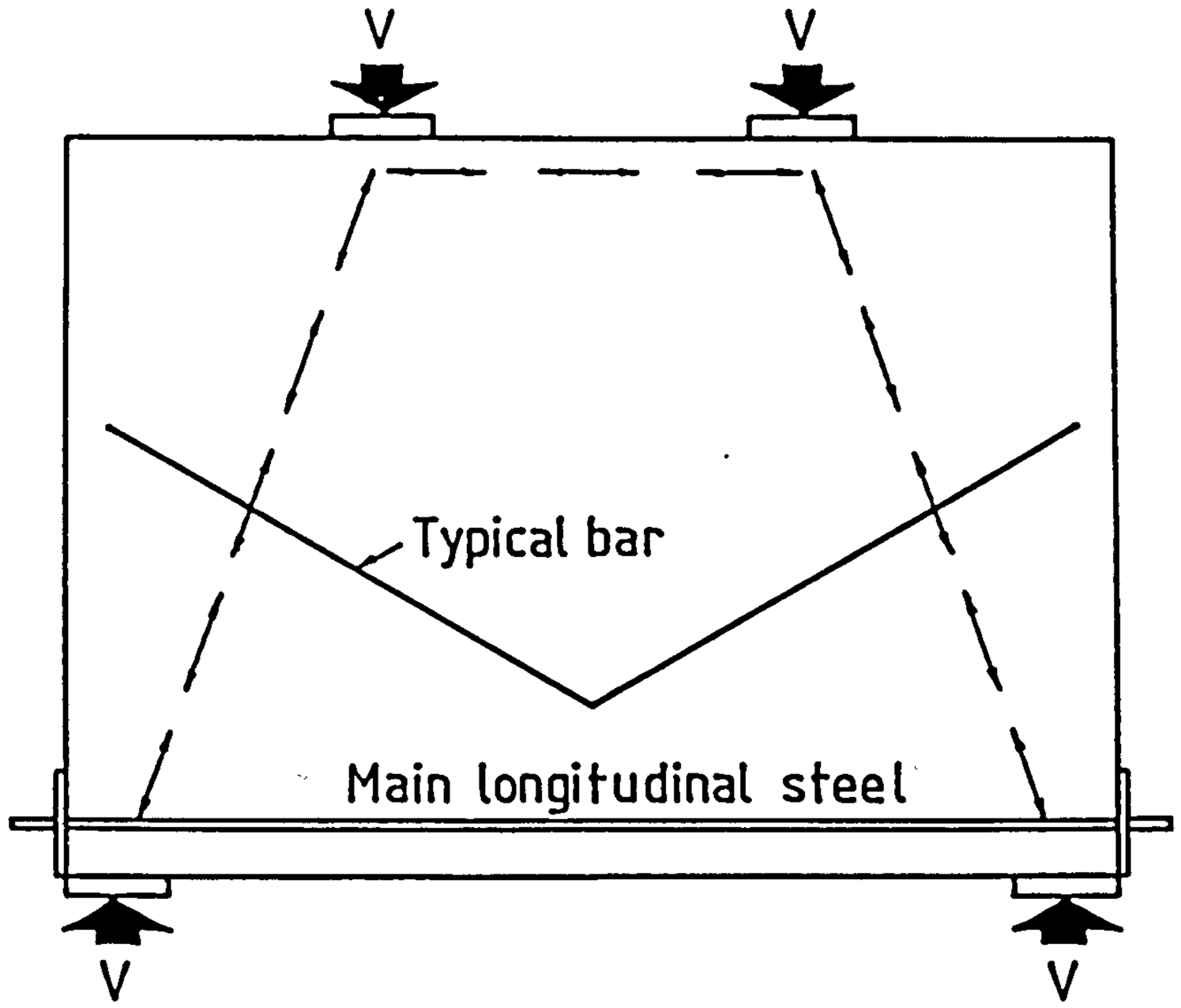

Meanings of symbols

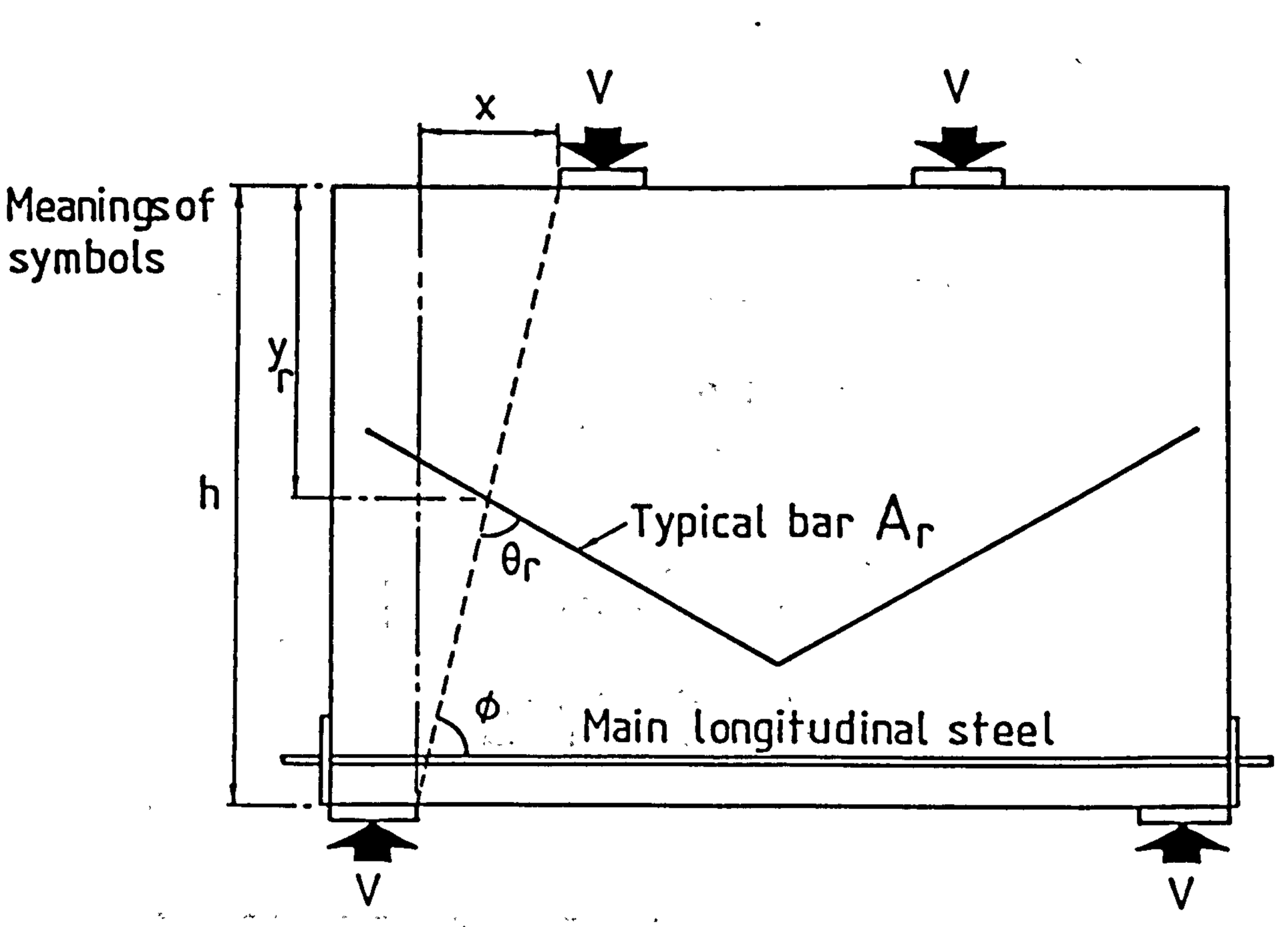

Figure 3.2 : Kong et al's model for deep beam without web-openings

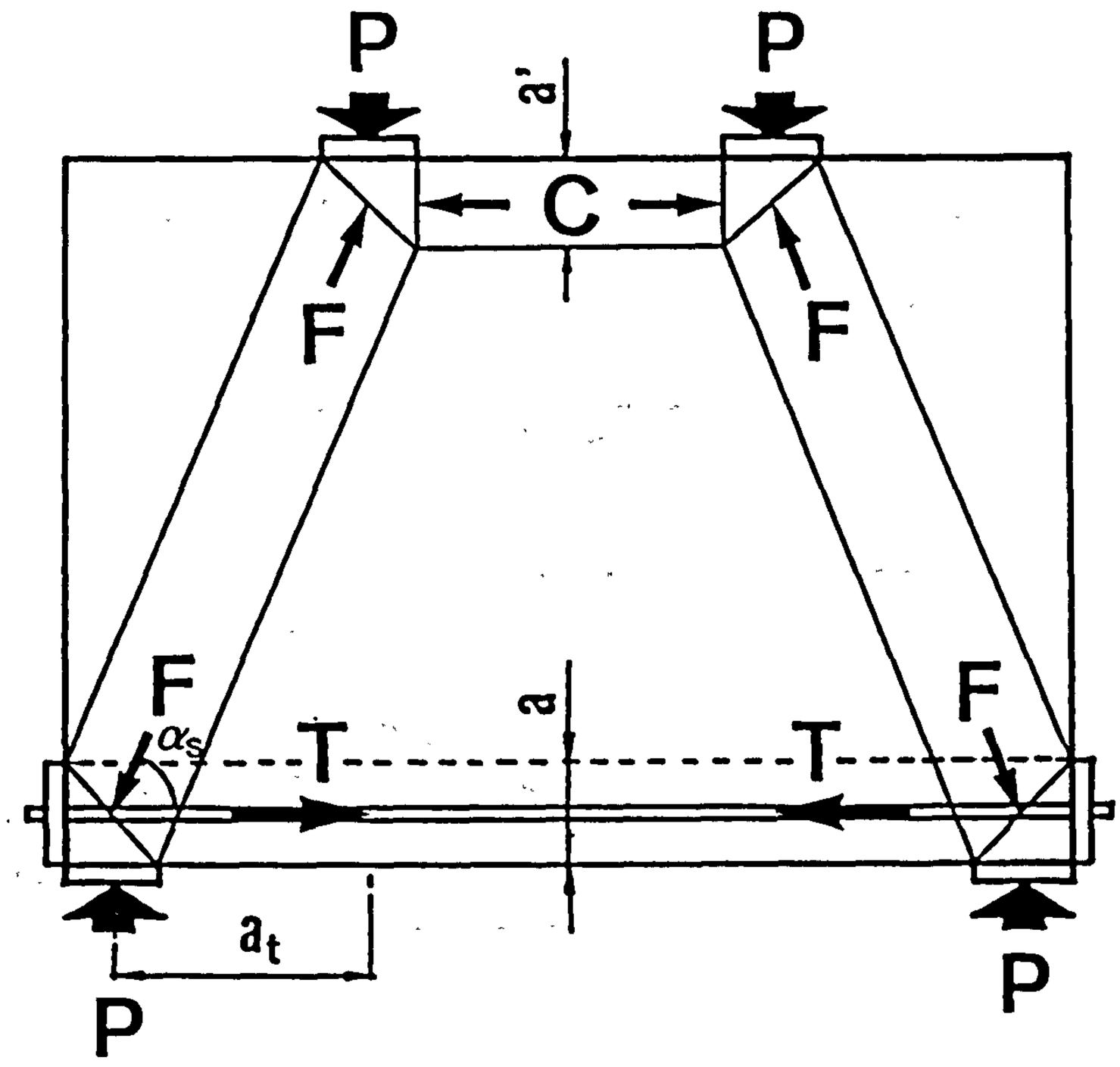

Figure 3.3 : Canadian Code deep beam strut model

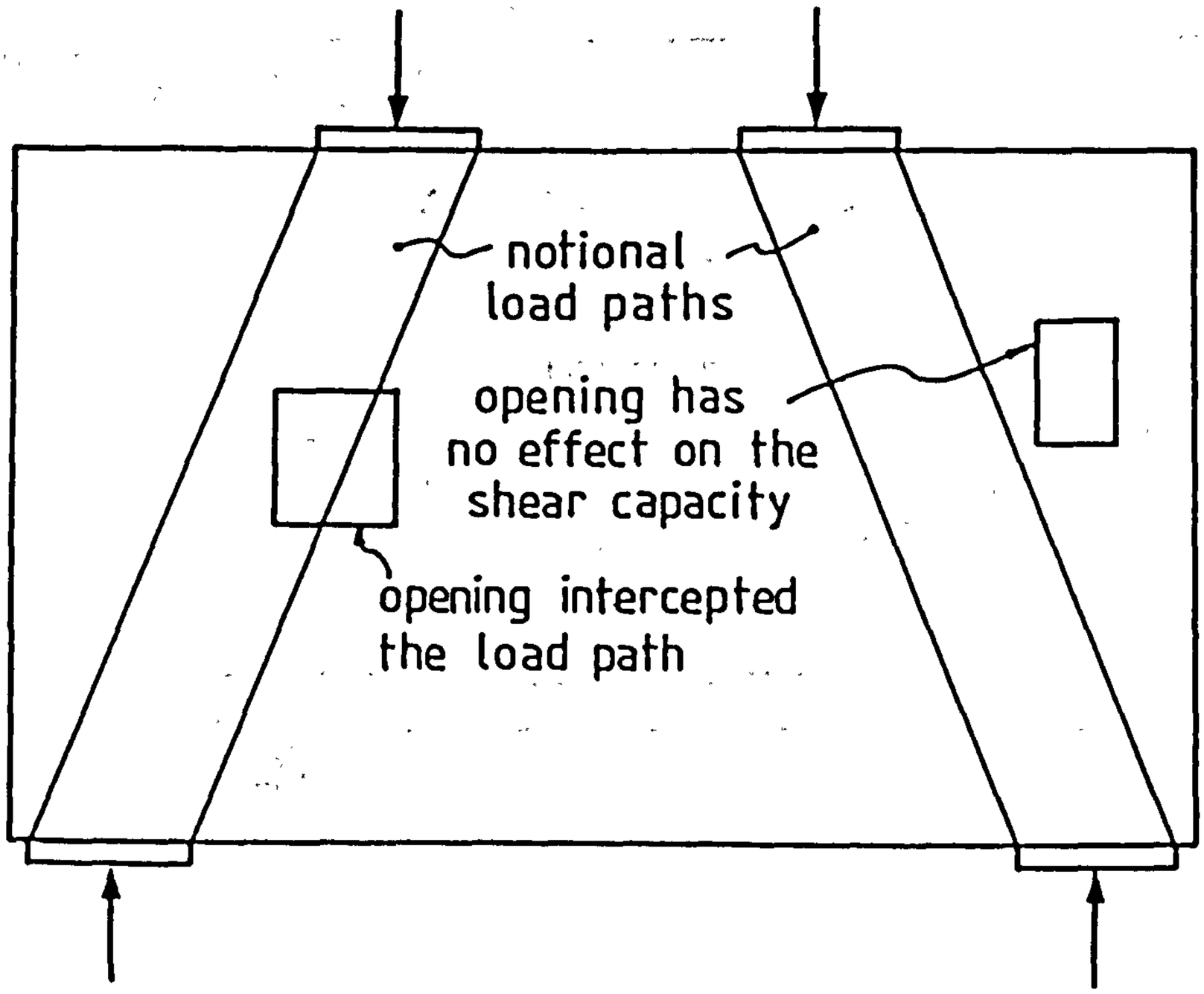

Figure 3.4 : Load paths proposed by Kong and Sharp [1977]

Structural idealization

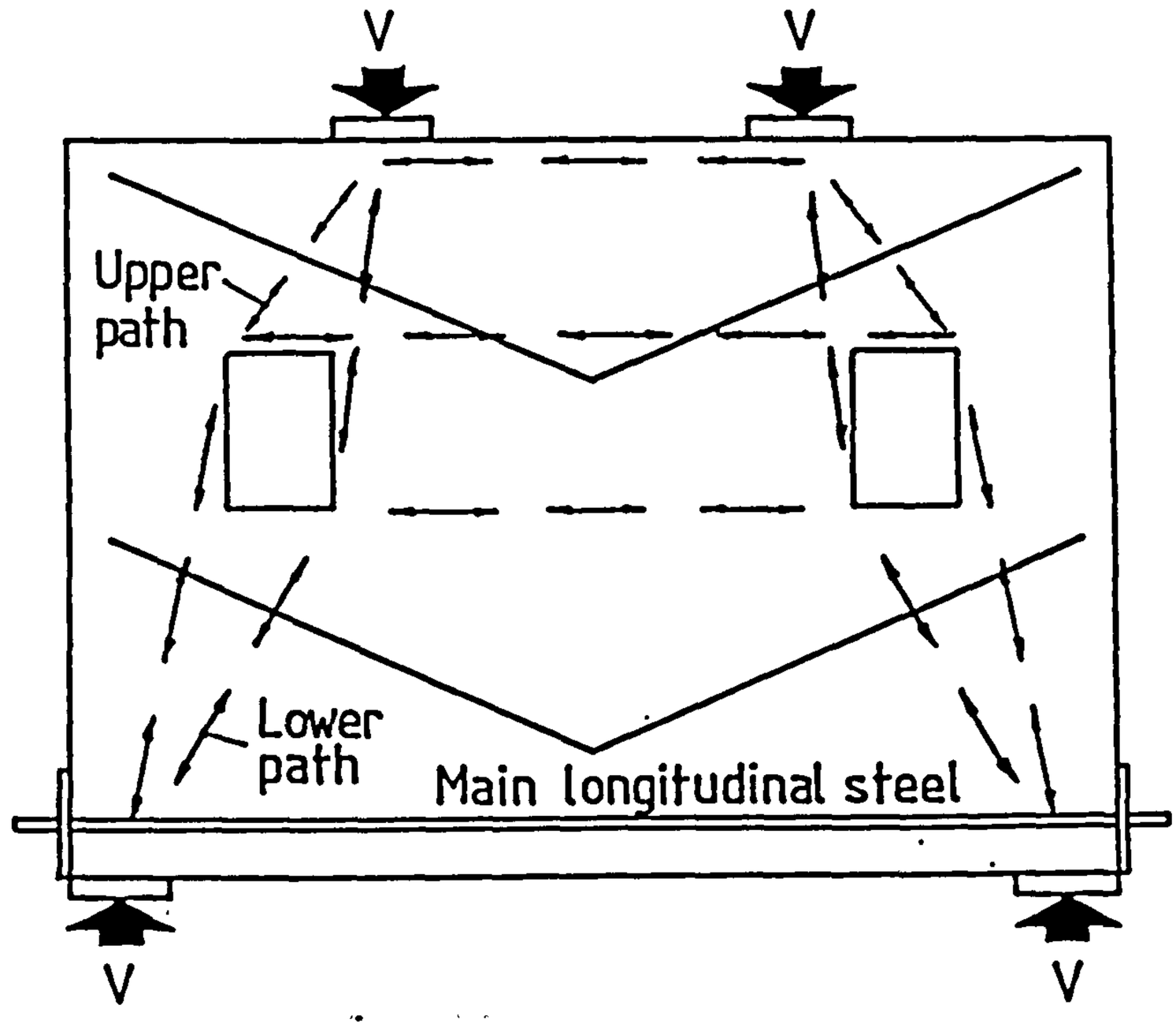

Meanings of symbols

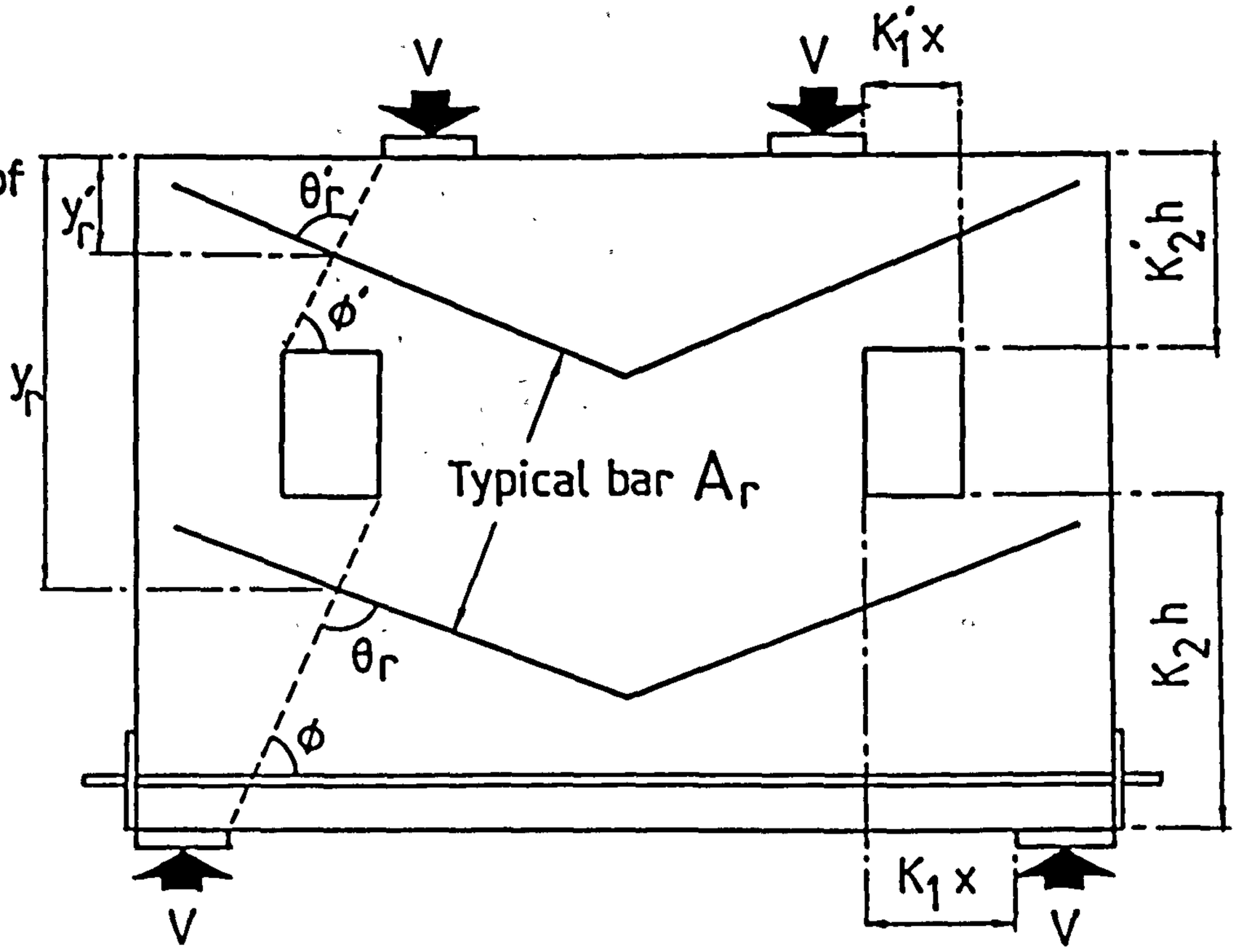

Figure 3.5 : Kong et al's model for deep beam with web-openings

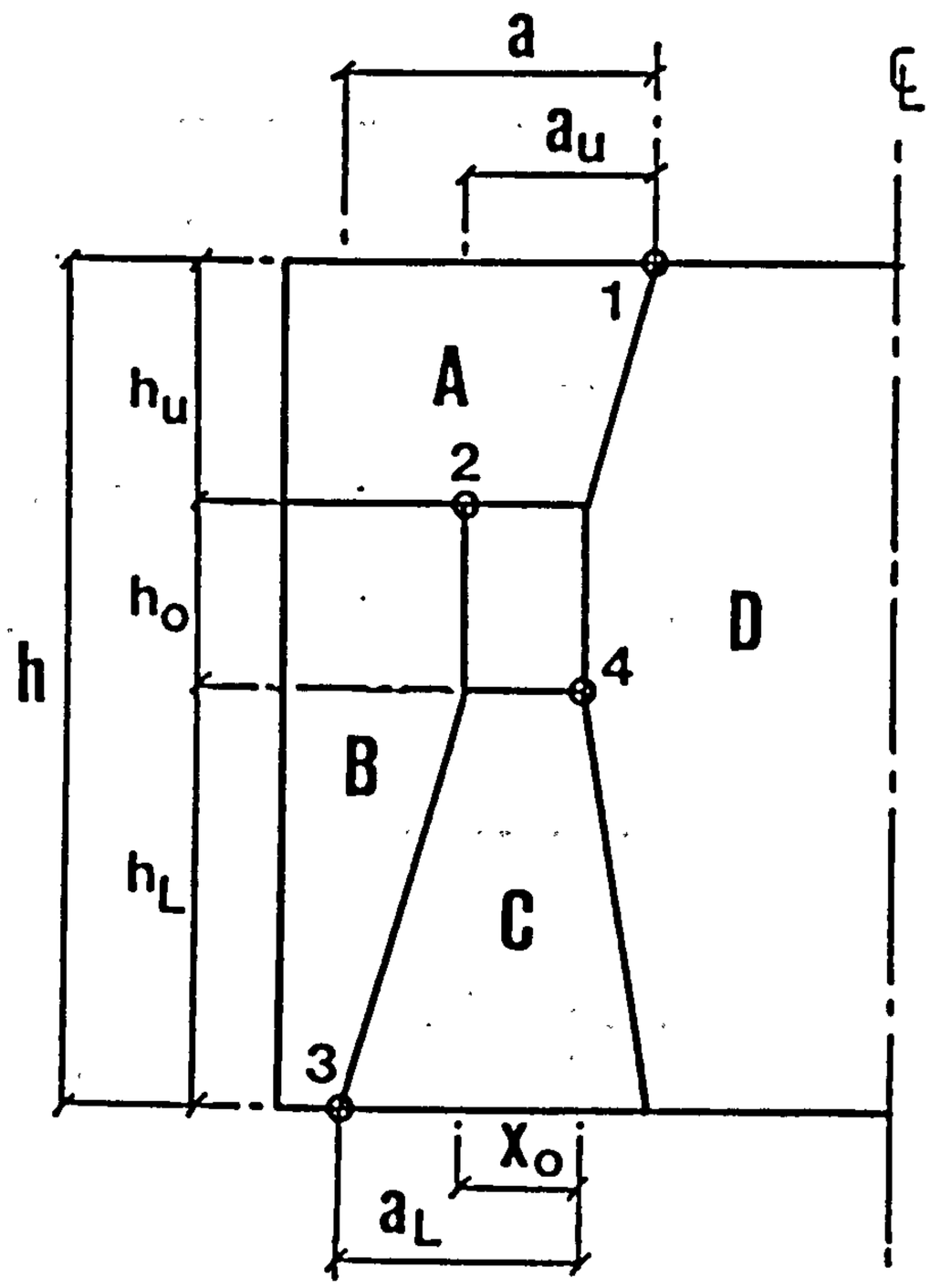

Figure 3.6 : Kubik's model for deep beams with web-openings

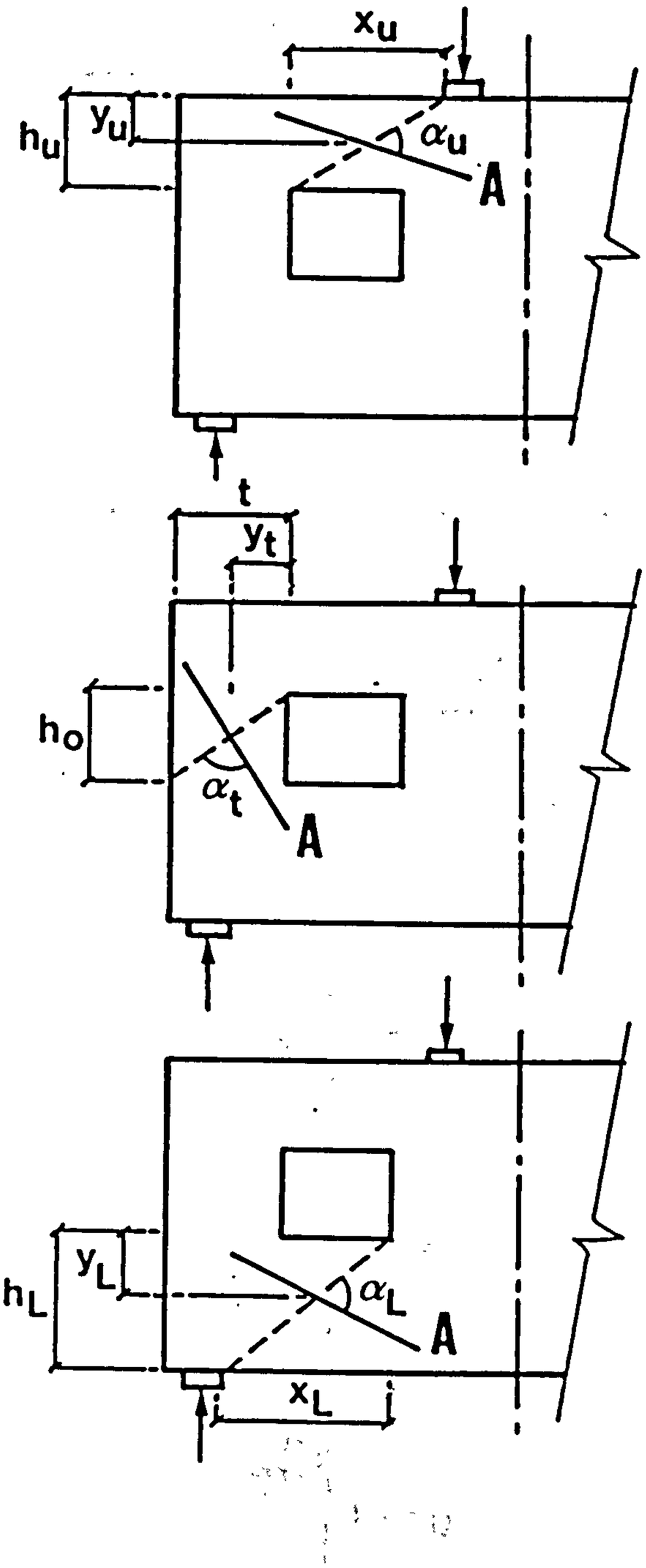

(a) Shear failure above the web-opening

(b) Shear failure beside the web-opening

(c) Shear failure below the web-opening

Figure 3.7 : Notations for shear failures in Kubik's model

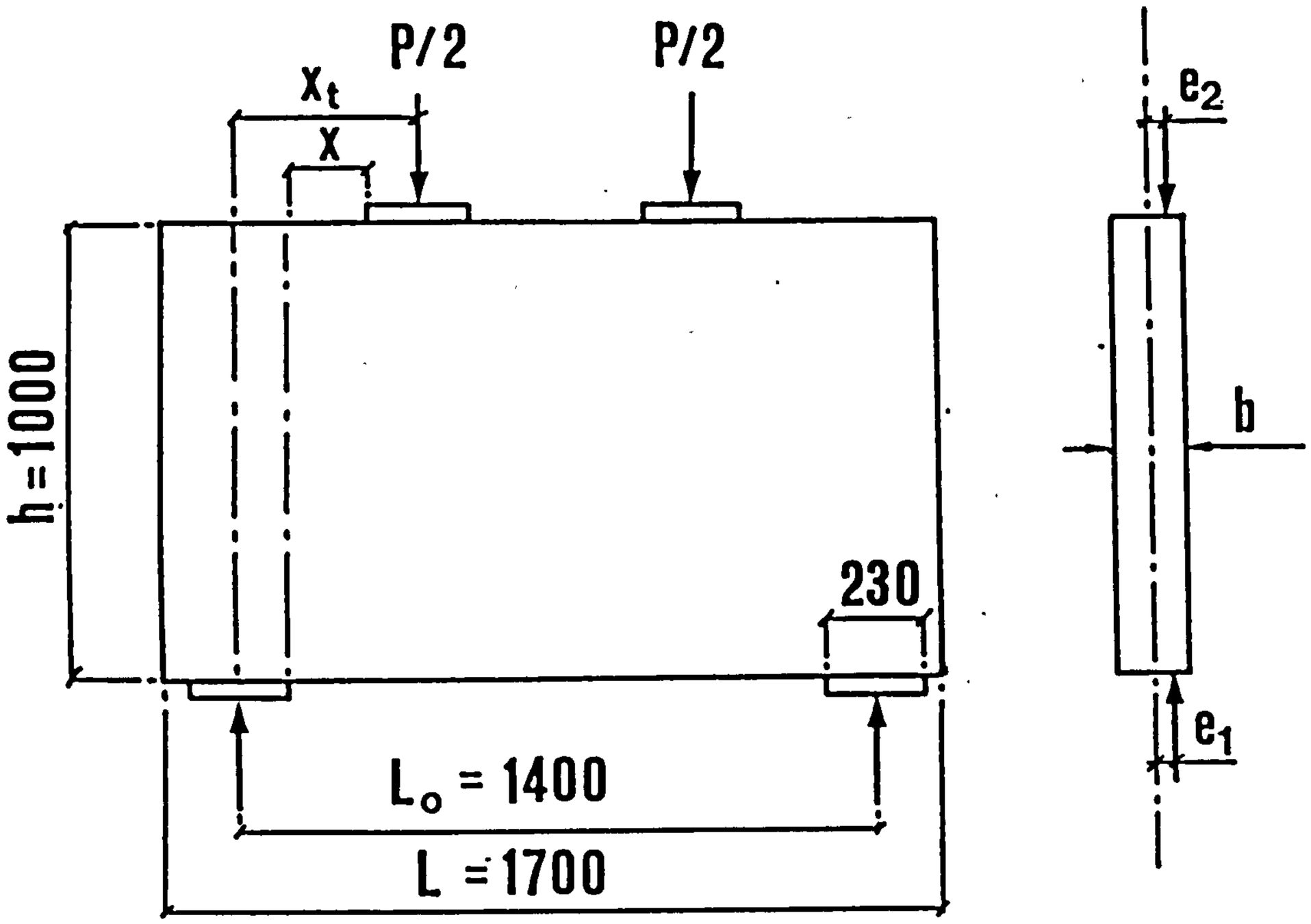

(a) General dimensions of test beams

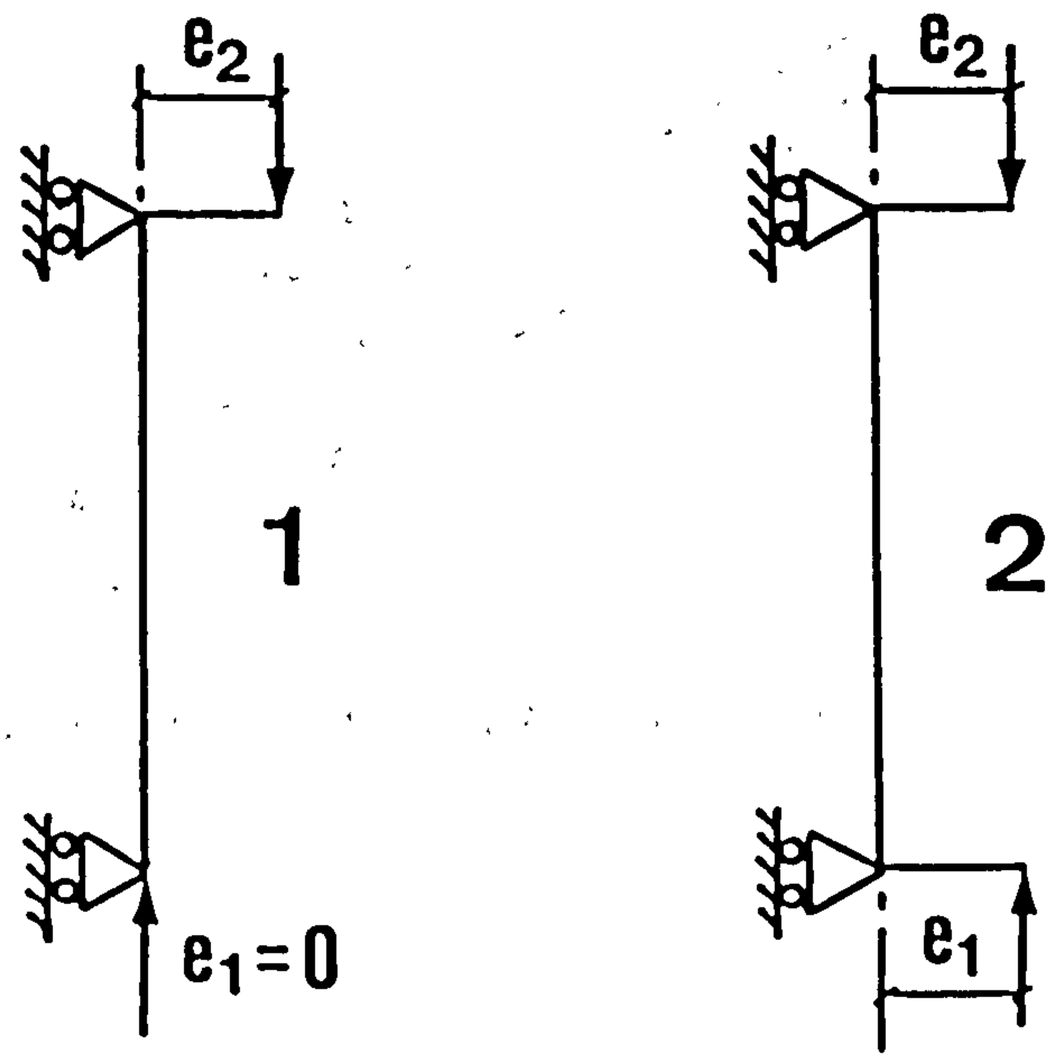

(b) Loading schemes 1 and 2

Figure 4.1 : Typical details of slender deep beam tests

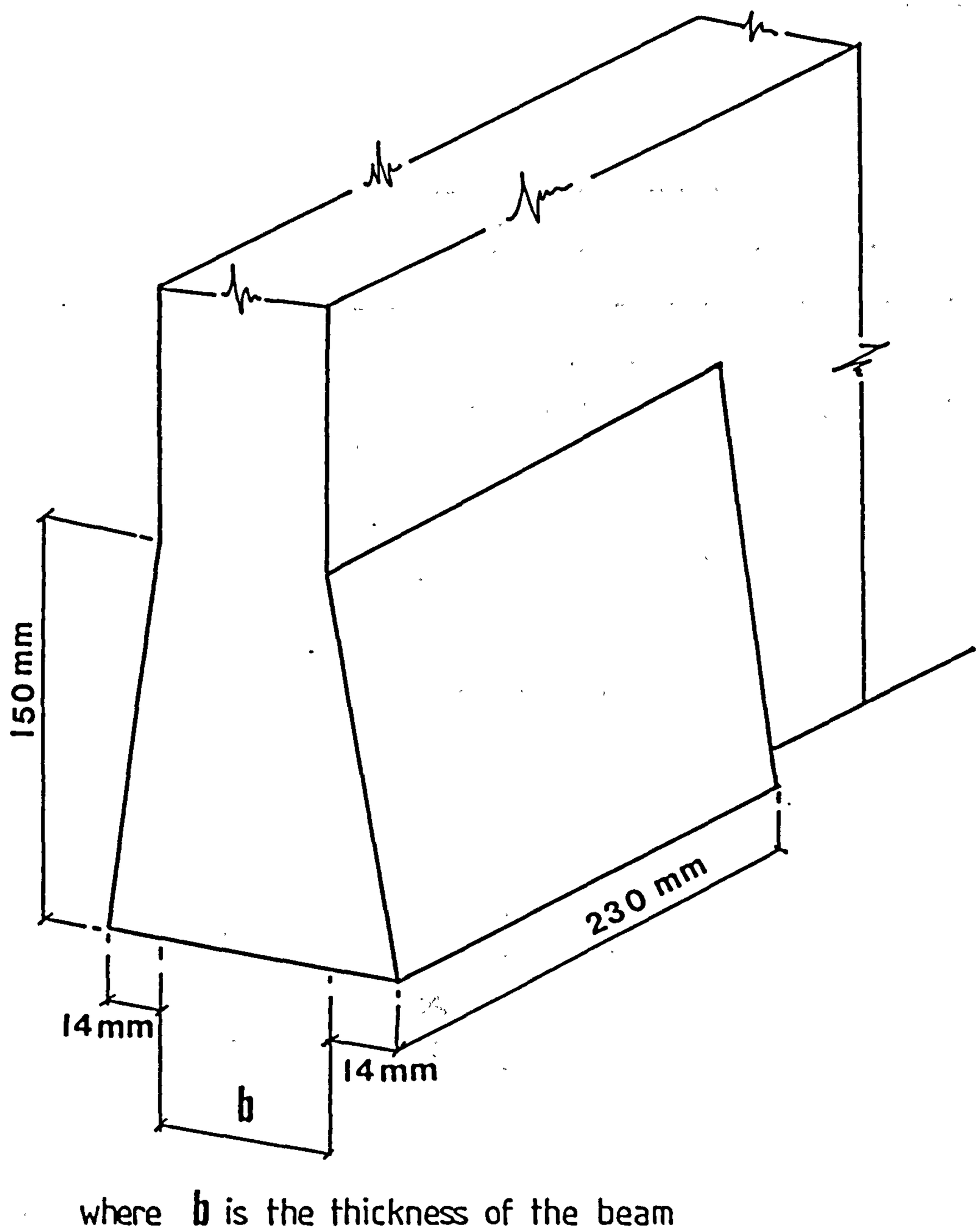

where b is the thickness of the beam

Figure 4.2 : Local thickening

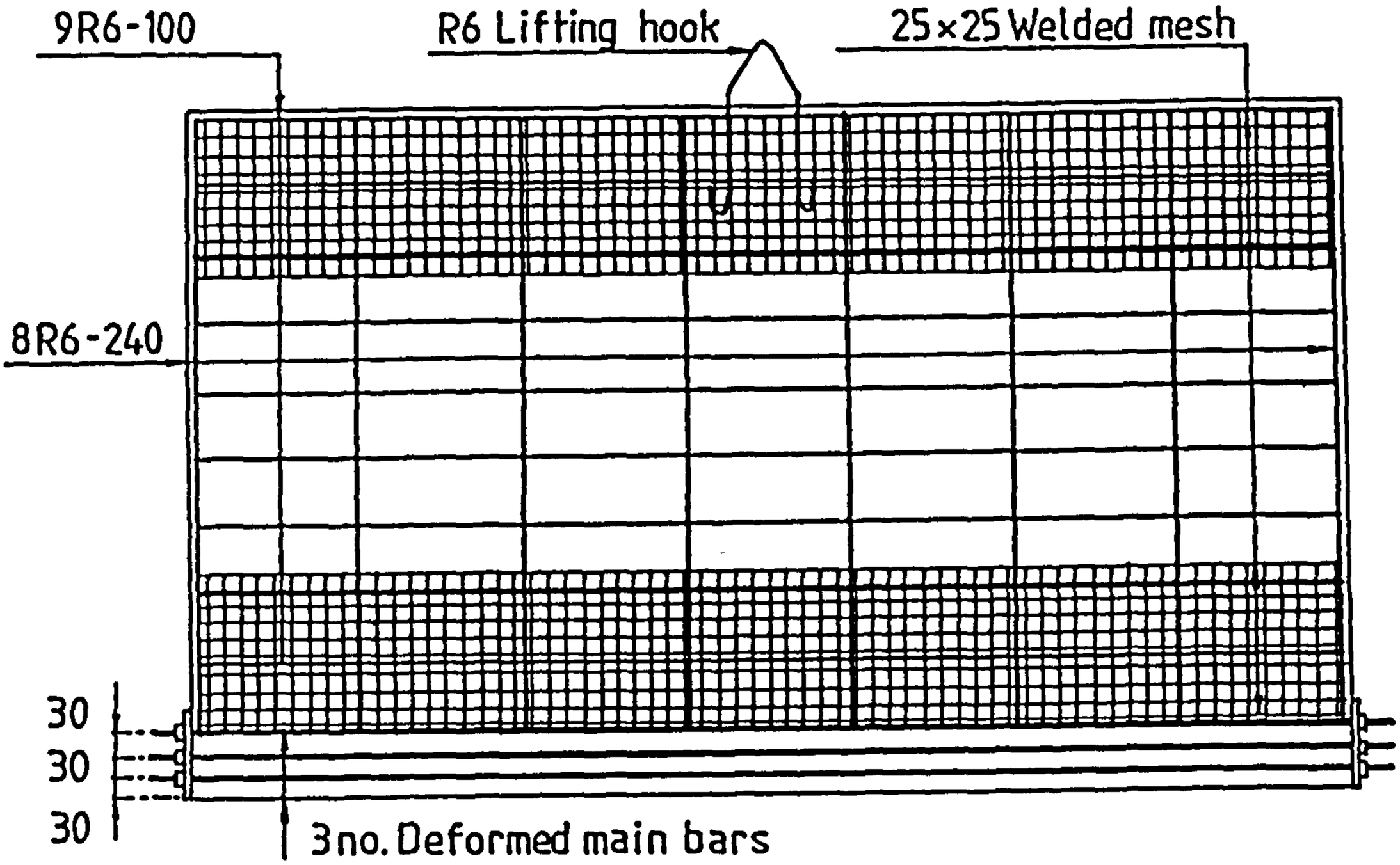

Typical steel arrangement

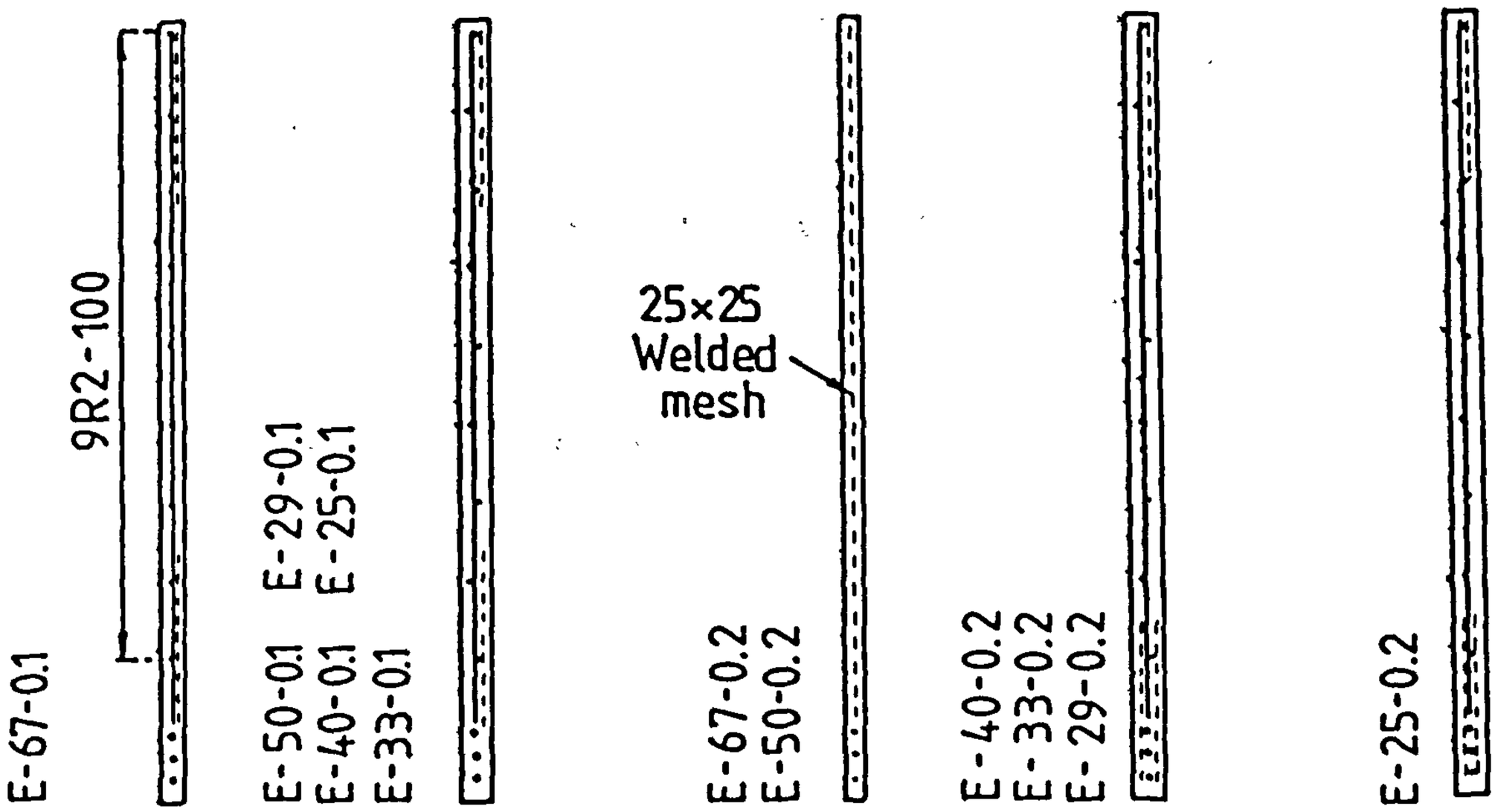

All web reinforcement are R6 unless stated otherwise
(All dimensions in mm)

Figure 4.3 : Steel arrangement in the E-Series test beams

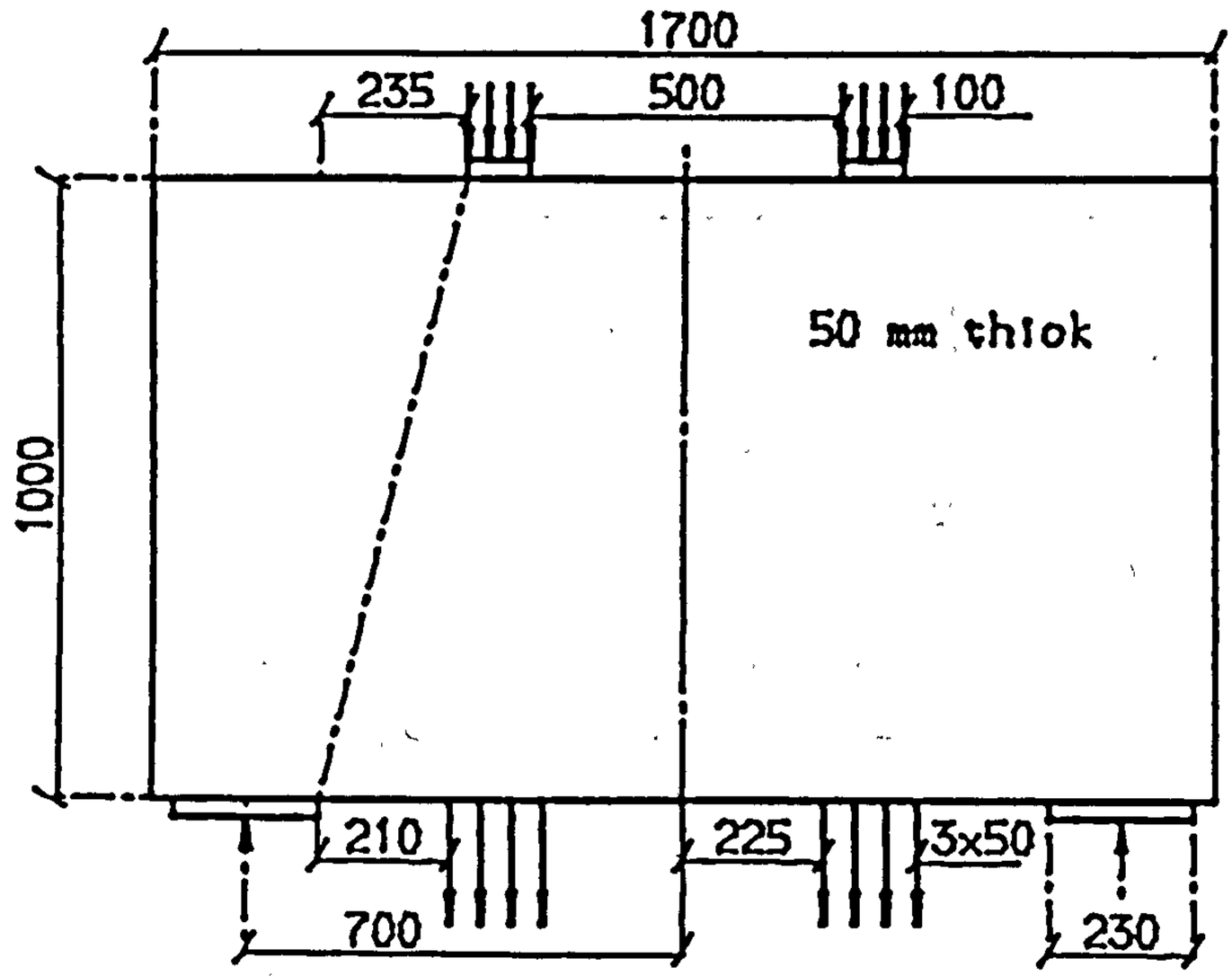

(All dimensions in mm)

Figure 4.4 : General dimensions of the CB-Series test beams

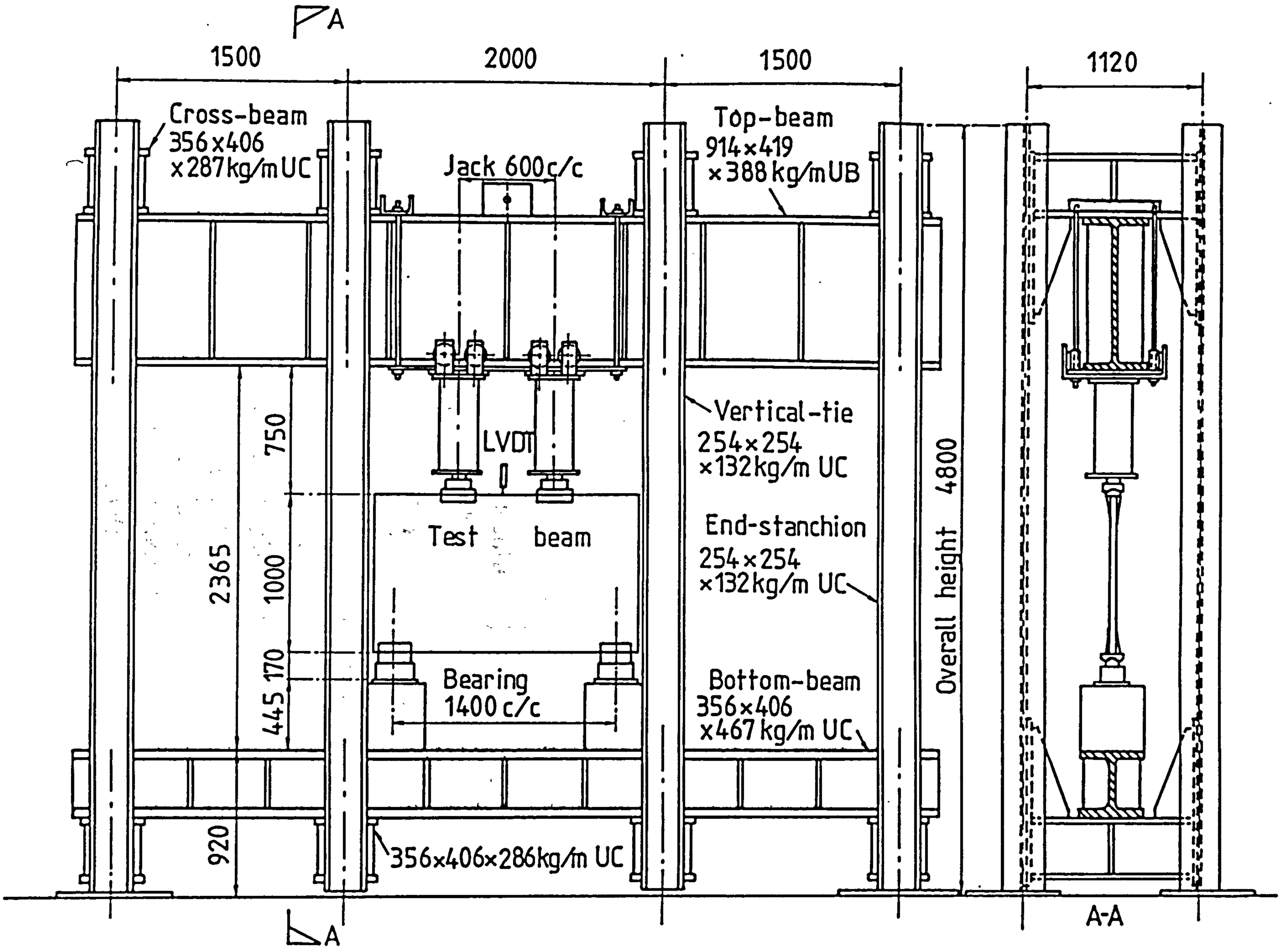

Figure 4.5 : General arrangement of the test rig

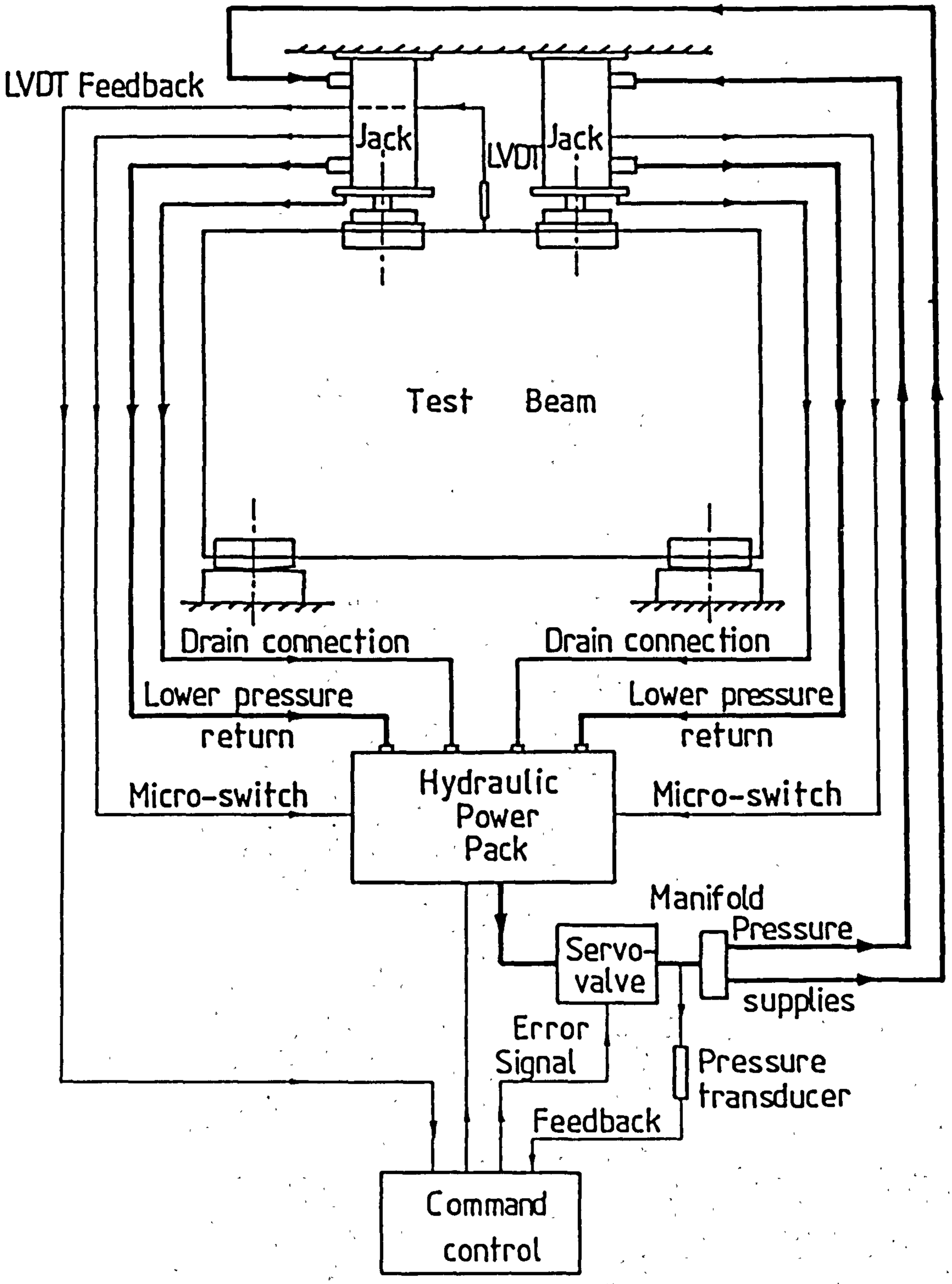

Figure 4.6 : The servo-hydraulic jacking system

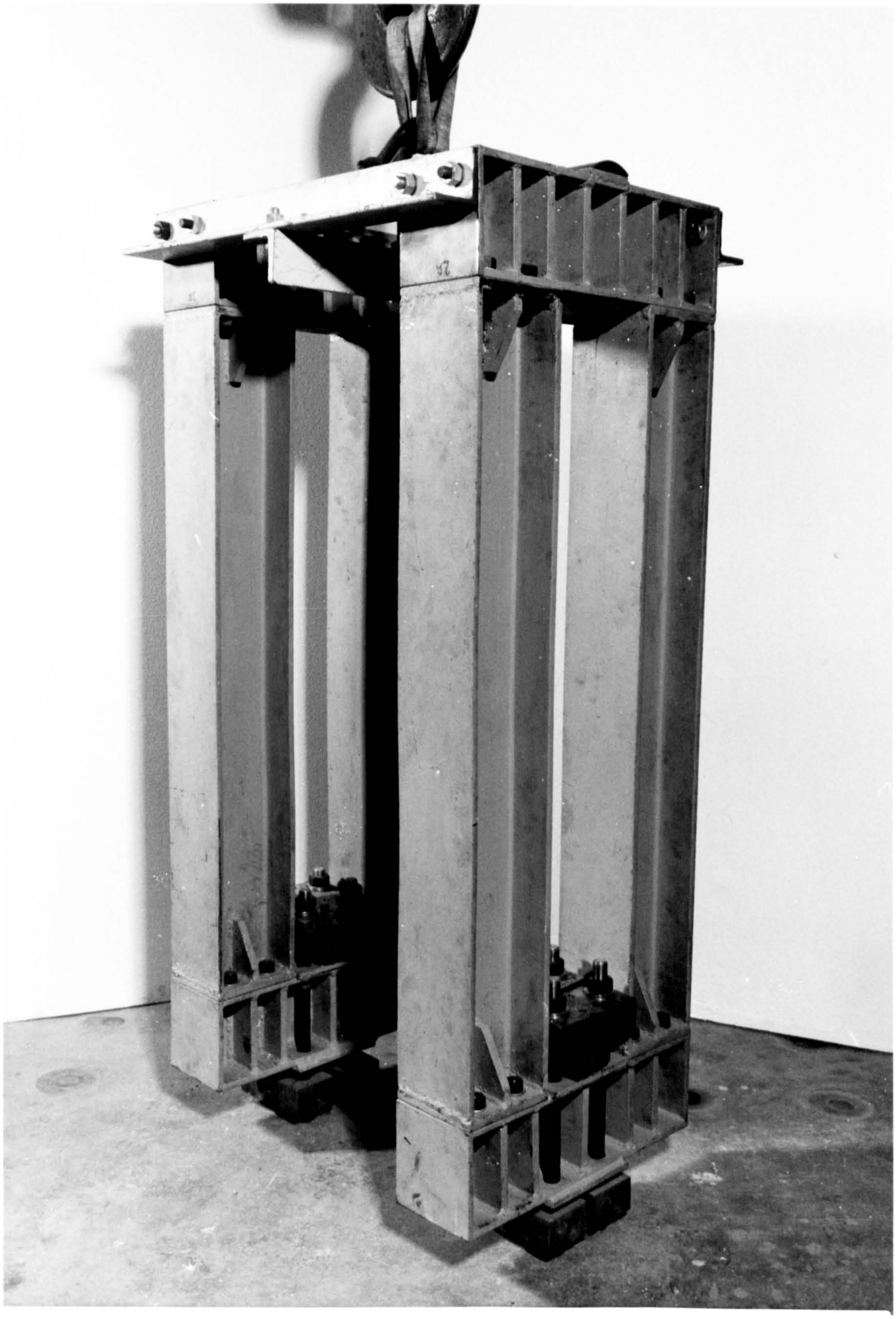

Figure 4.7 : The combined top and bottom loading system

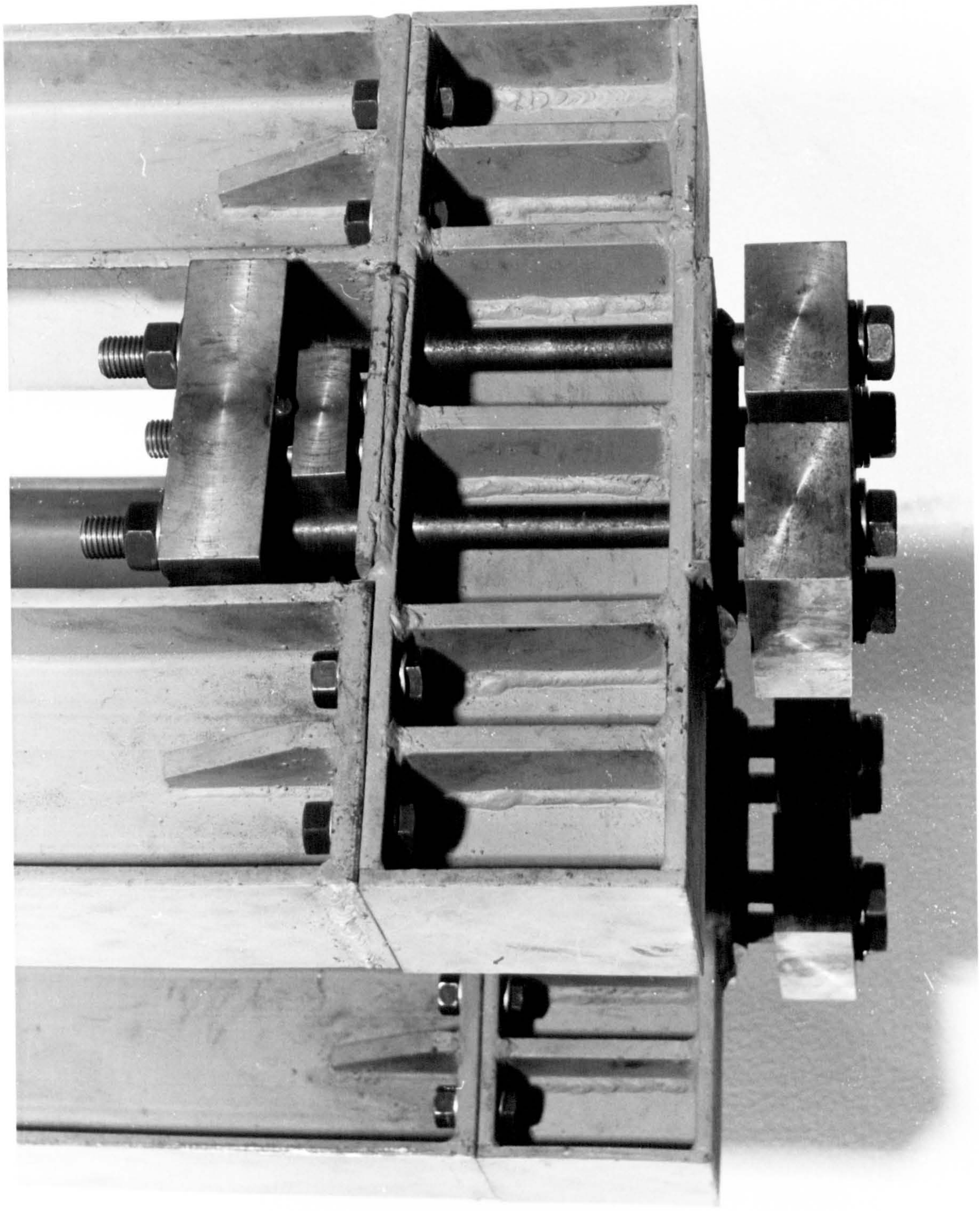

Figure 4.8 : Bottom yoke set up (CB-Series tests)

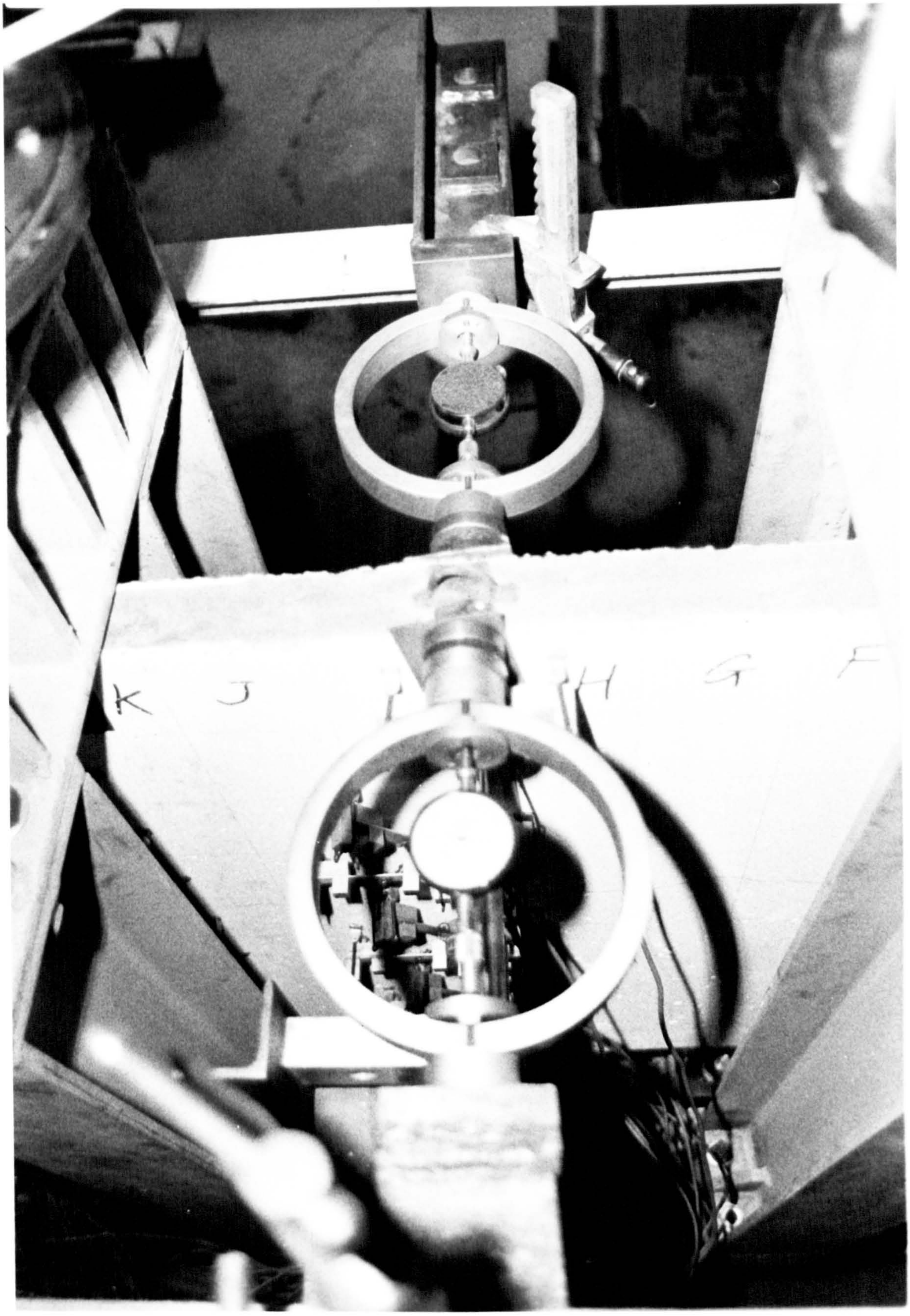

Figure 4.9 : Proving rings set up (CB-Series tests)

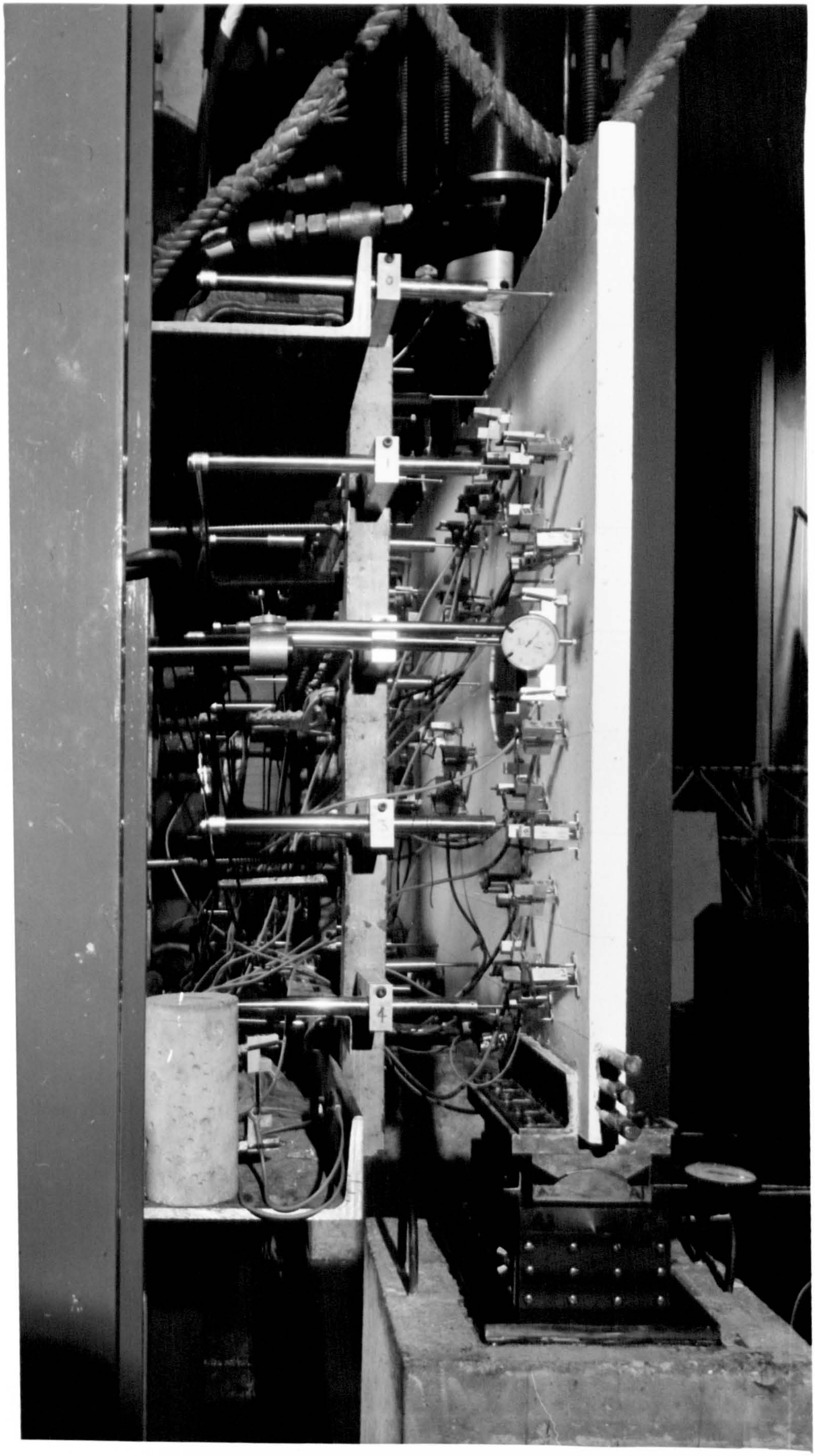

Figure 4.10 : Displacement transducers set up

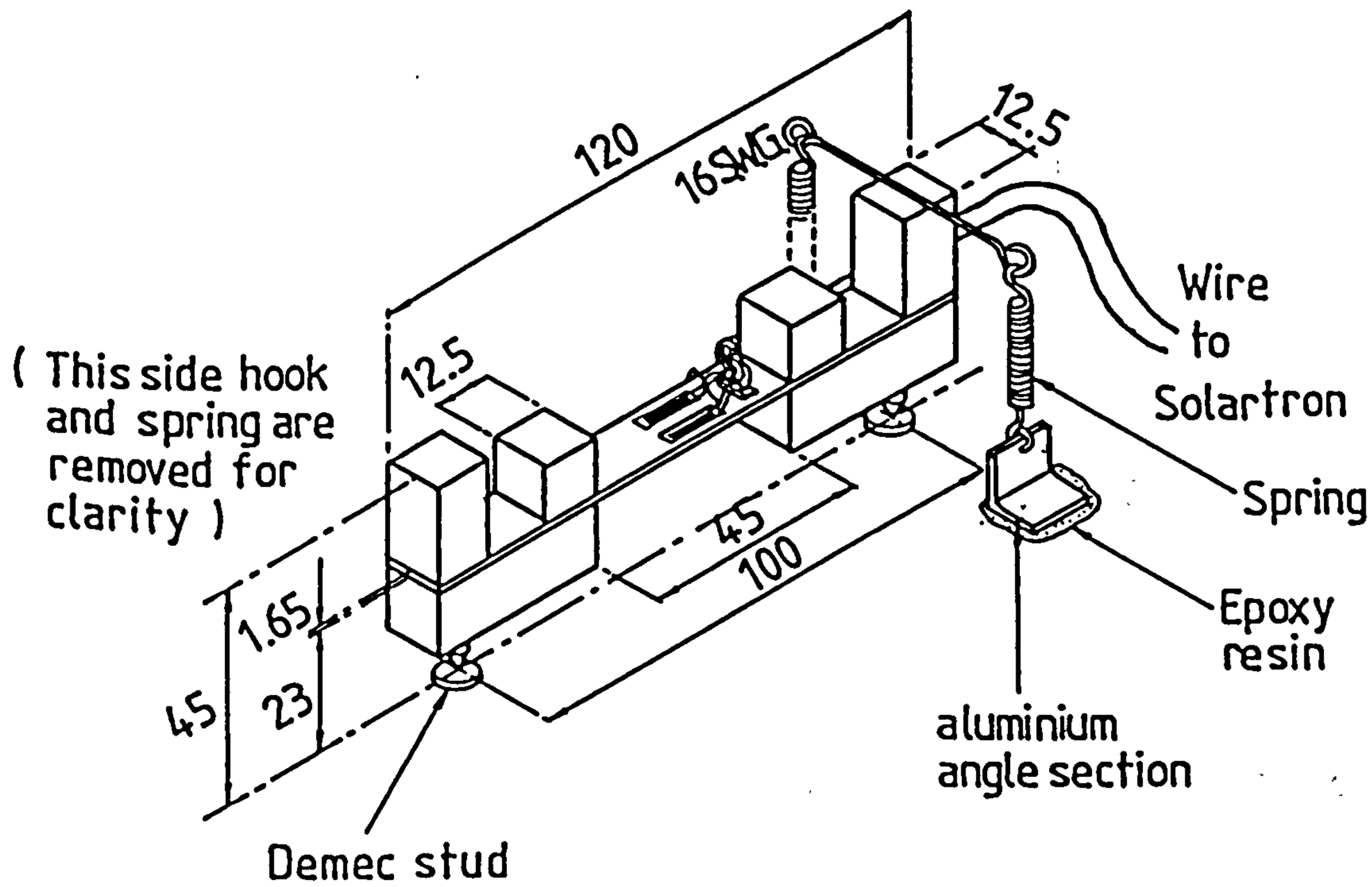

Figure 4.11 : Details of the electrical demountable strain transducers

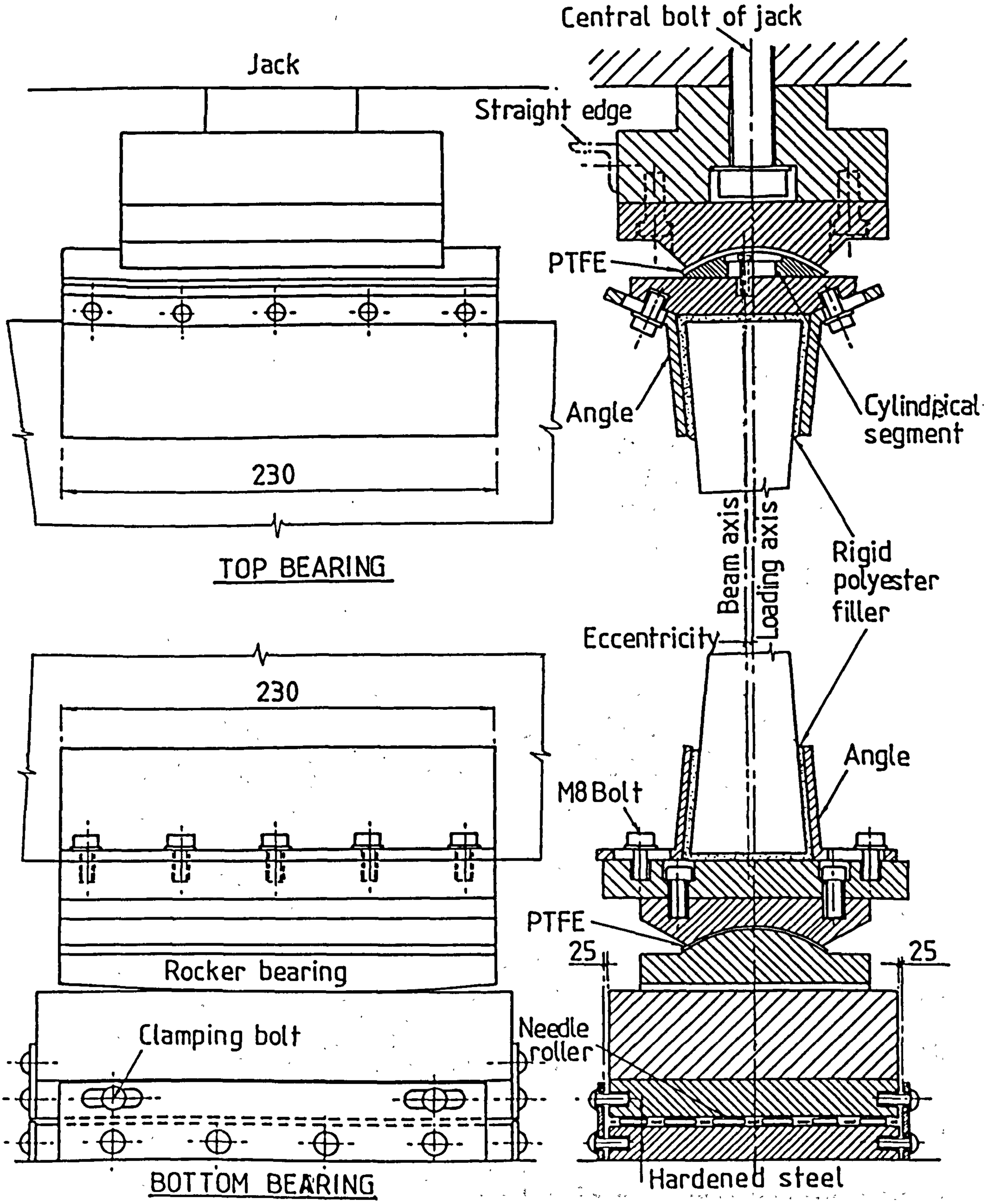

Figure 4.12 : Top and bottom bearings

Figure 5.1 : Overall view of the buckling test set up

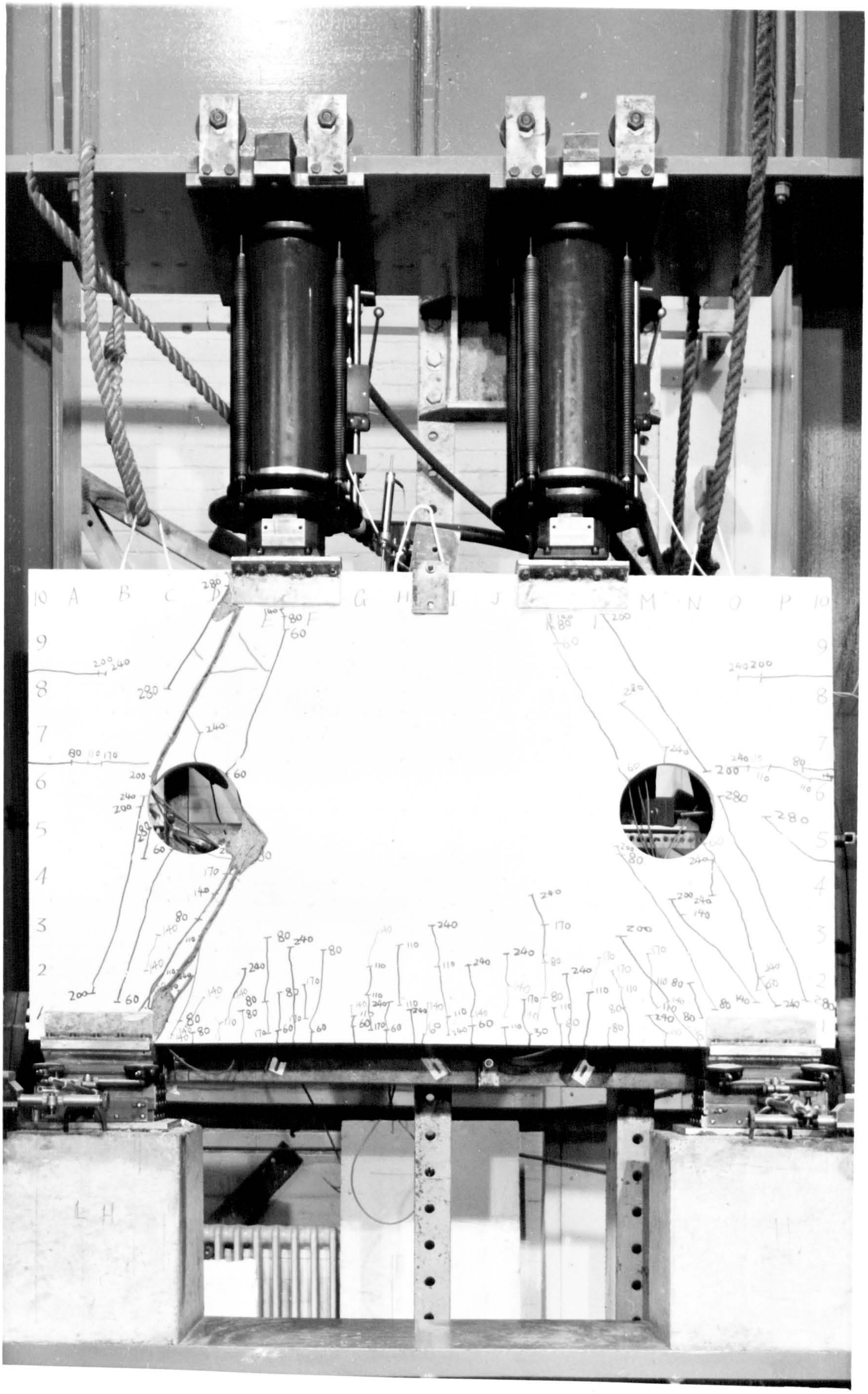

Figure 5.2 : Deep beam with circular web-openings (W-Series tests)

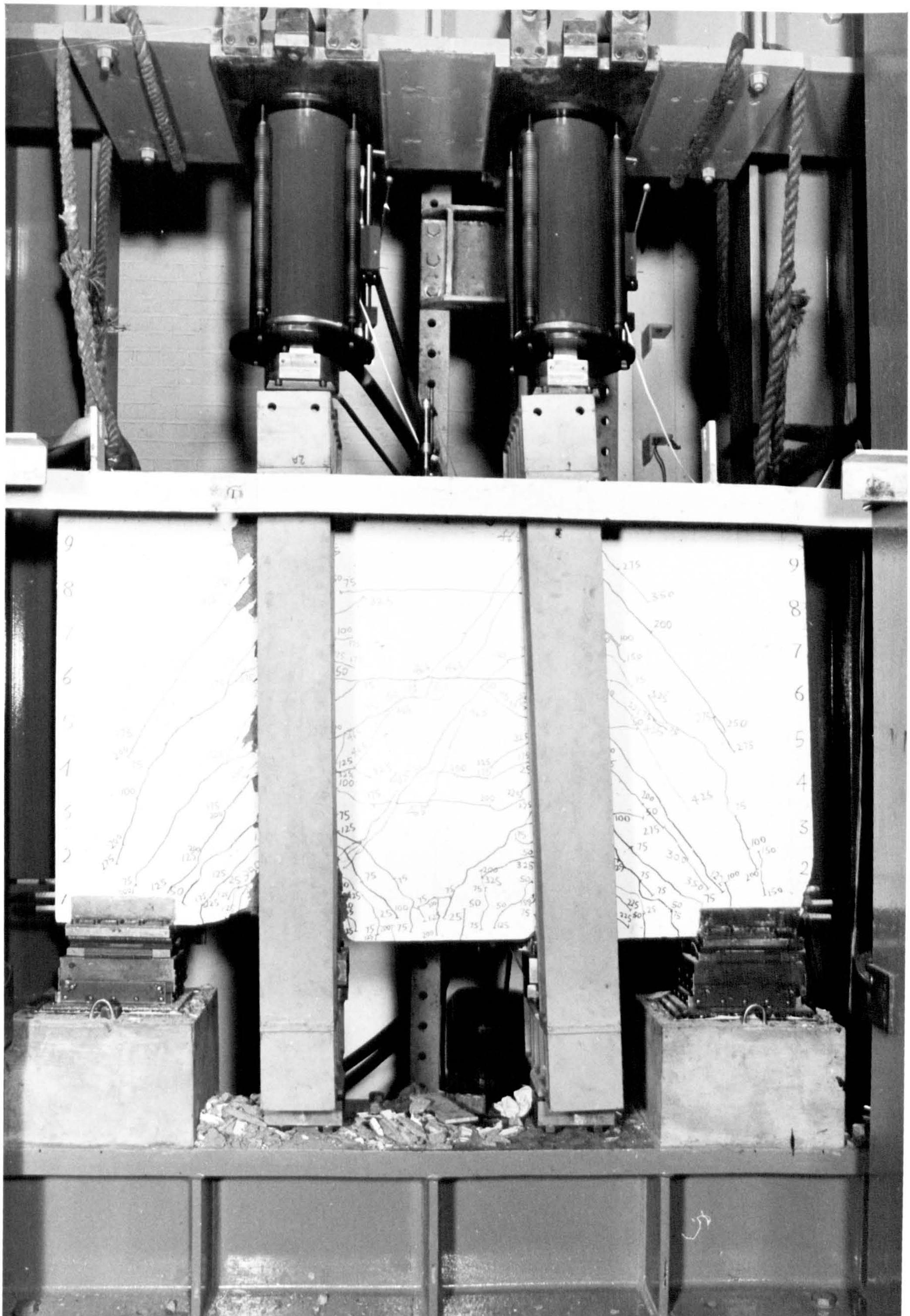

Figure 5.3 : Test set up of the CB-Series beams

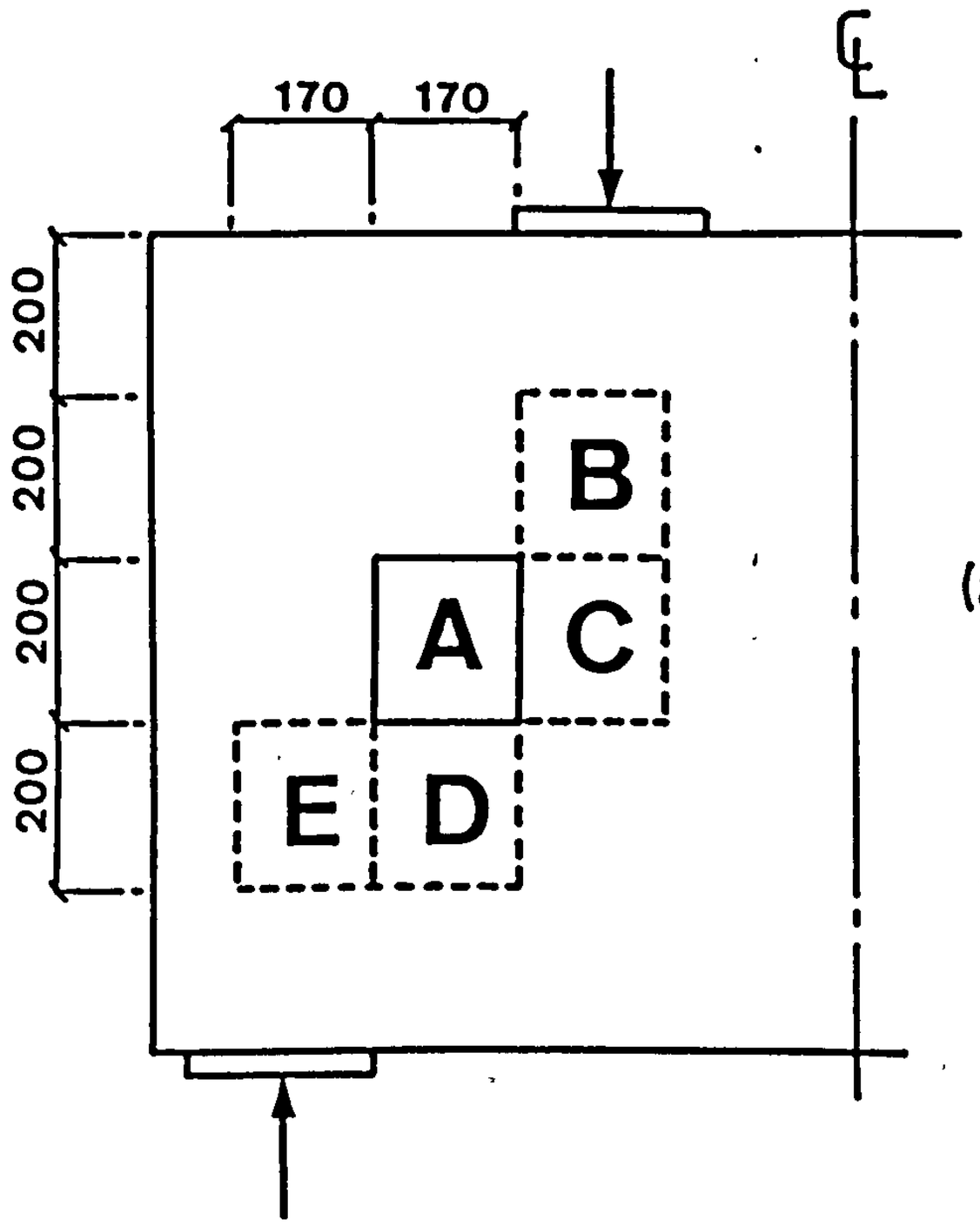

(a) rectangular web-openings

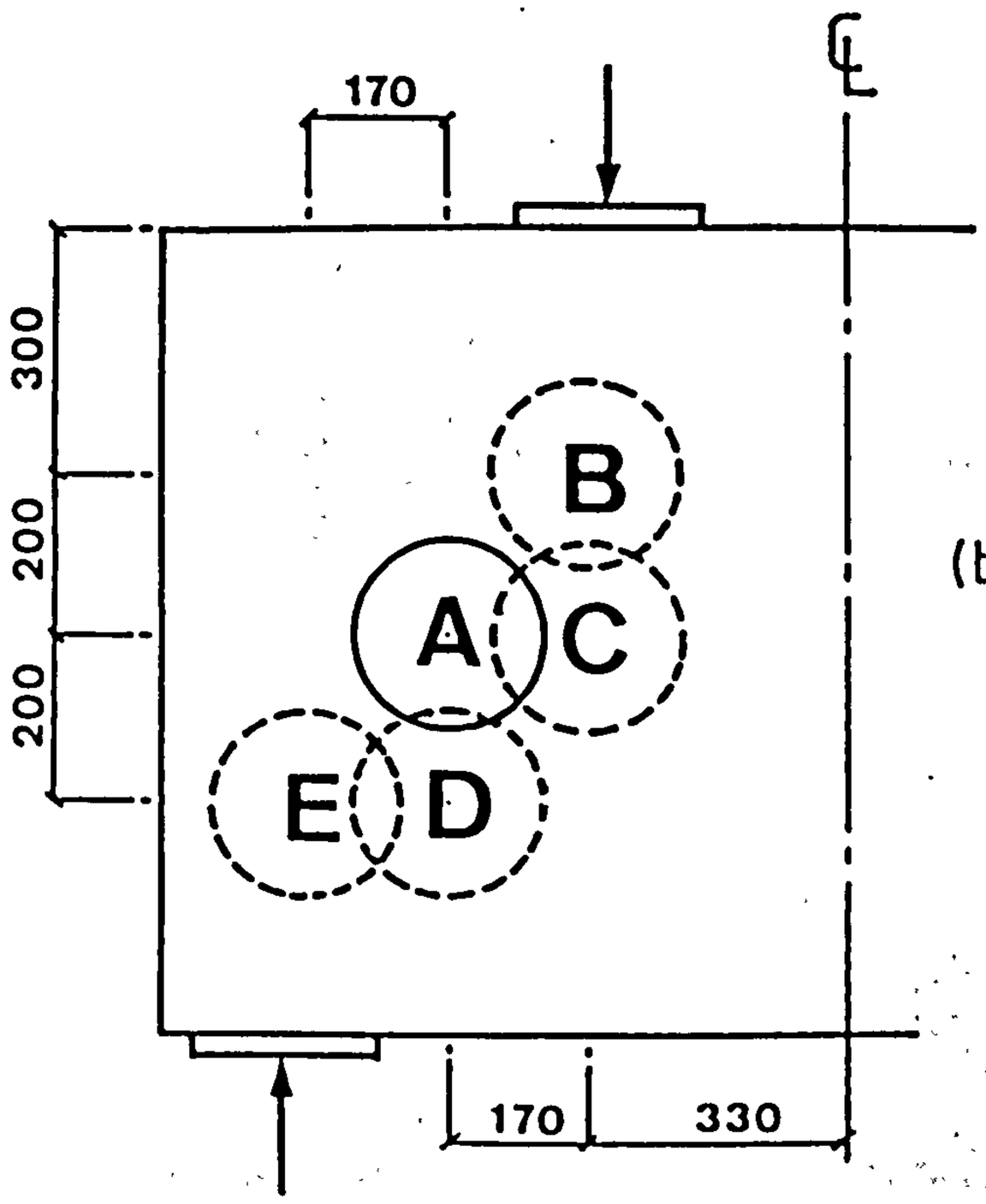

(b) circular web-openings

Figure 5.4 : Positions of the web-openings in the W-Series beams

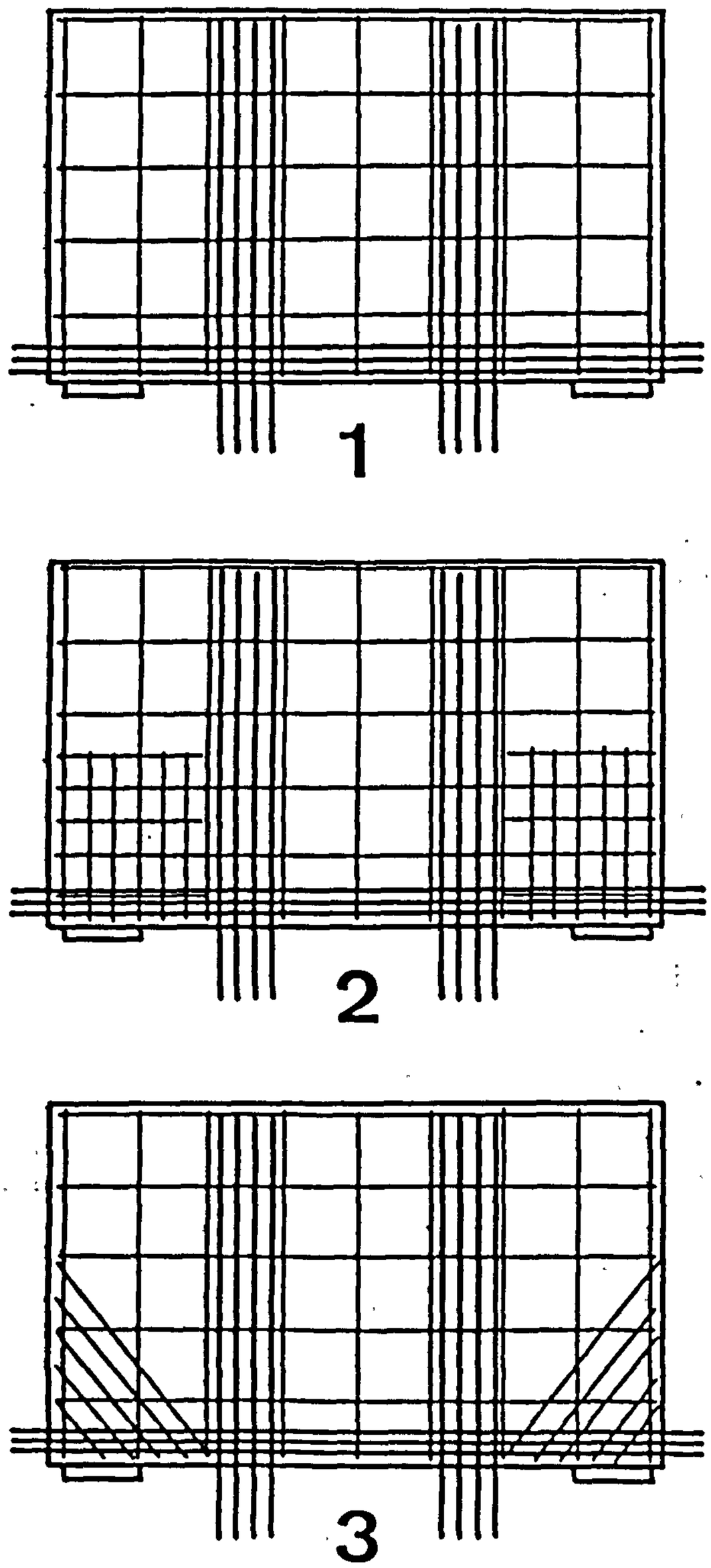

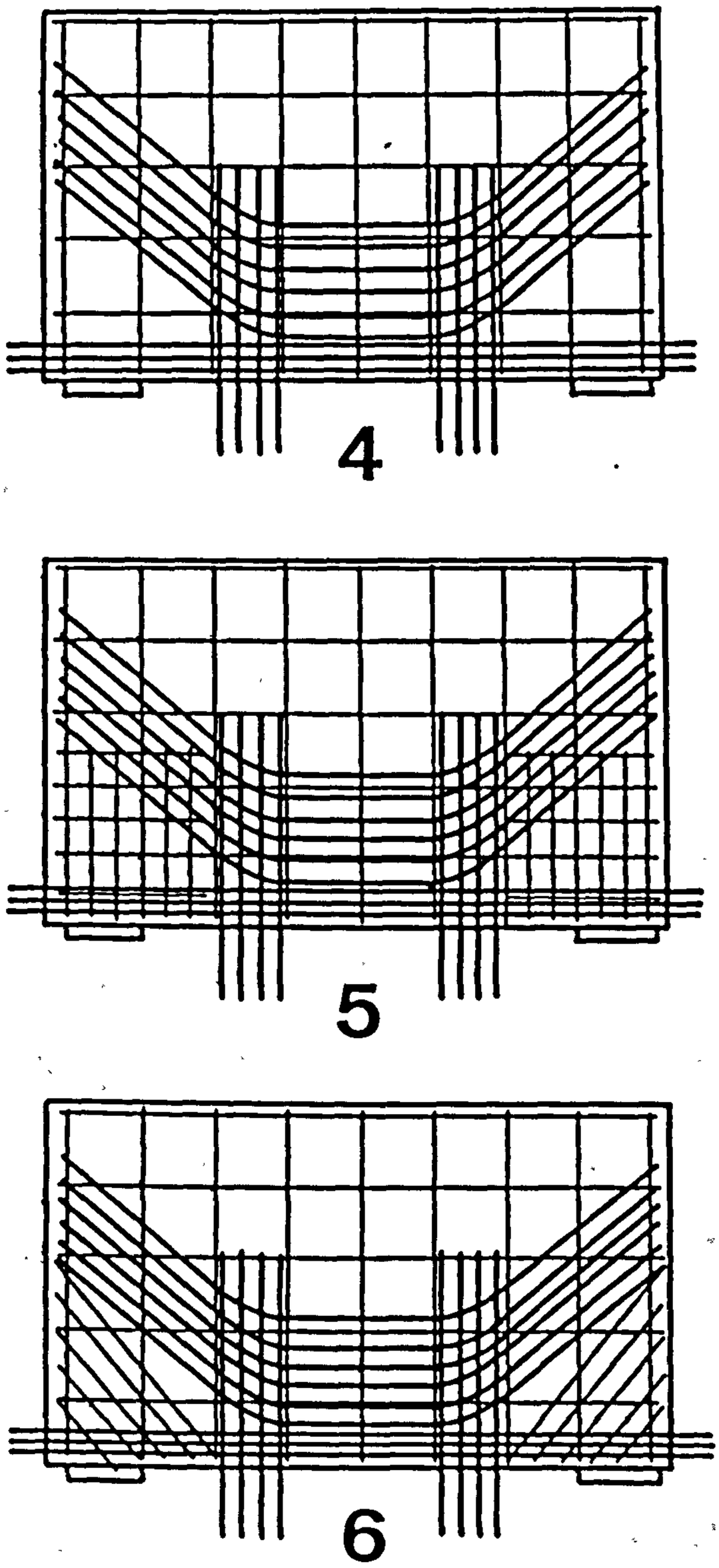

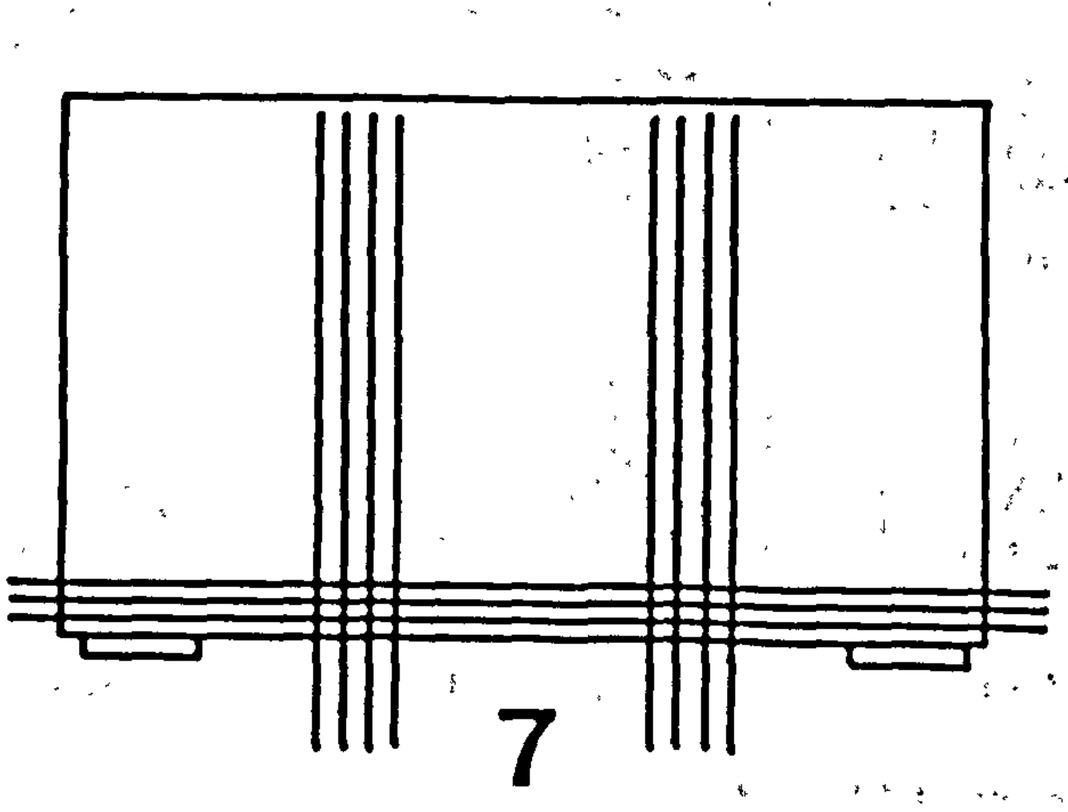

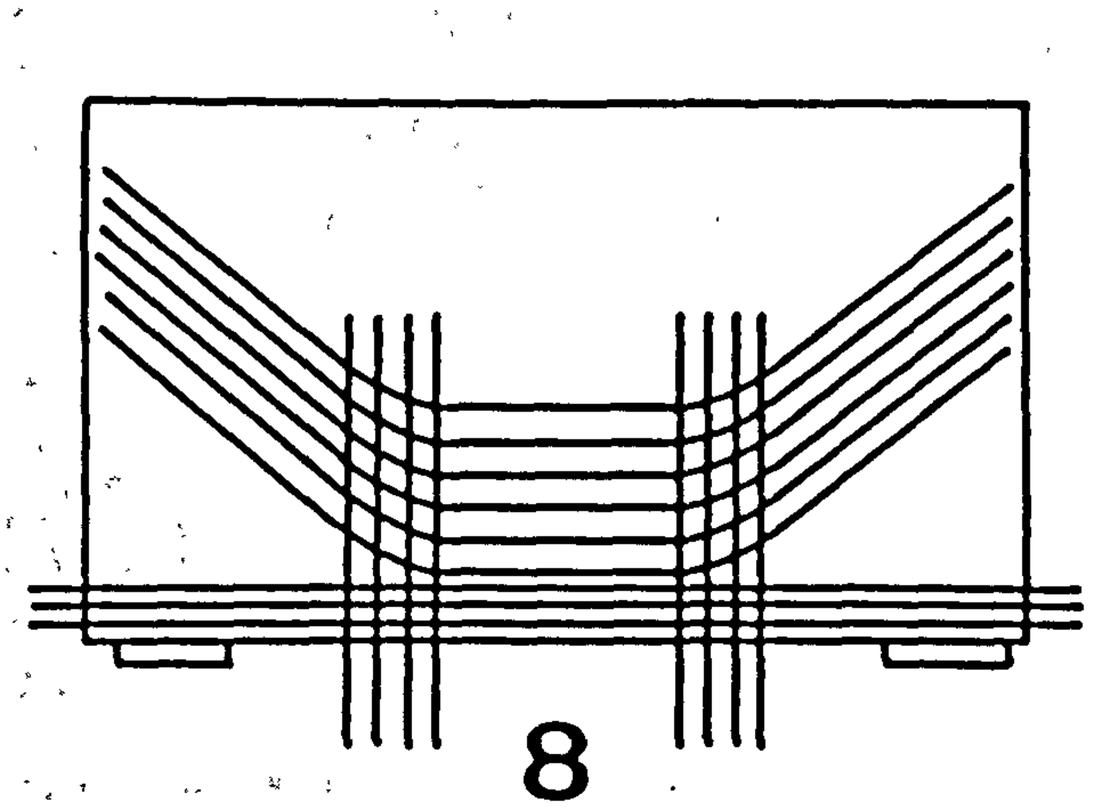

Figure 5.5 : Steel arrangements in the CB-Series beams

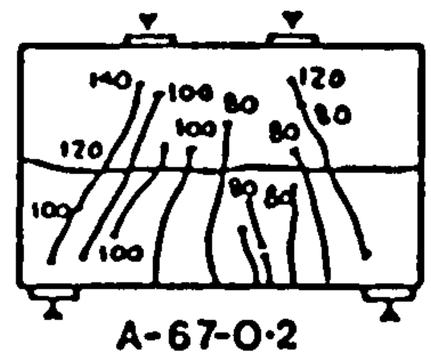
A-67-0·2

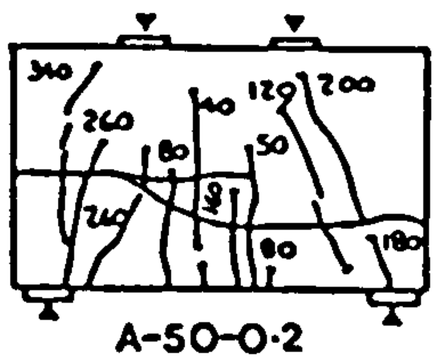
A-50-0·2

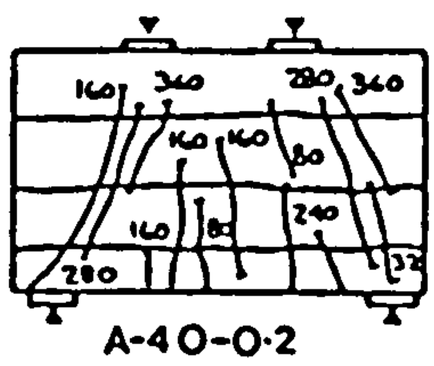
A-40-0·2

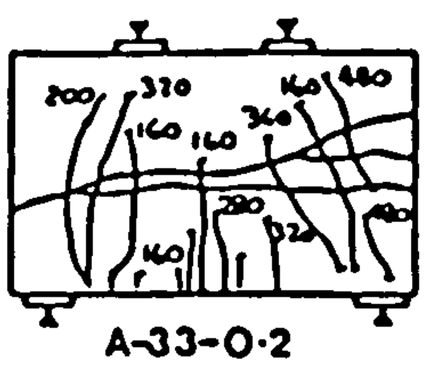
A-33-0·2

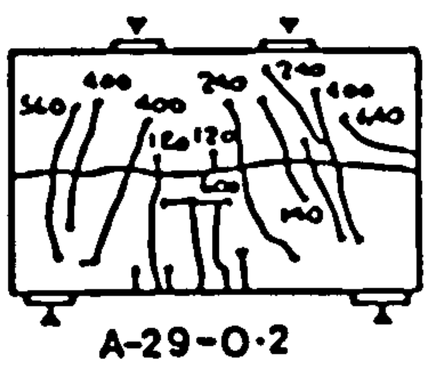
A-29-0·2

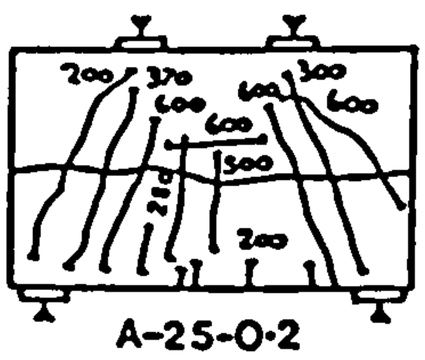
A-25-0·2

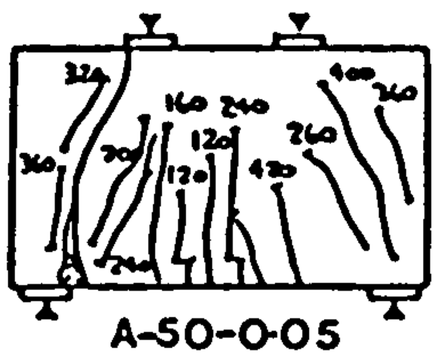
A-50-0·05

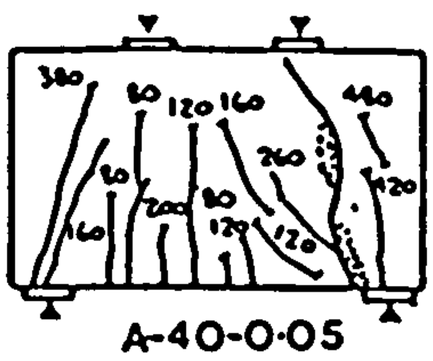
A-40-0·05

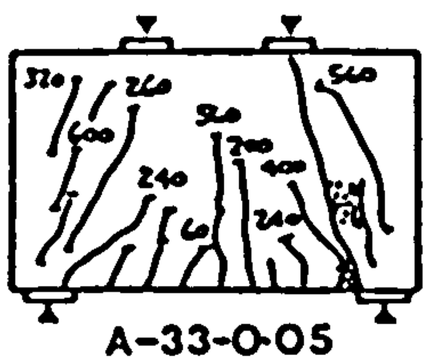
A-33-0·05

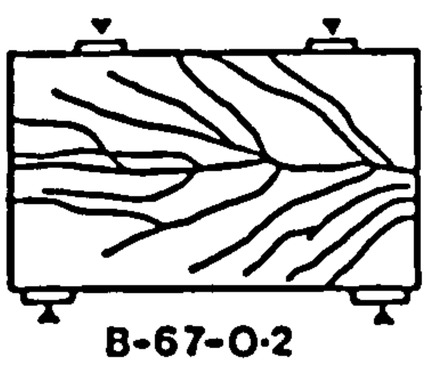
B-67-0·2

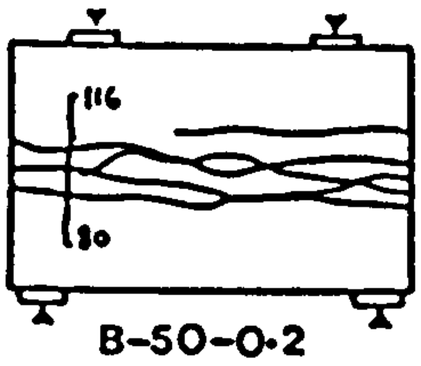
B-50-0·2

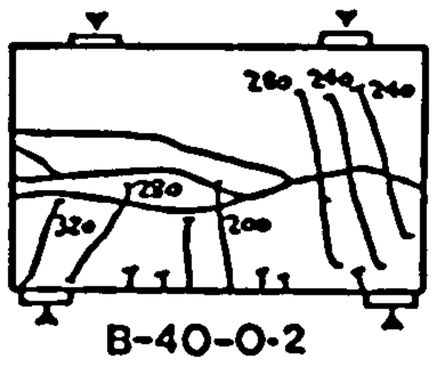
B-40-0·2

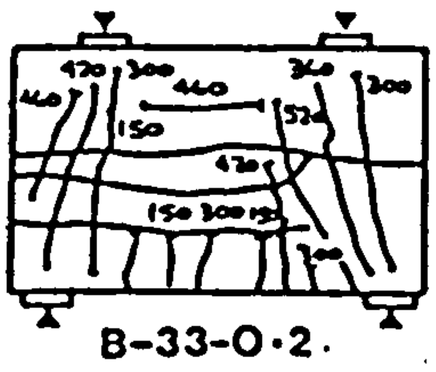
B-33-0·2

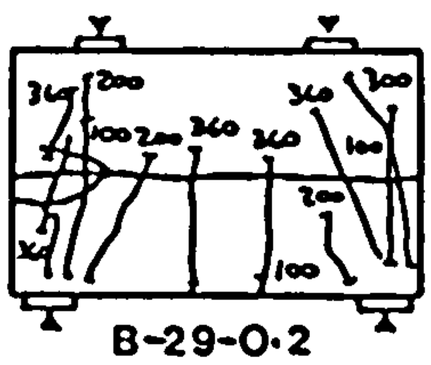
B-29-0·2

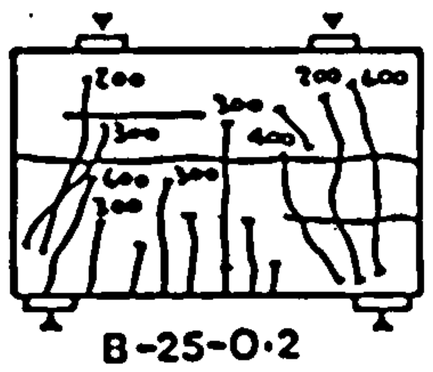
B-25-0·2

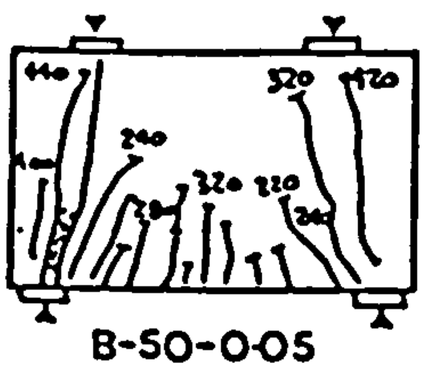
B-50-0·05

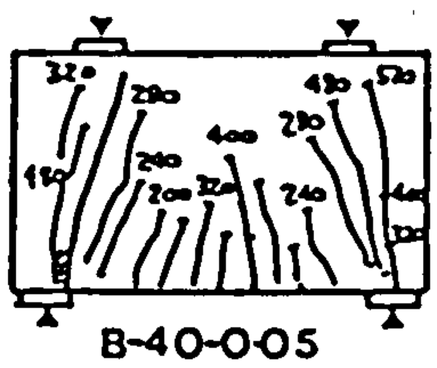
B-40-0·05

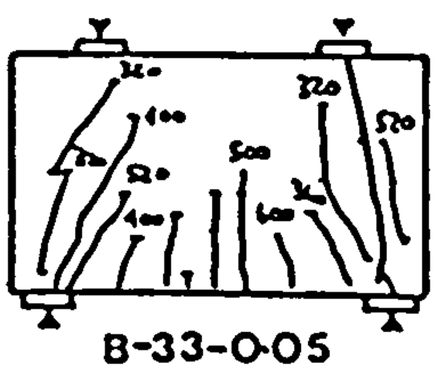
B-33-0·05

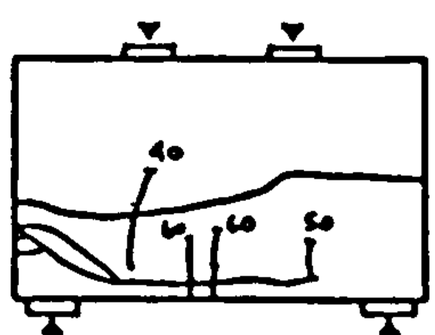
C-67-0·1

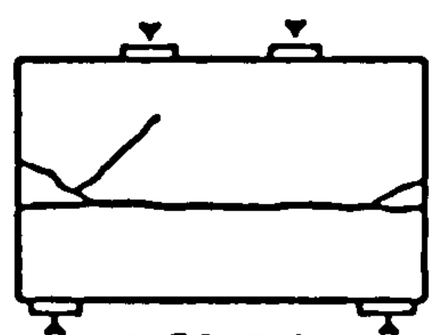
C-50-0·1

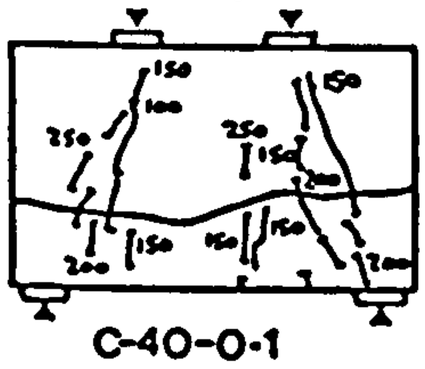
C-40-0·1

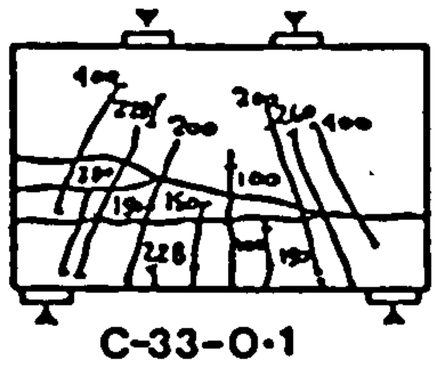
C-33-0·1

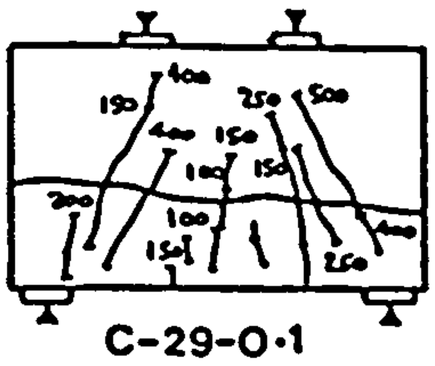
C-29-0·1

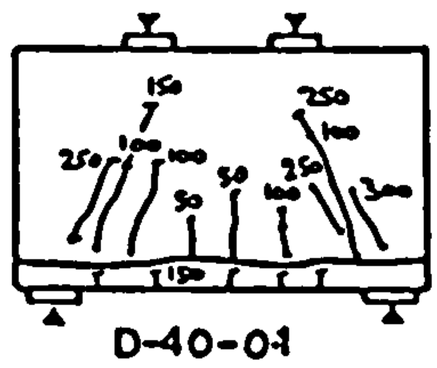
D-40-0·1

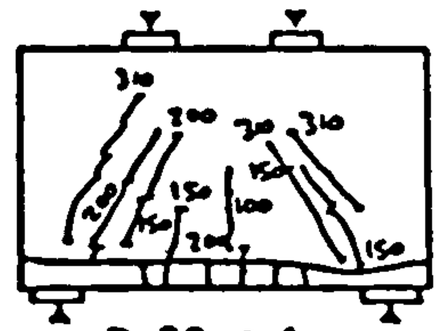
D-33-0·1

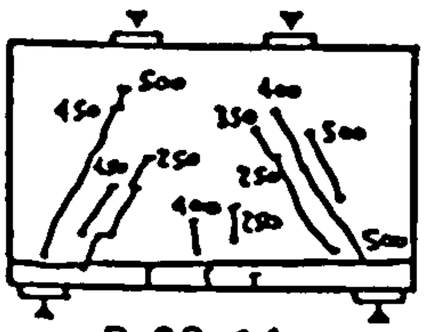
D-29-0·1

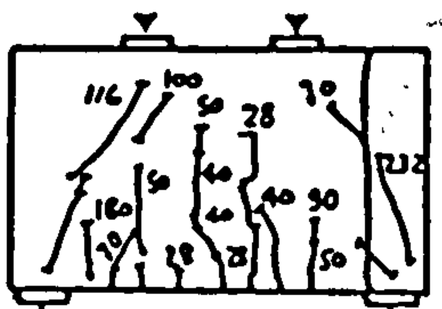
E-67-0·1

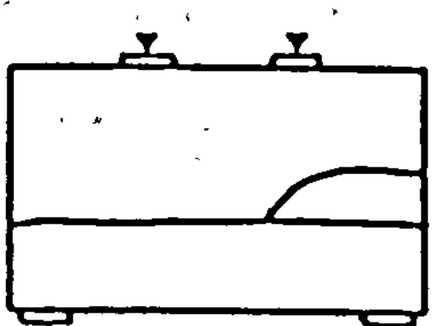
E-50-0·1

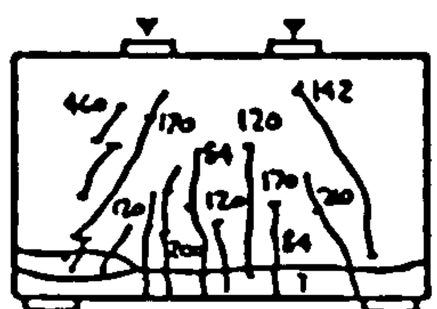
E-40-0·1

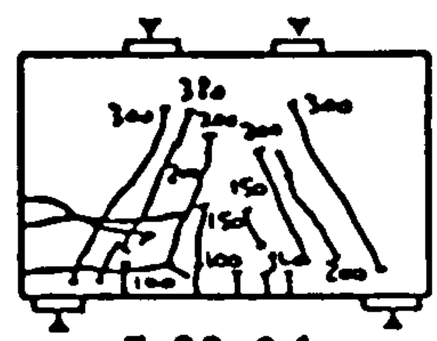
E-33-0·1

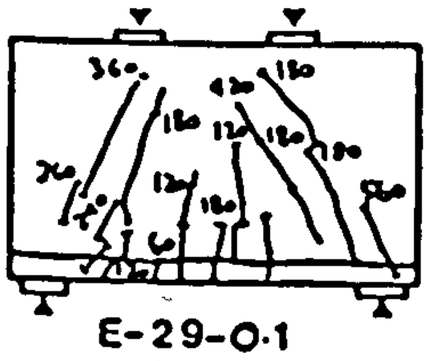
E-29-0·1

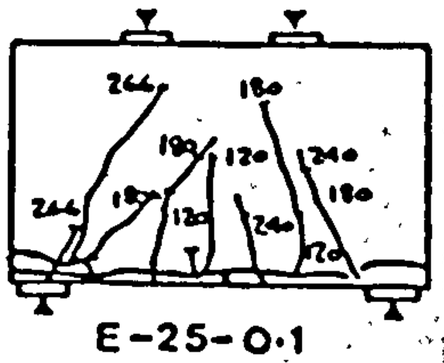
E-25-0·1

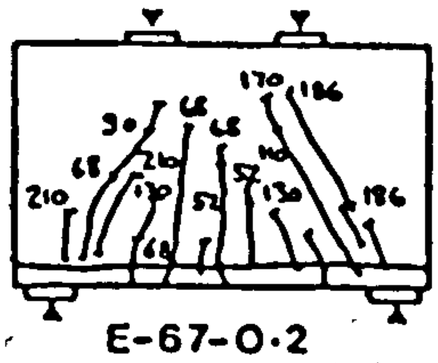
E-67-0·2

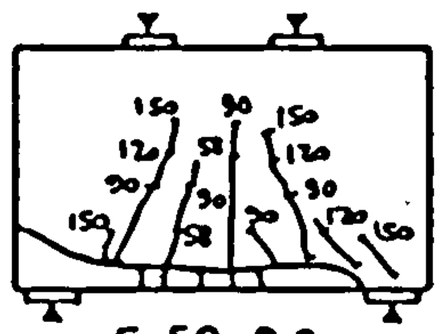
E-50-0·2

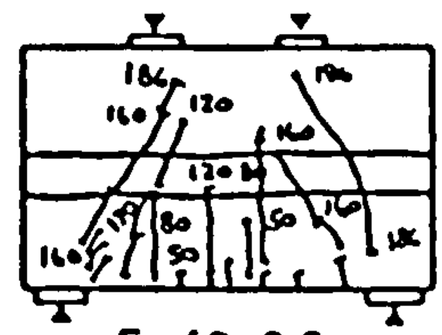
E-40-0·2

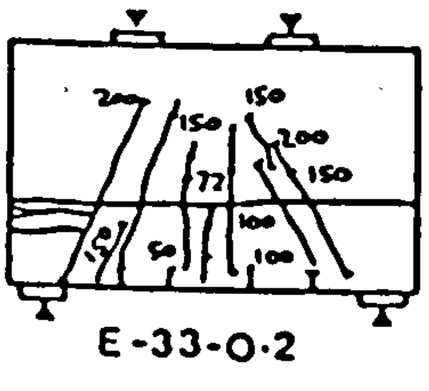
E-33-0·2

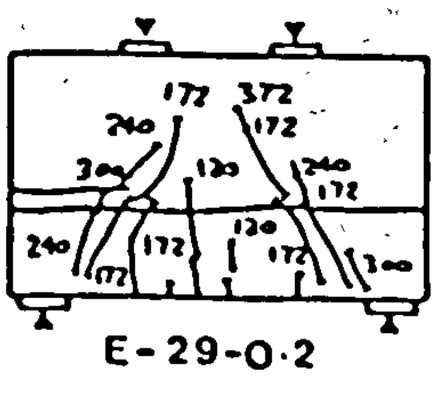
E-29-0·2

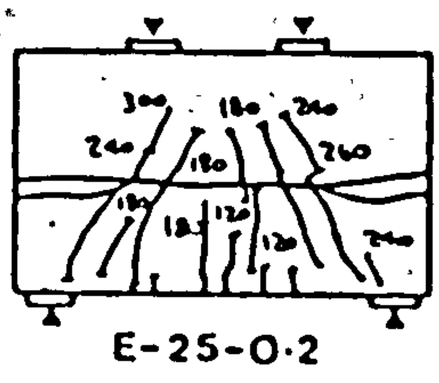
E-25-0·2

Figure 6.1 : Crack patterns at failure (A to E Series beams)

(shows also load in kN at which each crack was first observed and the extent of the crack at that load; Beam notation as in Table 4.1, [Kong et al, 1986b])

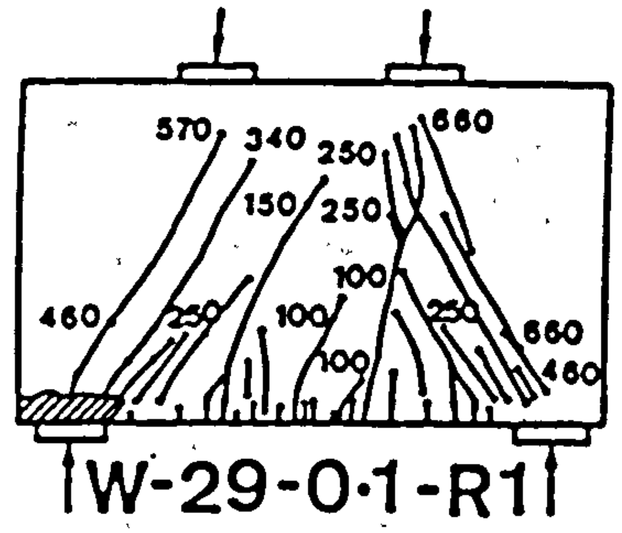

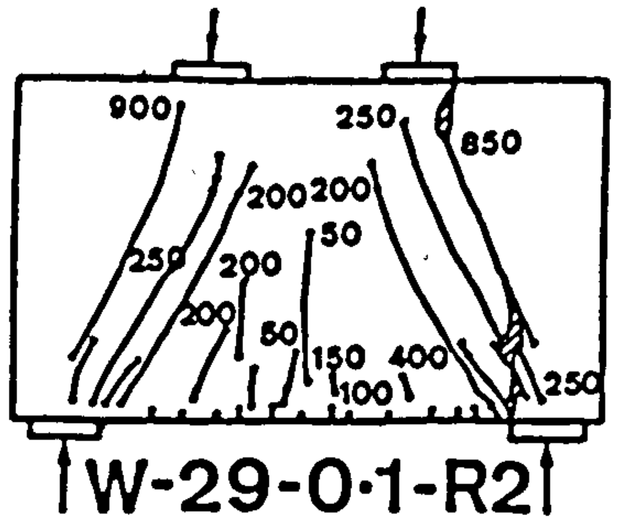

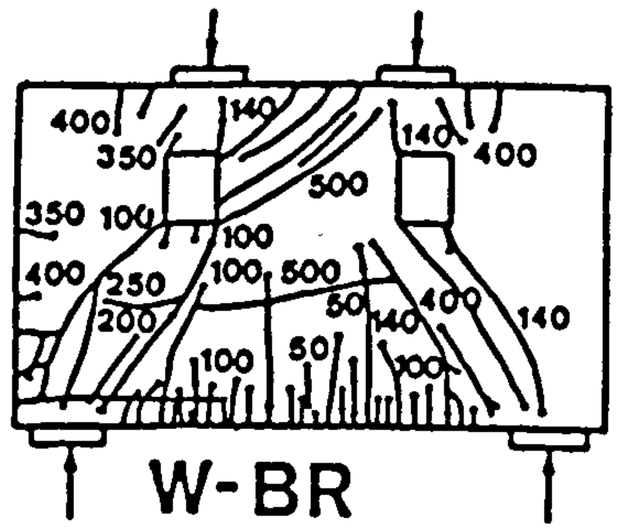

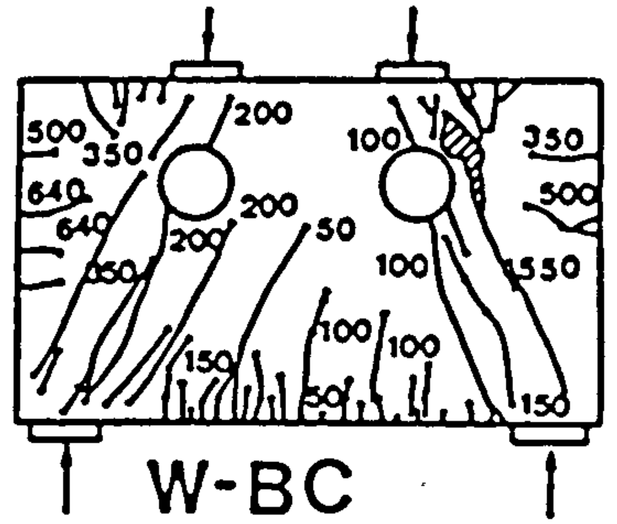

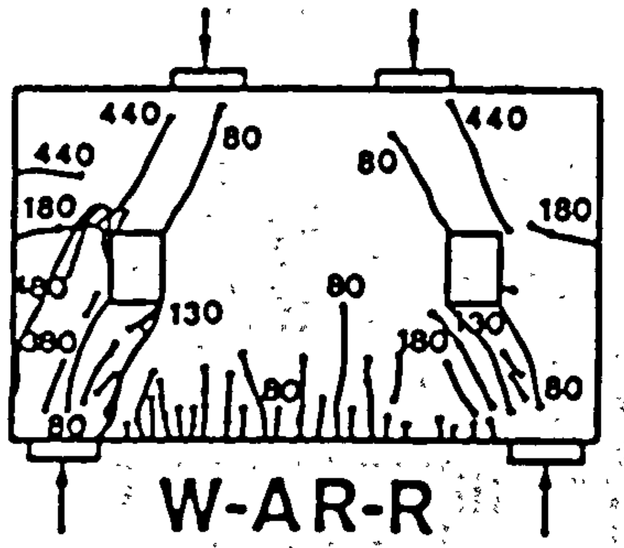

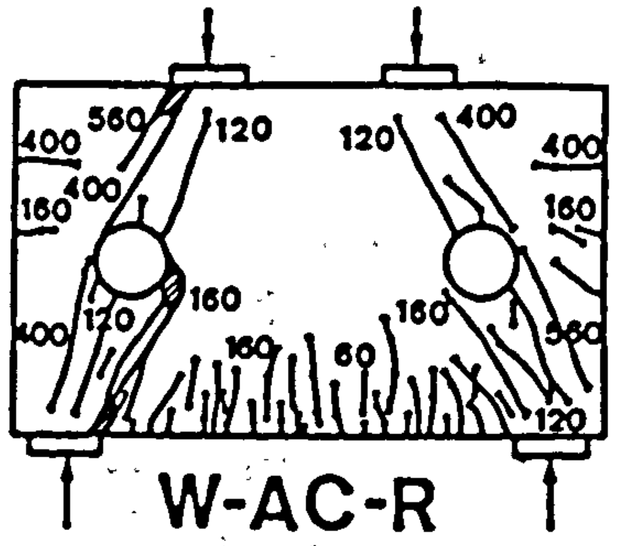

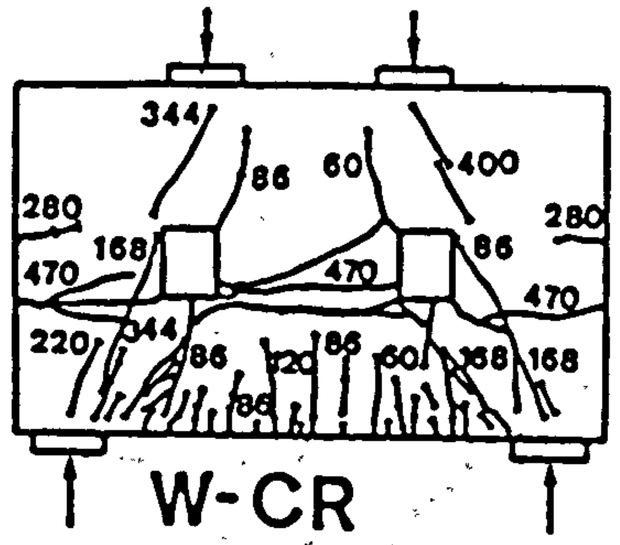

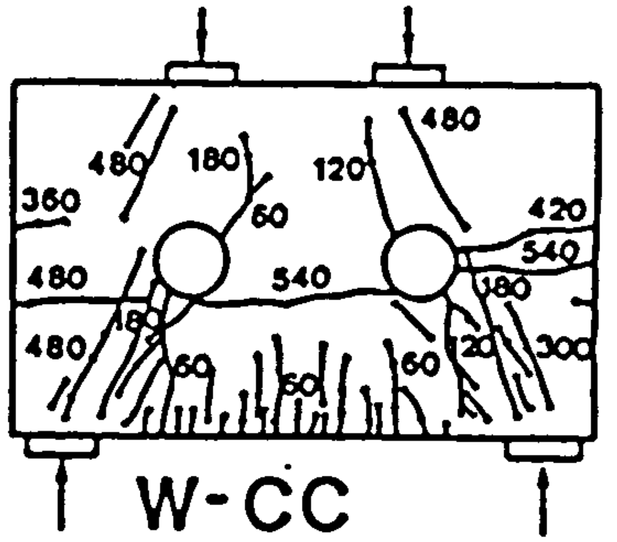

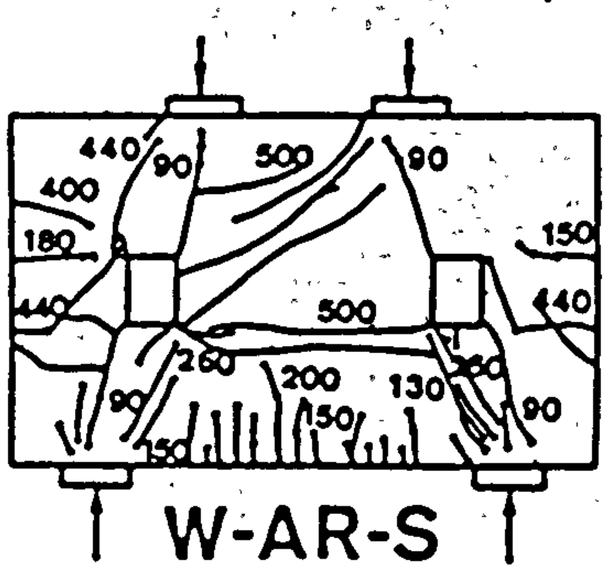

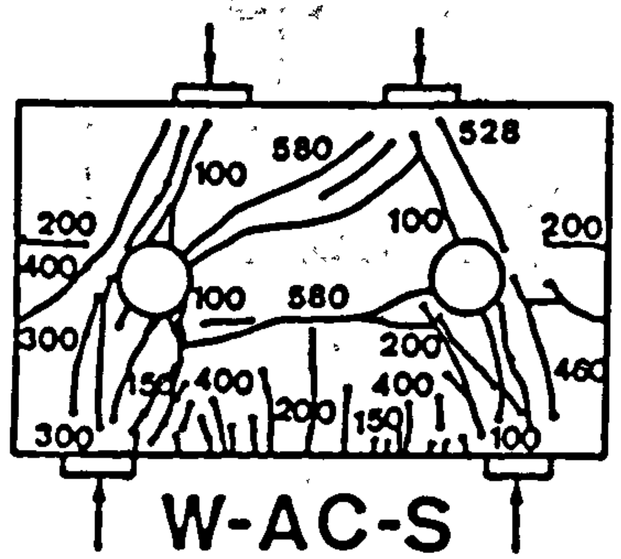

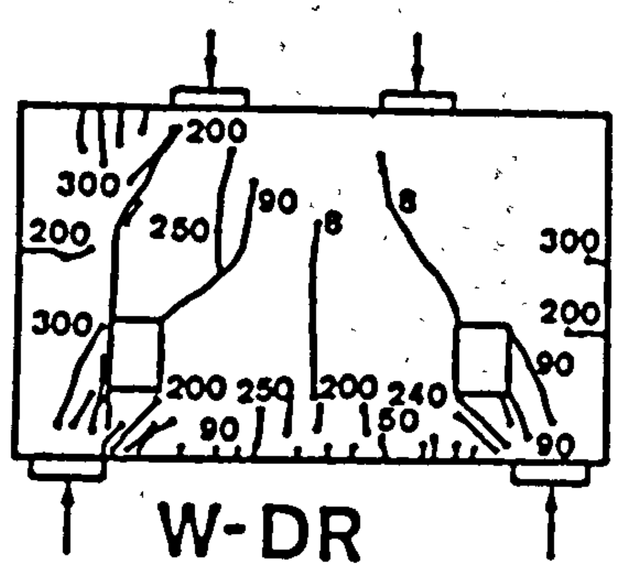

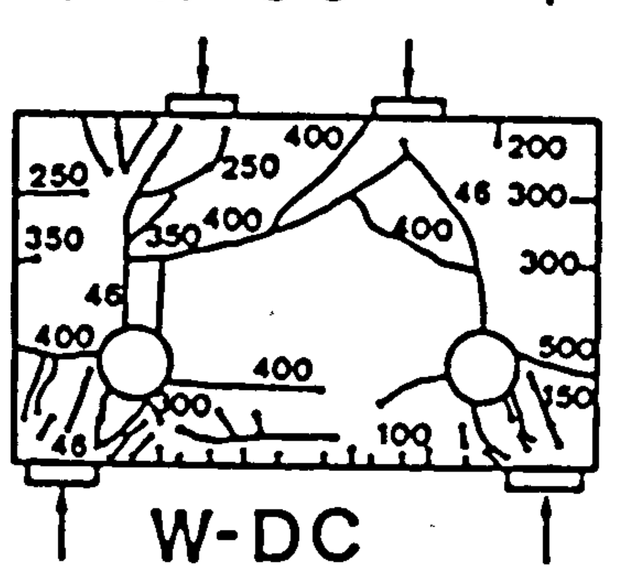

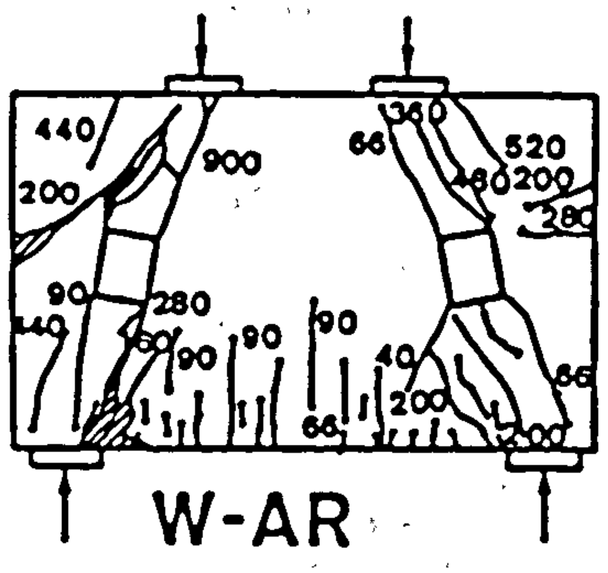

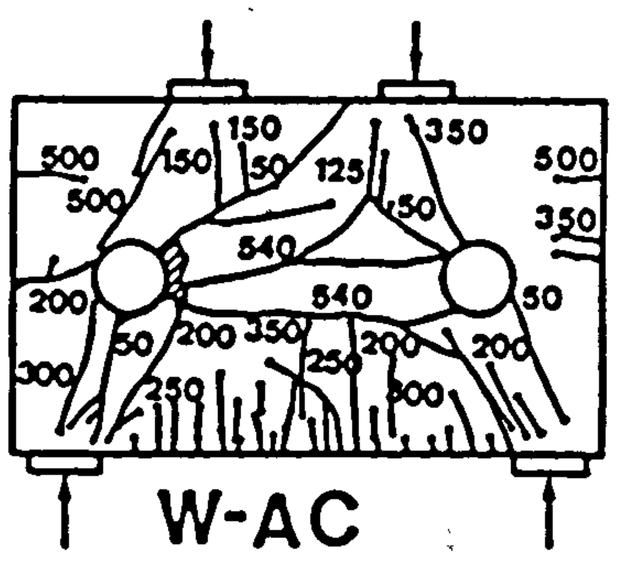

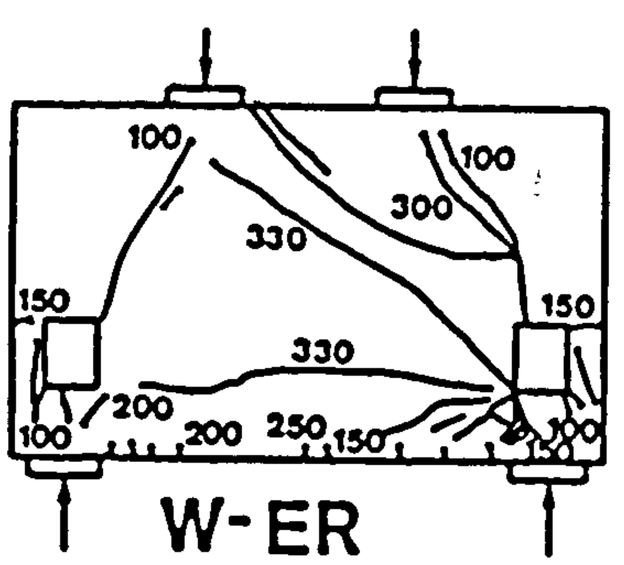

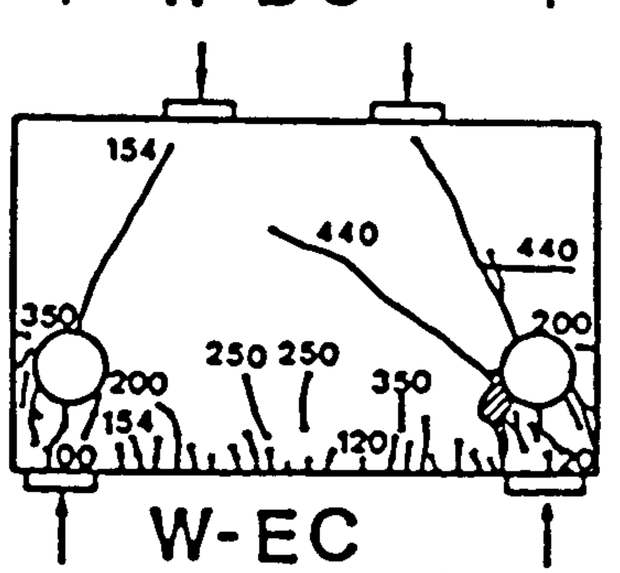

Figure 6.2 : Crack patterns at failure (W-Series beams)

(shows also load in kN at which each crack was first observed and the extent of the crack at that load; Beam notation as in Table 4.2)

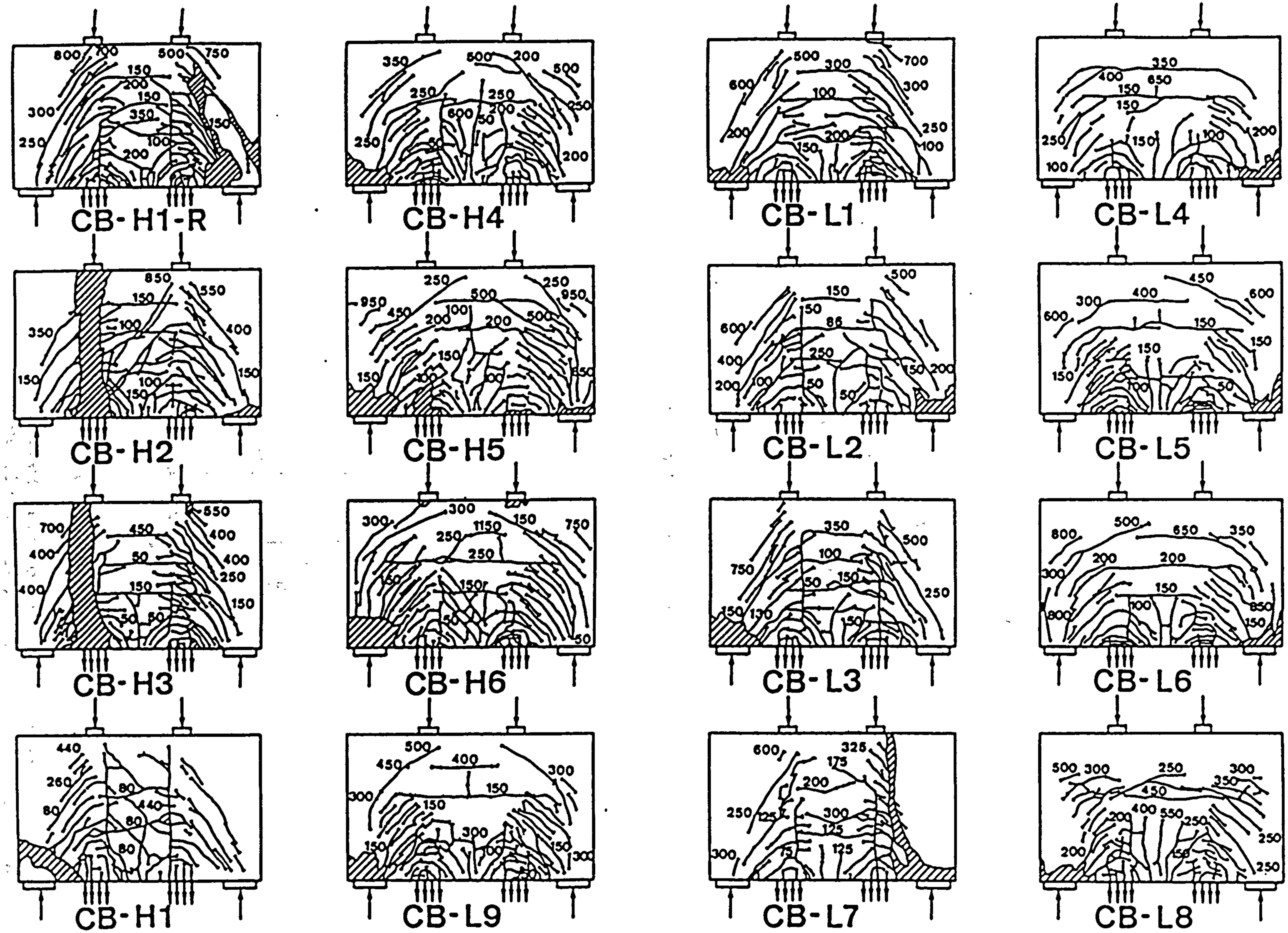

Figure 6.3 : Crack patterns at failure (CB-Series beams)

(shows also load in kN at which each crack was first observed and the extent of the crack at that load; Beam notation as in. Table 4.3)

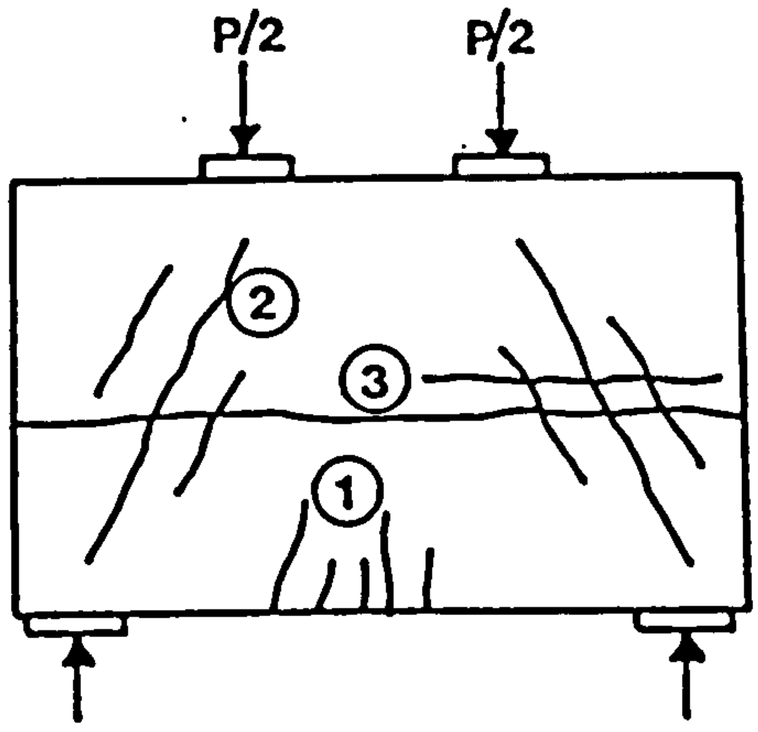

Figure 6.4 : Typical sequence of crack development

(A to E Series beams, [Kong et al, 1986b])

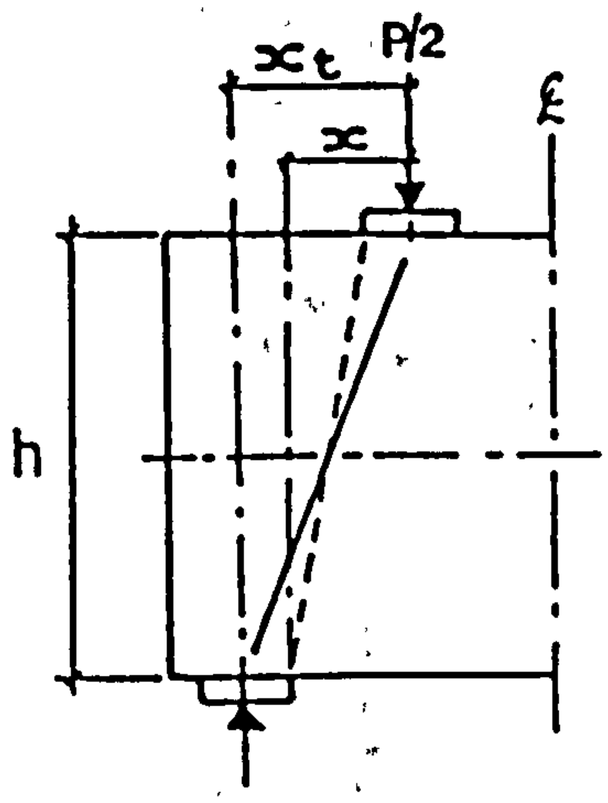

Figure 6.5 : Representation of critical diagonal crack

(dotted line for stocky deep beams; full line for slender deep beams, [Kong et al, 1986b])

Effectiveness of web reinforcement	Mode of failure	
Poor	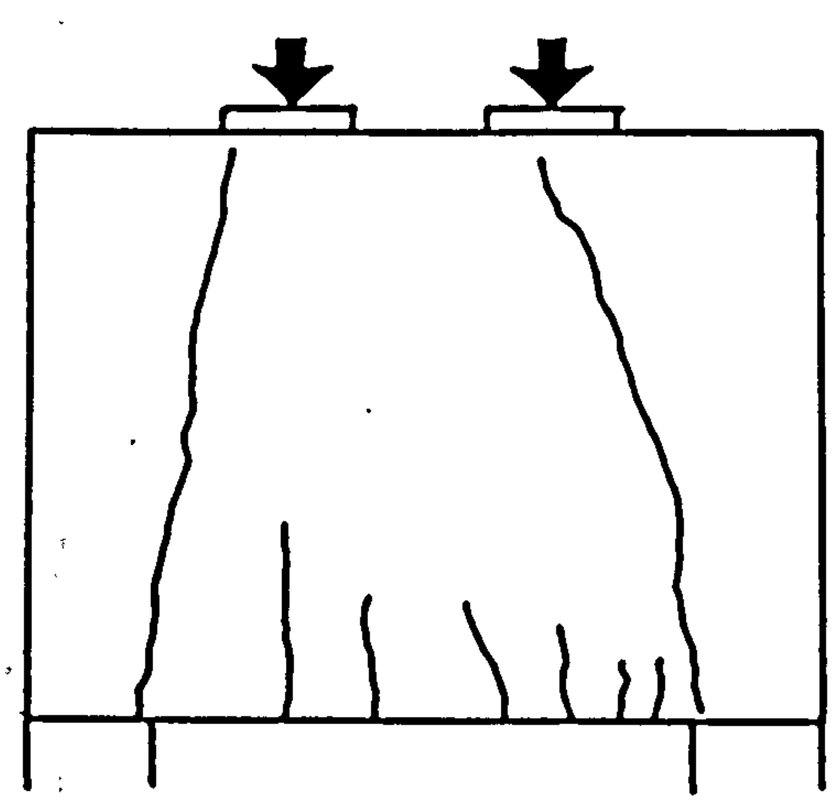	Splitting from top to bottom
Fair	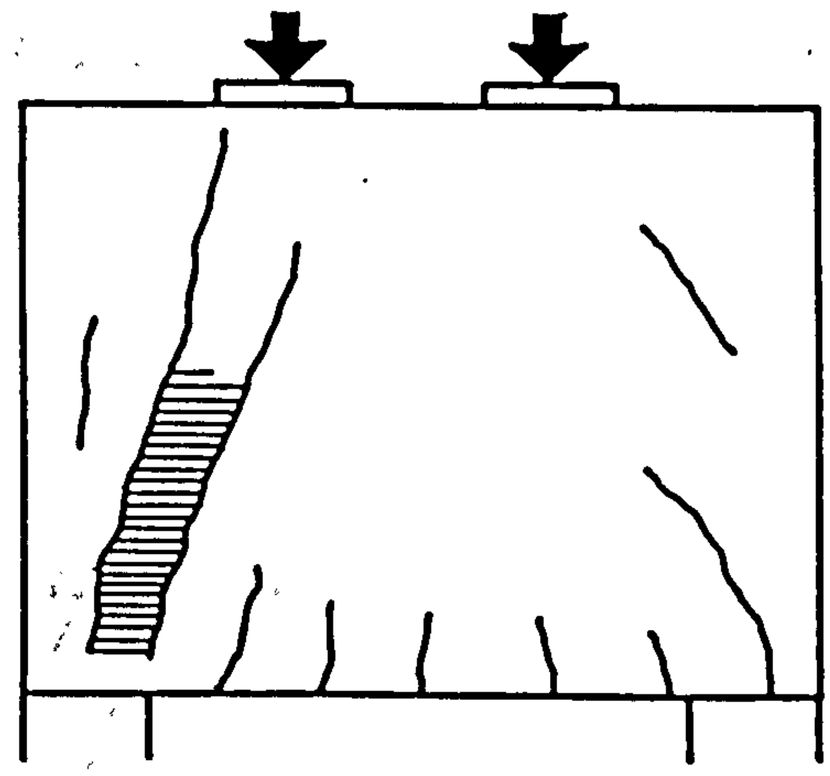	Crushing of strut-like portion
High	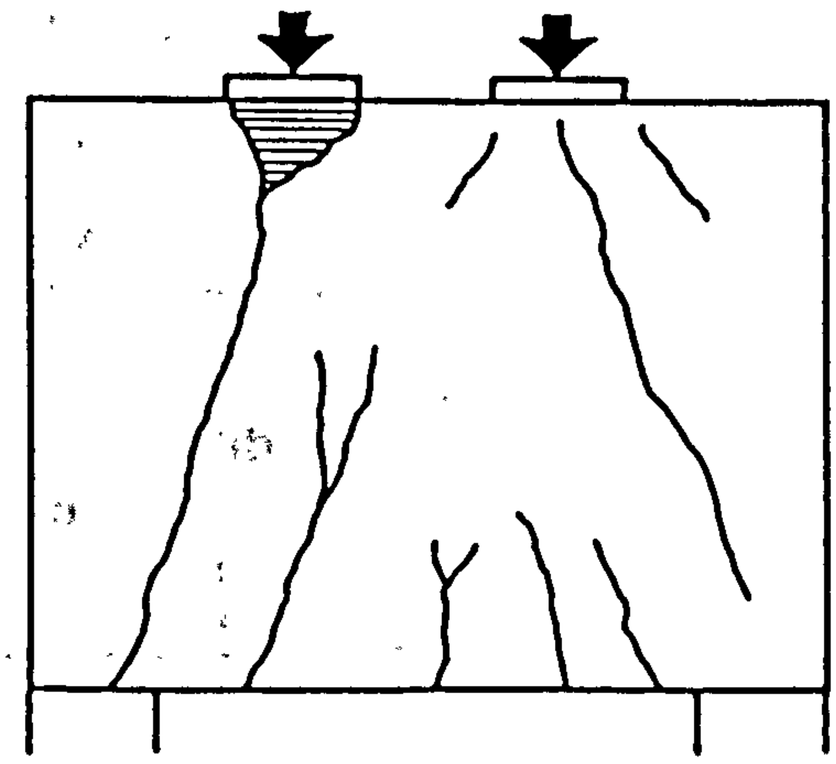	Crushing of bearing

Figure 6.6 : Typical modes of failure in stocky deep beams

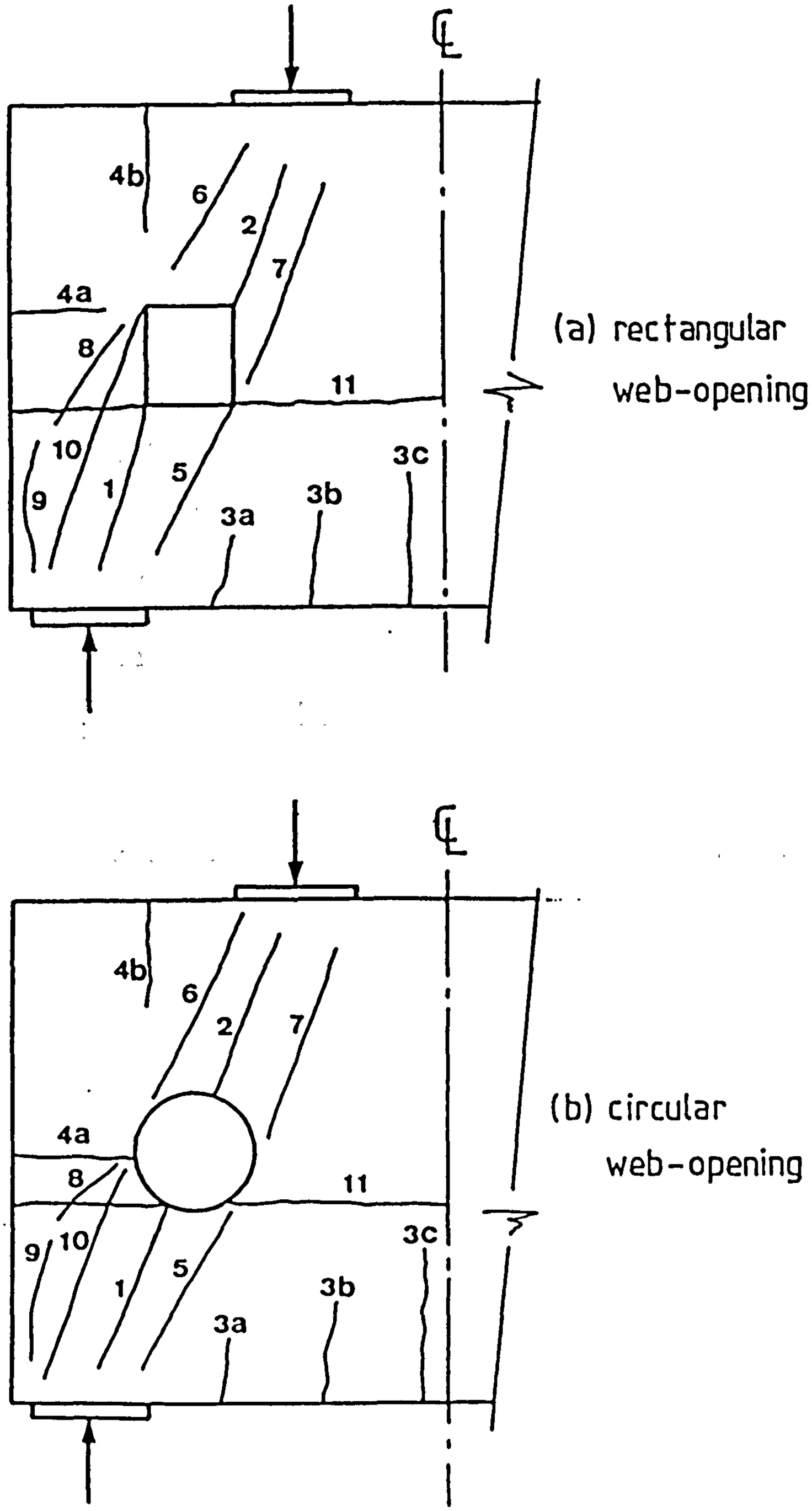

Figure 6.7 : Typical sequence of crack development (W-Series beams)

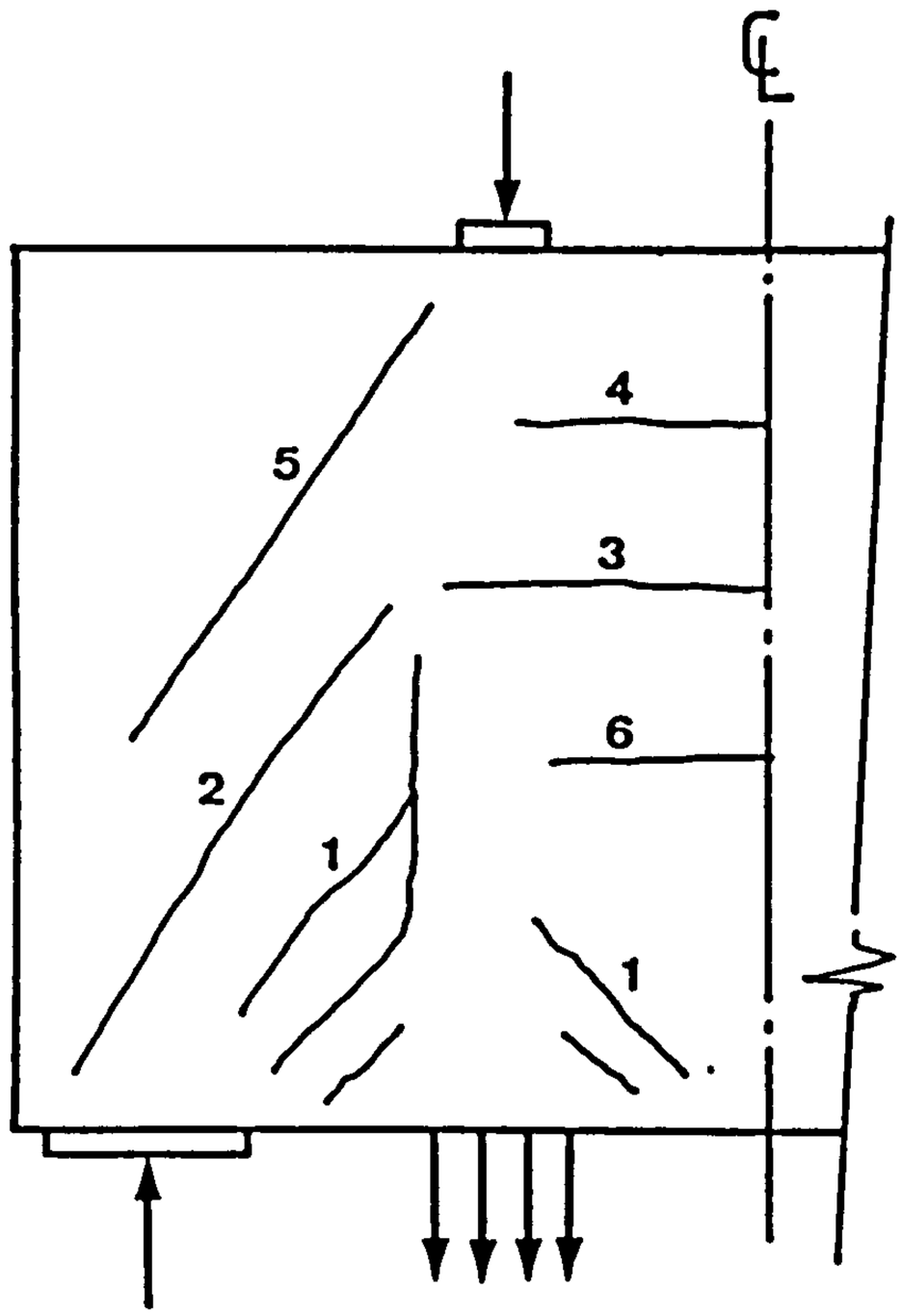

Figure 6.8 : Typical sequence of crack development (CB-Series beams)

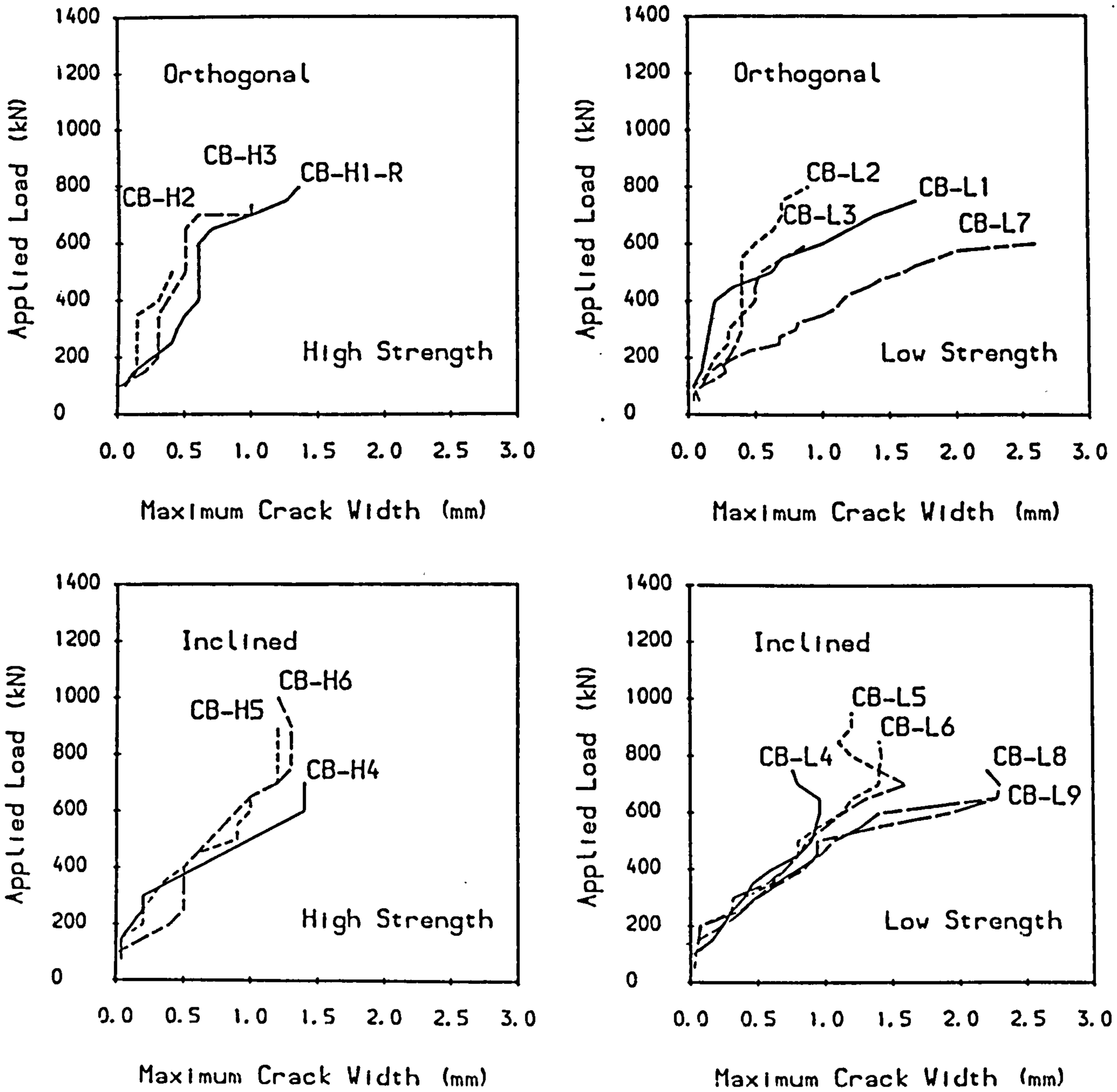

Figure 6.9 : Maximum crack width development (CB-Series beams)

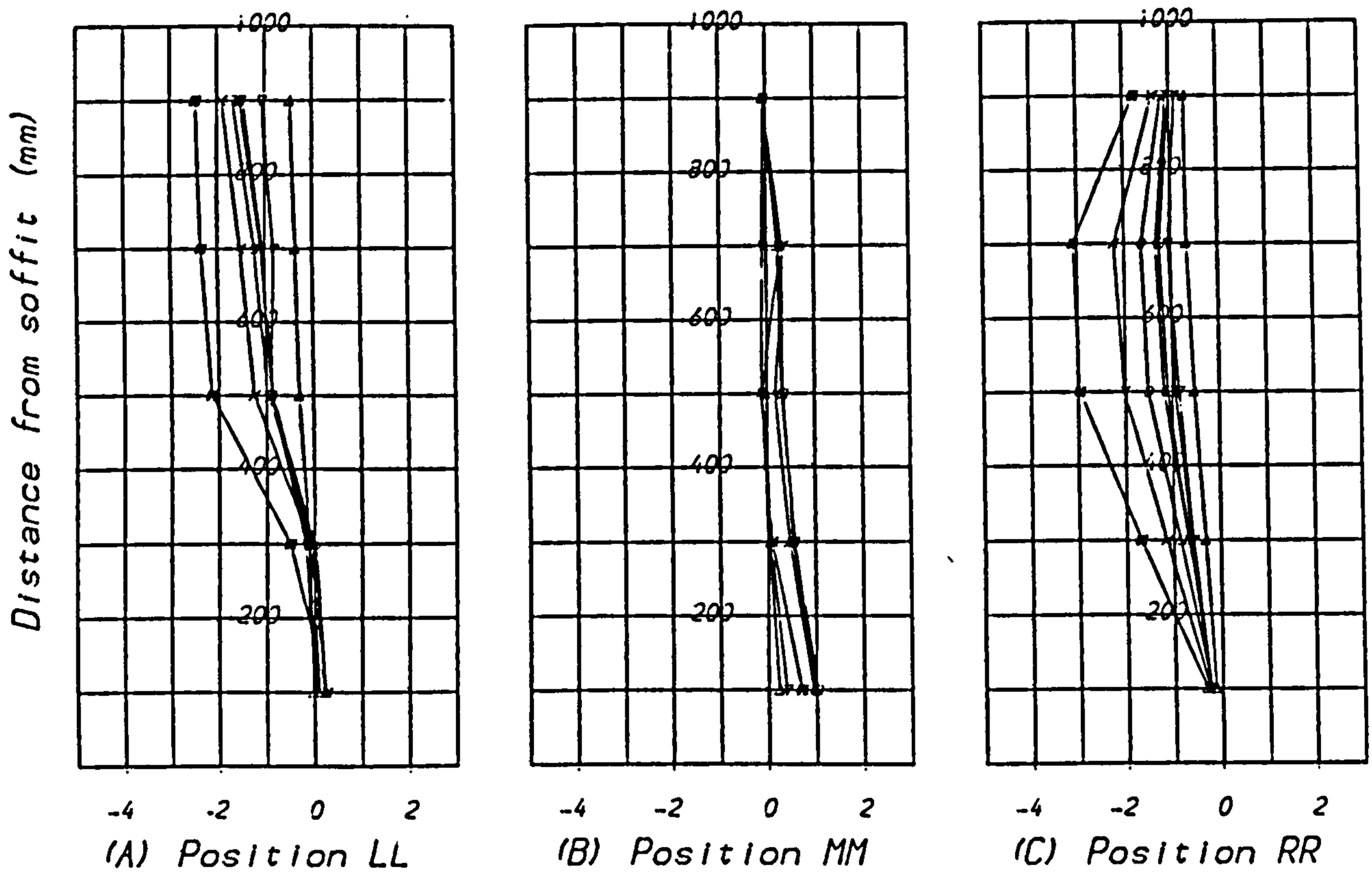

Figure 6.10(a) : Lateral displacement profiles of Beam E-67-0.1

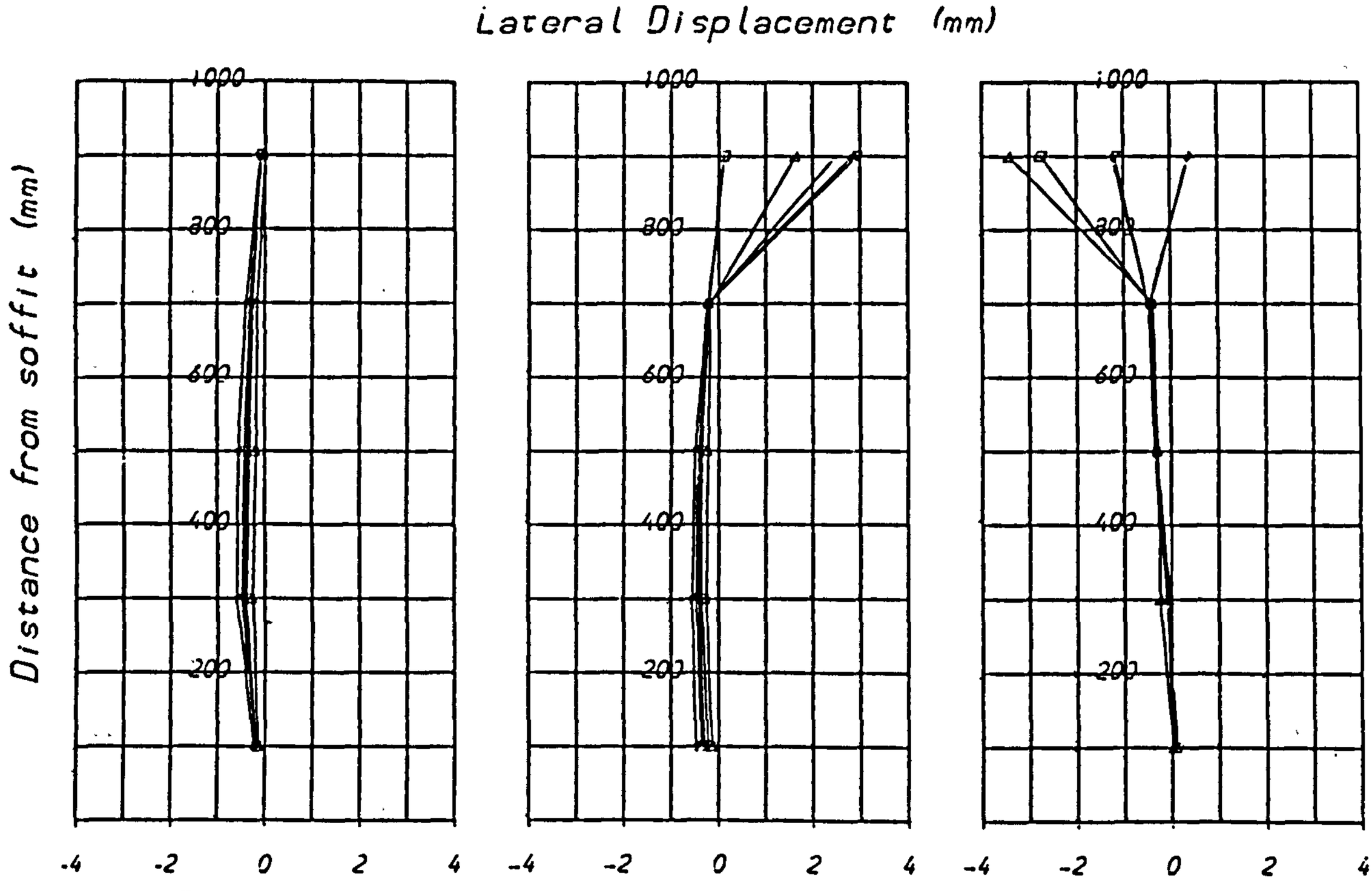

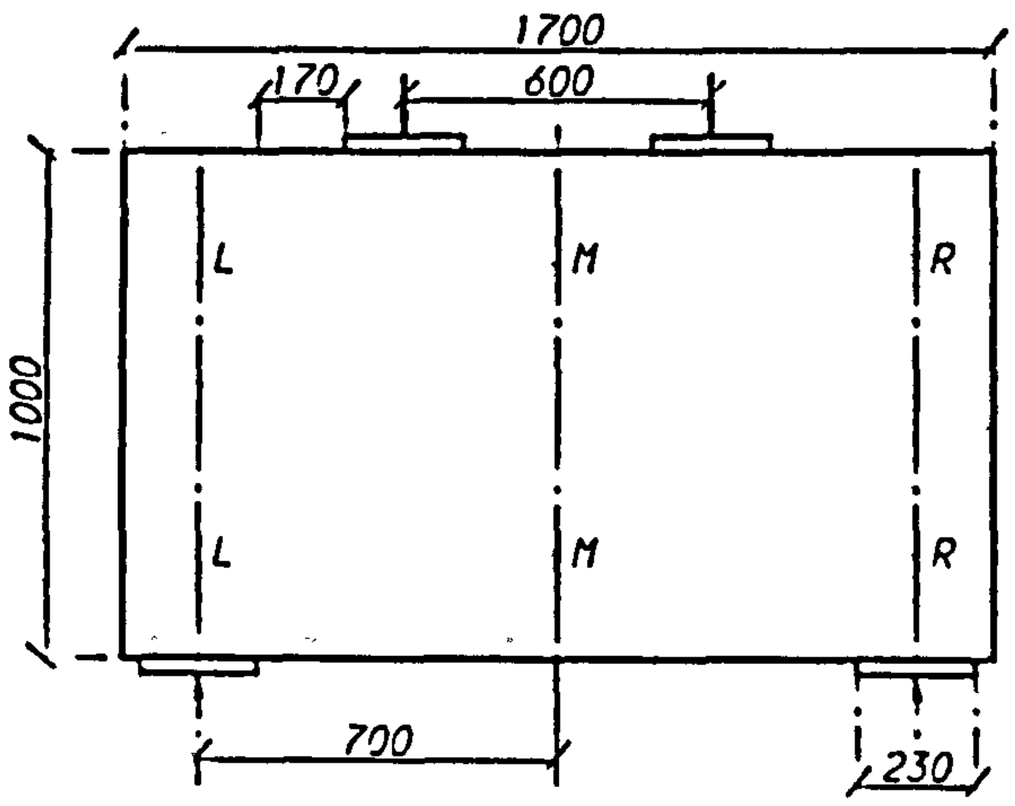

Top and Bottom eccentricities = -2.0 mm
20 mm thick

(All dimensions in mm)

6 kN
20 kN
40 kN
60 kN
80 kN
100 kN

Failure Load 200 kN

Figure 6.10(b) : Lateral displacement profiles of Beam E-50-0.1

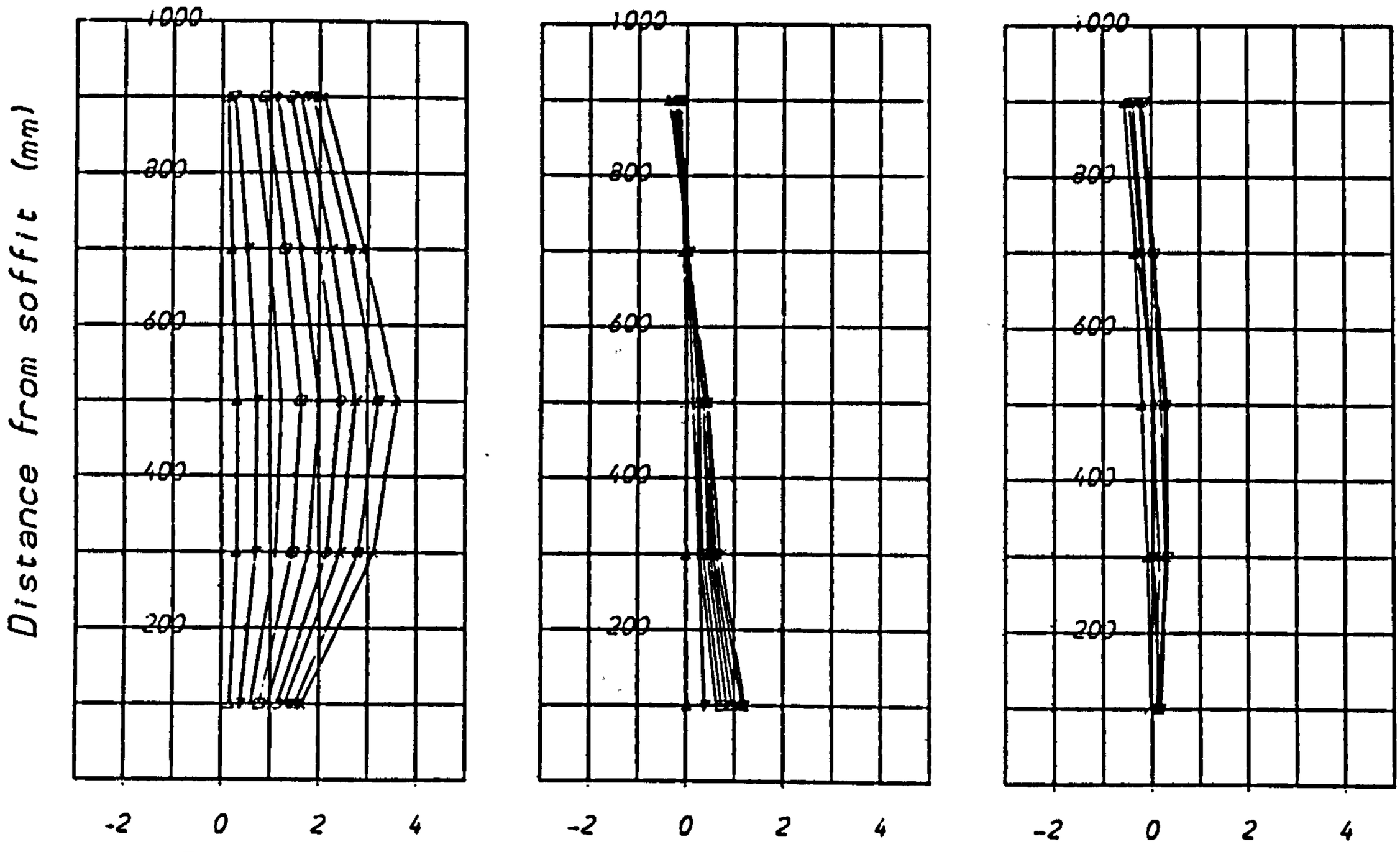

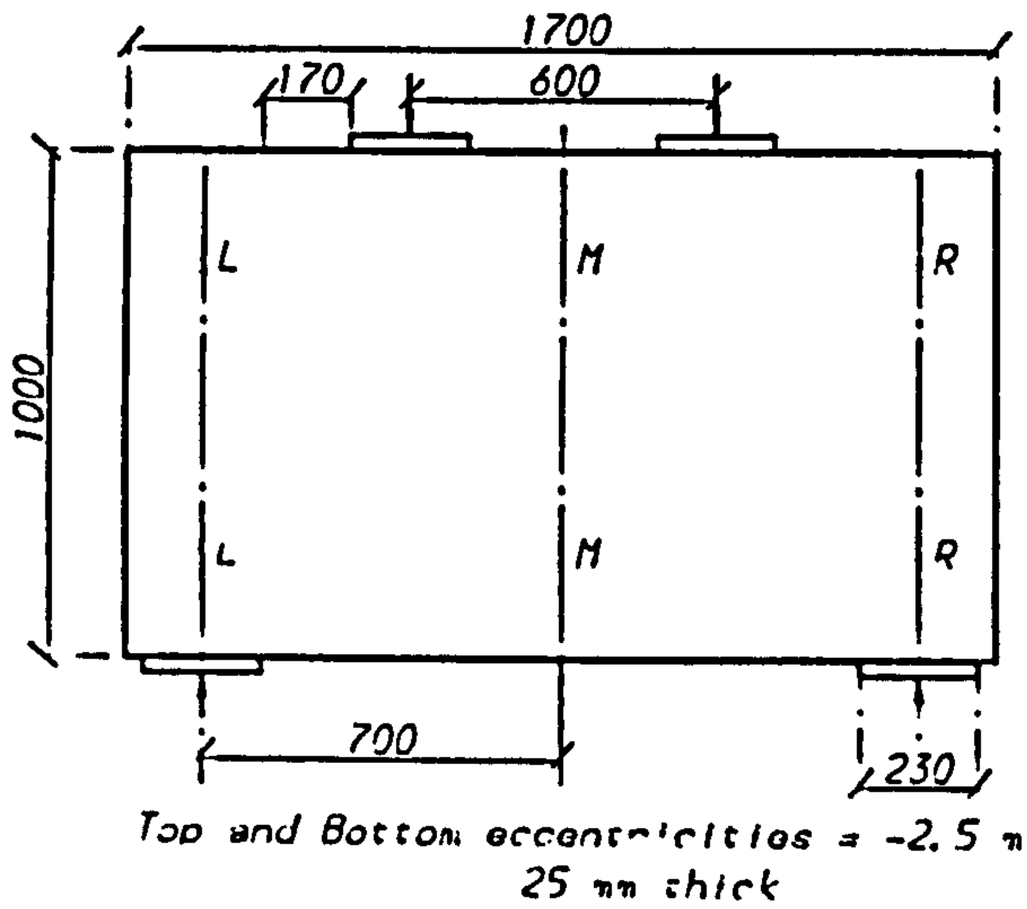

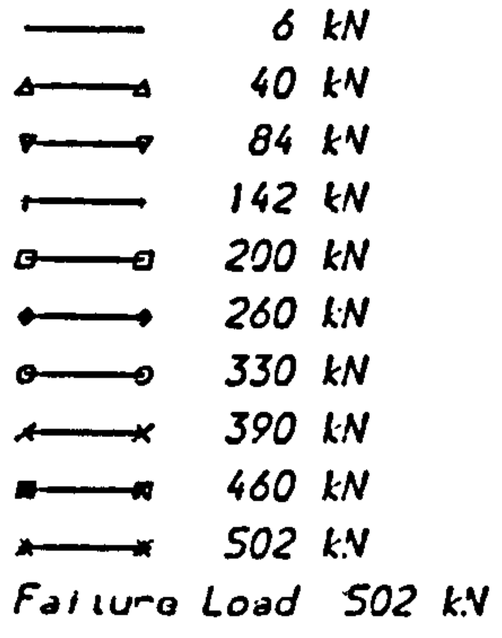

Top and Bottom eccentricities = -2.5 mm
25 mm thick

(All dimensions in mm)

Figure 6.10(c) : Lateral displacement profiles of Beam E-40-0.1

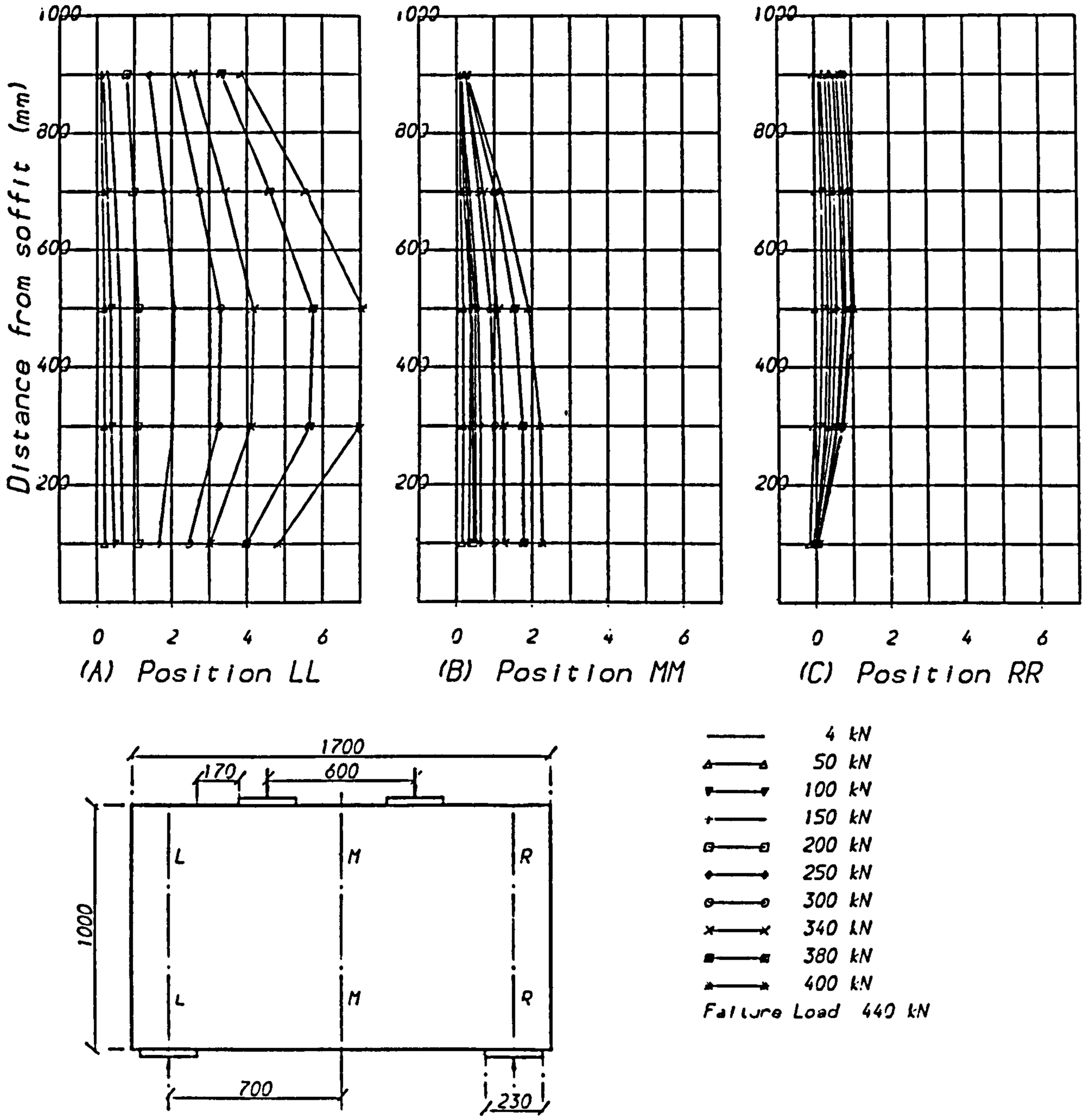

Figure 6.10(d) : Lateral displacement profiles of Beam E-33-0.1

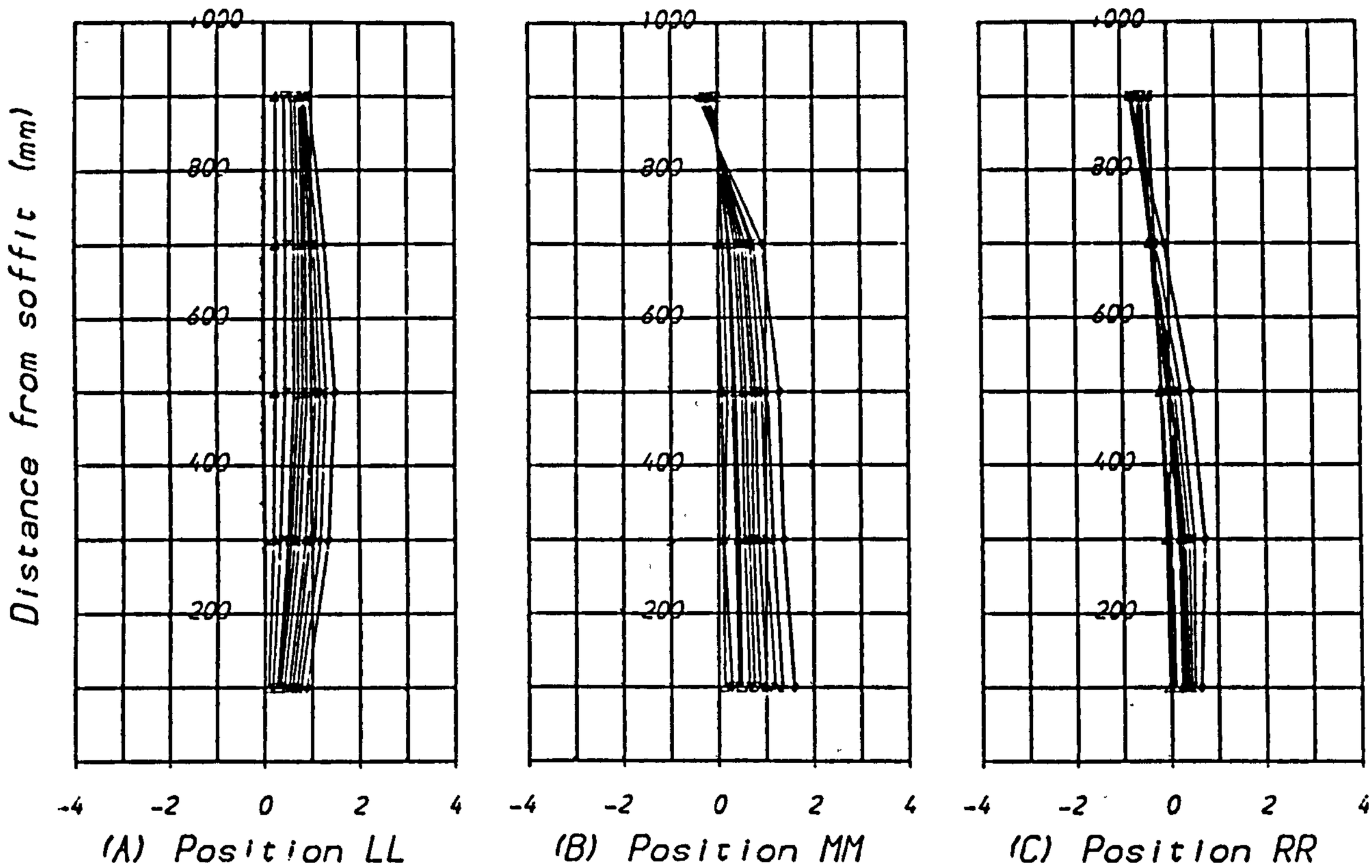

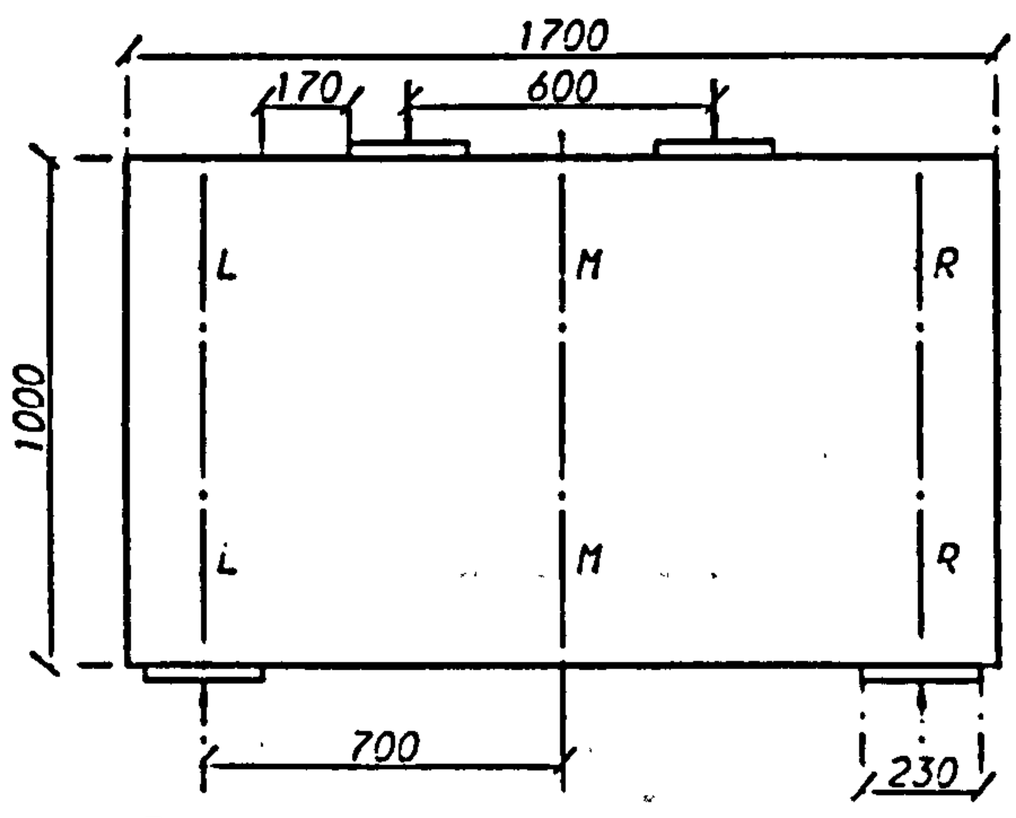

6 kN
60 kN
120 kN
180 kN
240 kN
300 kN
360 kN
420 kN
480 kN
560 kN
620 kN
700 kN

Failure Load 700 kN

Top and Bottom eccentricities = -3.5 mm
35 mm thick

(All dimensions in mm)

Figure 6.10(e) : Lateral displacement profiles of Beam E-29-0.1

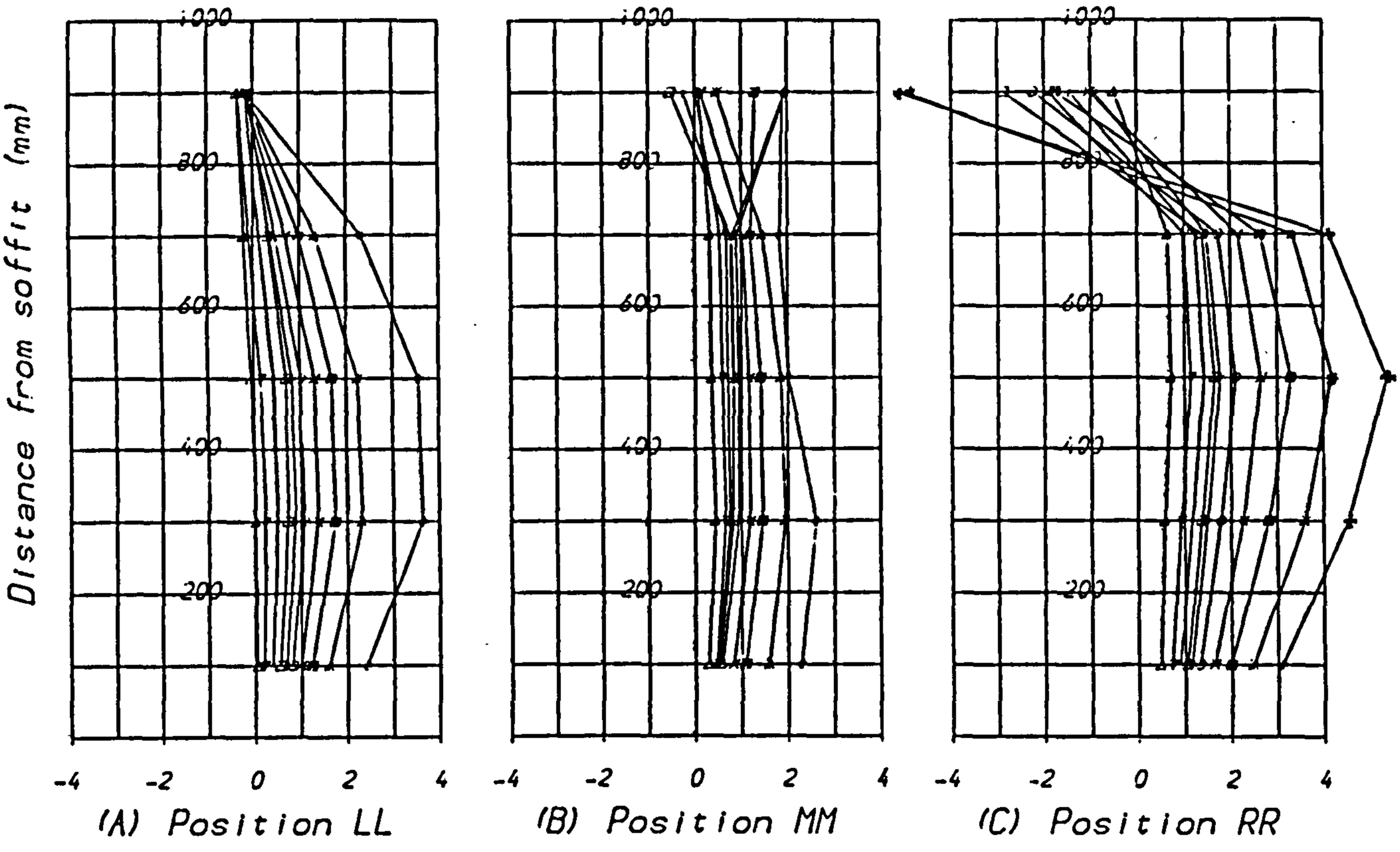

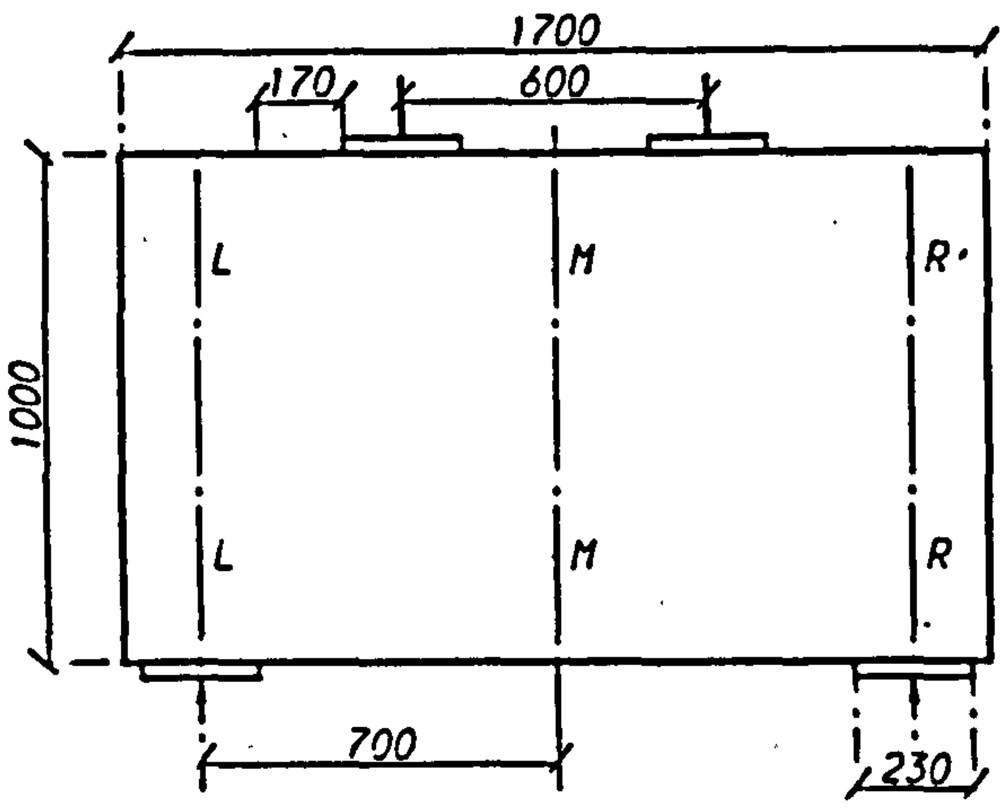

Top and Bottom eccentricities = -4.0 mm
40 mm thick

(All dimensions in mm)

	4 kN
	60 kN
	120 kN
	180 kN
	240 kN
	266 kN
	320 kN
	380 kN
	440 kN
	500 kN
	560 kN

Failure Load 560 kN

Figure 6.10(f) : Lateral displacement profiles of Beam E-25-0.1

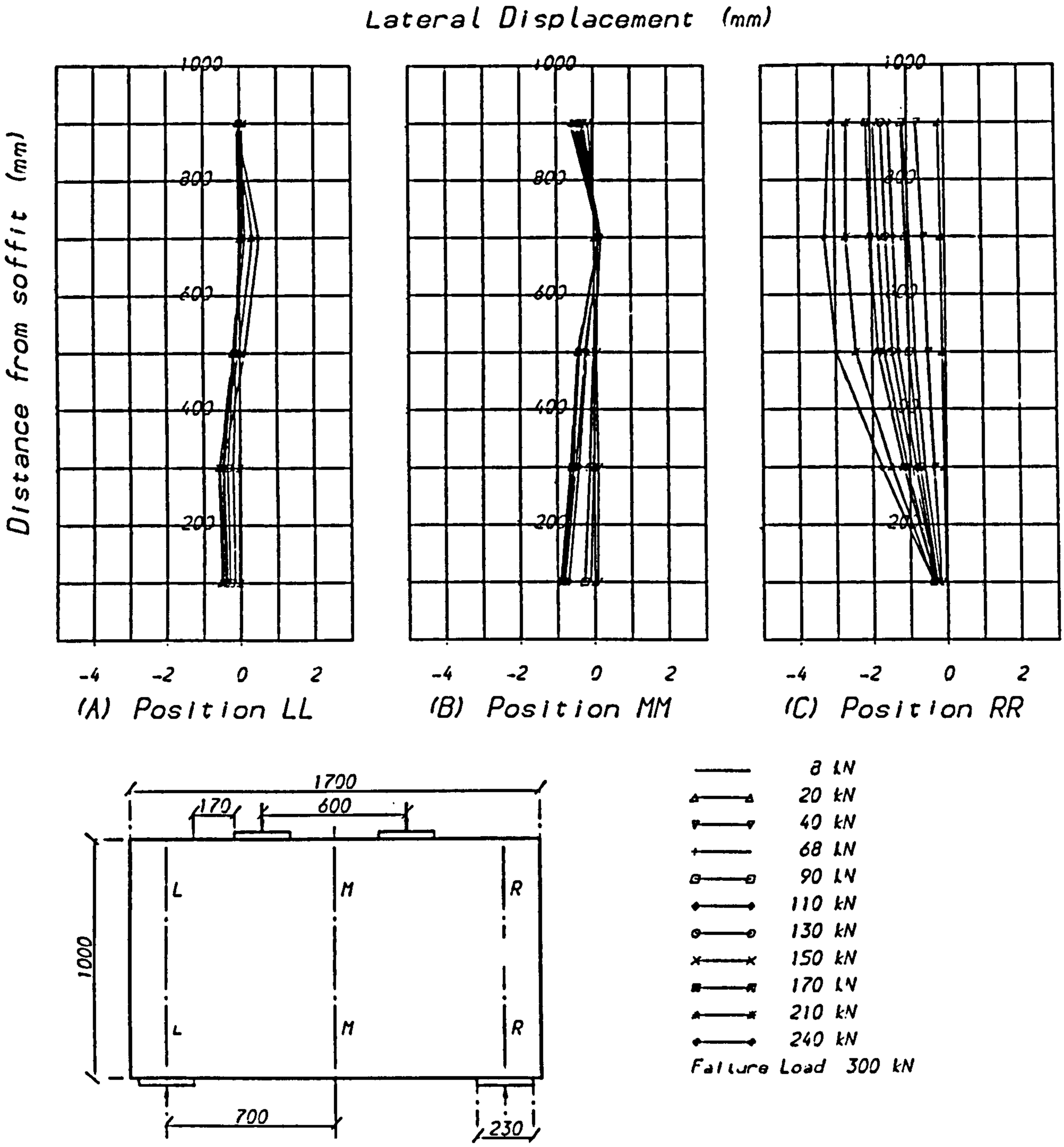

Figure 6.10(g) : Lateral displacement profiles of Beam E-67-0.2

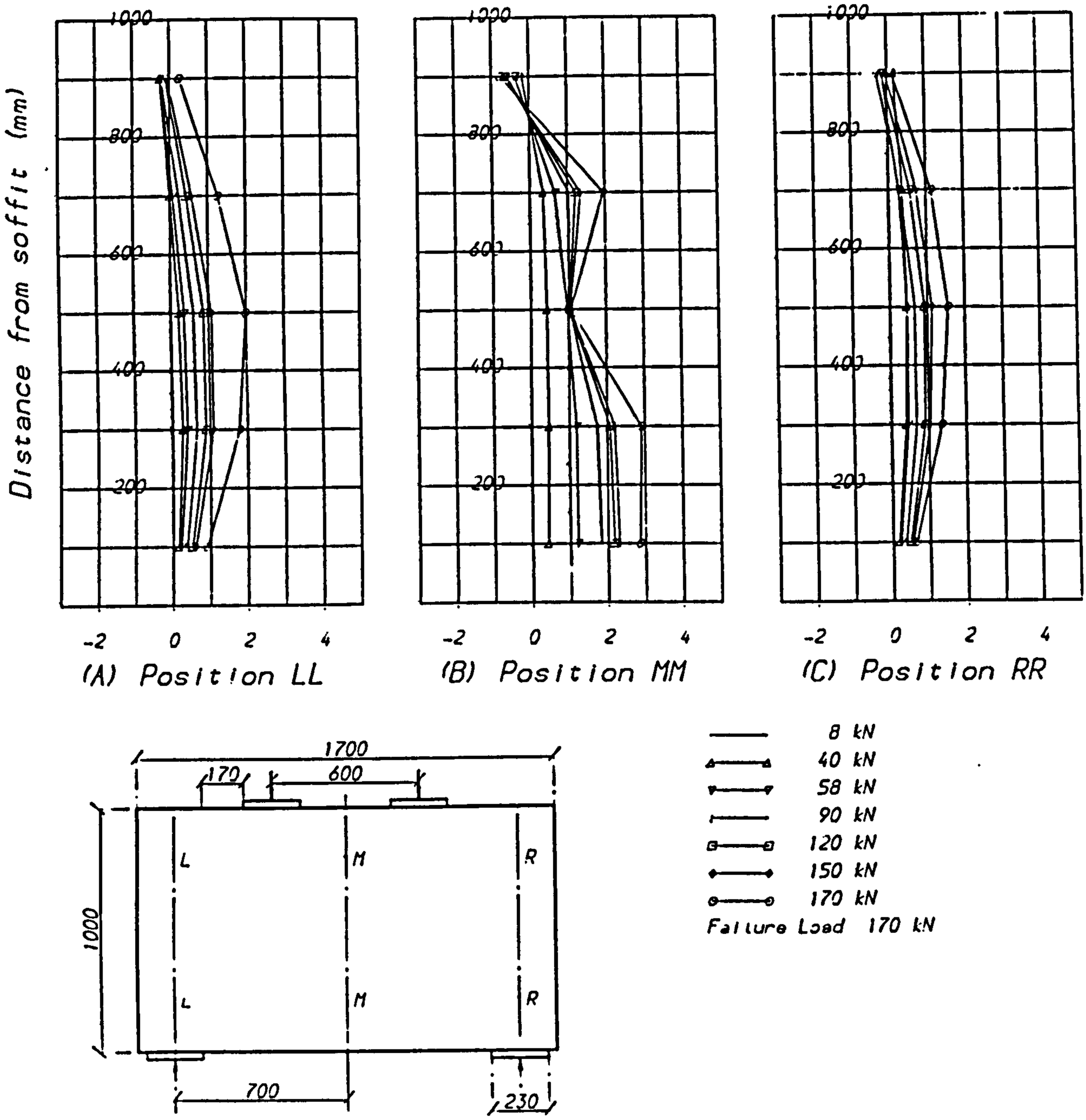

Figure 6.10(h) : Lateral displacement profiles of Beam E-50-0.2

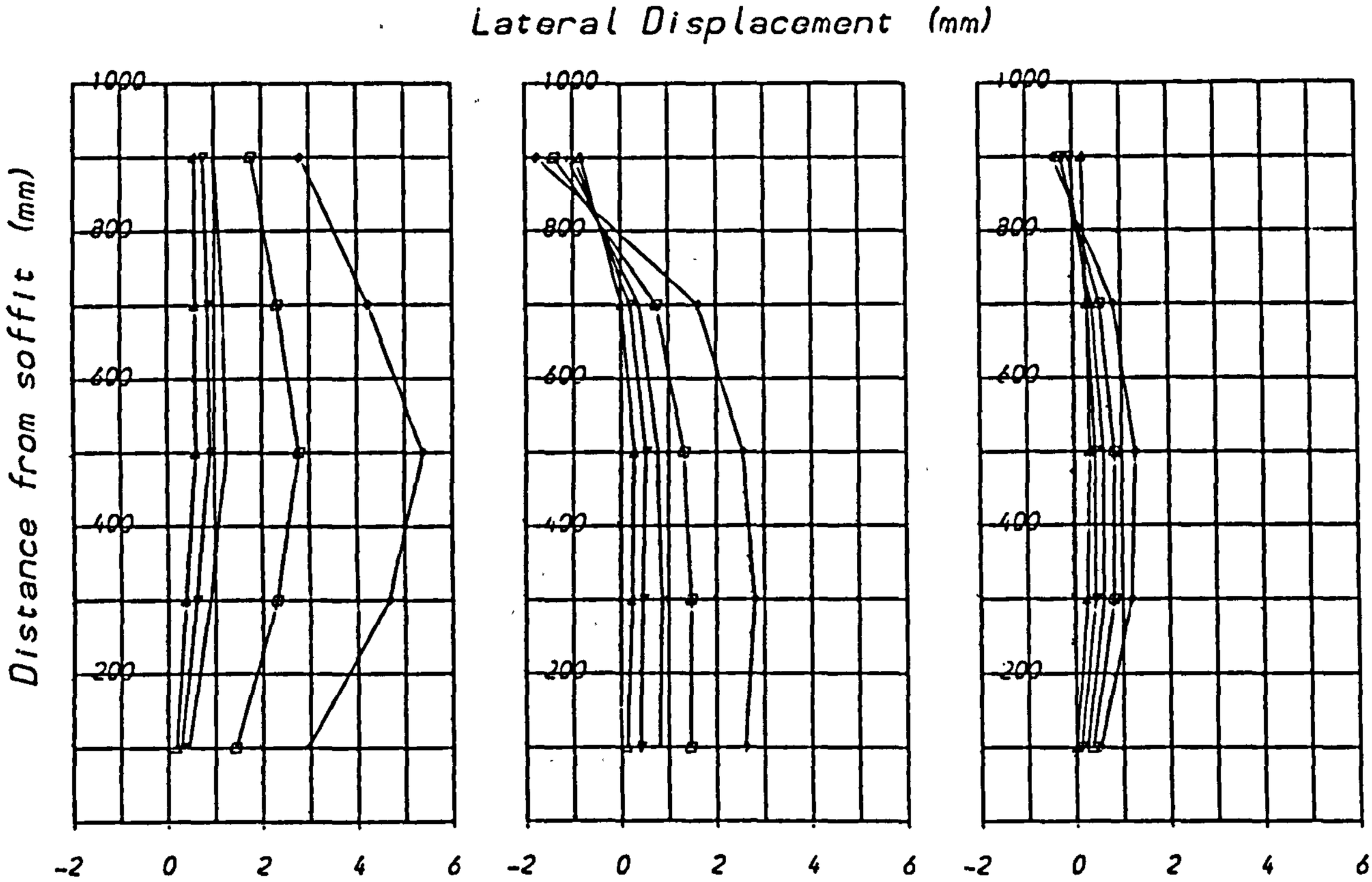

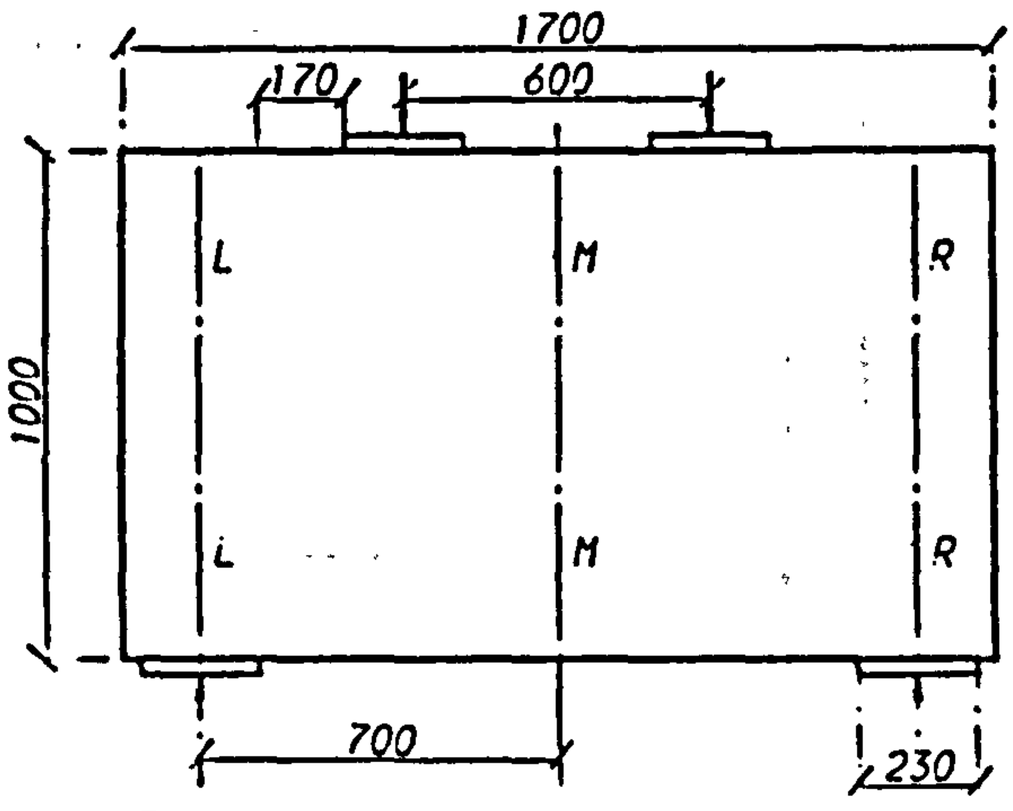

6 kN
50 kN
80 kN
120 kN
160 kN
186 kN
Failure Load 210 kN

Top and Bottom eccentricities = -5.0 mm
25 mm thick

(All dimensions in mm)

Figure 6.10(i) : Lateral displacement profiles of Beam E-40-0.2

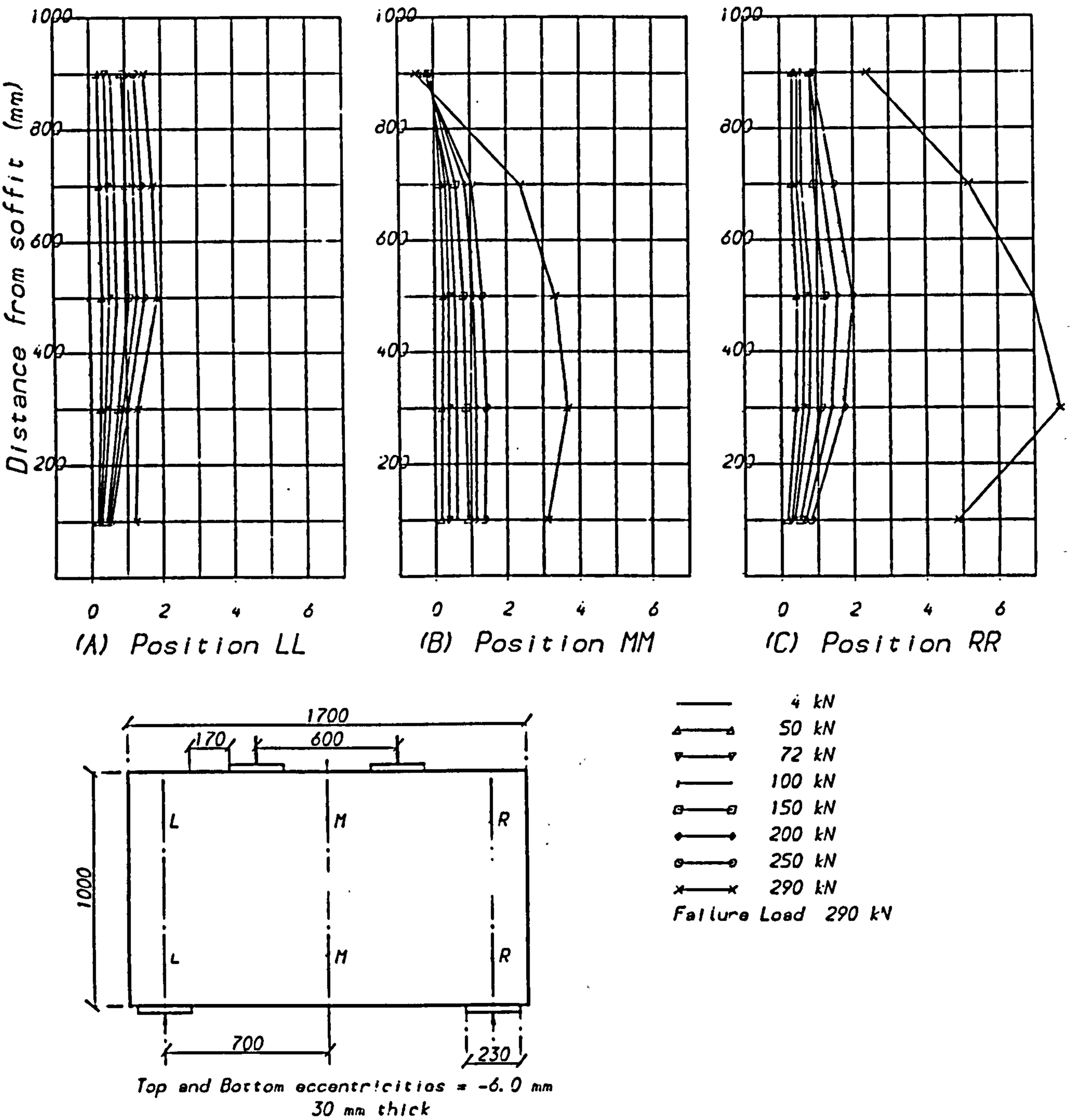

Figure 6.10(j) : Lateral displacement profiles of Beam E-33-0.2

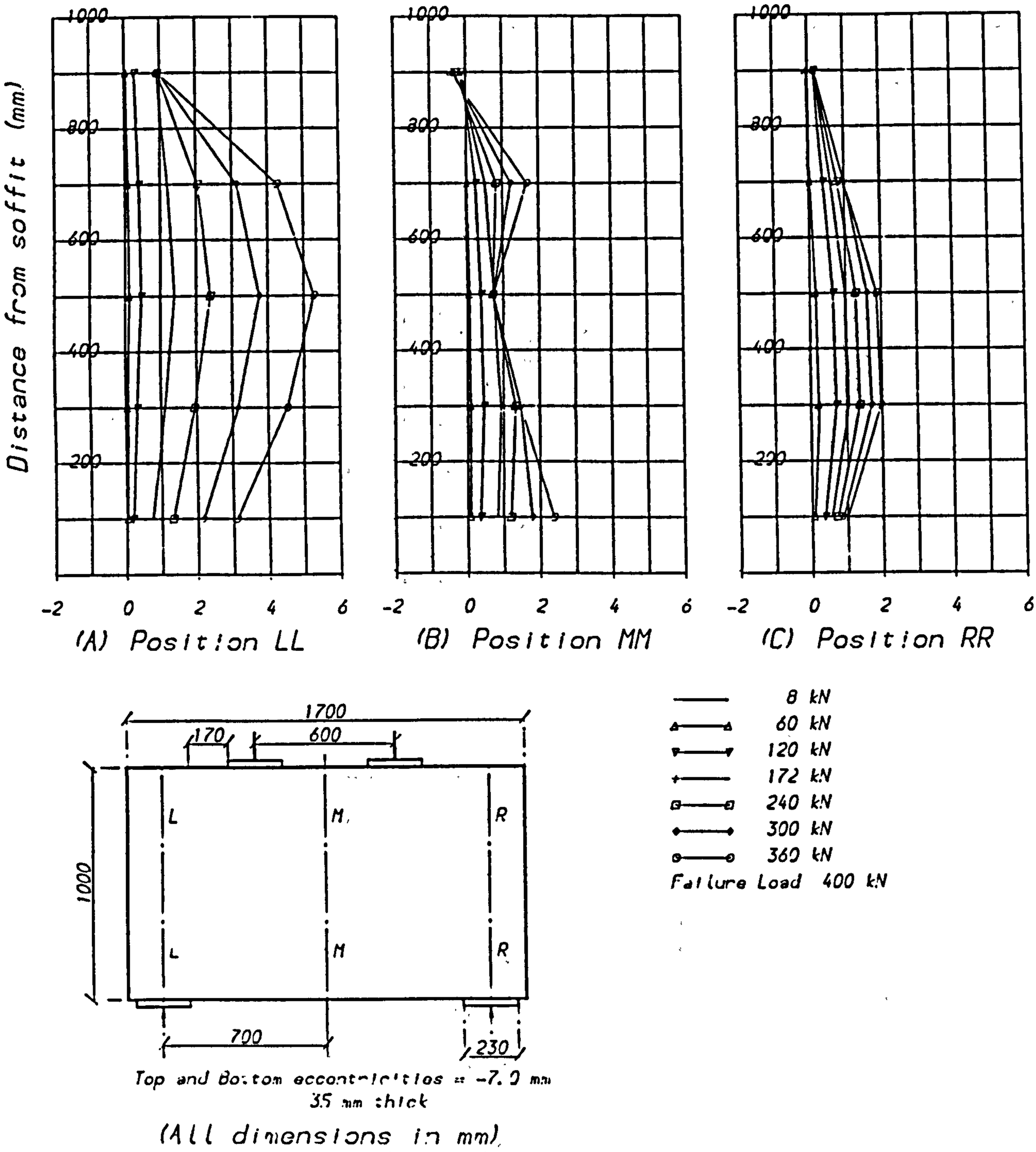

Figure 6.10(k) : Lateral displacement profiles of Beam E-29-0.2

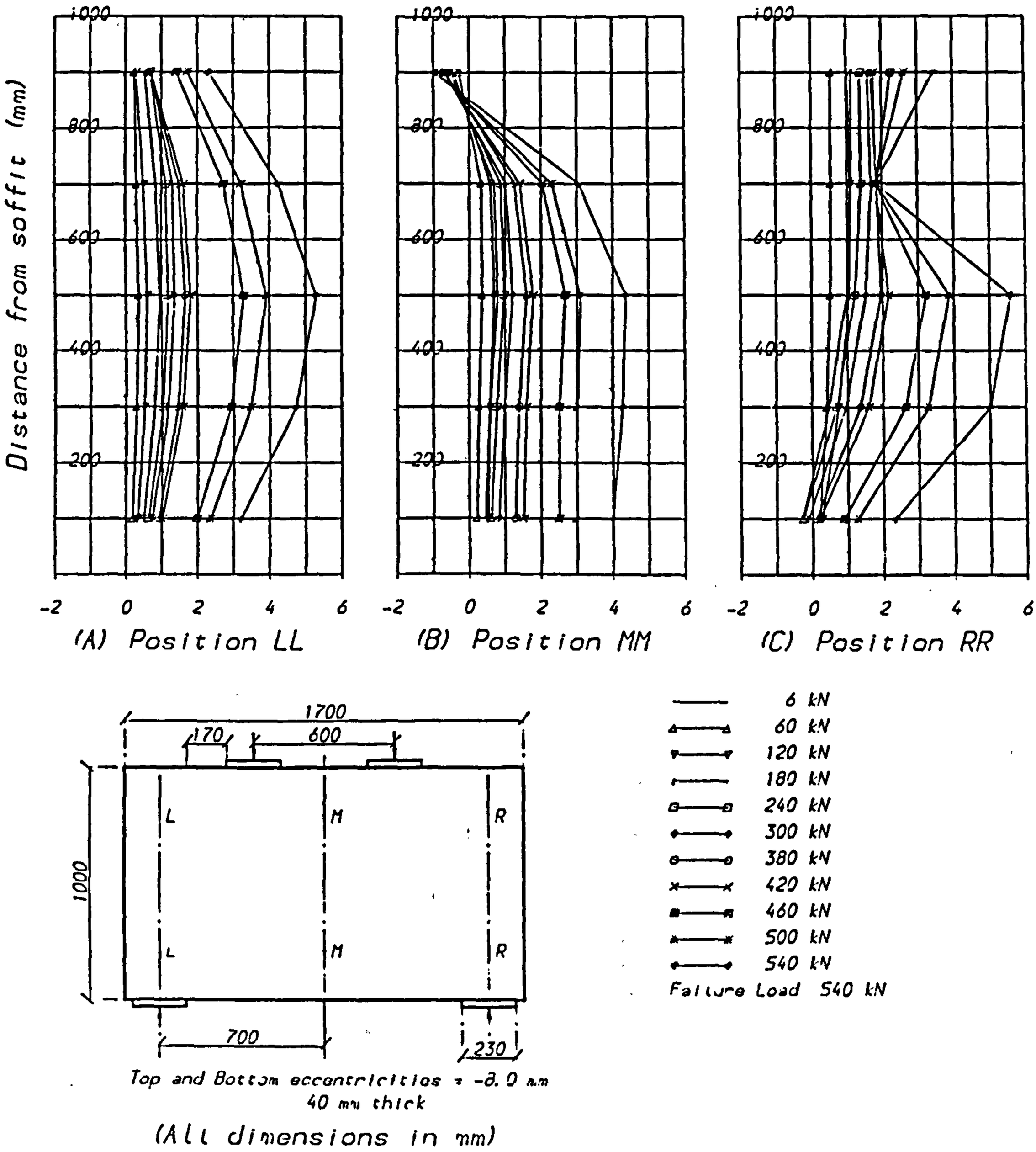

Figure 6.10(1) : Lateral displacement profiles of Beam E-25-0.2

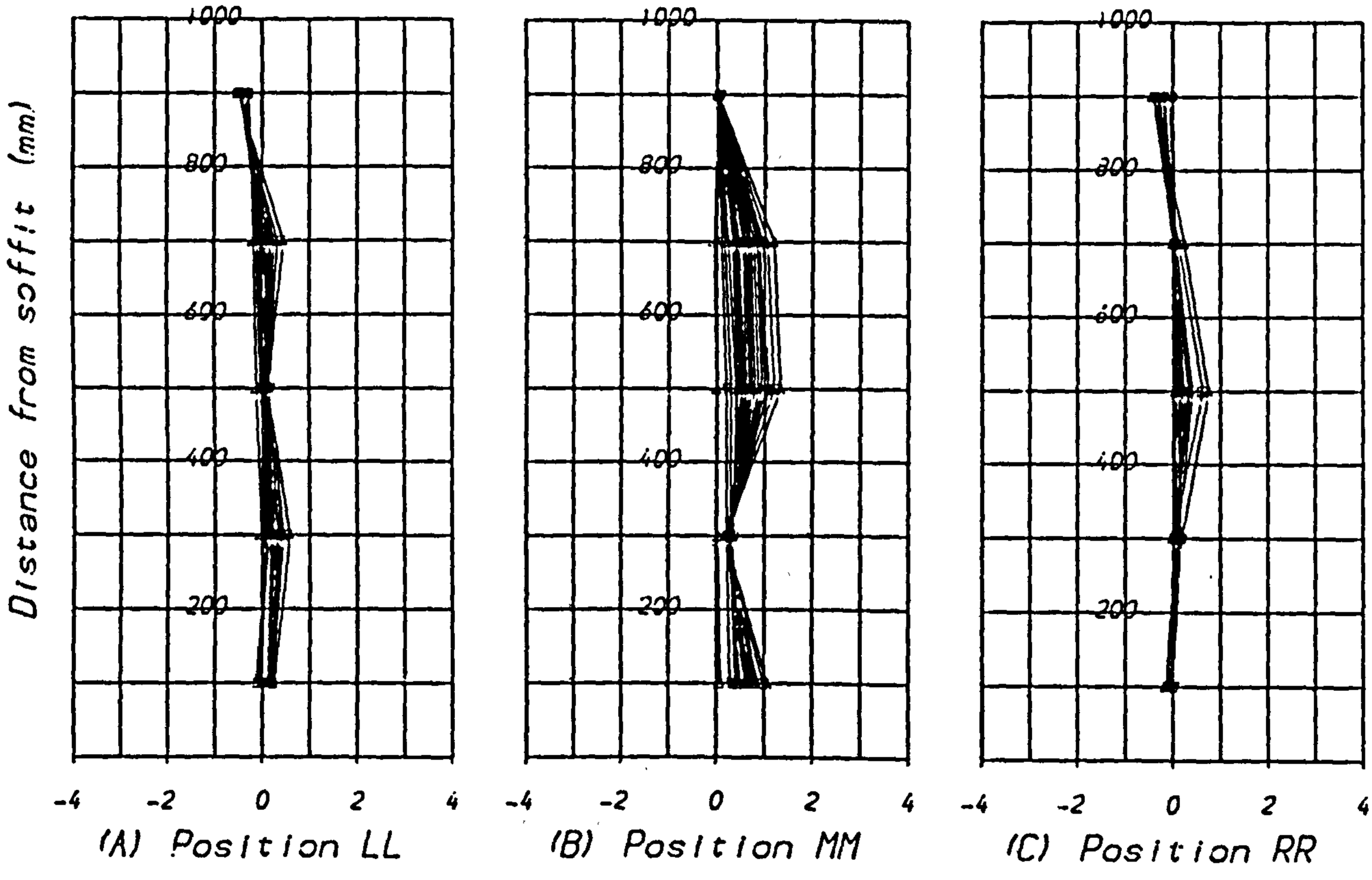

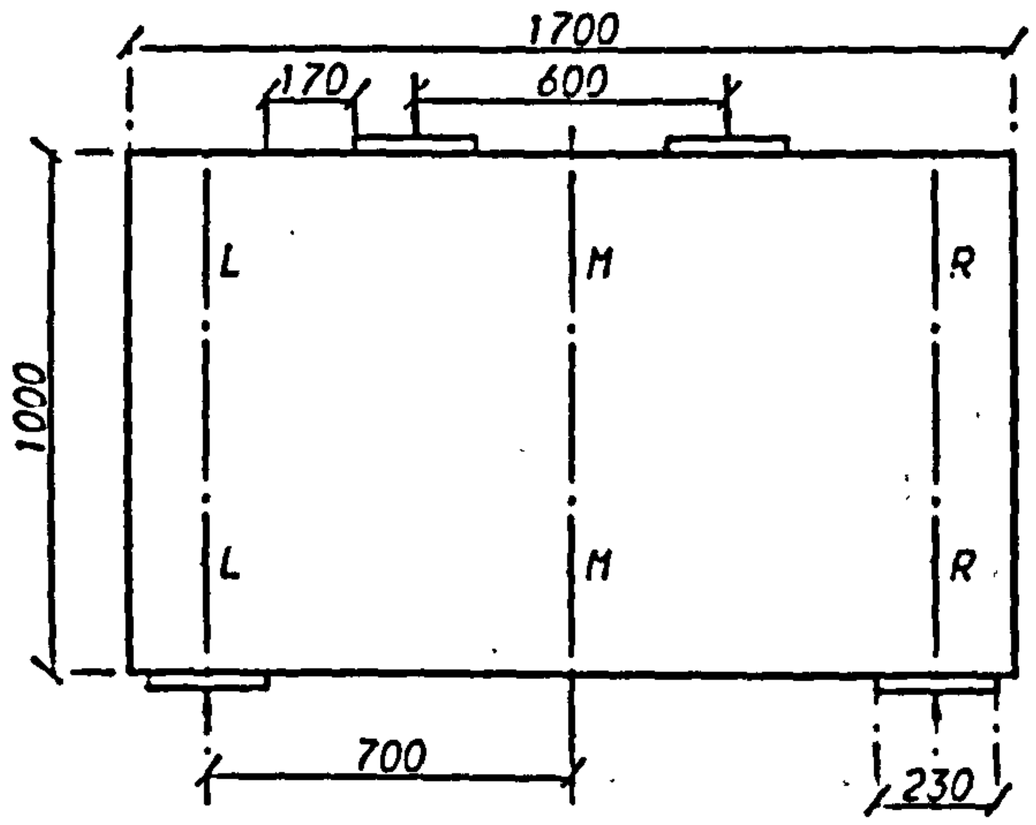

Top and Bottom eccentricities = -3.5 mm
35 mm thick
(All dimensions in mm)

	4 kN		750 kN
	50 kN		800 kN
	100 kN		850 kN
	150 kN		900 kN
	200 kN	Failure Load 950 kN	
	250 kN		
	300 kN		
	350 kN		
	400 kN		
	450 kN		
	500 kN		
	550 kN		
	600 kN		
	650 kN		
	700 kN		

Figure 6.11(a) : Lateral displacement profiles of Beam W-29-0.1-R2

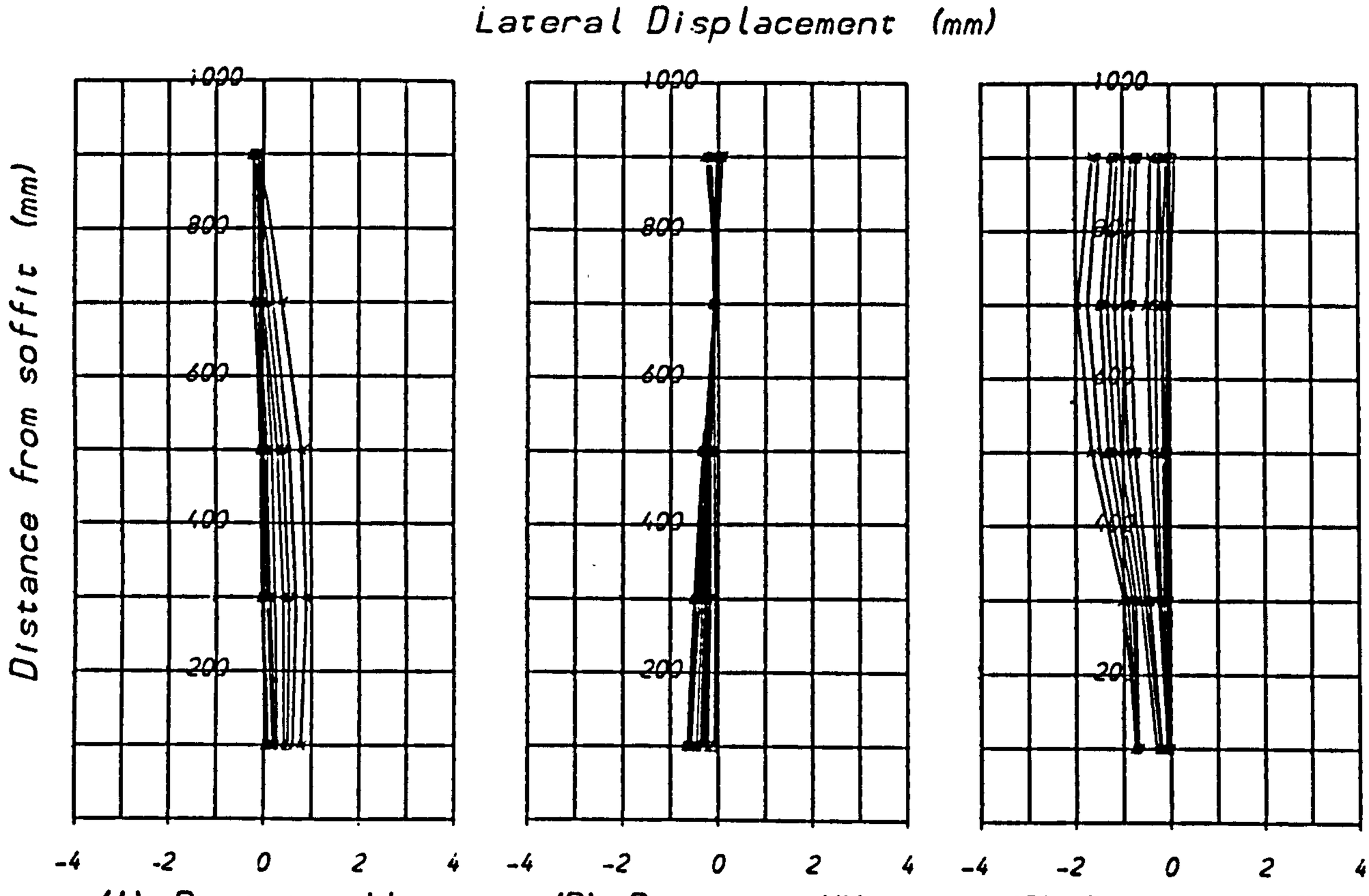

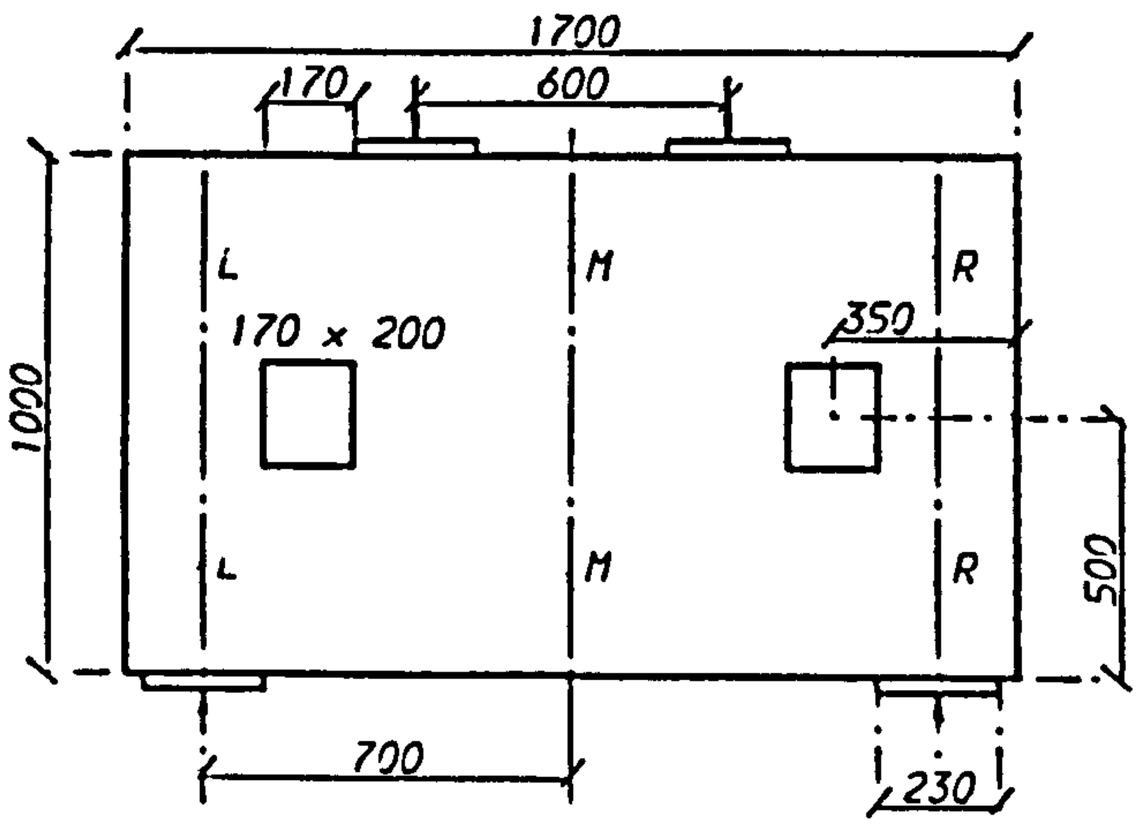

Top and Bottom eccentricities = -3.5 mm
55 mm thick
(All dimensions in mm)

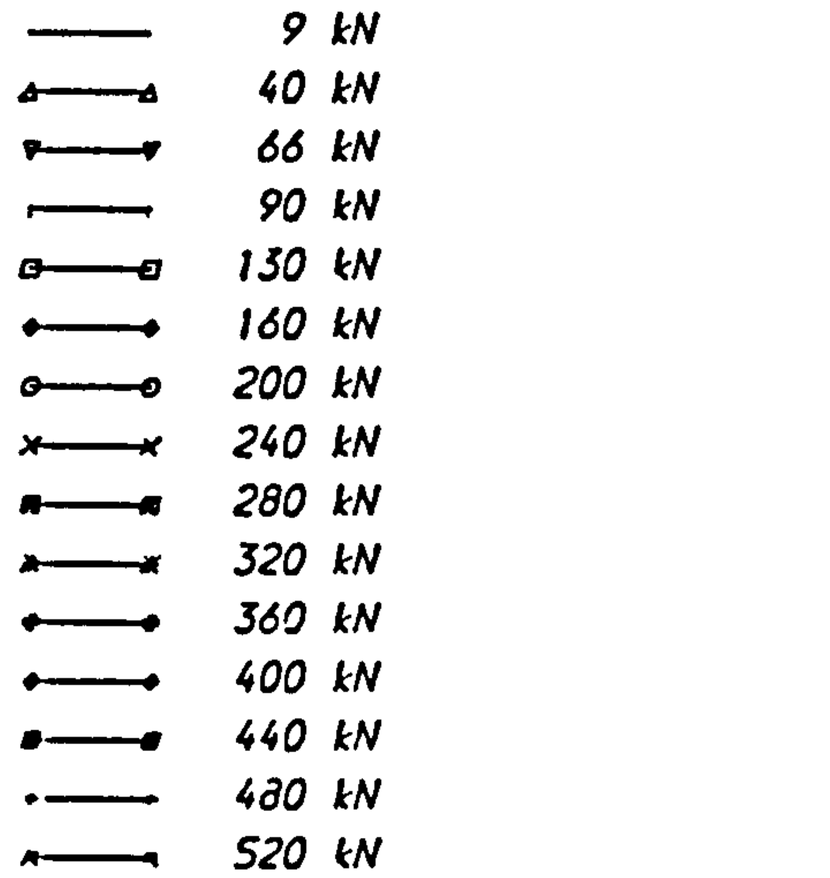

Figure 6.11(b) : Lateral displacement profiles of Beam W-AR

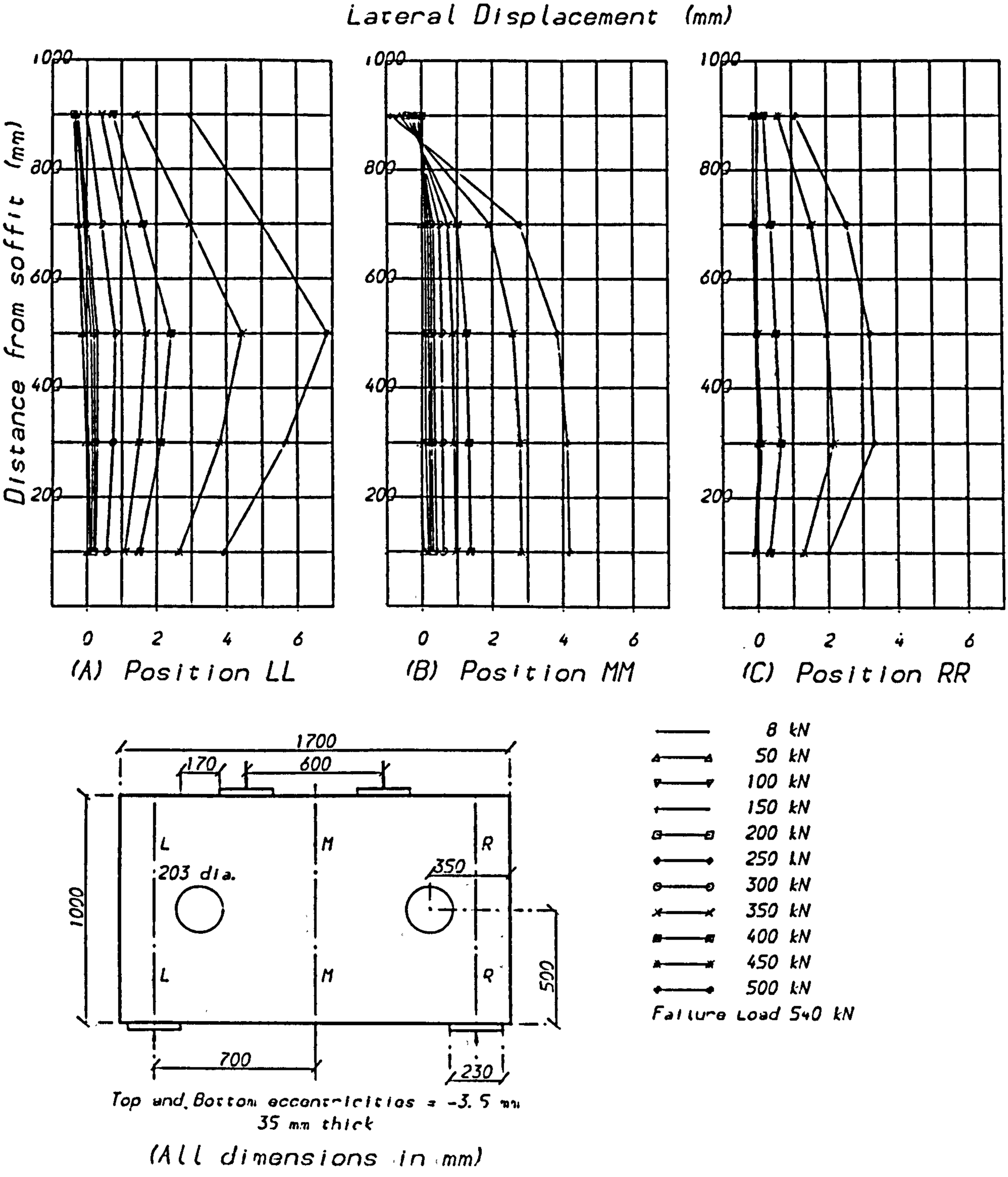

Figure 6.11(c) : Lateral displacement profiles of Beam W-AC

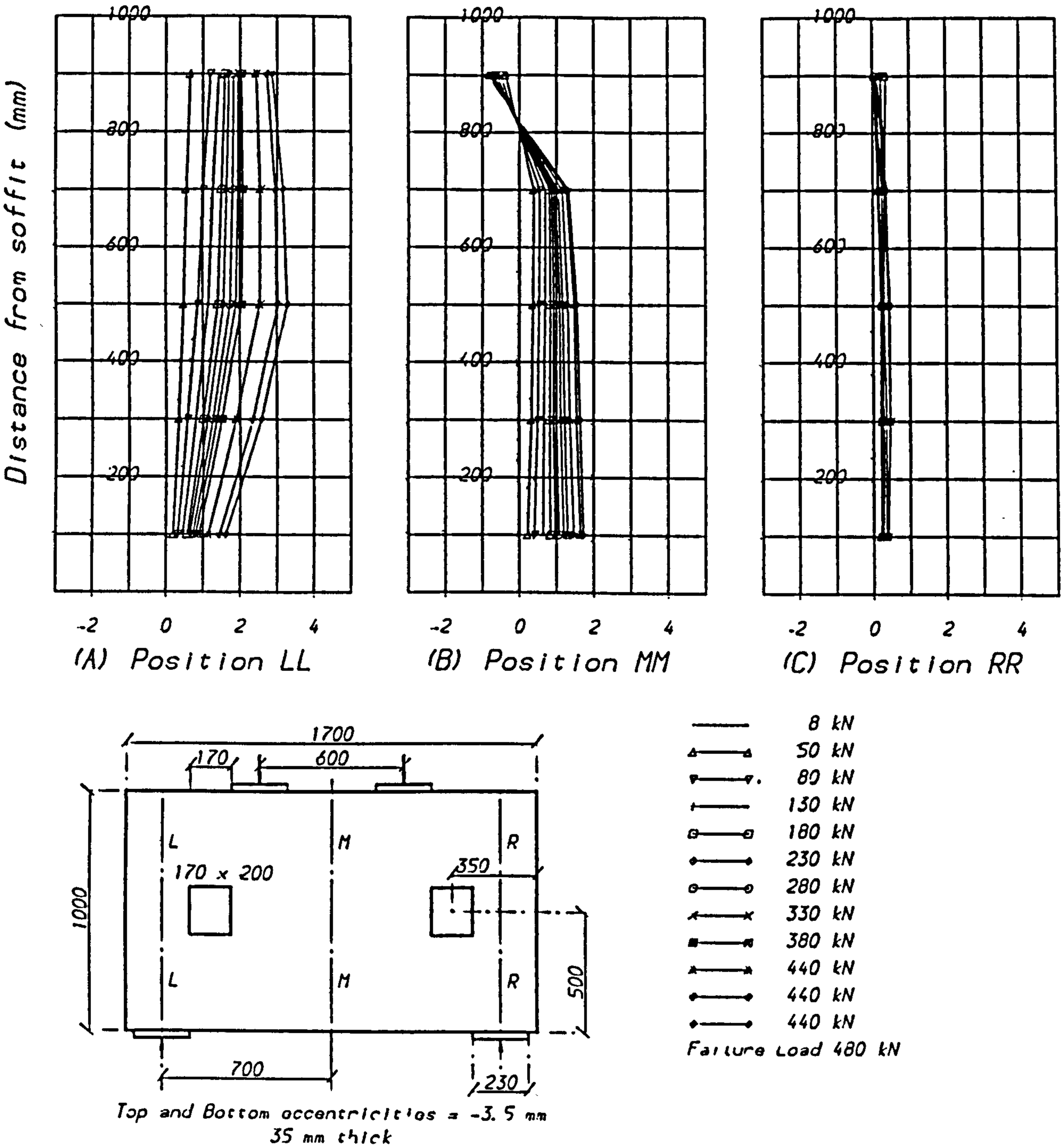

Figure 6.11(d) : Lateral displacement profiles of Beam W-AR-R

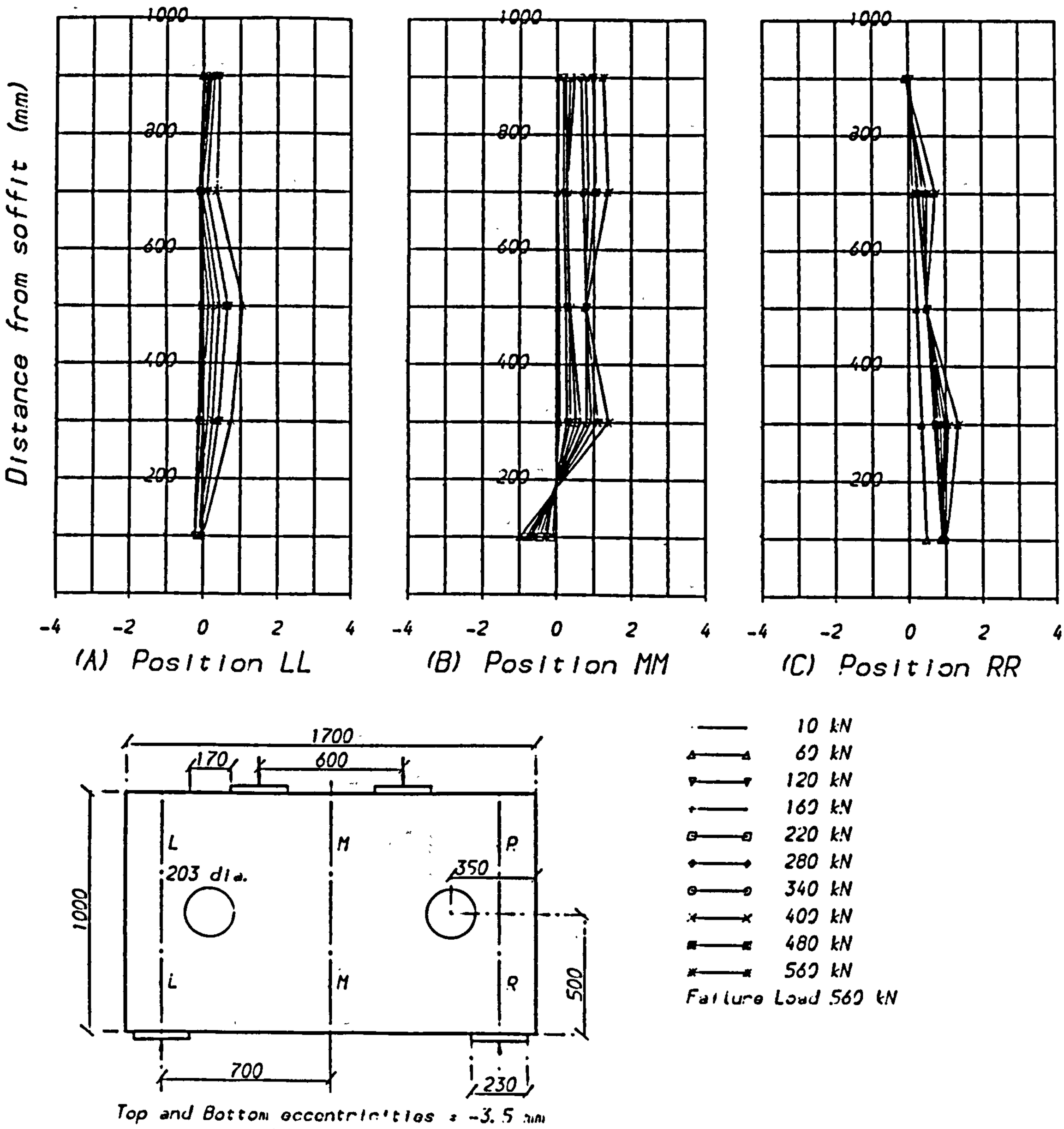

Figure 6.11(e) : Lateral displacement profiles of Beam W-AC-R

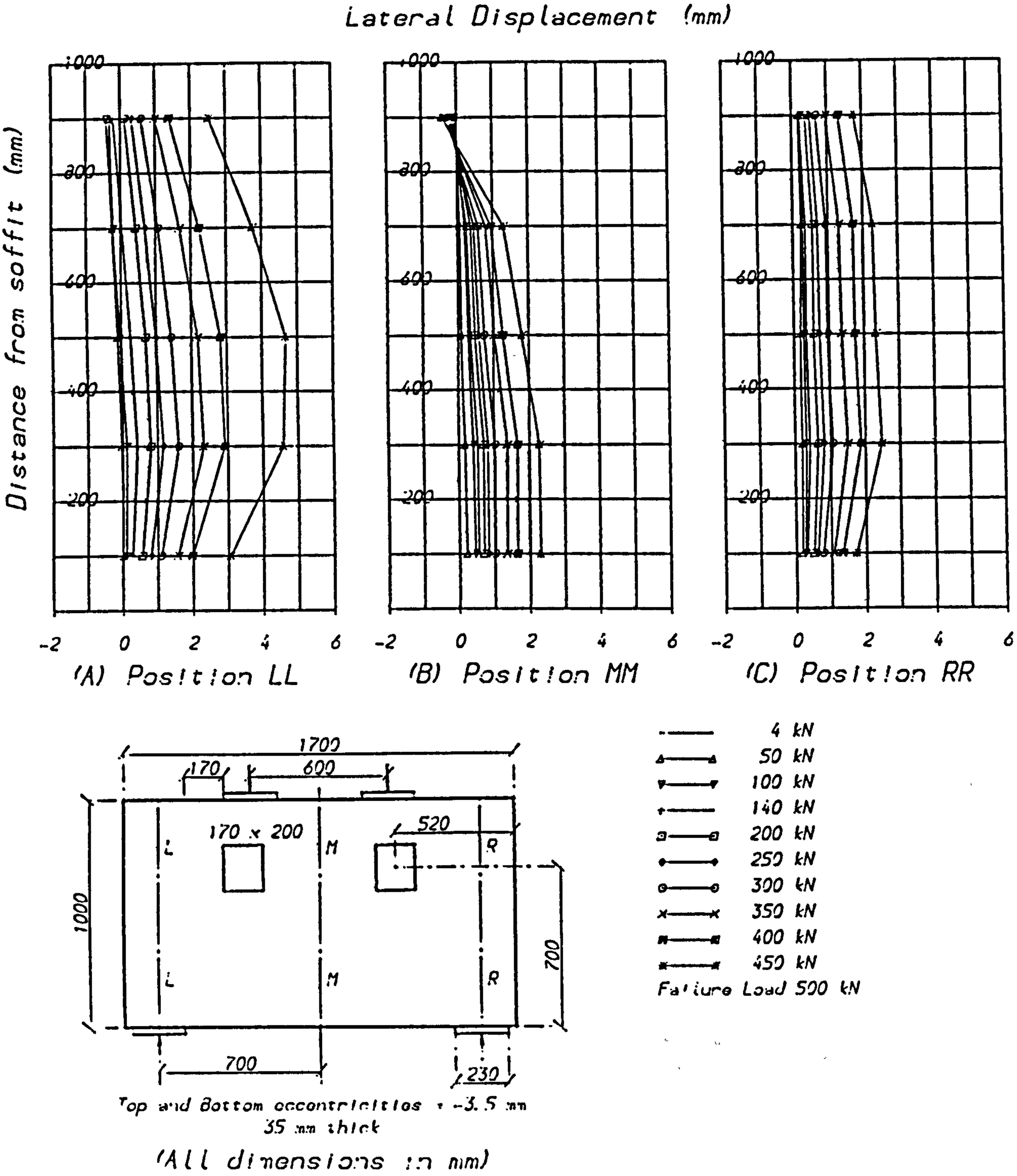

Figure 6.11(f) : Lateral displacement profiles of Beam W-BR

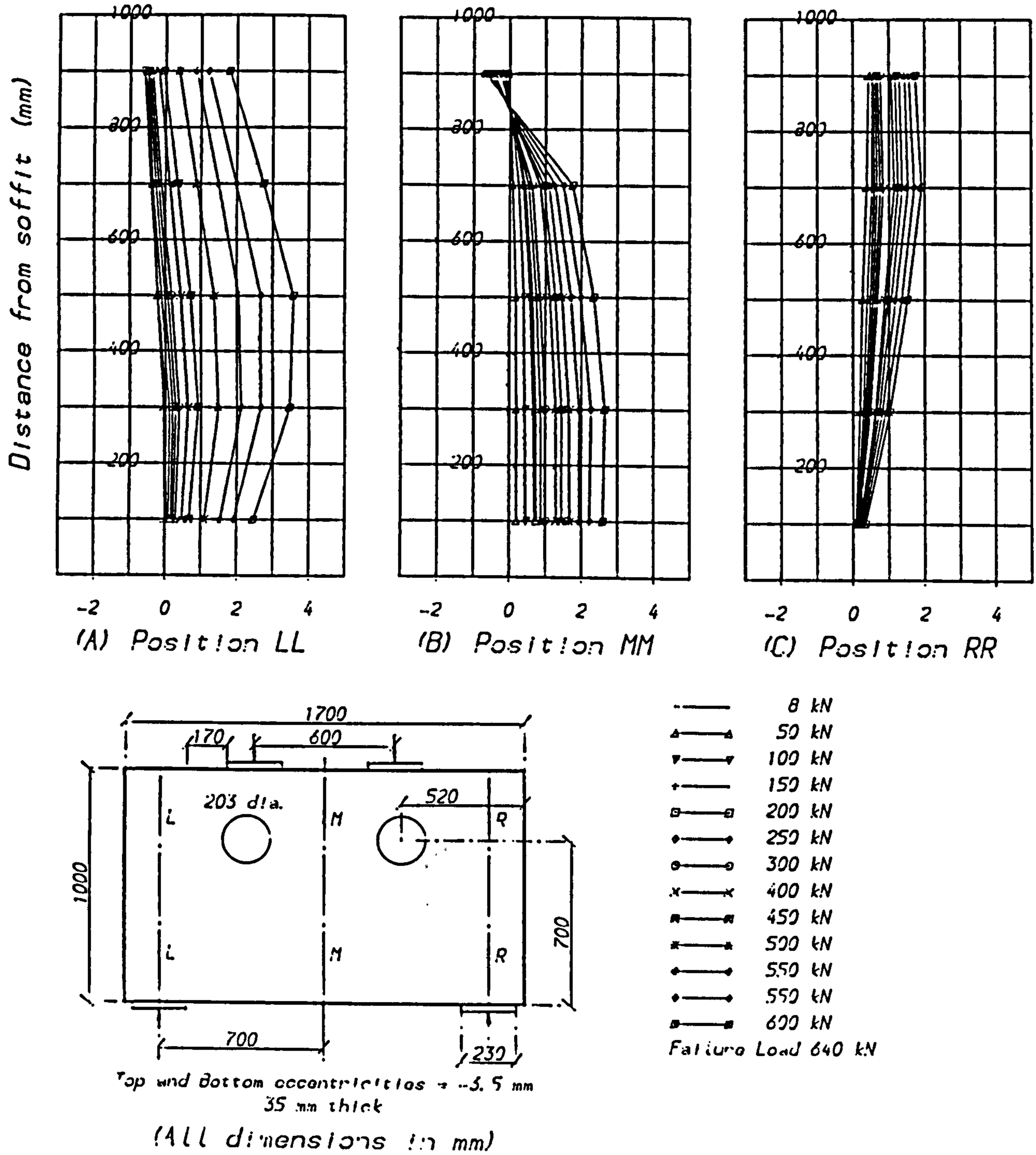

Figure 6.11(g) : Lateral displacement profiles of Beam W-BC

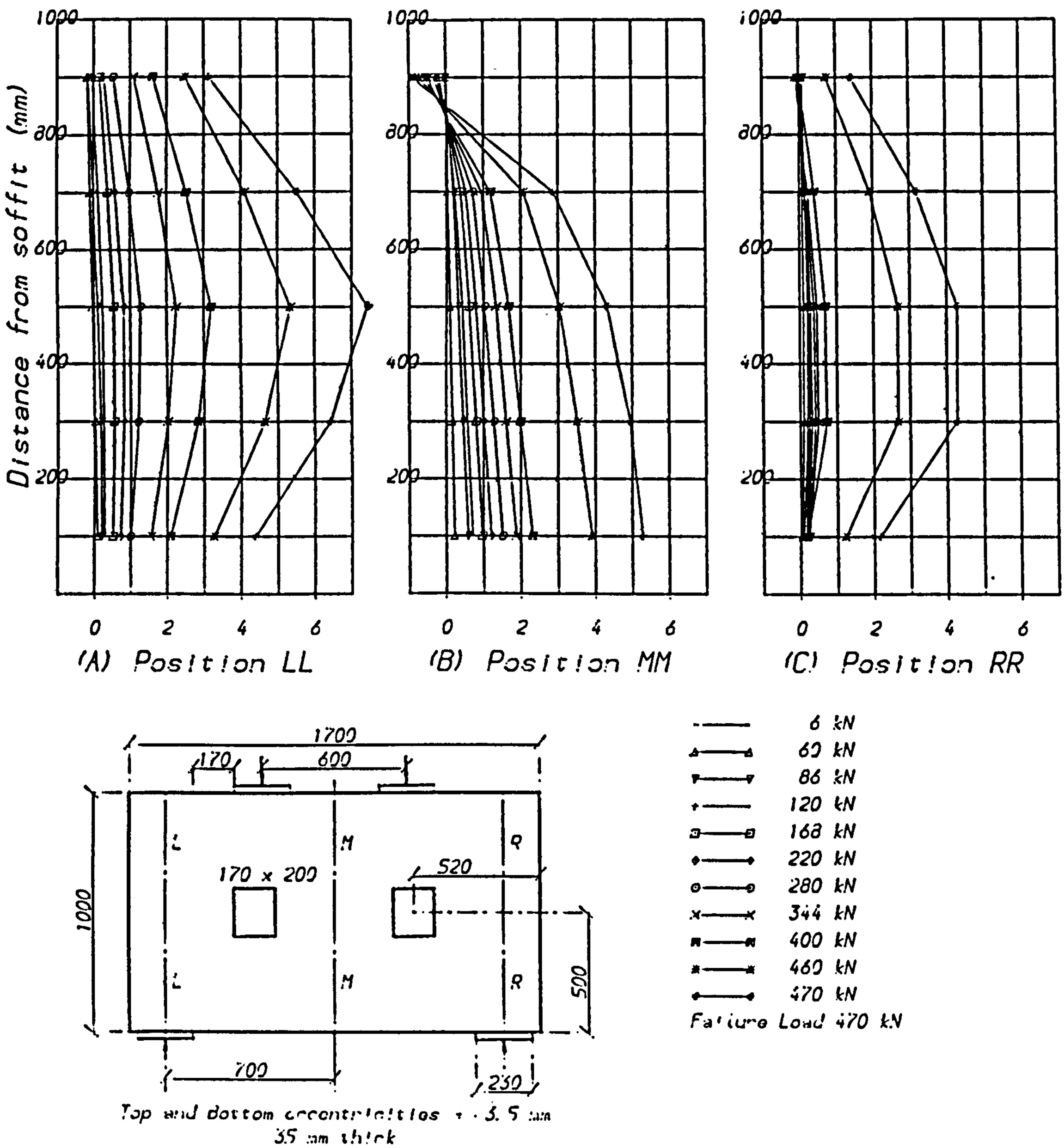

Figure 6.11(h) : Lateral displacement profiles of Beam W-CR

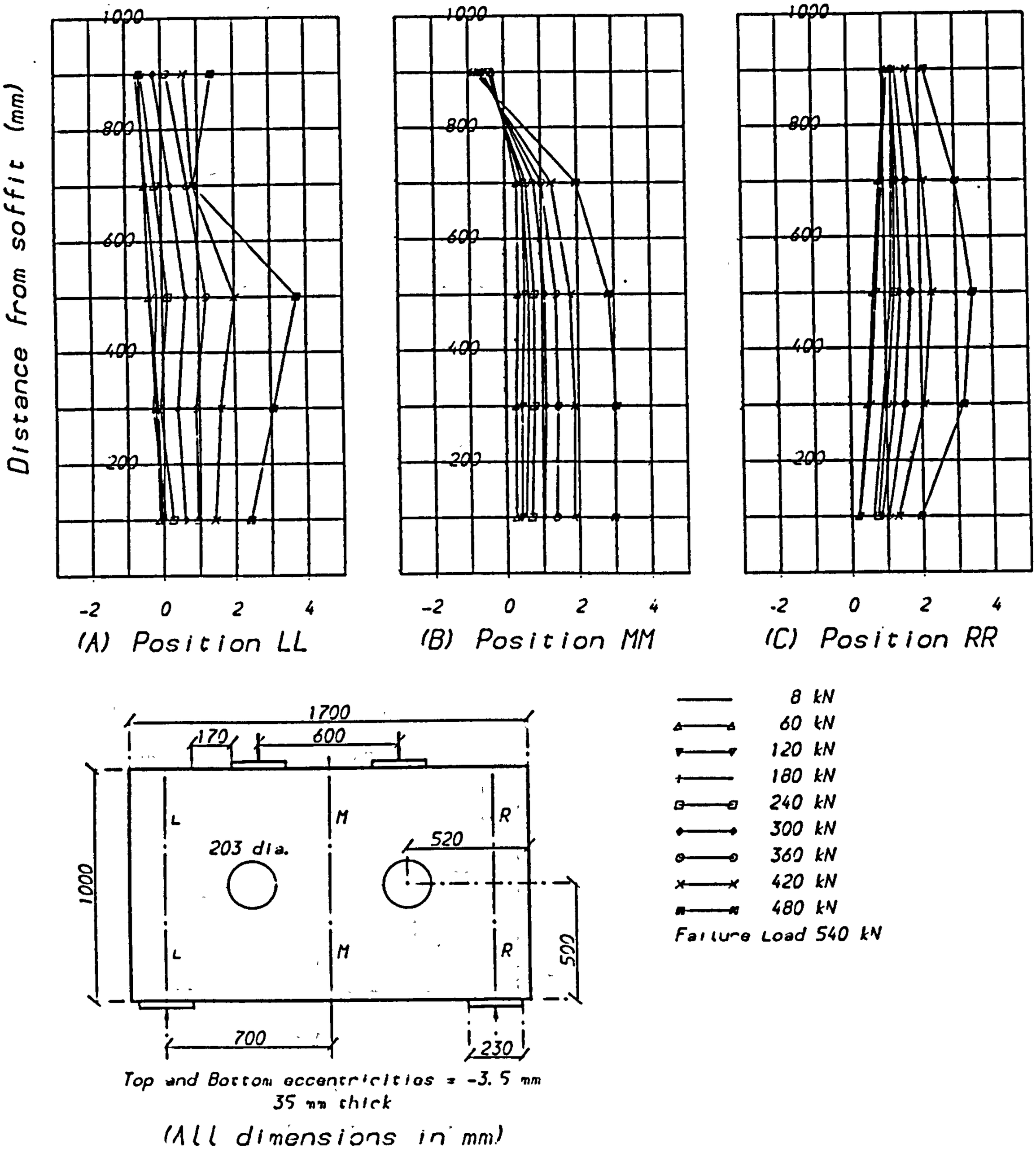

Figure 6.11(i) : Lateral displacement profiles of Beam W-CC

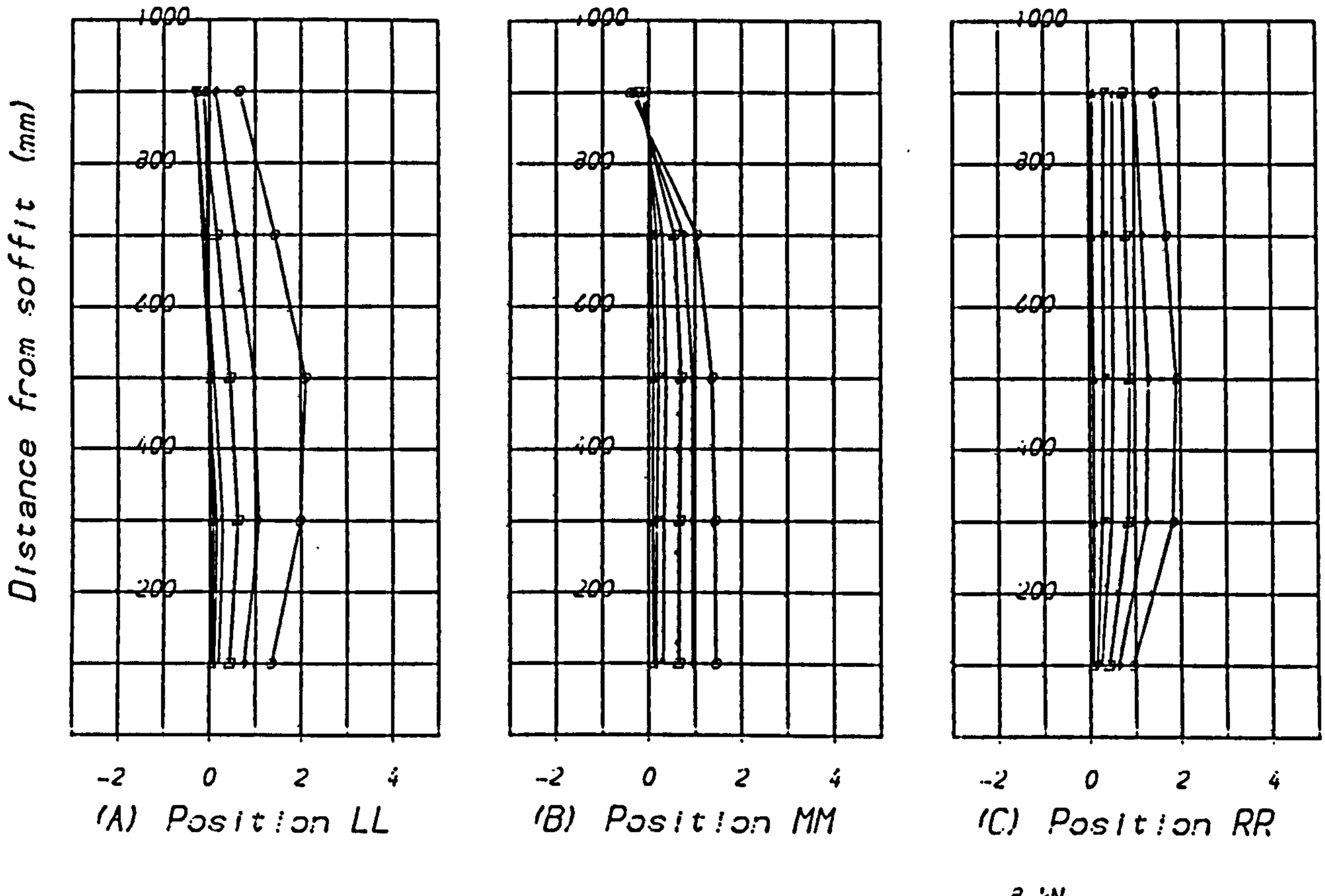

Figure 6.11(j) : Lateral displacement profiles of Beam W-DR

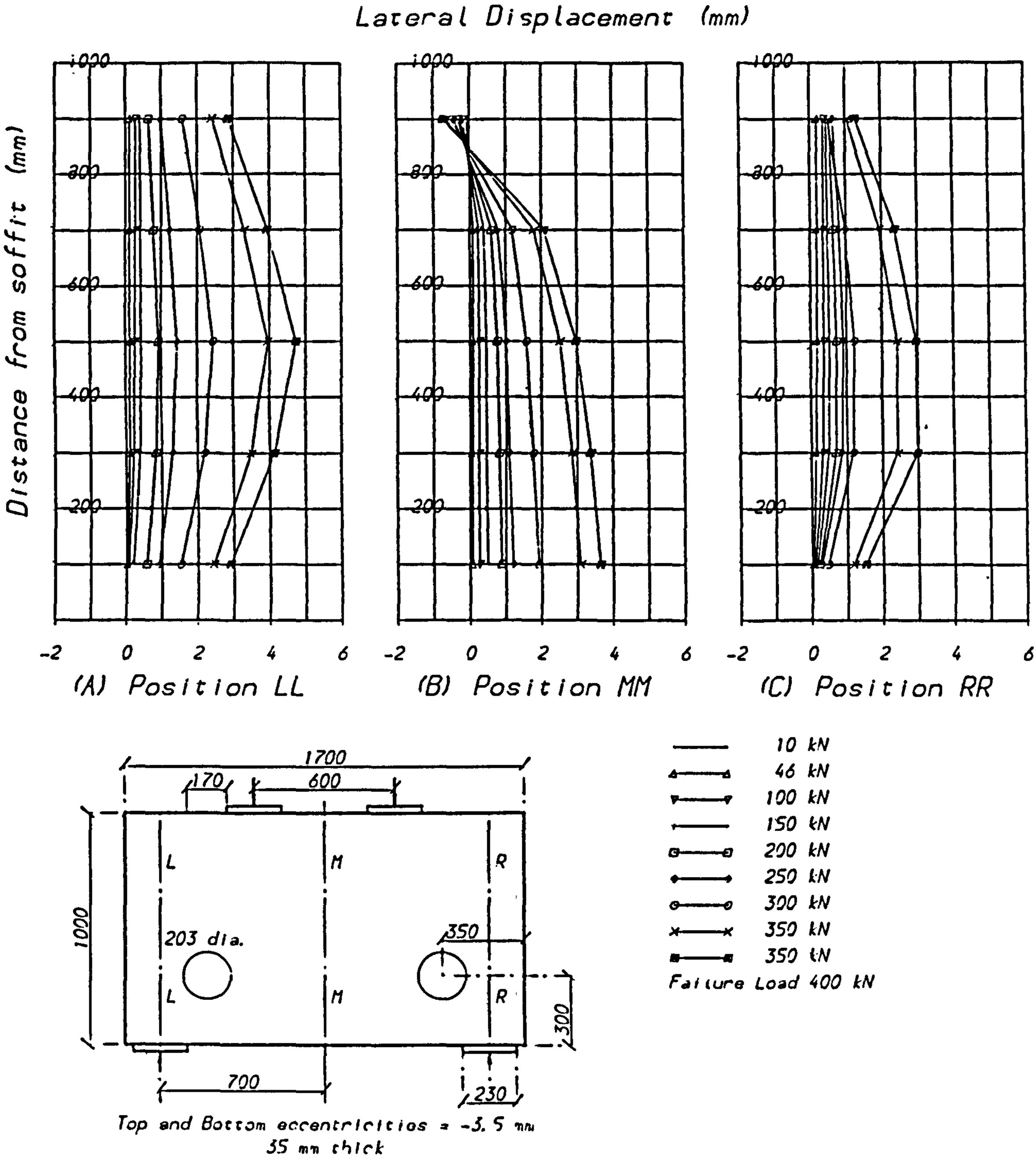

Figure 6.11(k) : Lateral displacement profiles of Beam W-DC

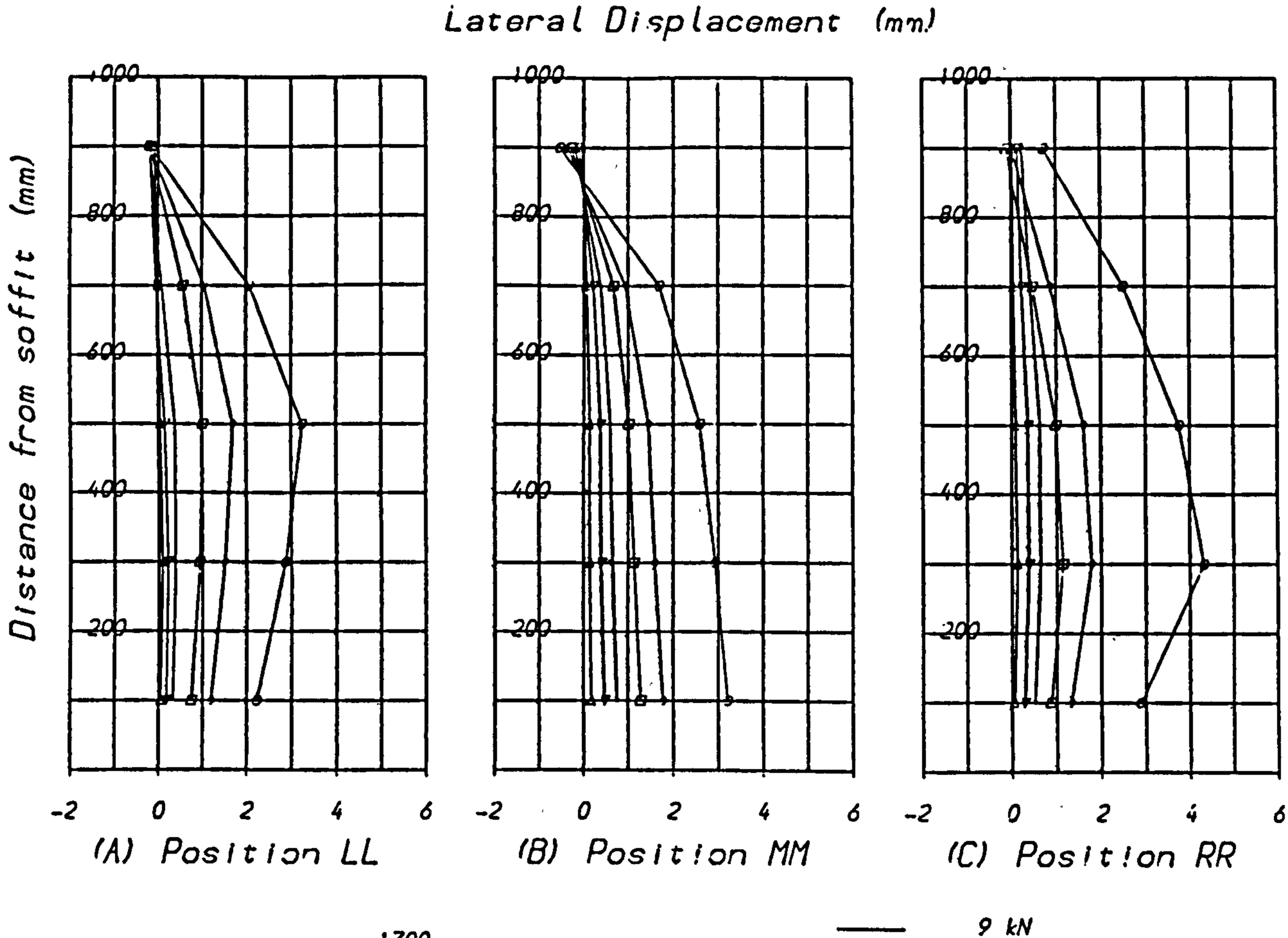

Figure 6.11(1) : Lateral displacement profiles of Beam W-ER

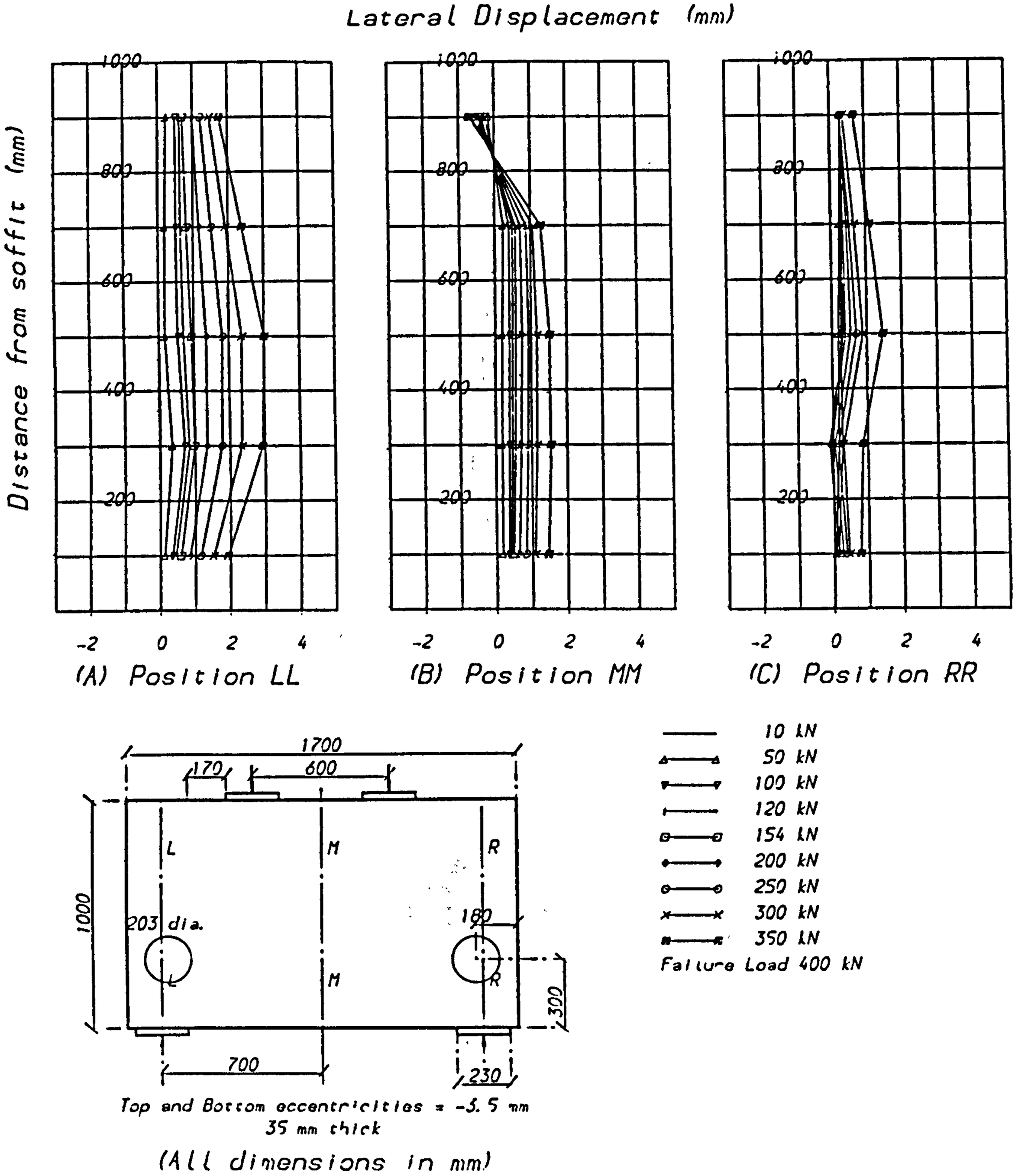

Figure 6.11(m) : Lateral displacement profiles of Beam W-EC

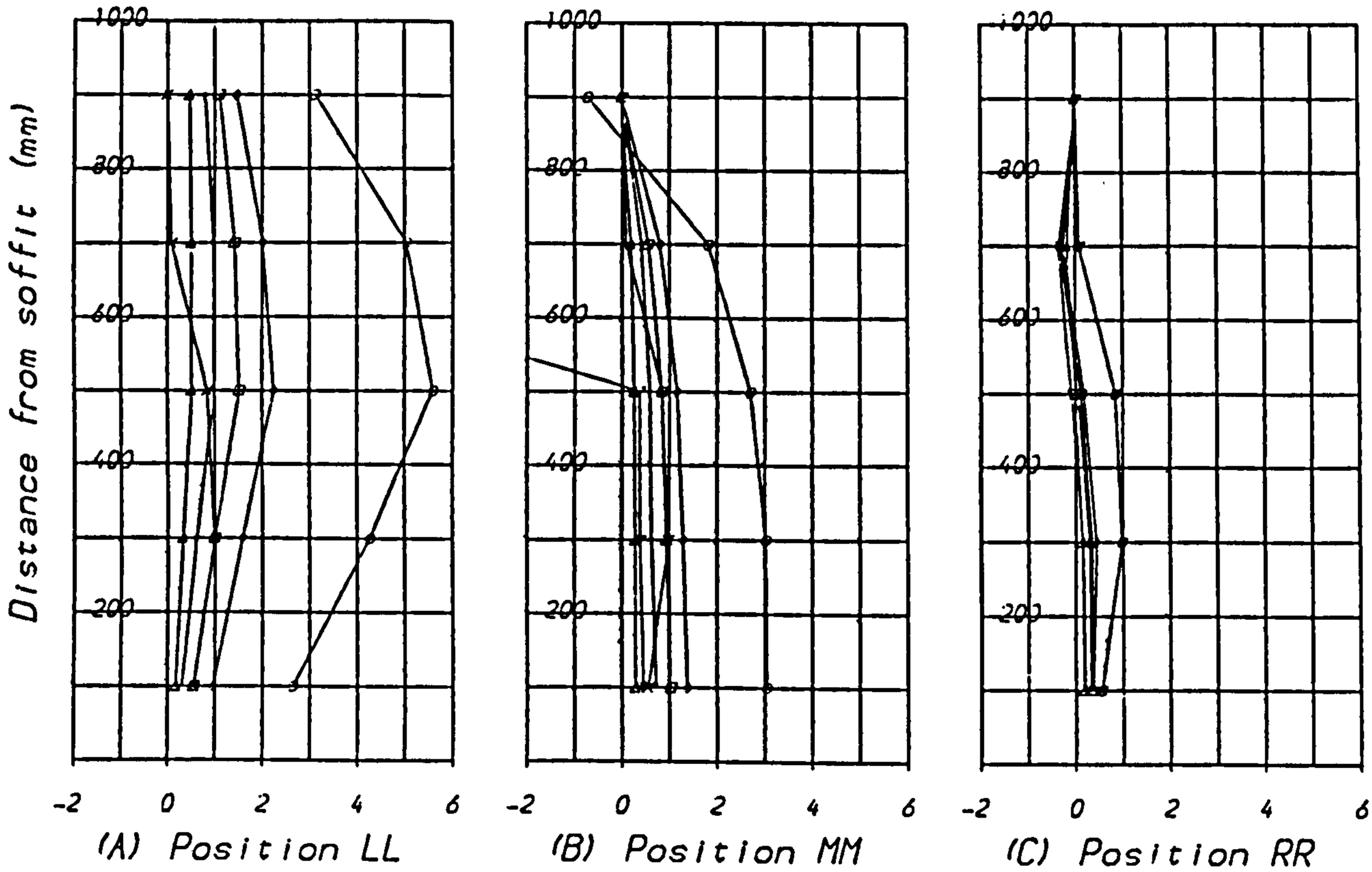

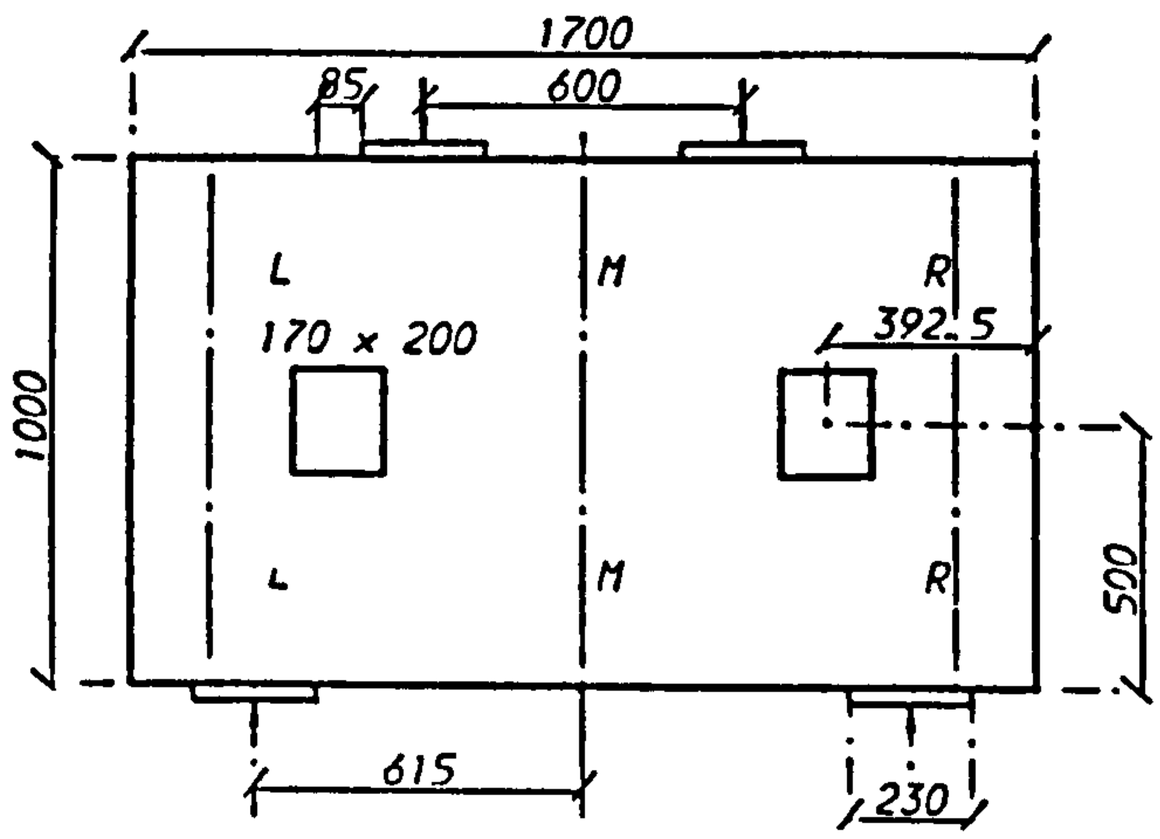

Top and Bottom eccentricities = -3.5 mm
35 mm thick
(All dimensions in mm)

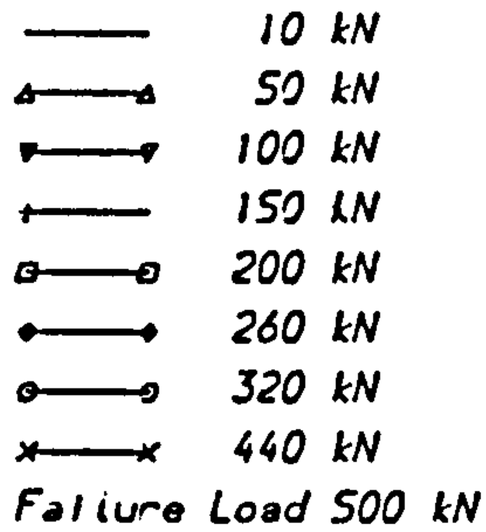

Figure 6.11(n) : Lateral displacement profiles of Beam W-AR-S

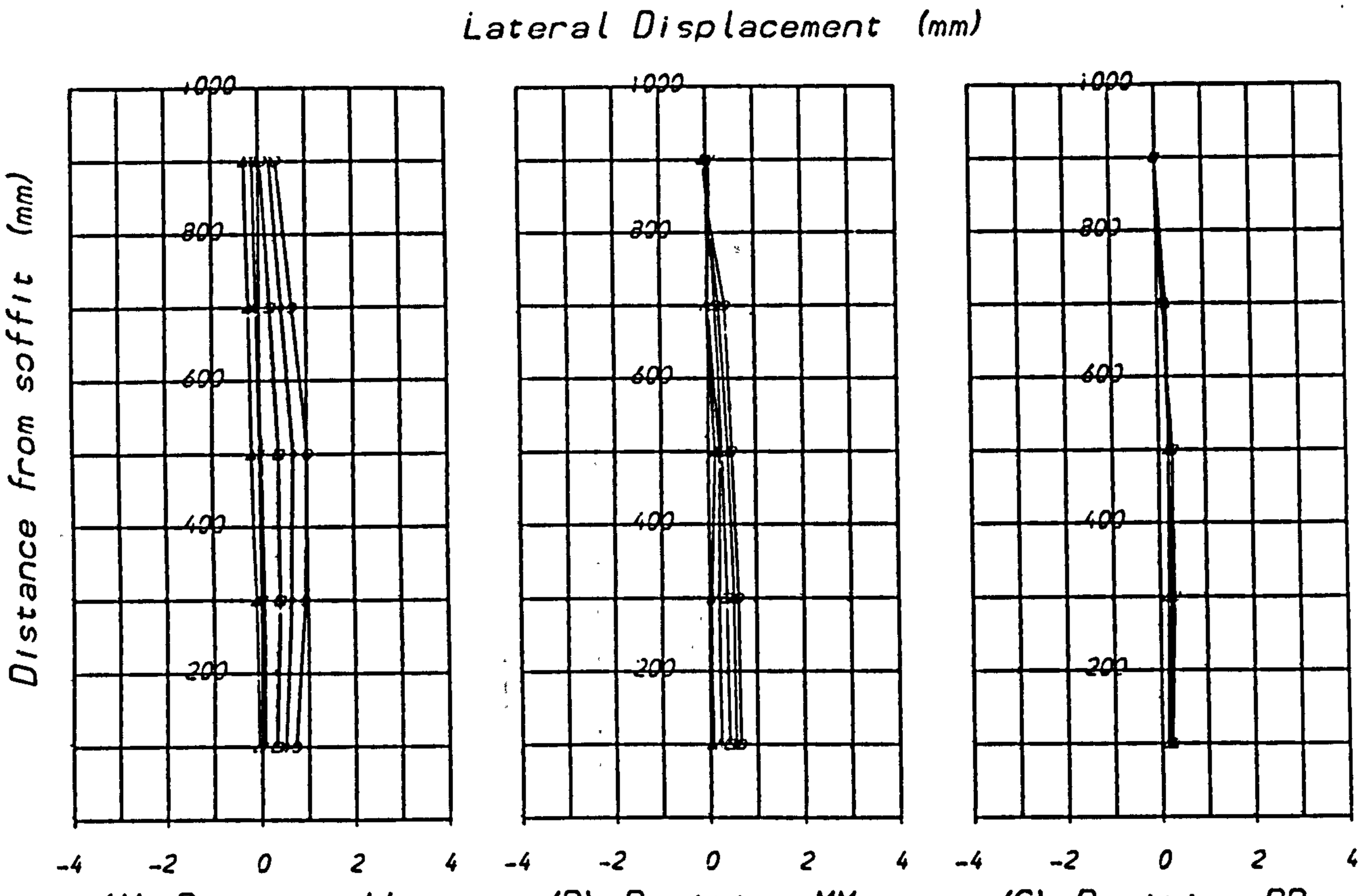

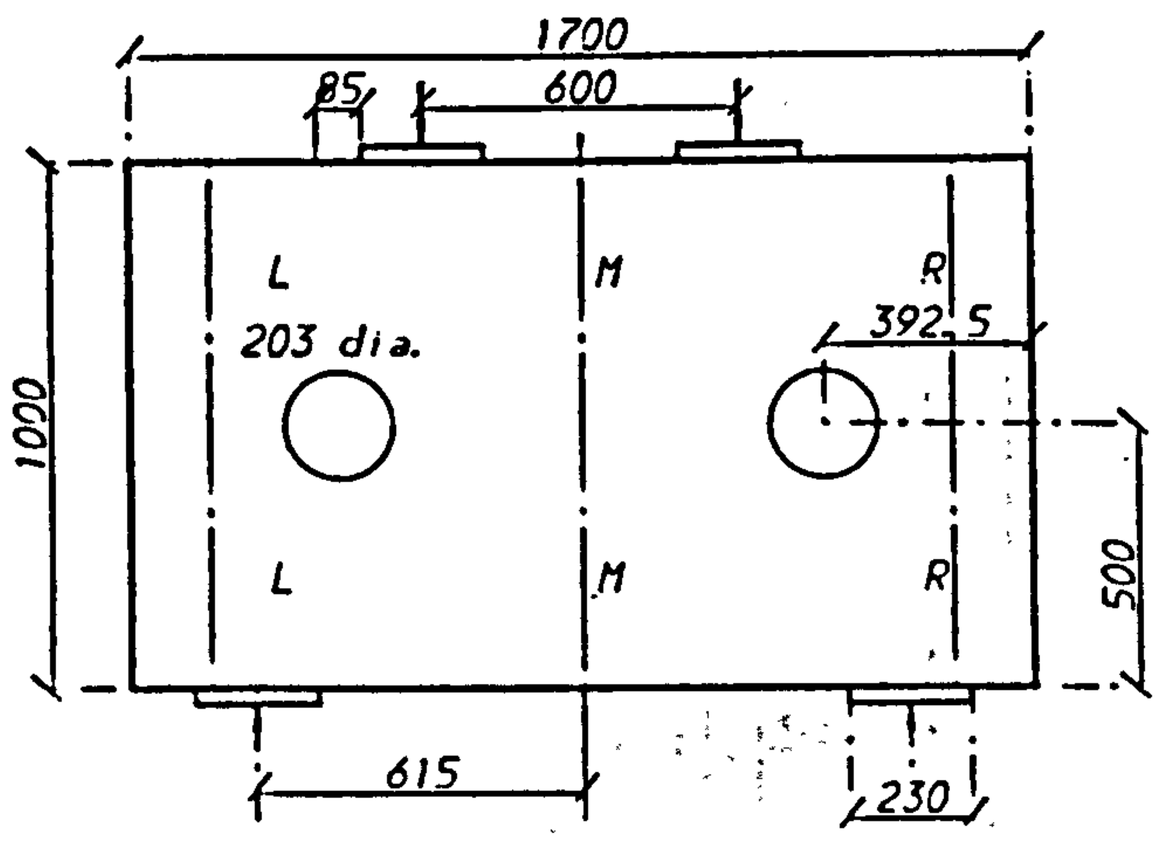

10 kN
50 kN
100 kN
150 kN
200 kN
250 kN
300 kN
Failure Load 580 kN

Top and Bottom eccentricities = -3.5 mm
35 mm thick

(All dimensions in mm)

Figure 6.11(o) : Lateral displacement profiles of Beam W-AC-S

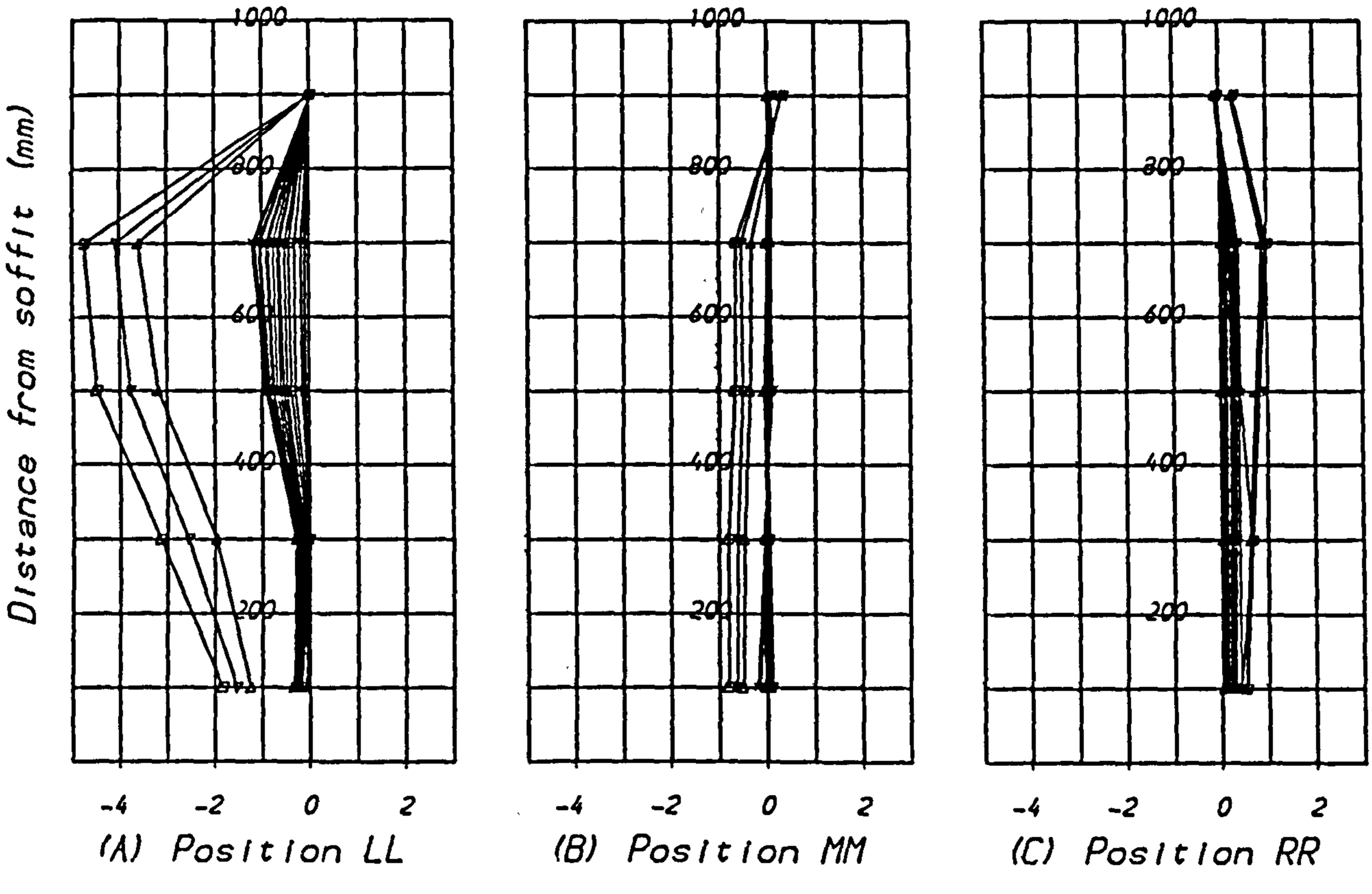

Figure 6.12(a) : Lateral displacement profiles of Beam CB-H1-R

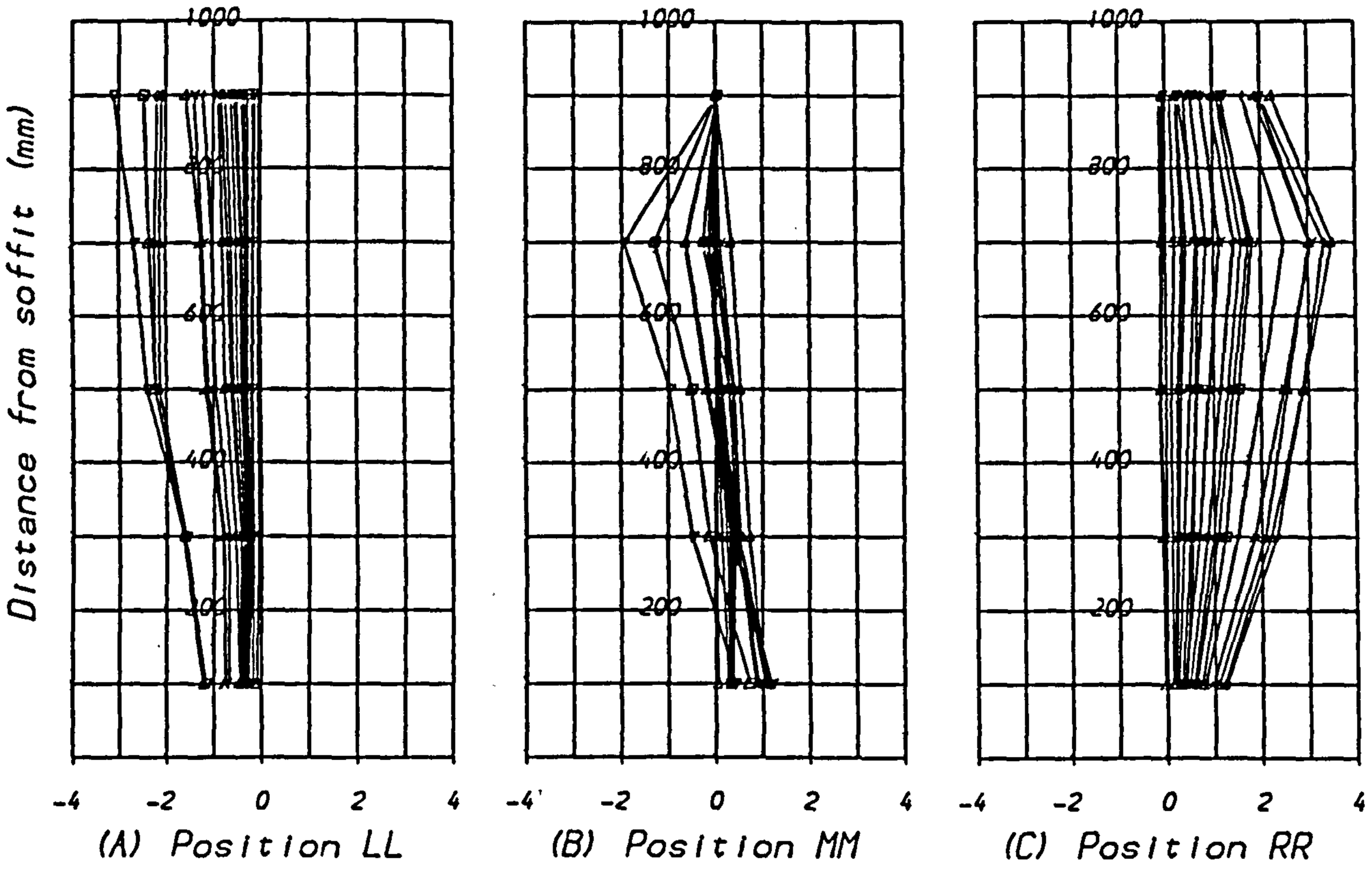

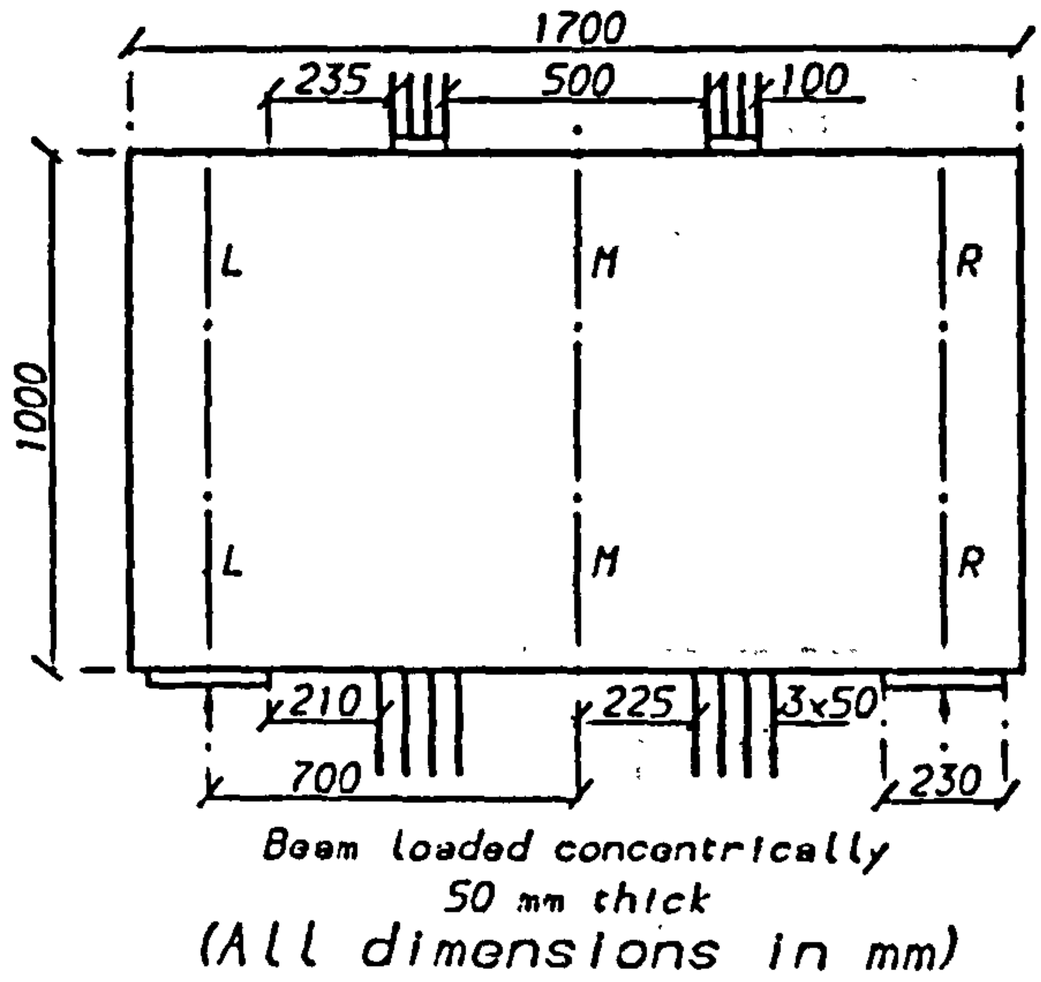

Figure 6.12(b) : Lateral displacement profiles of Beam CB-H2

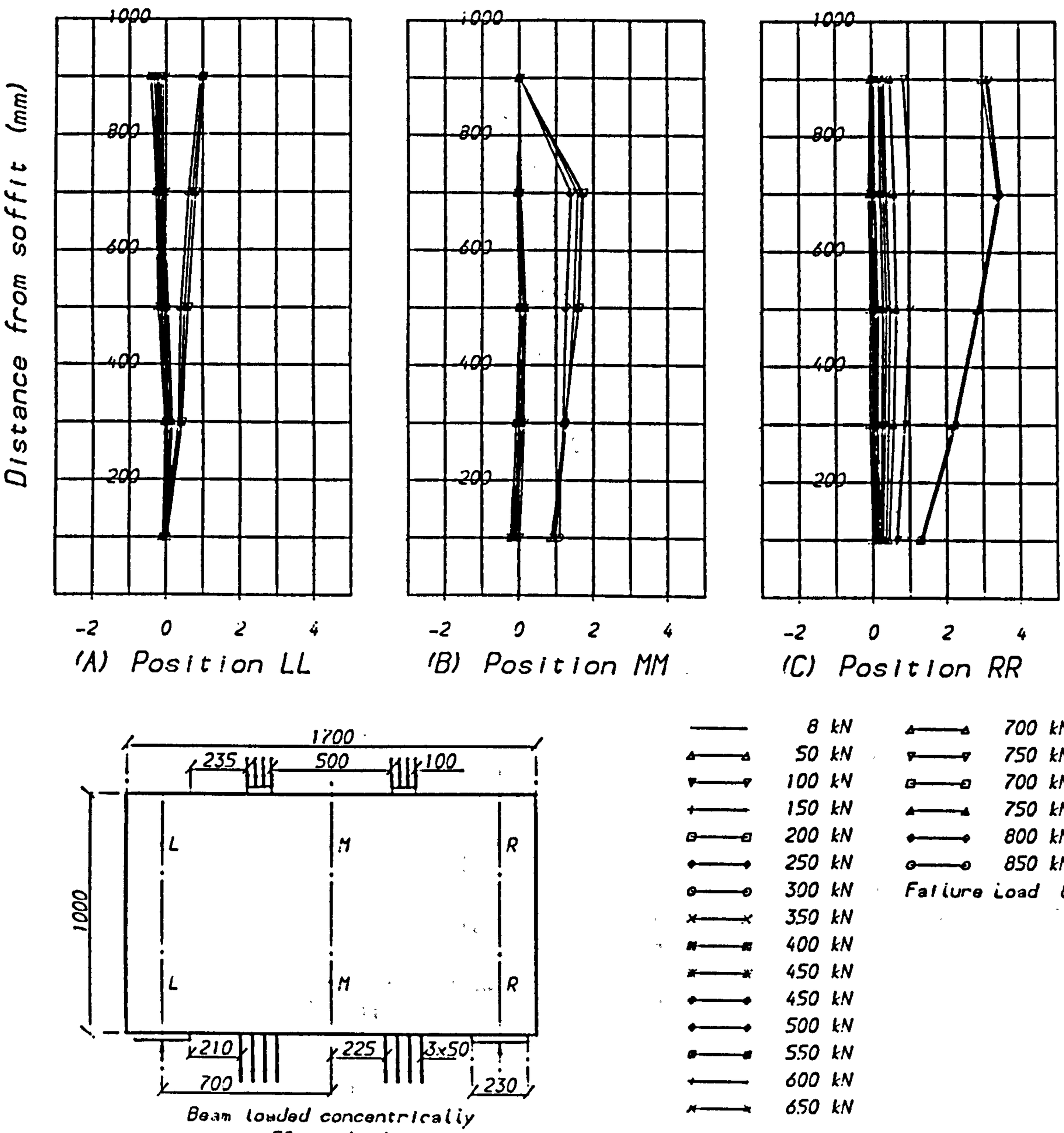

Figure 6.12(c) : Lateral displacement profiles of Beam CB-H3

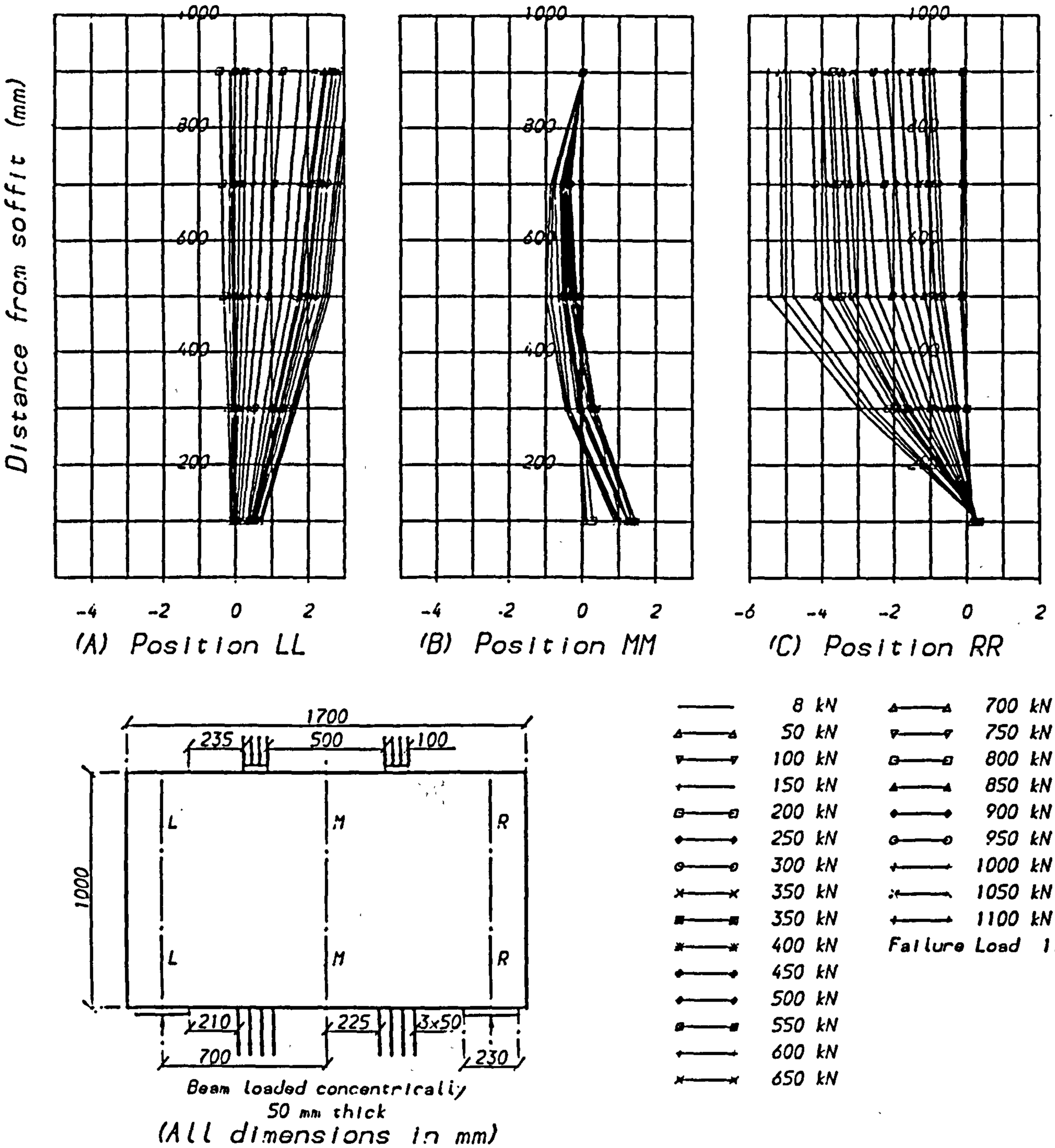

Figure 6.12(d) : Lateral displacement profiles of Beam CB-H4

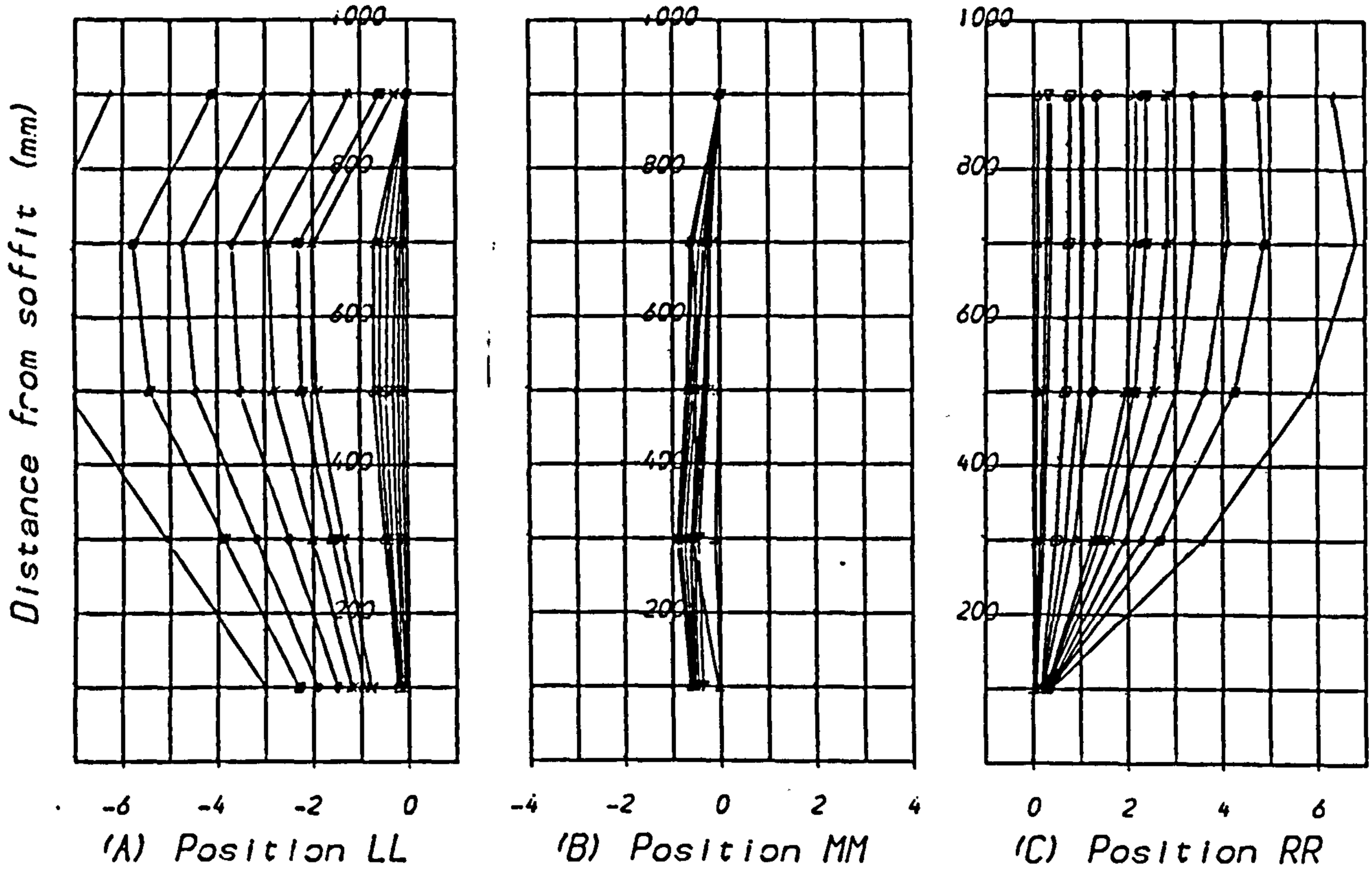

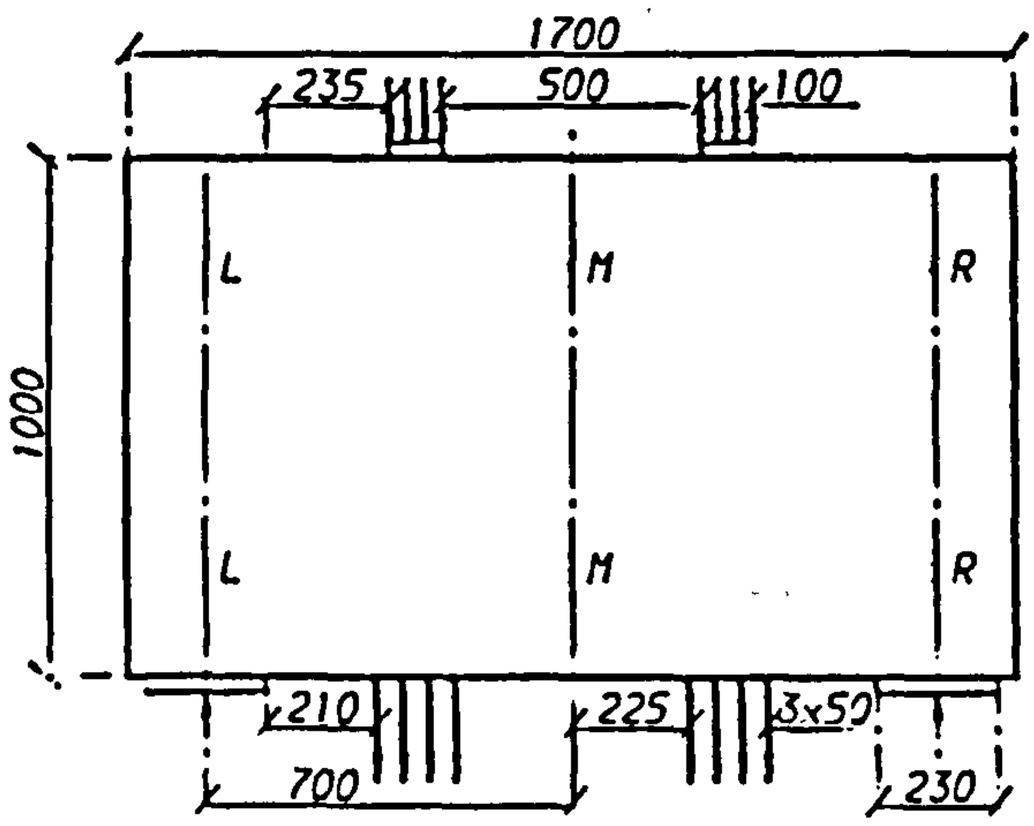

Beam loaded concentrically
50 mm thick
(All dimensions in mm)

8 kN
50 kN
100 kN
150 kN
200 kN
250 kN
300 kN
350 kN
350 kN
400 kN
450 kN
500 kN
550 kN
600 kN

Failure Load 1000 kN

Figure 6.12(e) : Lateral displacement profiles of Beam CB-H5

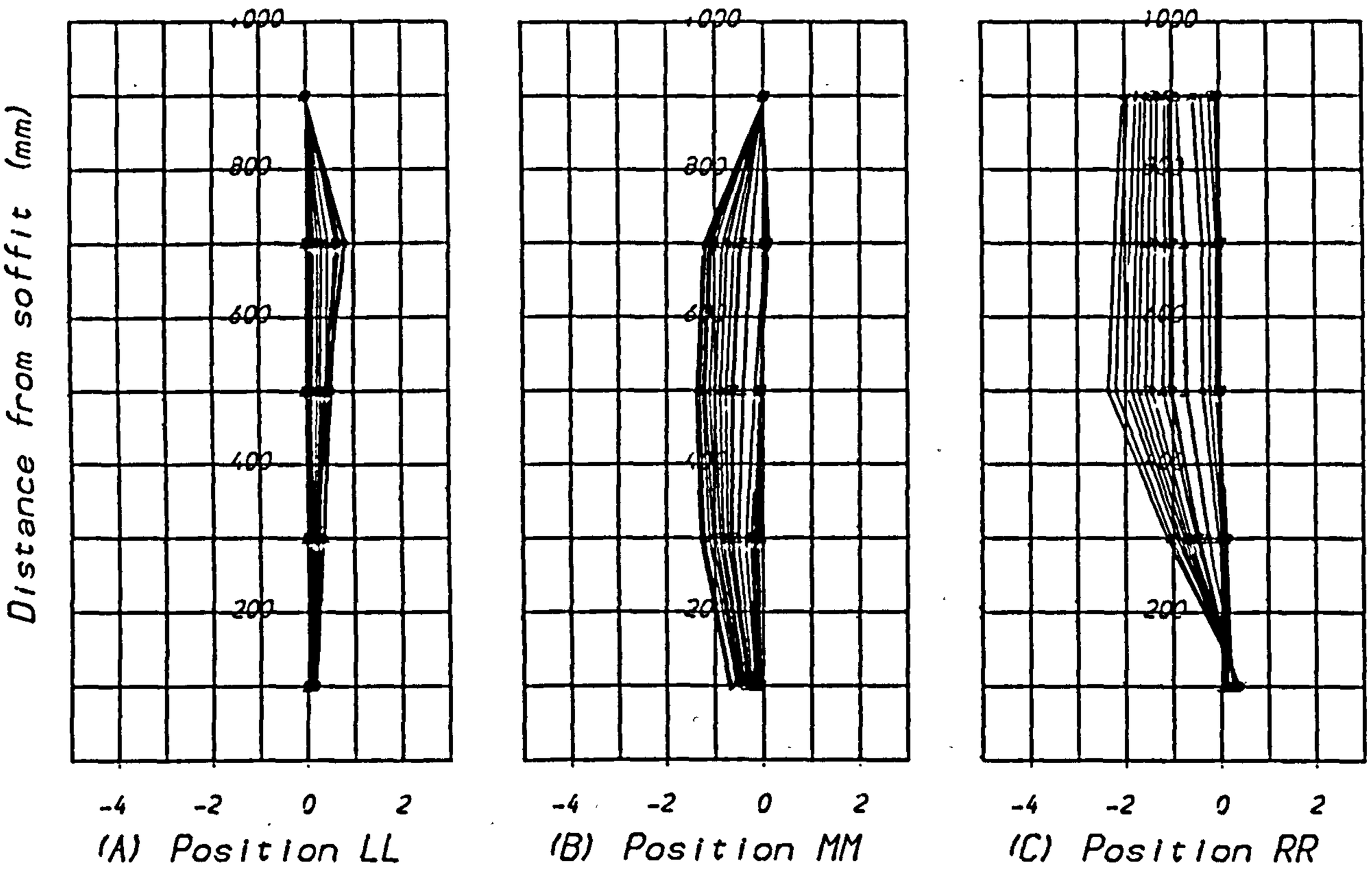

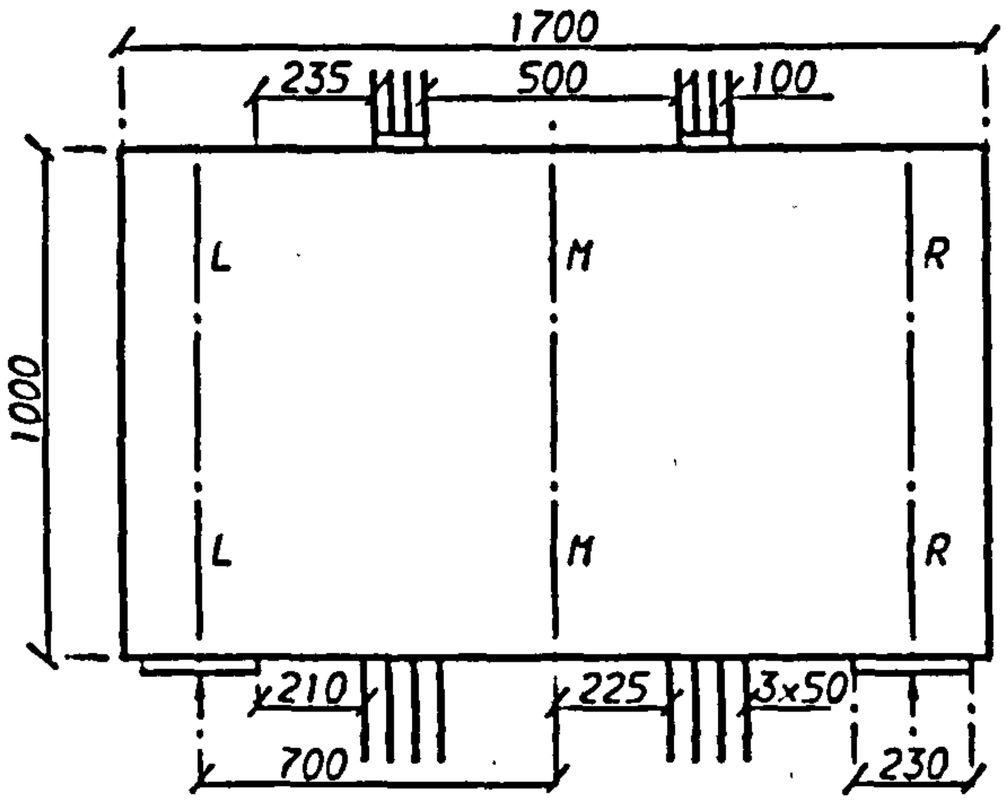

Beam loaded concentrically
50 mm thick
(All dimensions in mm)

———	8 kN	———	700 kN
———	50 kN	———	750 kN
———	100 kN	———	800 kN
———	150 kN	———	850 kN
———	200 kN	———	900 kN
———	250 kN	———	950 kN
———	300 kN	———	1000 kN
———	350 kN	———	1050 kN
———	400 kN	———	1100 kN
———	400 kN	———	1150 kN
———	450 kN	———	1200 kN
———	500 kN	Failure Load	1200 kN
———	550 kN		
———	600 kN		
———	650 kN		

Figure 6.12(f) : Lateral displacement profiles of Beam CB-H6

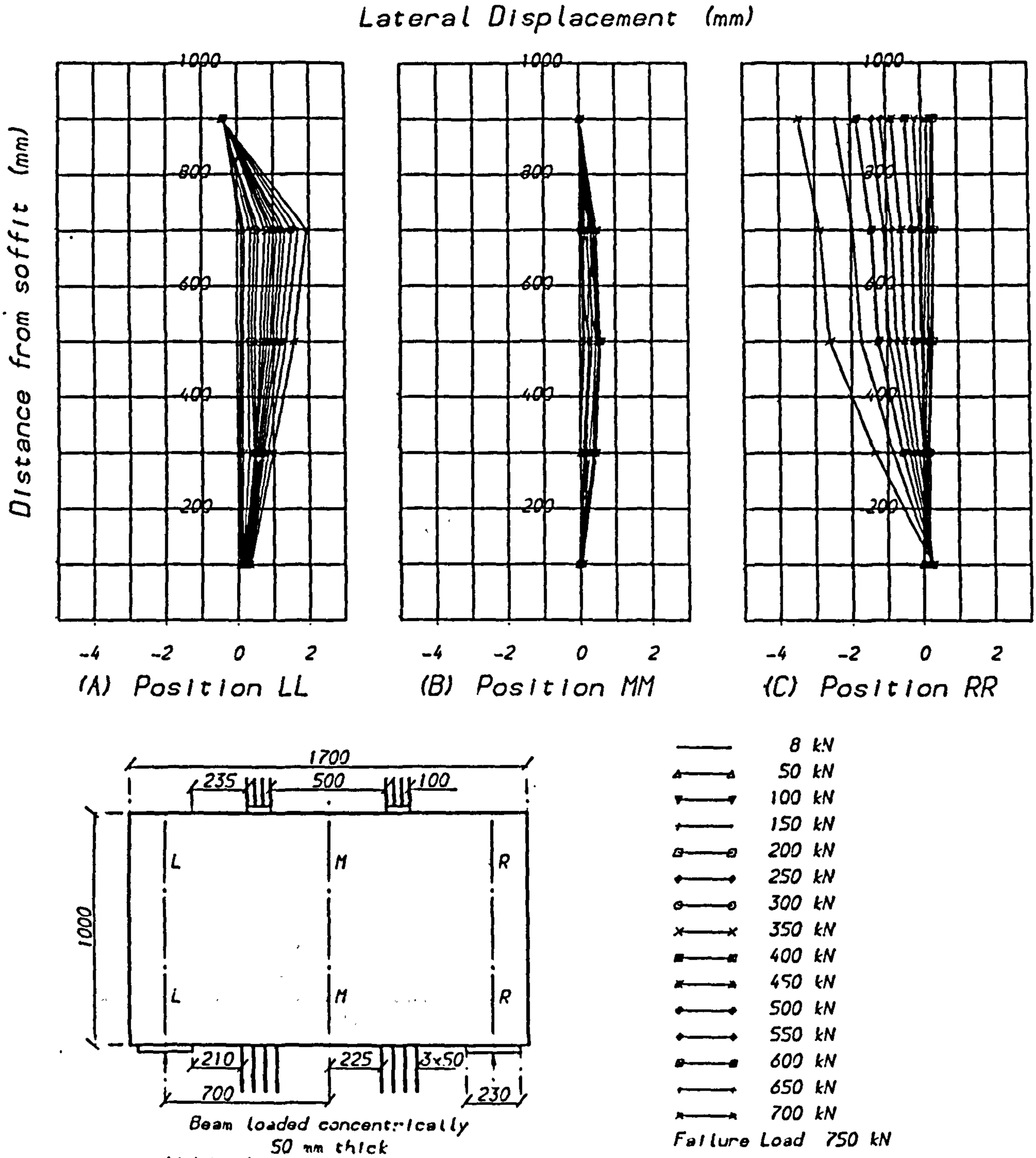

Figure 6.12(g) : Lateral displacement profiles of Beam CB-L1

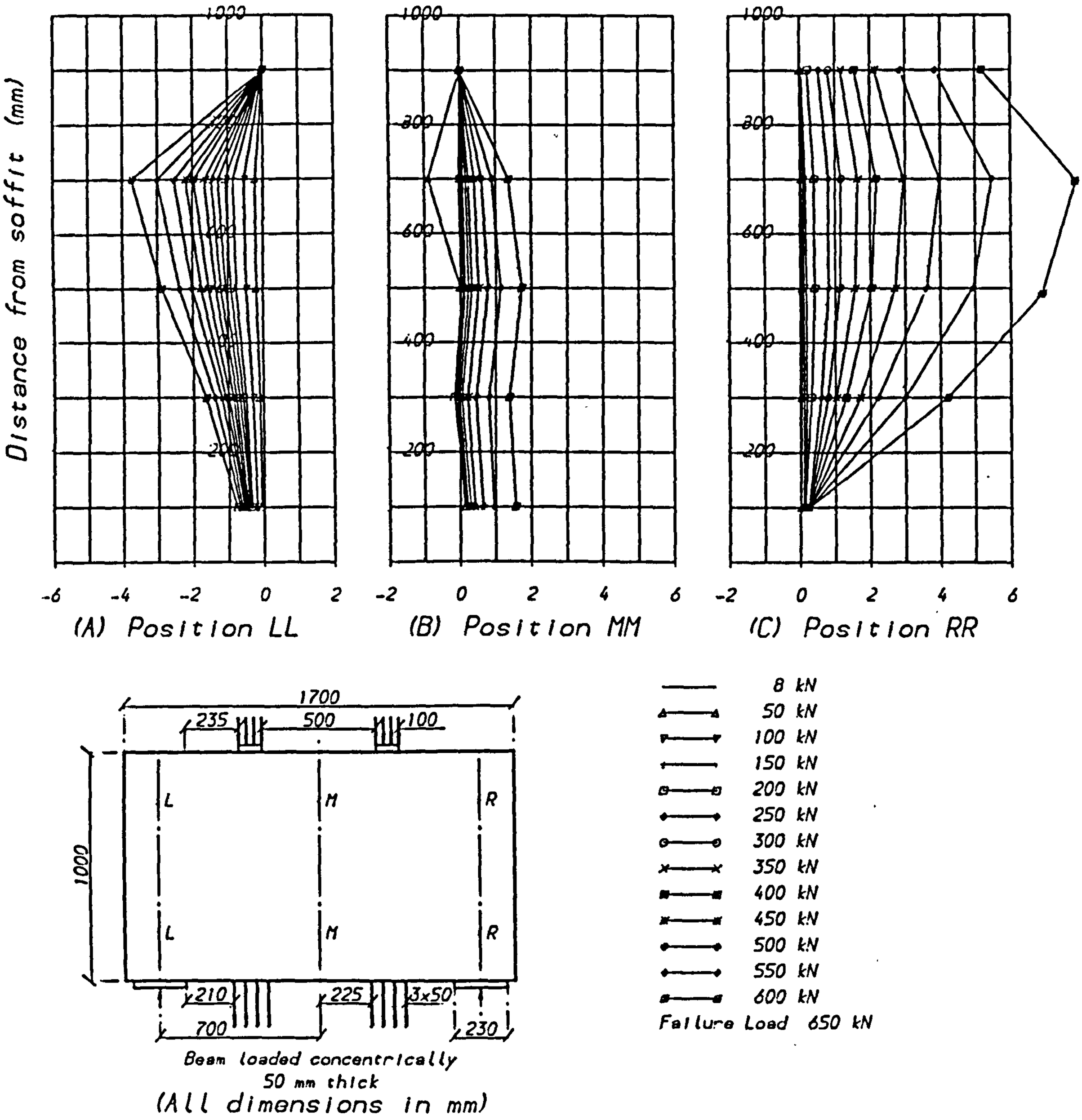

Figure 6.12(h) : Lateral displacement profiles of Beam CB-L2

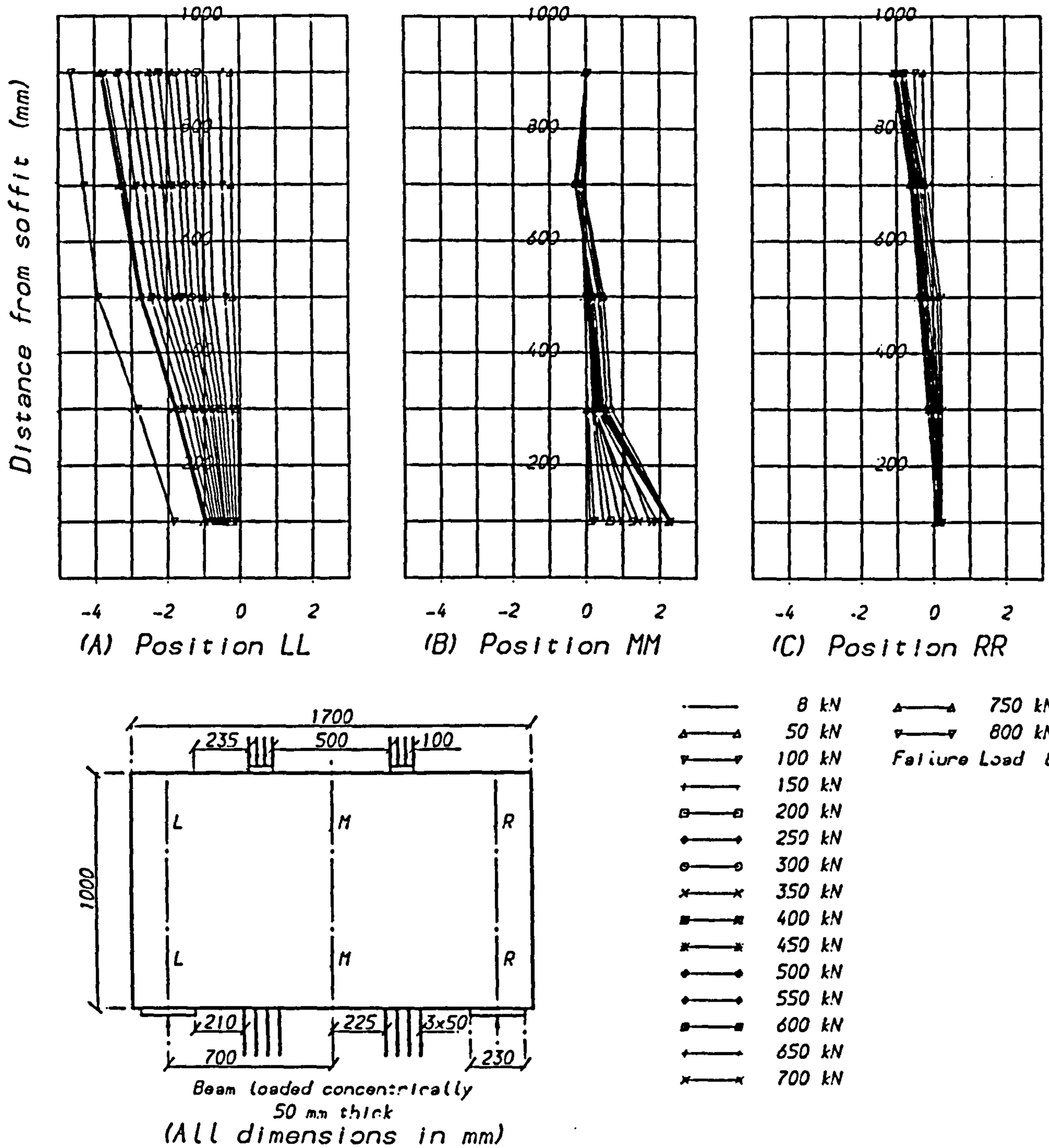

Figure 6.12(i) : Lateral displacement profiles of Beam CB-L3

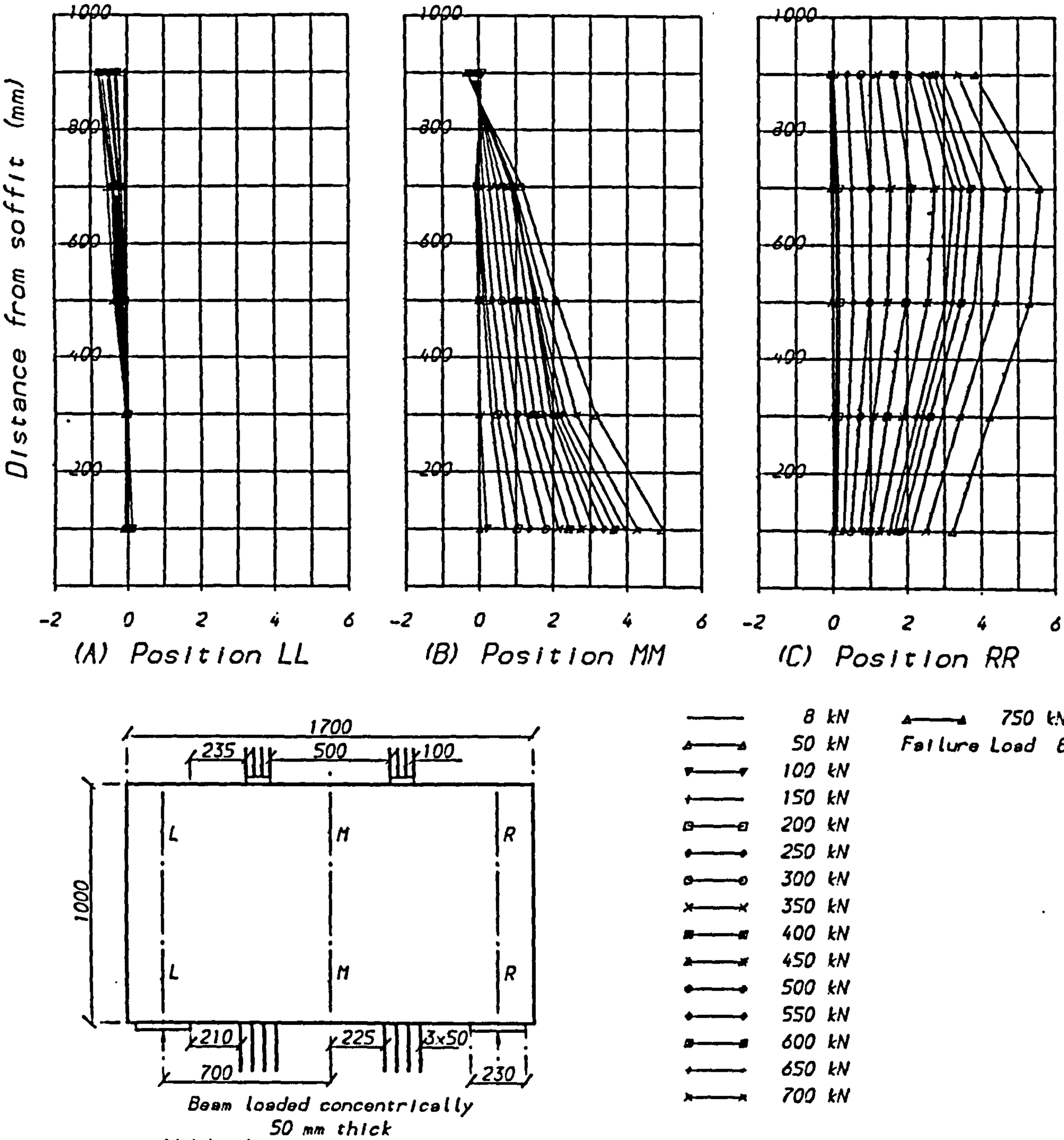

Figure 6.12(j) : Lateral displacement profiles of Beam CB-L4

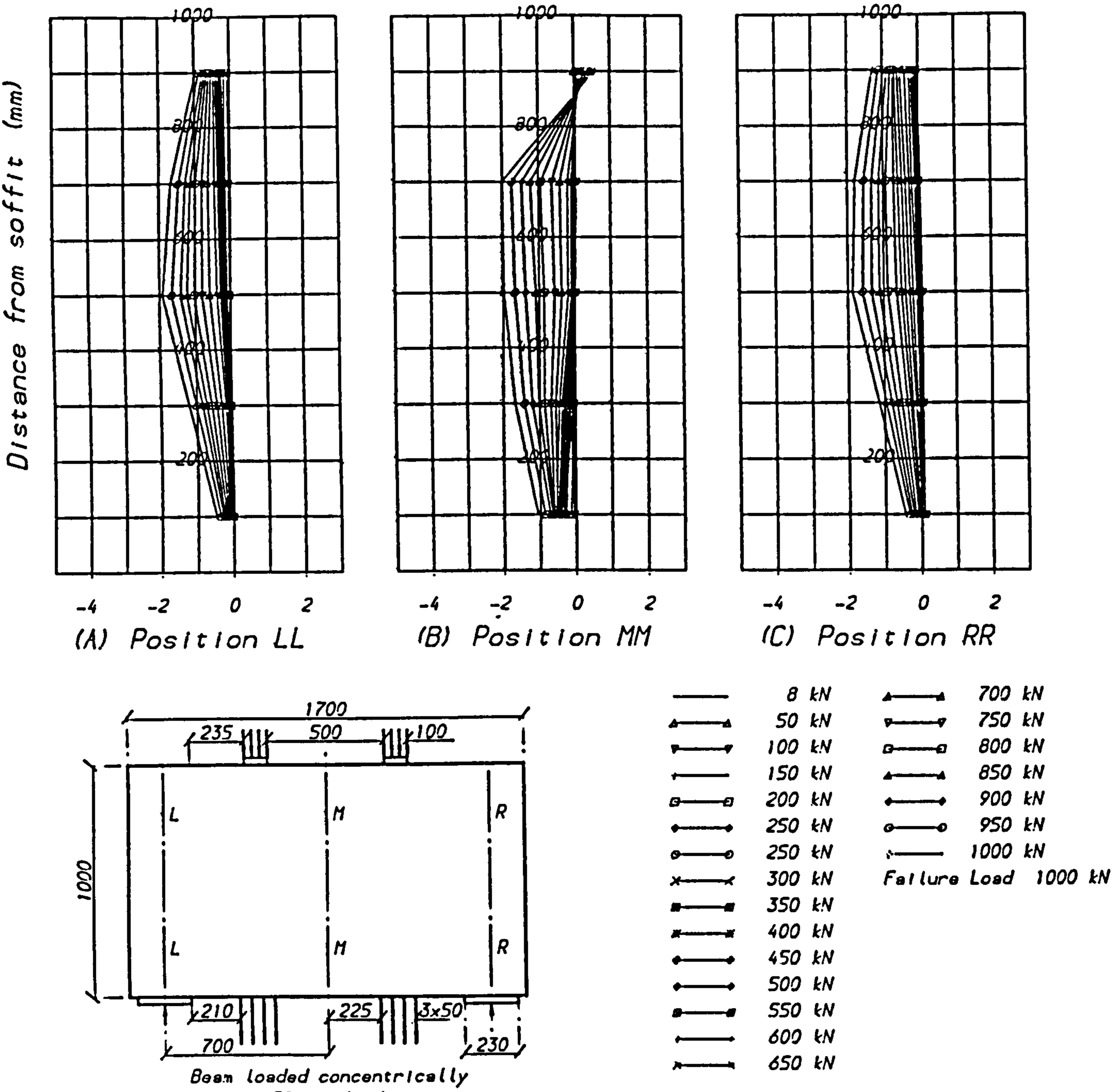

Figure 6.12(k) : Lateral displacement profiles of Beam CB-L5

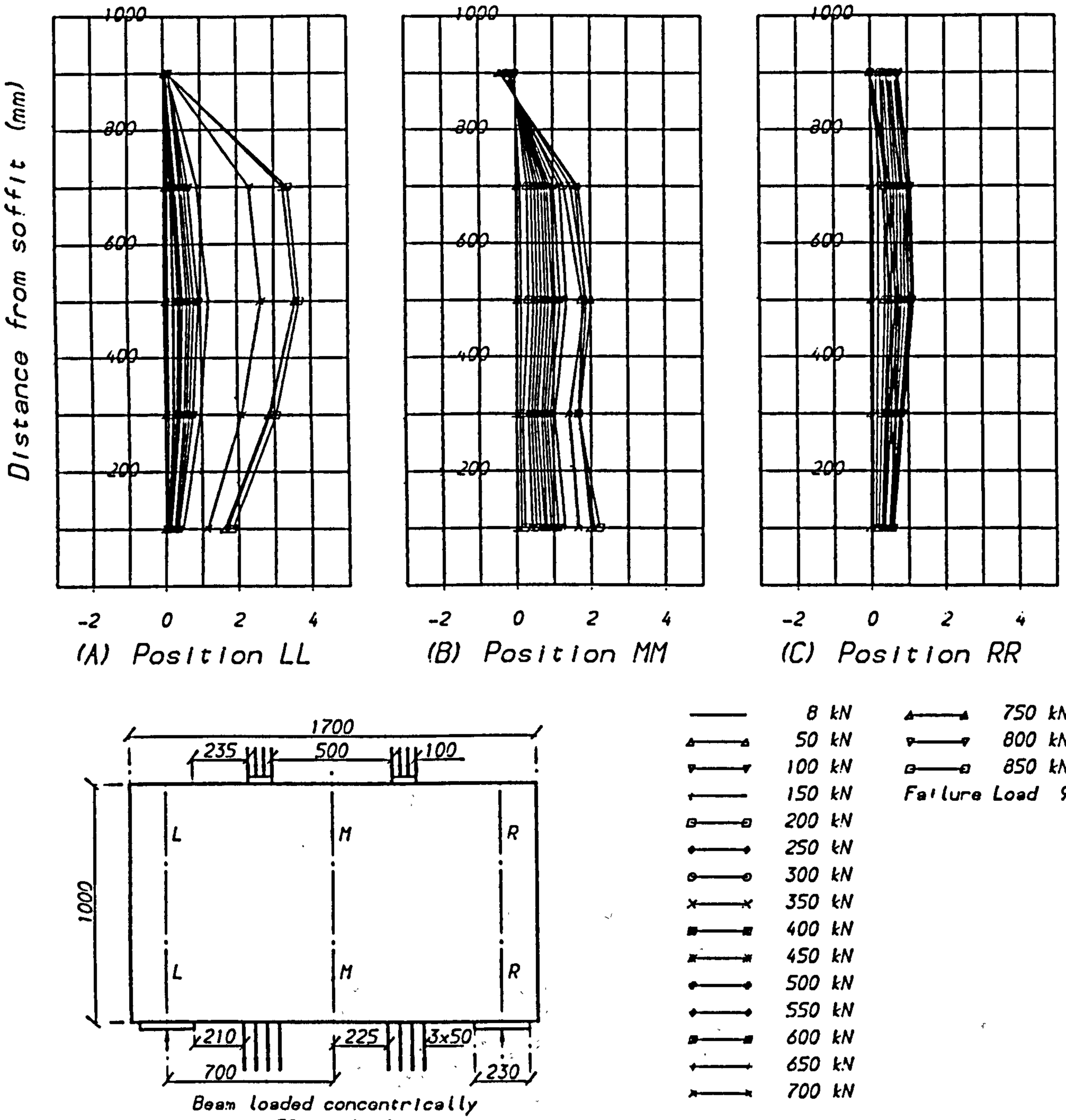

Figure 6.12(1) : Lateral displacement profiles of Beam CB-L6

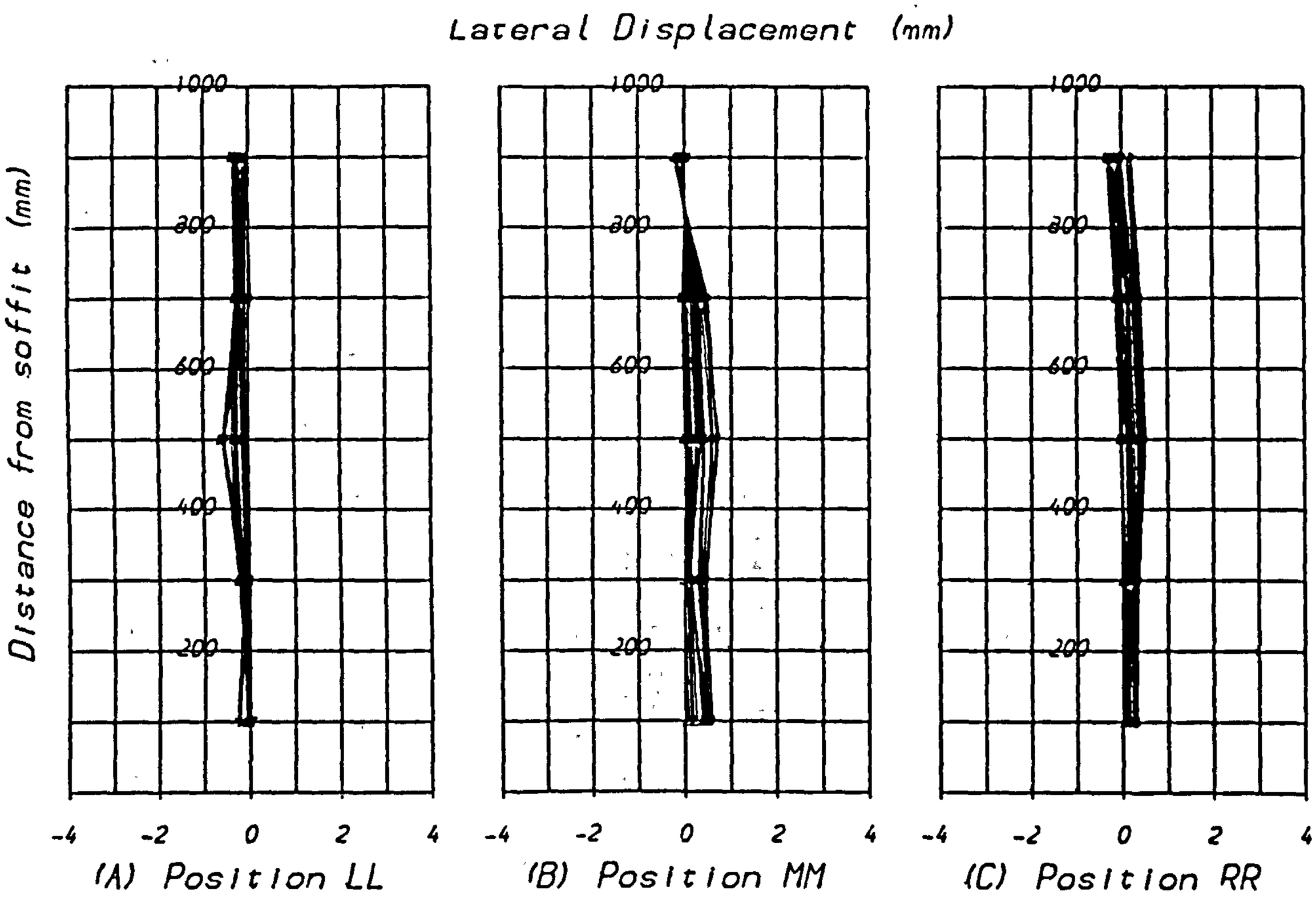

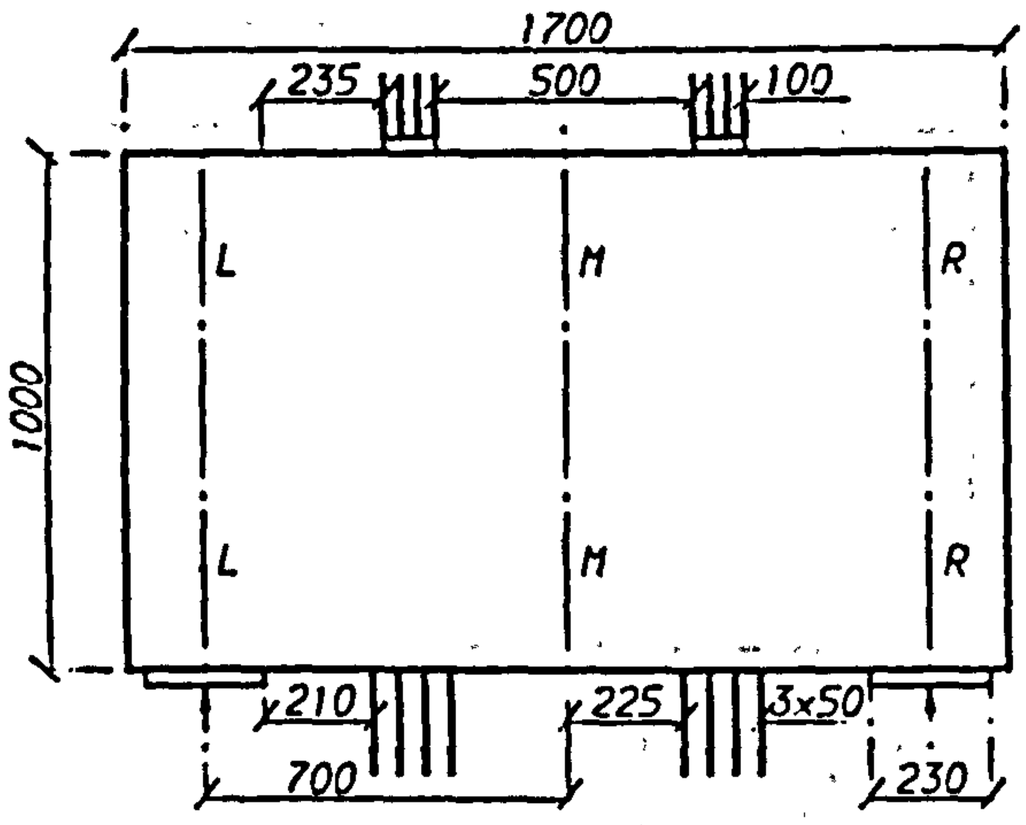

Beam loaded concentrically
50 mm thick
(All dimensions in mm)

	8 kN		375 kN
	25 kN		400 kN
	50 kN		425 kN
	75 kN		450 kN
	100 kN		475 kN
	125 kN		475 kN
	150 kN		500 kN
	175 kN		525 kN
	200 kN		550 kN
	225 kN		575 kN
	250 kN		600 kN
	275 kN	Failure Load	620 kN
	300 kN		
	325 kN		
	350 kN		

Figure 6.12(m) : Lateral displacement profiles of Beam CB-L7

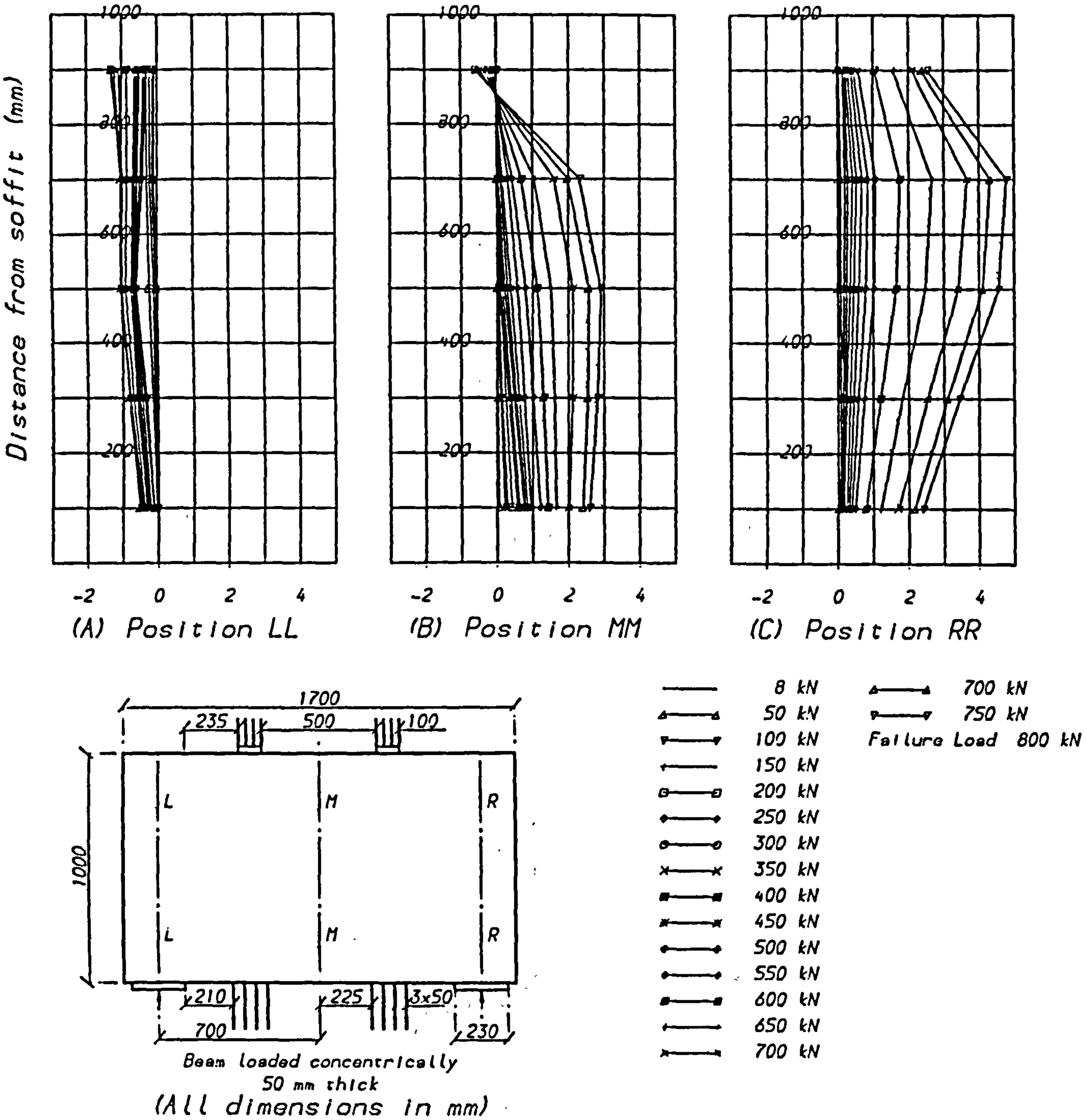

Figure 6.12(n) : Lateral displacement profiles of Beam CB-L8

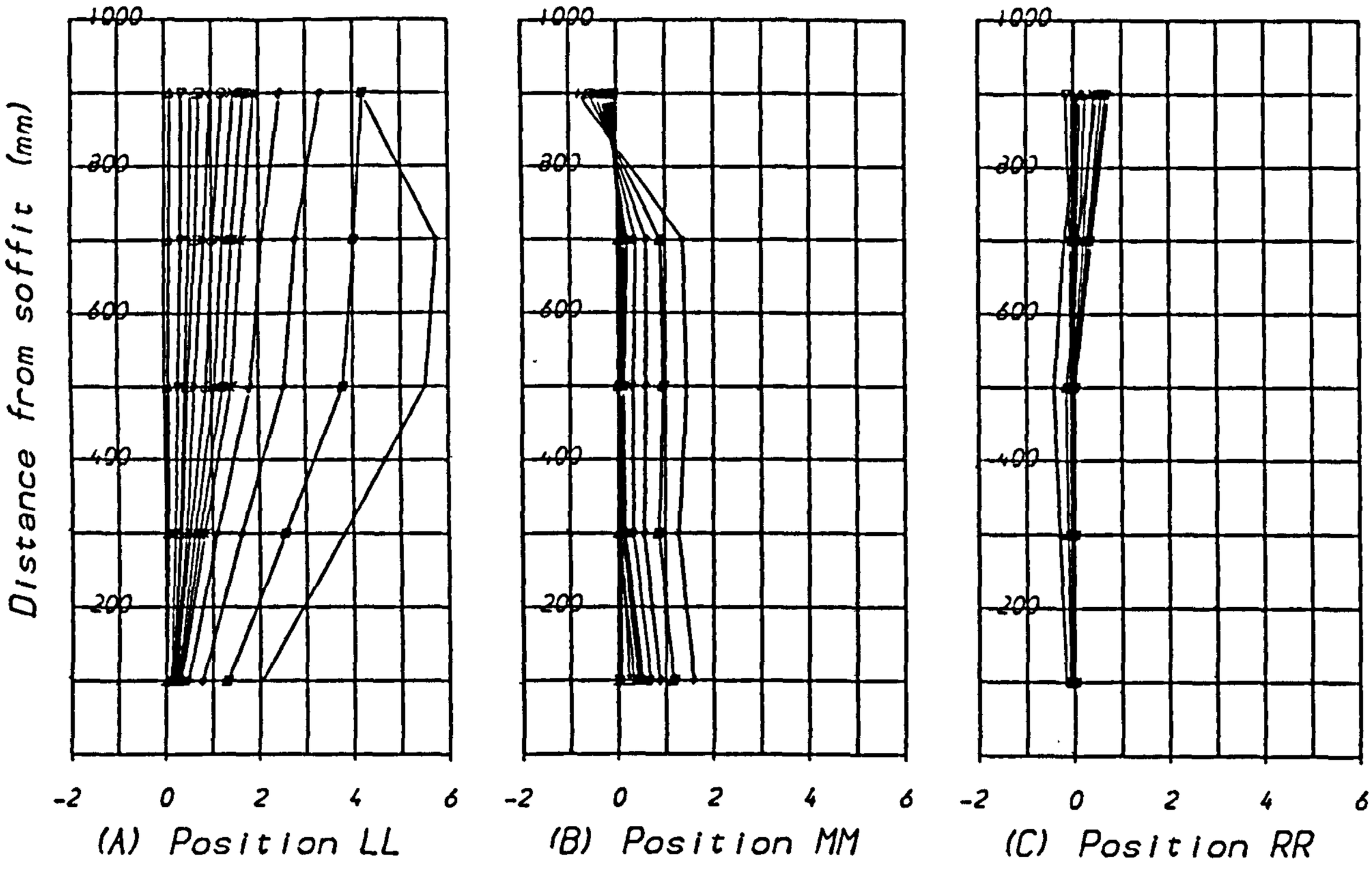

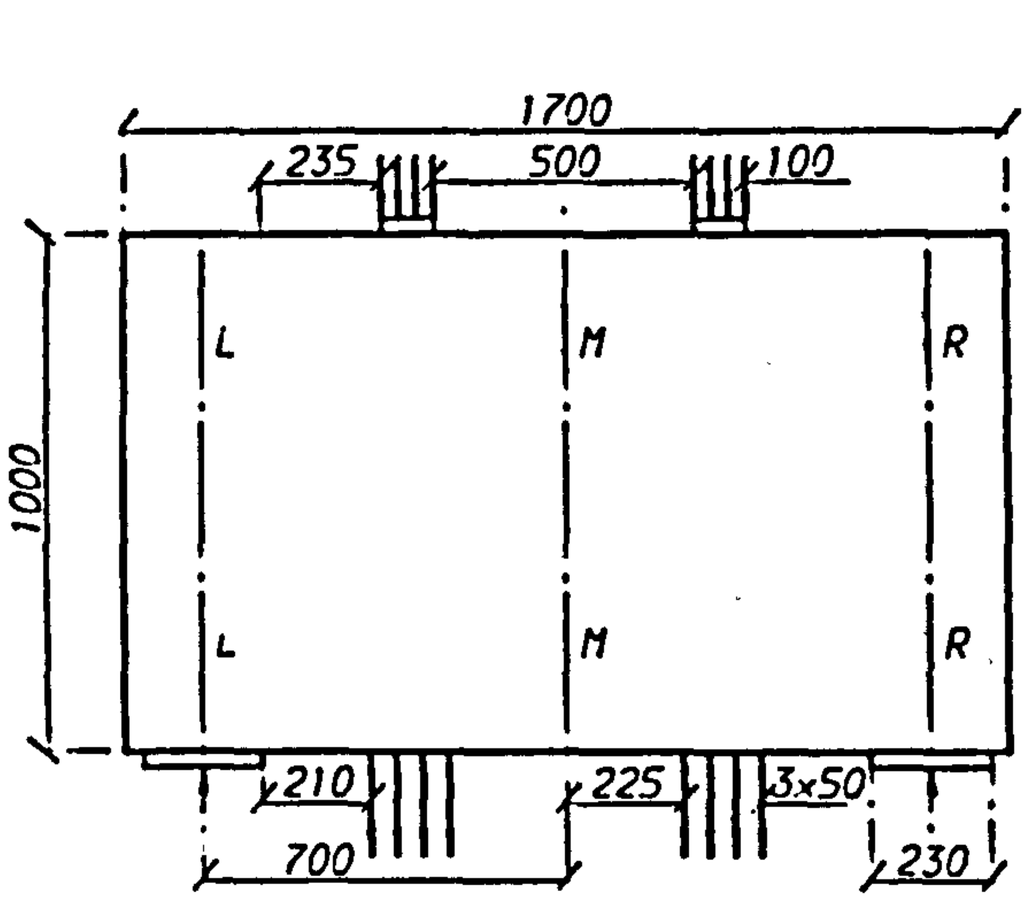

Beam loaded concentrically
50 mm thick
(All dimensions in mm)

———	8 kN
——▲——	50 kN
——▼——	100 kN
——+——	150 kN
——□——	200 kN
——◆——	250 kN
——○——	300 kN
——×——	350 kN
——■——	400 kN
——✱——	450 kN
——●——	500 kN
——◆——	550 kN
——■——	600 kN
——◆——	650 kN

Failure Load 650 kN

Figure 6.12(o) : Lateral displacement profiles of Beam CB-L9

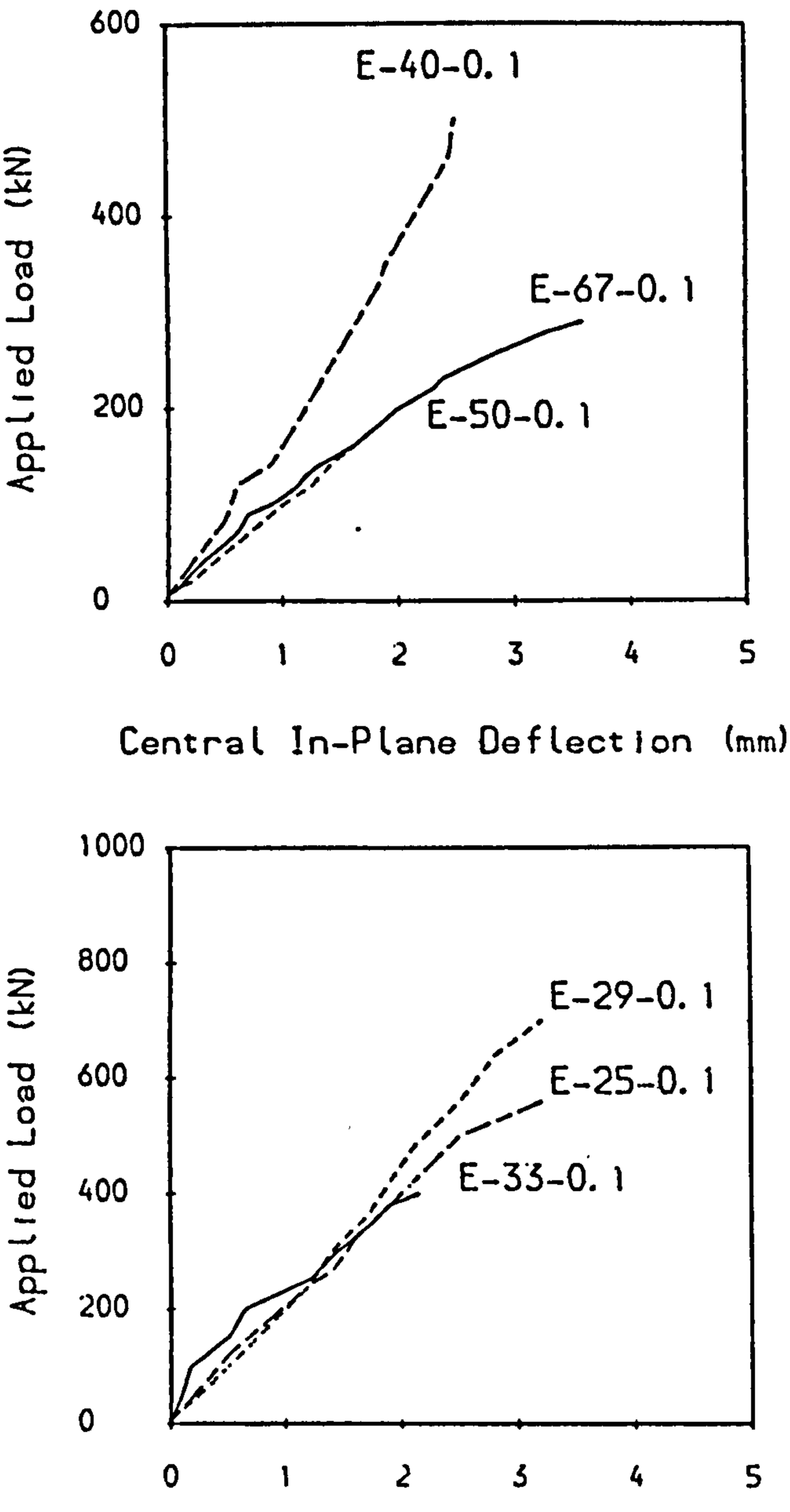

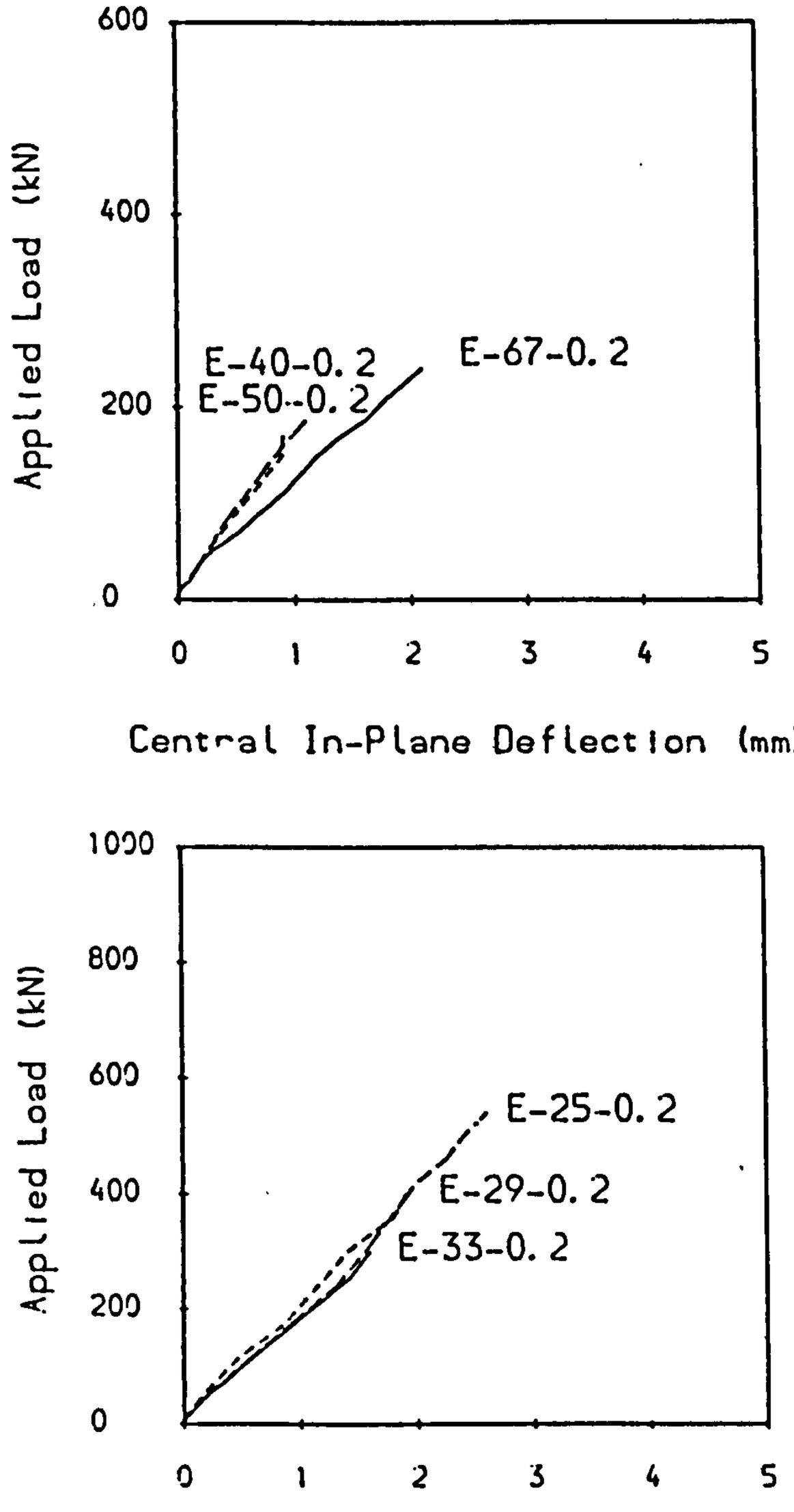

Figure 6.13 : Load-deflection curves (E-Series beams)

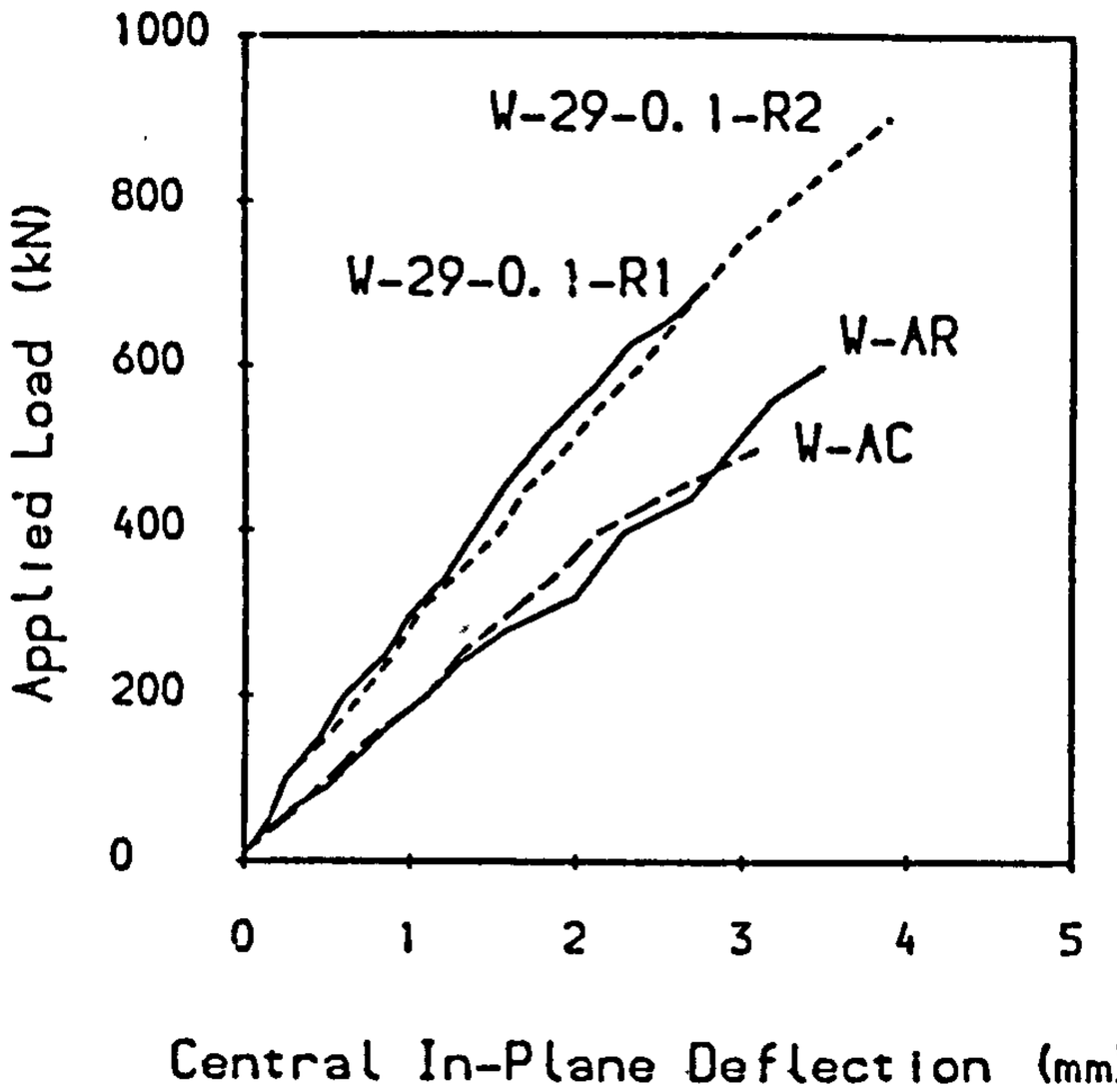

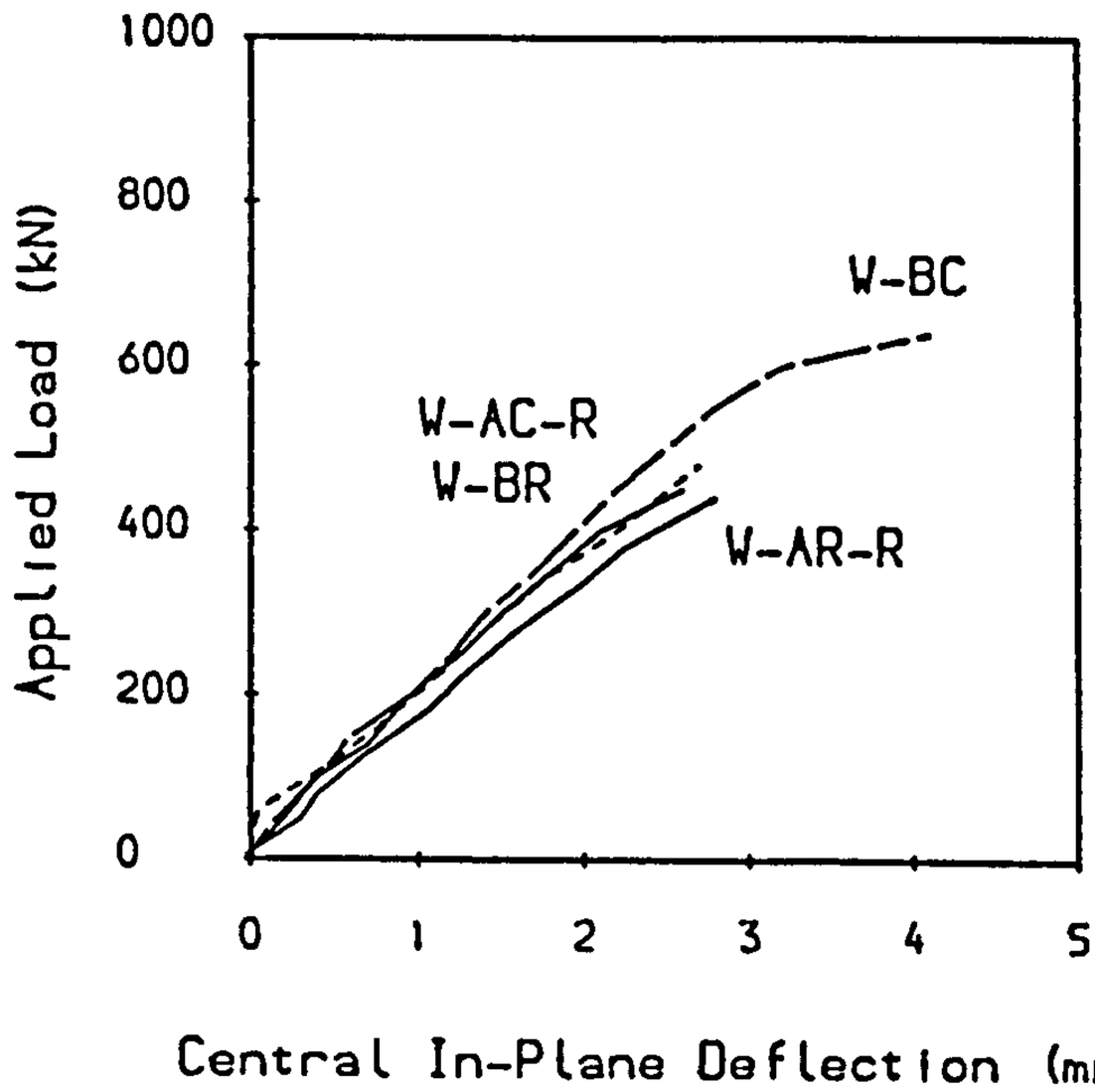

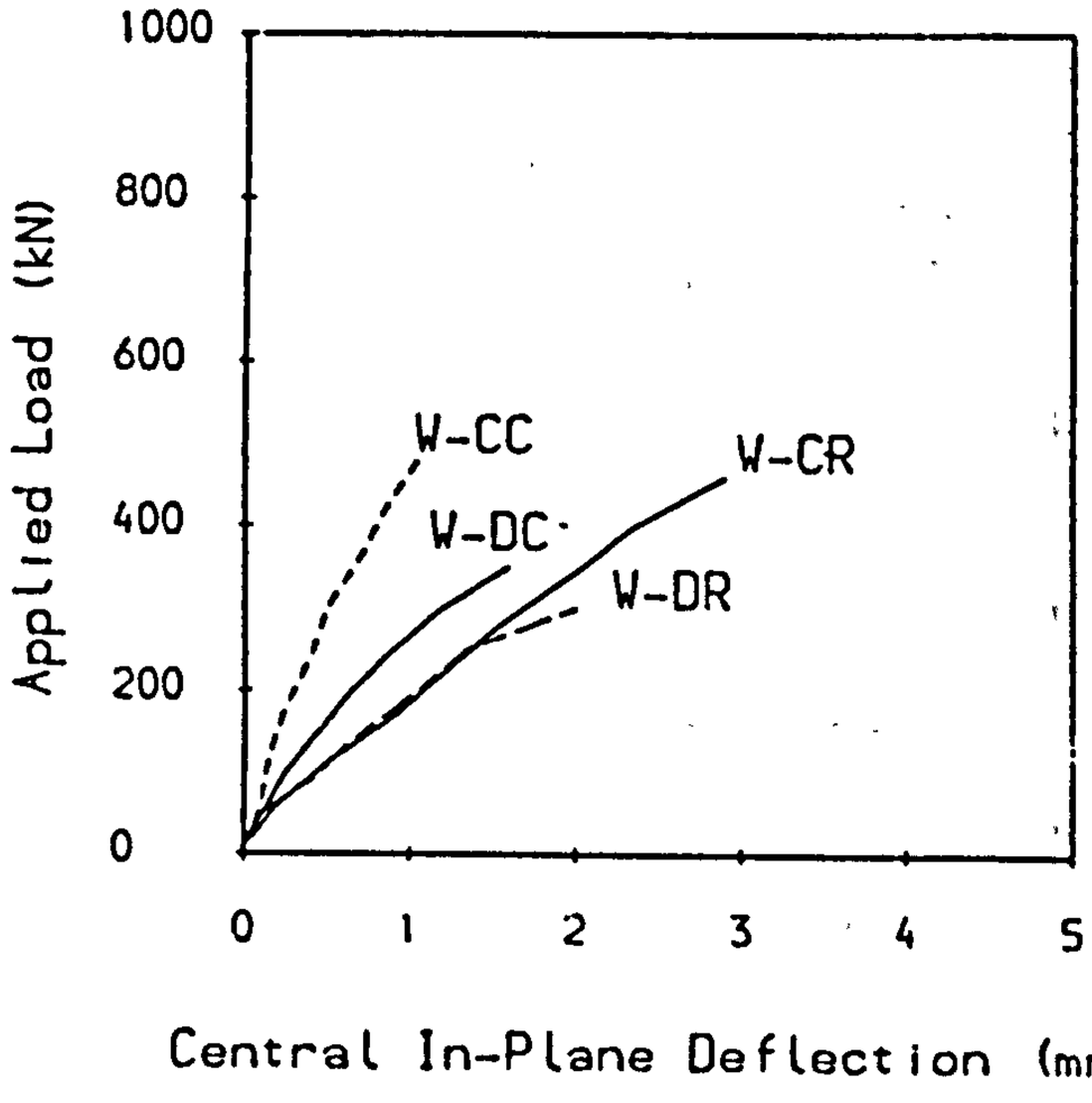

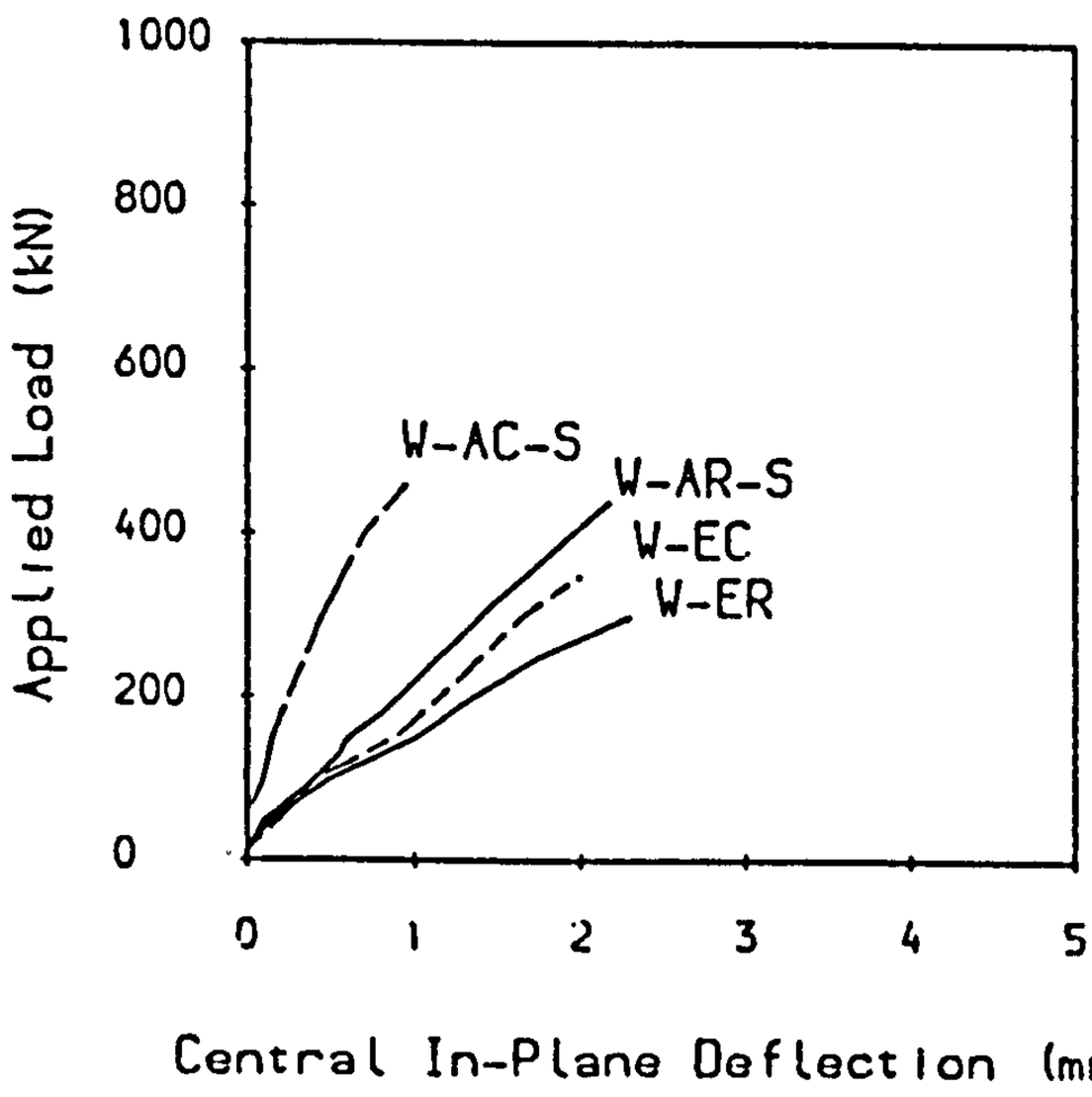

Figure 6.14 : Load-deflection curves (W-Series beams)

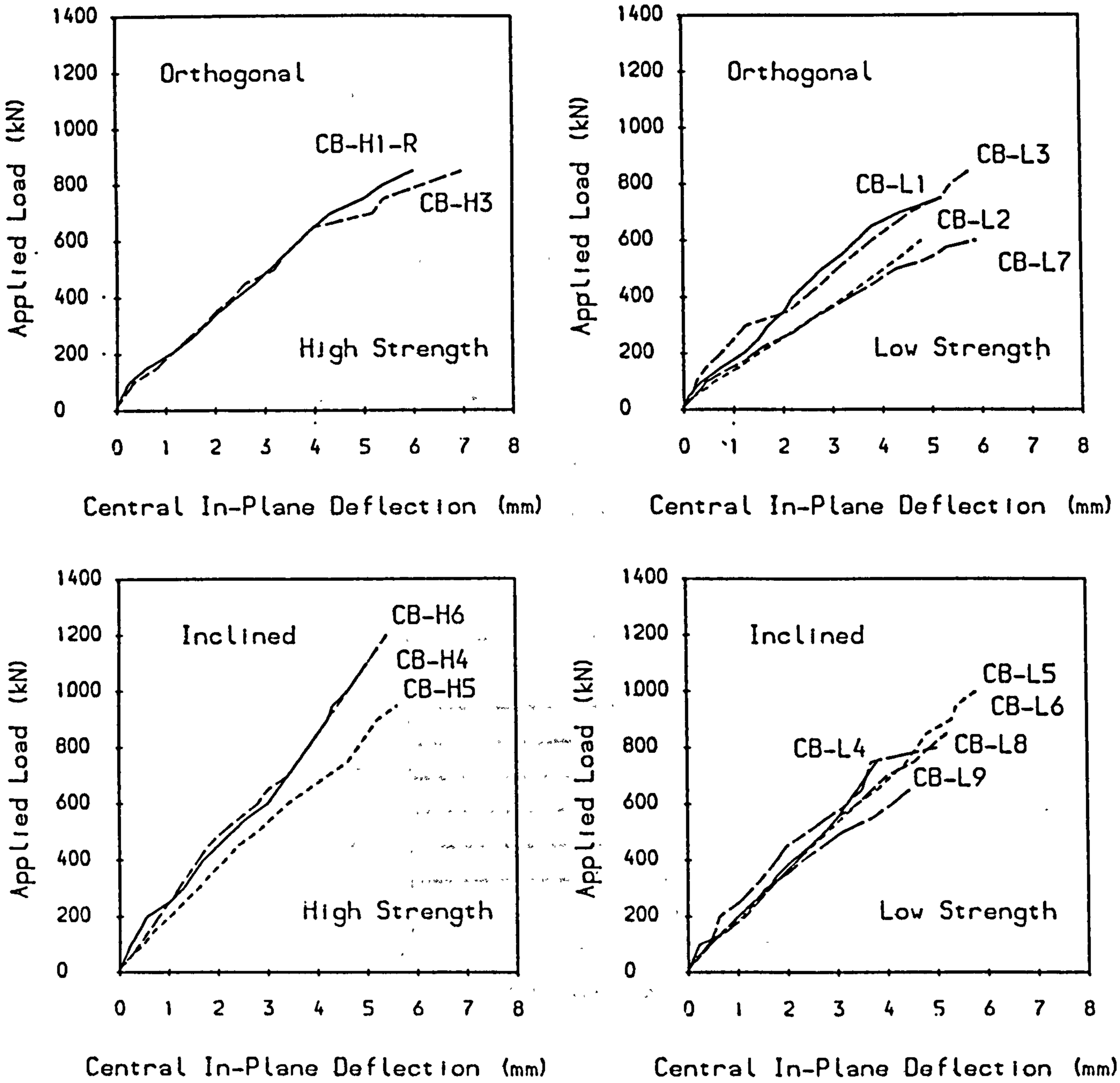

Figure 6.15 : Load-deflection curves (CB-Series beams)

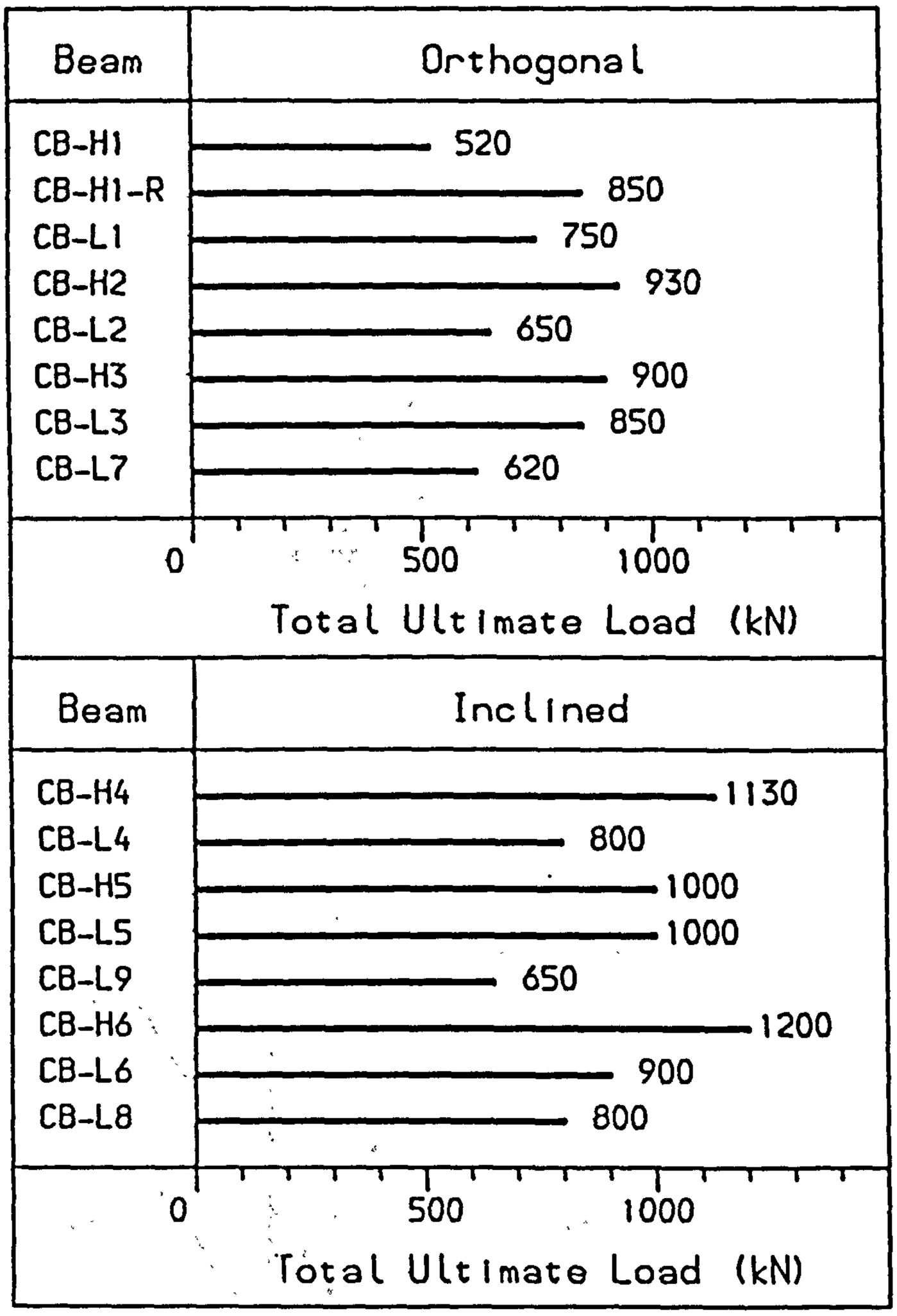

Figure 6.16 : Comparison of the total ultimate loads (CB-Series beams)

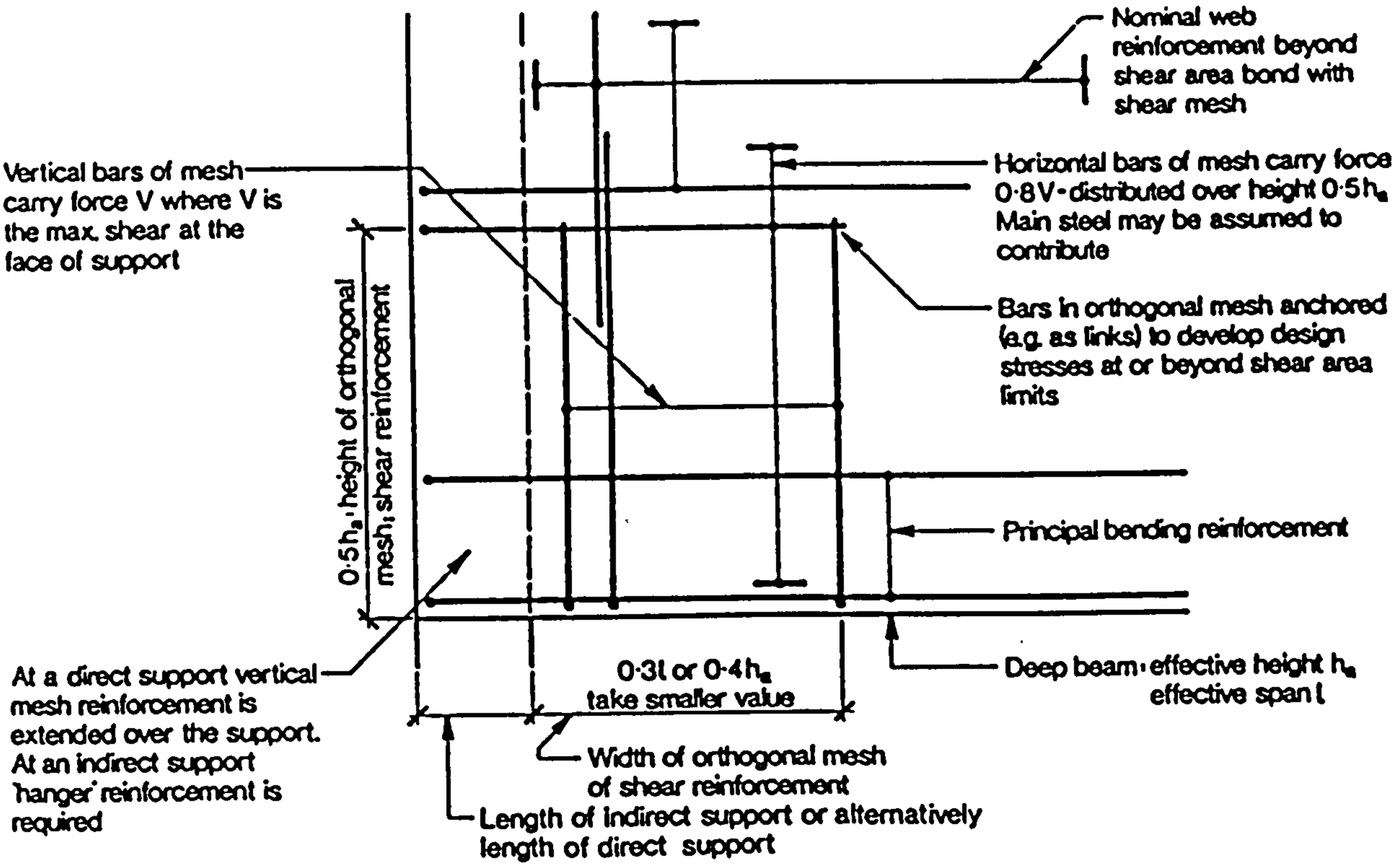

Figure 6.17 : Shear reinforcement for indirect and bottom loads at end support (CIRIA Guide, Fig.26 [1977])

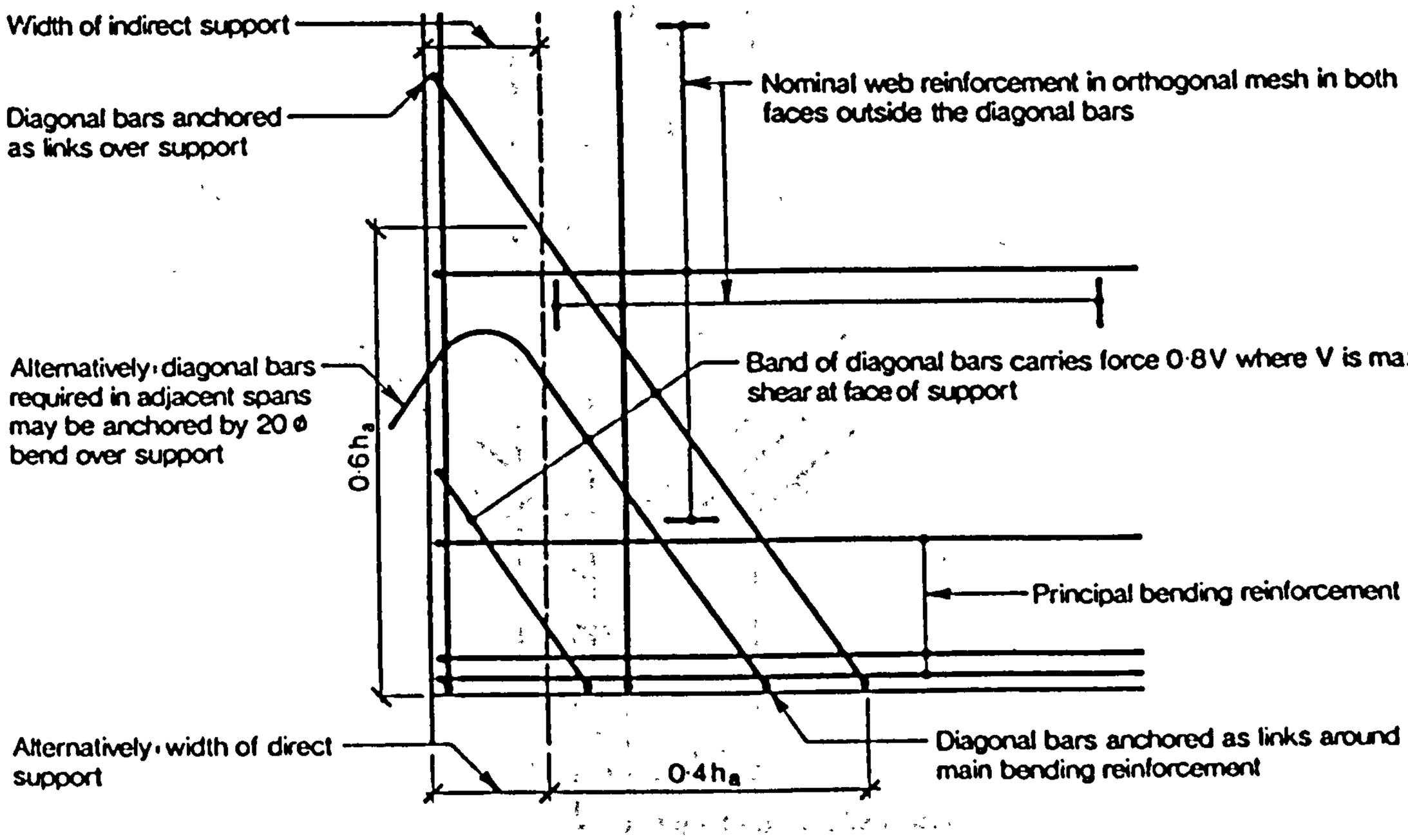

Figure 6.18 : Alternative shear reinforcement for indirect and bottom loads (CIRIA Guide, Fig.27 [1977])

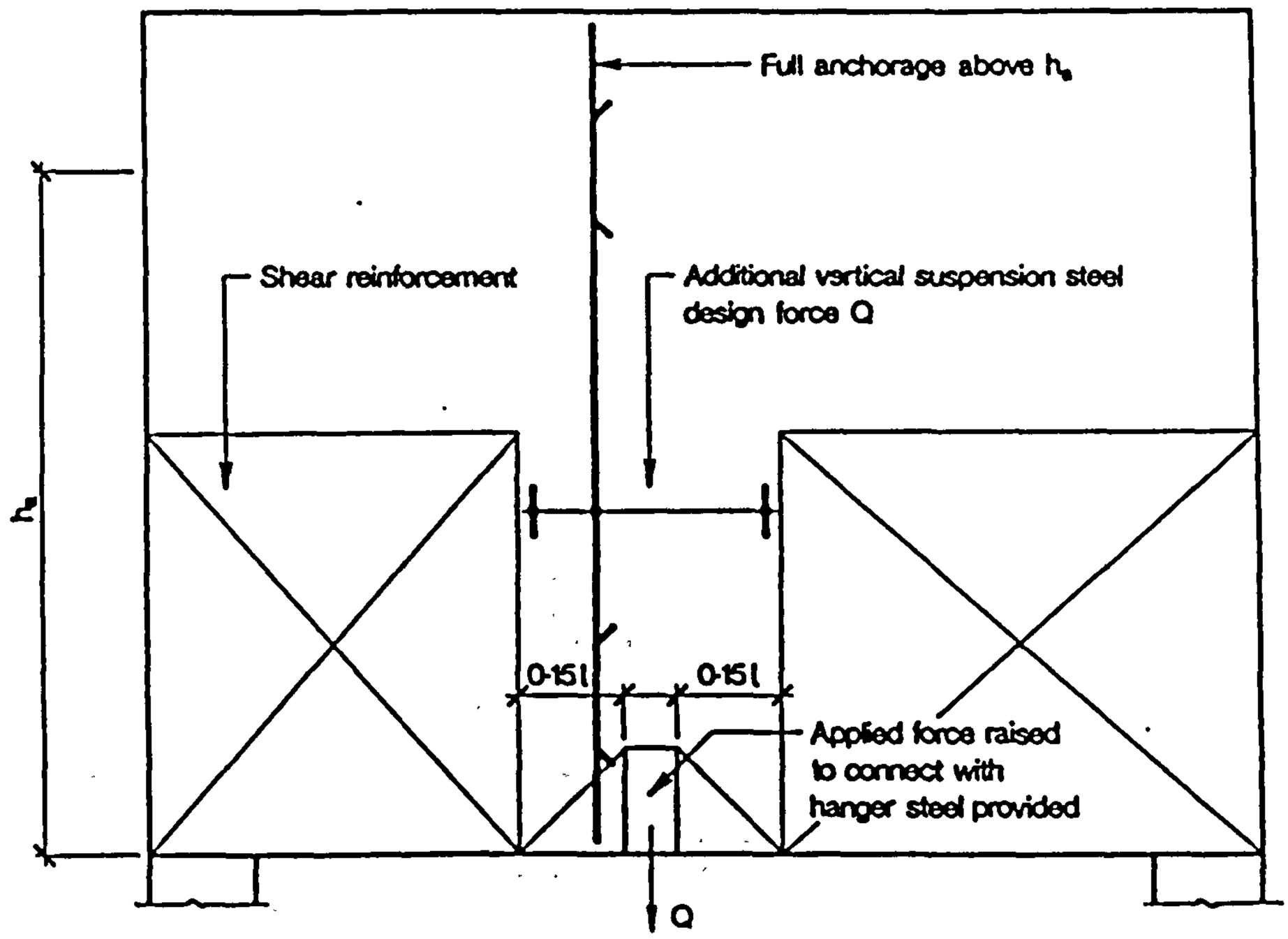

Figure 6.19 : Shear and hanger reinforcement for concentrated bottom loads (CIRIA Guide, Fig.28 [1977])

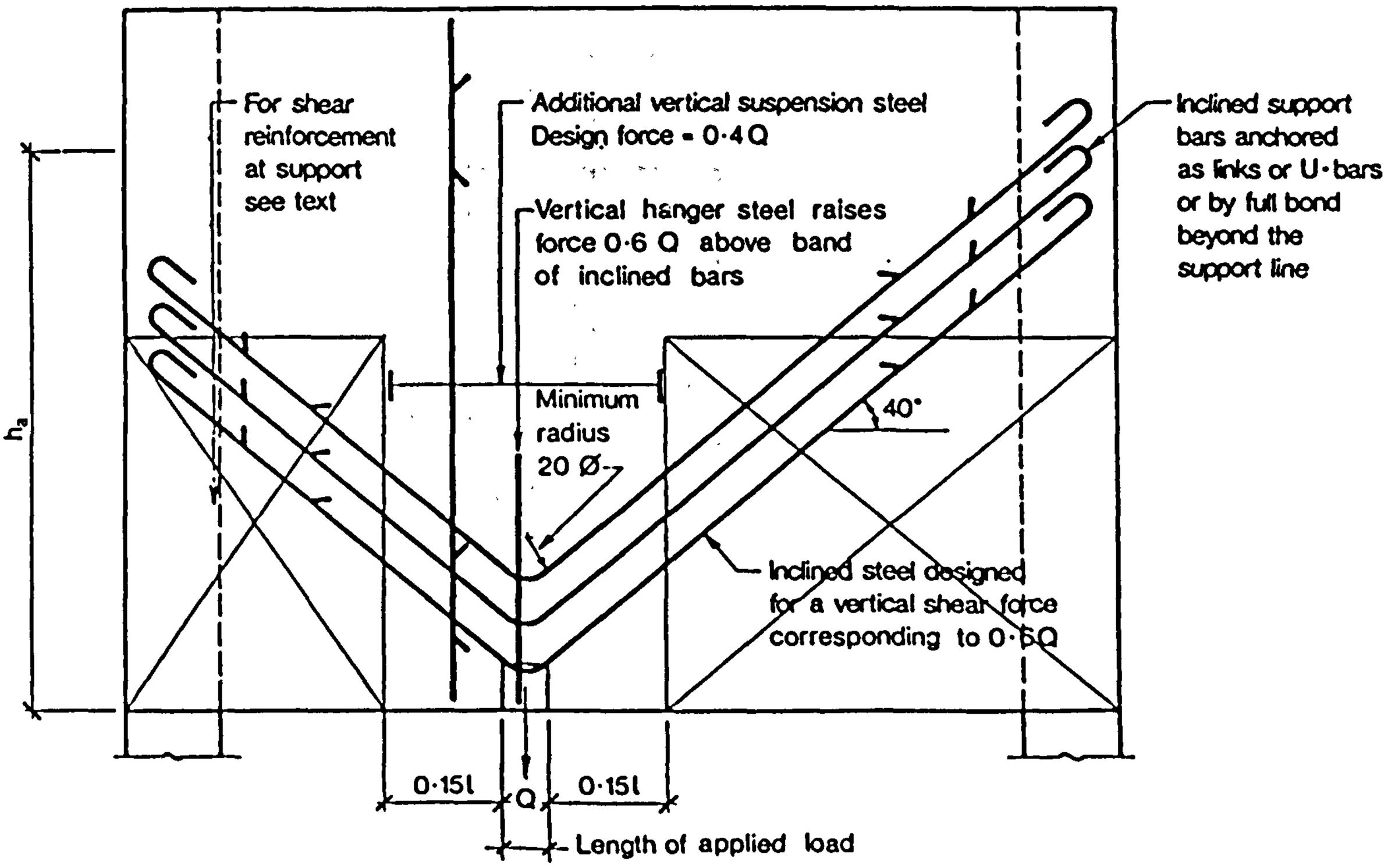

Figure 6.20 : Use of diagonal shear and hanger reinforcement (CIRIA Guide, Fig.29 [1977])

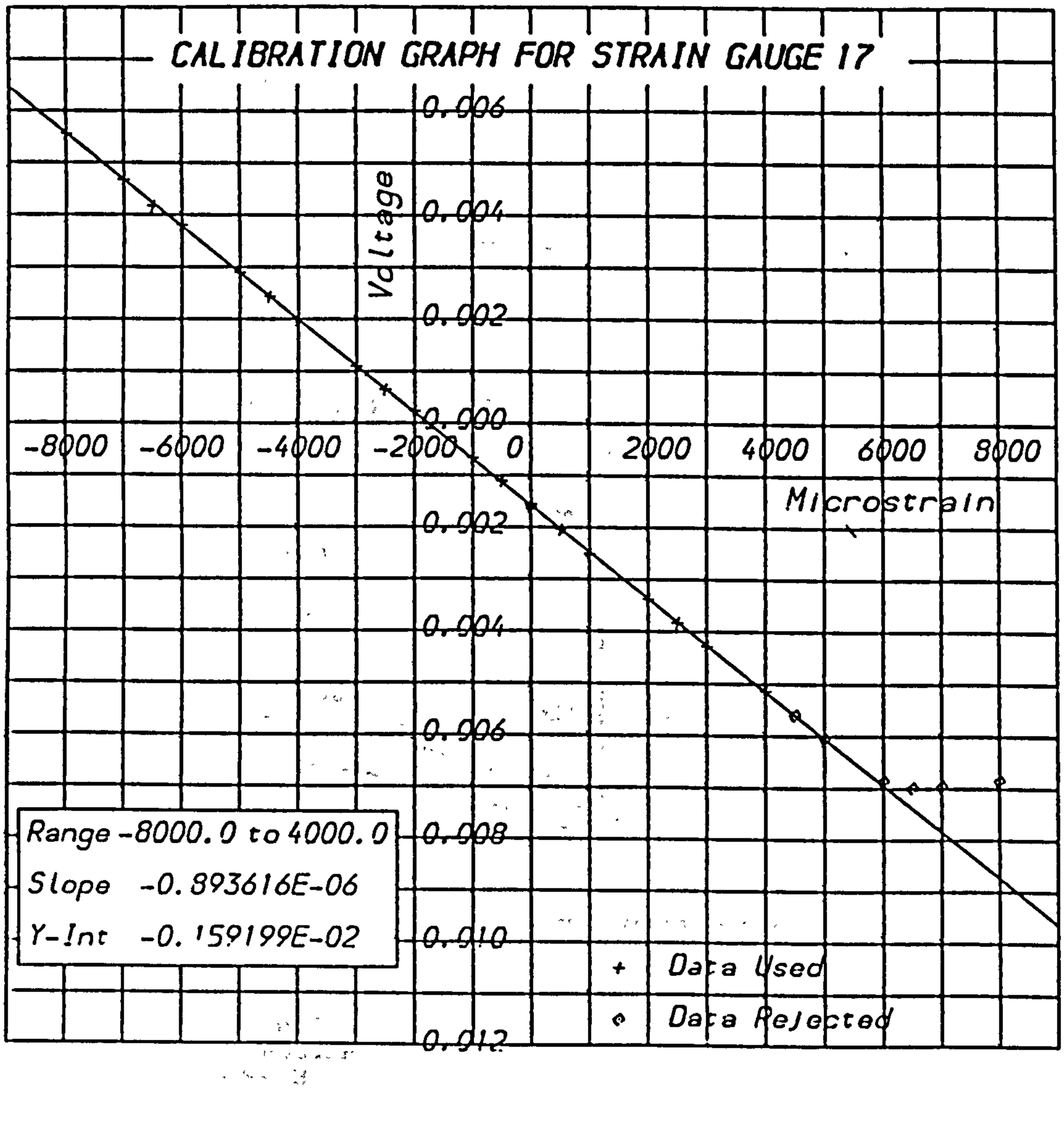

Figure 6.21 : Typical calibration graph for the strain transducers

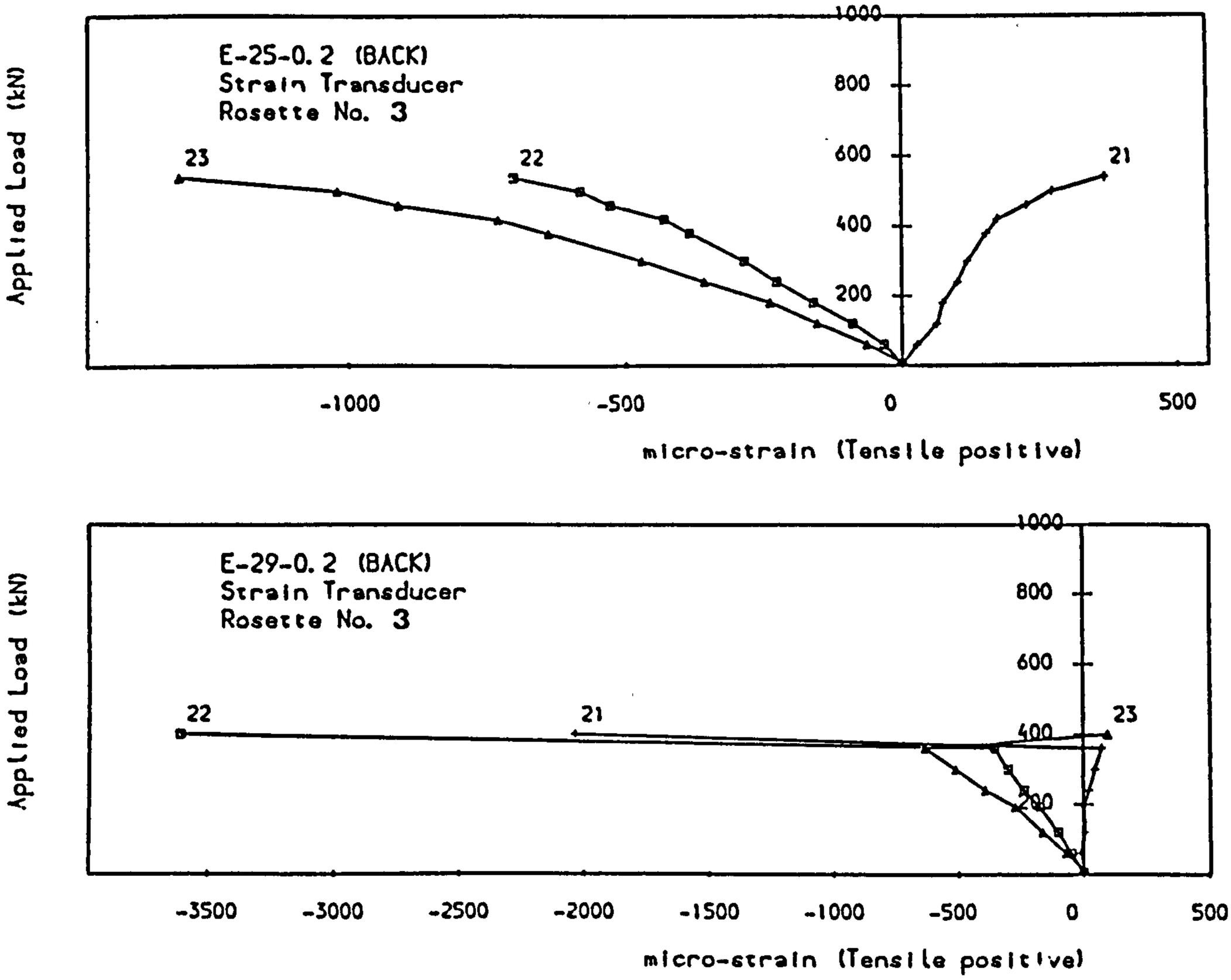

Figure 6.22 : Typical results of direct strain (E-Series beams)

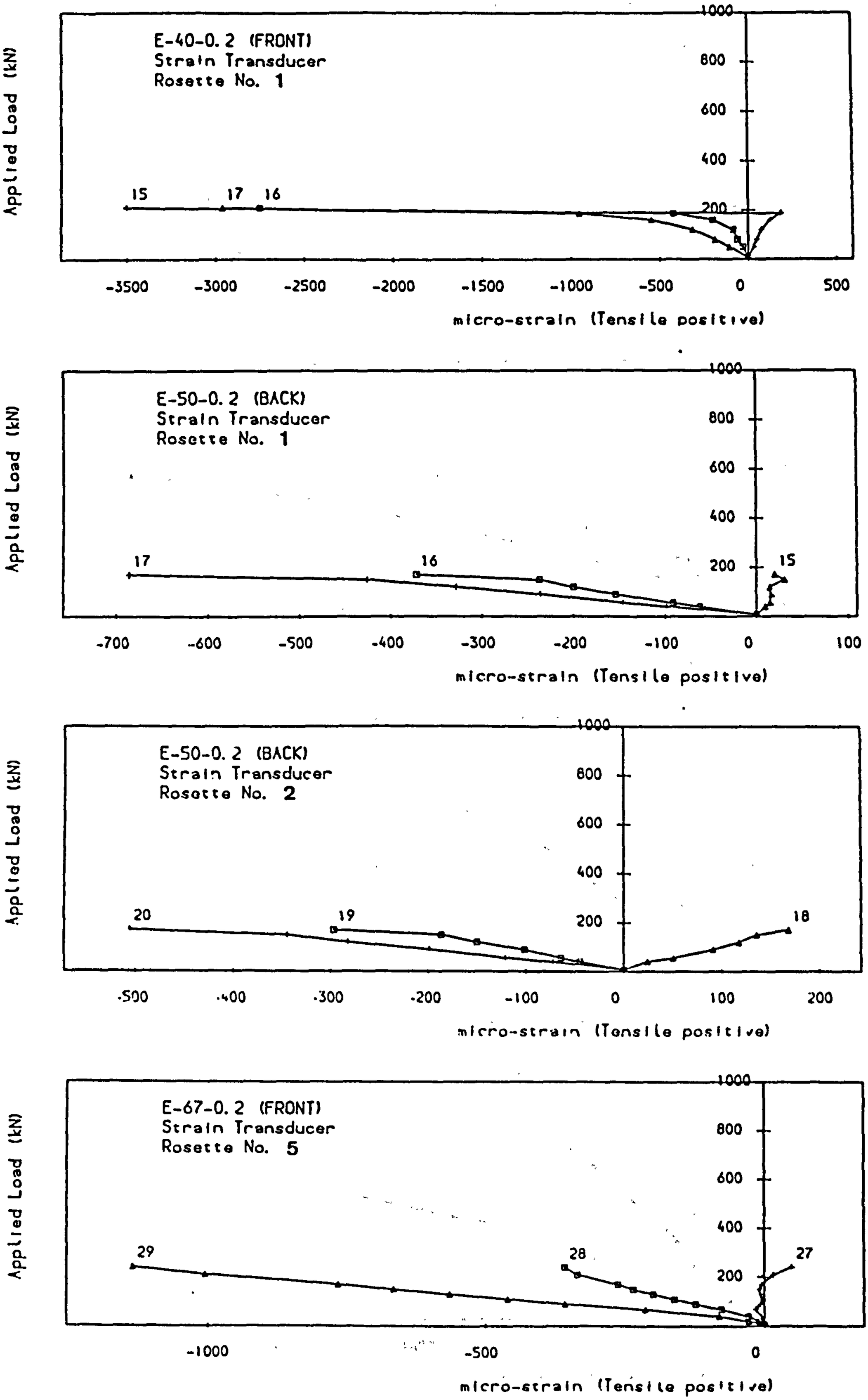

Figure 6.22 : Typical results of direct strain (E-Series beams) [cont'd]

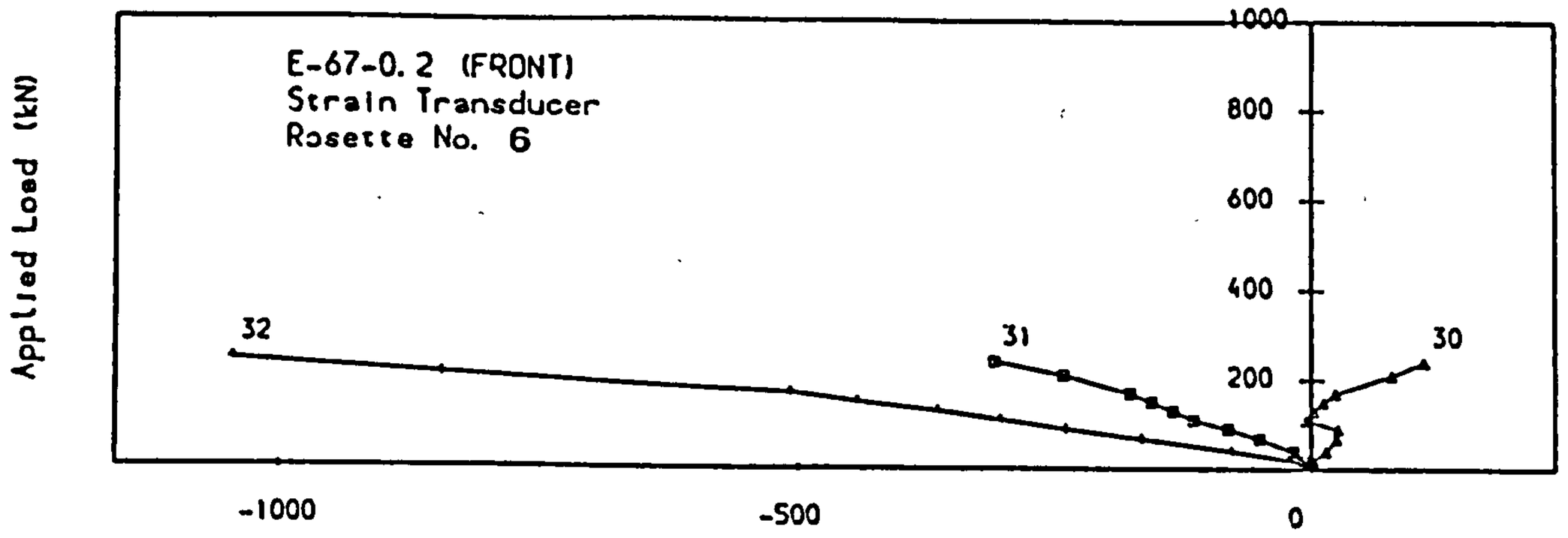

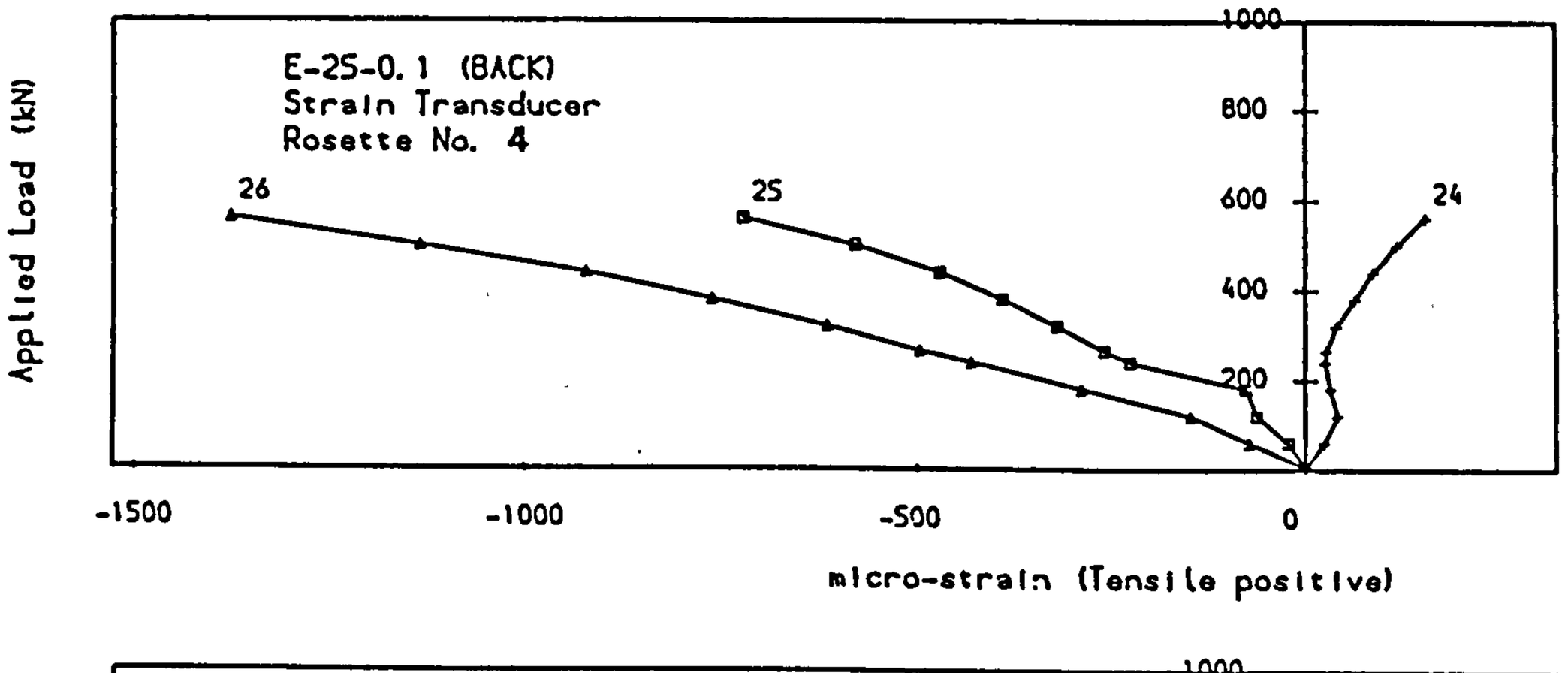

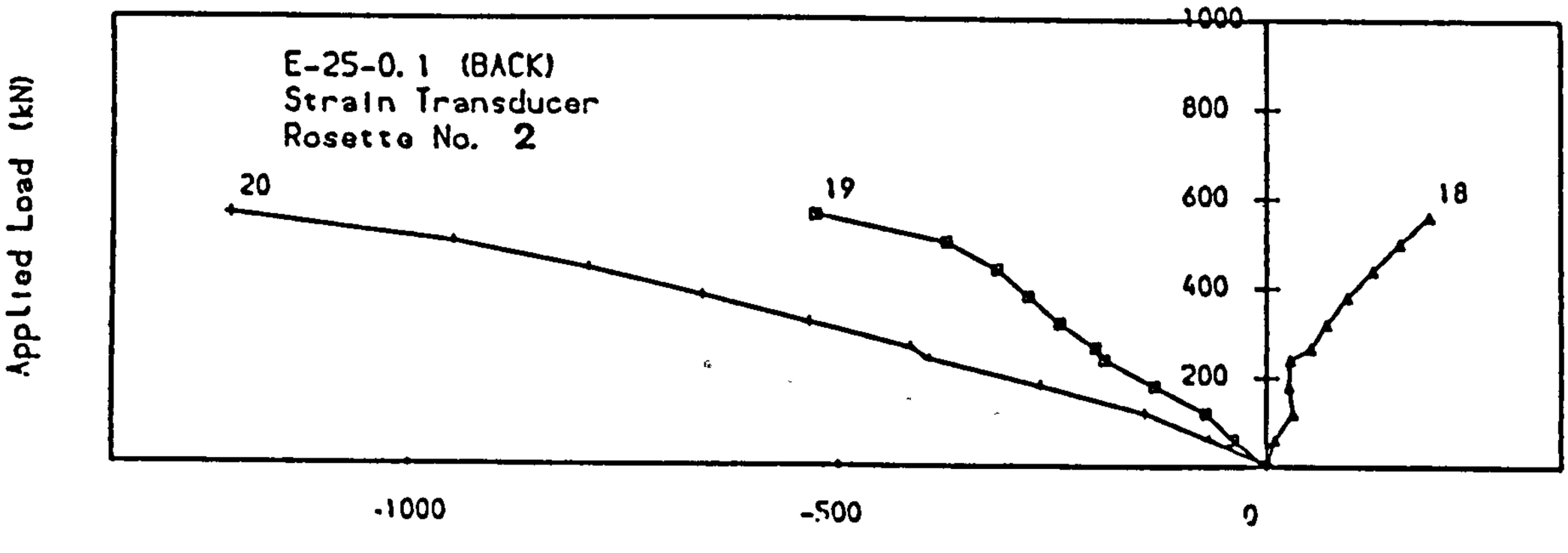

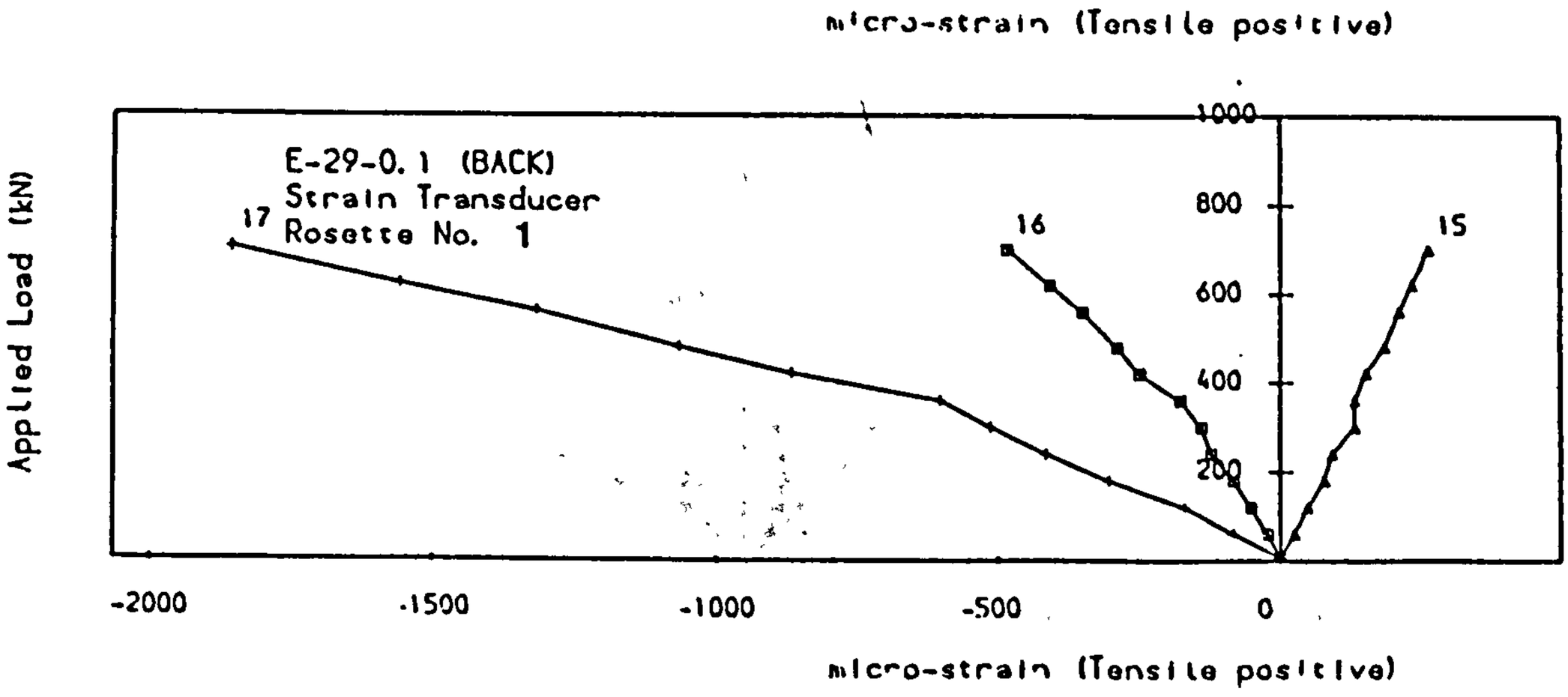

Figure 6.22 : Typical results of direct strain (E-Series beams) [cont'd]

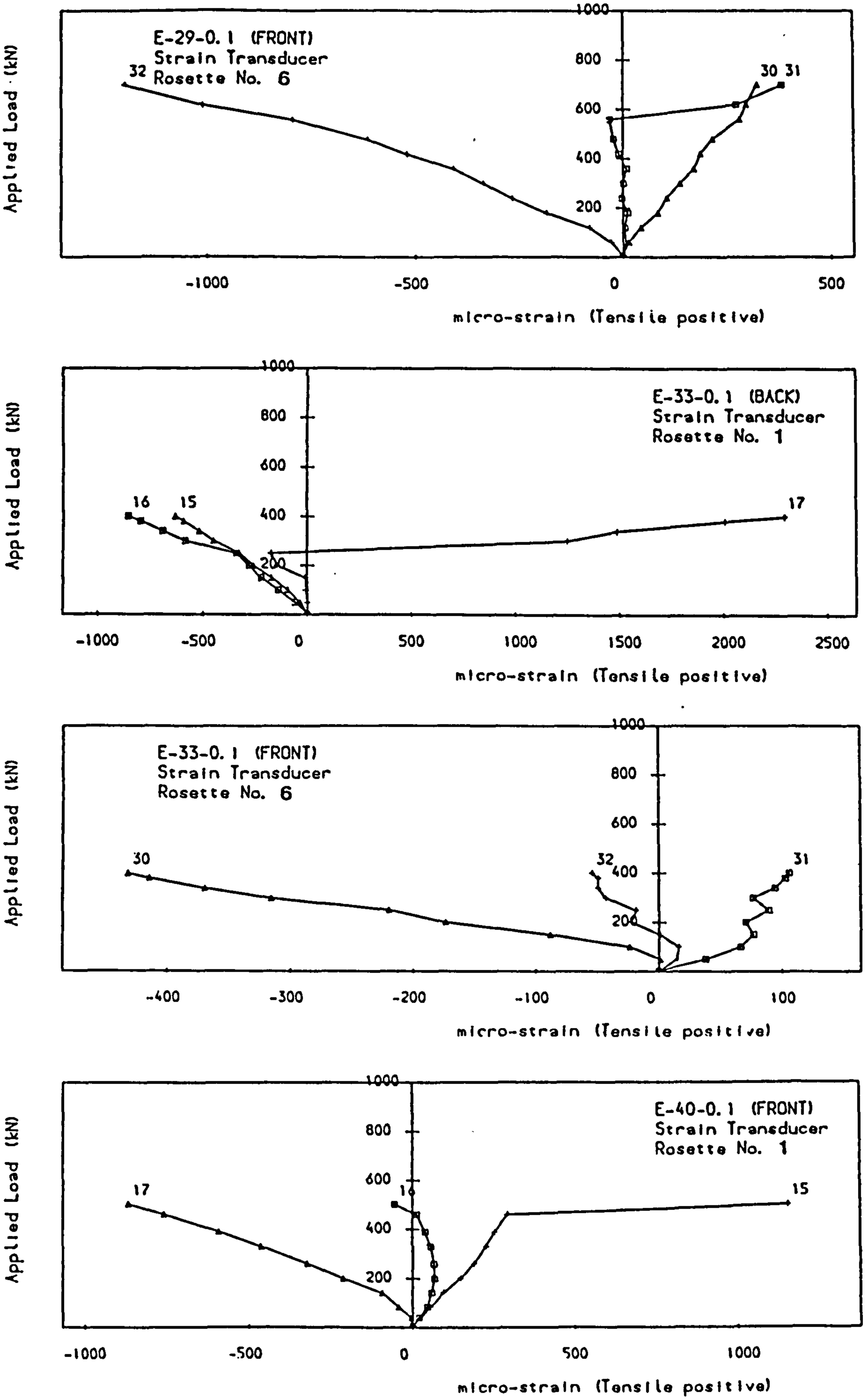

Figure 6.22 : Typical results of direct strain (E-Series beams) [cont'd]

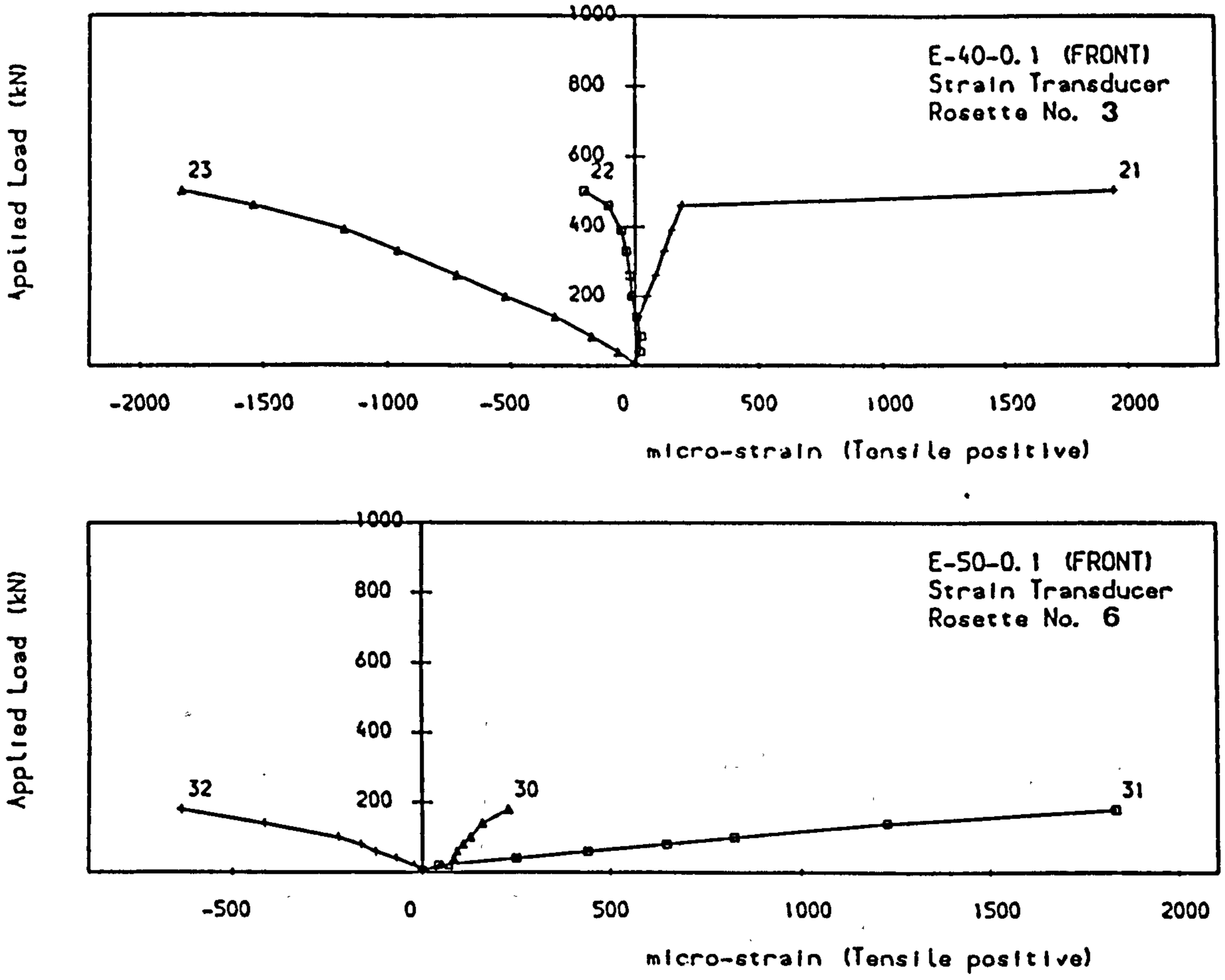

Figure 6.22 : Typical results of direct strain (E-Series beams) [cont'd]

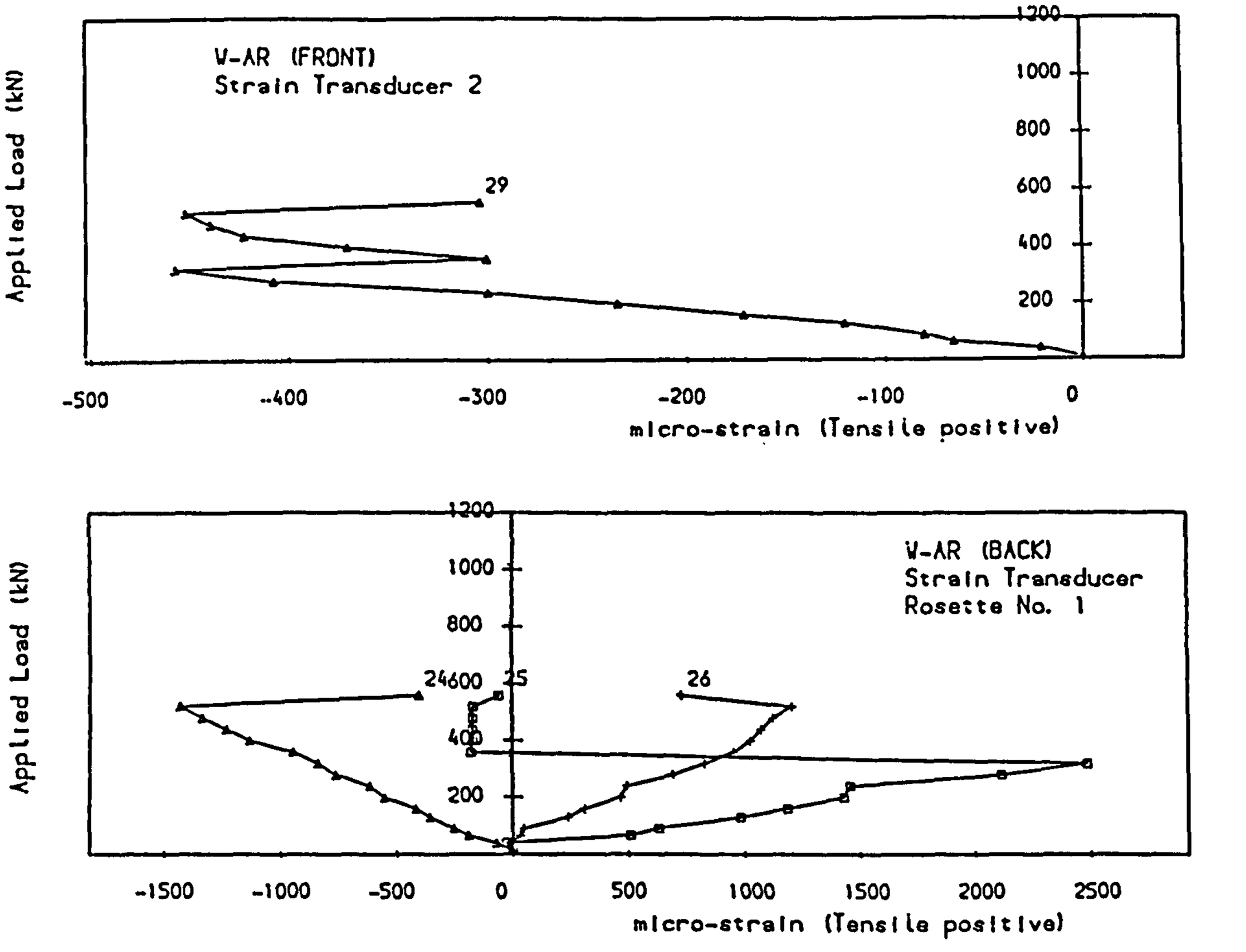

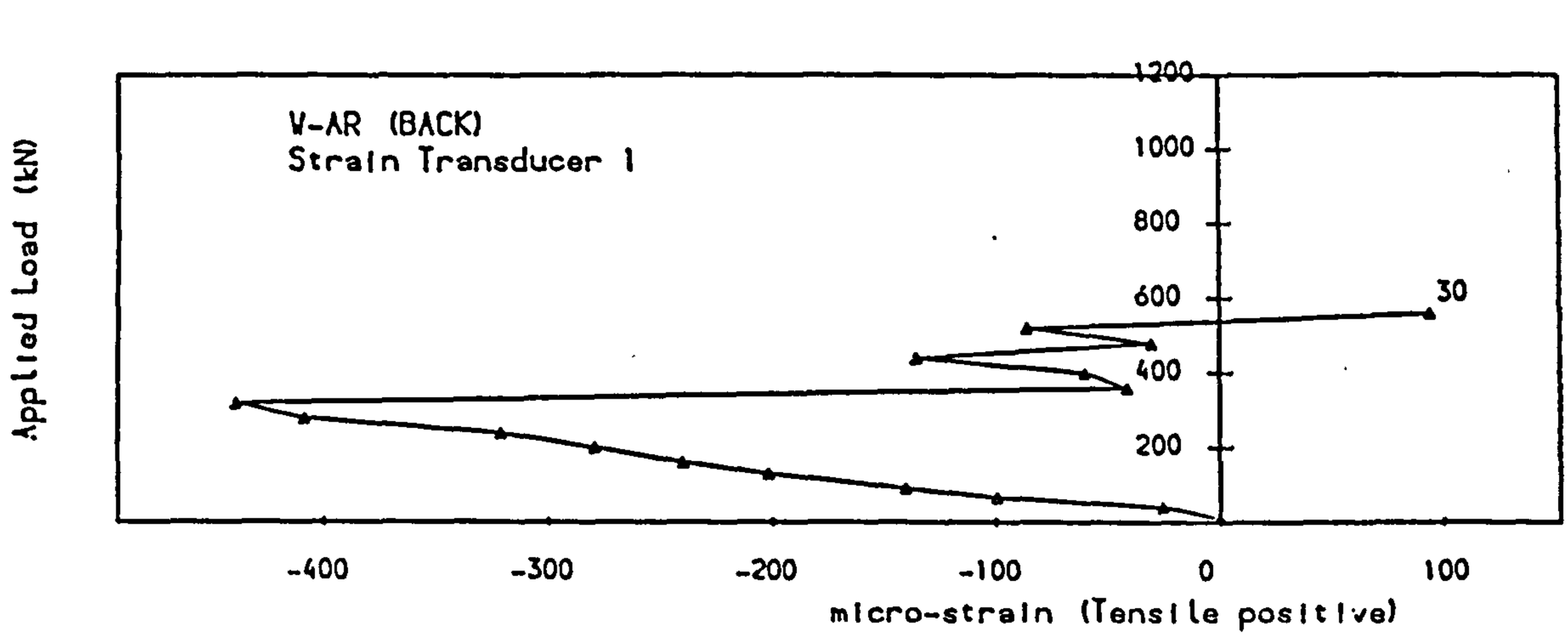

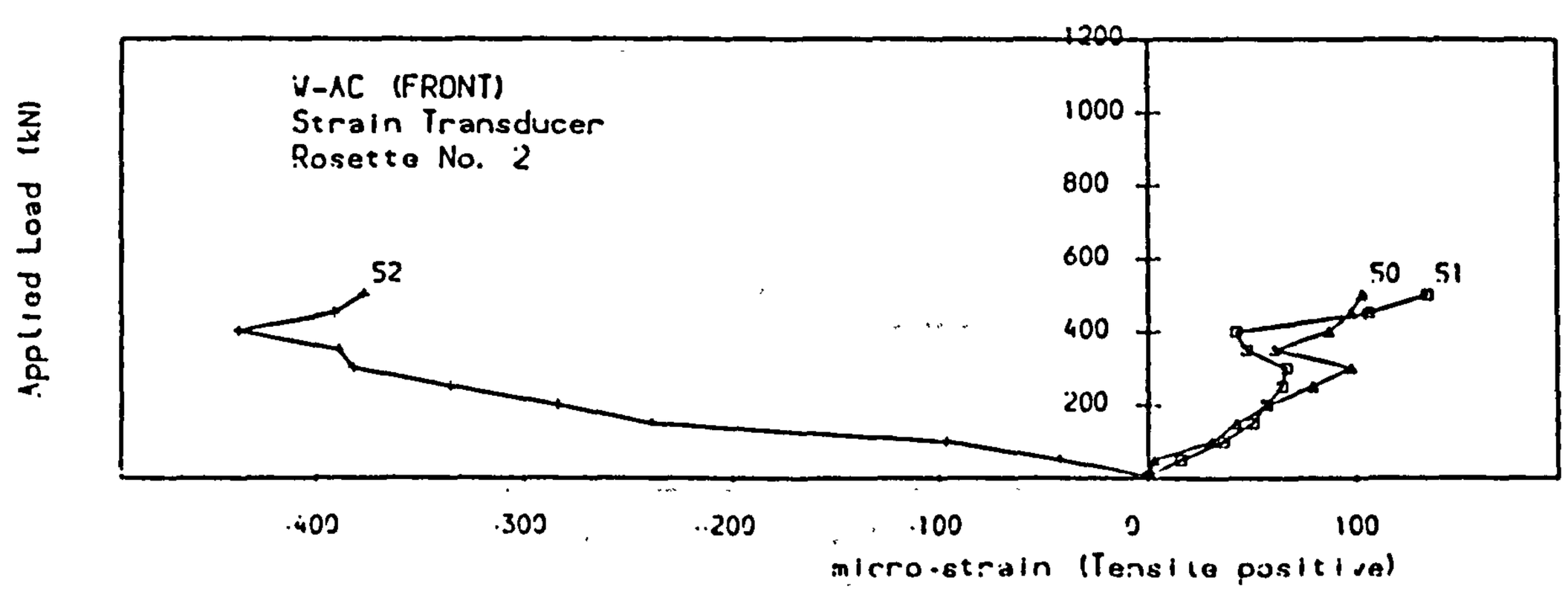

Figure 6.23 : Typical results of direct strain (W-Series beams)

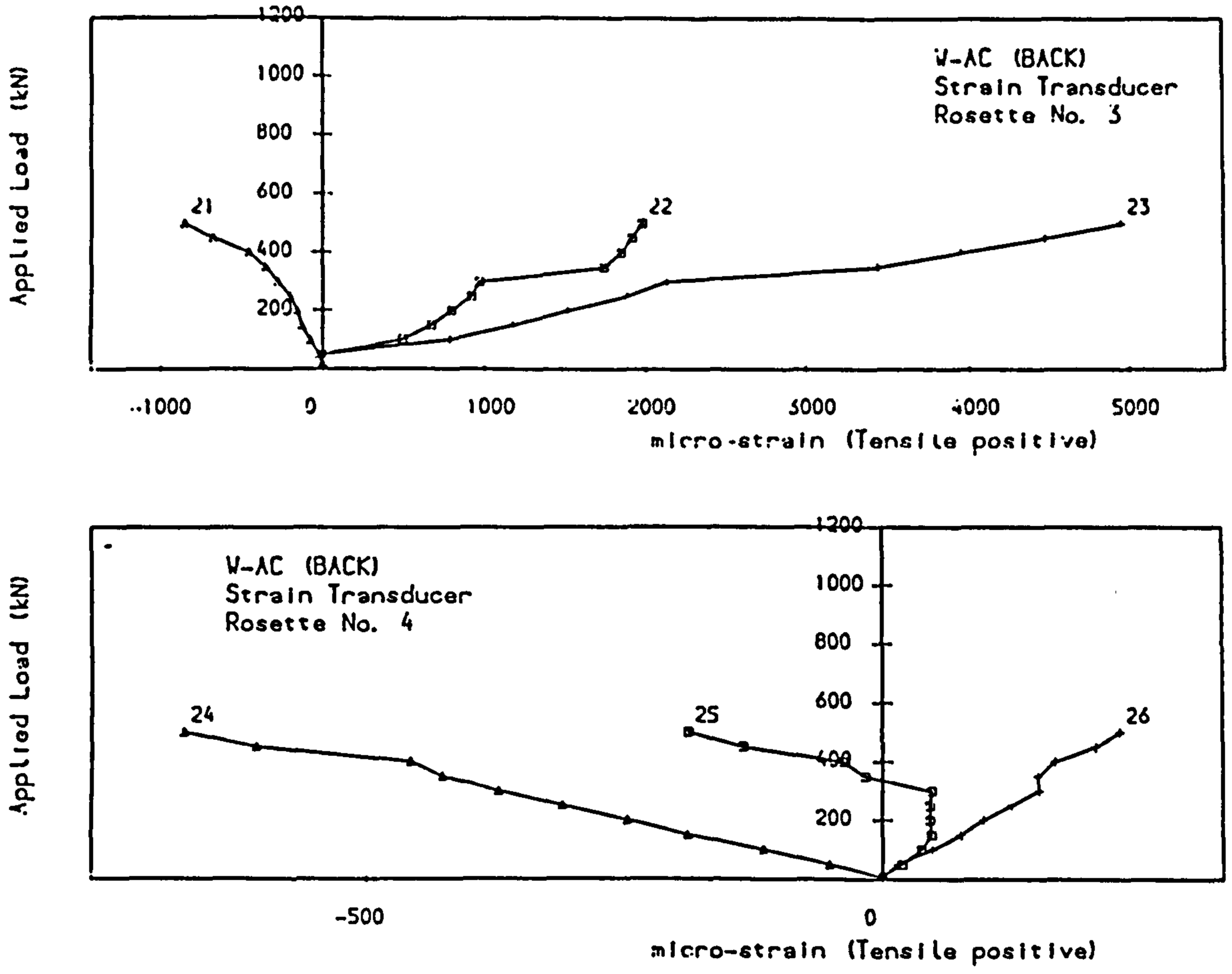

Figure 6.23 : Typical results of direct strain (W-Series beams) [cont'd]

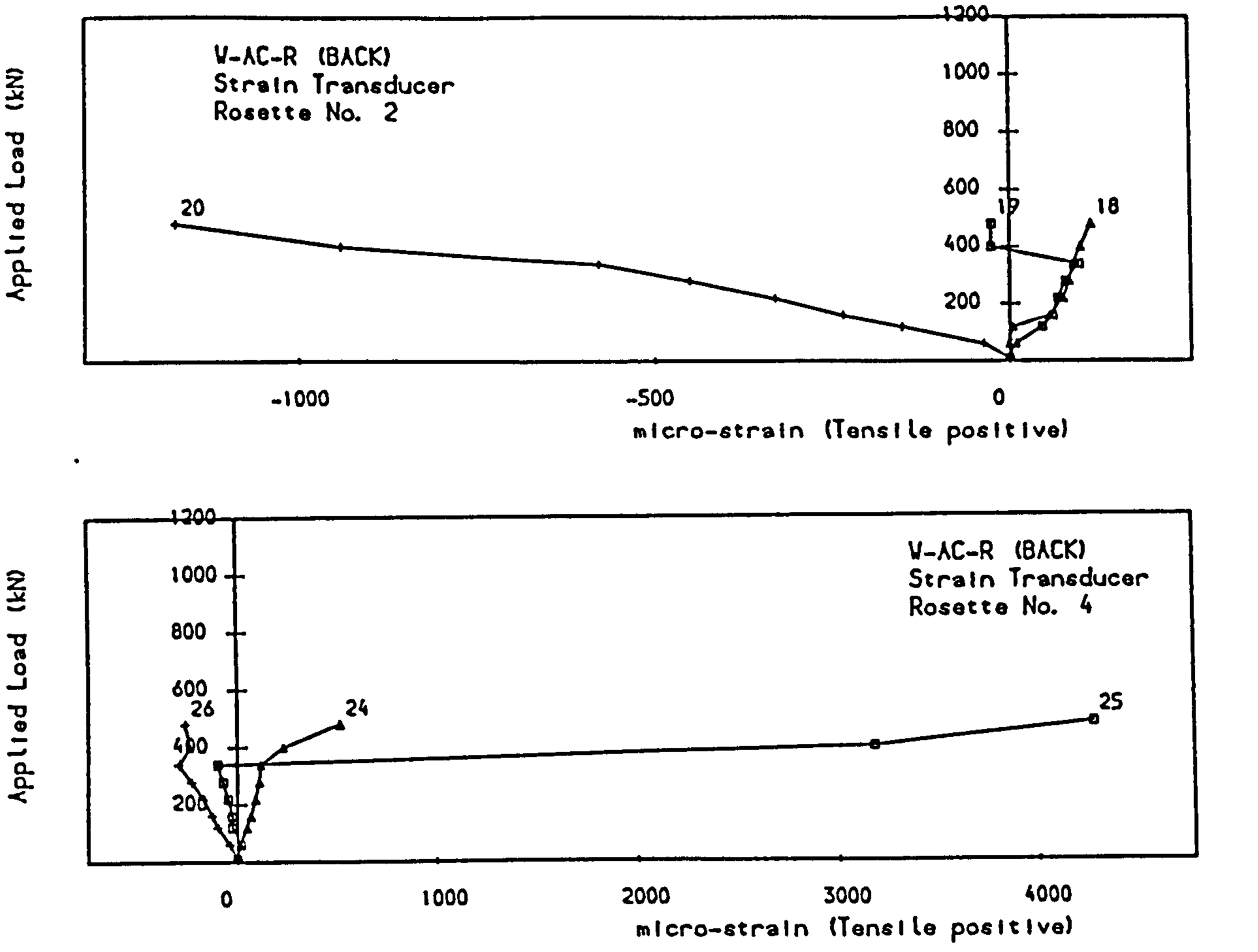

Figure 6.23 : Typical results of direct strain (W-Series beams) [cont'd]

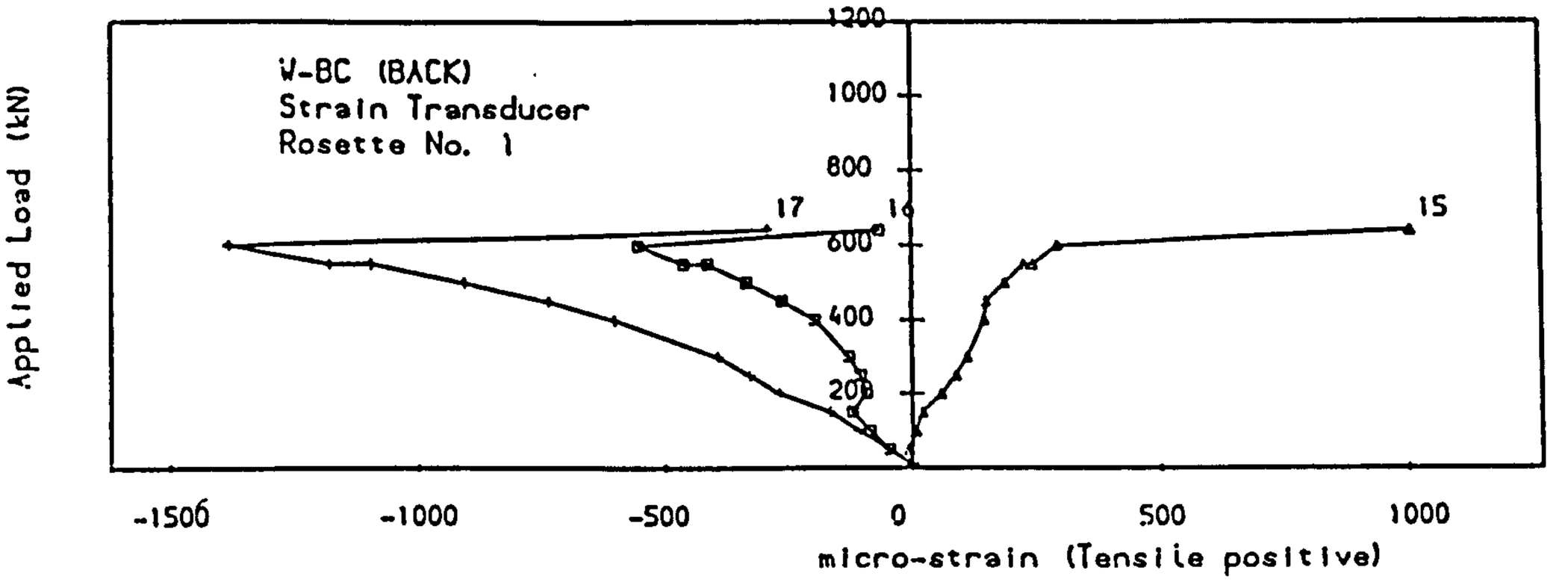

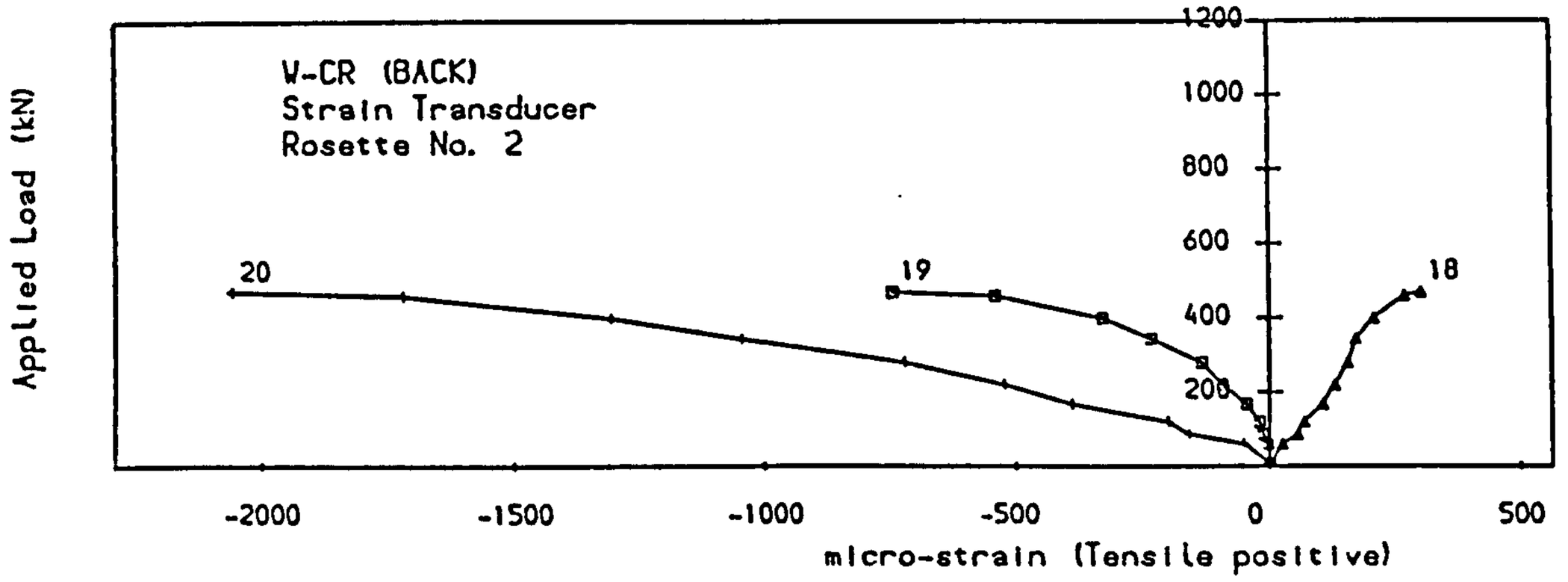

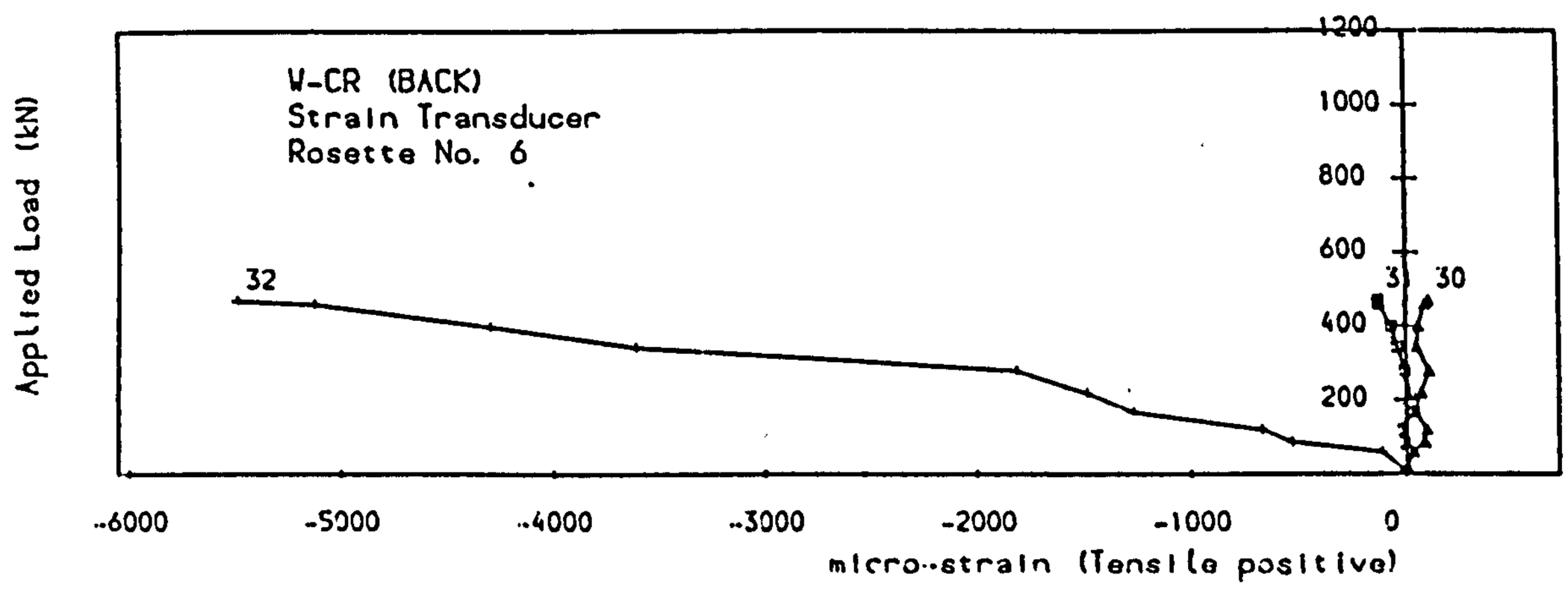

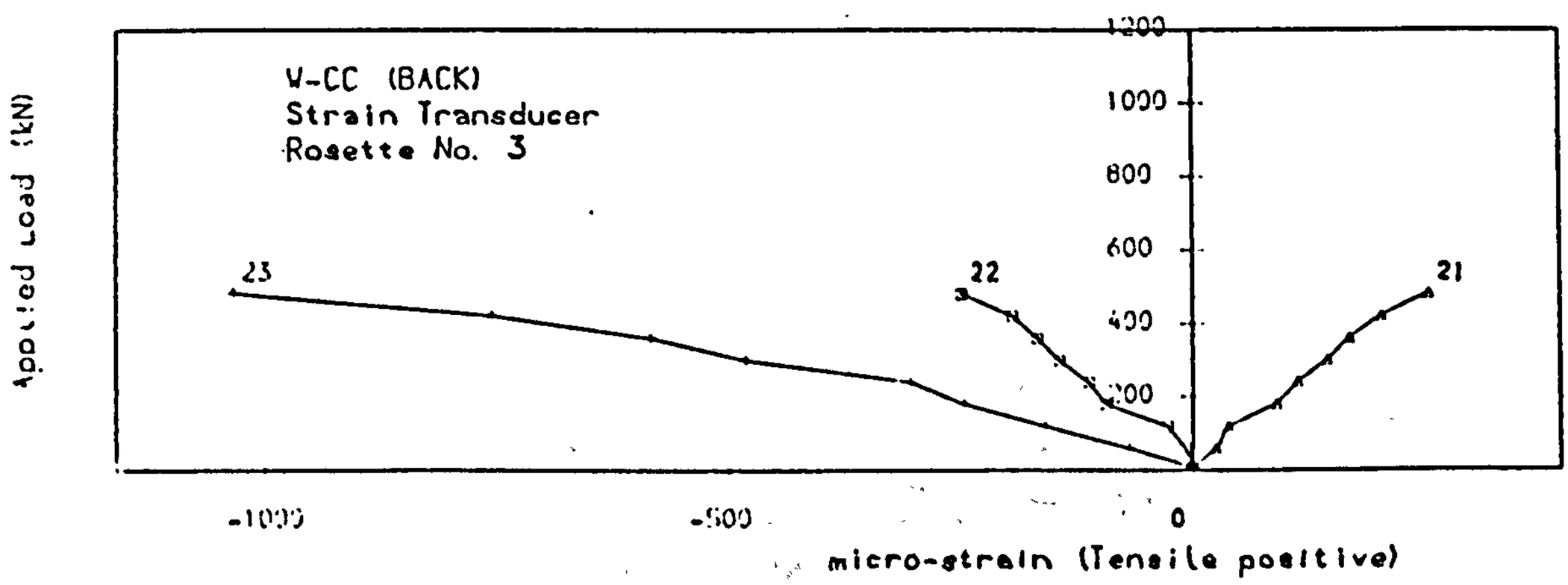

Figure 6.23 : Typical results of direct strain (W-Series beams) [cont'd]

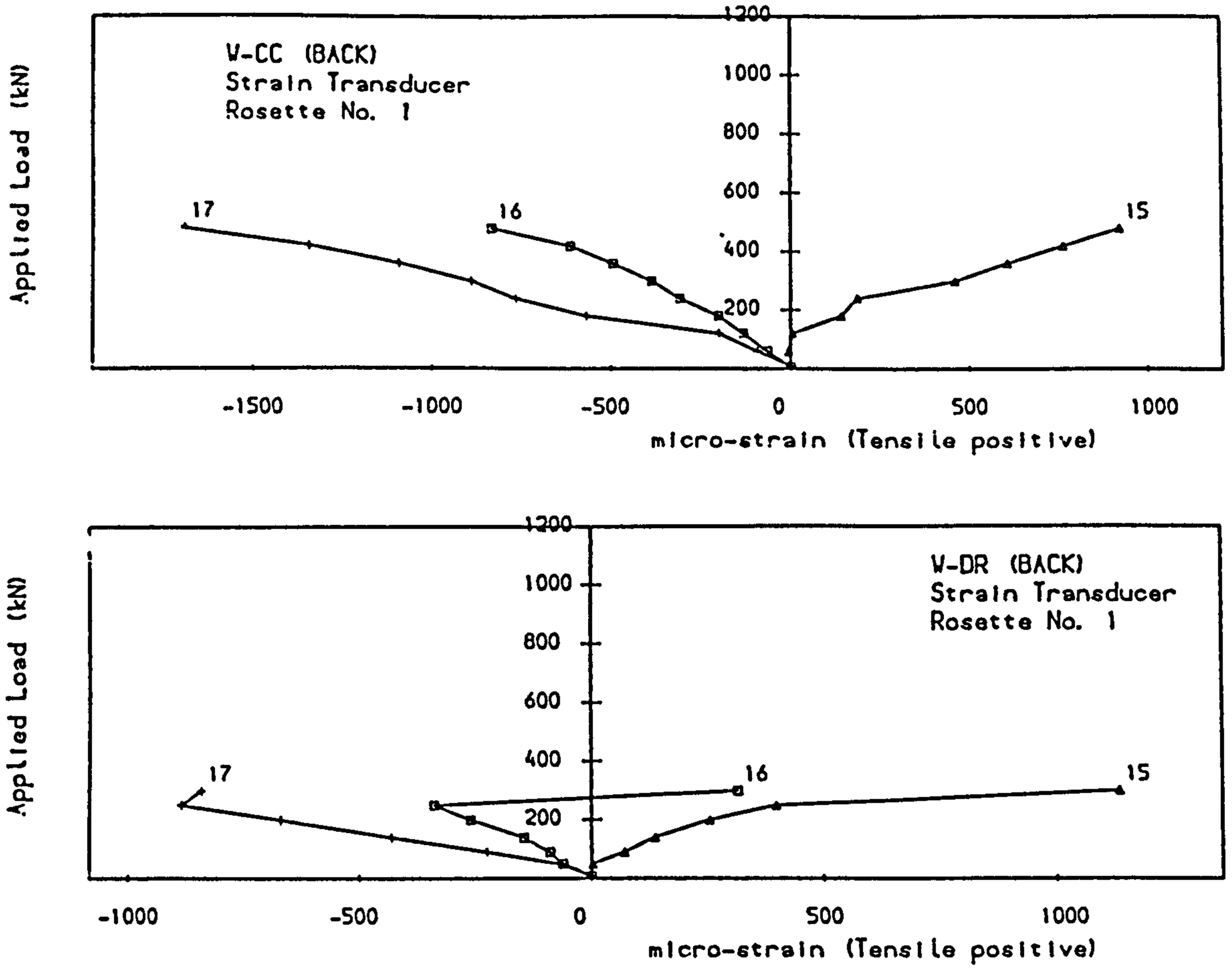

Figure 6.23 : Typical results of direct strain (W-Series beams) [cont'd]

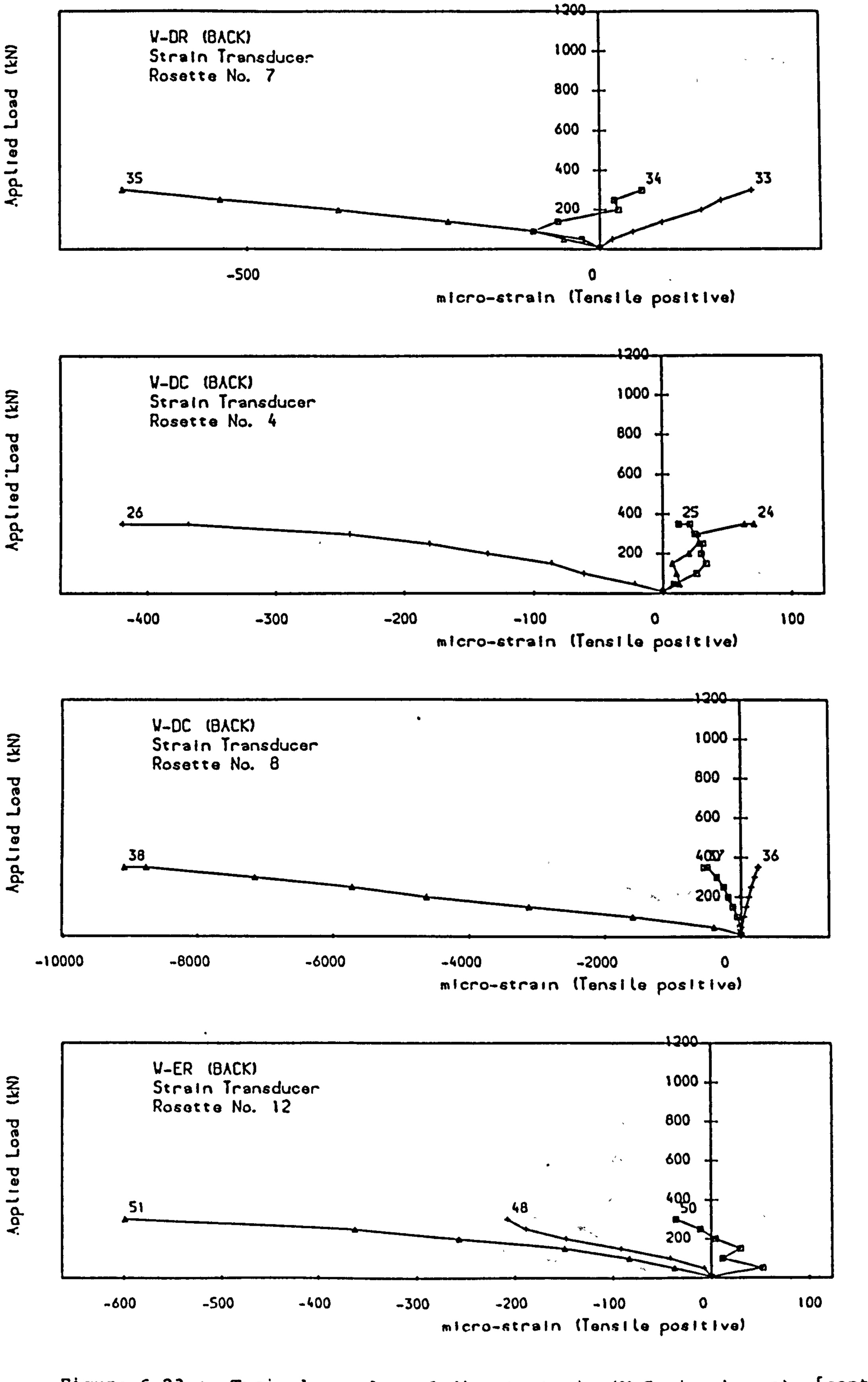

Figure 6.23 : Typical results of direct strain (W-Series beams) [cont'd]

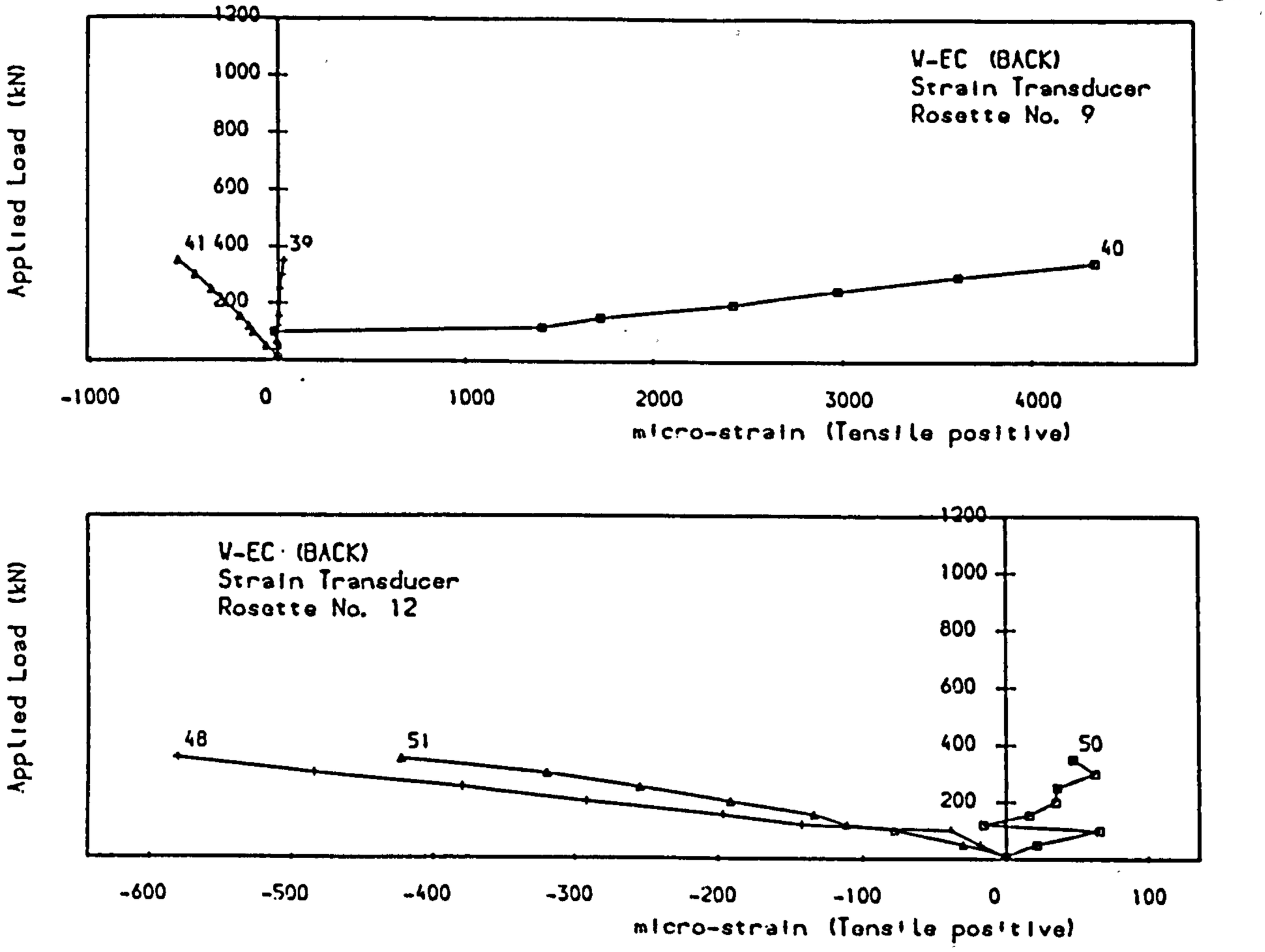

Figure 6.23 : Typical results of direct strain (W-Series beams) [cont'd]

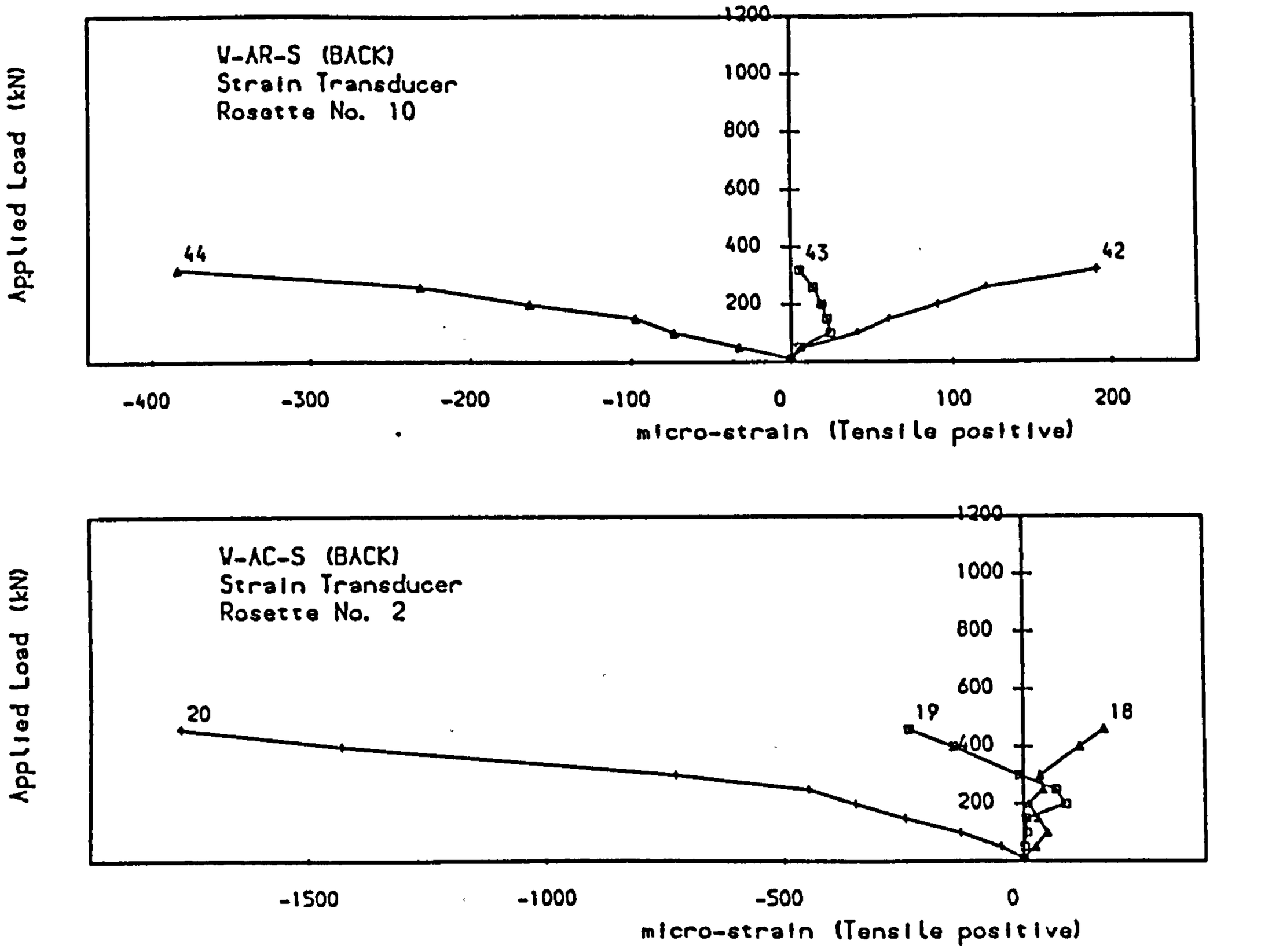

Figure 6.23 : Typical results of direct strain (W-Series beams) [cont'd]

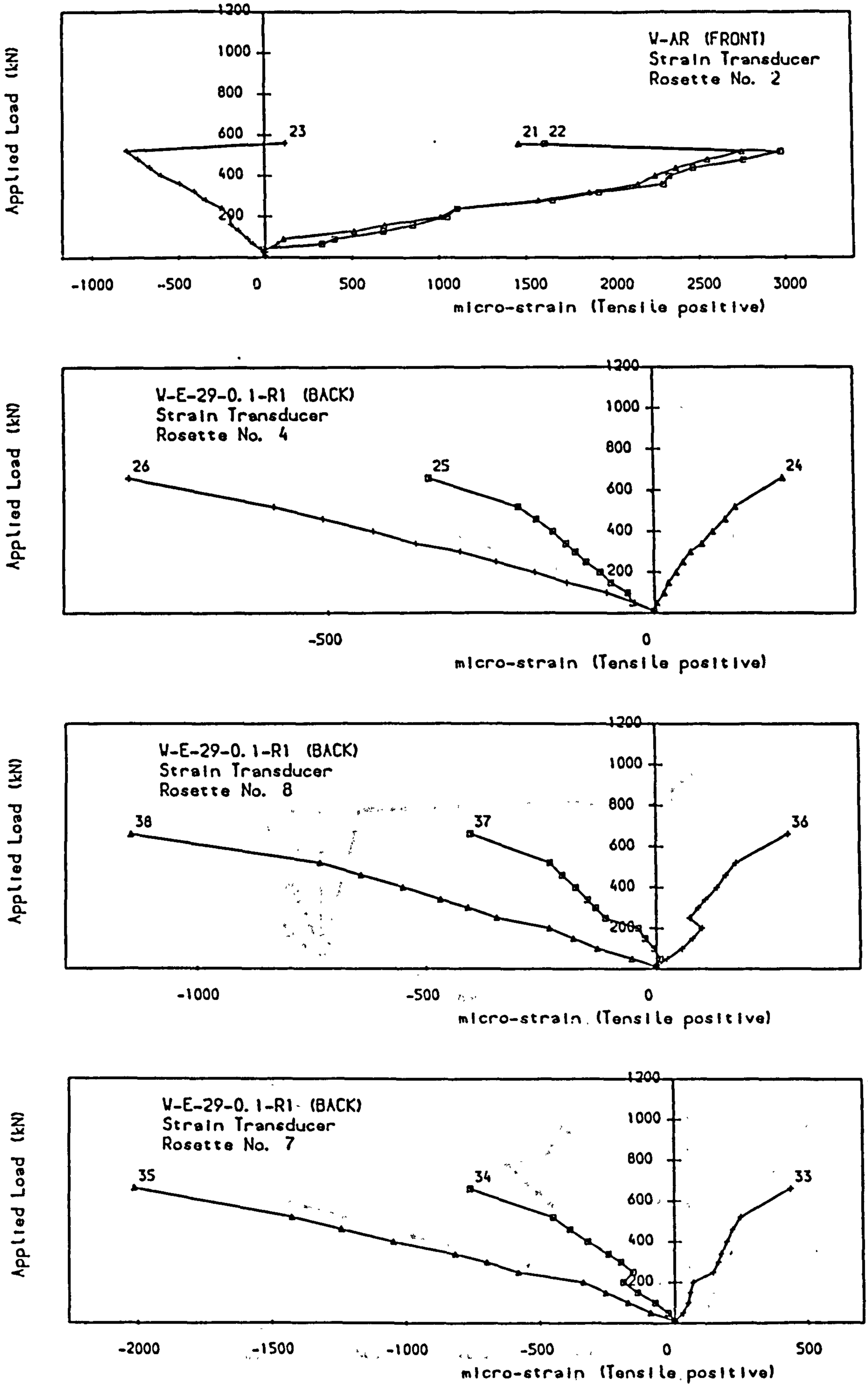

Figure 6.23 : Typical results of direct strain (W-Series beams) [cont'd]

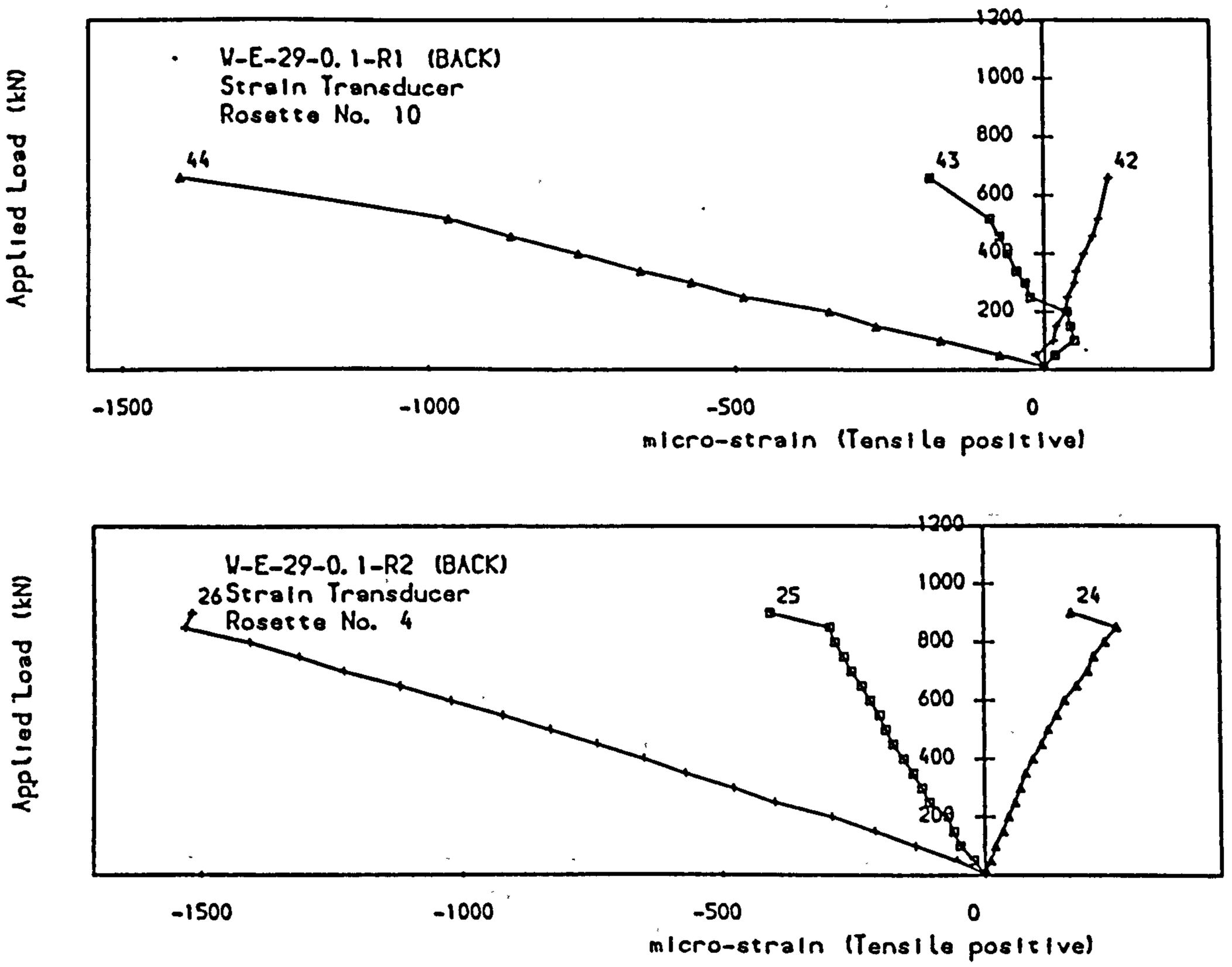

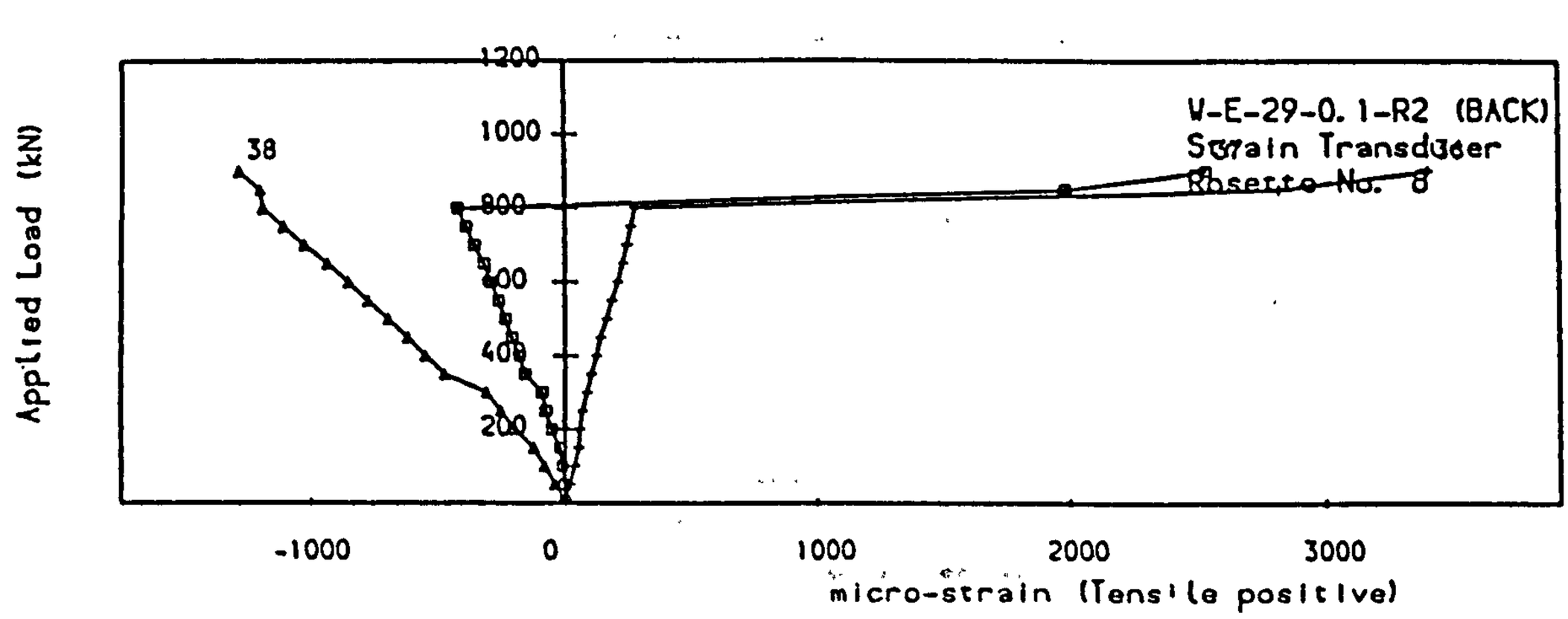

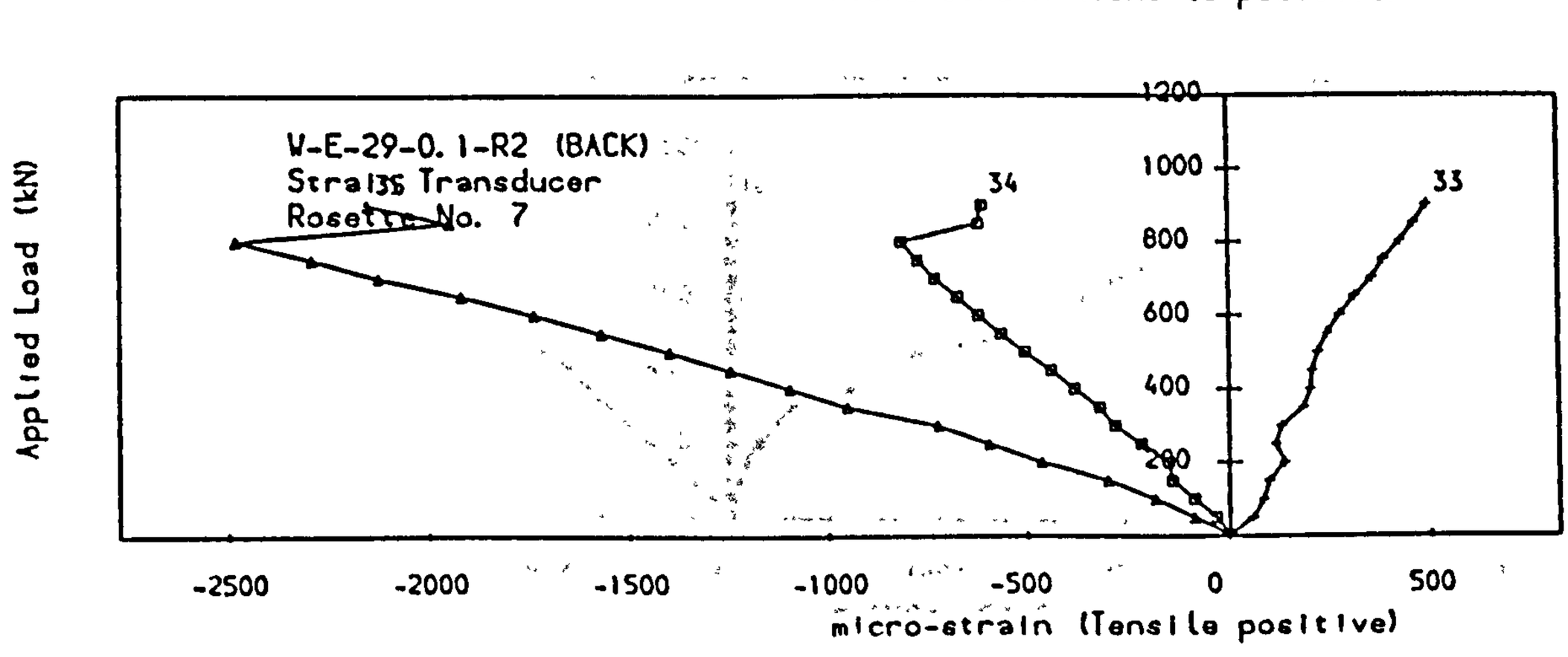

Figure 6.23 : Typical results of direct strain (W-Series beams) [cont'd]

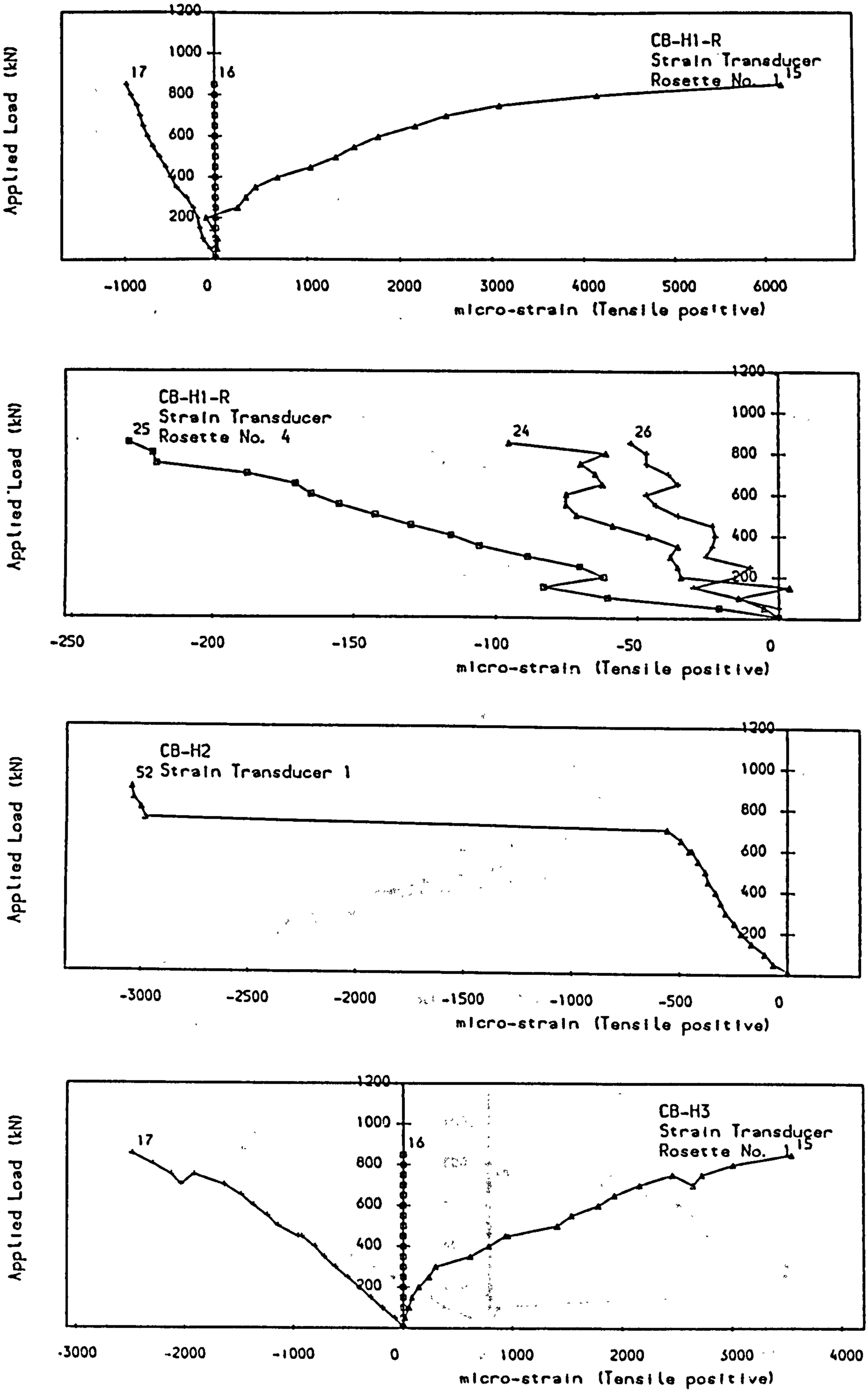

Figure 6.24 : Typical results of direct strain (CB-Series beams)

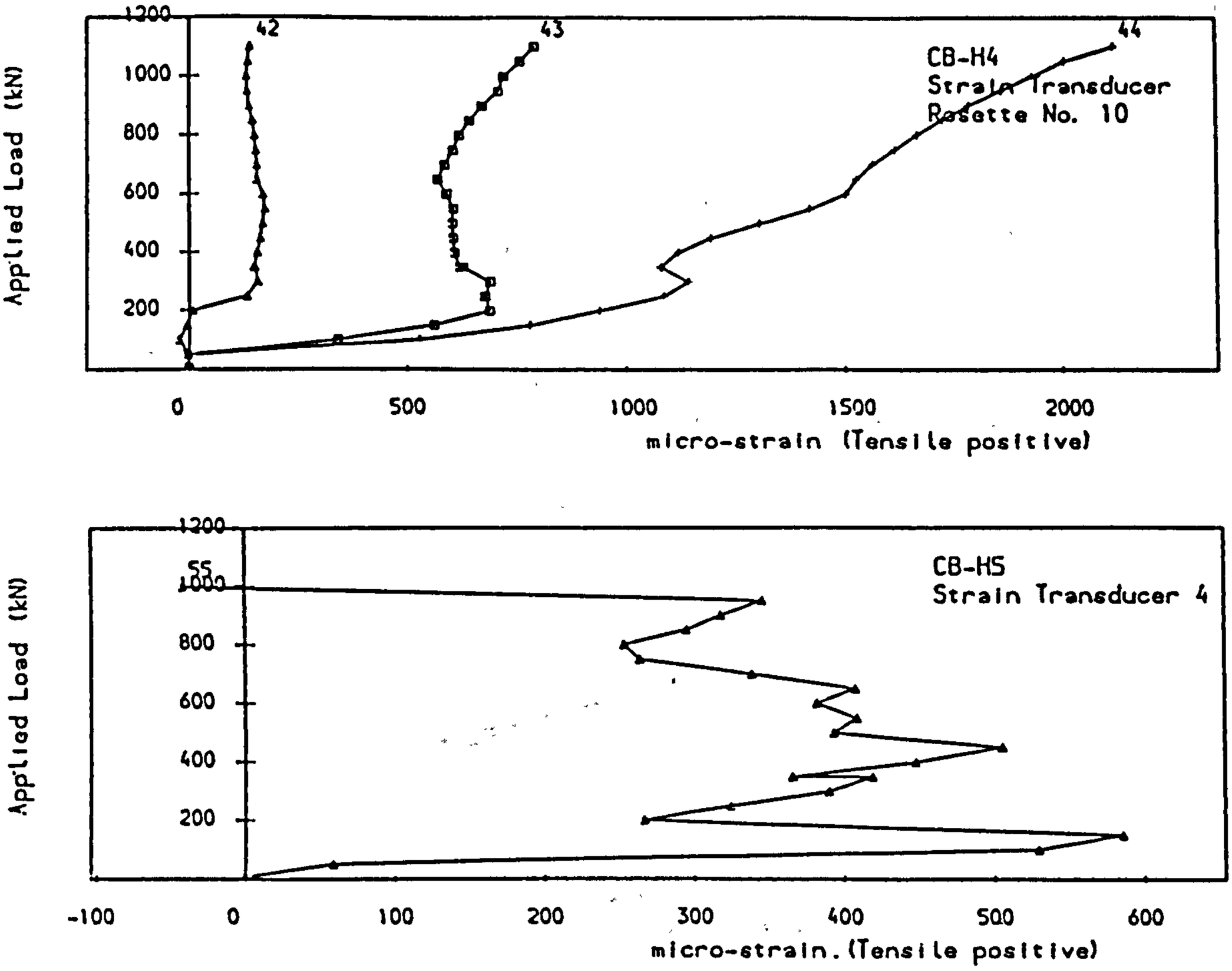

Figure 6.24 : Typical results of direct strain (CB-Series beams) [cont'd]

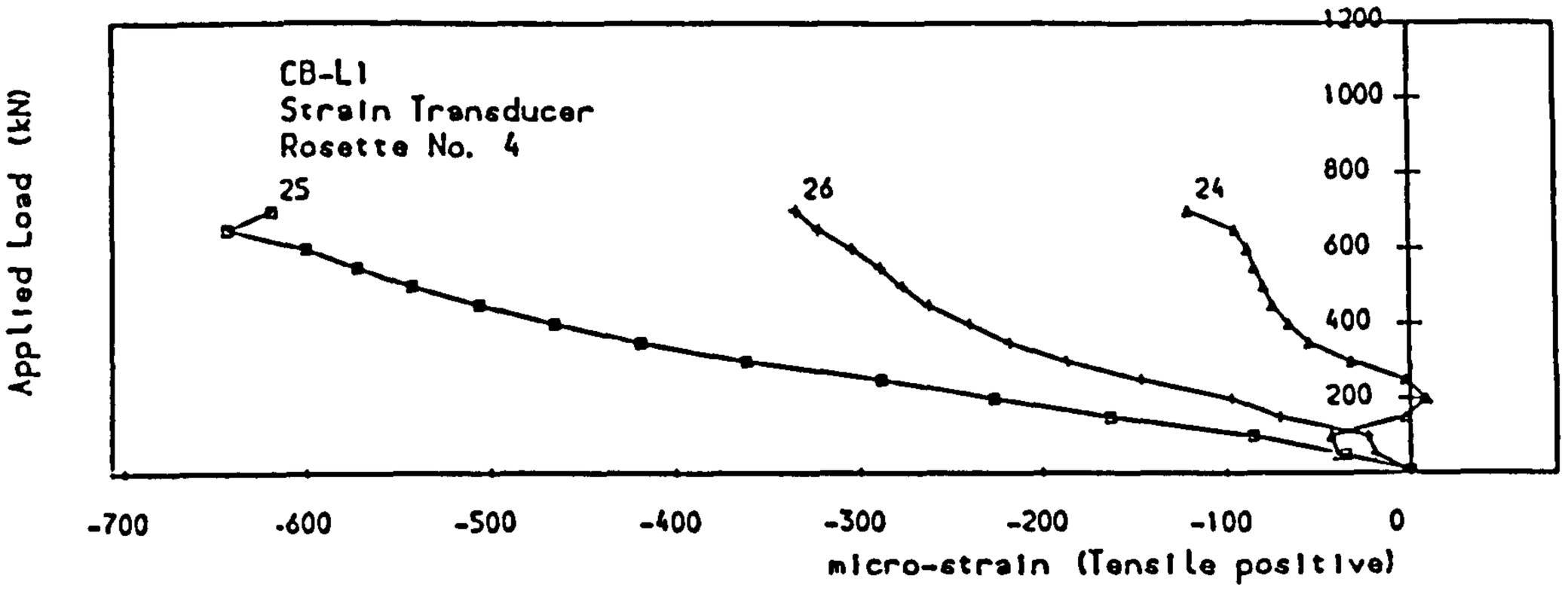

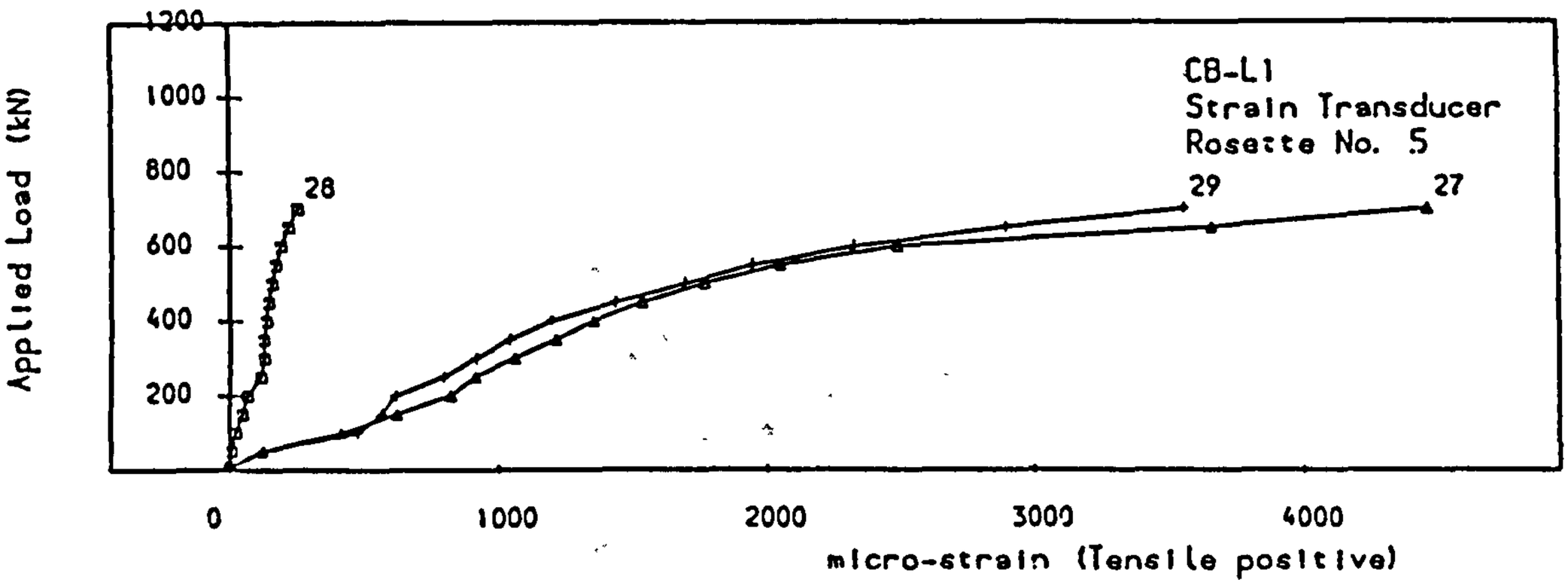

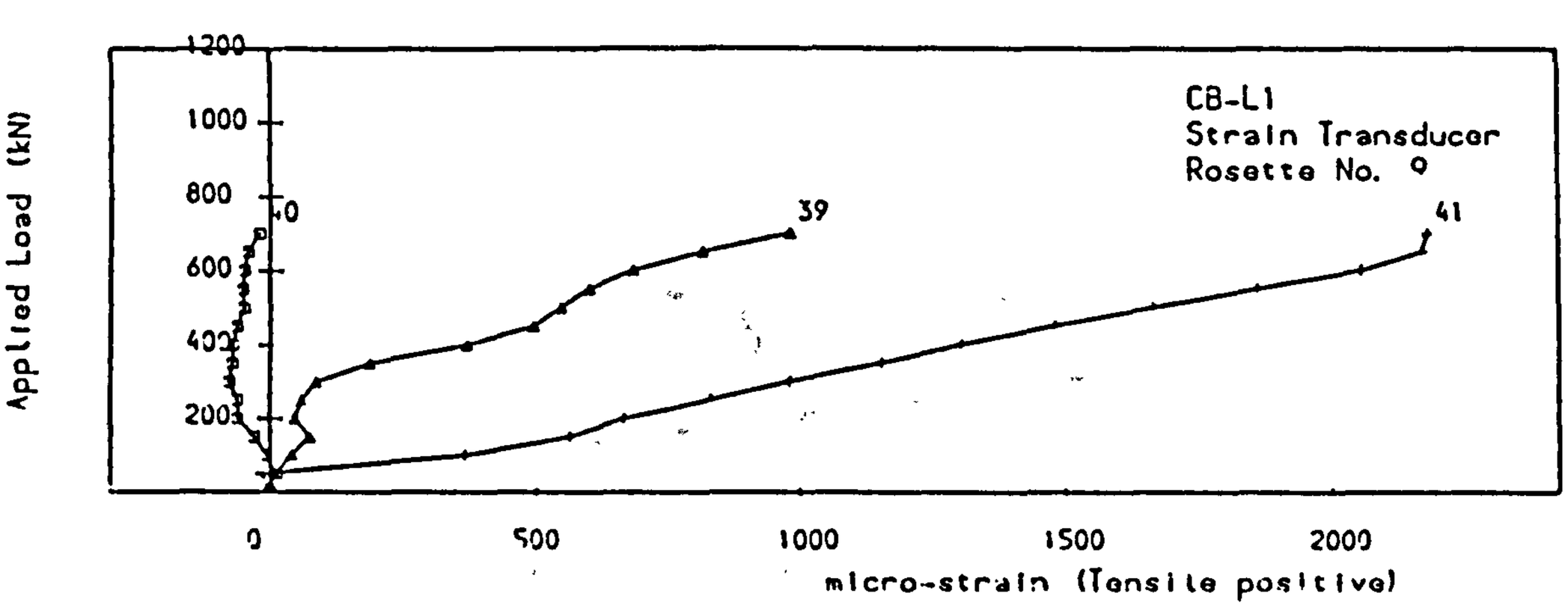

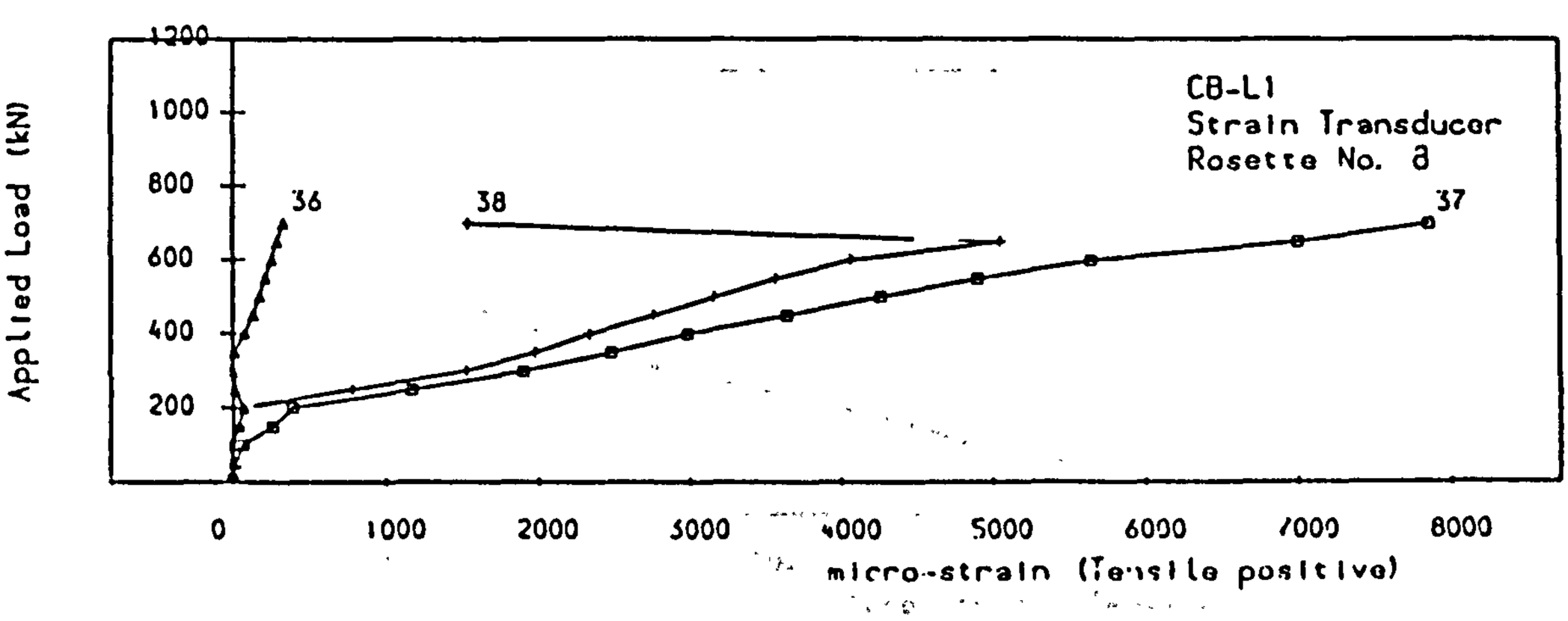

Figure 6.24 : Typical results of direct strain (CB-Series beams) [cont'd]

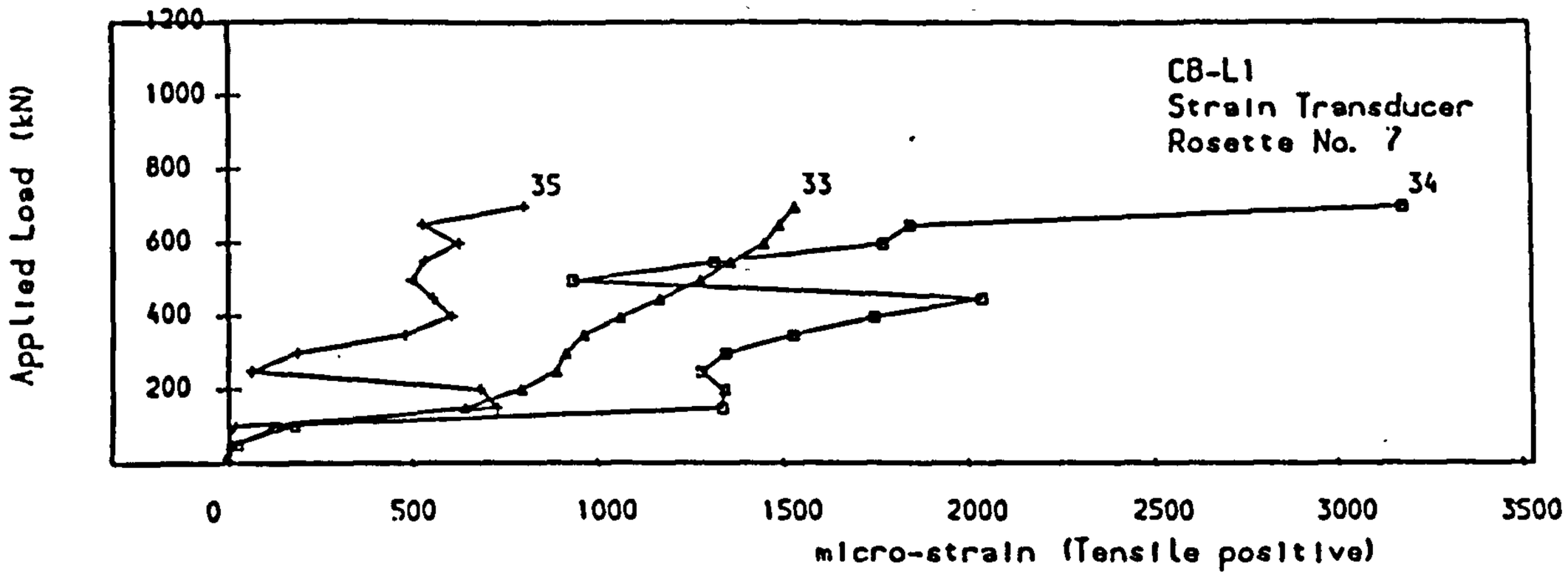

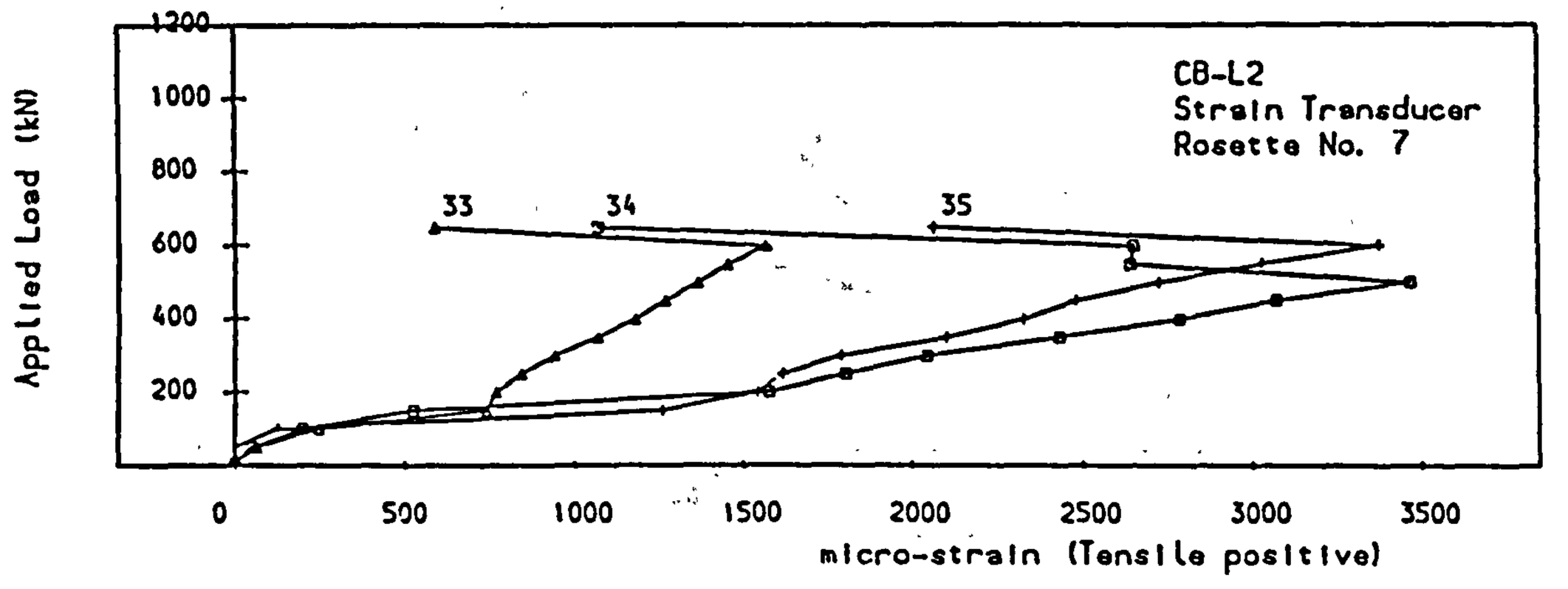

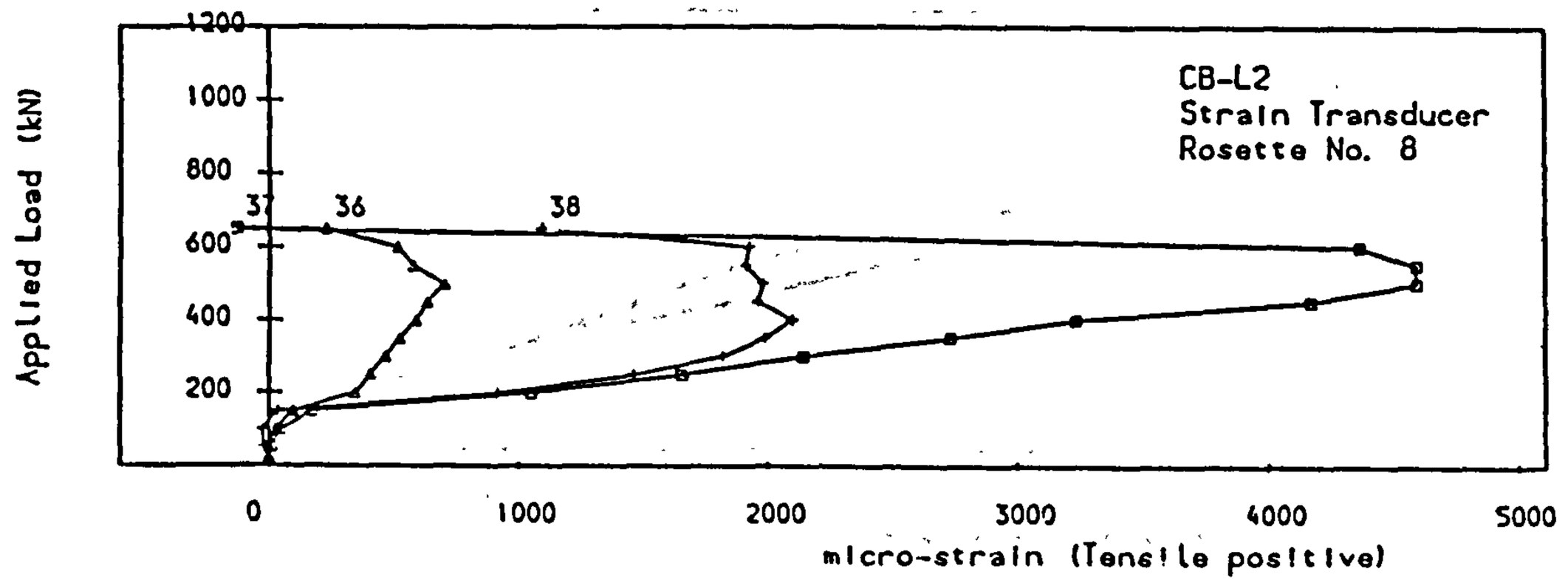

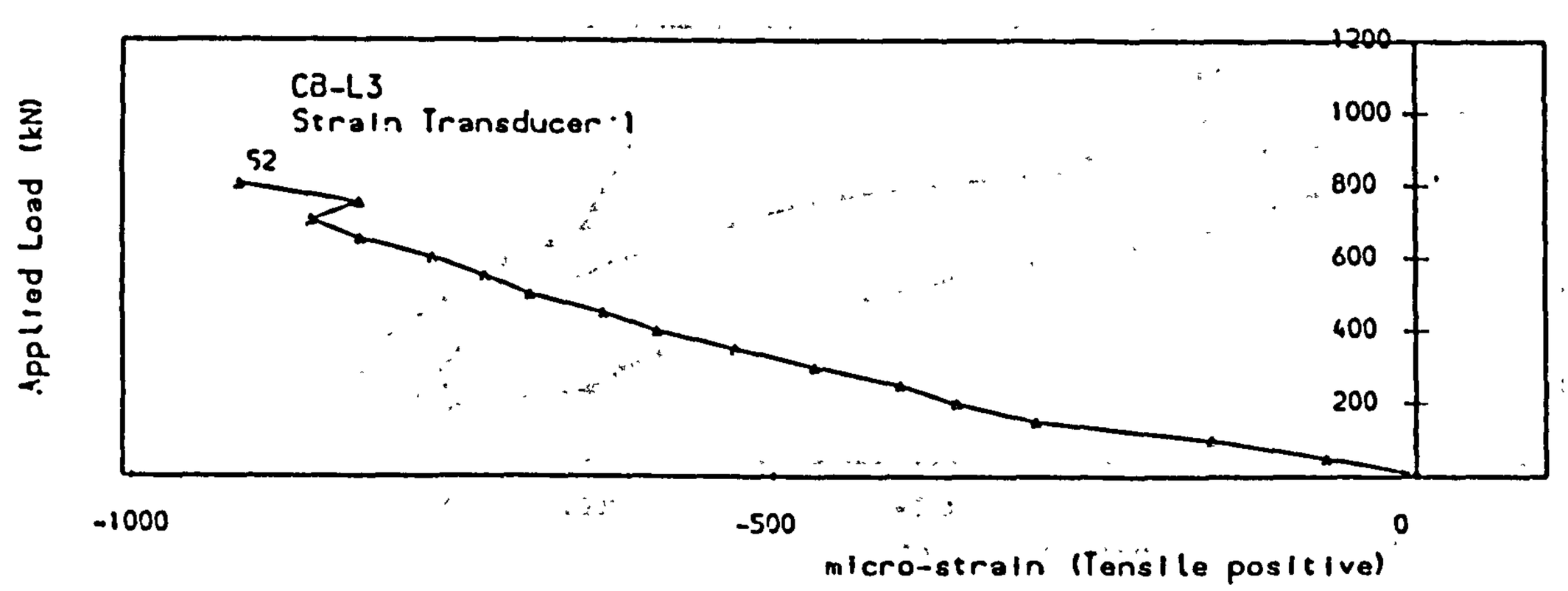

Figure 6.24 : Typical results of direct strain (CB-Series beams) [cont'd]

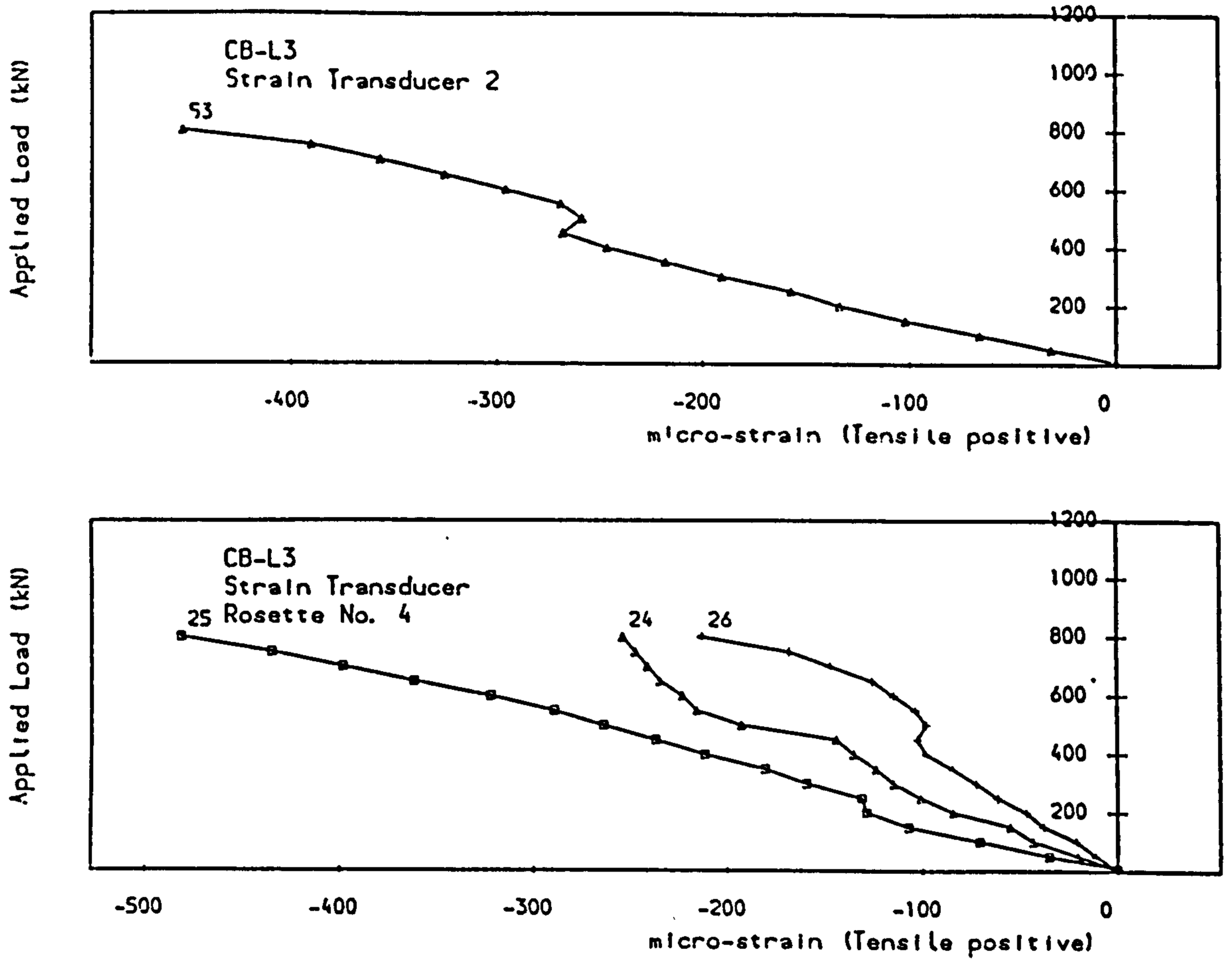

Figure 6.24 : Typical results of direct strain (CB-Series beams) [cont'd]

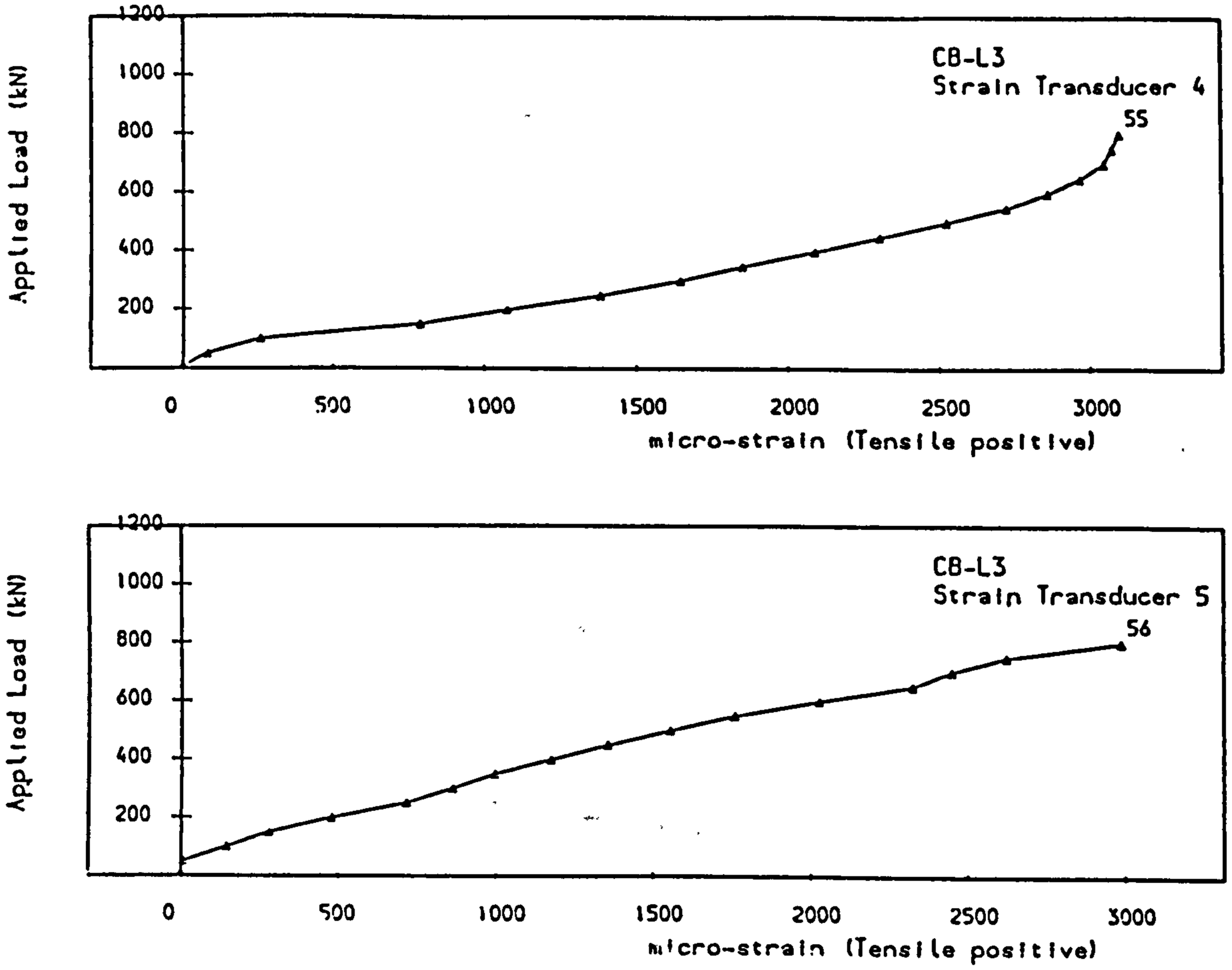

Figure 6.24 : Typical results of direct strain (CB-Series beams) [cont'd]

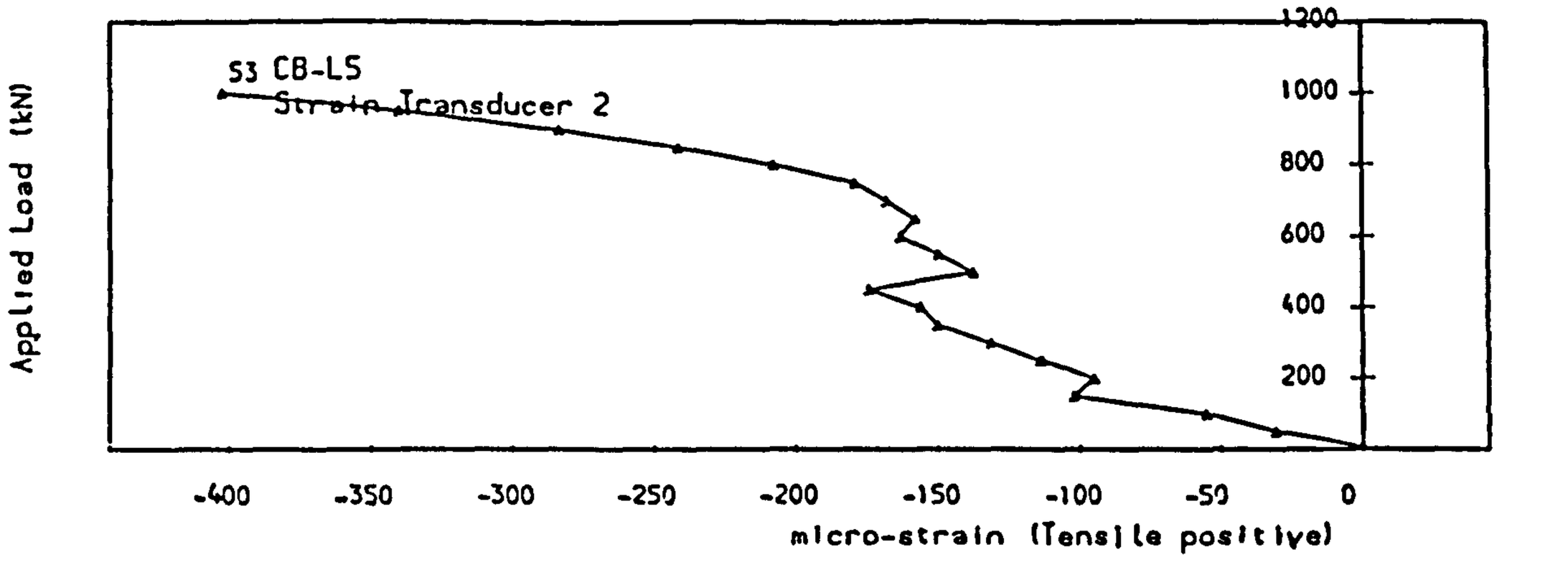

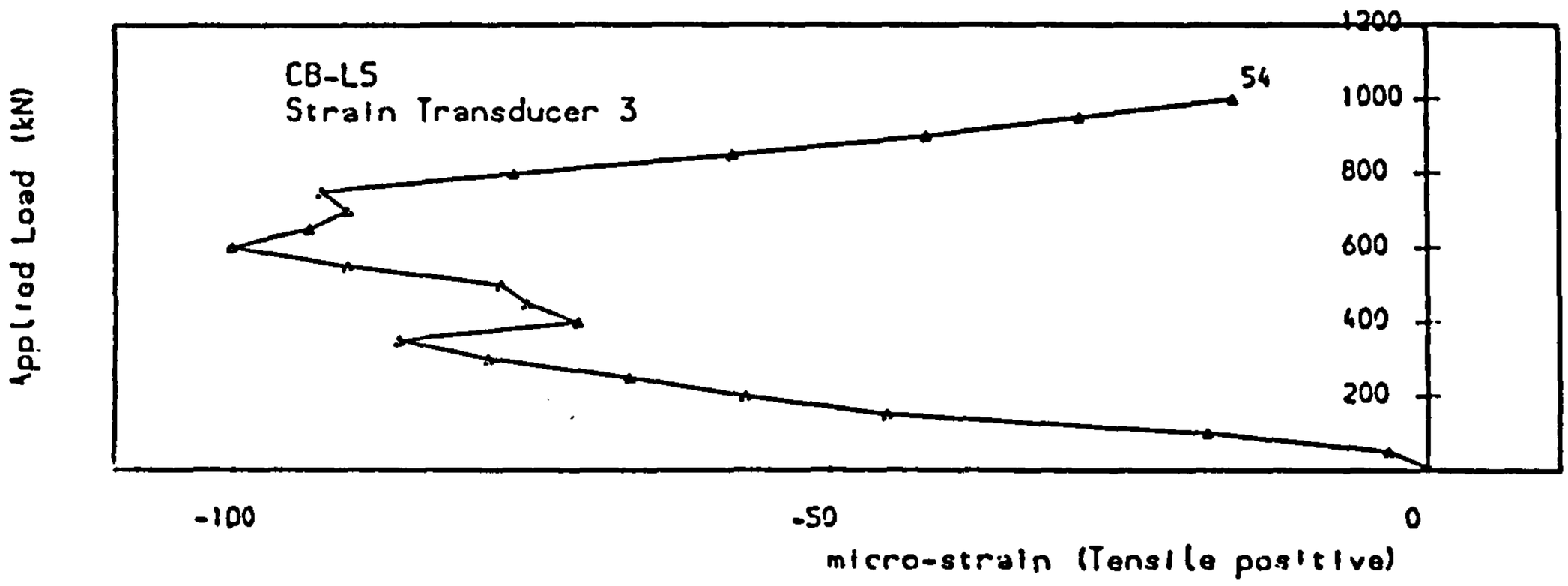

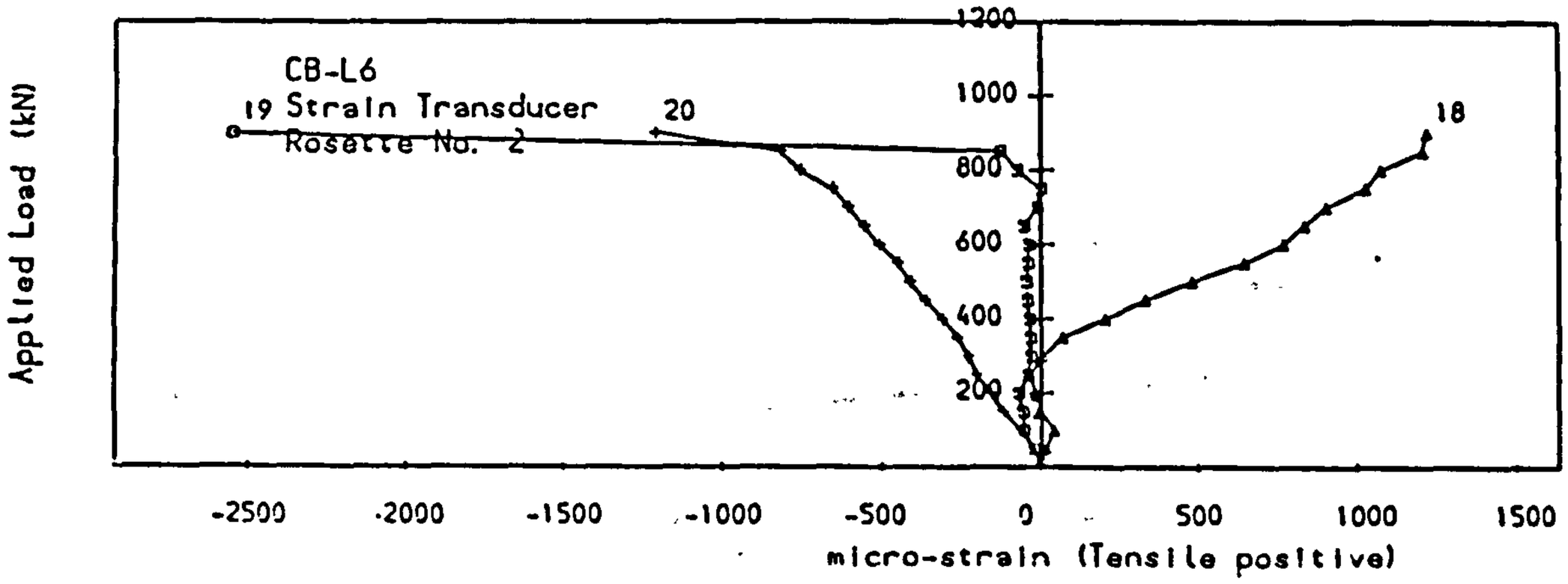

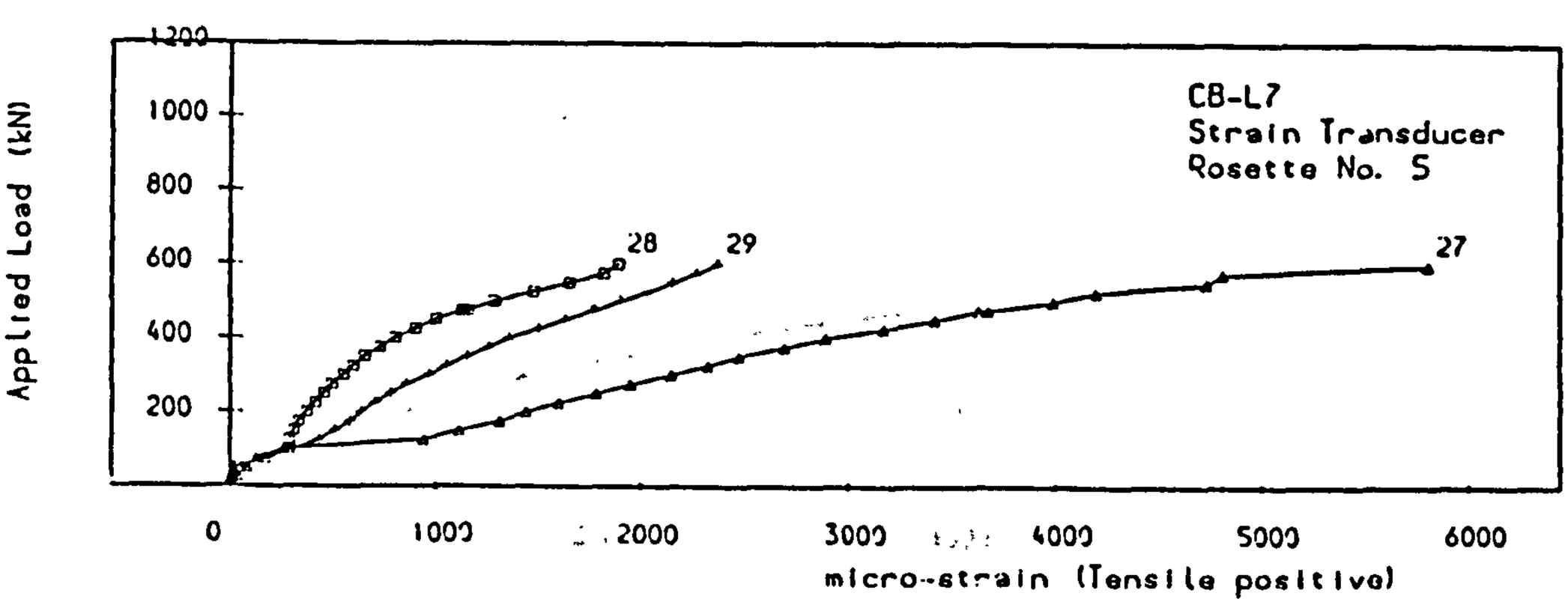

Figure 6.24 : Typical results of direct strain (CB-Series beams) [cont'd]

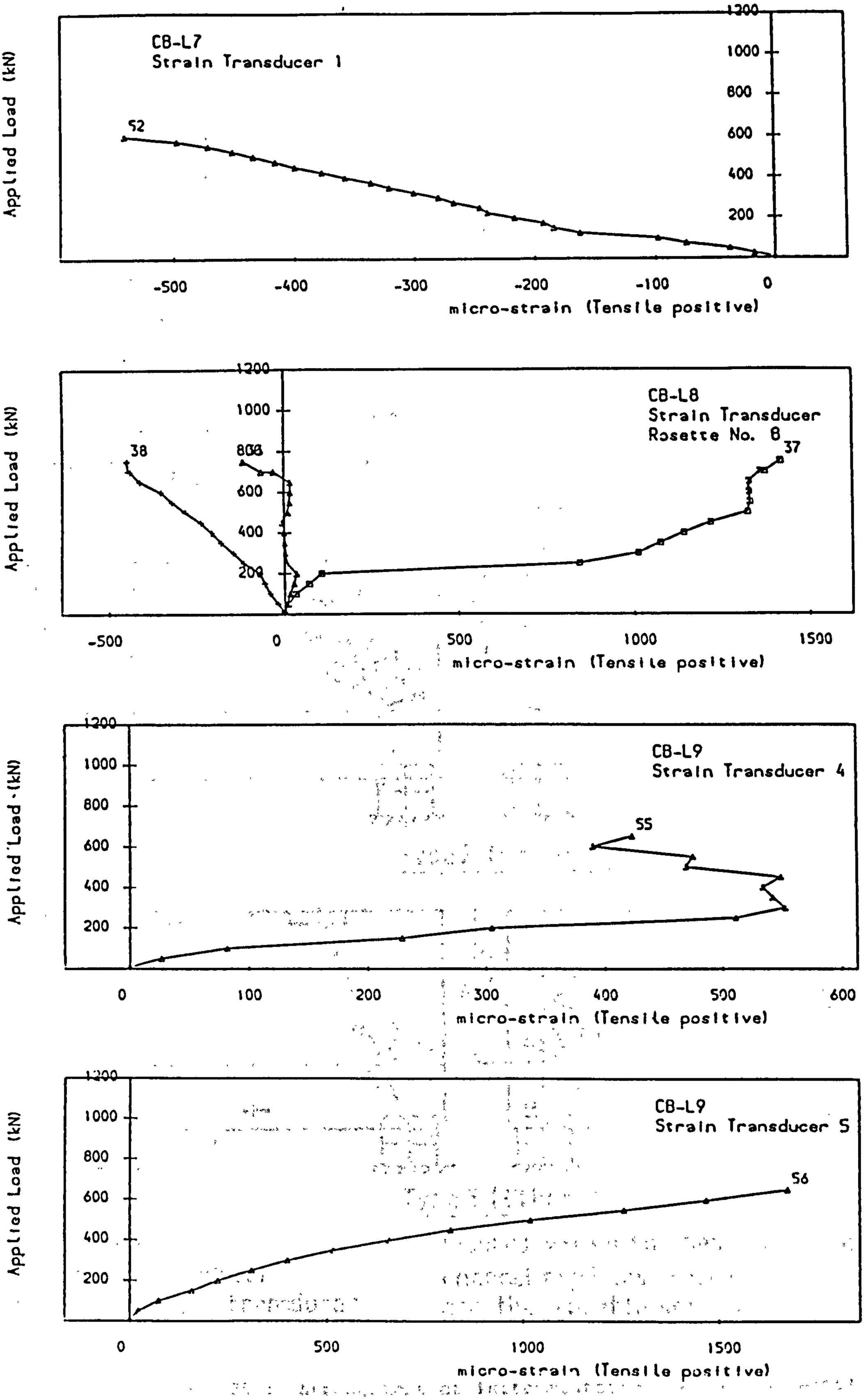

Figure 6.24 : Typical results of direct strain (CB-Series beams) [cont'd]

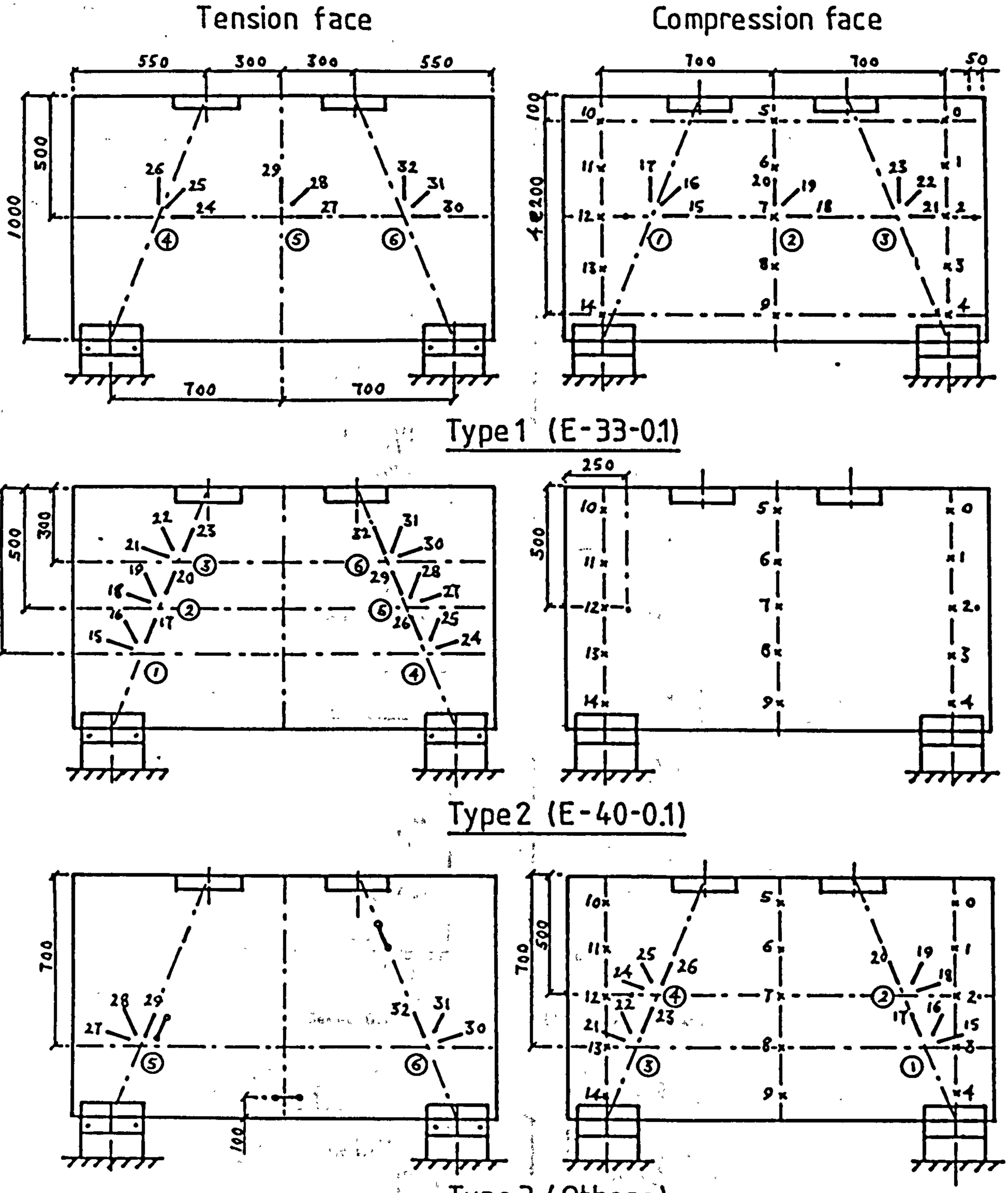

Figure 6.25 : Arrangement of instrumentation (E-Series beams)

(All dimensions in mm)

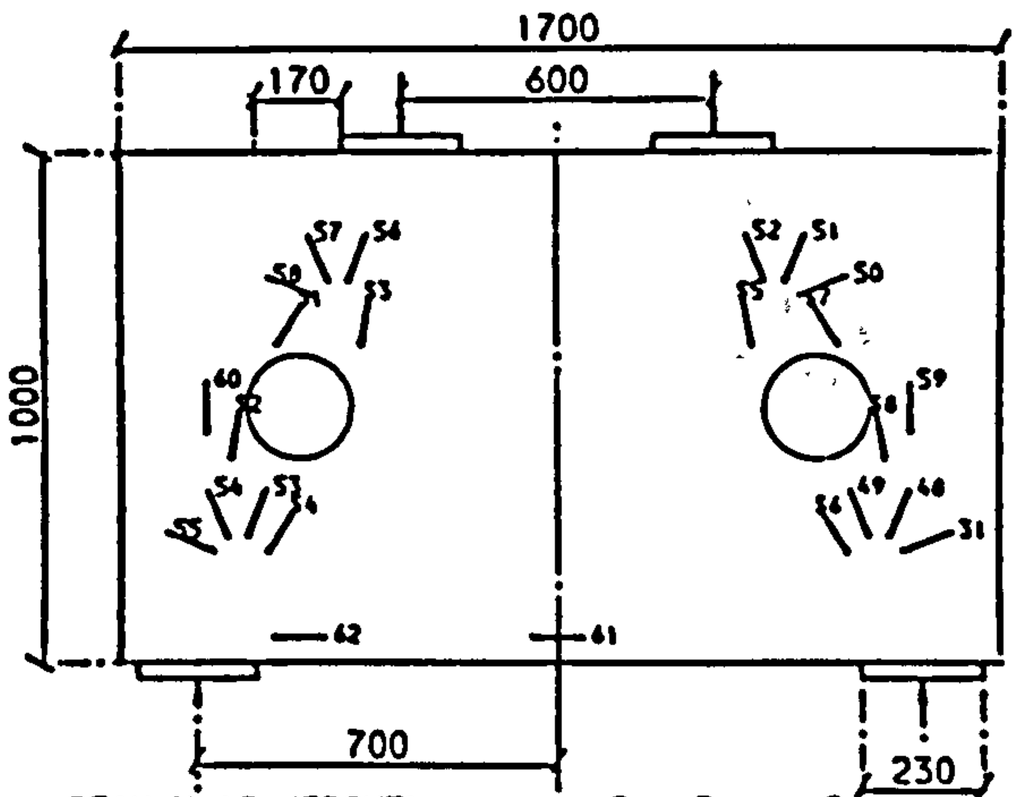

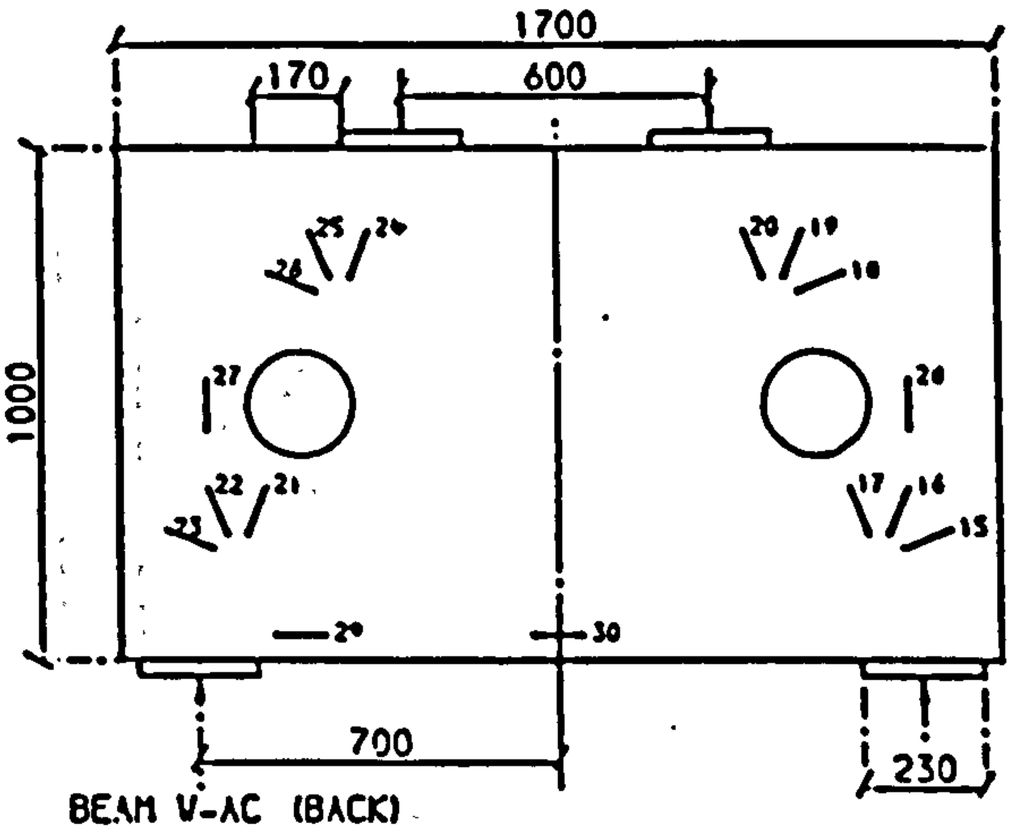

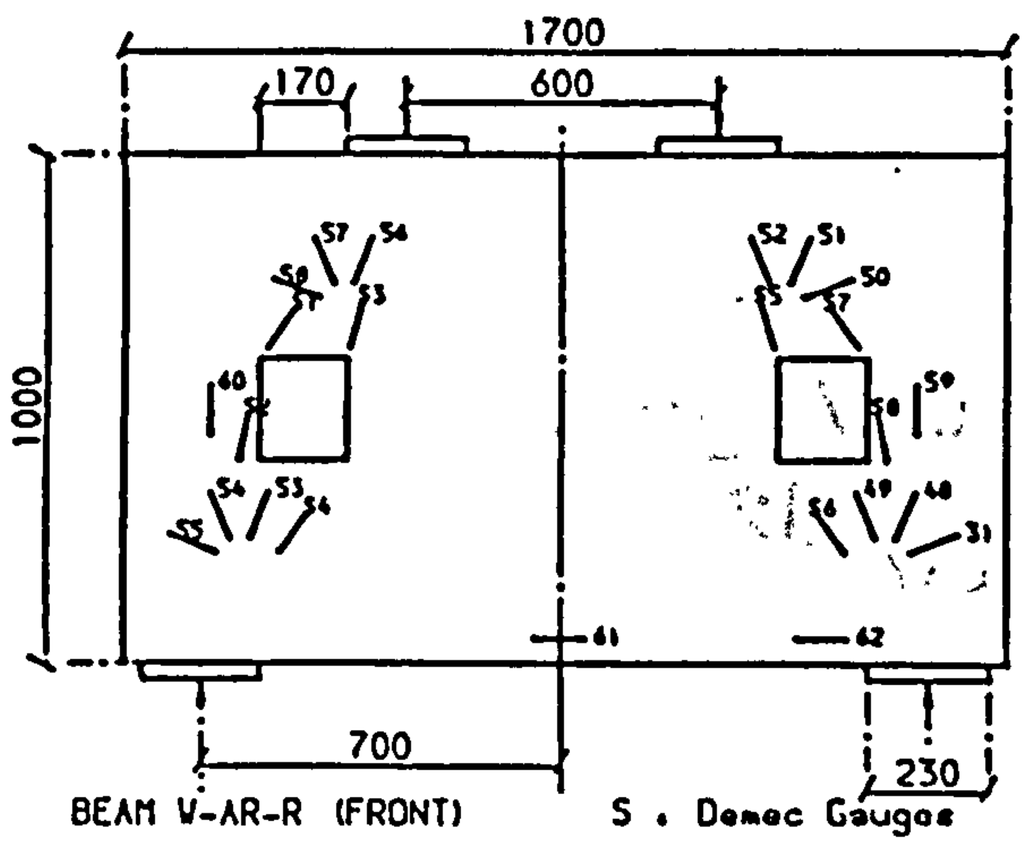

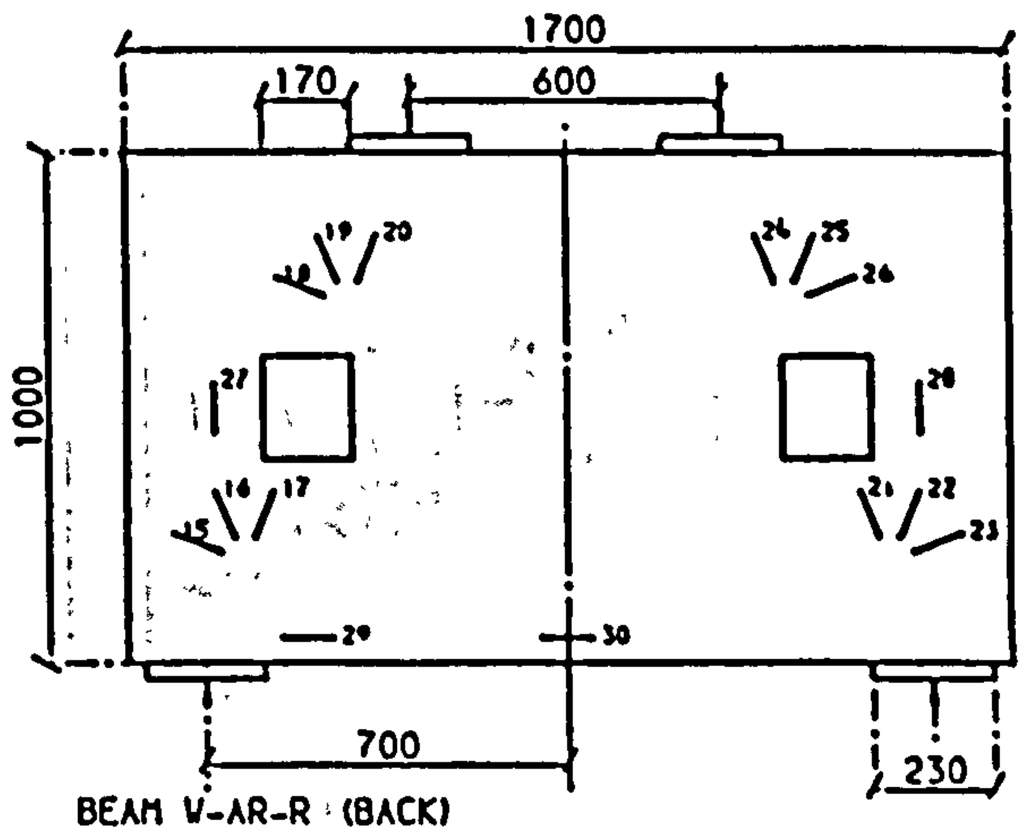

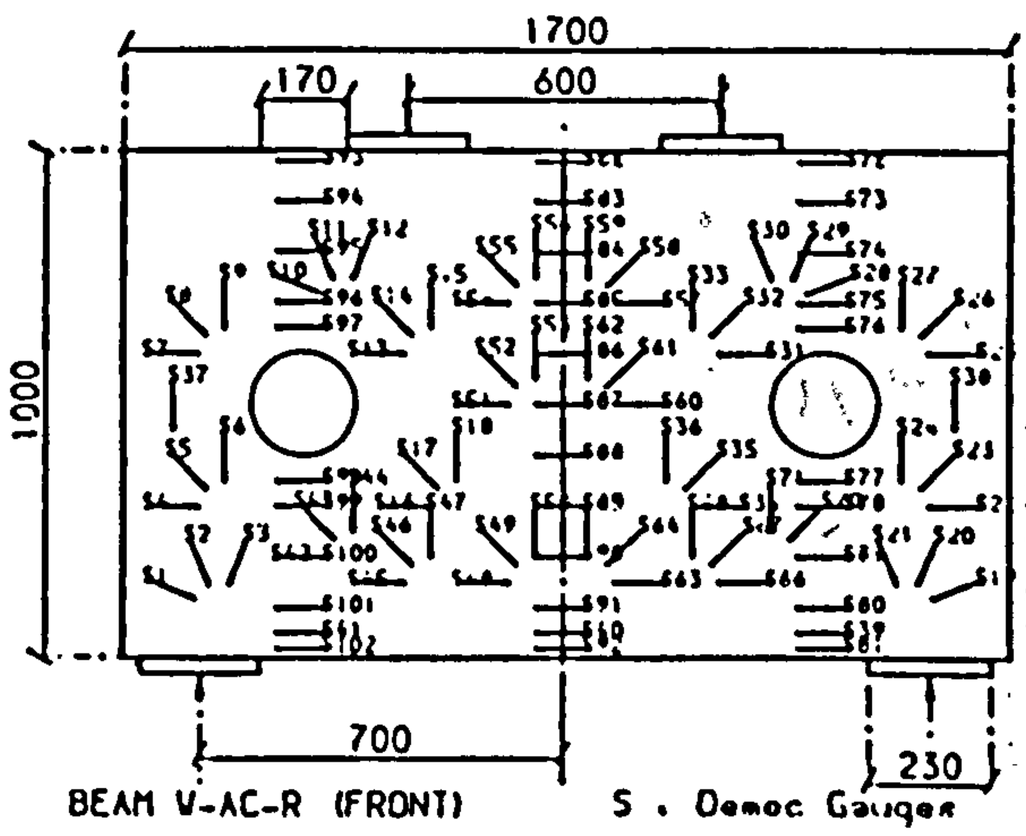

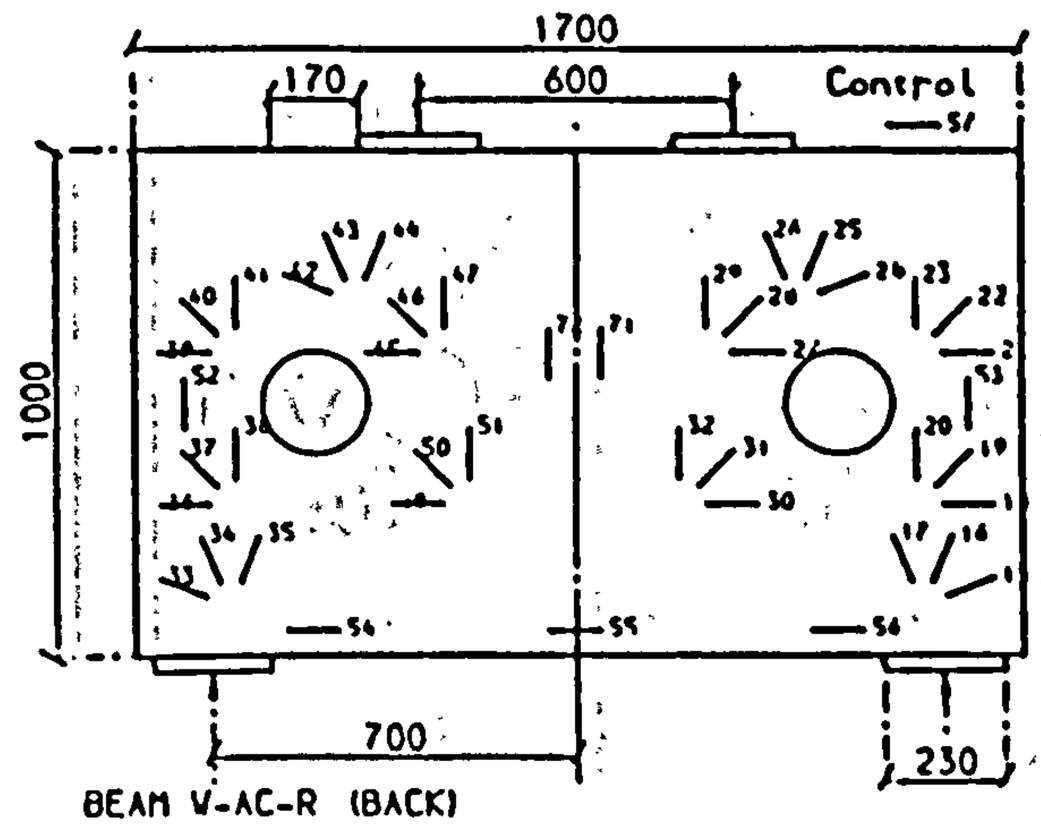

Figure 6.26 : Position of strain gauges (W-Series beams)

(All dimensions in mm)

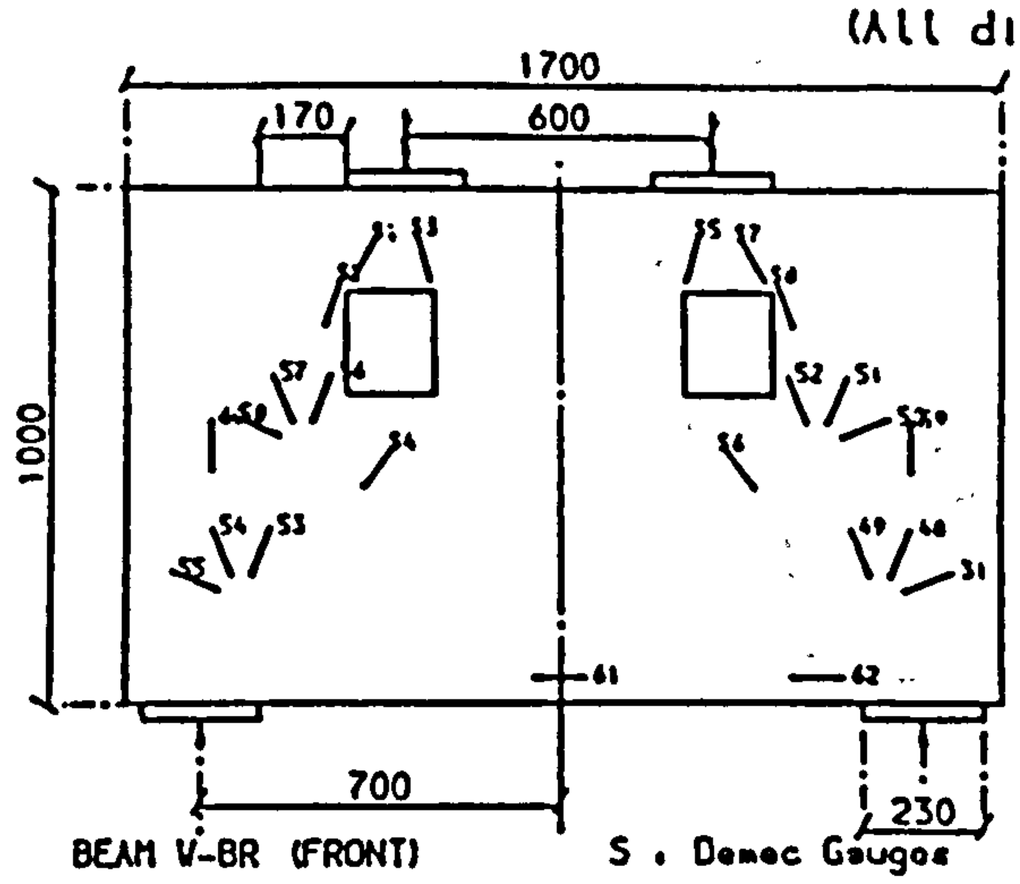

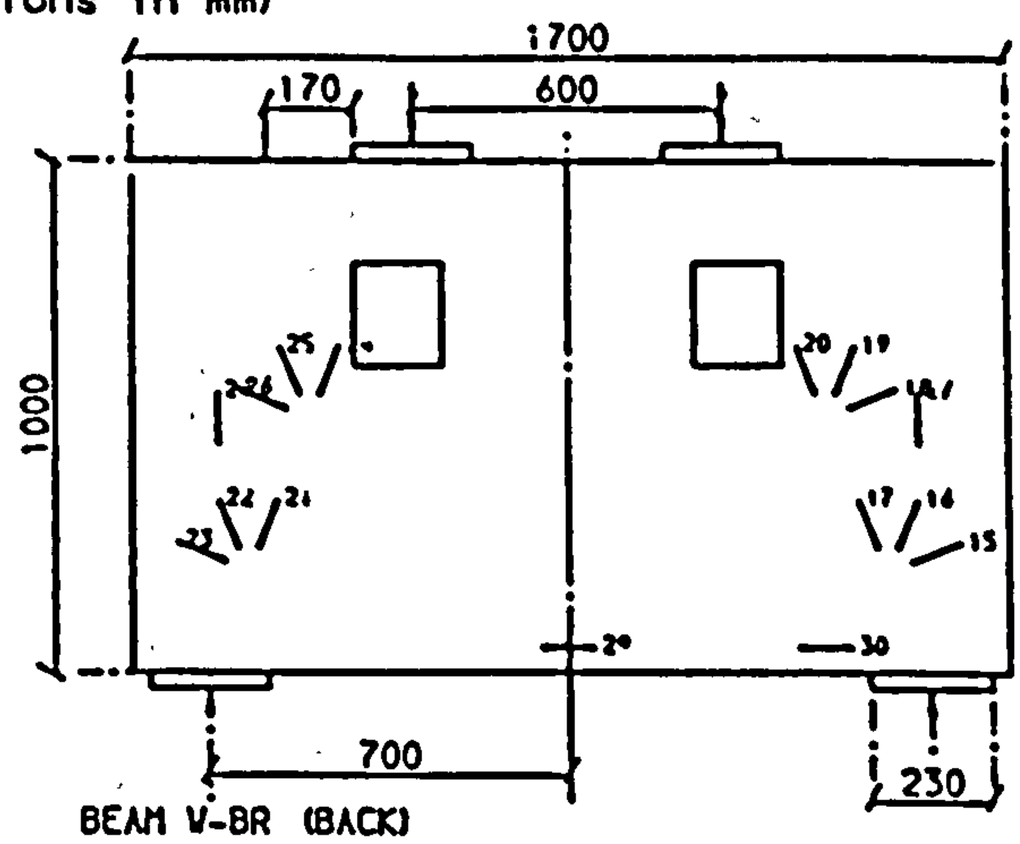

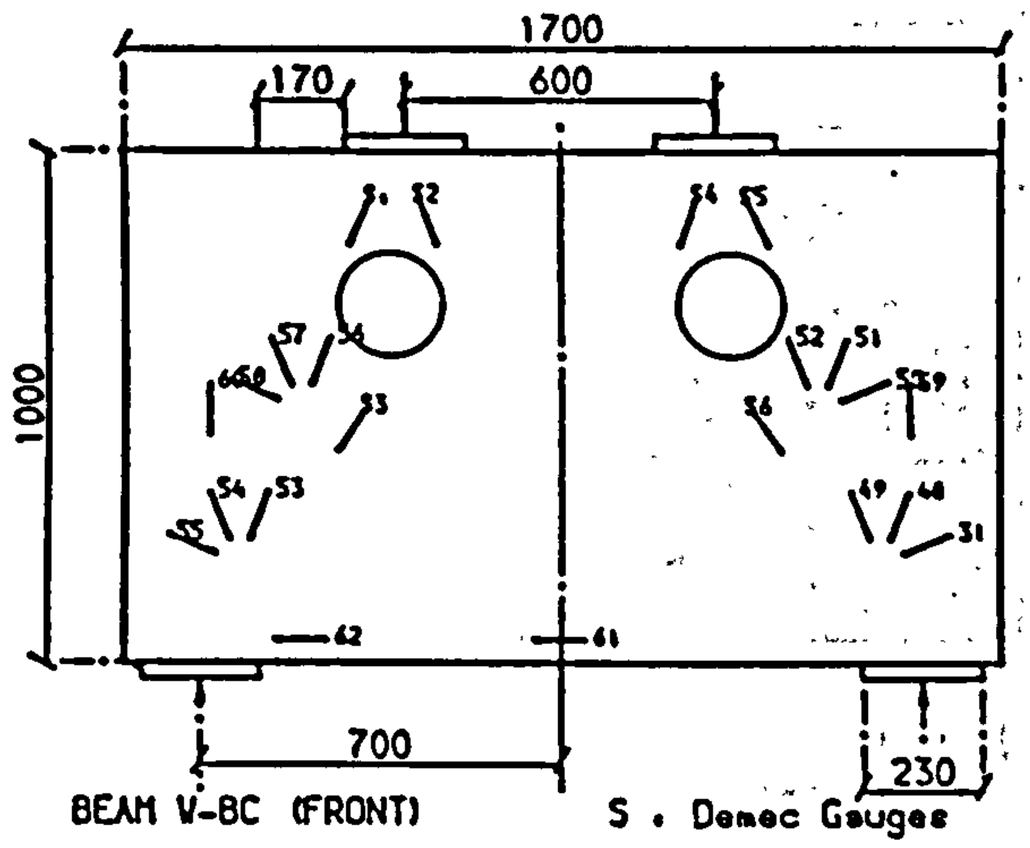

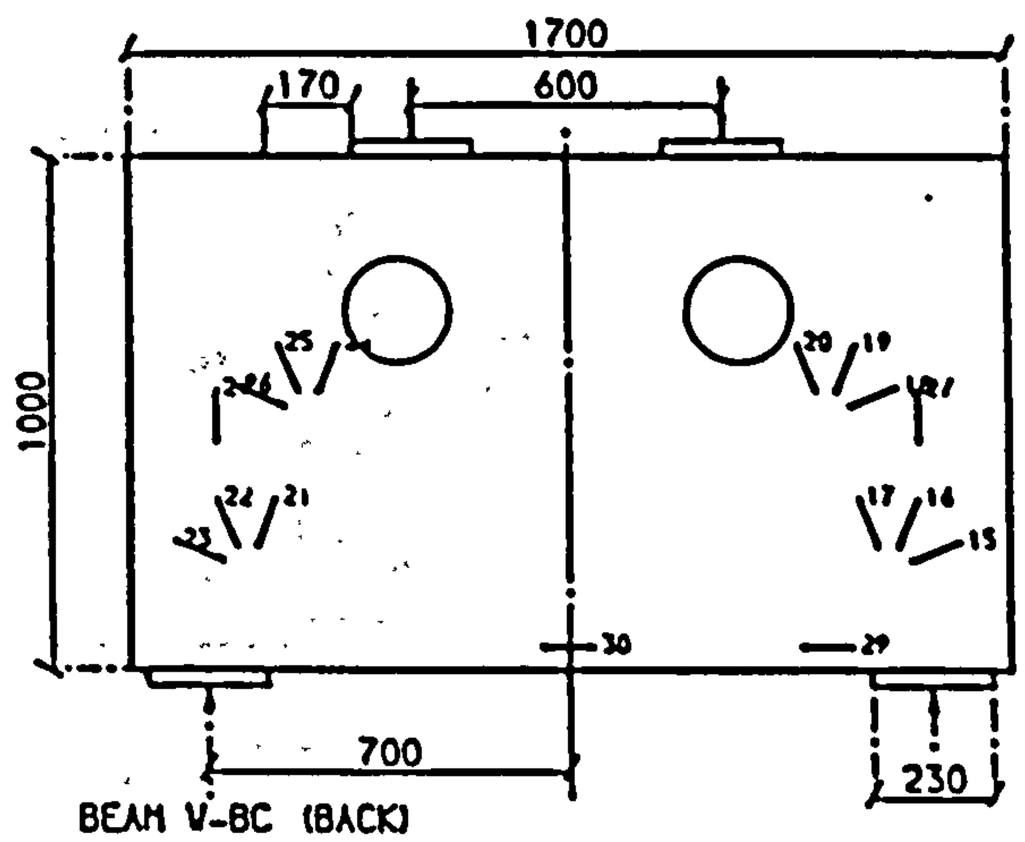

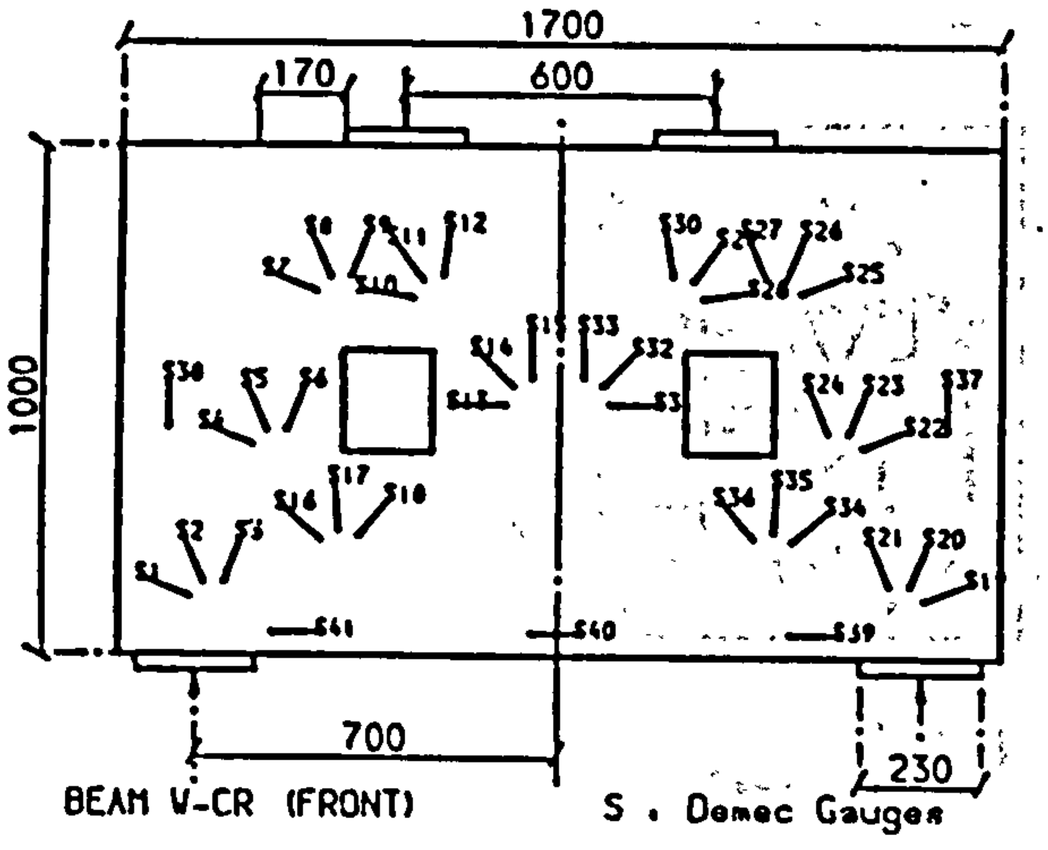

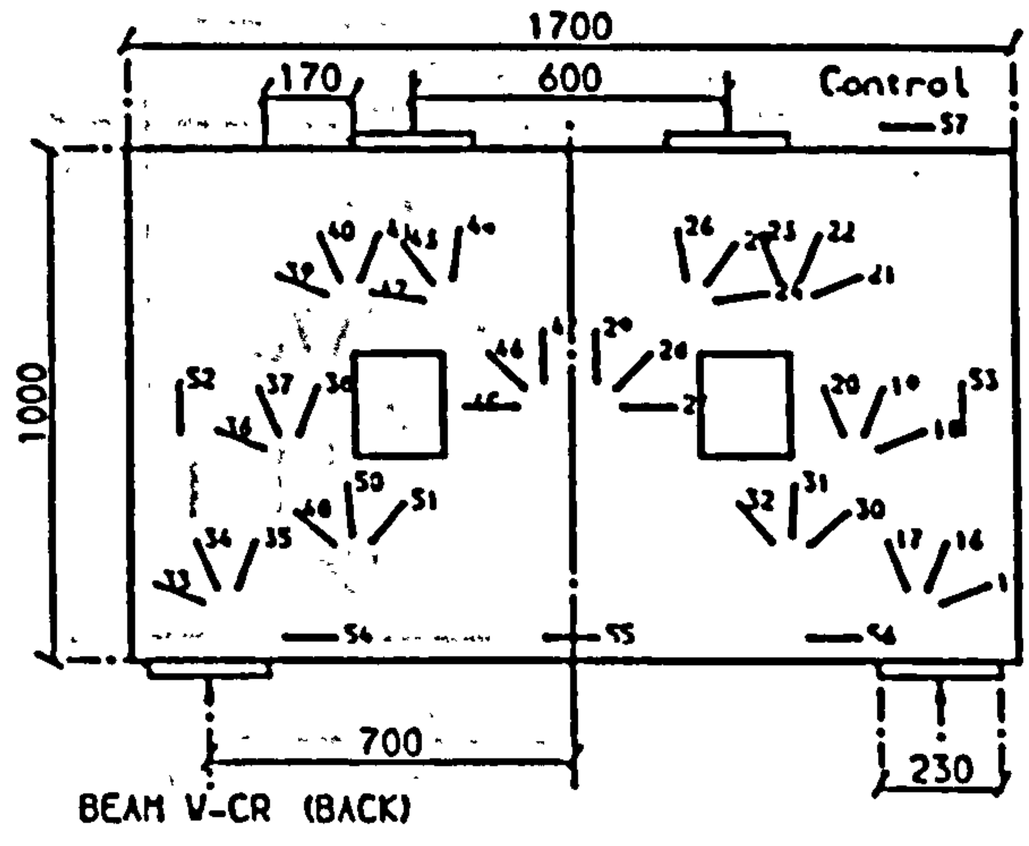

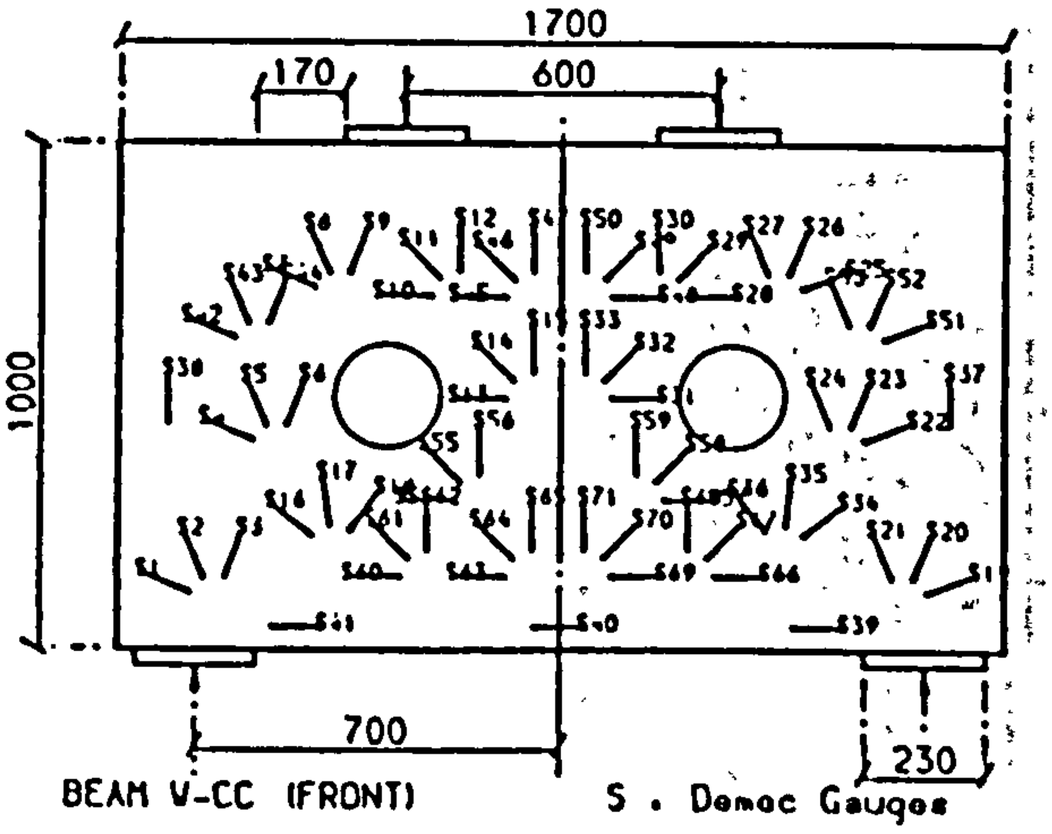

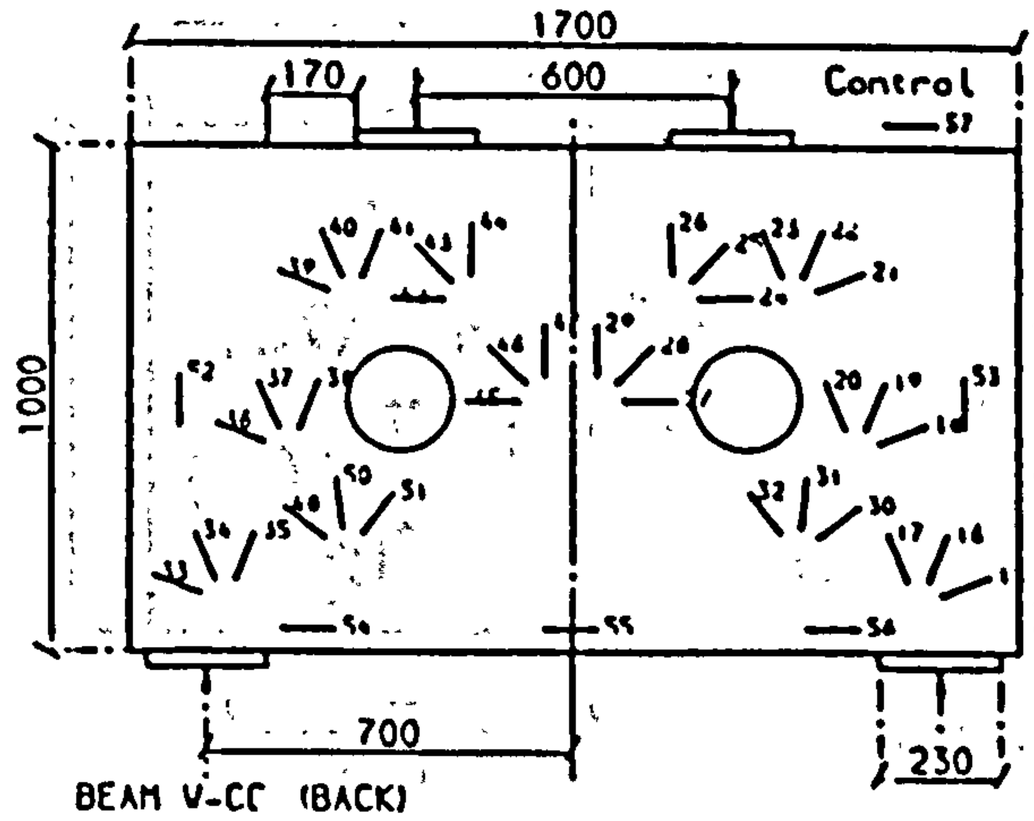

Figure 6.26 : Position of strain gauges (W-Series beams) [cont'd]

(All dimensions in mm)

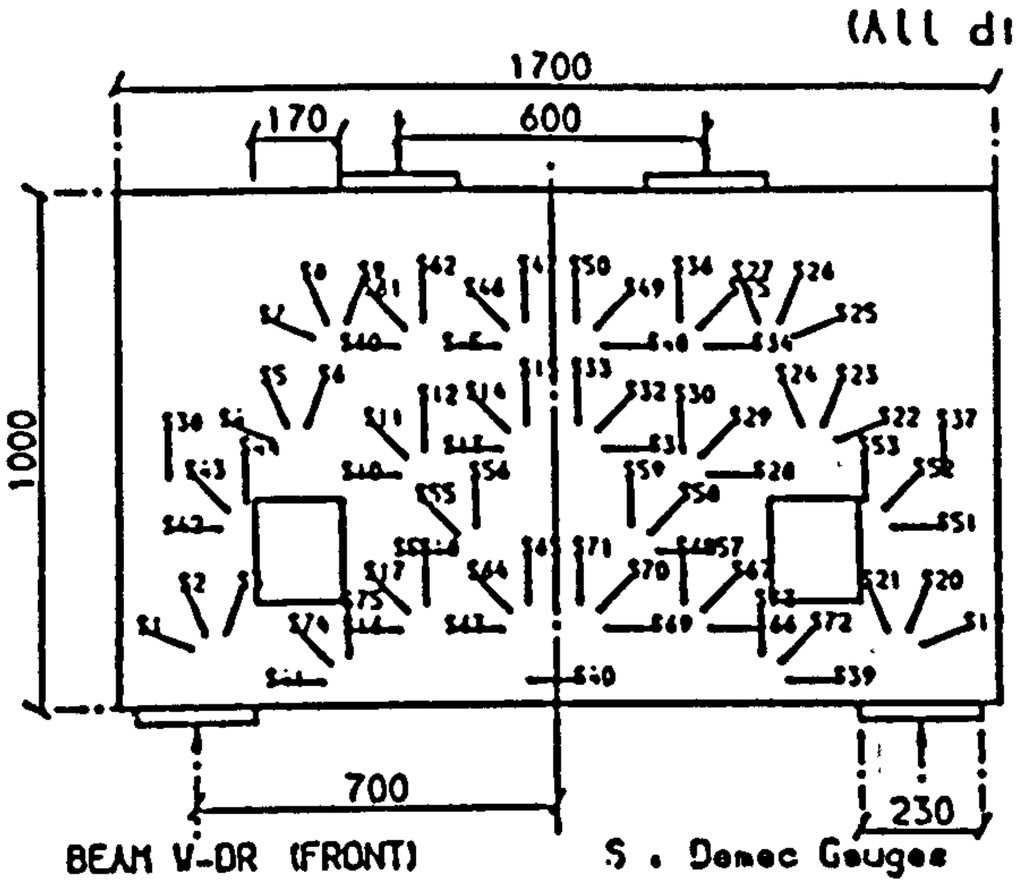

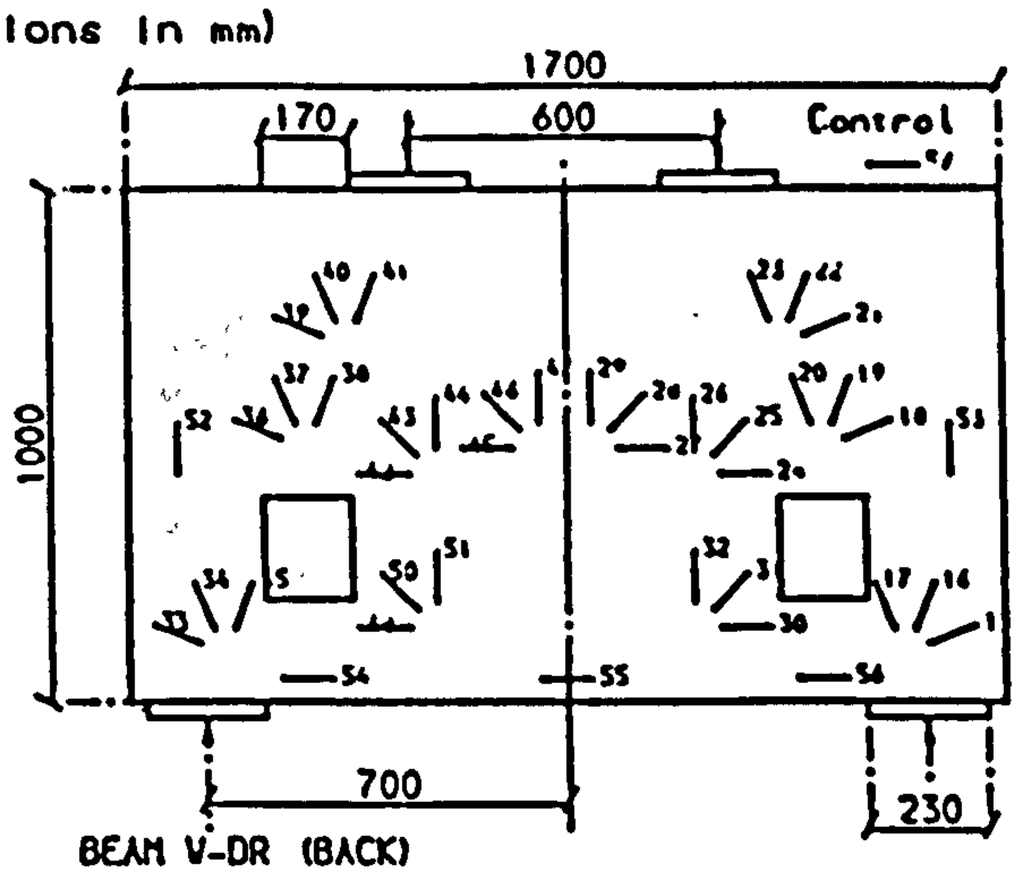

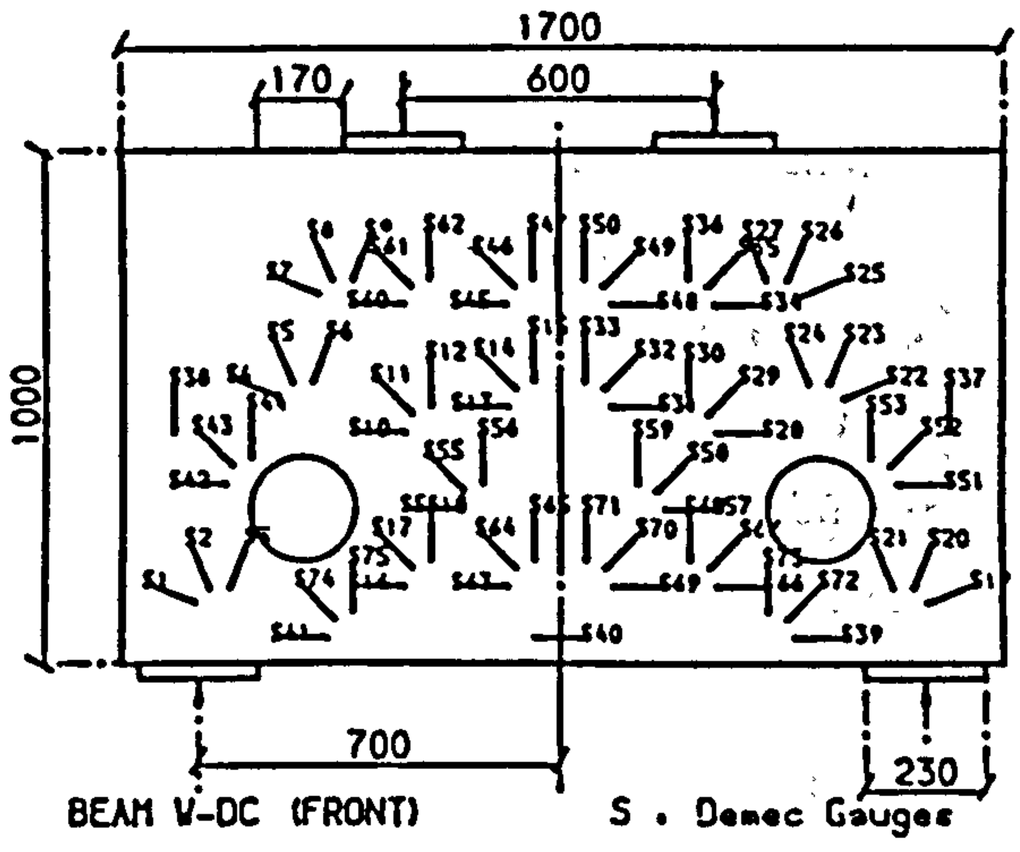

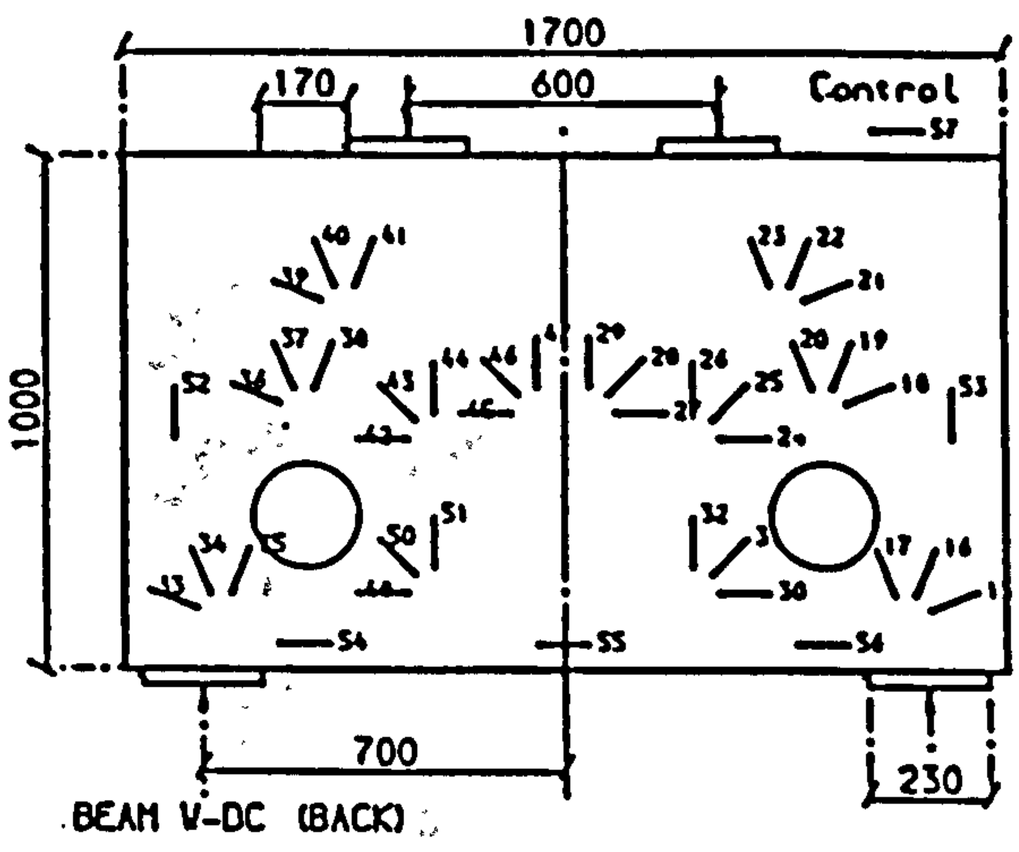

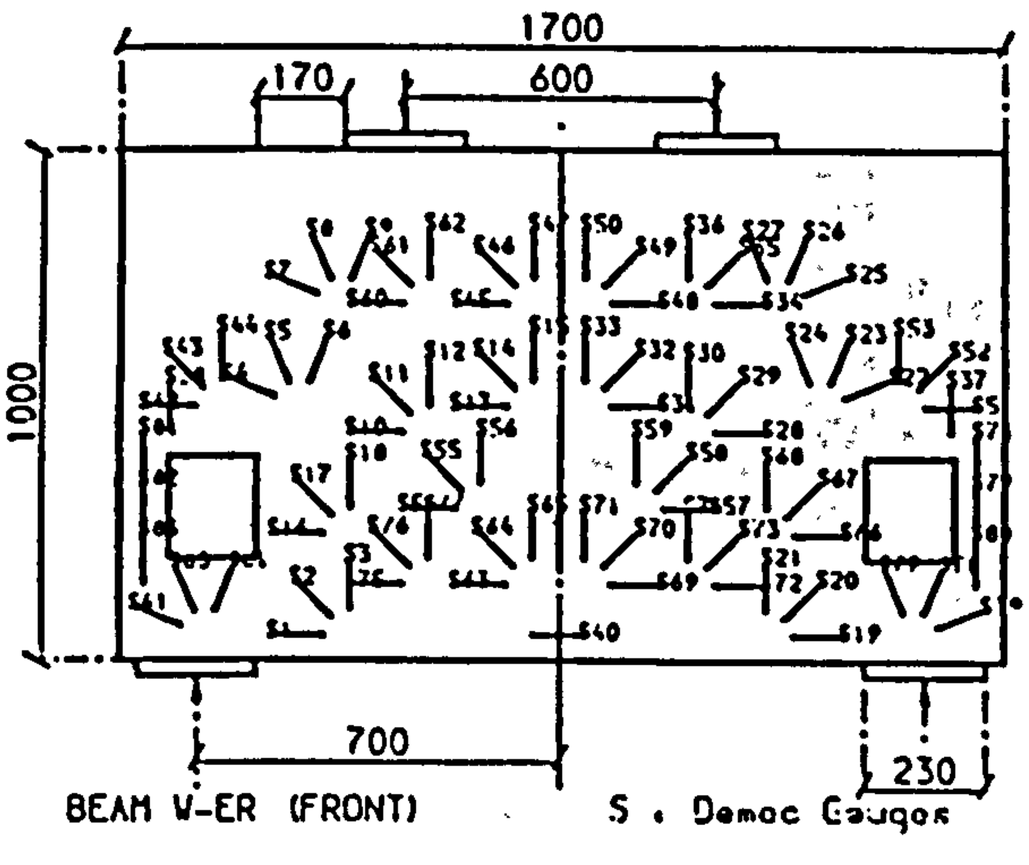

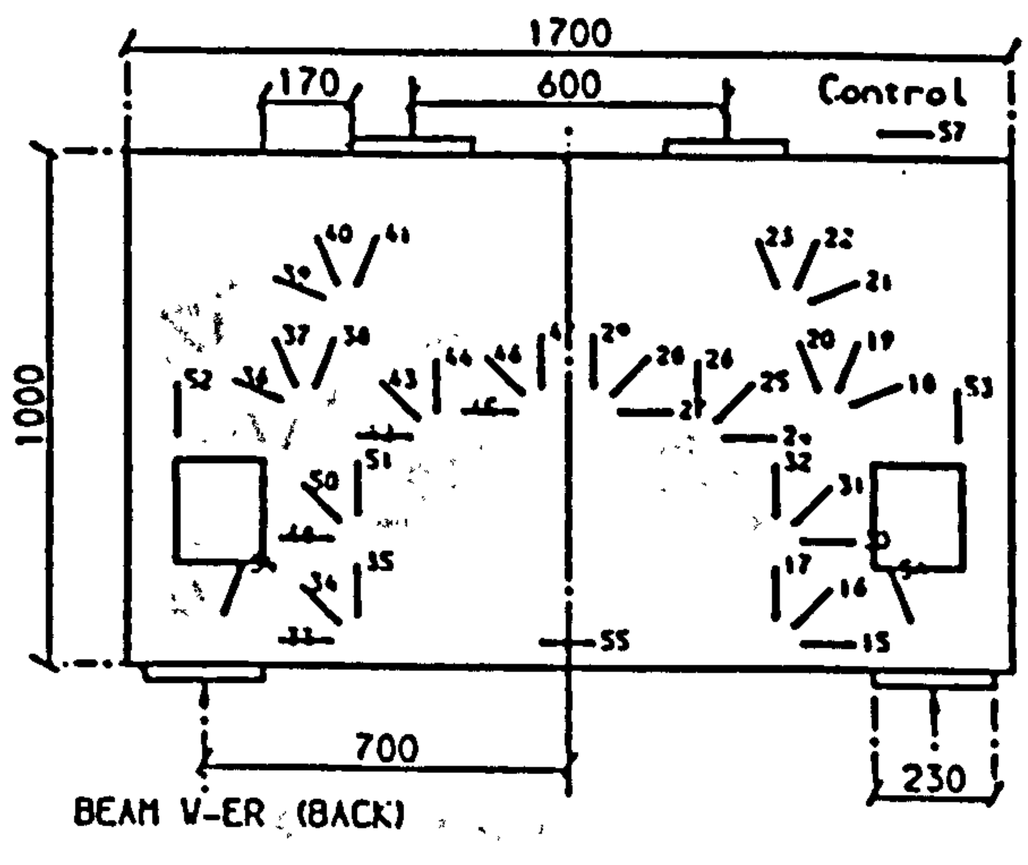

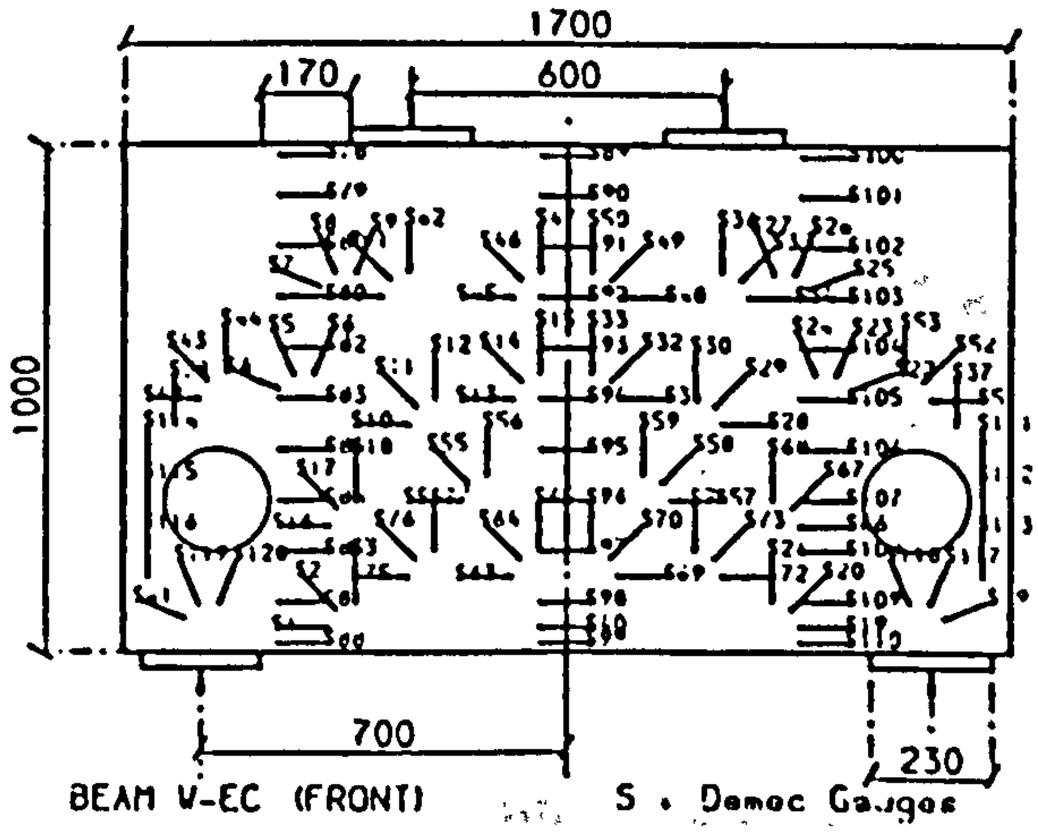

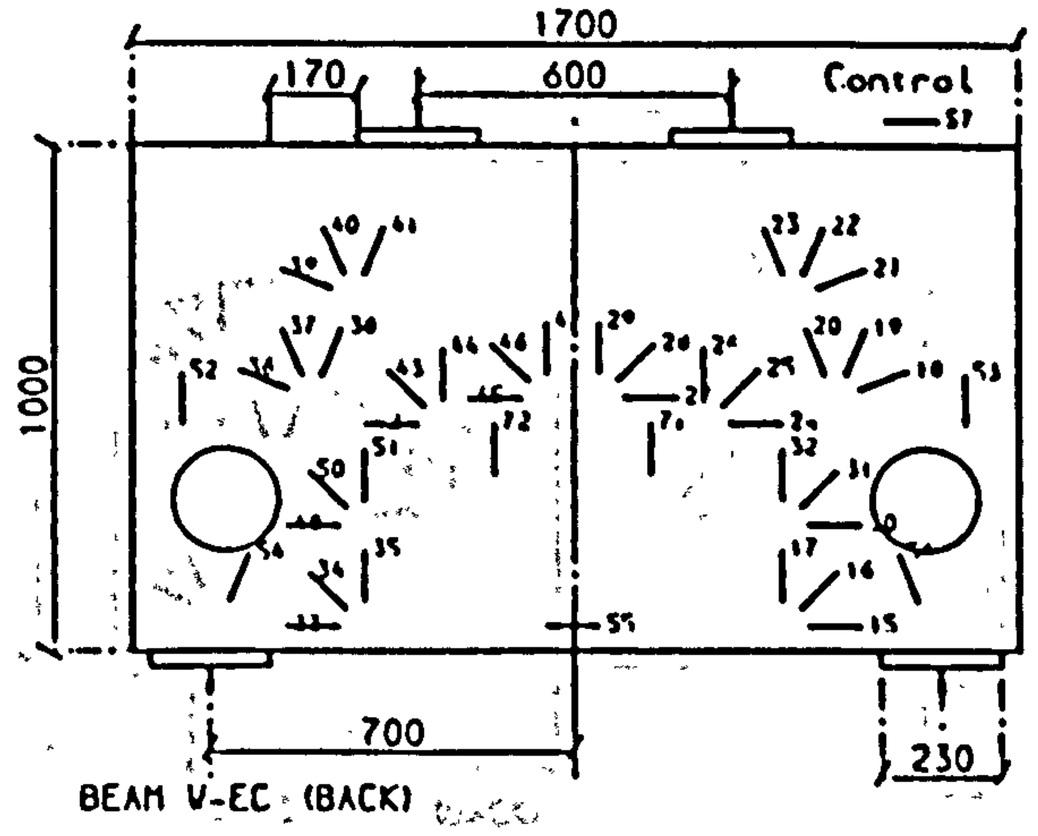

Figure 6.26 : Position of strain gauges (W-Series beams) [cont'd]

(All dimensions in mm)

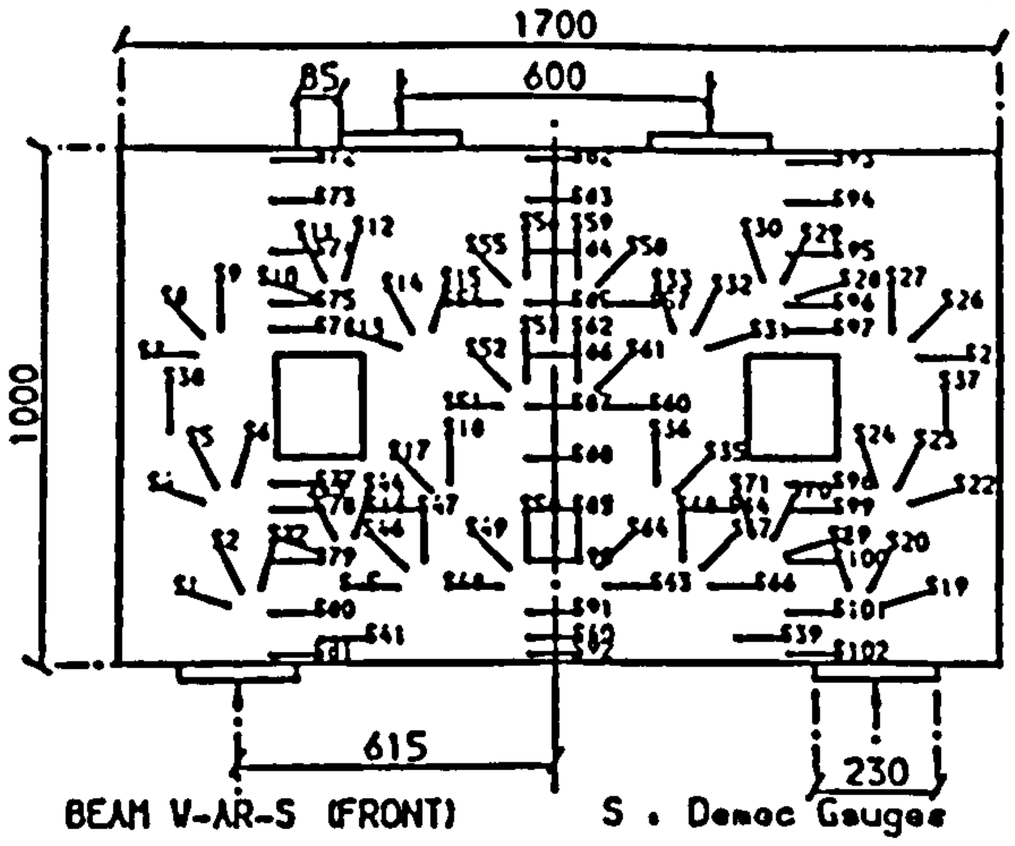

BEAM V-AC-S (FRONT) S . Demec Gauges

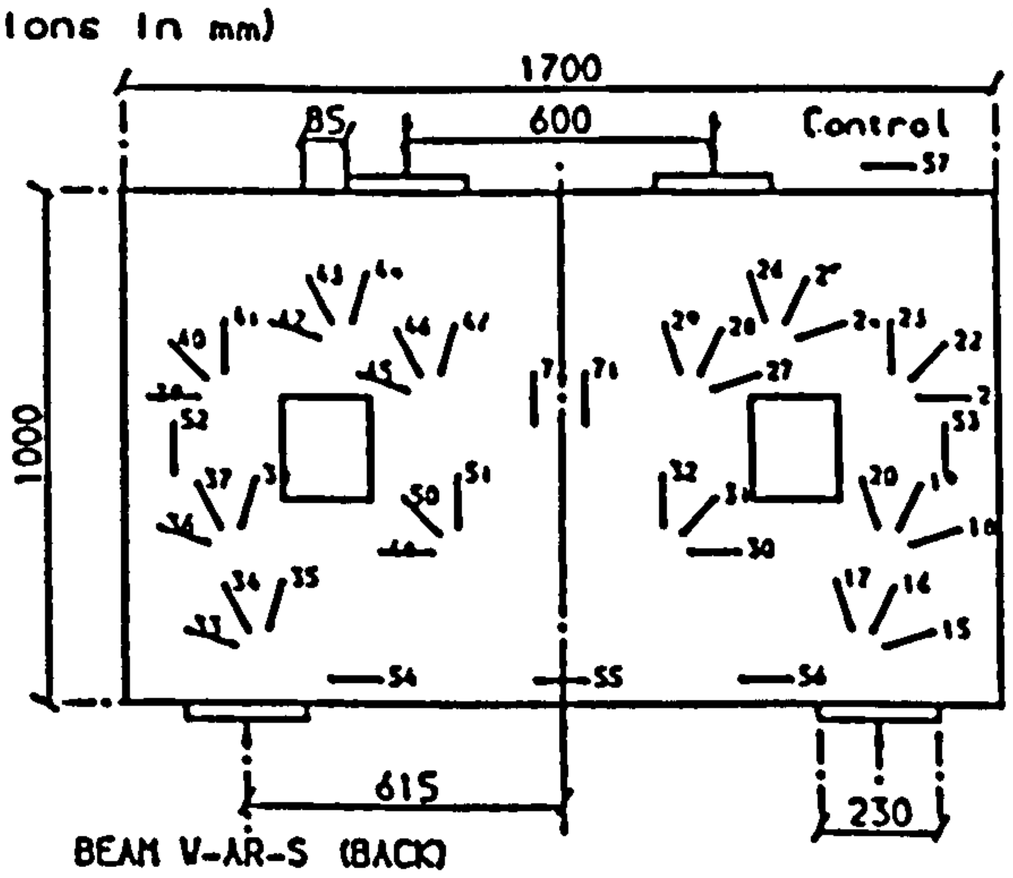

BEAM V-AC-S (BACK)

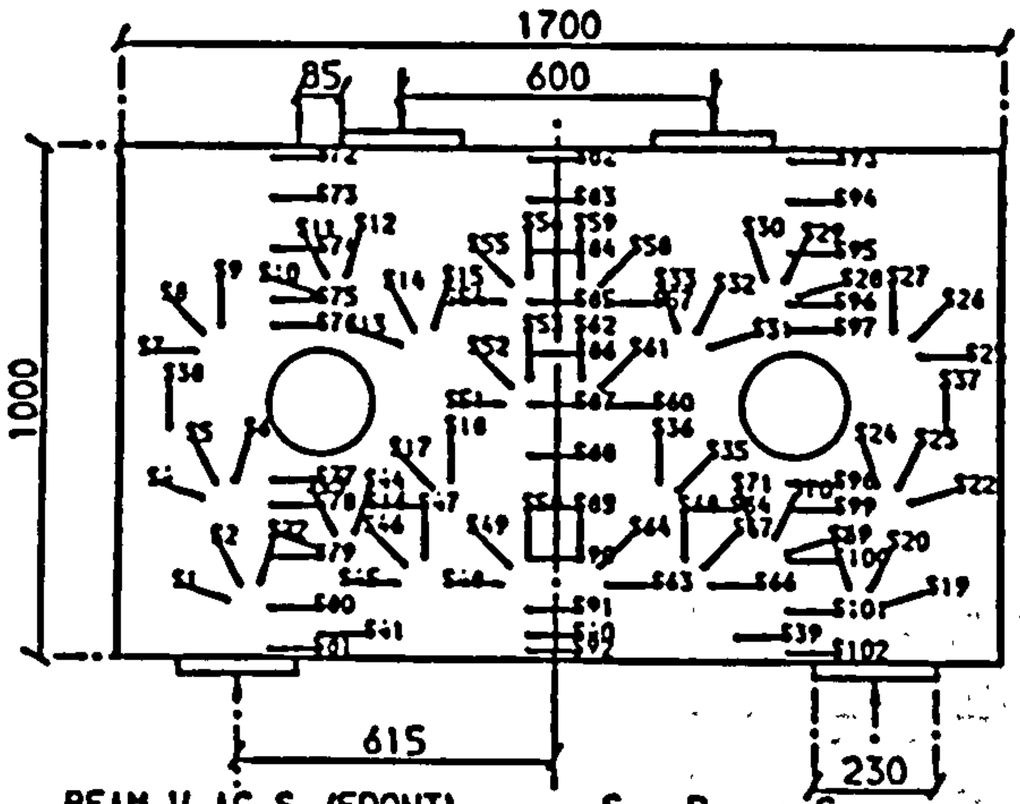

BEAM V-AR-S (FRONT) S . Demec Gauges

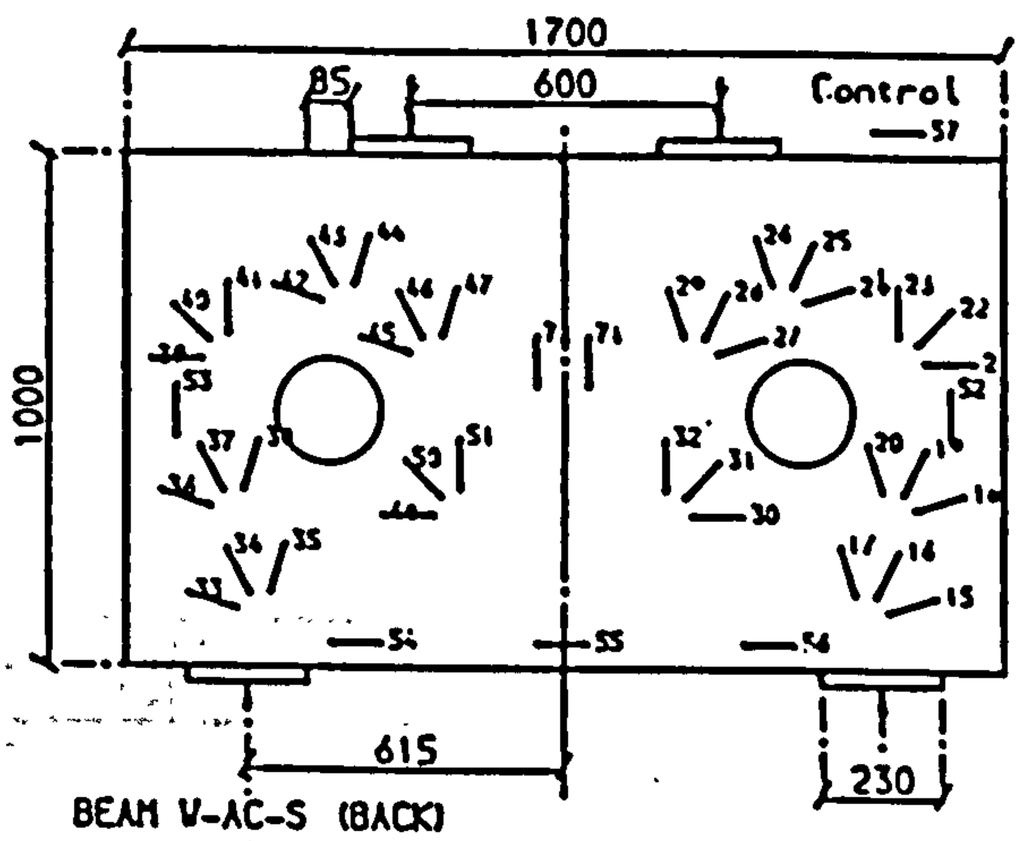

BEAM V-AR-S (BACK)

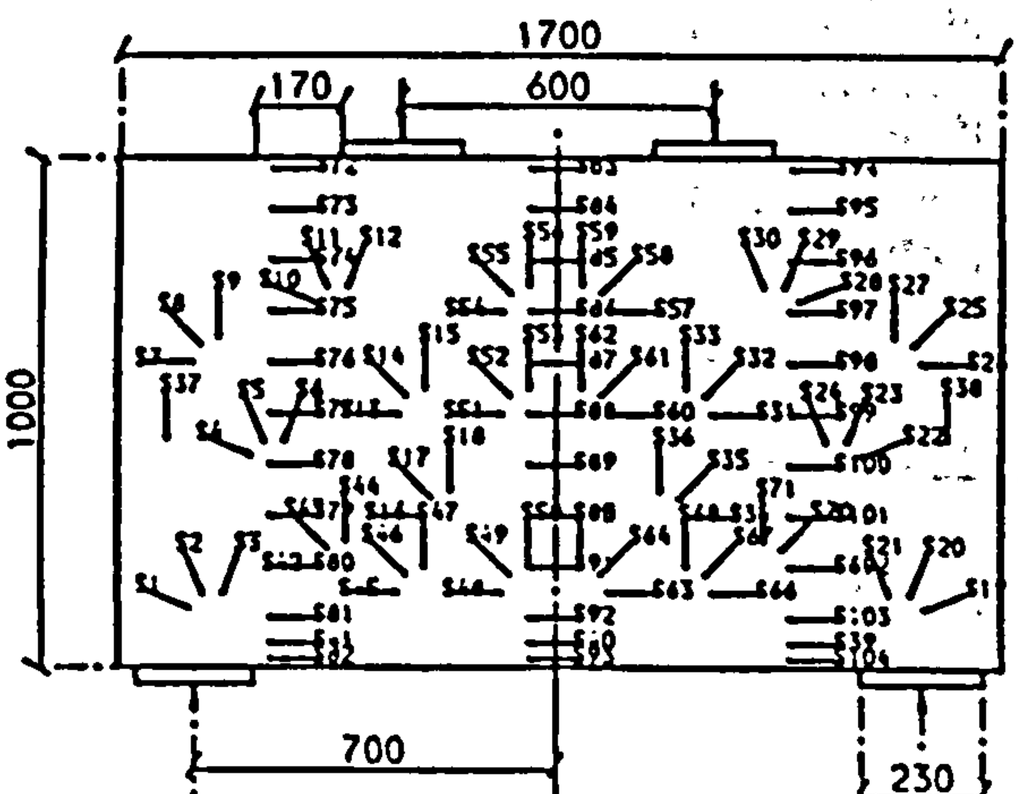

BEAM V-29-0.1-R1 (FRONT) S . Demec Gauges

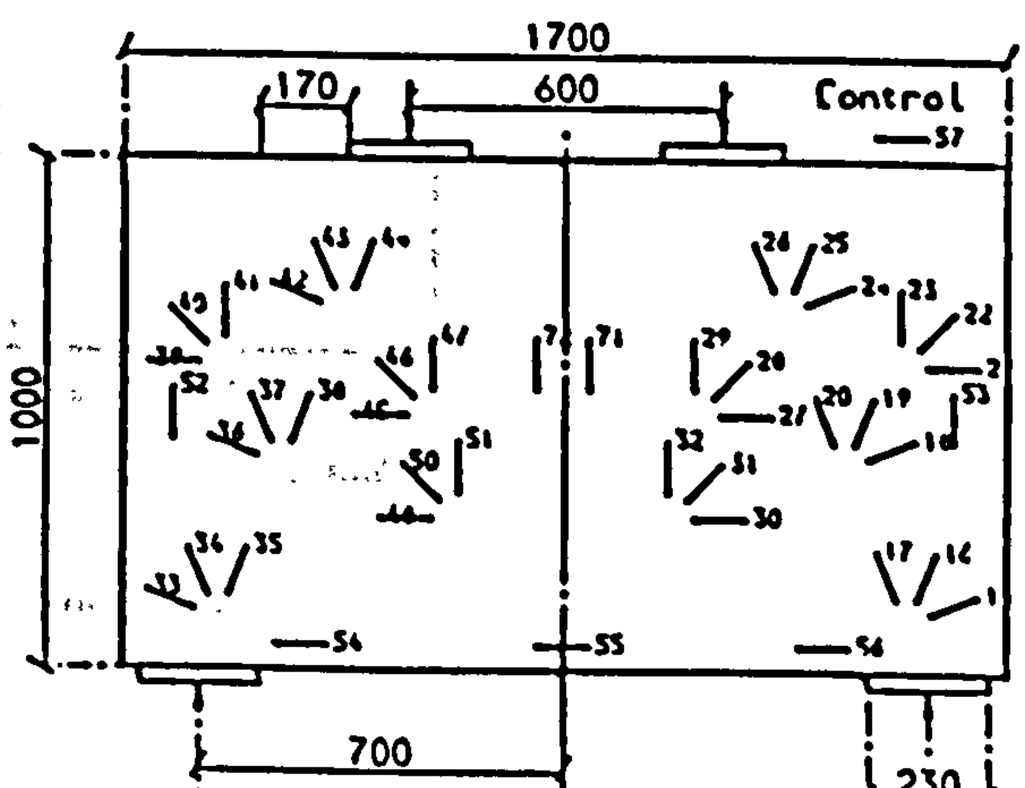

BEAM V-29-0.1-R1 (BACK)

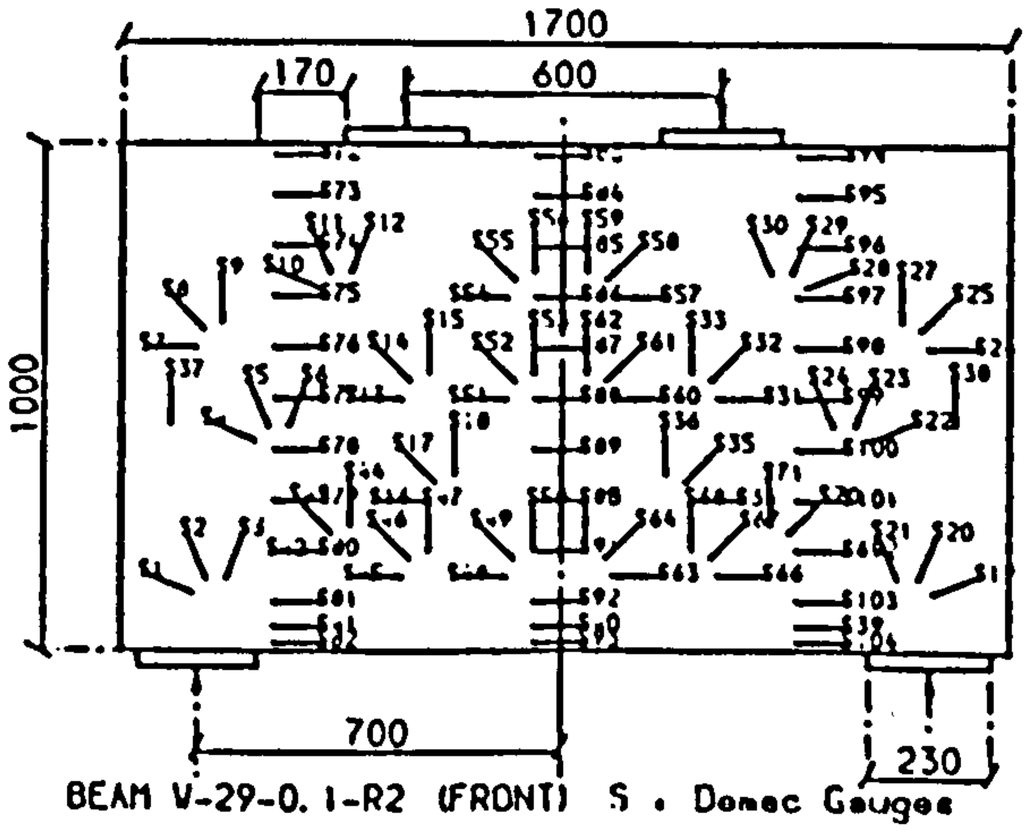

BEAM V-29-0.1-R2 (FRONT) S . Demec Gauges

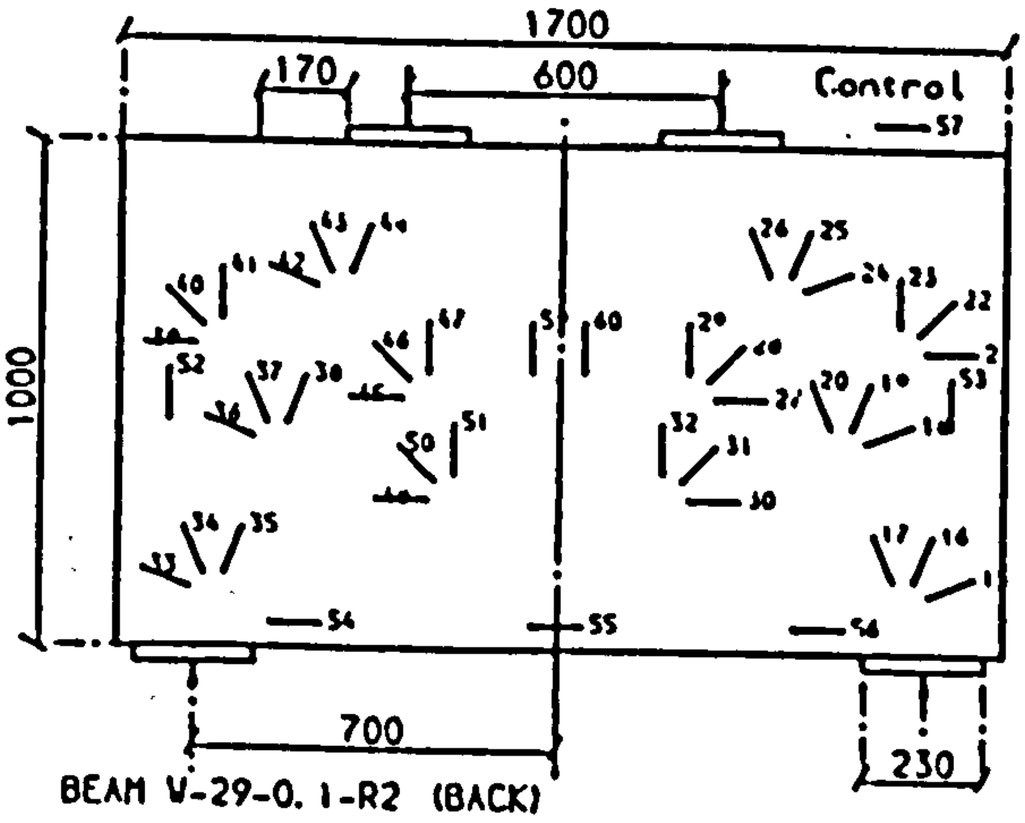

BEAM V-29-0.1-R2 (BACK)

Figure 6.26 : Position of strain gauges (W-Series beams) [cont'd]

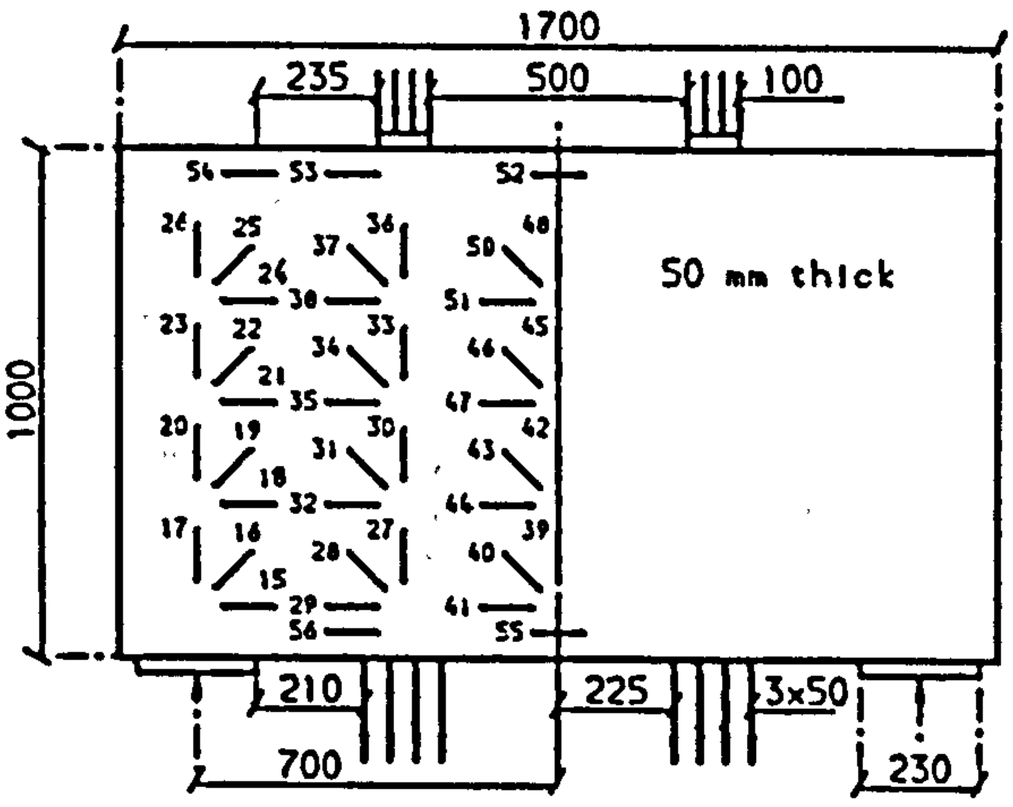

(All dimensions in mm)

Figure 6.27 : Typical position of strain gauges (CB-Series beams)

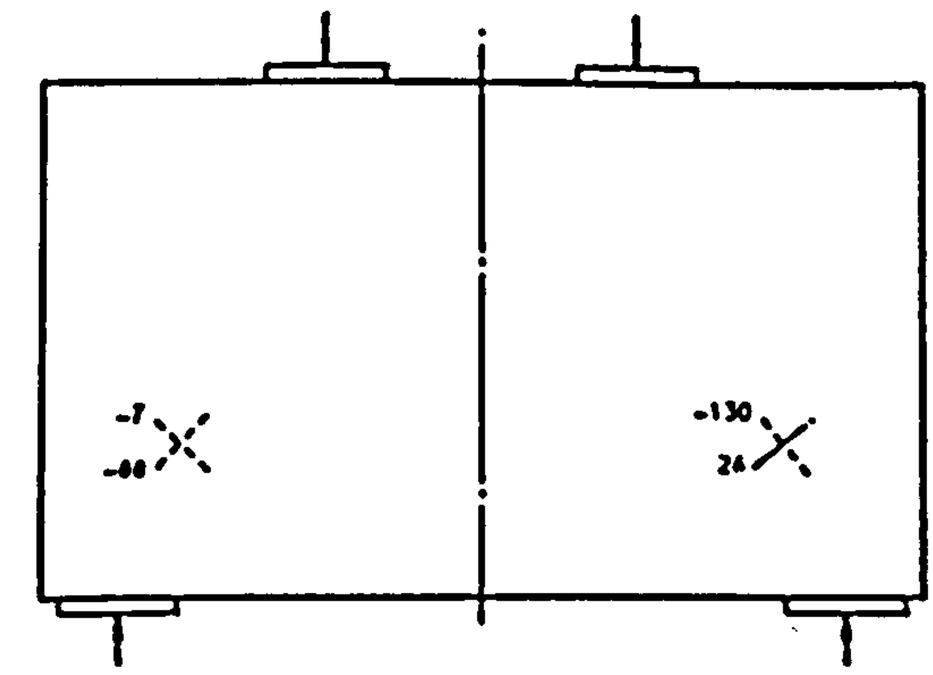

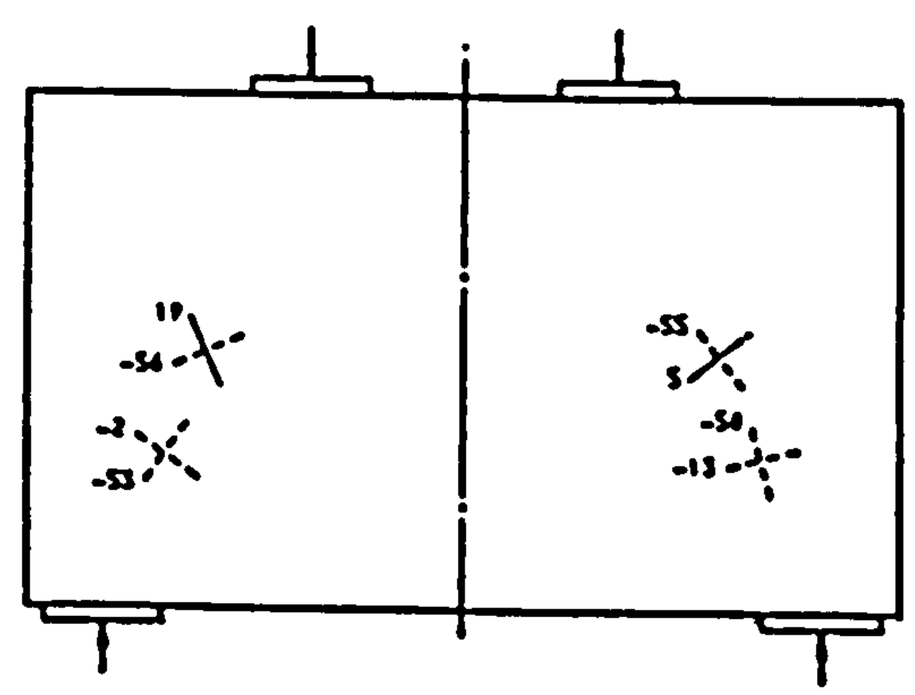

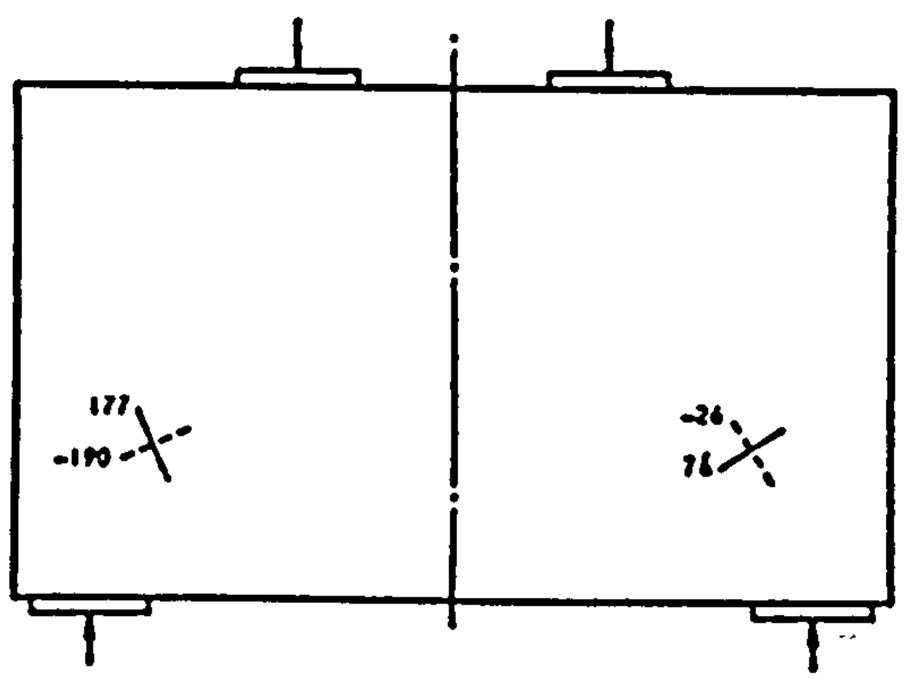

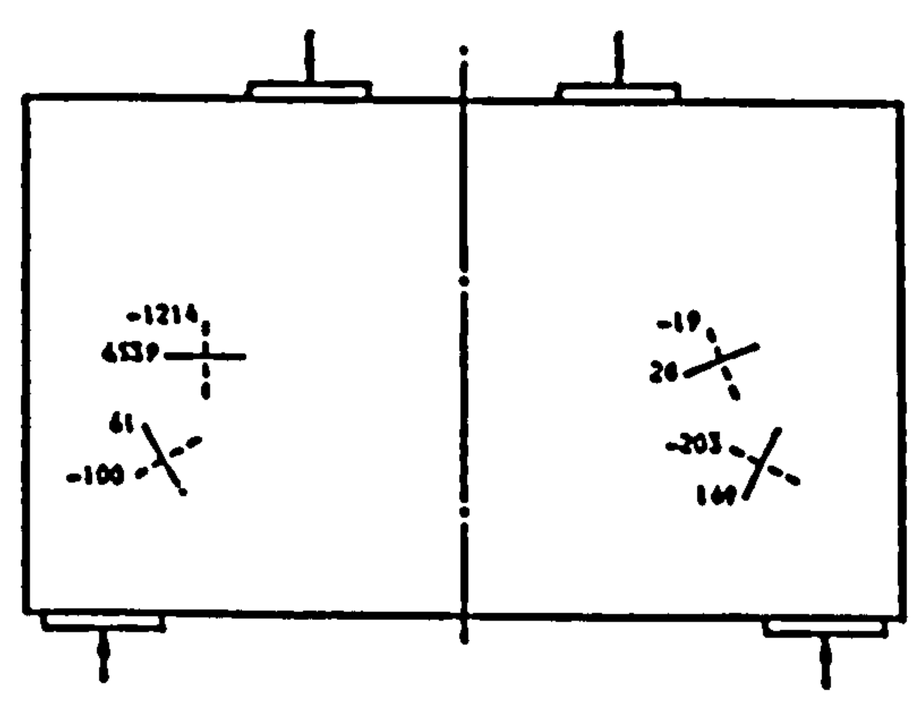

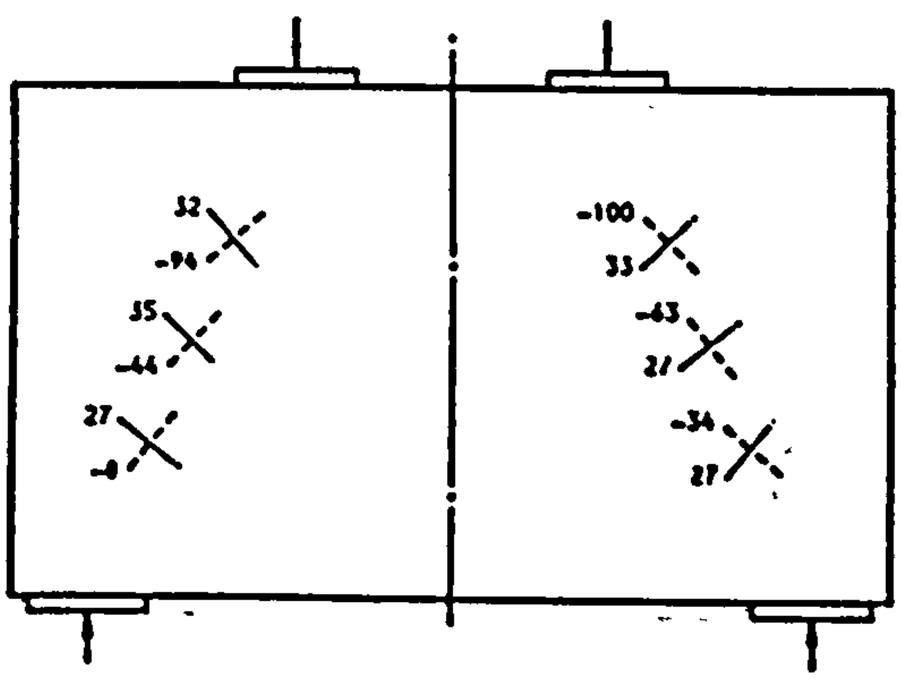

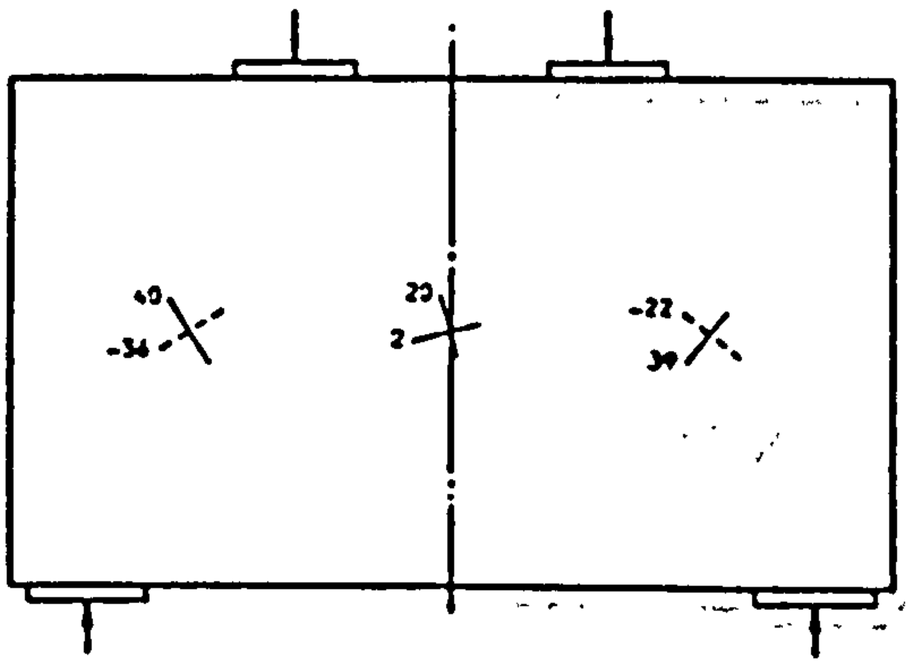

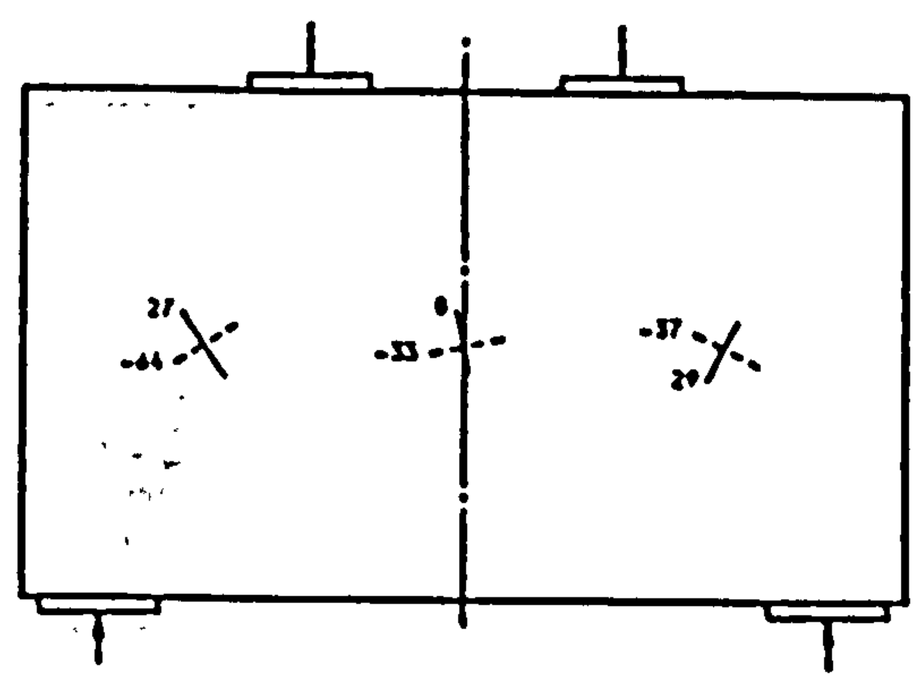

Figure 6.28 : Principal strains after the first load increments (E-Series beams)

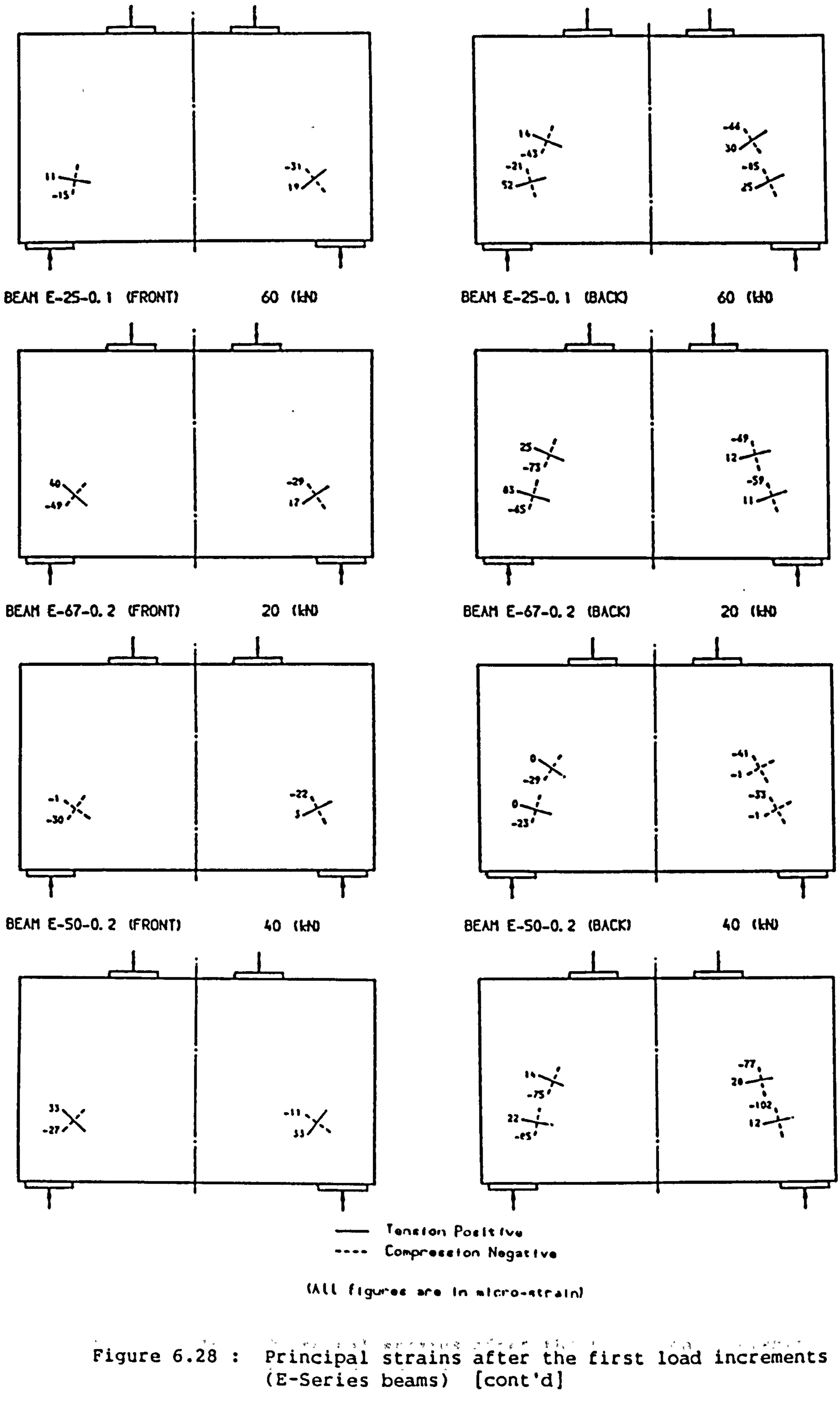

Figure 6.28 : Principal strains after the first load increments (E-Series beams) [cont'd]

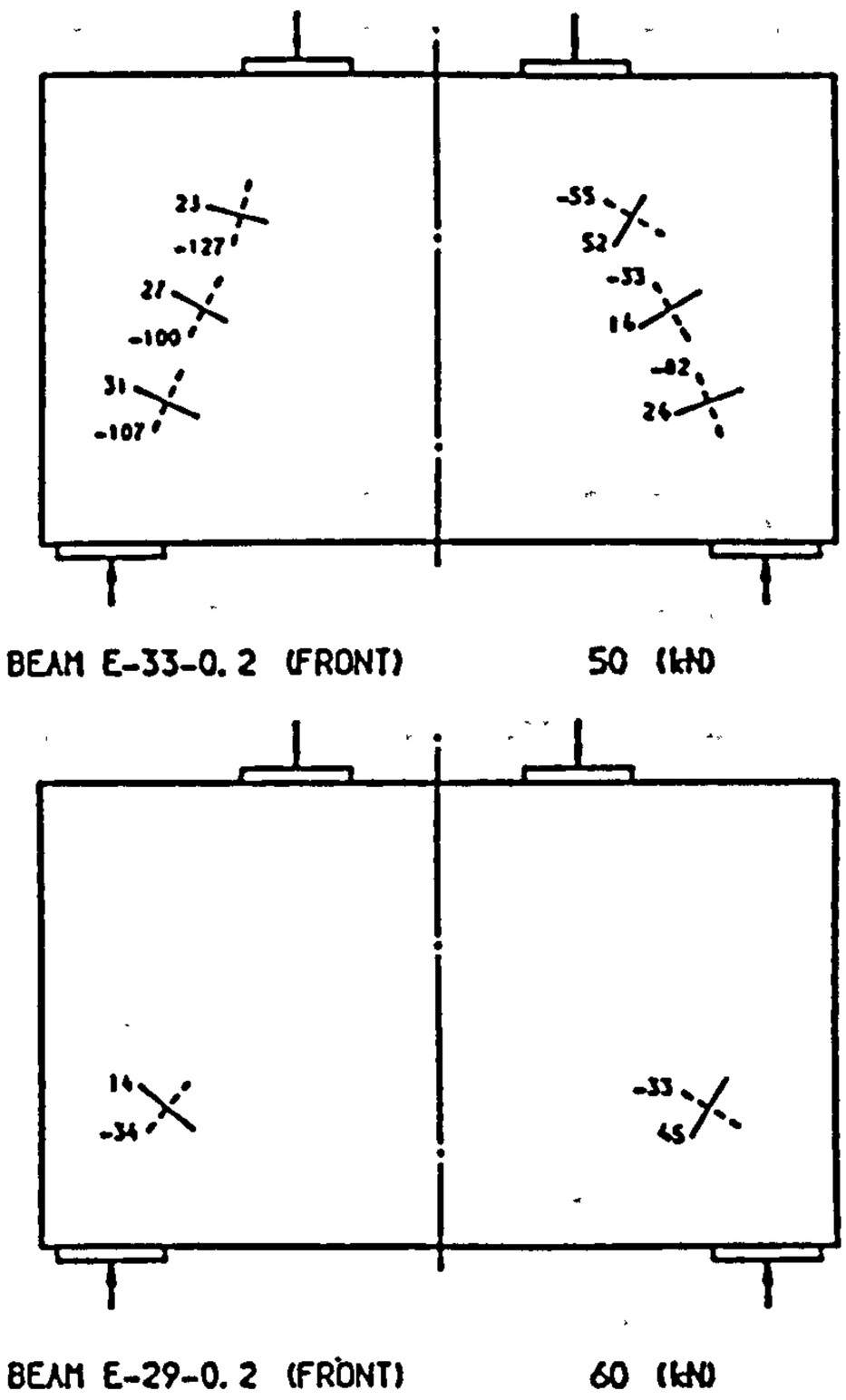

Figure 6.28 : Principal strains after the first load increments (E-Series beams) [cont'd]

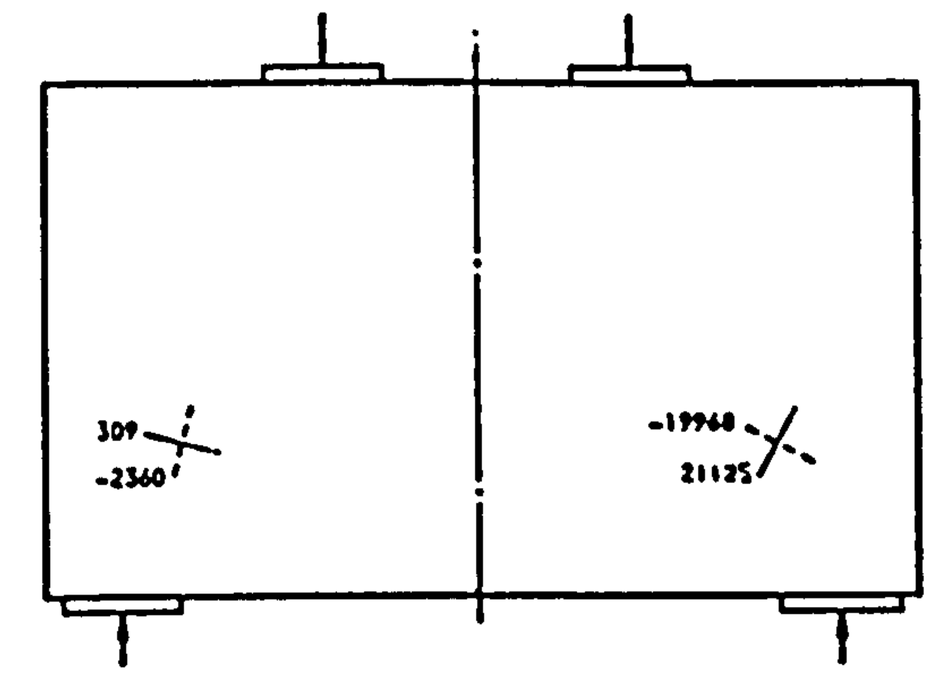

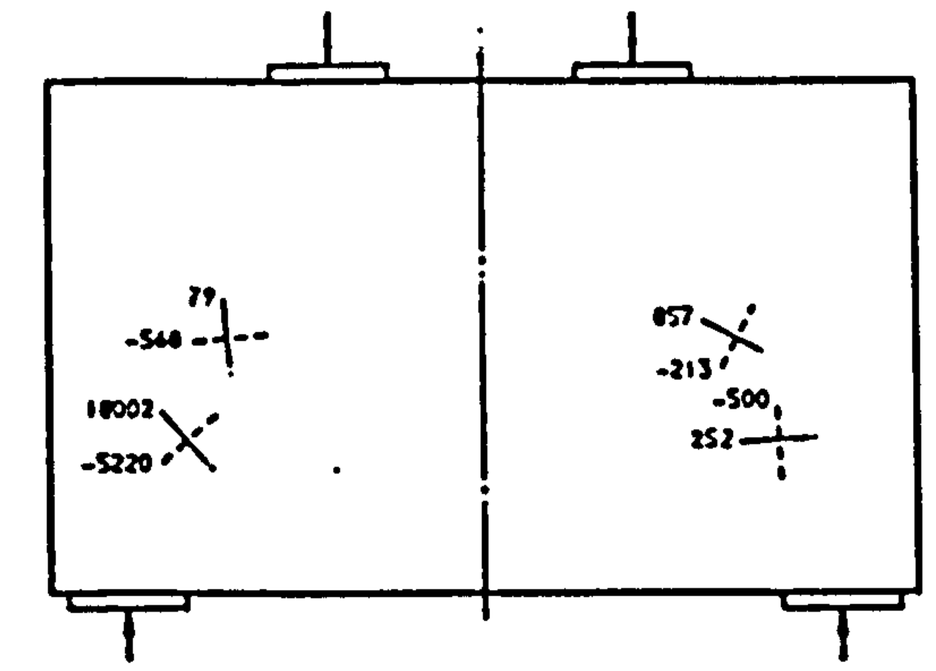

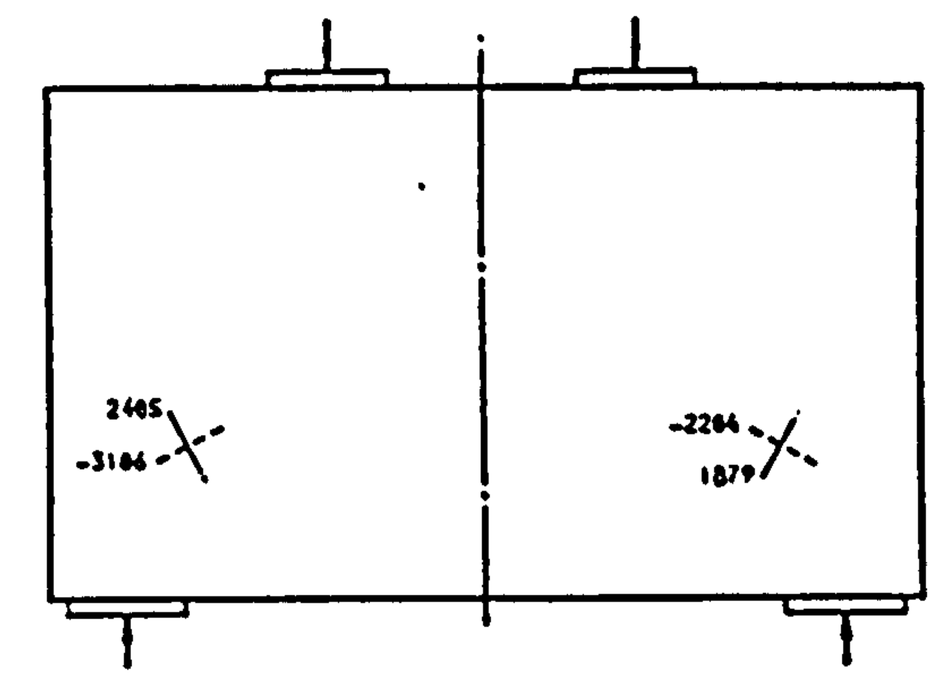

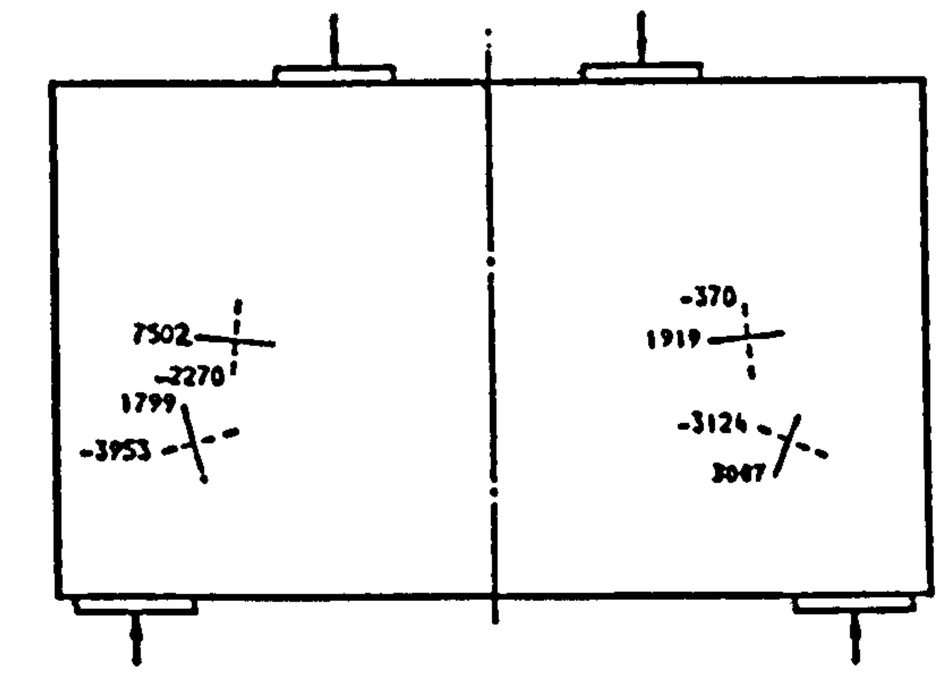

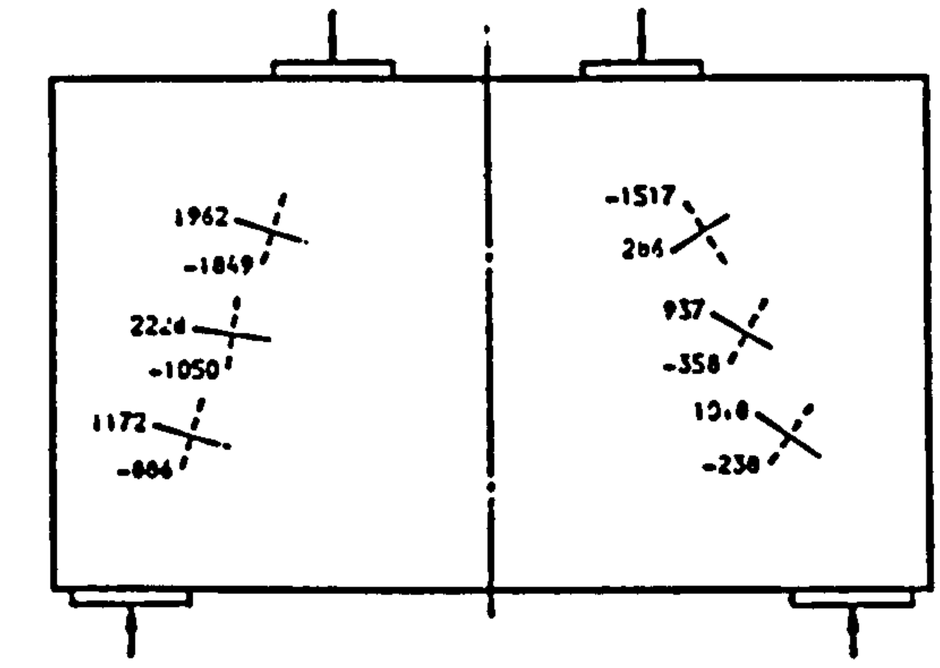

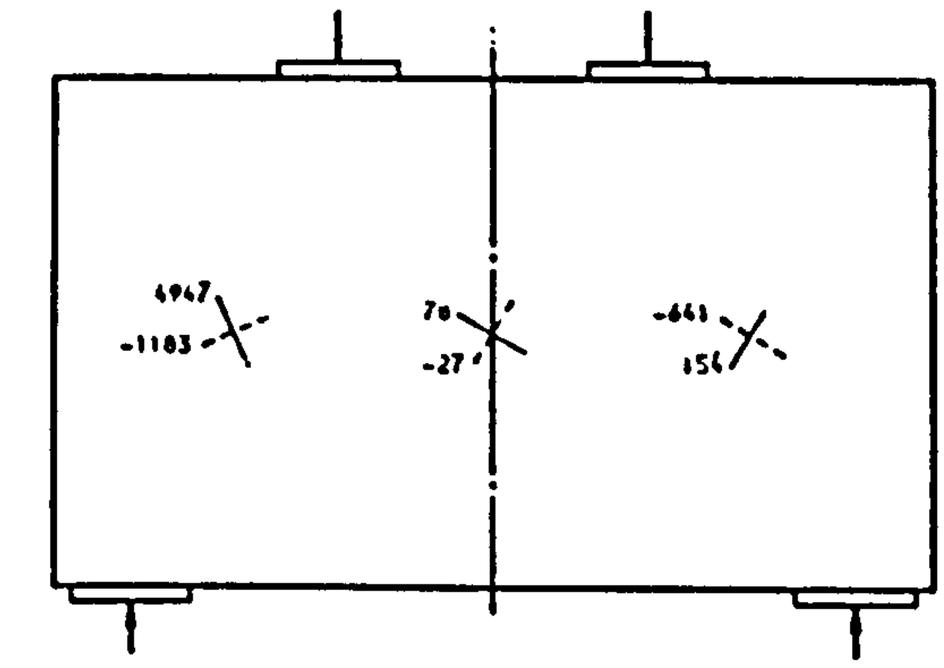

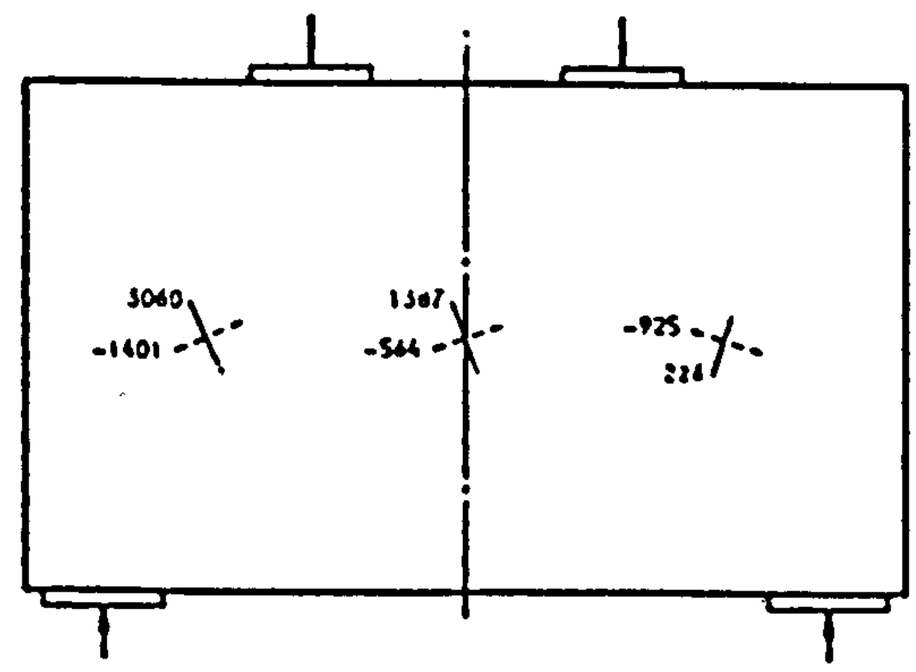

—— Tension Positive
---- Compression Negative

(All figures are in micro-strain)

Figure 6.29 : Principal strains after the last load increments (E-Series beams)

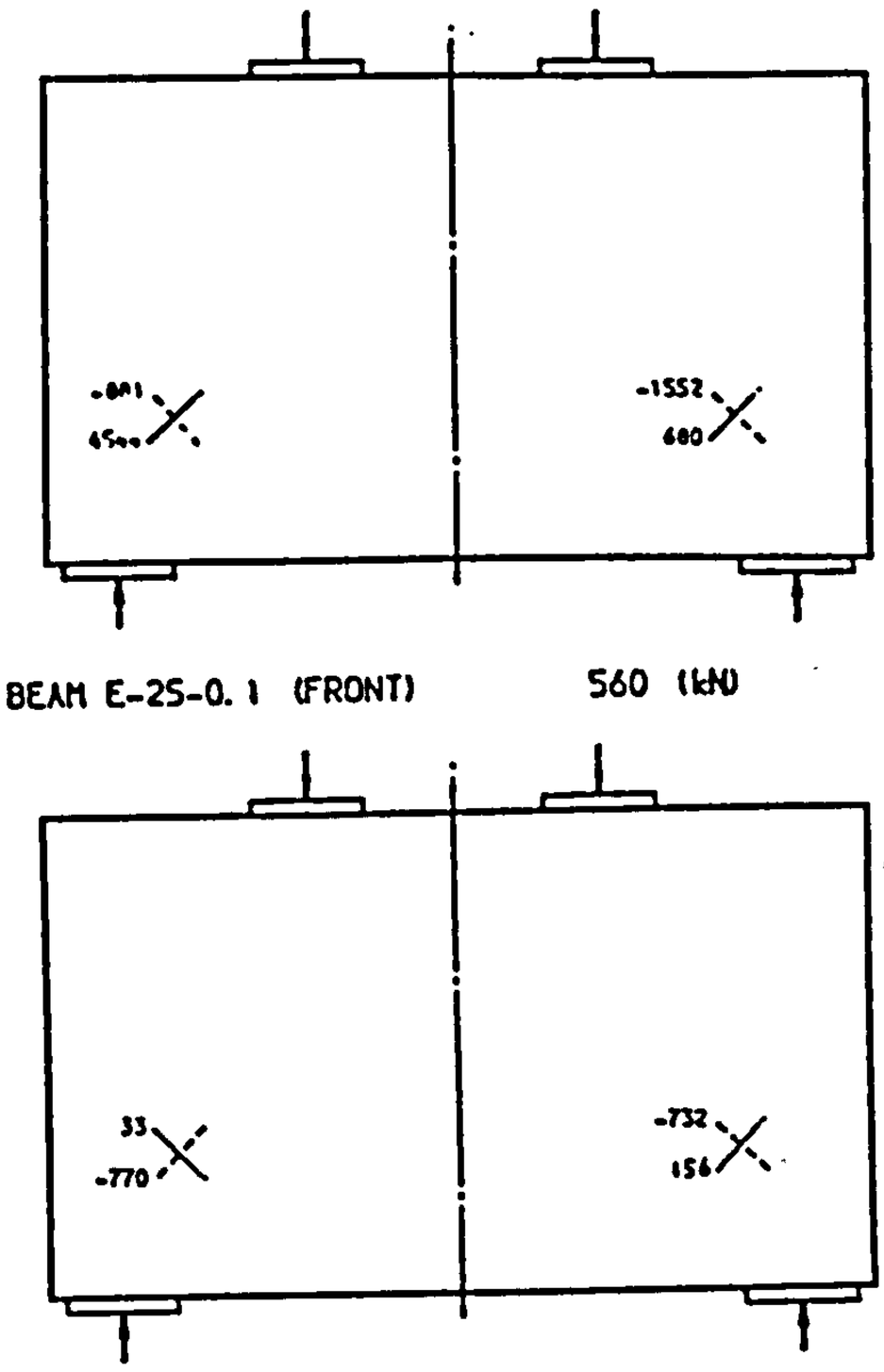

Figure 6.29 : Principal strains after the last load increments (E-Series beams) [cont'd]

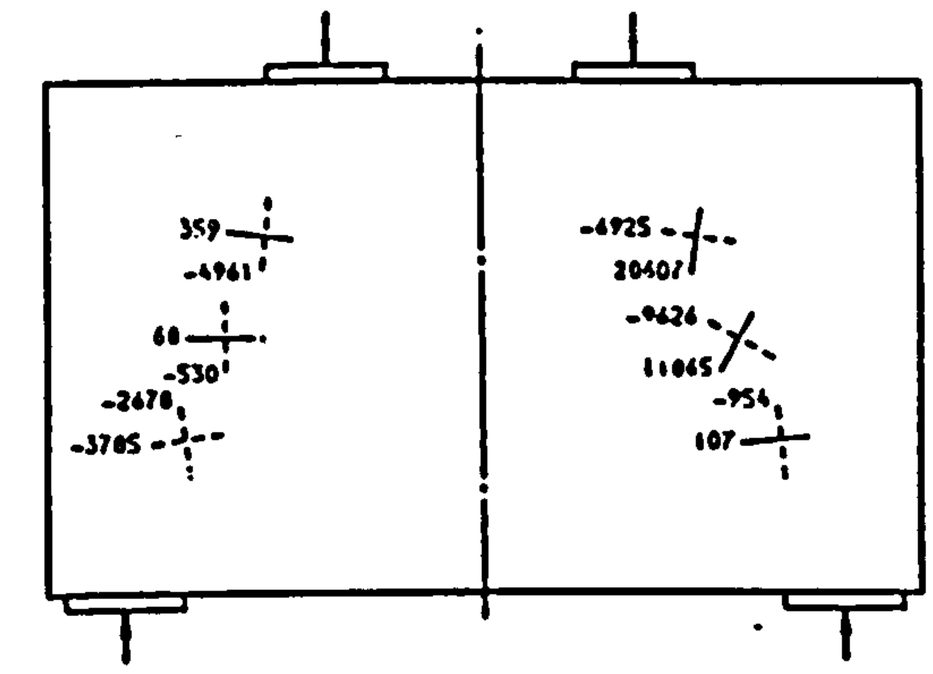

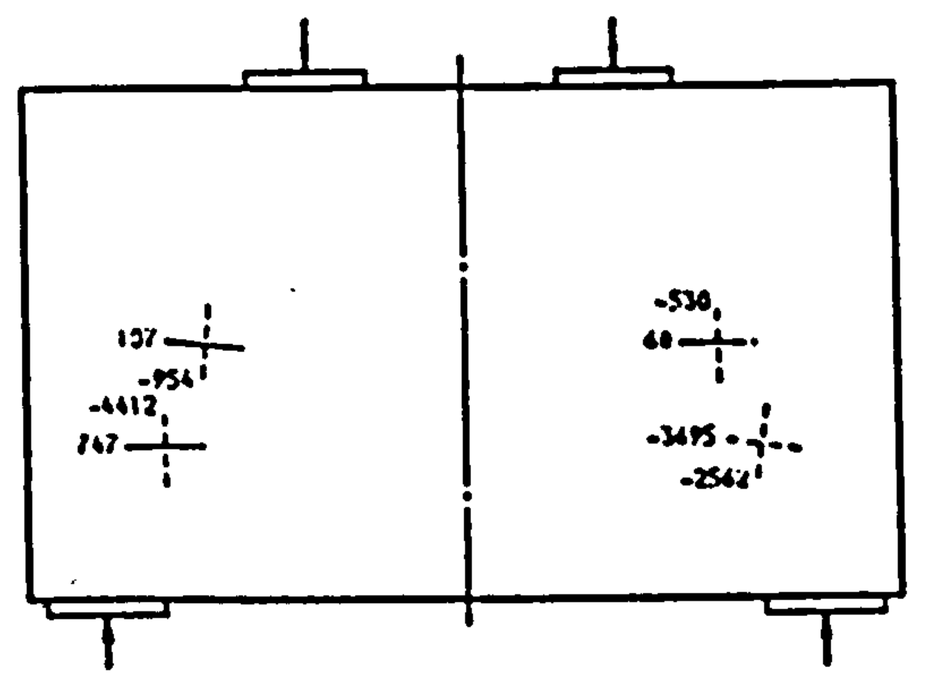

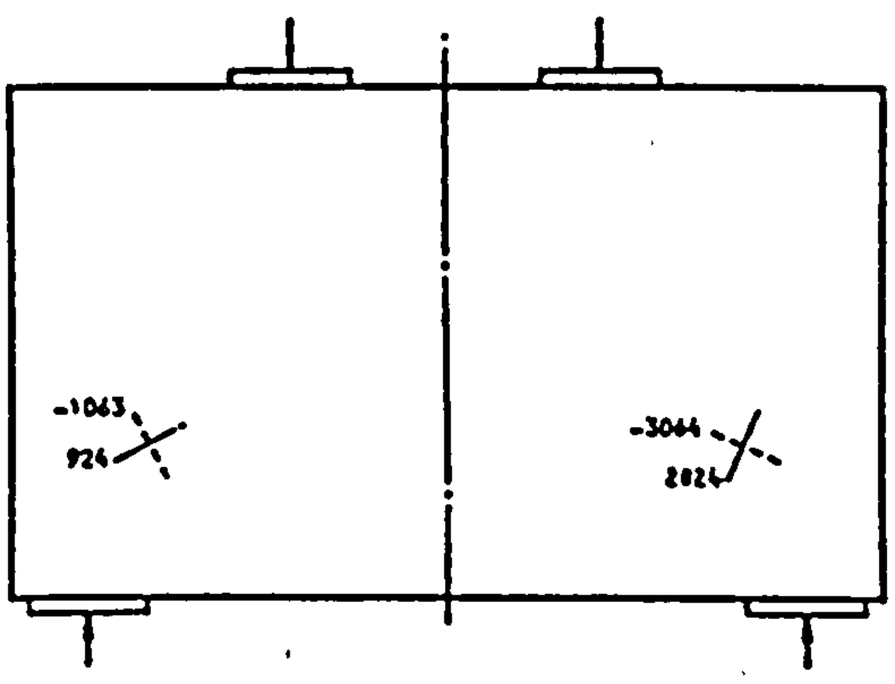

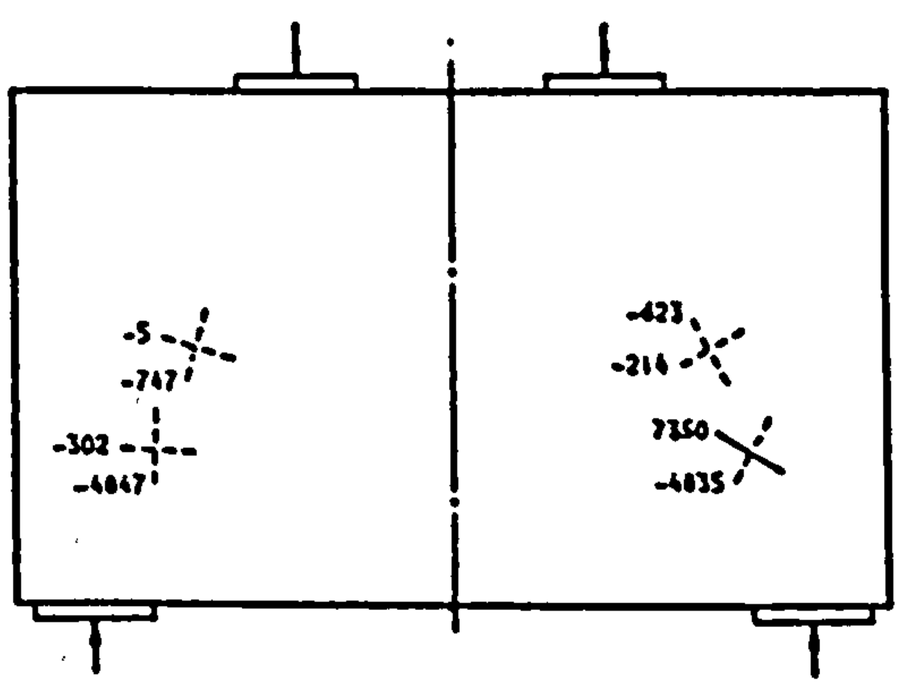

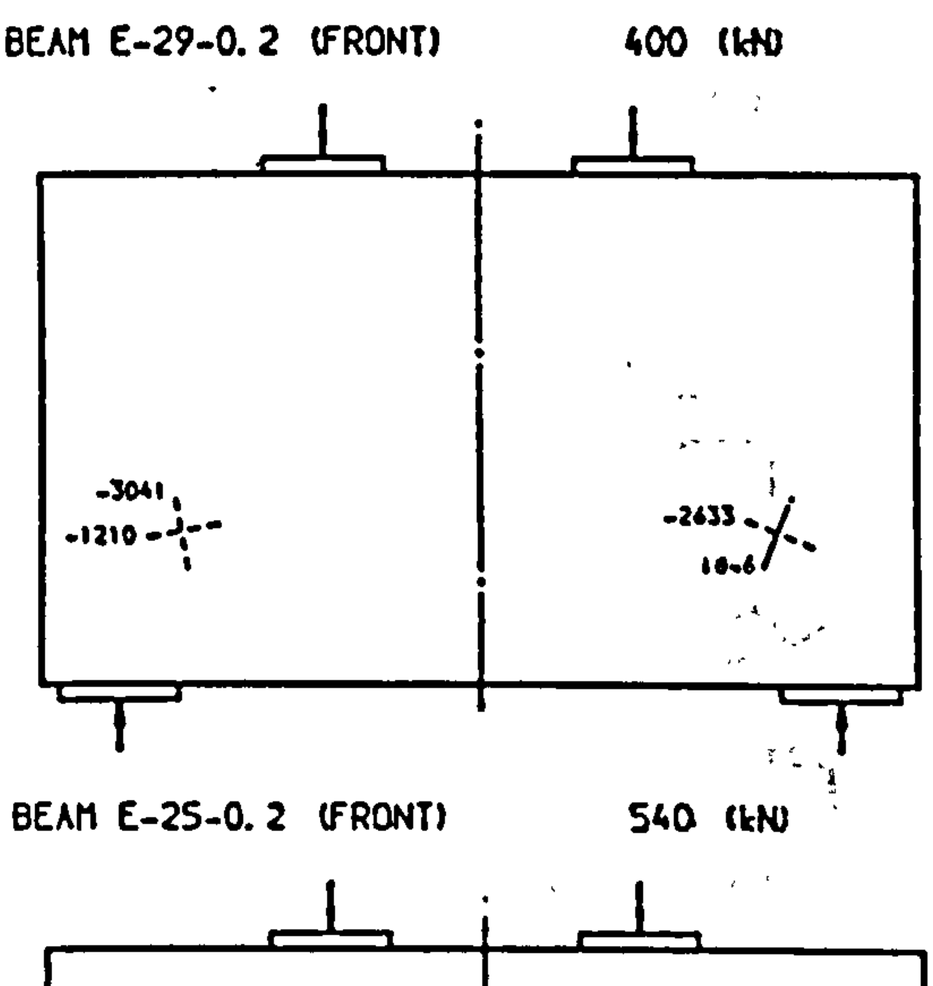

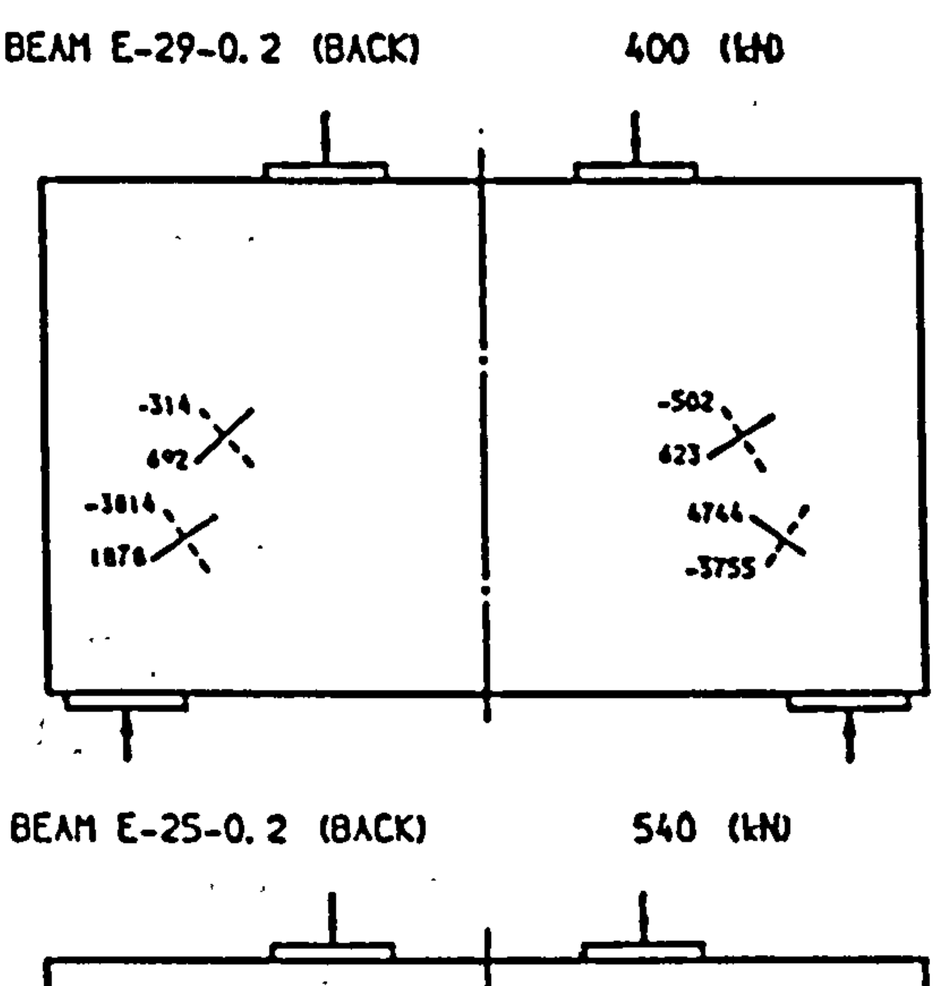

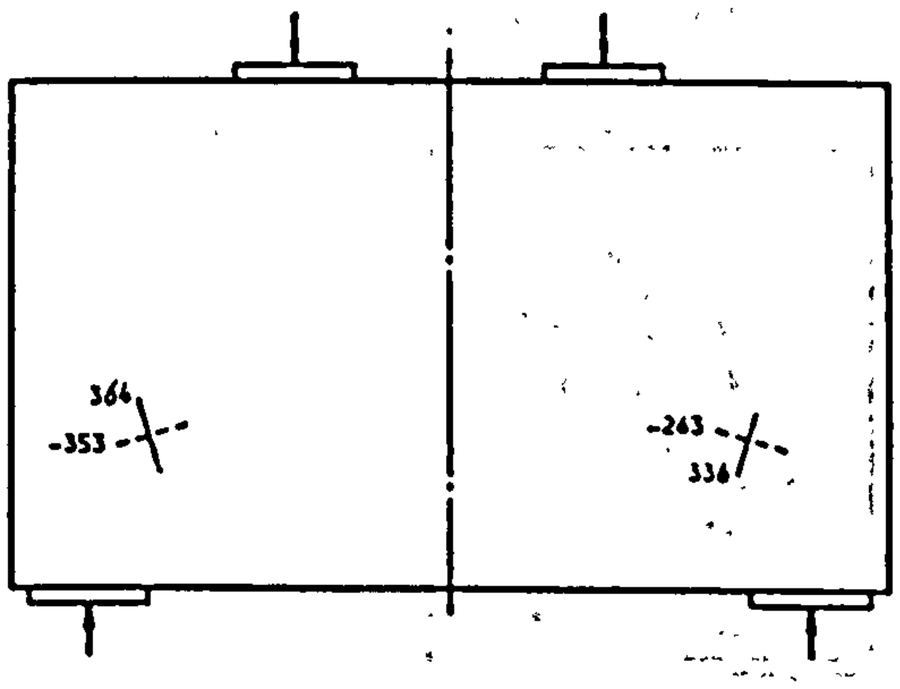

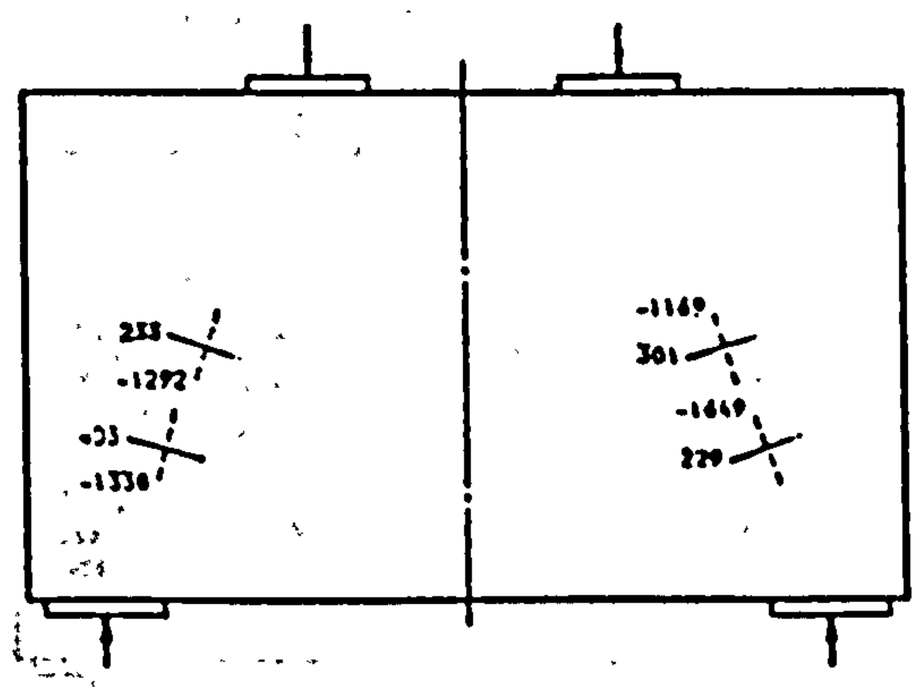

— Tension Positive
---- Compression Negative

(All figures are in micro-strain)

Figure 6.29 : Principal strains after the last load increments (E-Series beams) [cont'd]

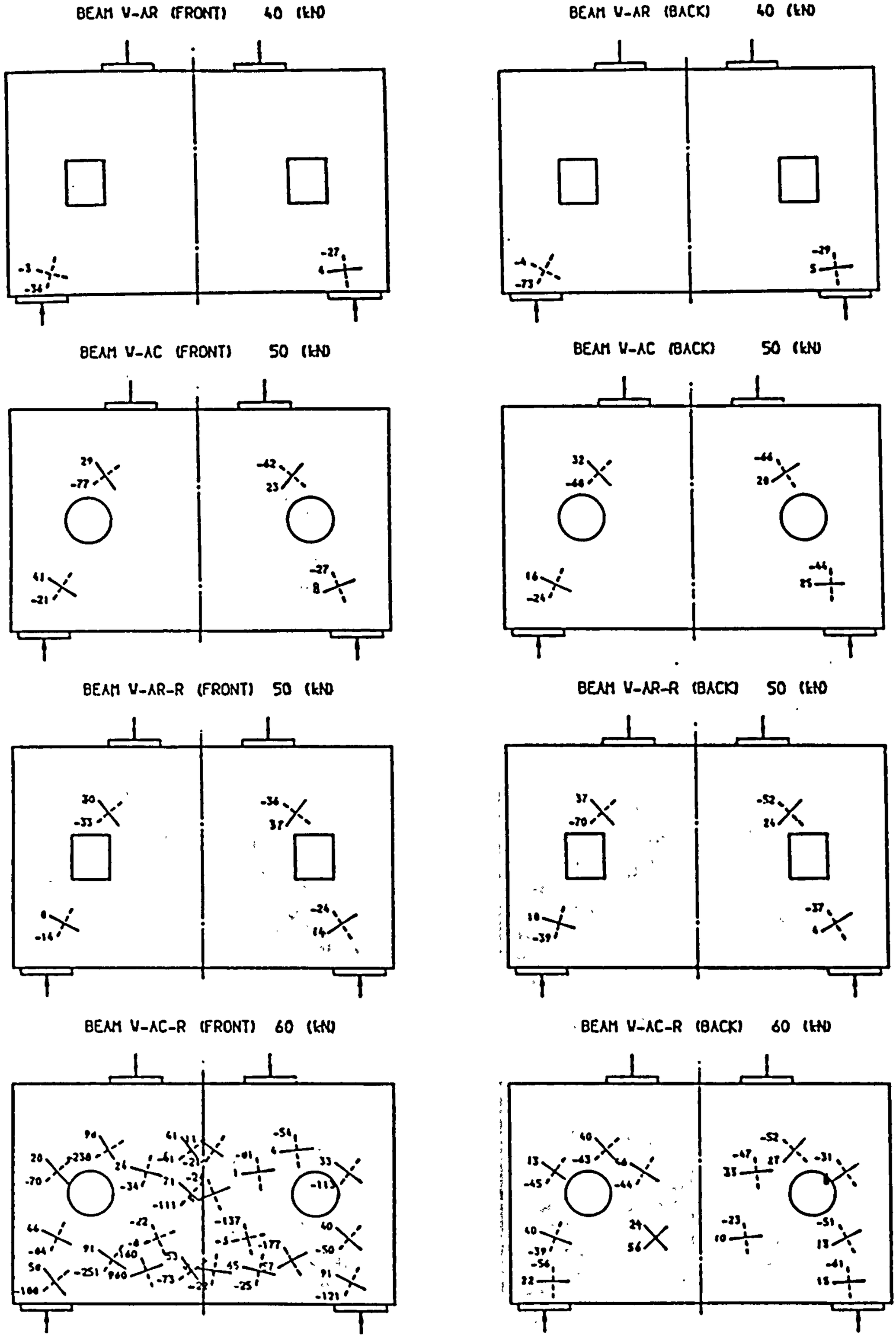

Figure 6.30 : Principal strains after the first load increments (W-Series beams)

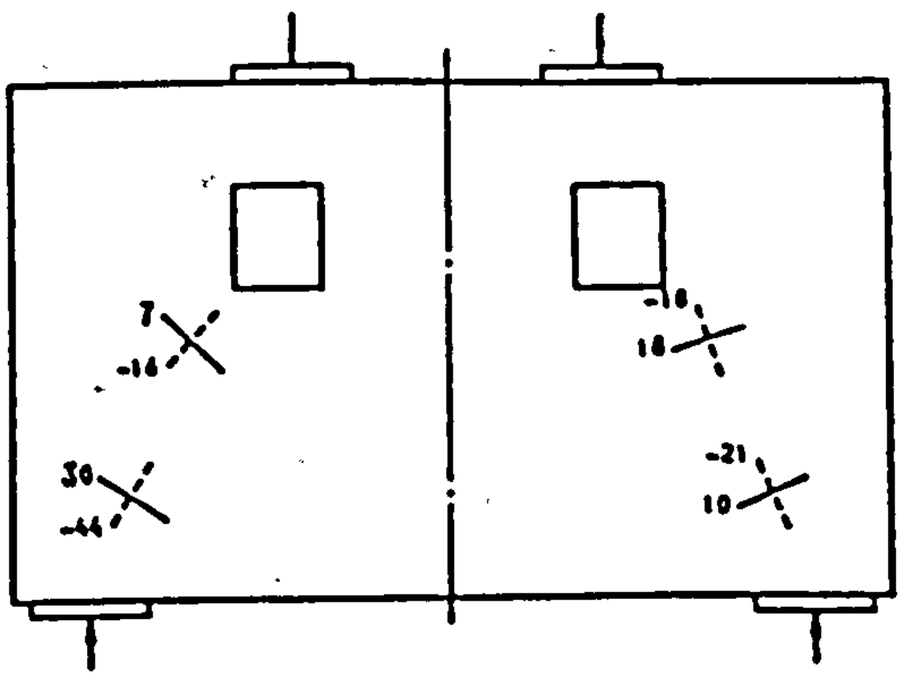

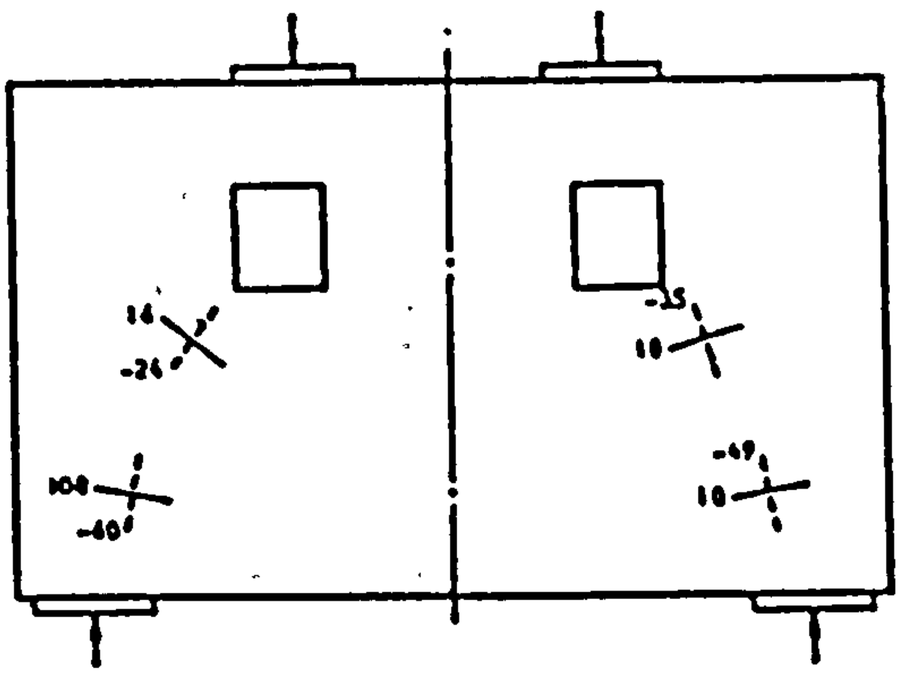

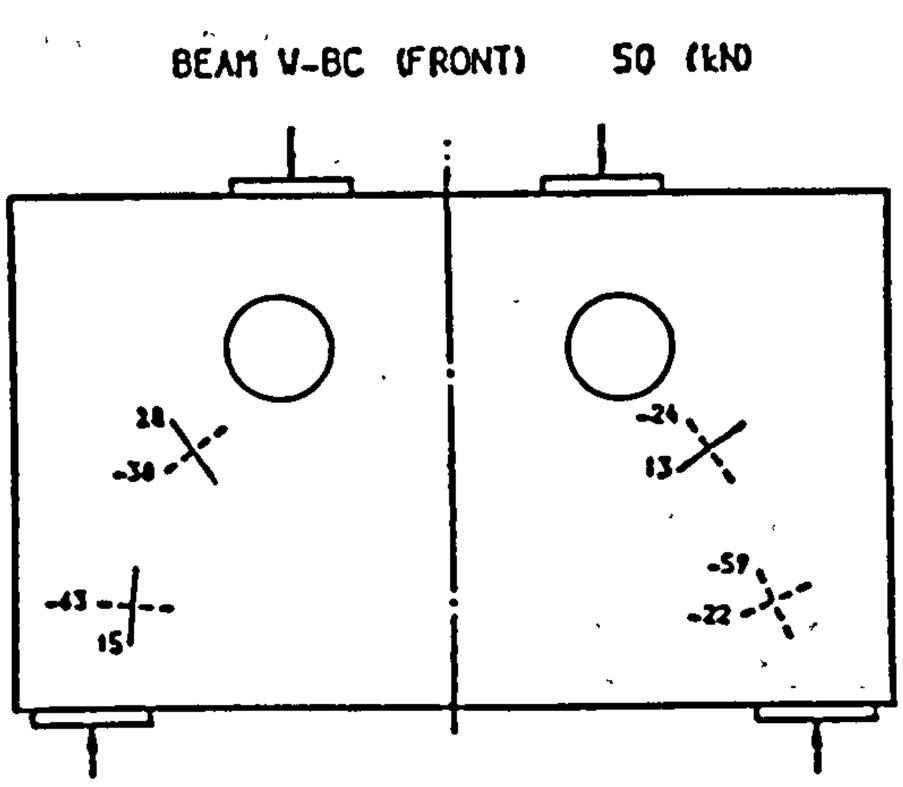

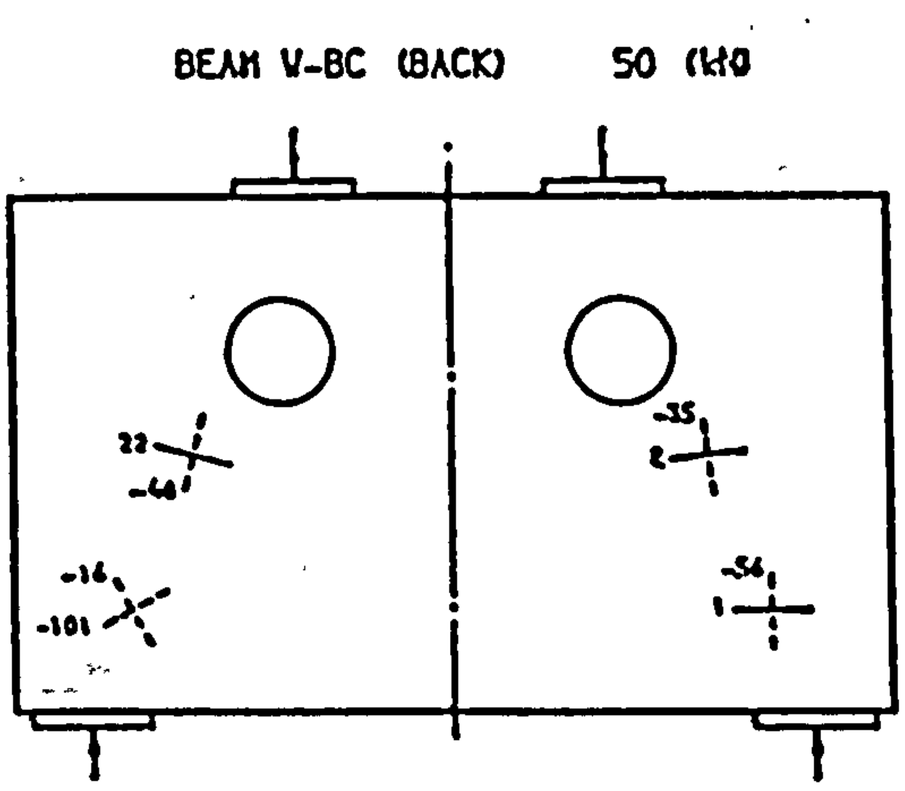

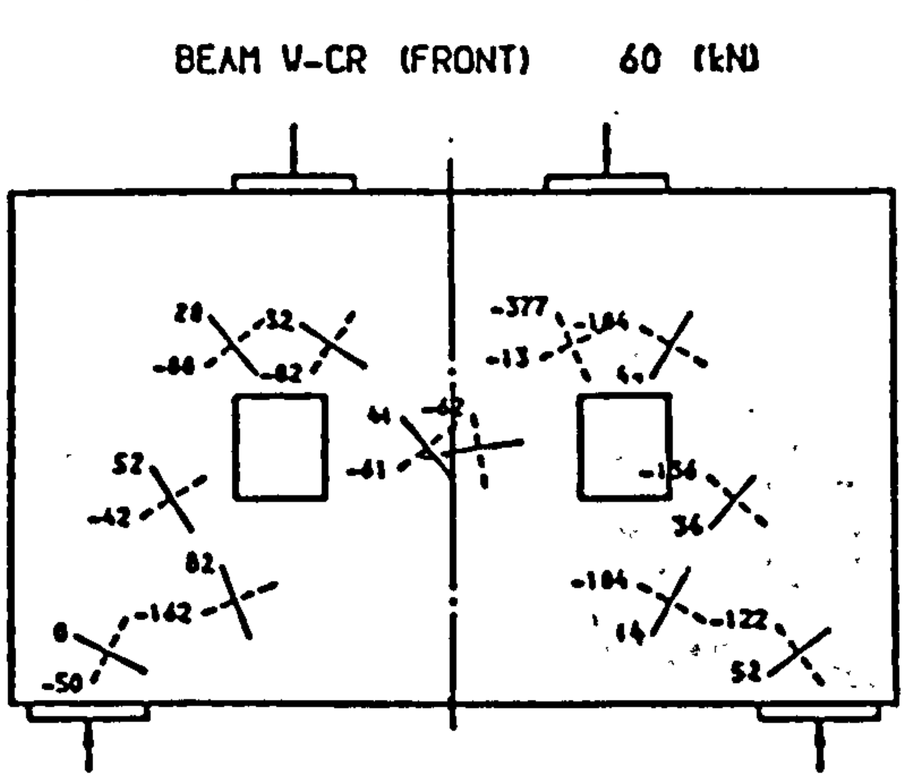

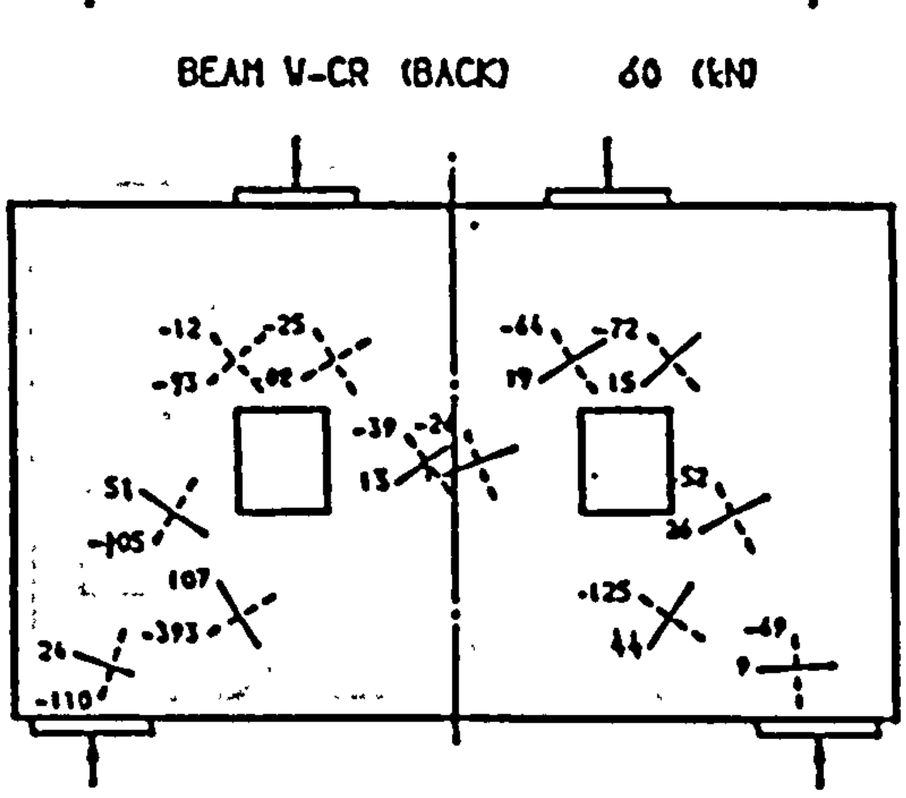

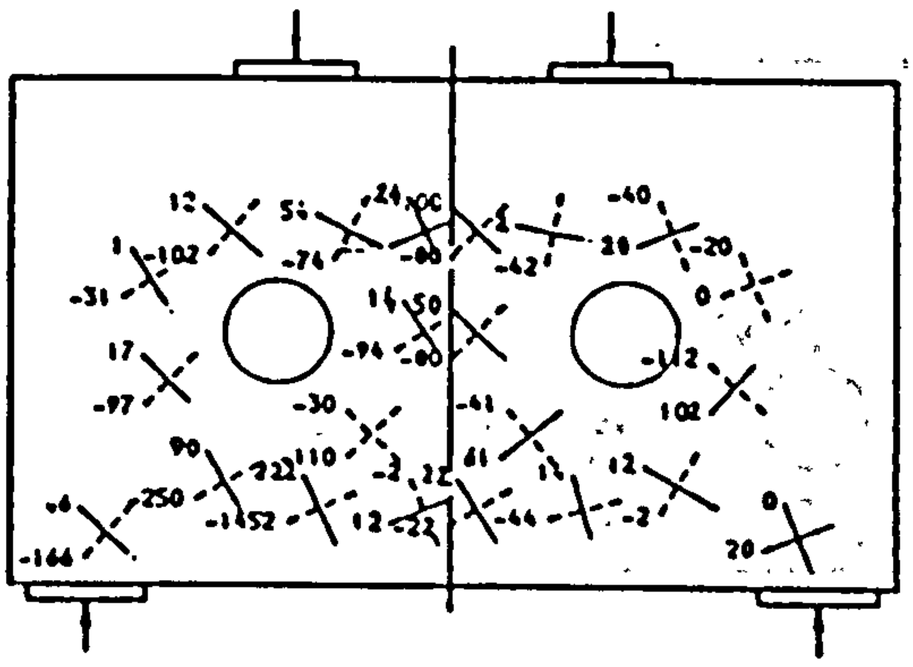

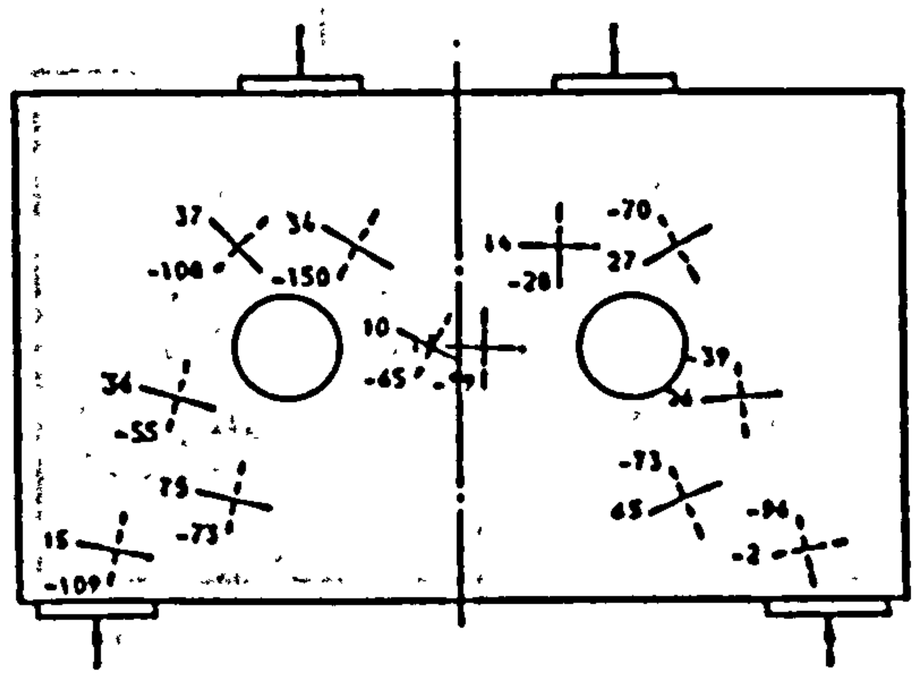

(All figures are in micro-strain)

Figure 6.30 : Principal strains after the first load increments (W-Series beams) [cont'd]

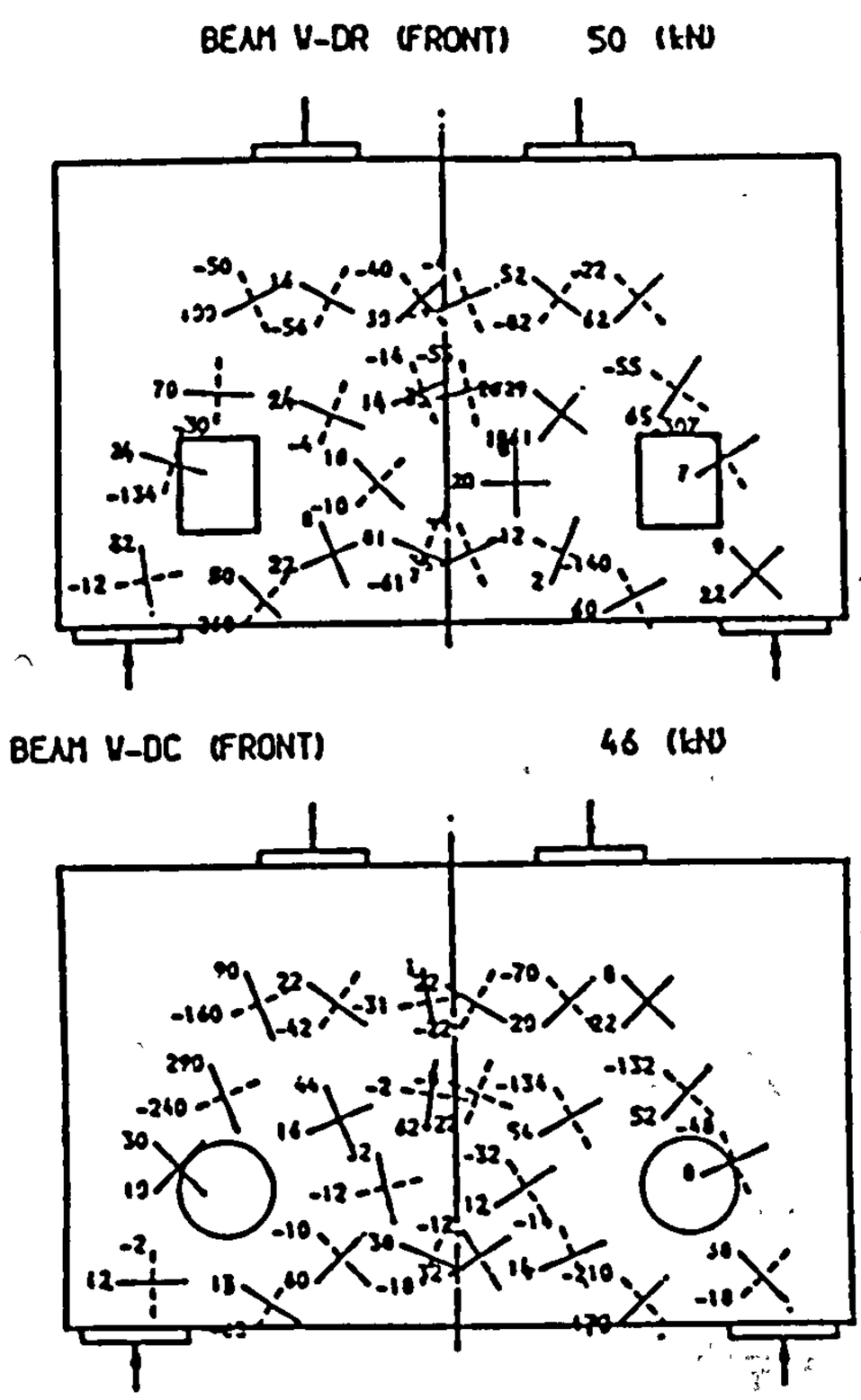

Figure 6.30 : Principal strains after the first load increments (W-Series beams) [cont'd]

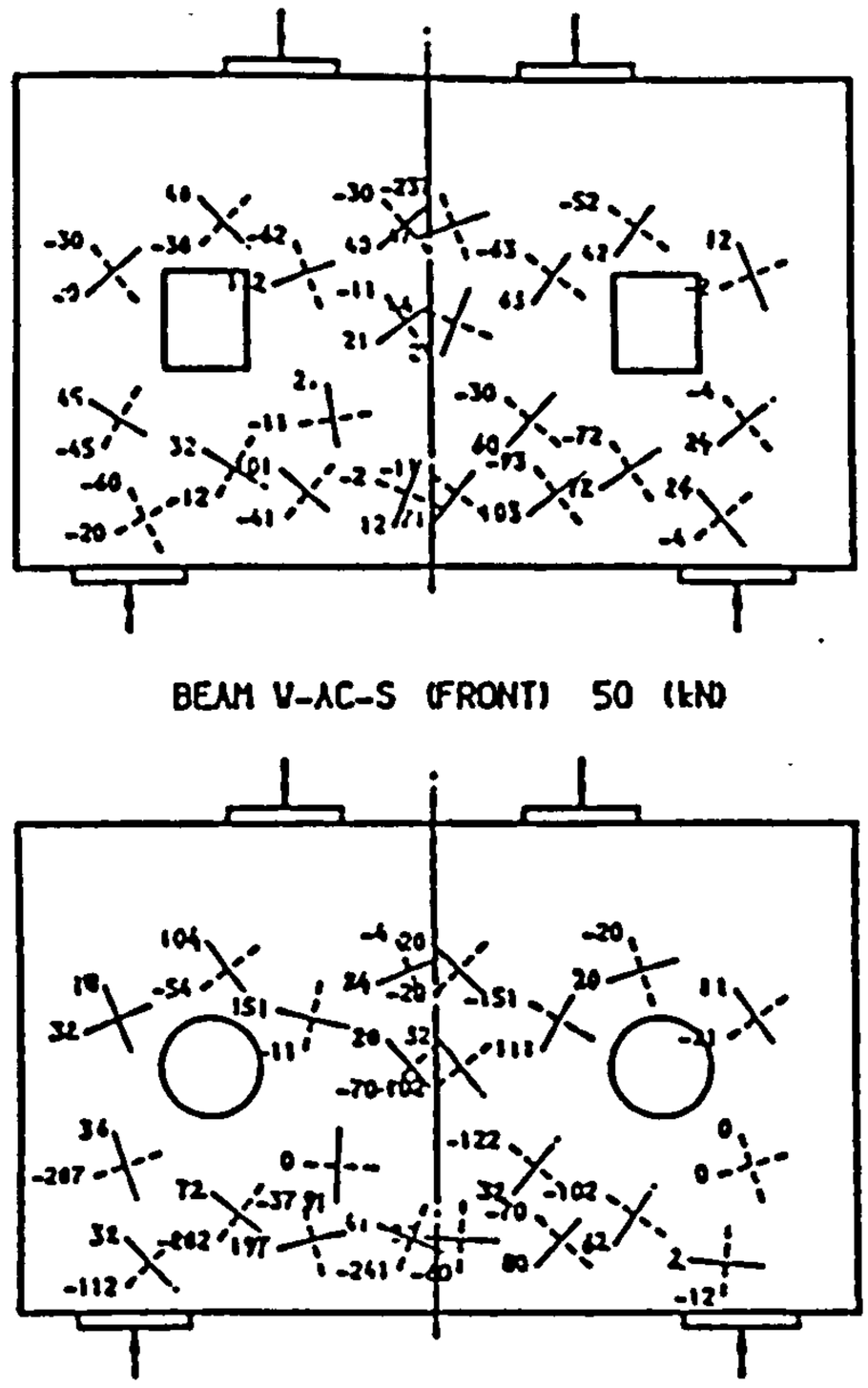

Figure 6.30 : Principal strains after the first load increments (W-Series beams) [cont'd]

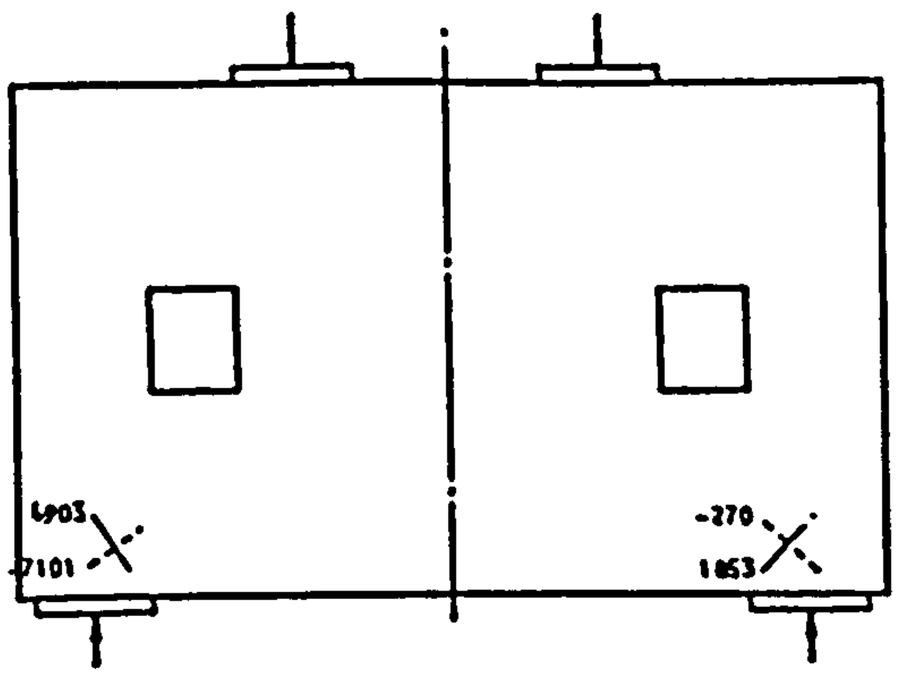

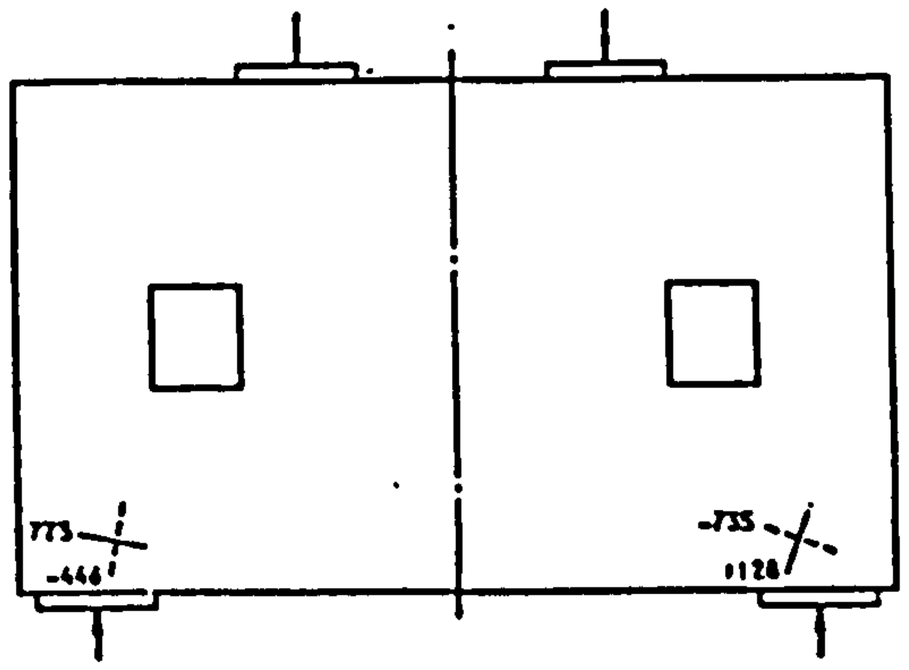

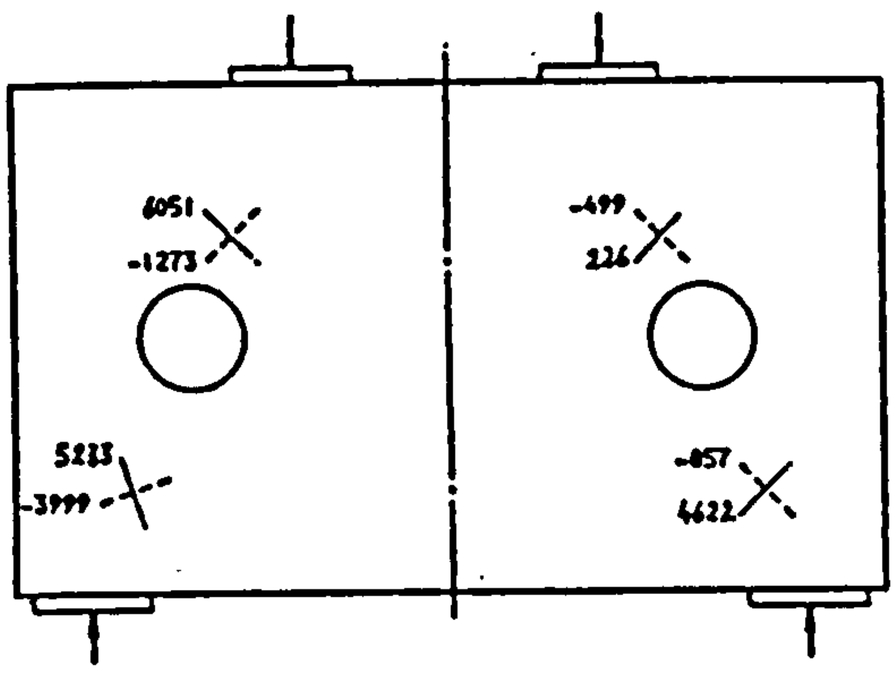

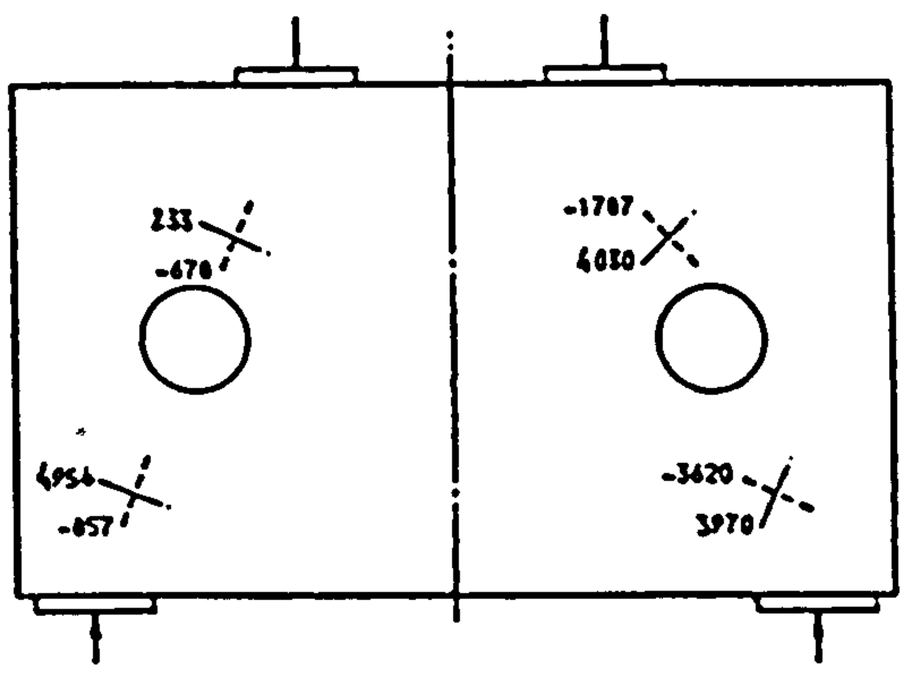

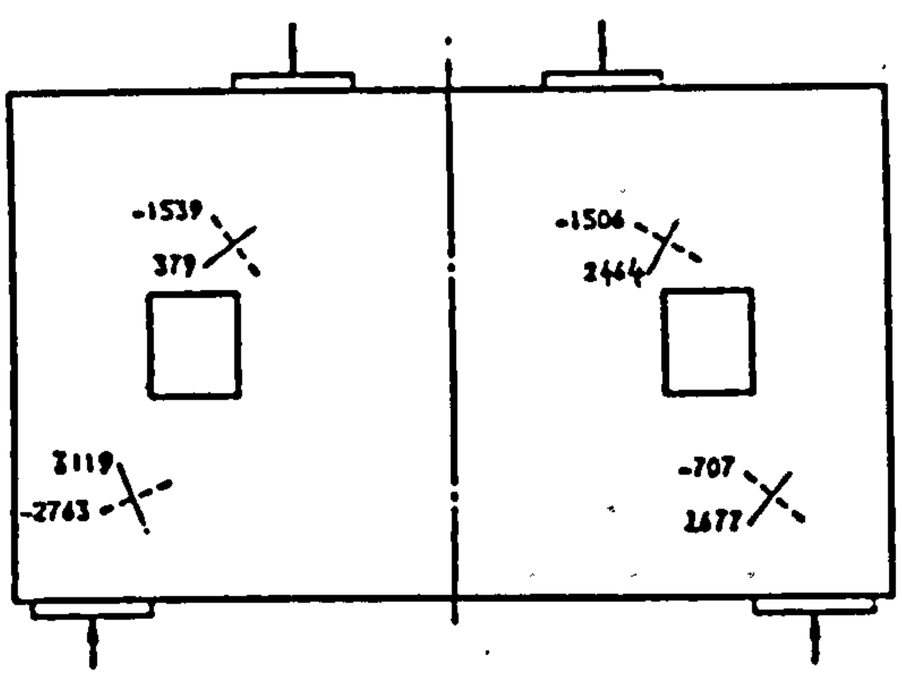

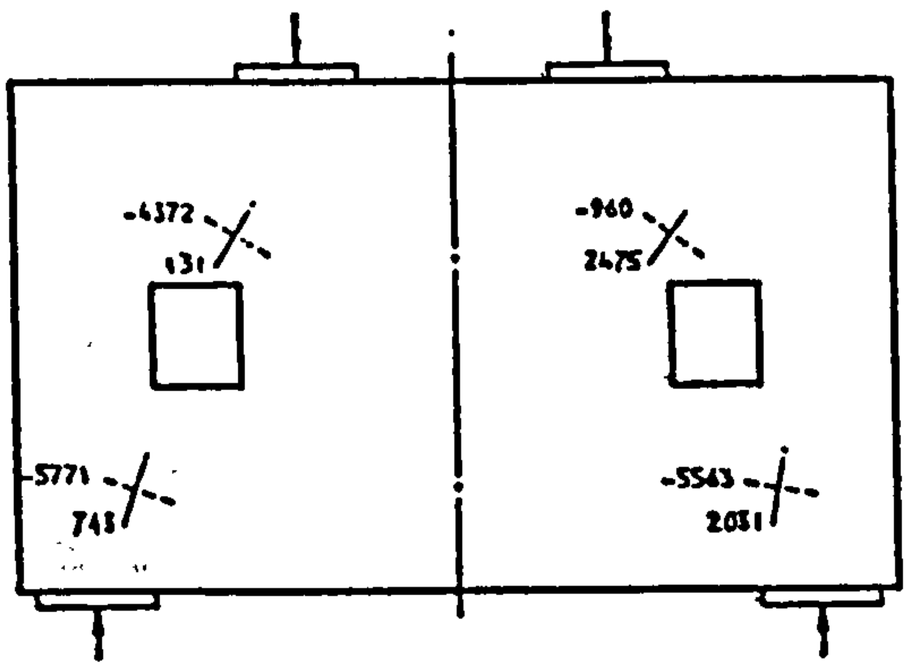

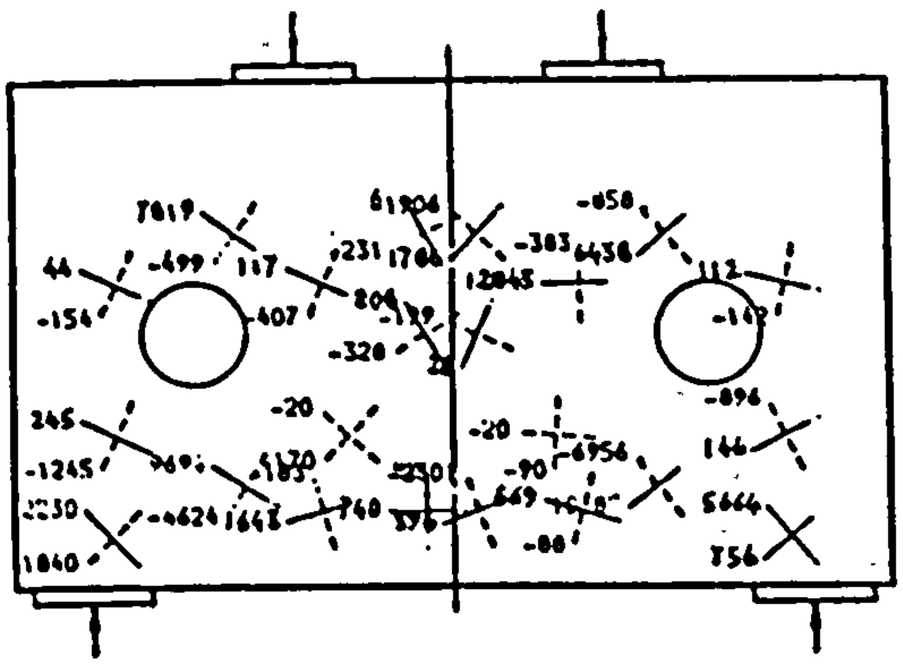

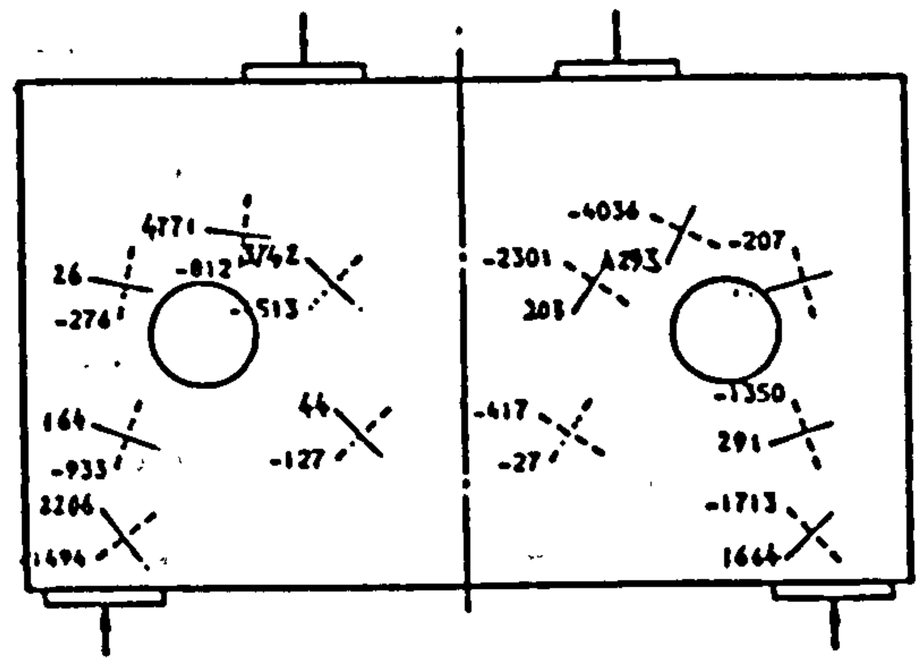

—— Tension Positive
---- Compression Negative

(All figures are in micro-strain)

Figure 6.31 : Principal strains after the last load increments (W-Series beams)

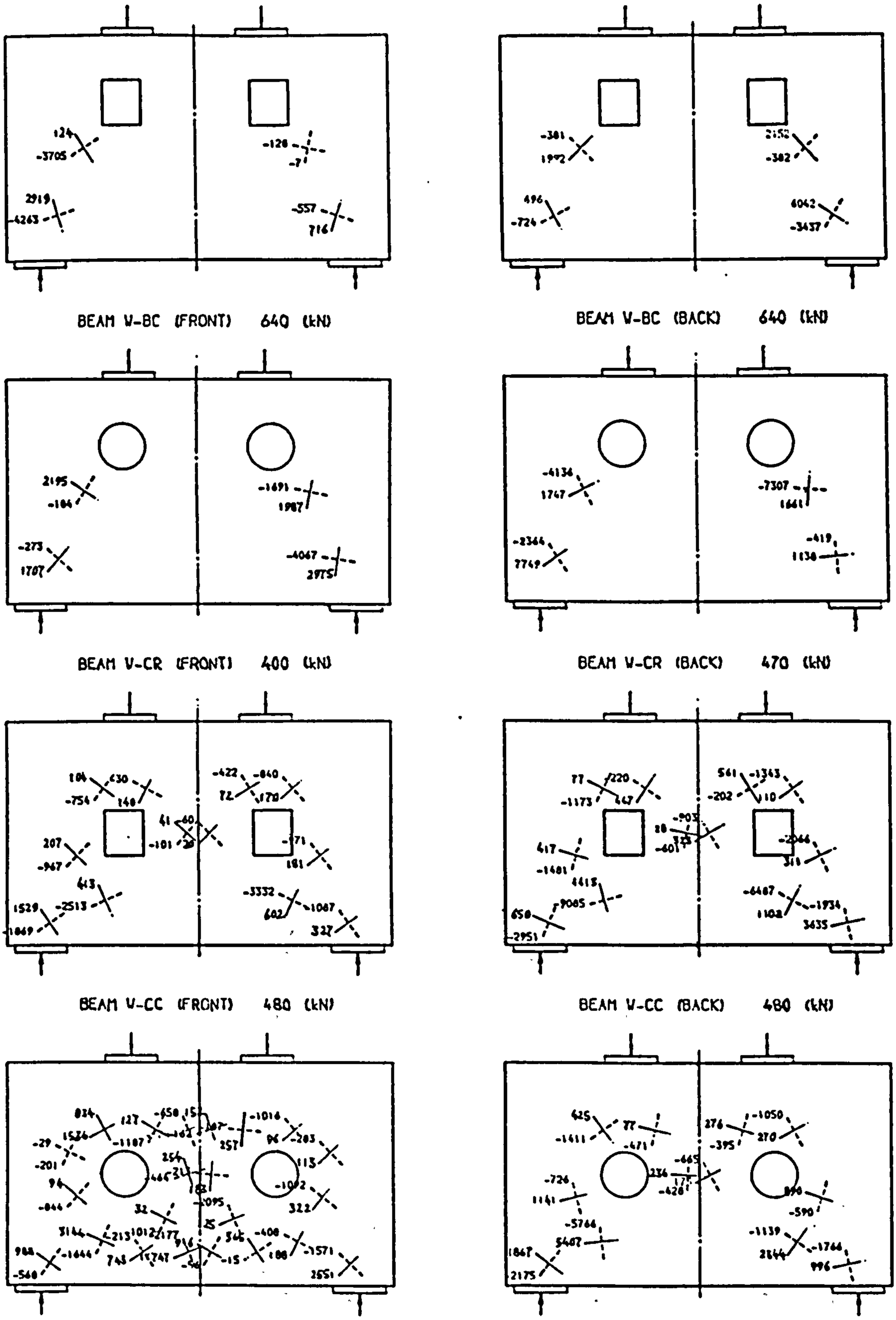

Figure 6.31 : Principal strains after the last load increments (W-Series beams) [cont'd]

BEAM V-DR (FRONT) 300 (kN)

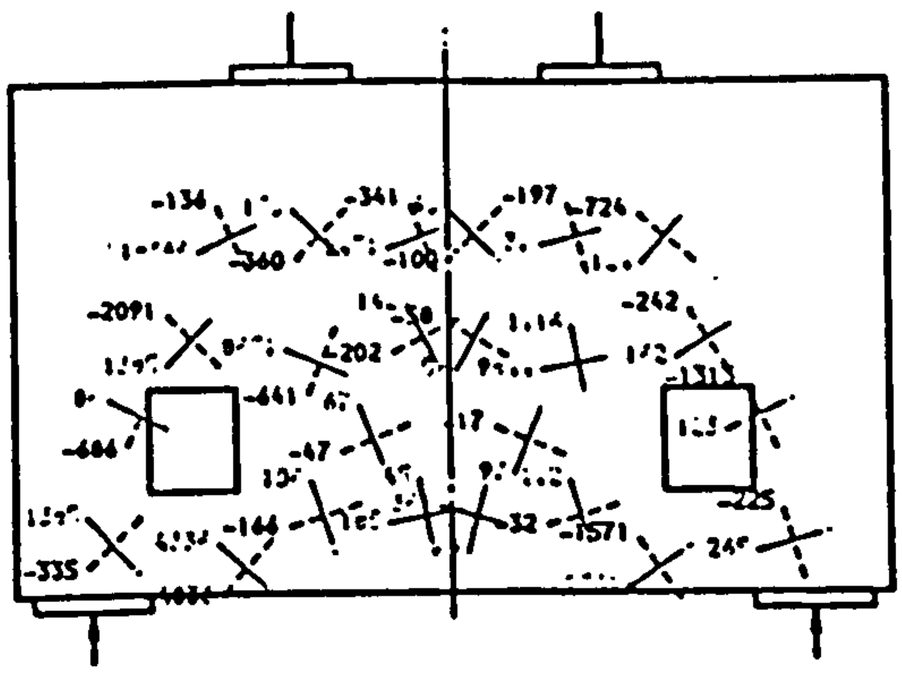

BEAM V-DR (BACK) 300 (kN)

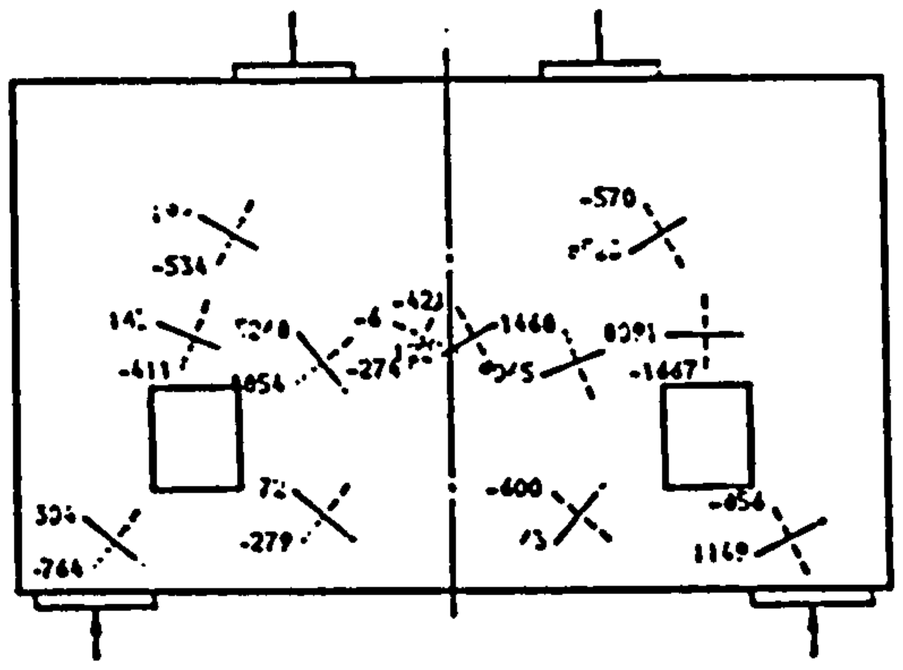

BEAM V-DC (FRONT) 350 (kN)

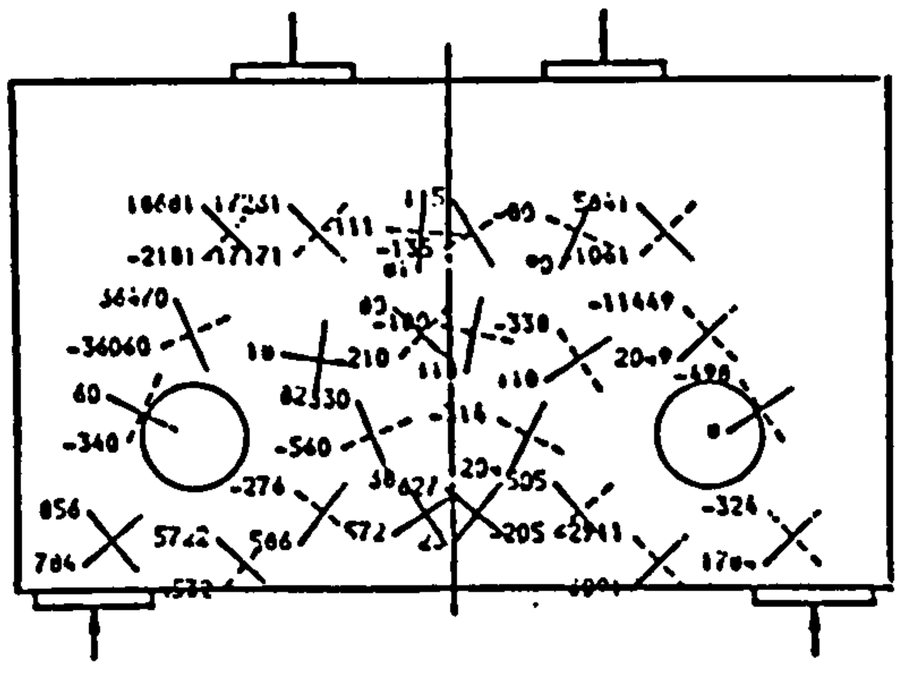

BEAM V-DC (BACK) 350 (kN)

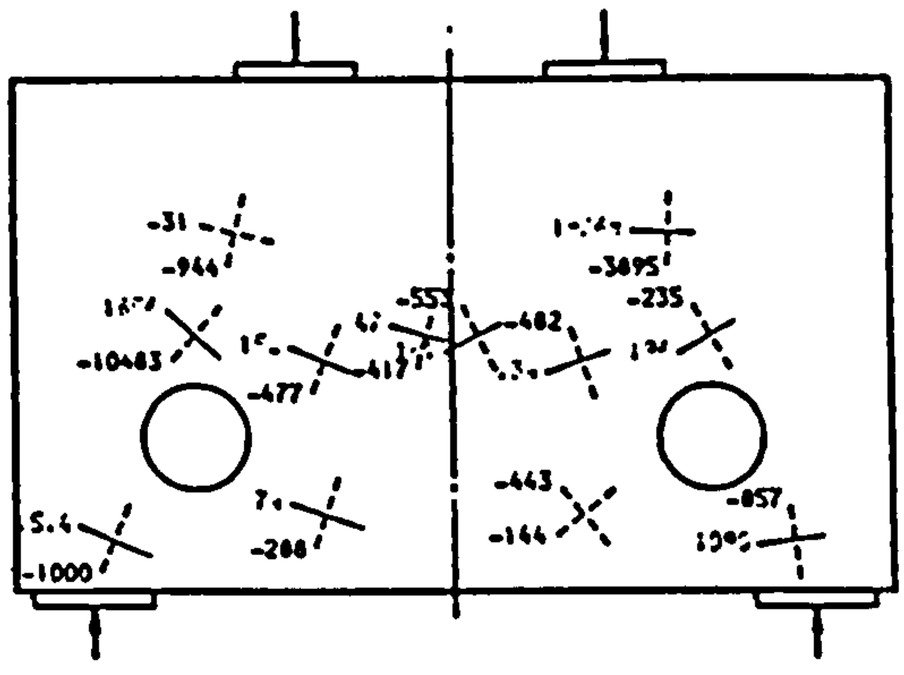

BEAM V-ER (FRONT) 300 (kN)

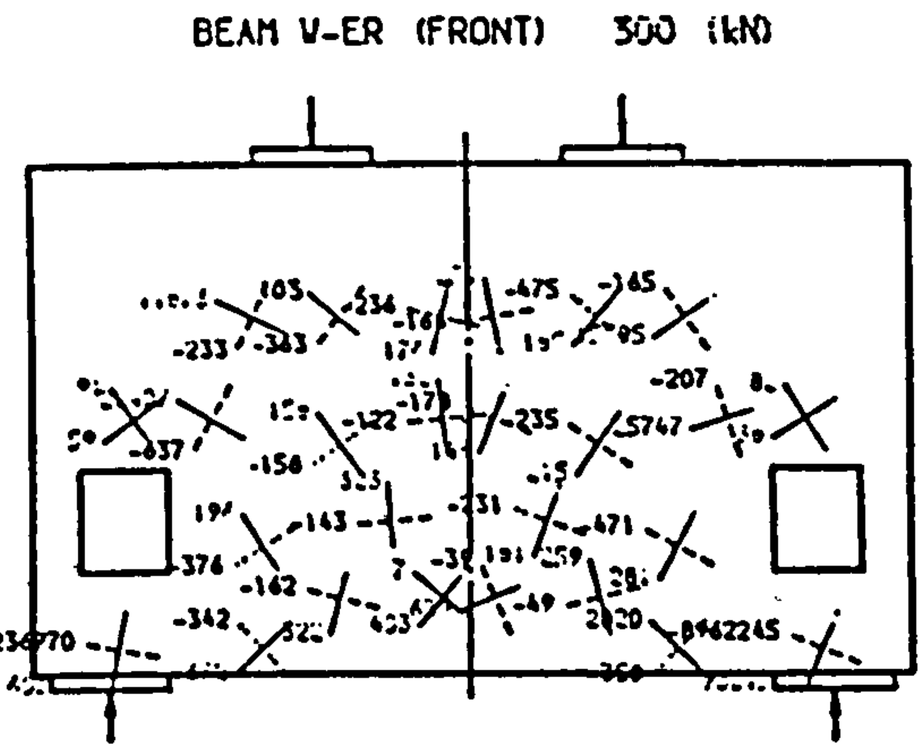

BEAM V-ER (BACK) 300 (kN)

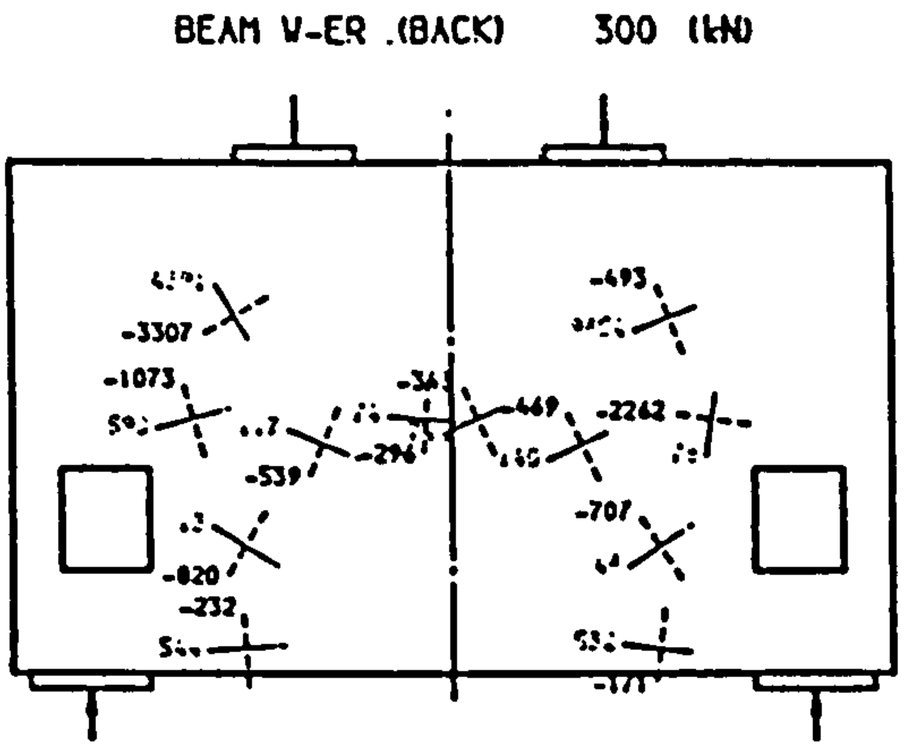

BEAM V-EC (FRONT) 350 (kN)

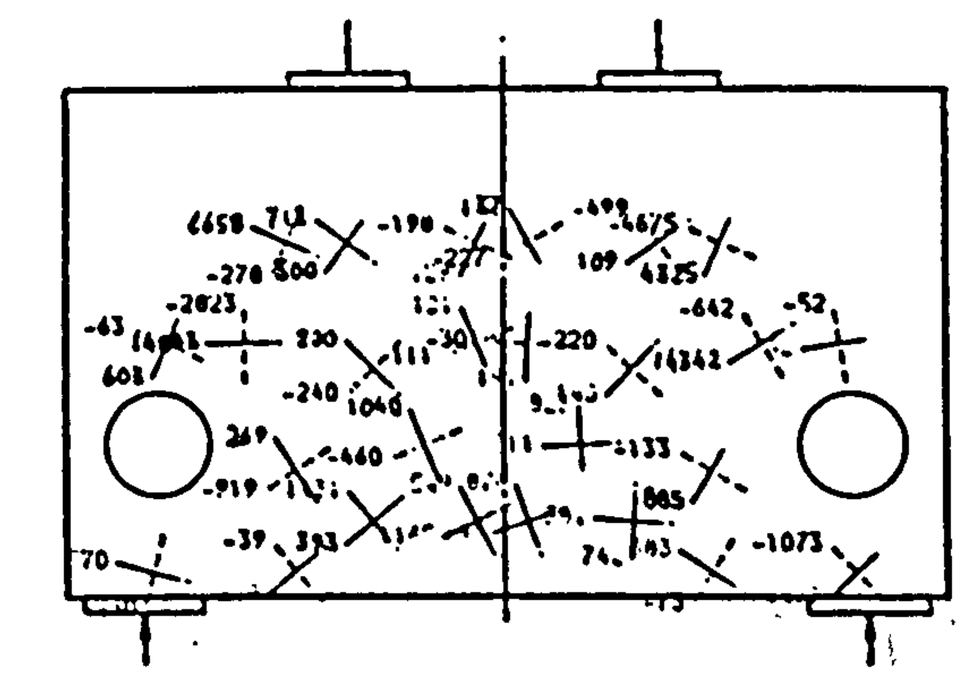

BEAM V-EC (BACK) 350 (kN)

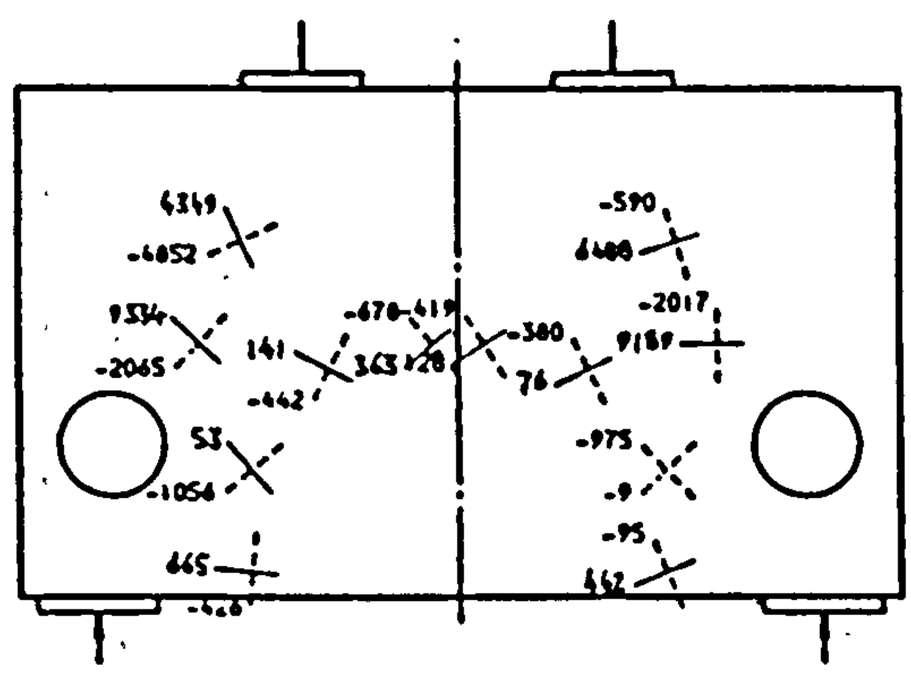

BEAM W-ER (FRONT) 300 (kN)

BEAM W-ER (BACK) 300 (kN)

— Tension Positive

---- Compression Negative

(All figures are in micro-strain)

Figure 6.31 : Principal strains after the last load increments (W-Series beams) [cont'd]

BEAM V-AR-S (FRONT) 320 (kN)

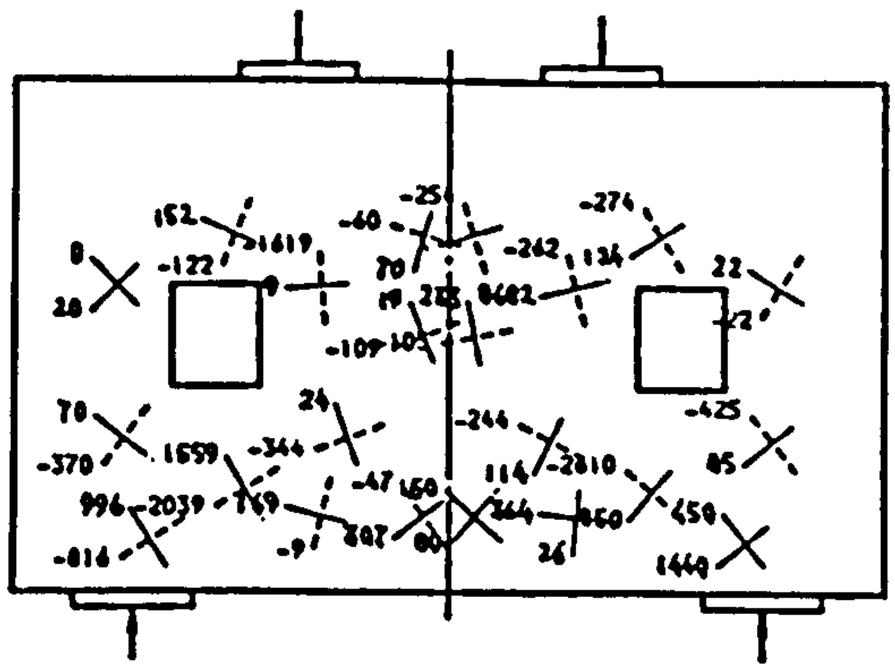

BEAM V-AR-S (BACK) 320 (kN)

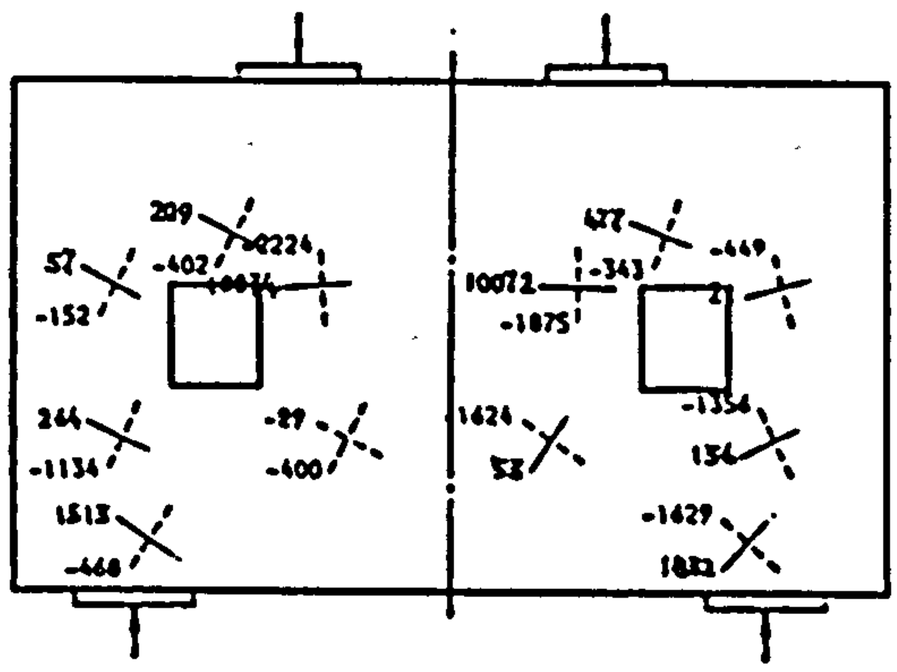

BEAM V-AC-S (FRONT) 460 (kN)

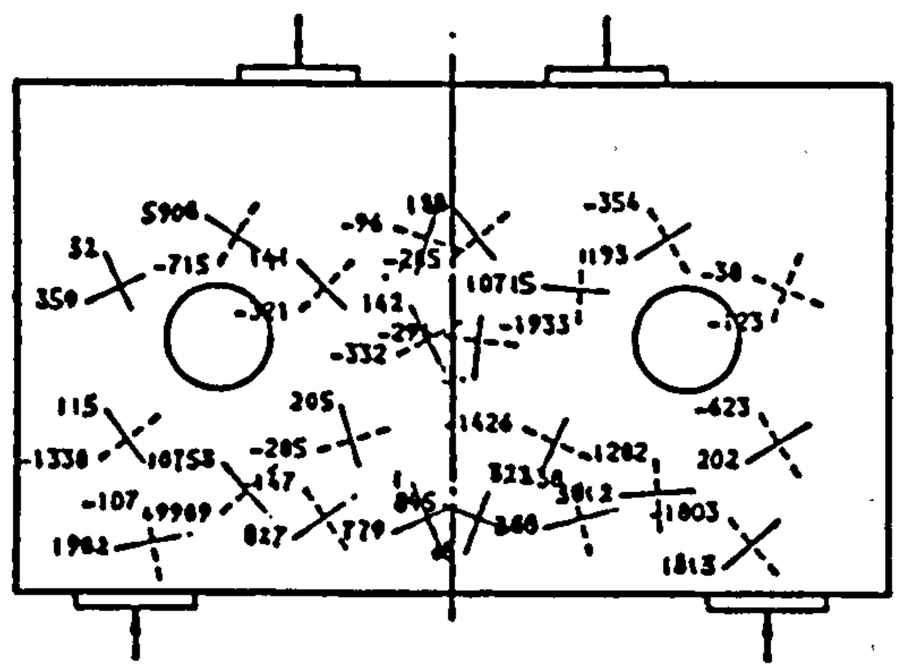

BEAM V-AC-S (BACK) 460 (kN)

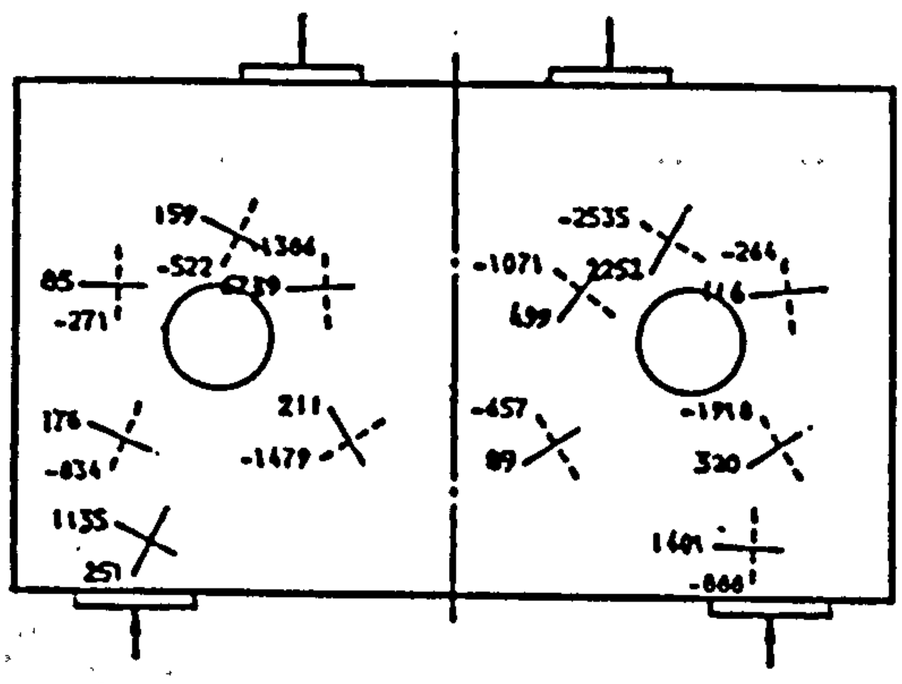

BEAM V-29-0.1-R1 (FRONT) 520 (kN)

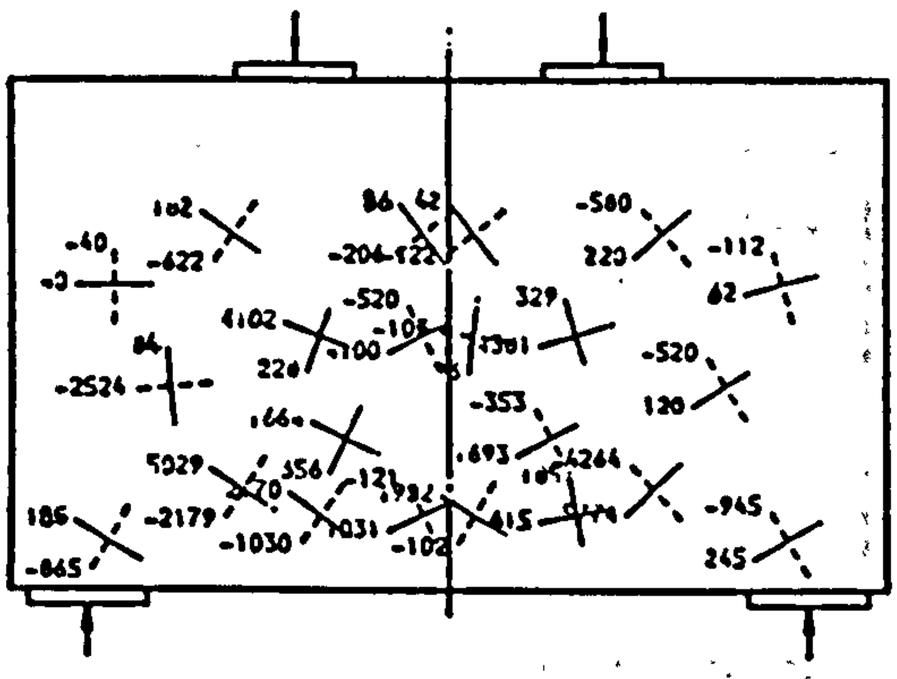

BEAM V-29-0.1-R1 (BACK) 660 (kN)

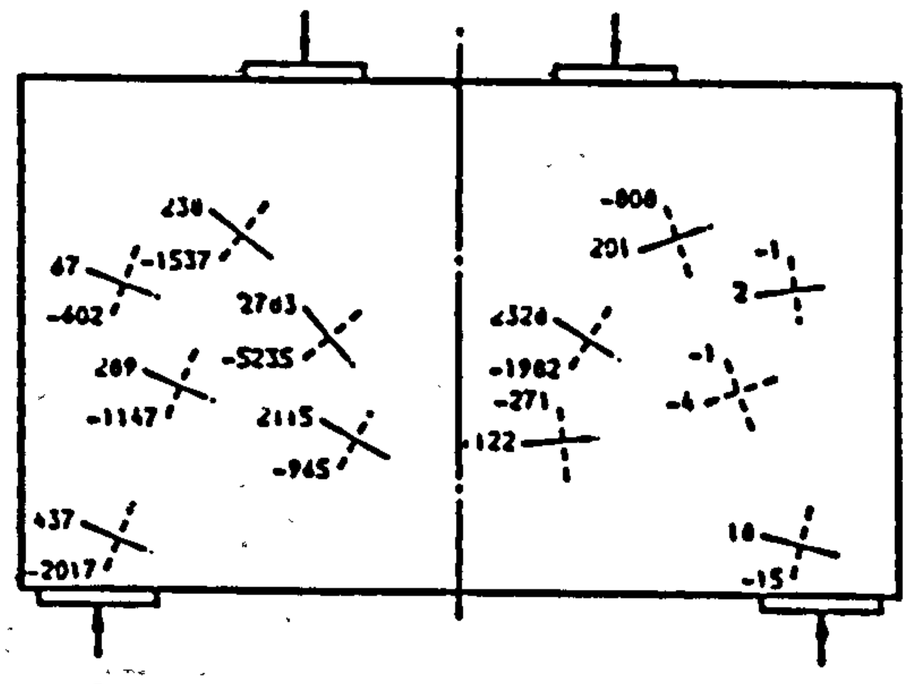

BEAM V-29-0.1-R2 (FRONT) 650 (kN)

BEAM V-29-0.1-R2 (BACK) 900 (kN)

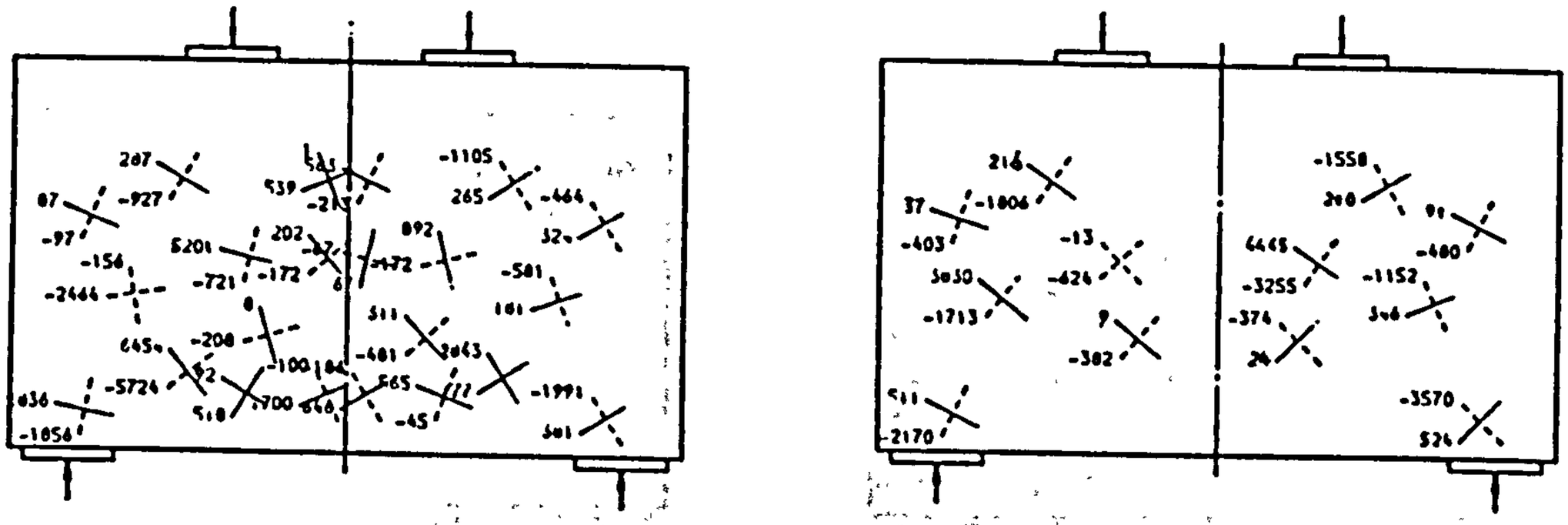

— Tension Positive

---- Compression Negative

(All figures are in micro-strain)

Figure 6.31 : Principal strains after the last load increments (W-Series beams). [cont'd]

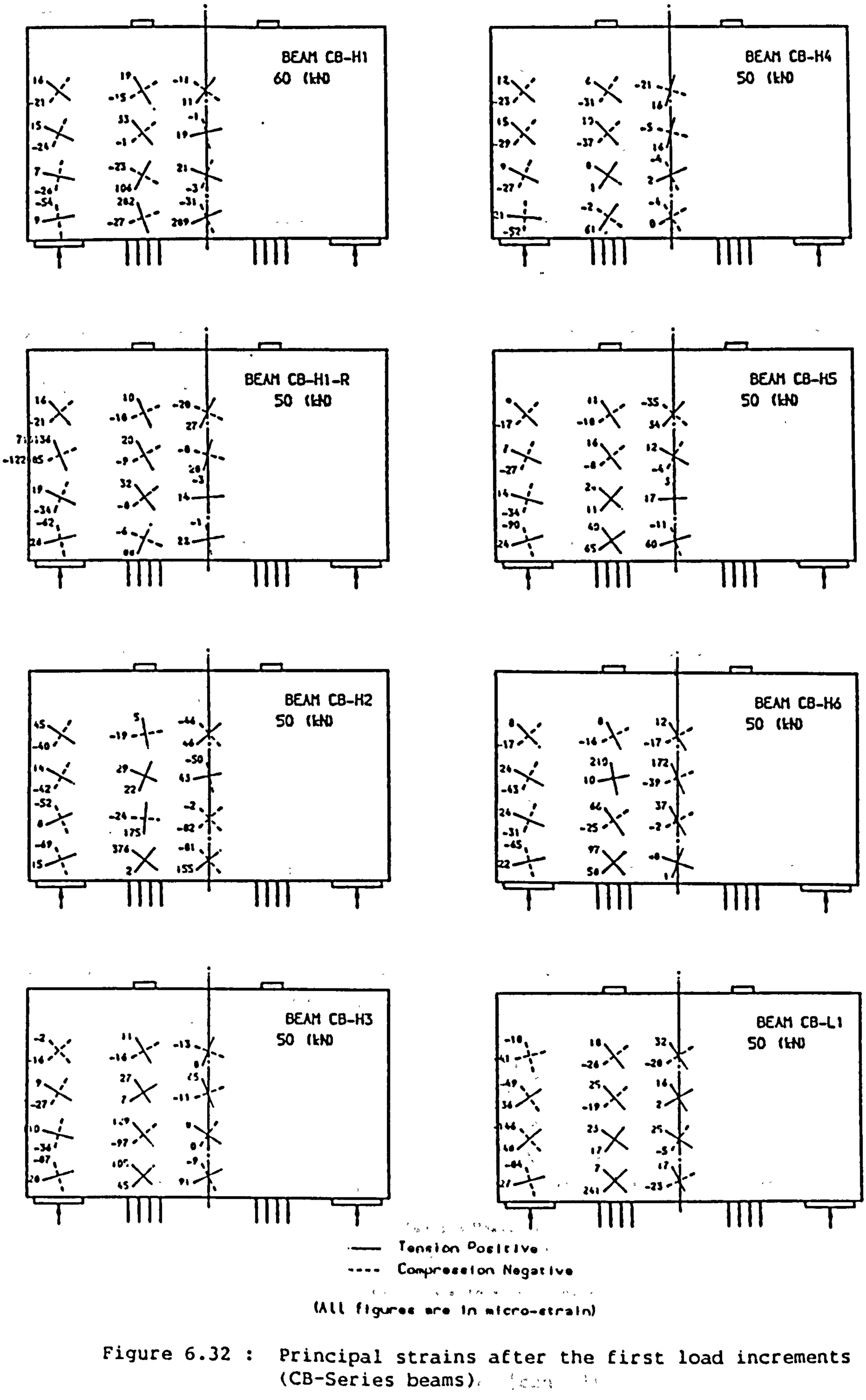

Figure 6.32 : Principal strains after the first load increments (CB-Series beams).

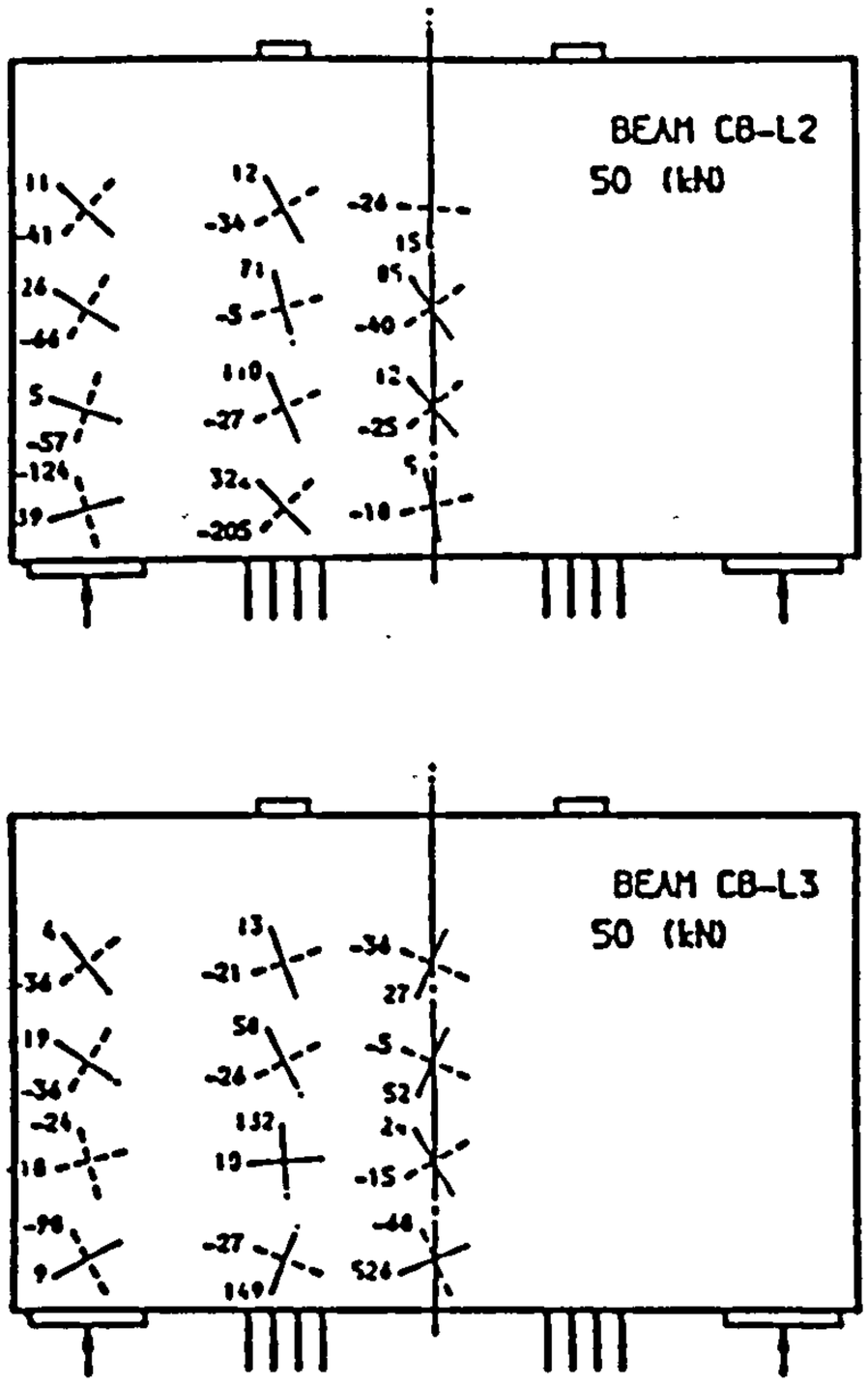

Figure 6.32 : Principal strains after the first load increments (CB-Series beams) [cont'd]

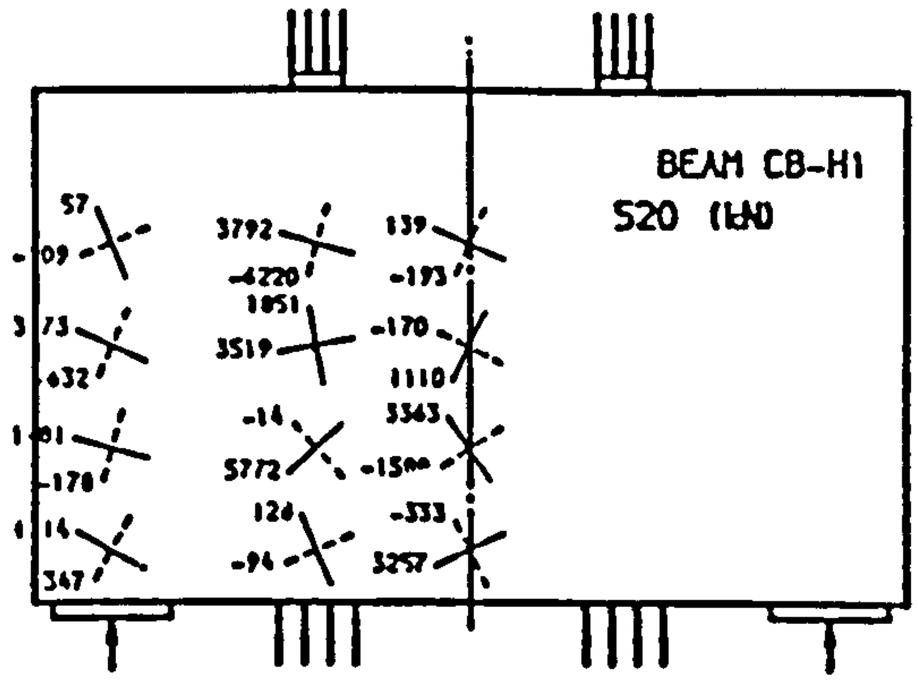

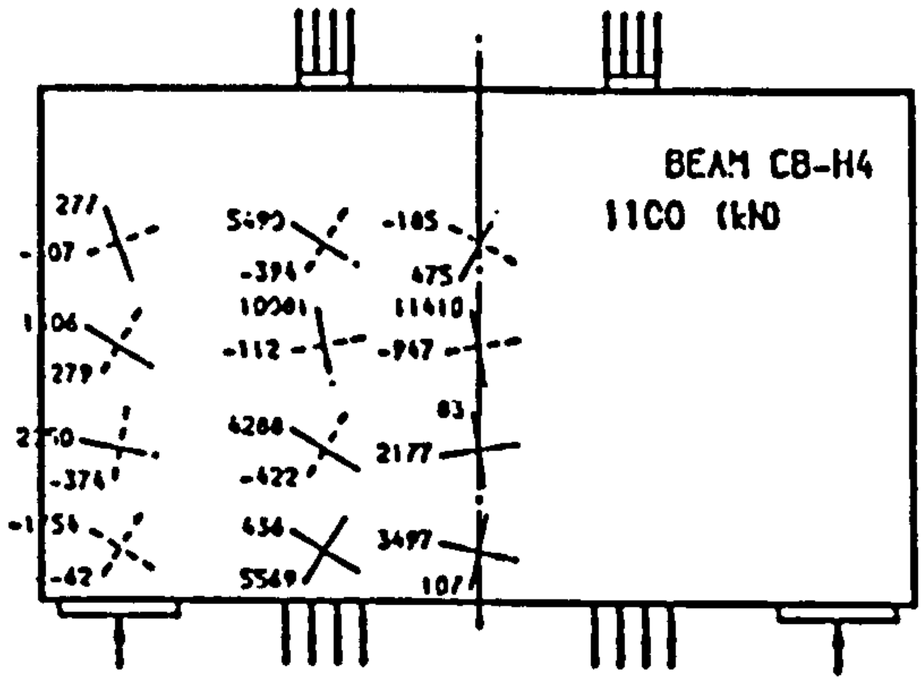

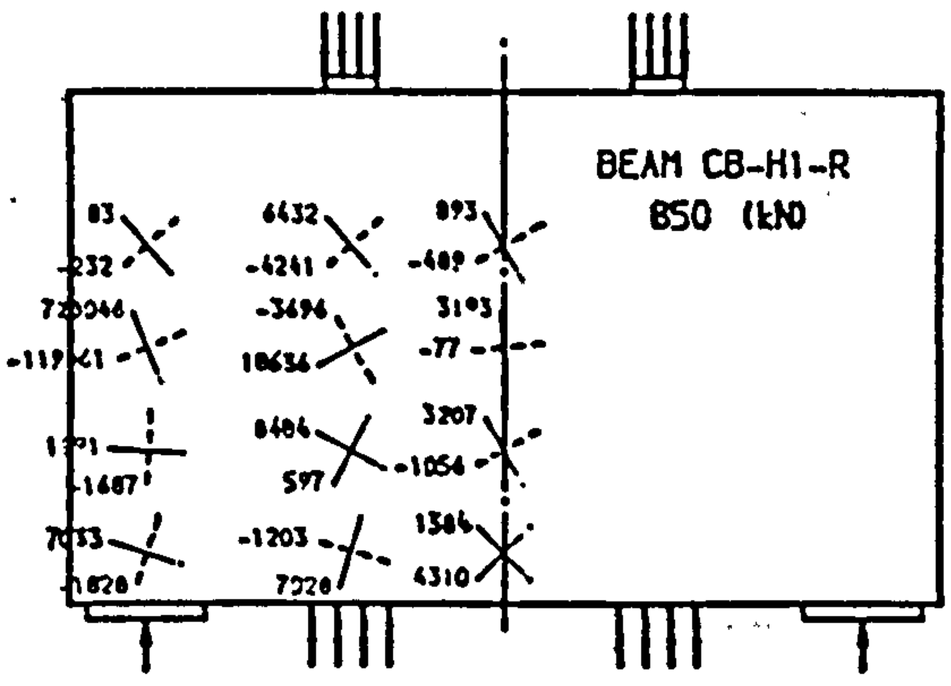

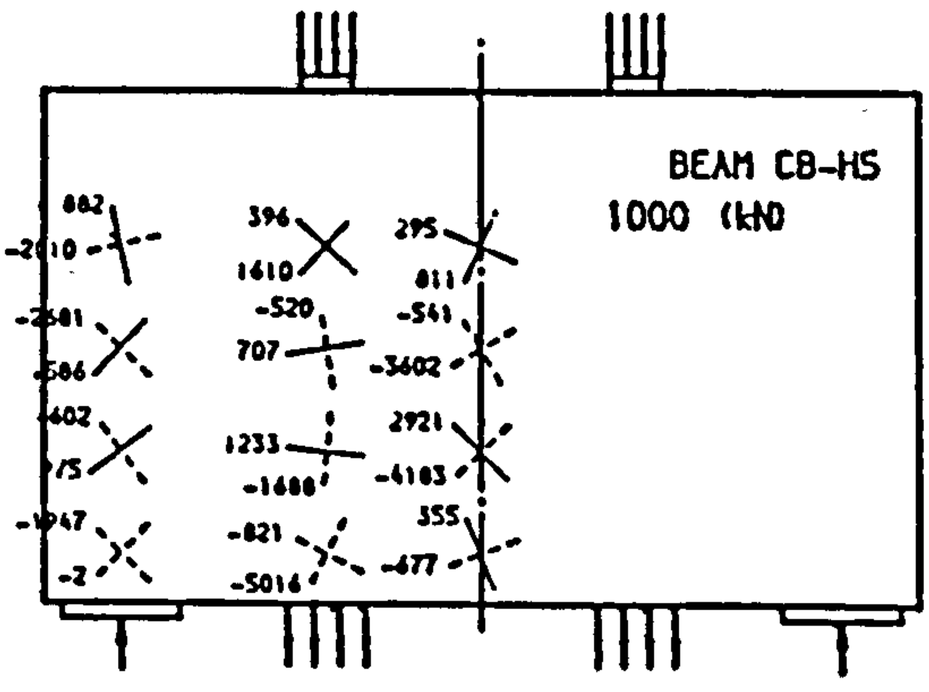

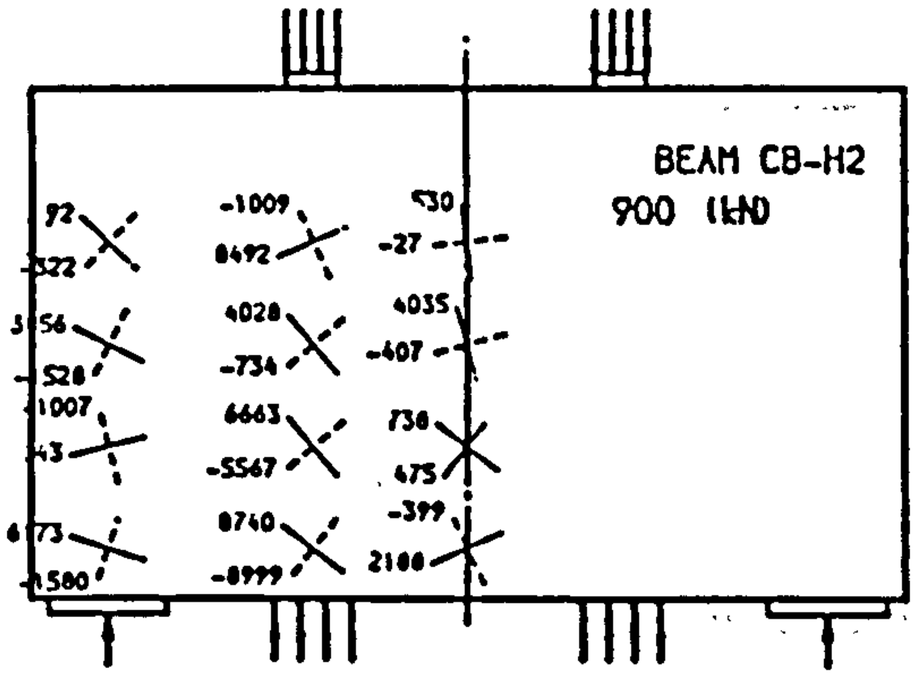

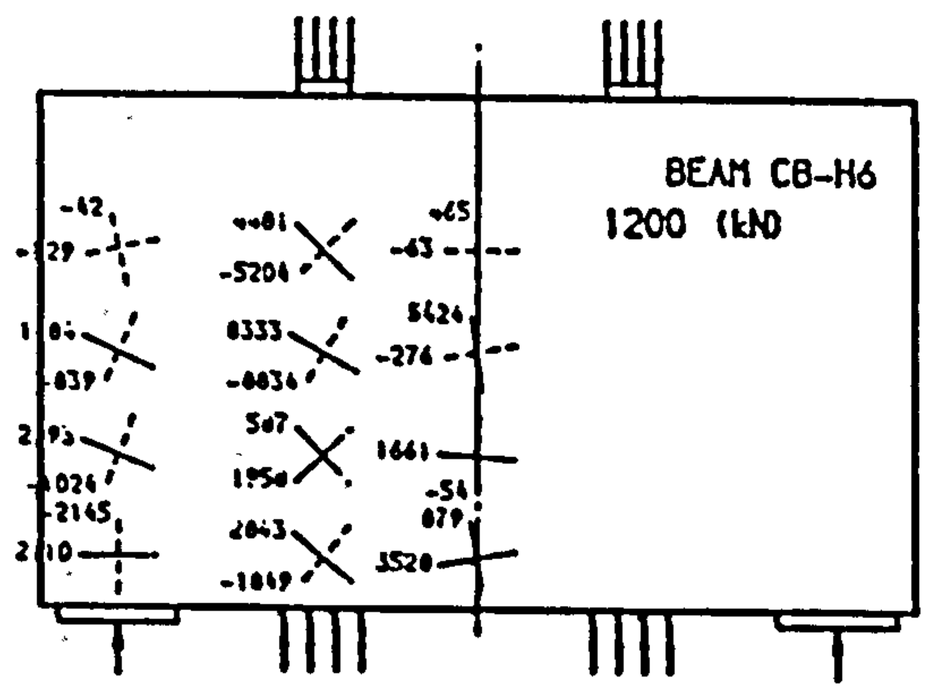

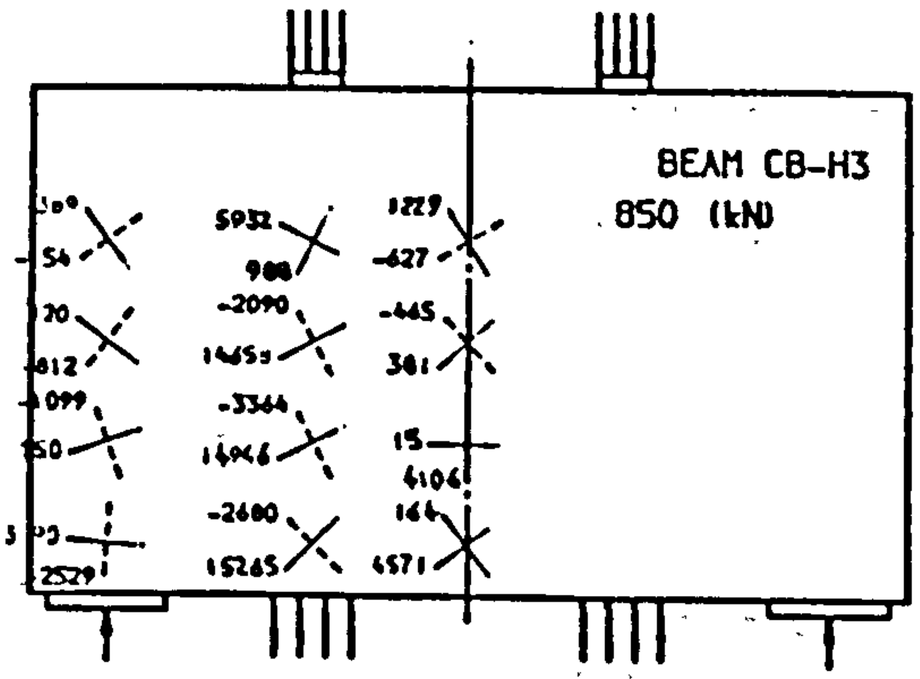

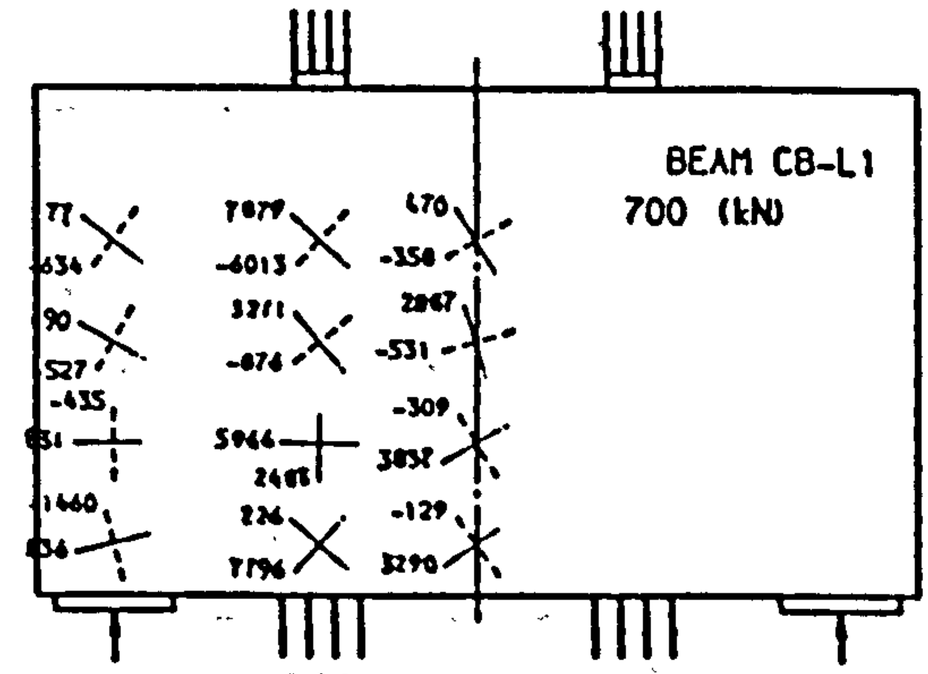

—— Tension Positive

---- Compression Negative

(All figures are in micro-strain)

Figure 6.33 : Principal strains after the last load increments (CB-Series beams)

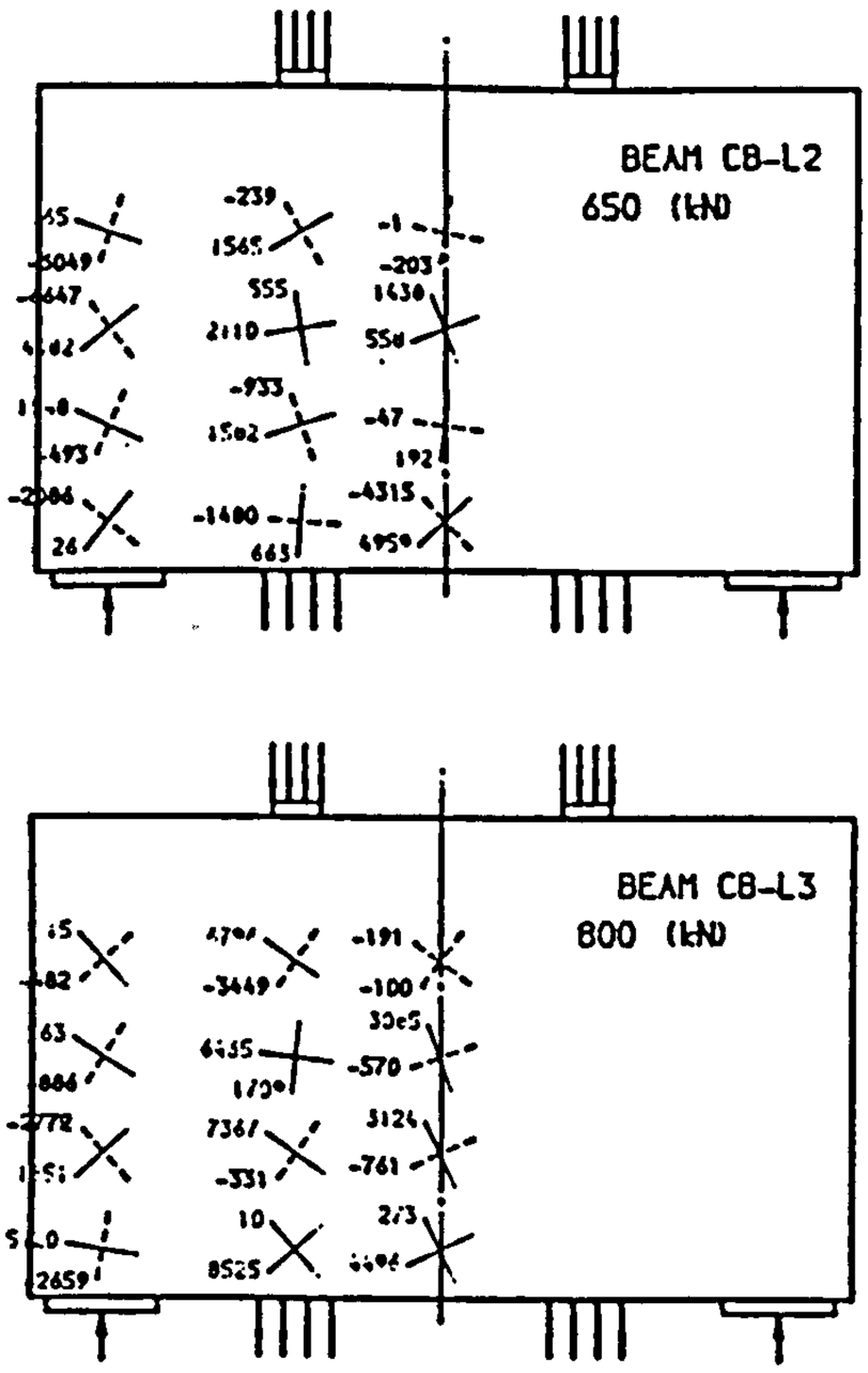

Figure 6.33 : Principal strains after the last load increments (CB-Series beams) [cont'd]

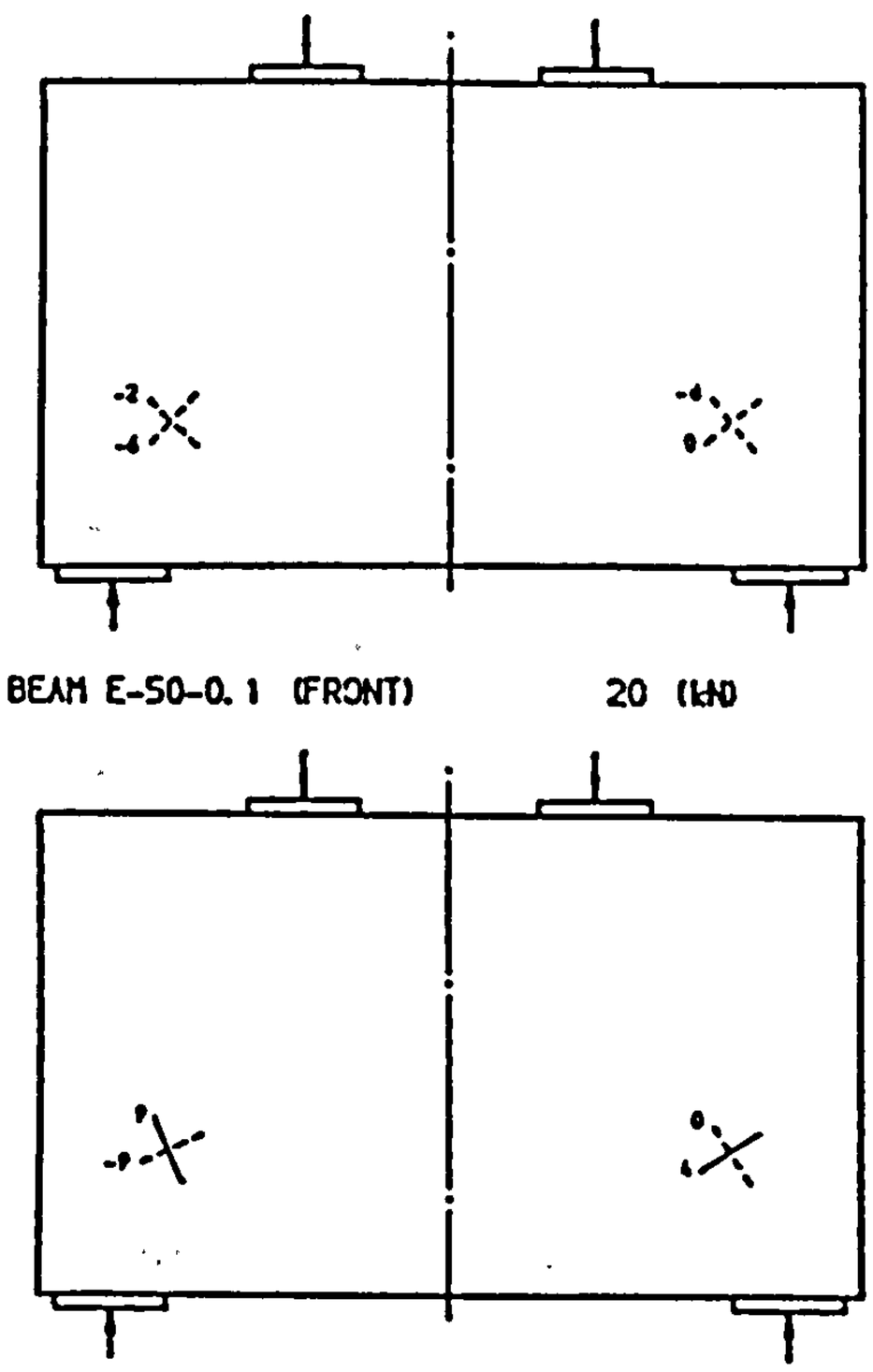

Figure 6.34 : Principal stresses after the first load increments (E-Series beams, theory of elasticity)

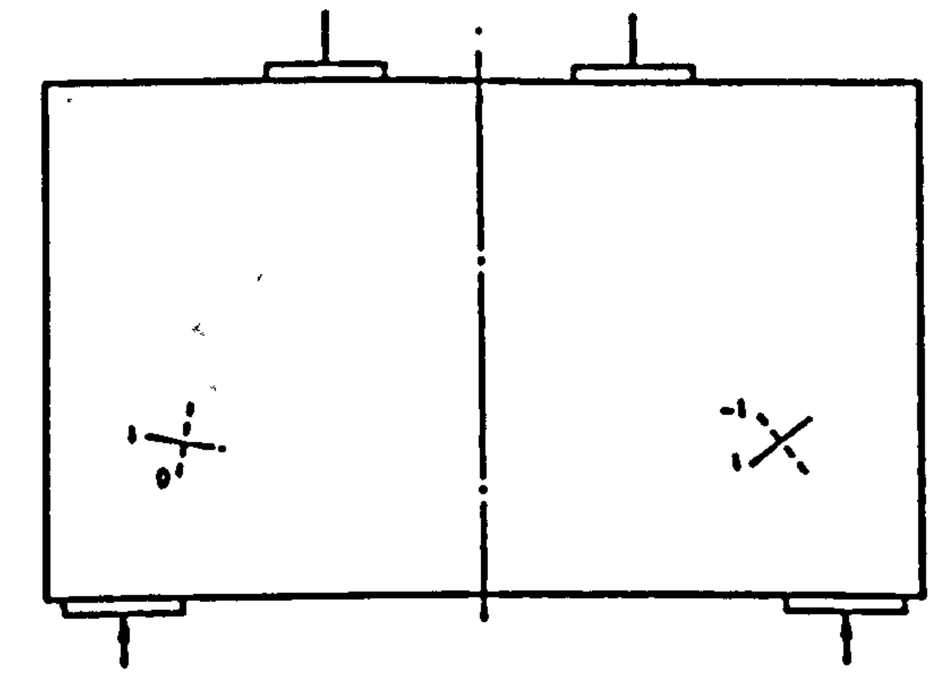

Figure 6.34 : Principal stresses after the first load increments (E-Series beams, theory of elasticity) [cont'd]

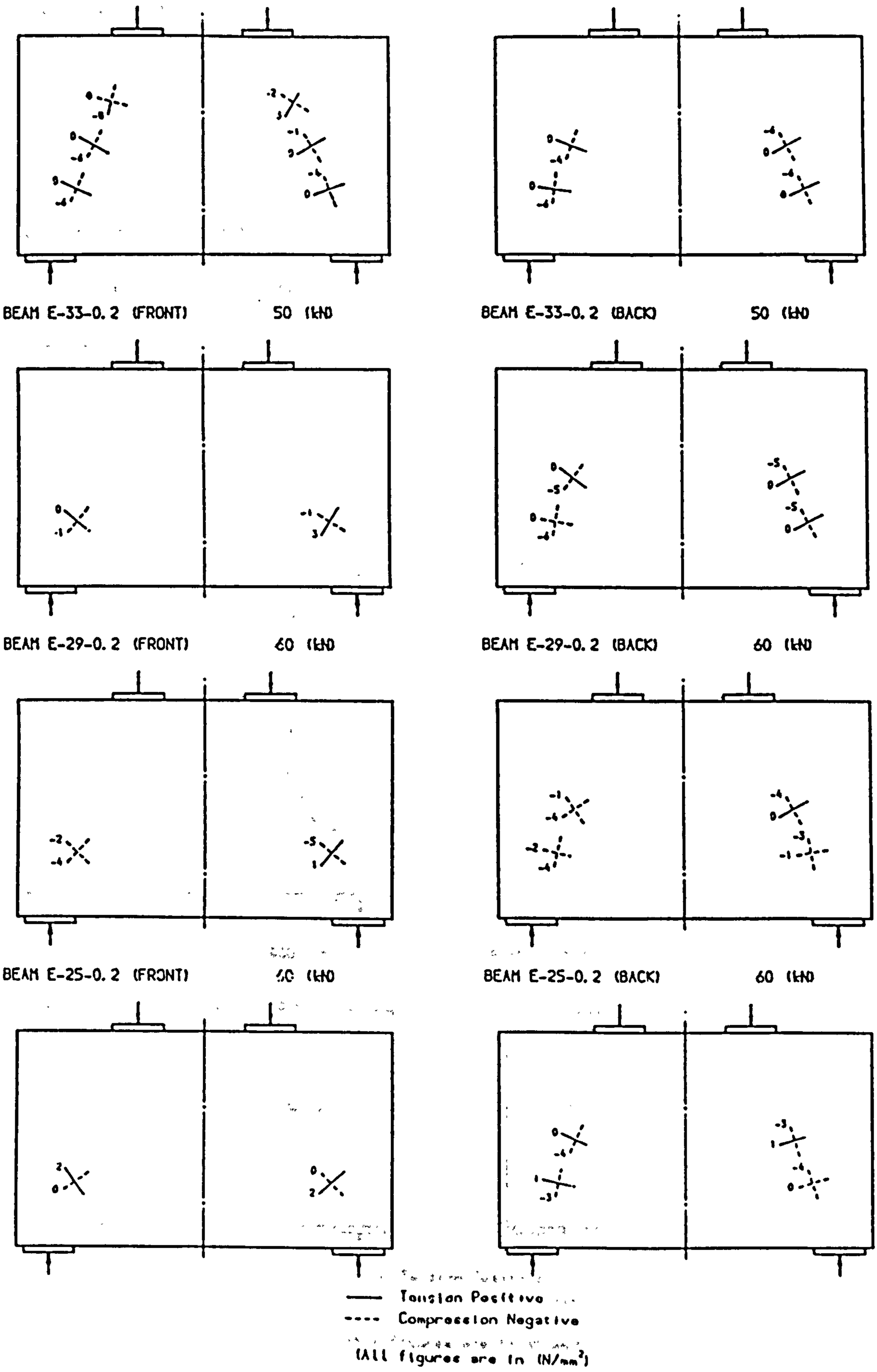

Figure 6.34 : Principal stresses after the first load increments (E-Series beams, theory of elasticity) [cont'd]

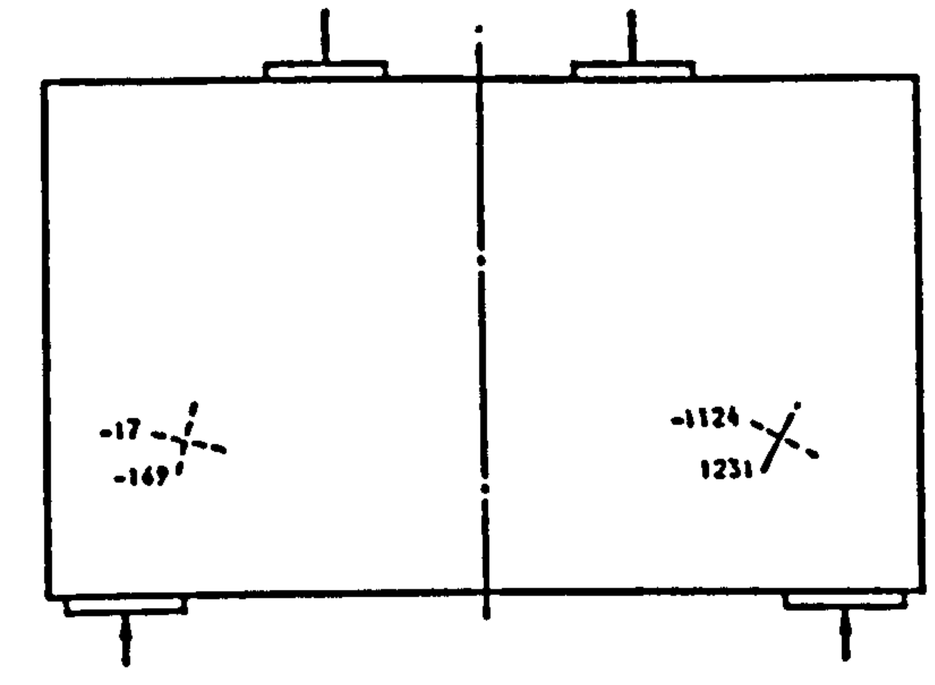

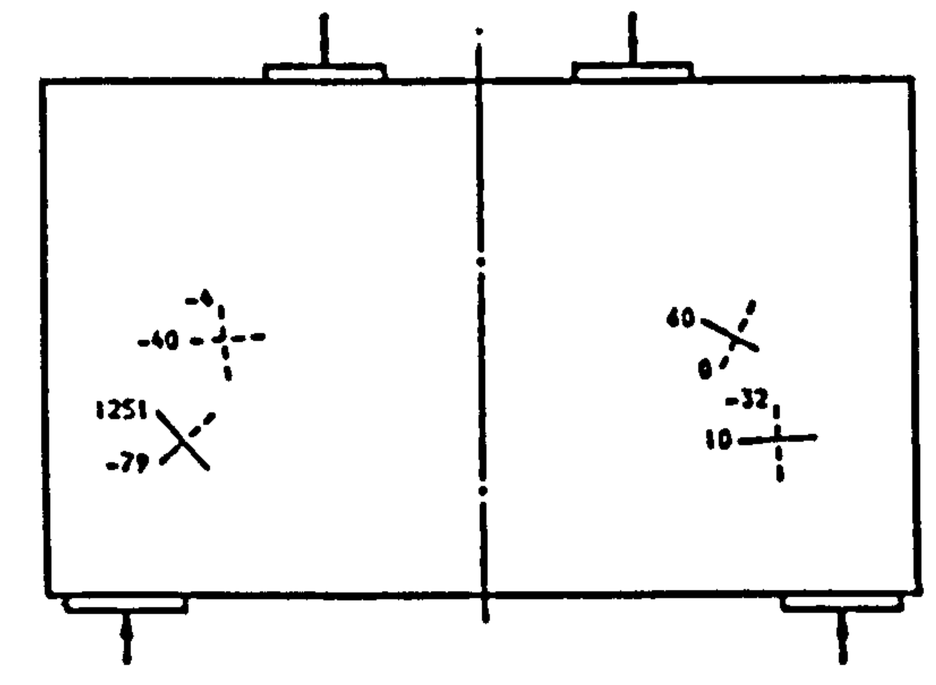

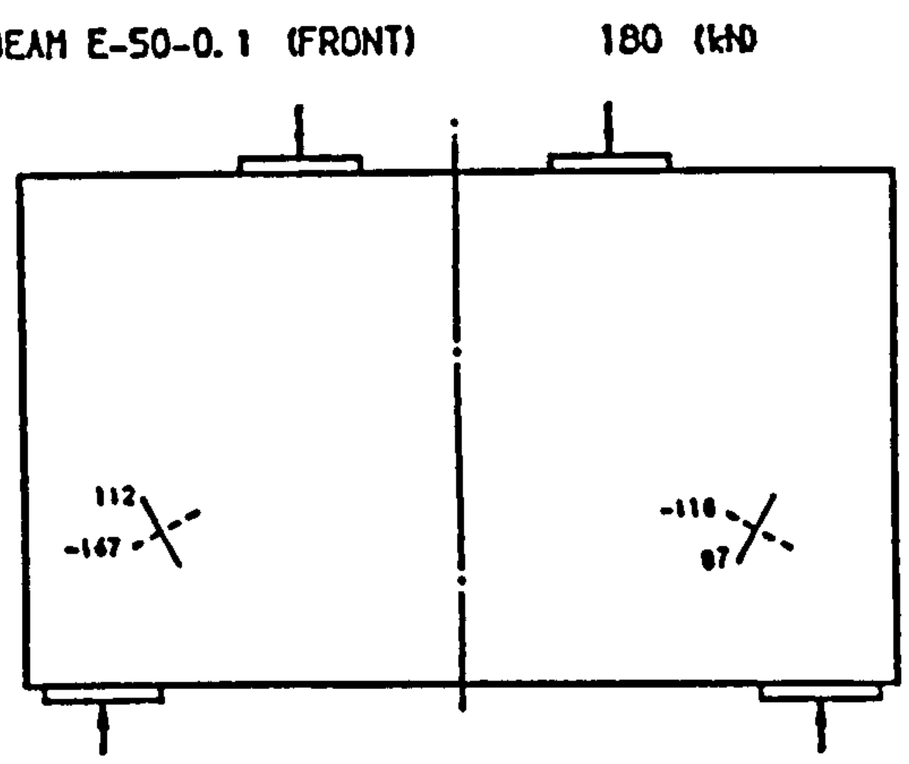

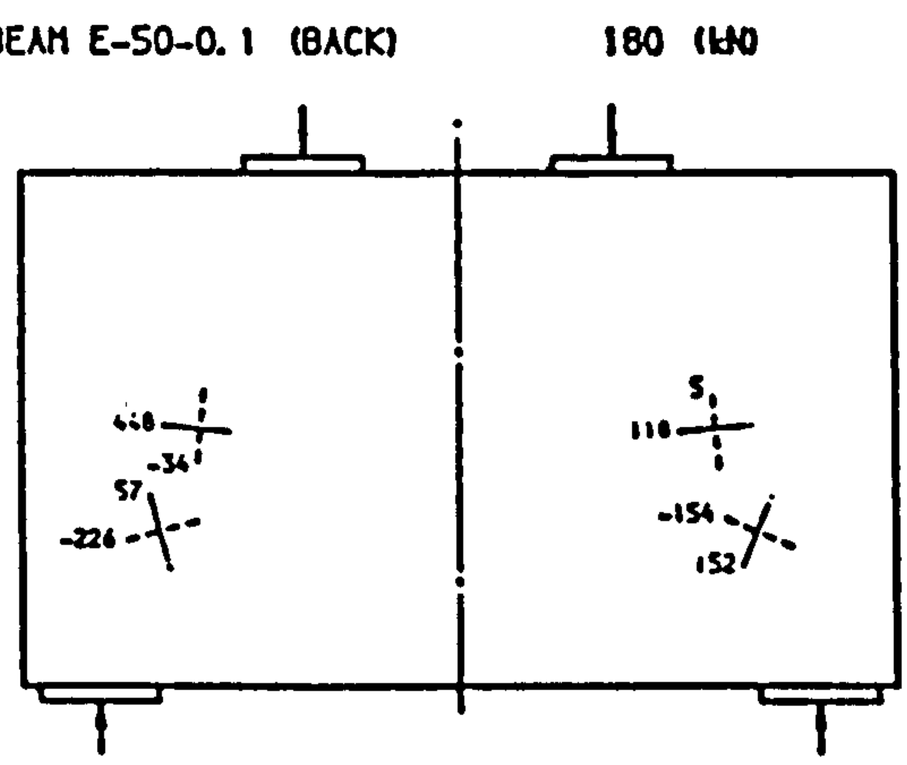

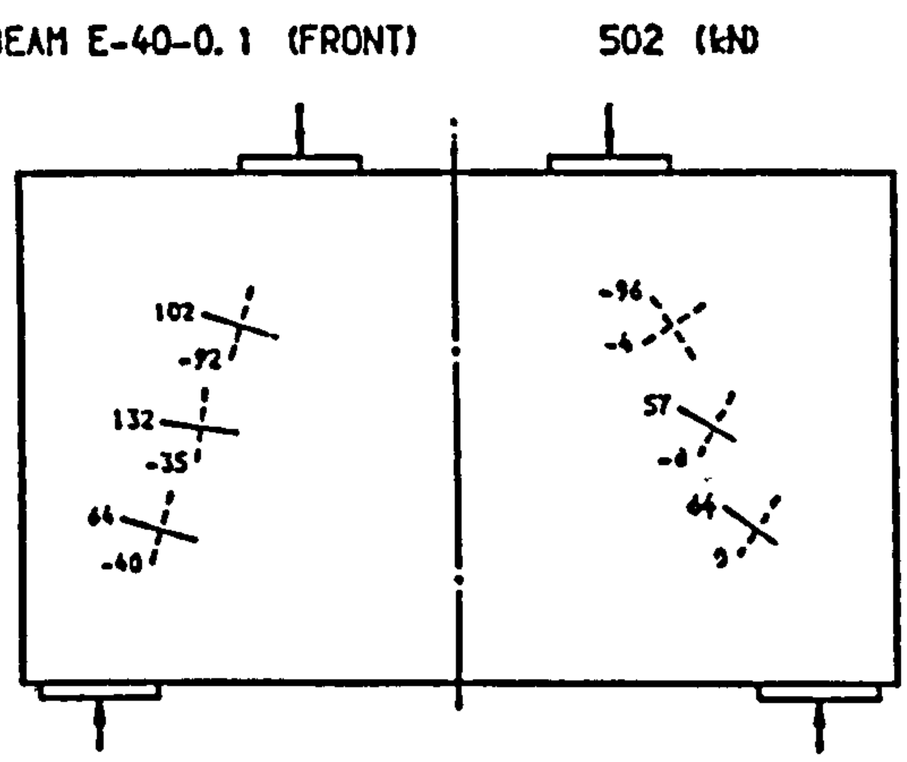

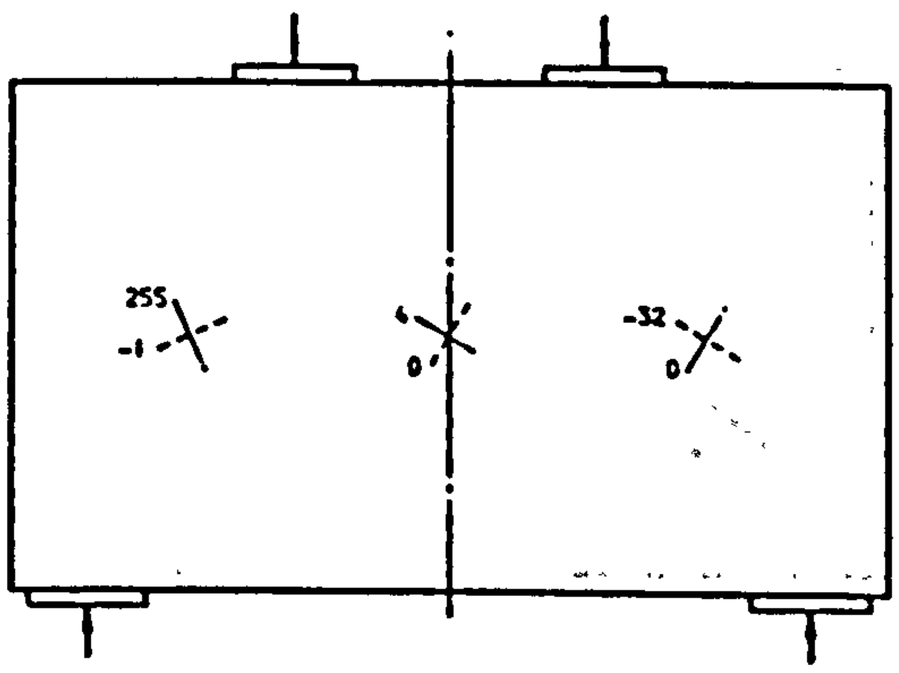

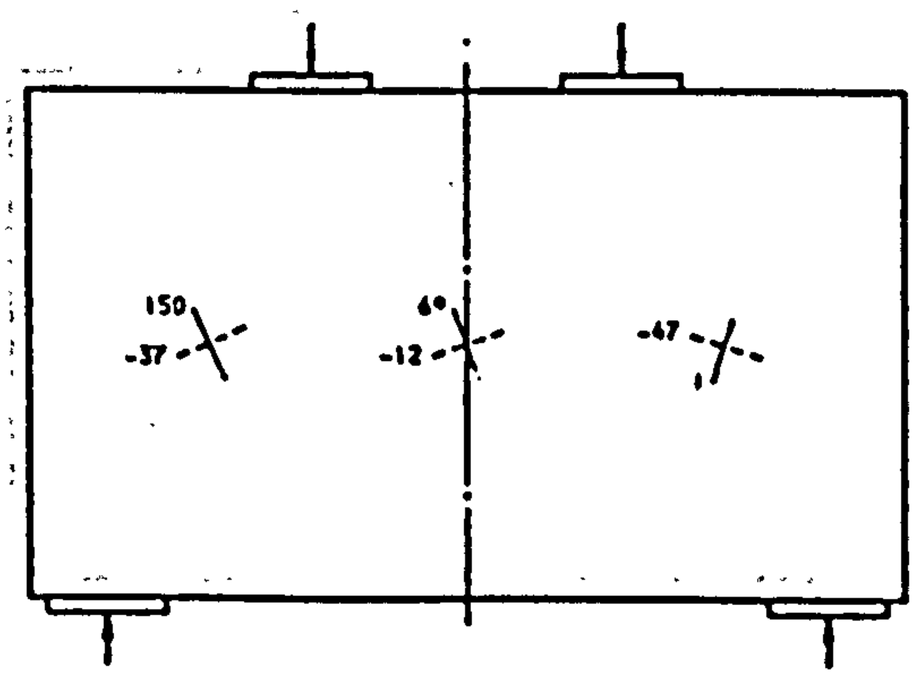

Tension Positive
Compression Negative

(All figures are in (N/mm^2))

Figure 6.35 : Principal stresses after the last load increments (E-Series beams, theory of elasticity)

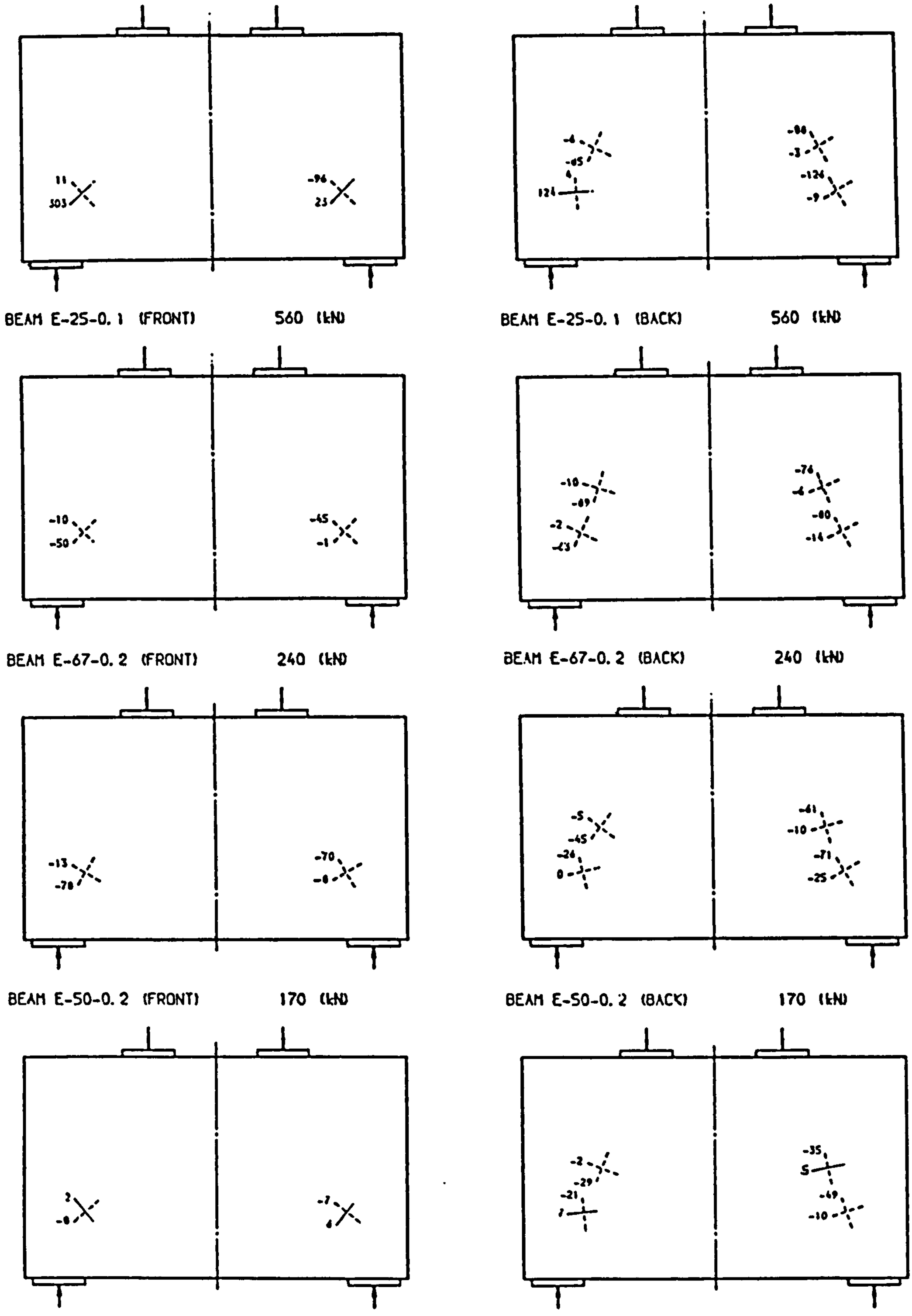

Figure 6.35 : Principal stresses after the last load increments (E-Series beams, theory of elasticity) [cont'd]

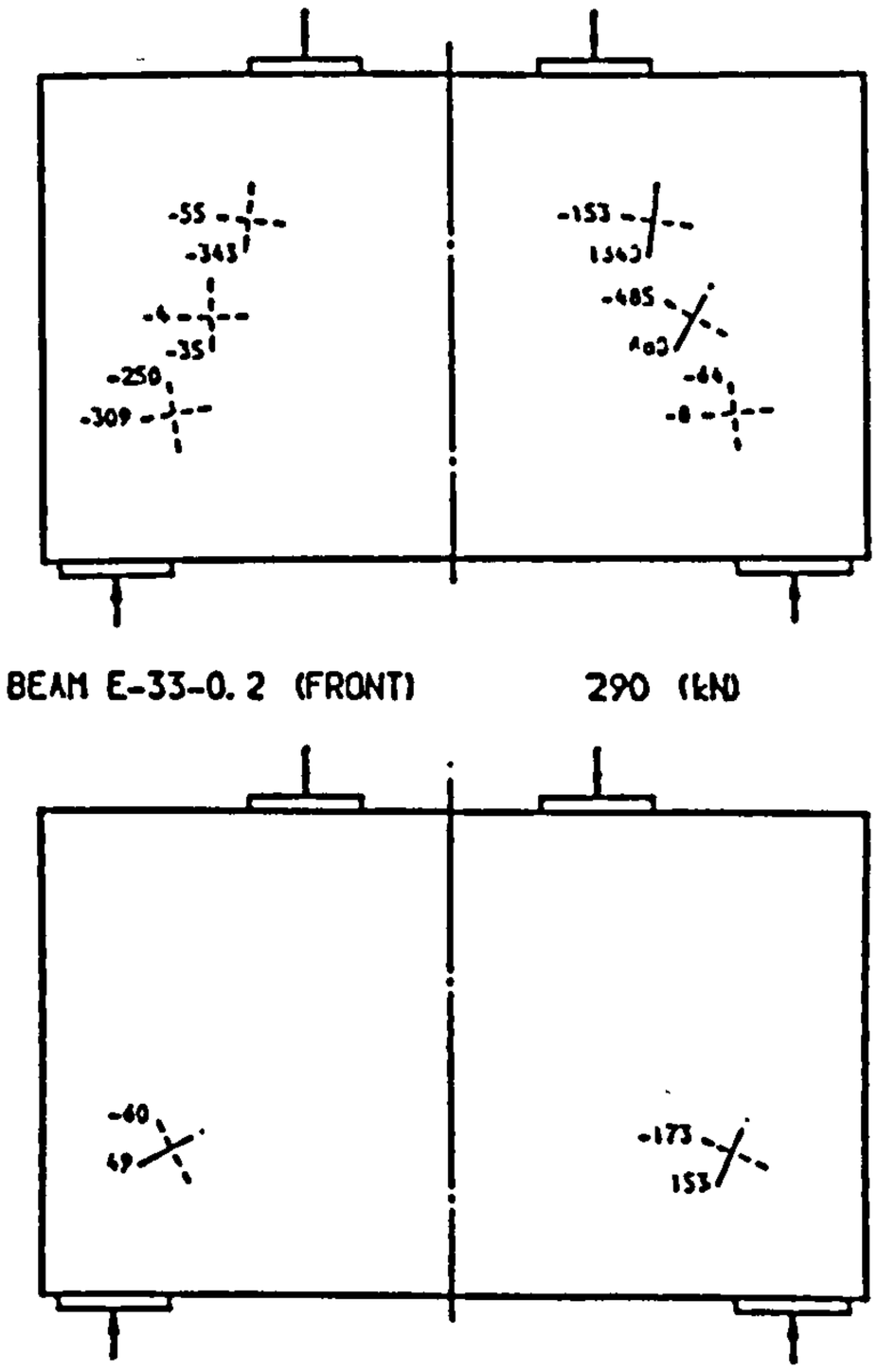

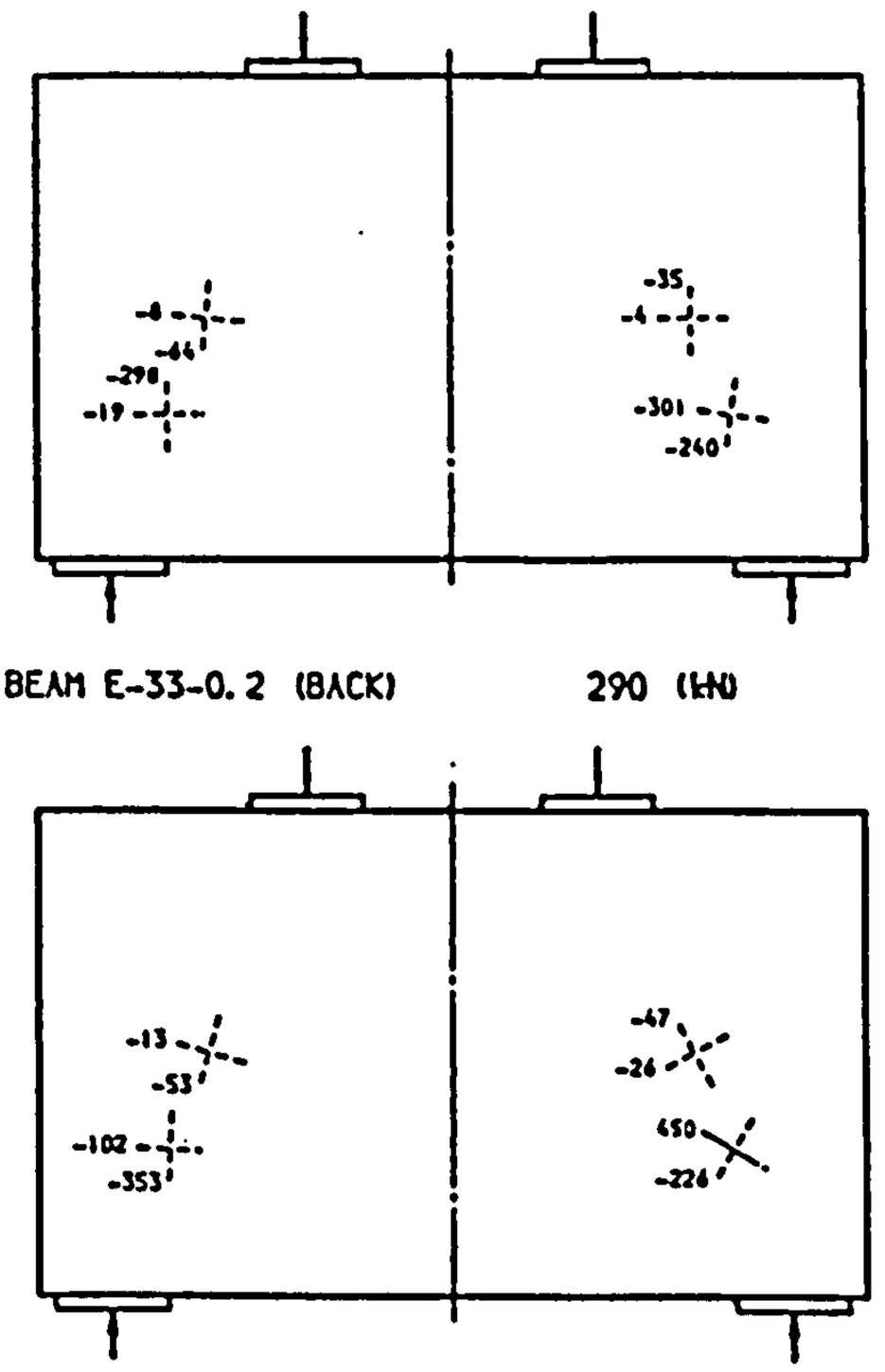

—— Tension Positive
---- Compression Negative

(All figures are in N/mm^2)

Figure 6.35 : Principal stresses after the last load increments (E-Series beams, theory of elasticity) [cont'd]

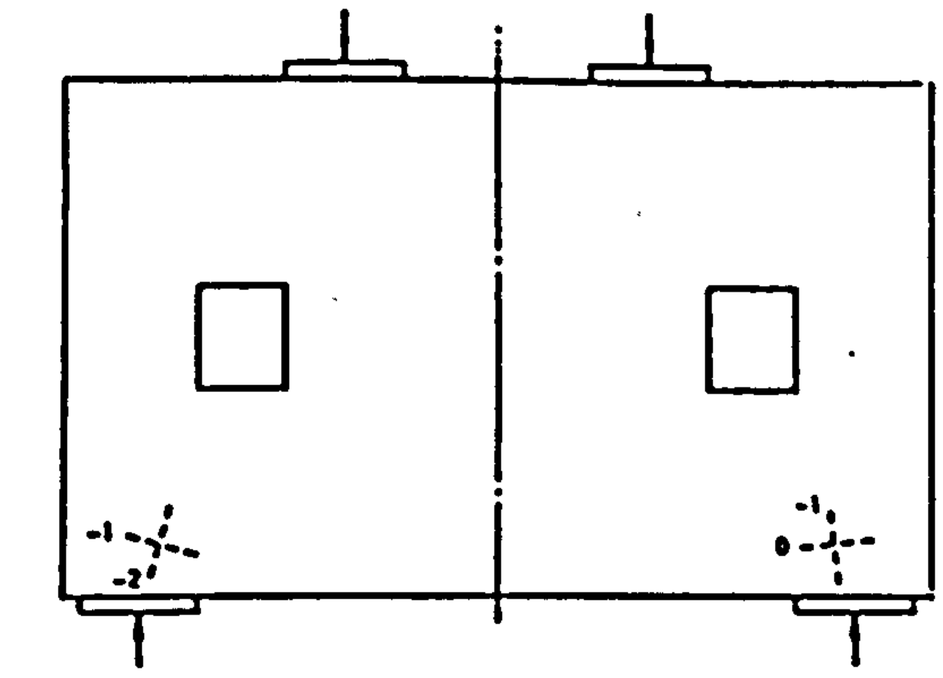

Figure 6.36 : Principal stresses after the first load increments (W-Series beams, theory of elasticity)

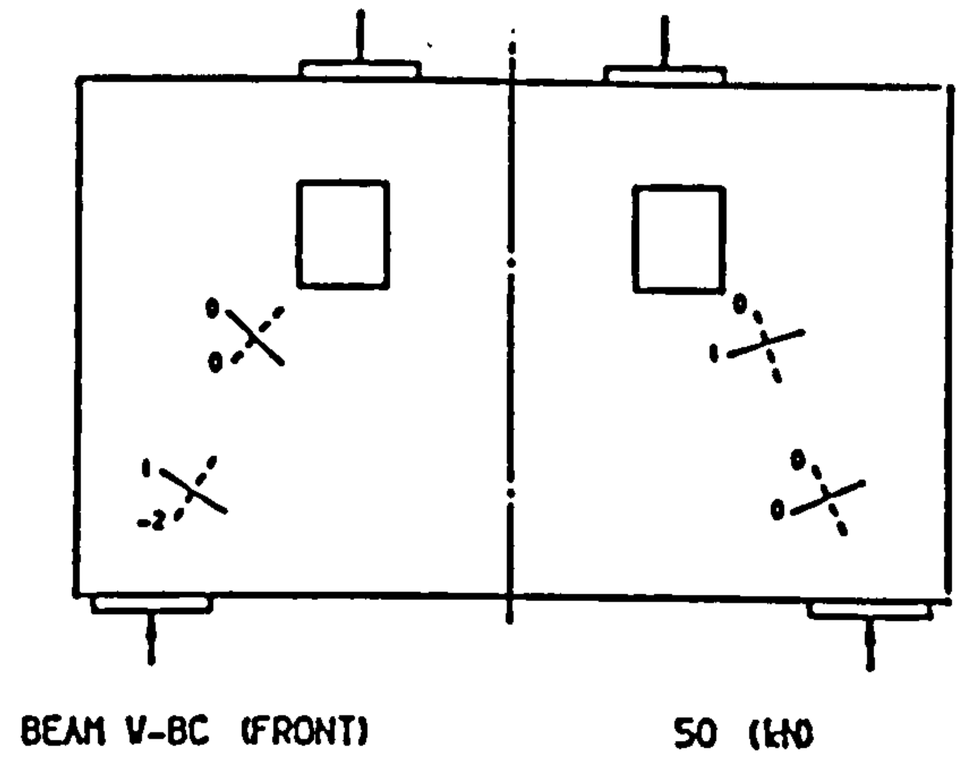

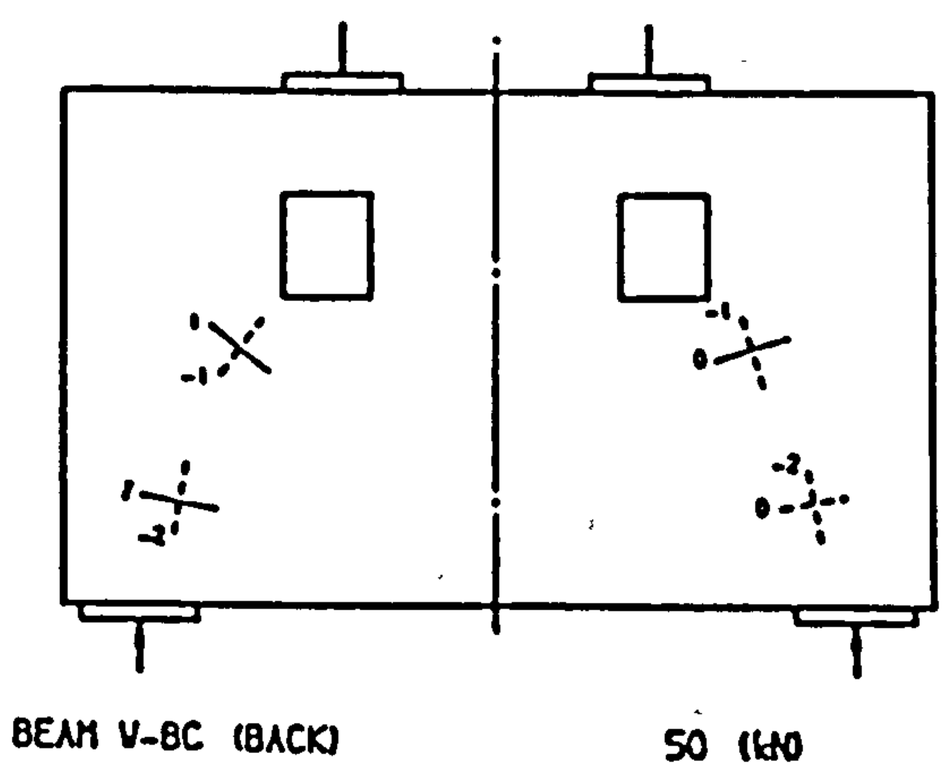

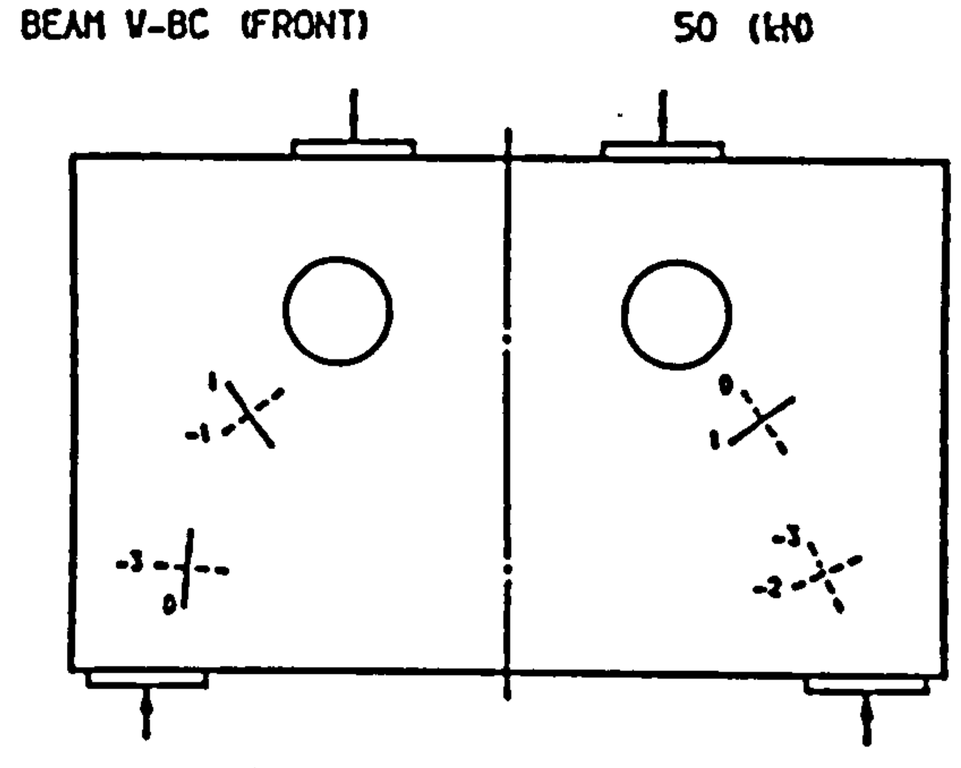

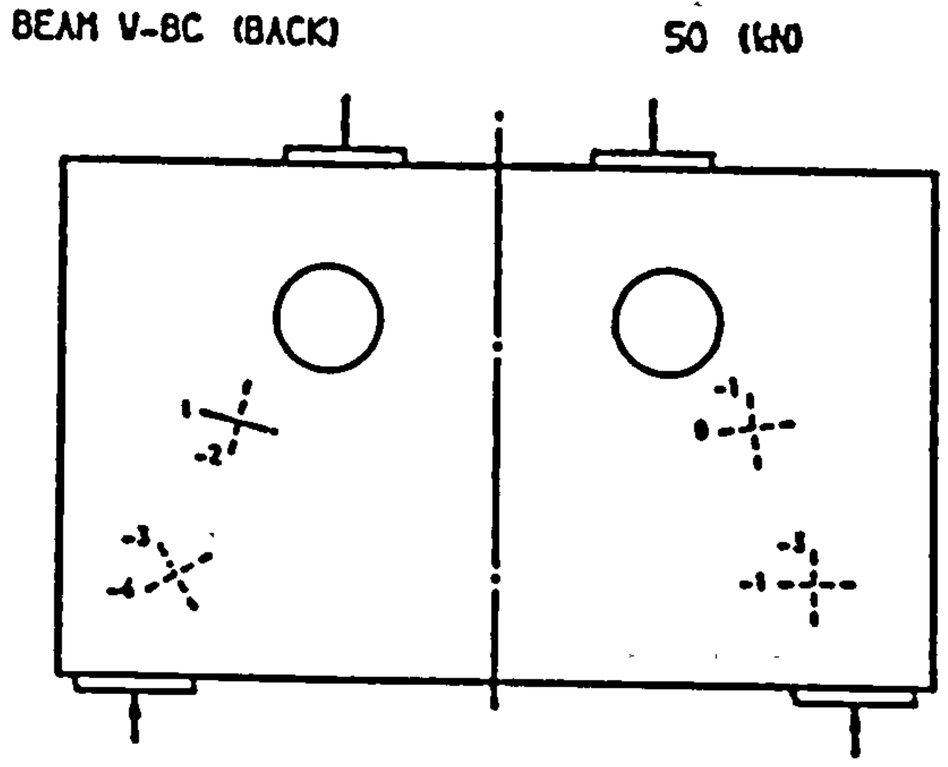

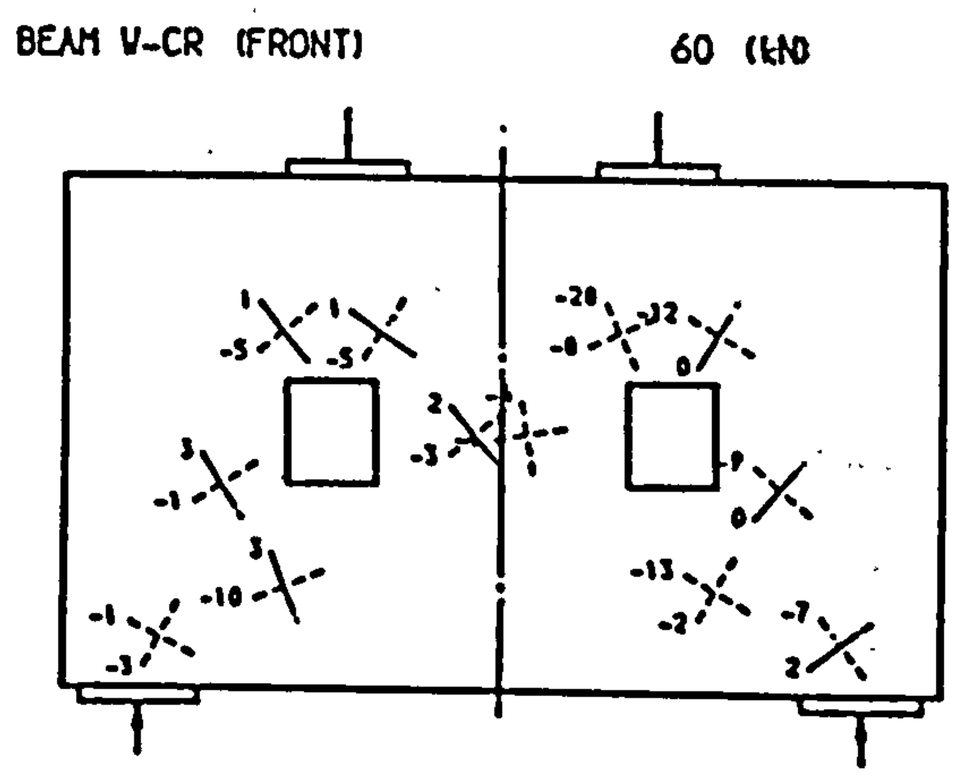

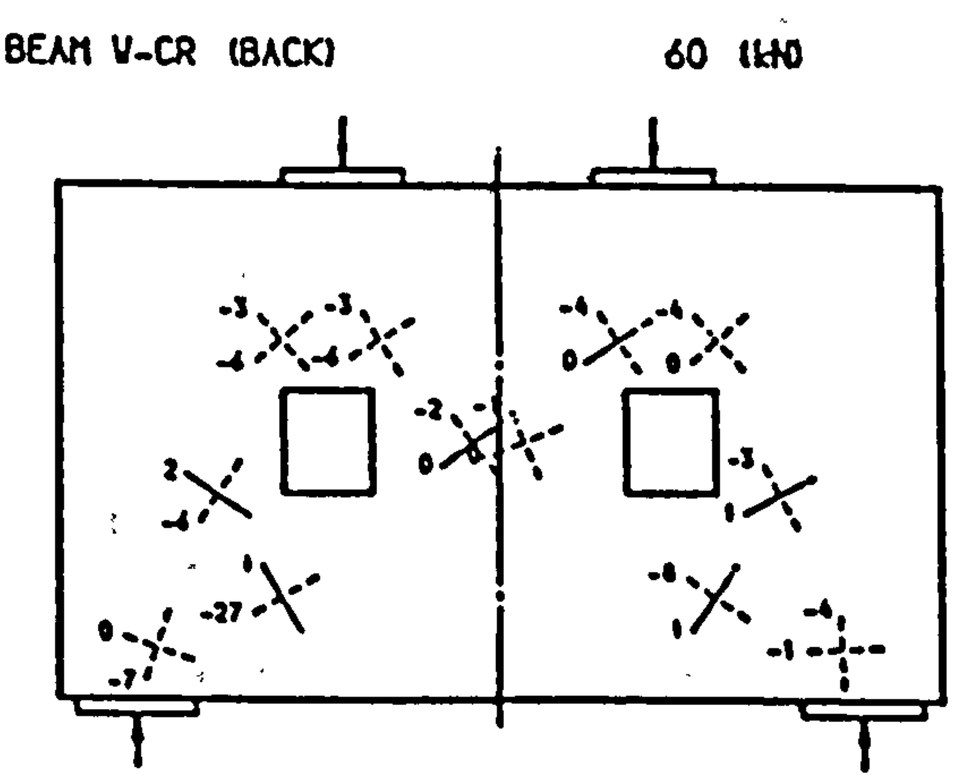

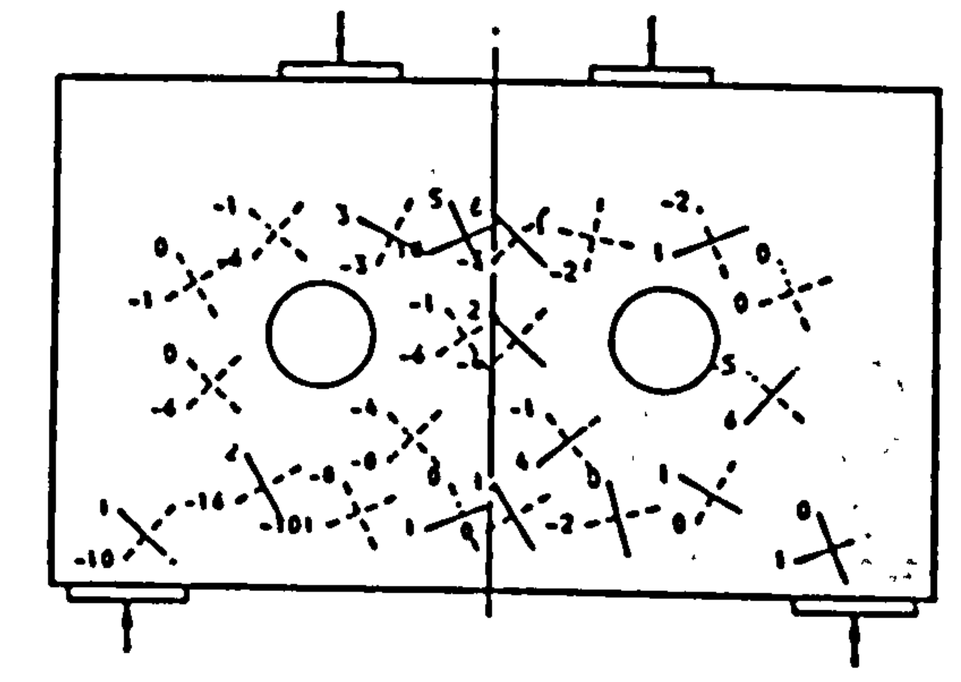

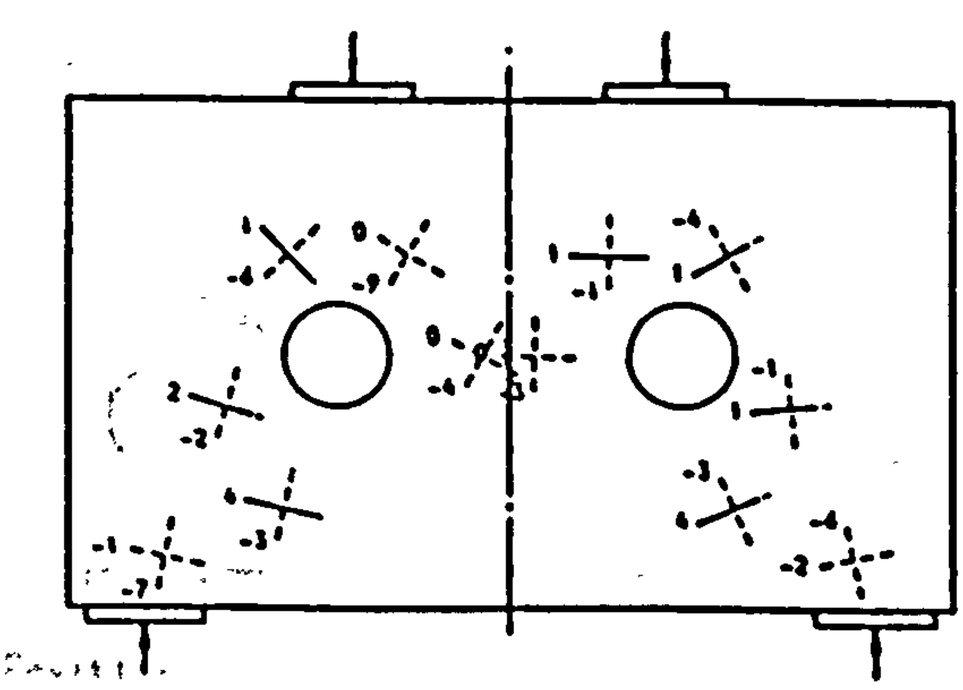

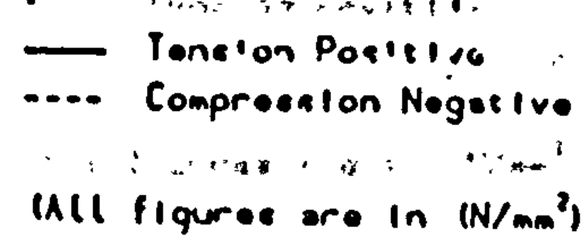

Figure 6.36 : Principal stresses after the first load increments (W-Series beams, theory of elasticity) [cont'd]

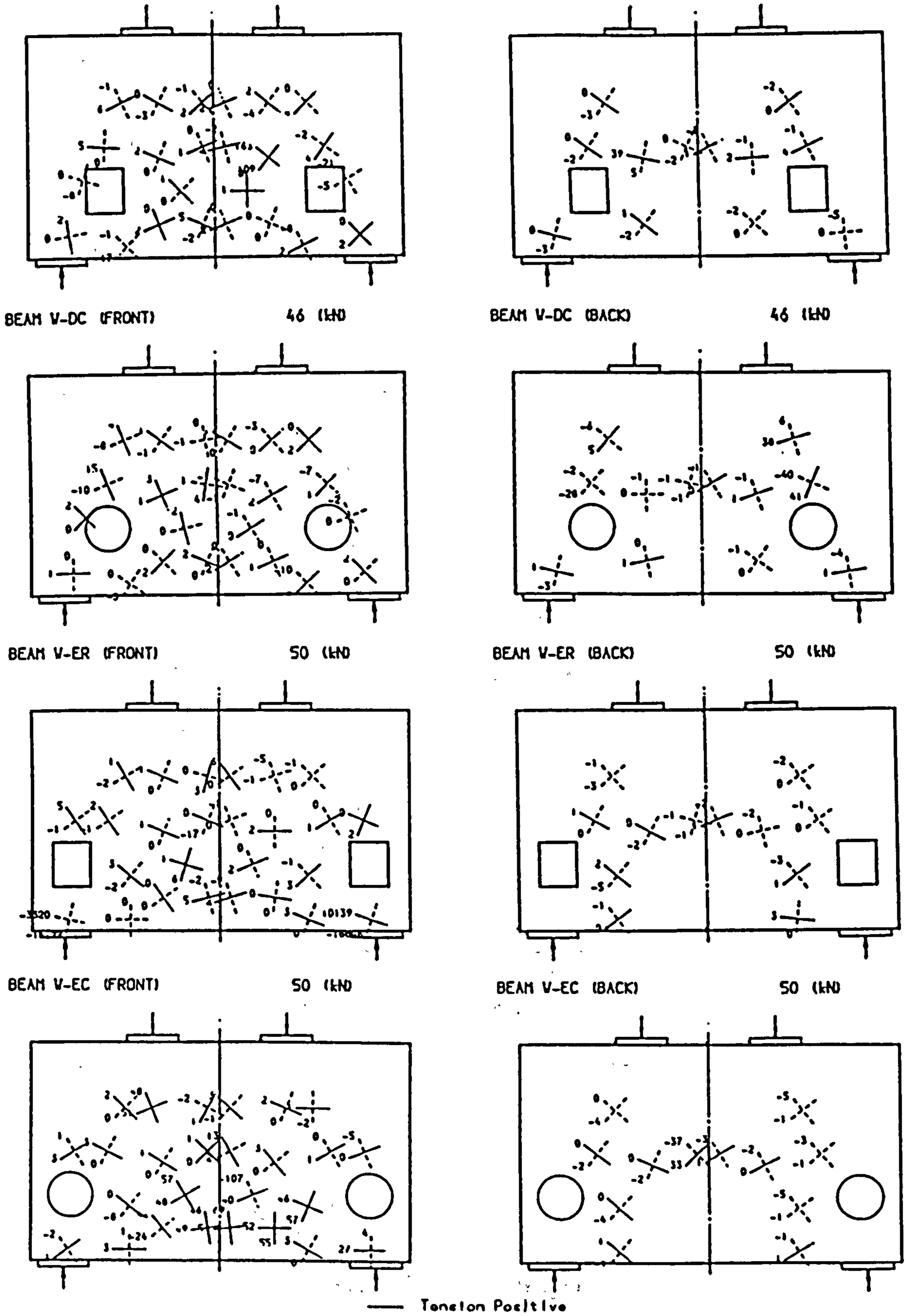

Figure 6.36 : Principal stresses after the first load increments (W-Series beams, theory of elasticity) [cont'd]

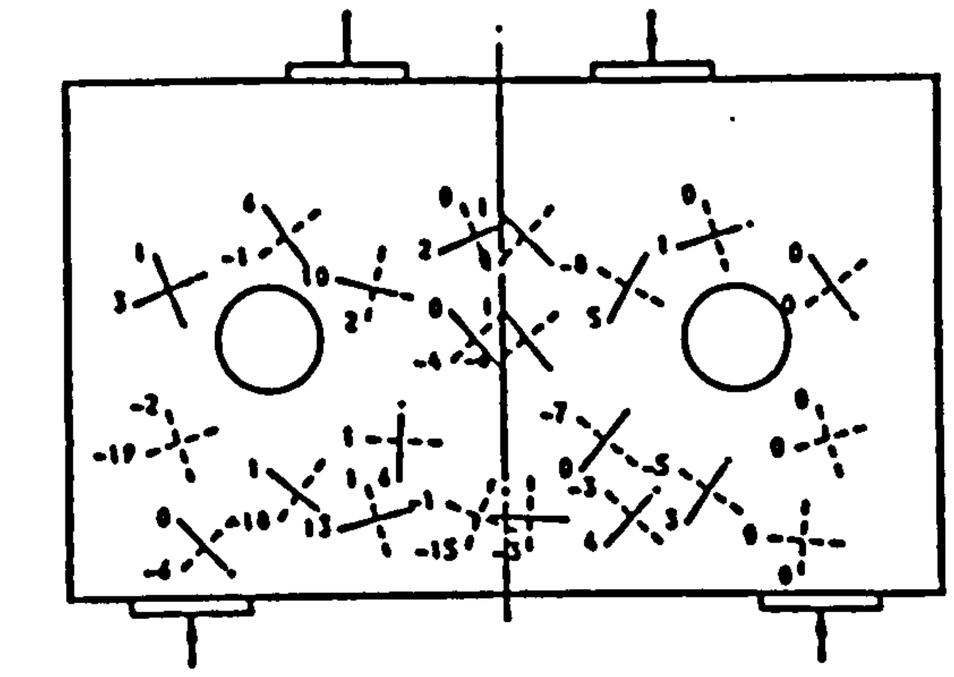

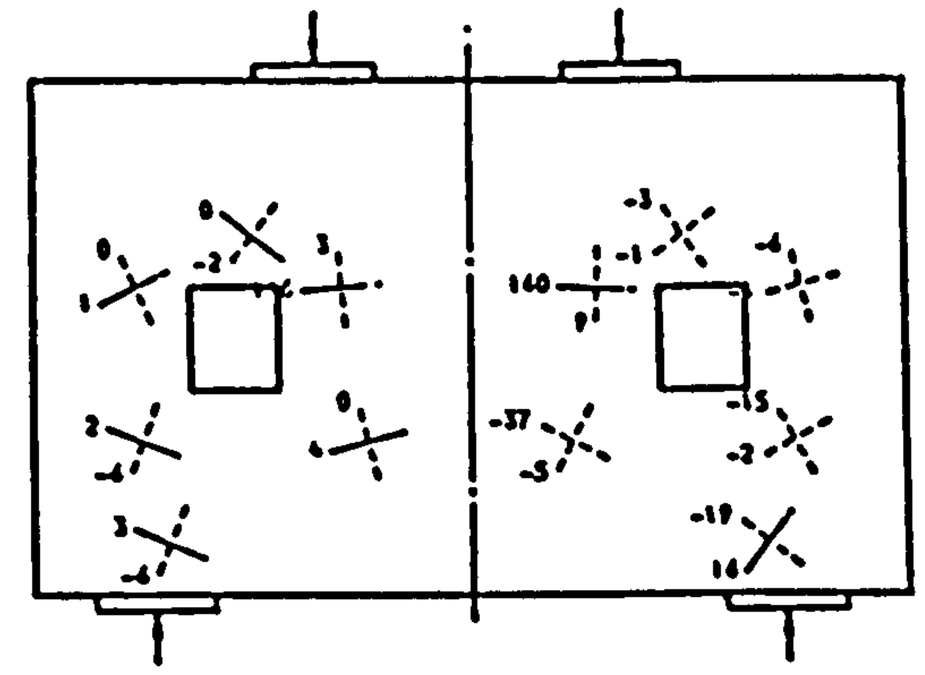

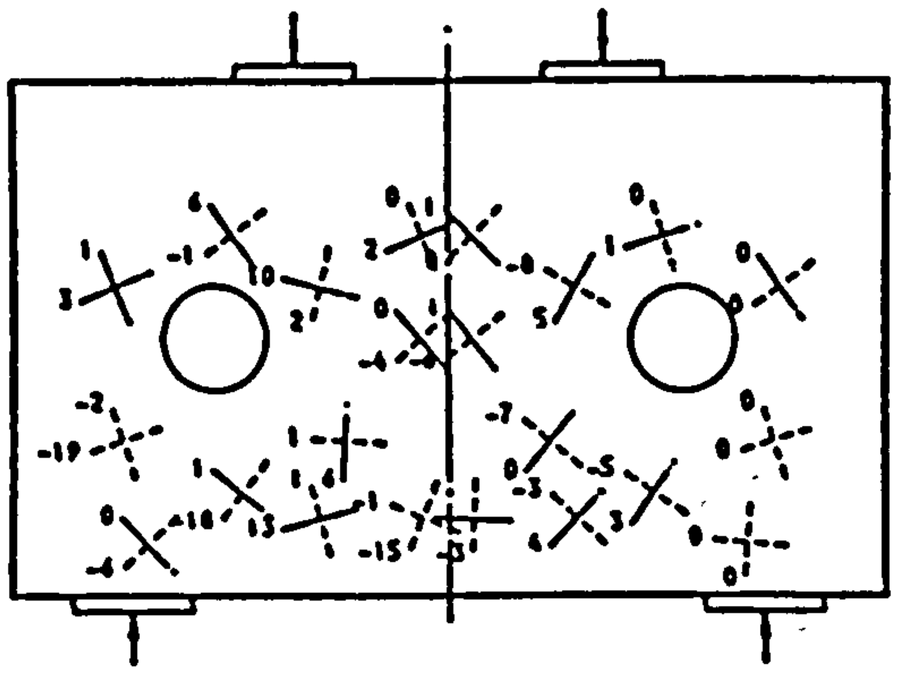

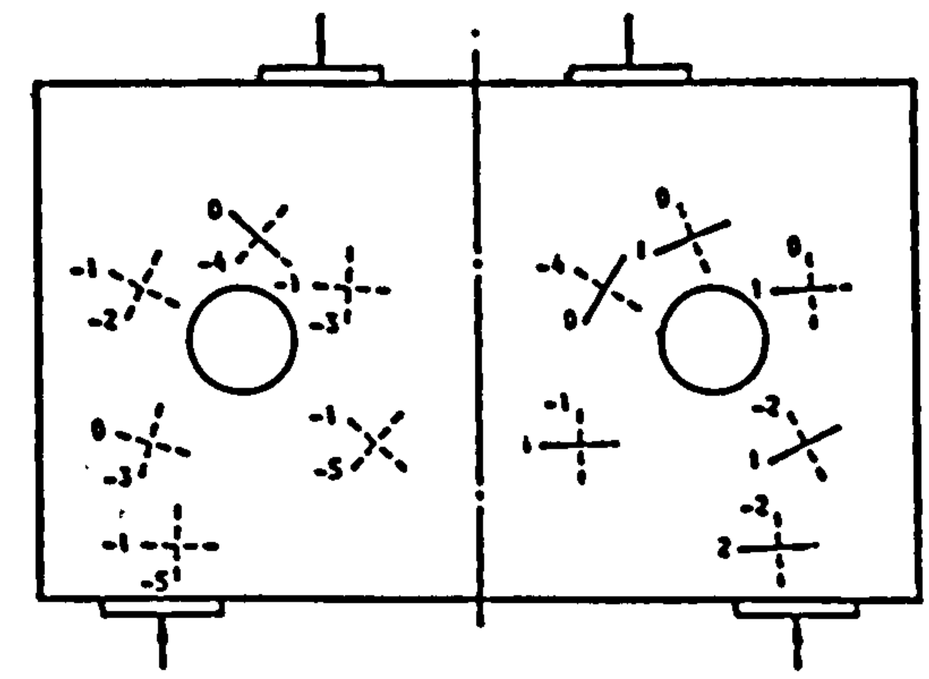

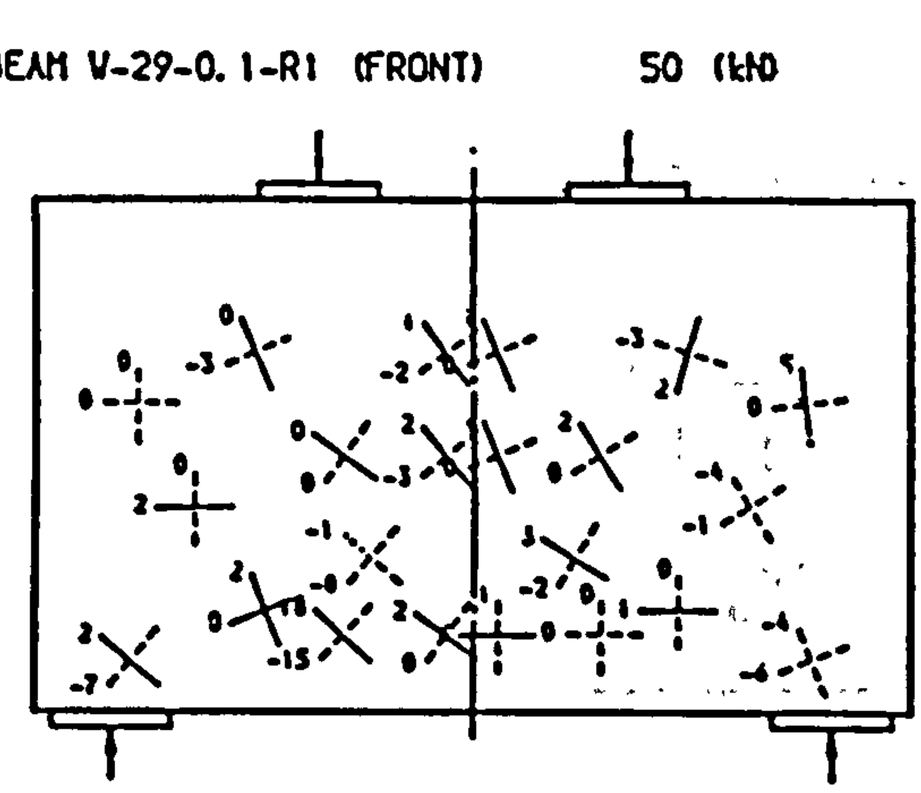

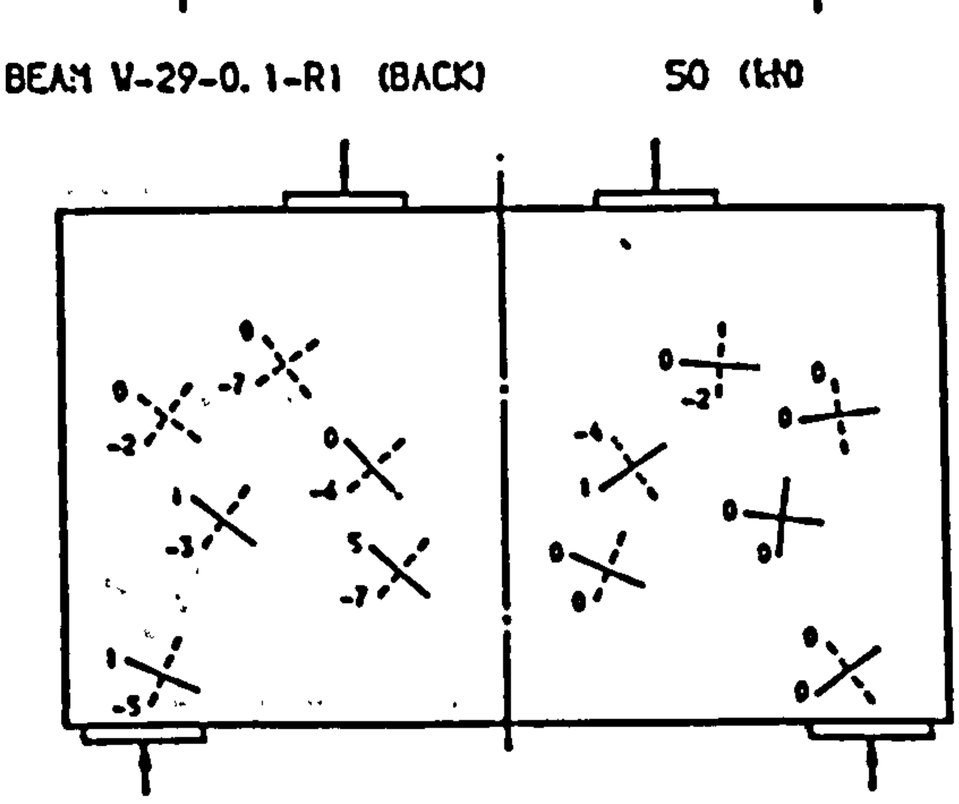

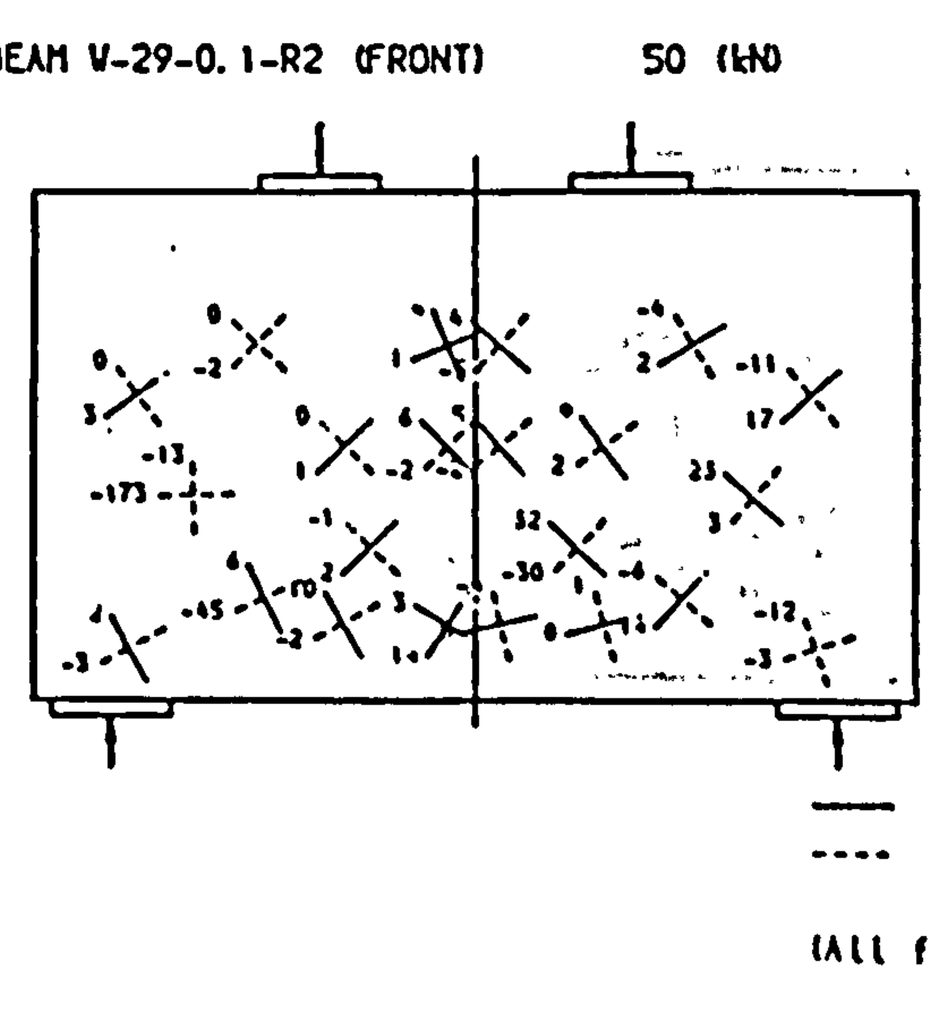

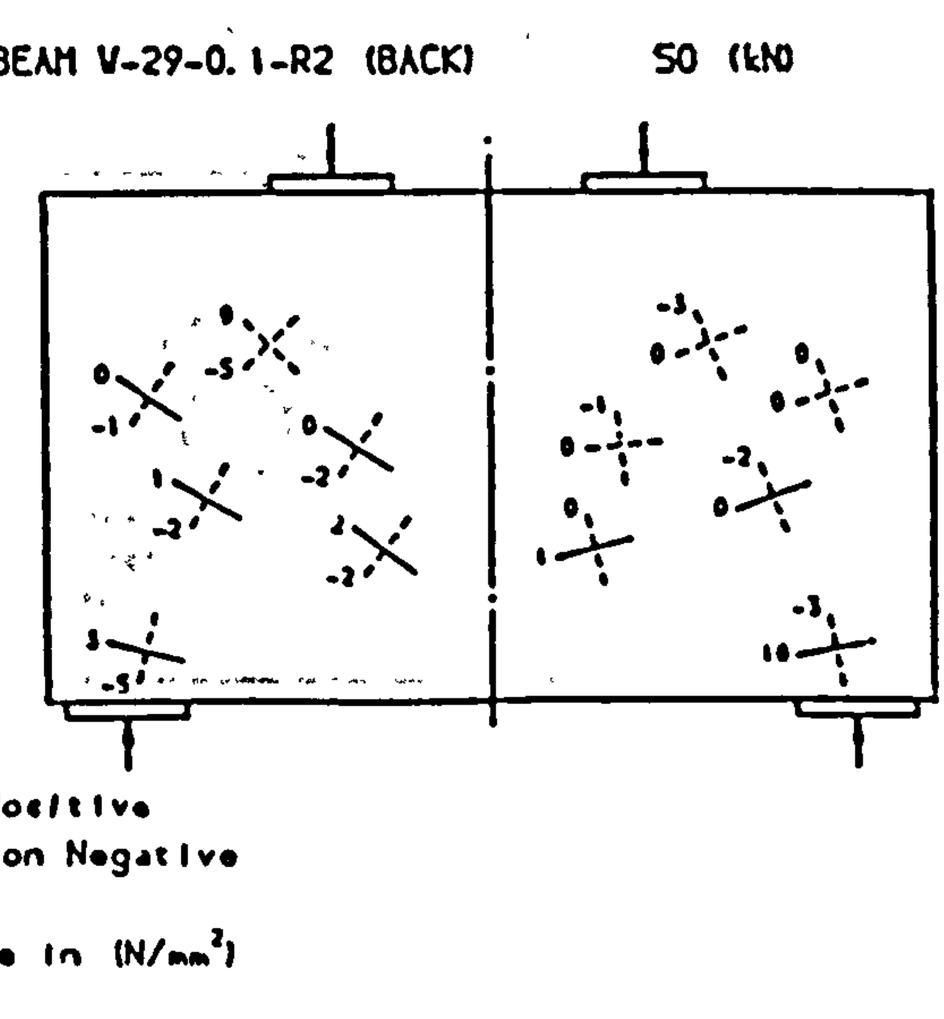

Figure 6.36 : Principal stresses after the first load increments (W-Series beams, theory of elasticity) [cont'd]

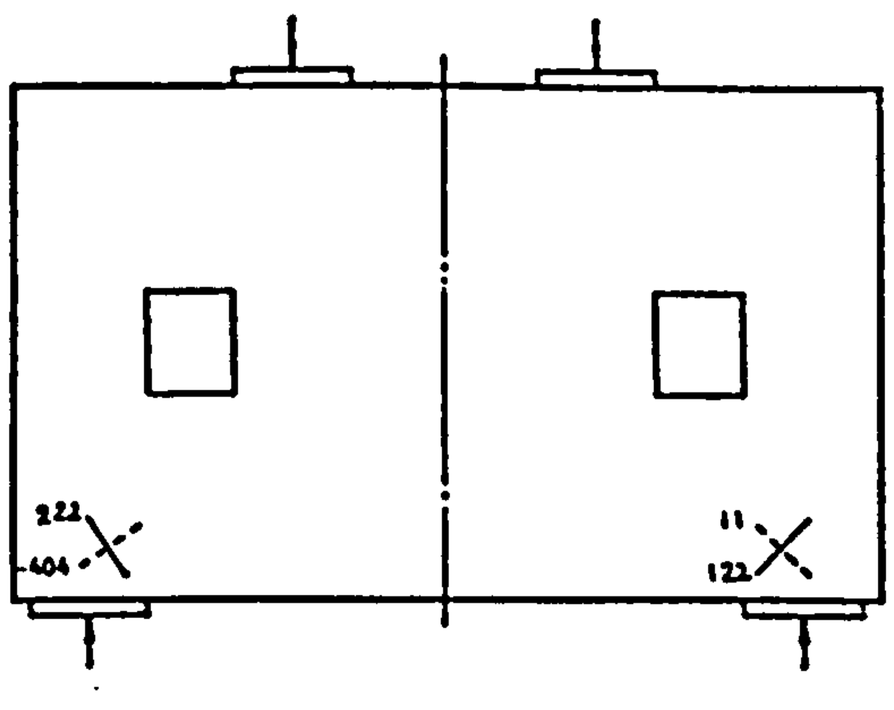

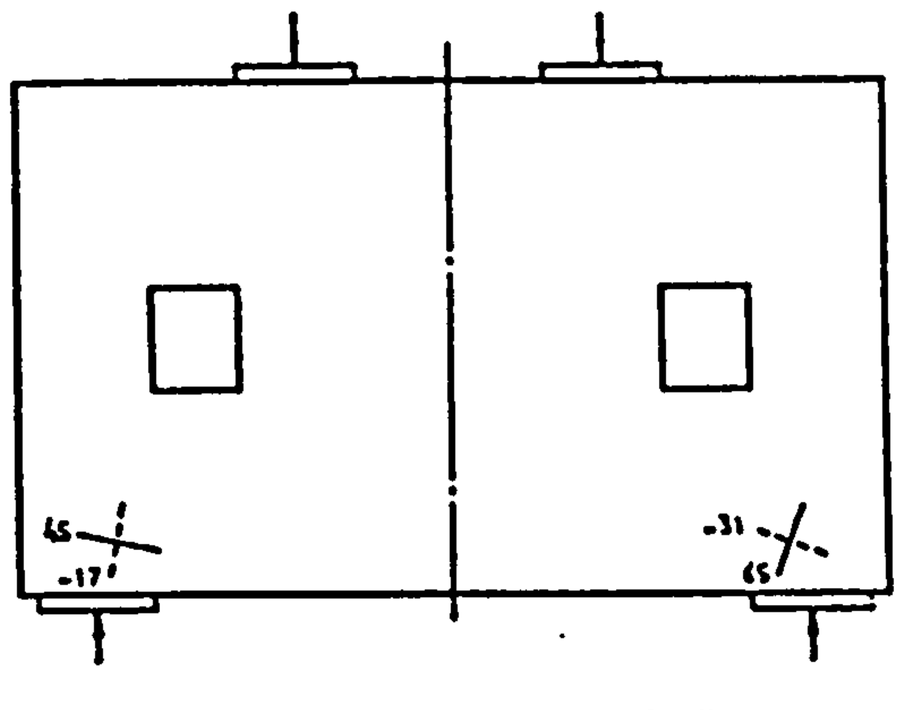

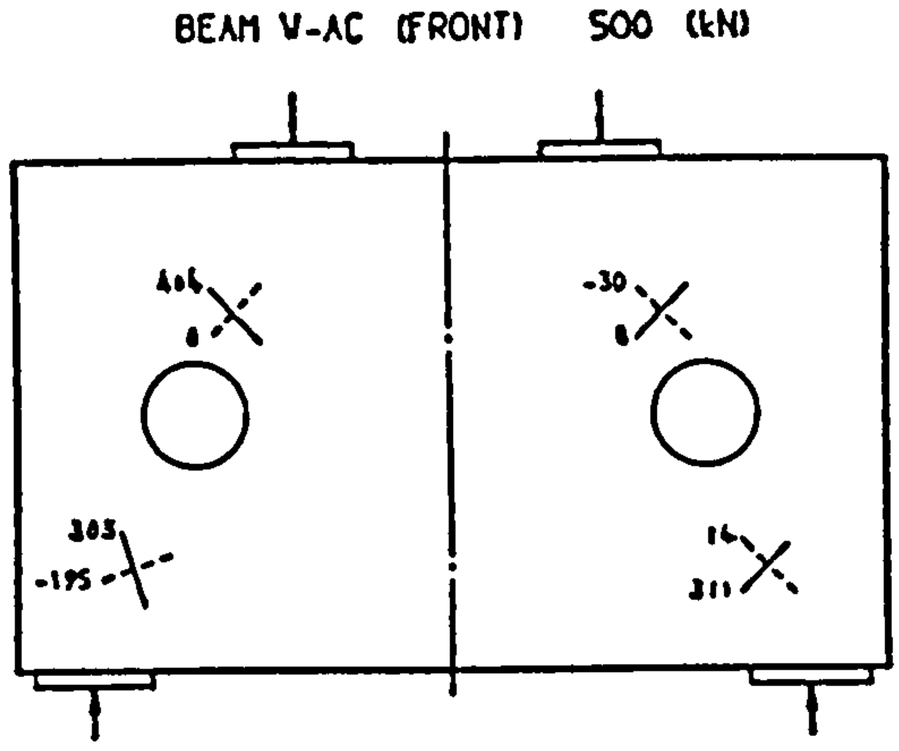

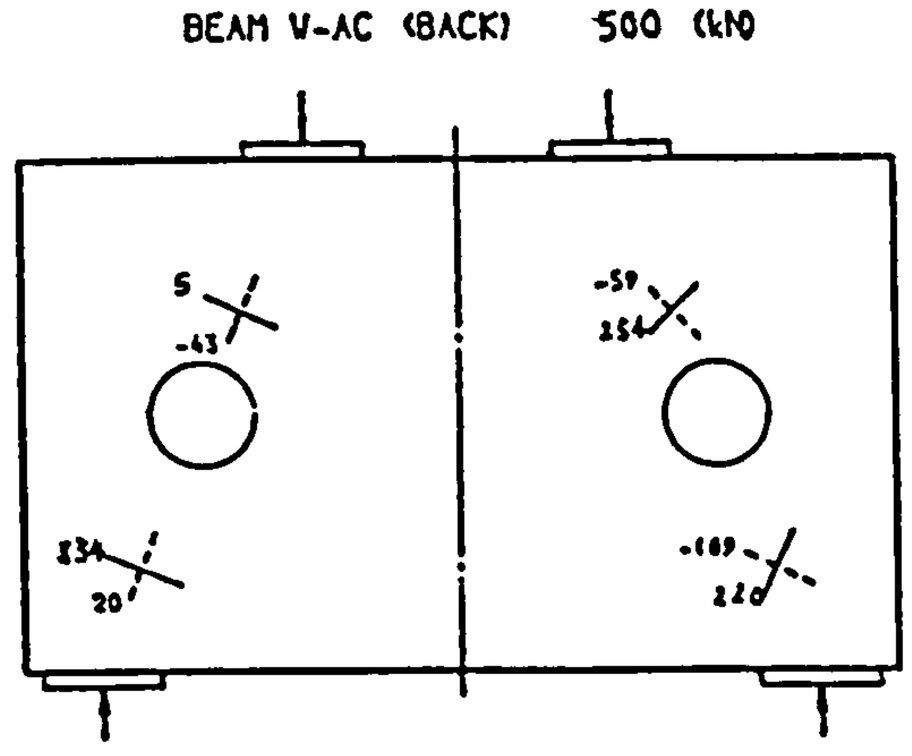

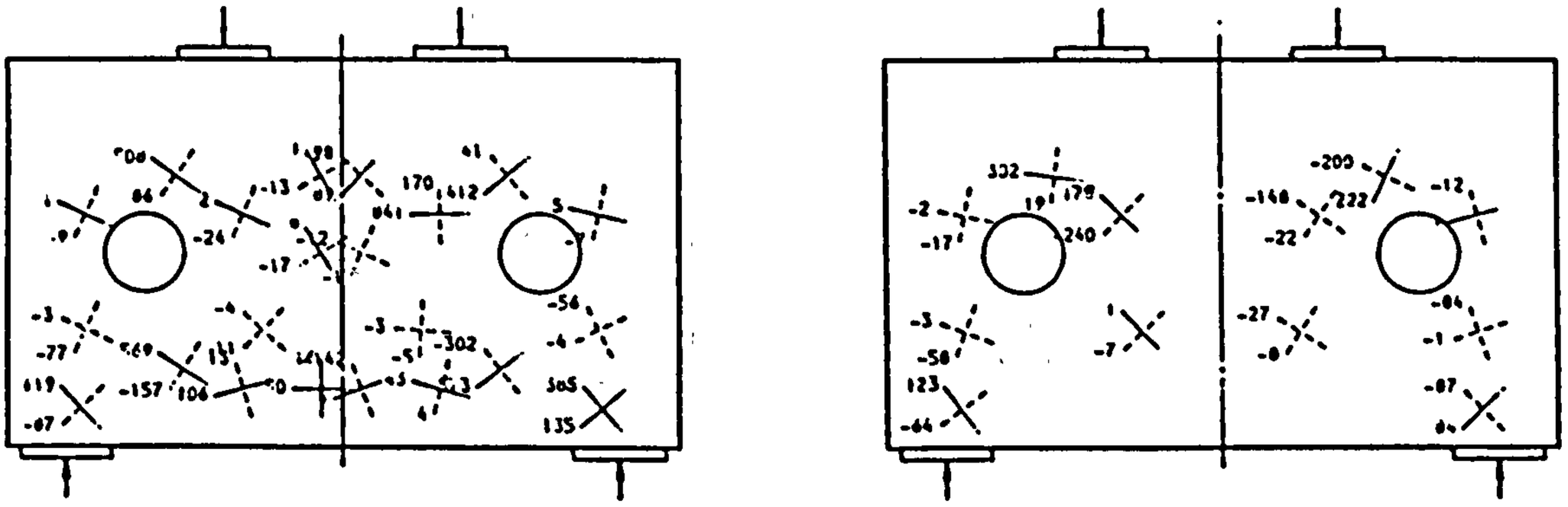

Figure 6.37 : Principal stresses after the last load increments (W-Series beams, theory of elasticity)

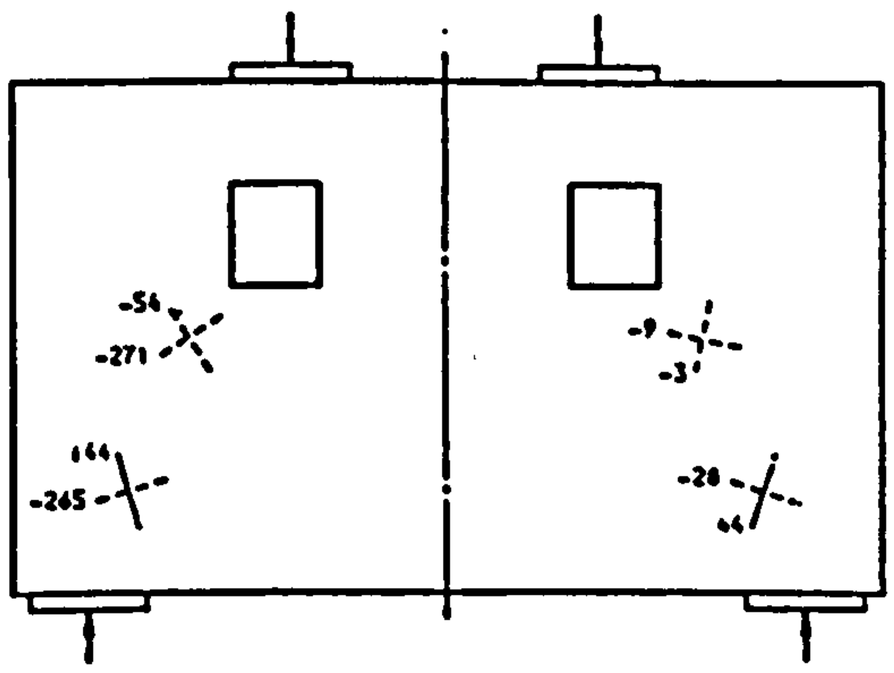

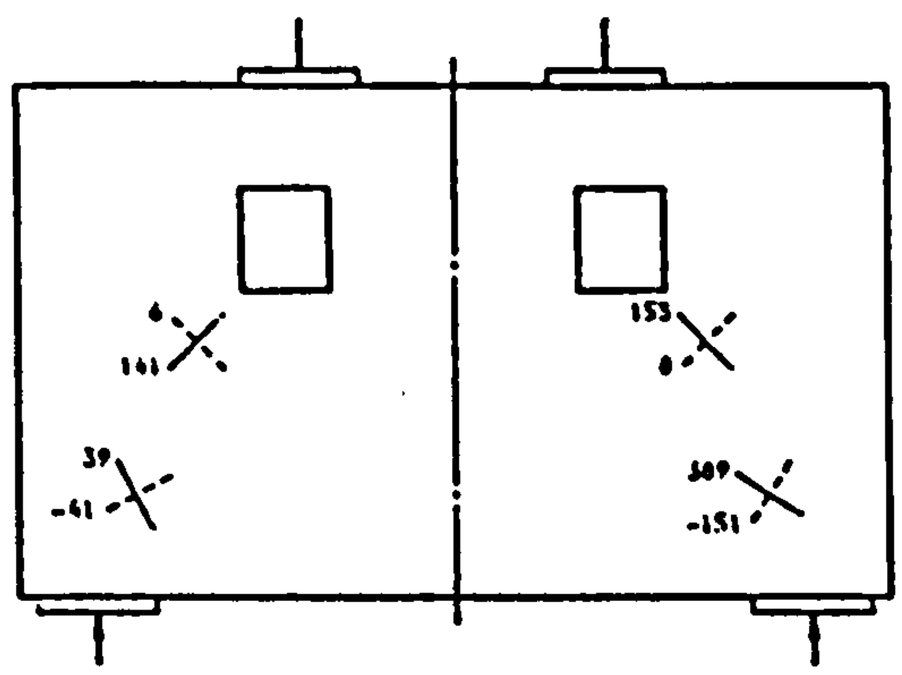

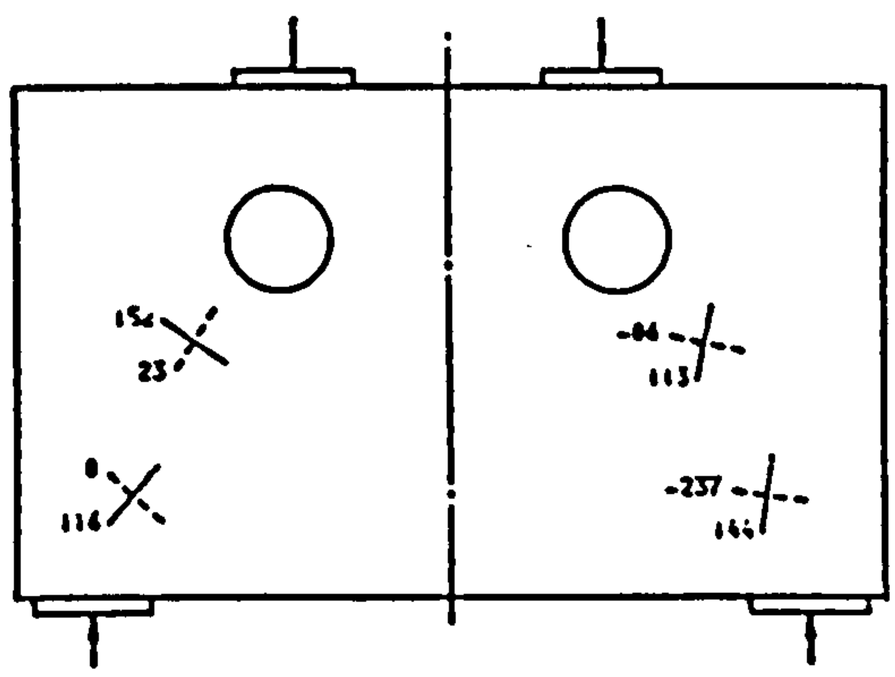

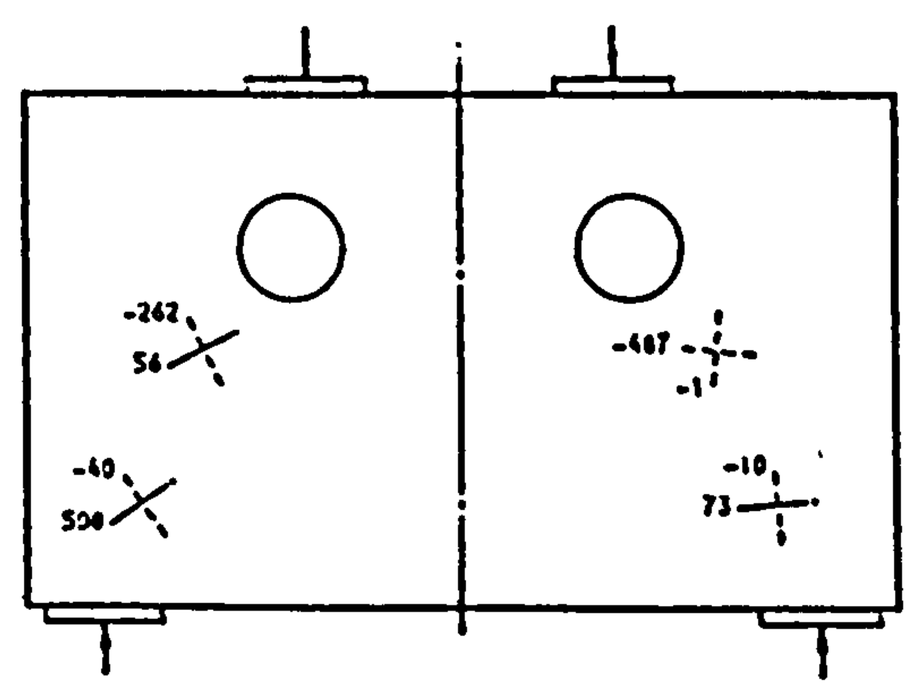

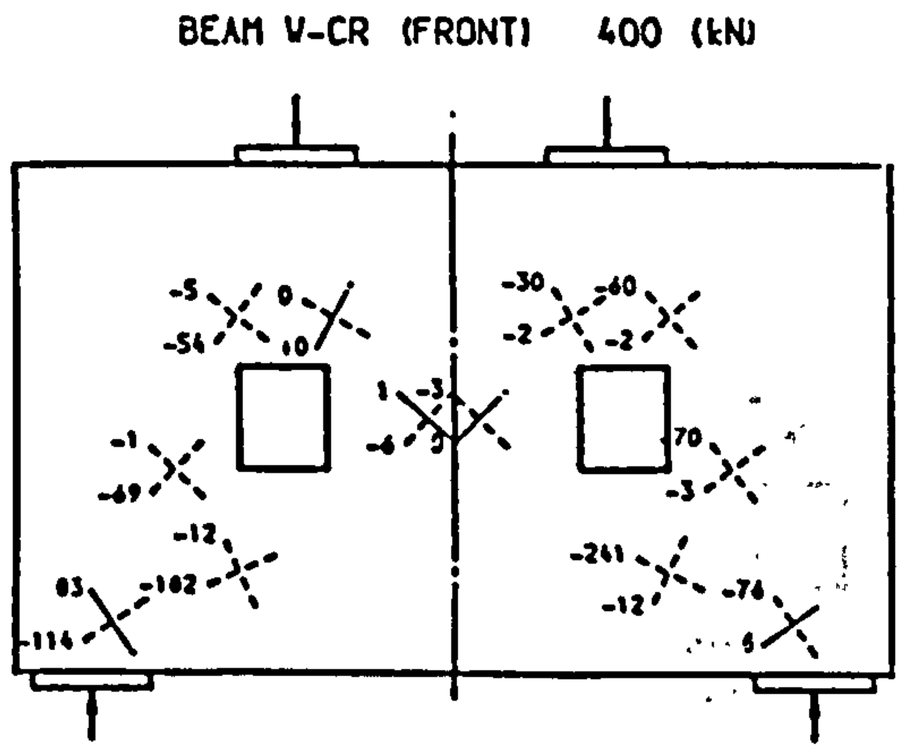

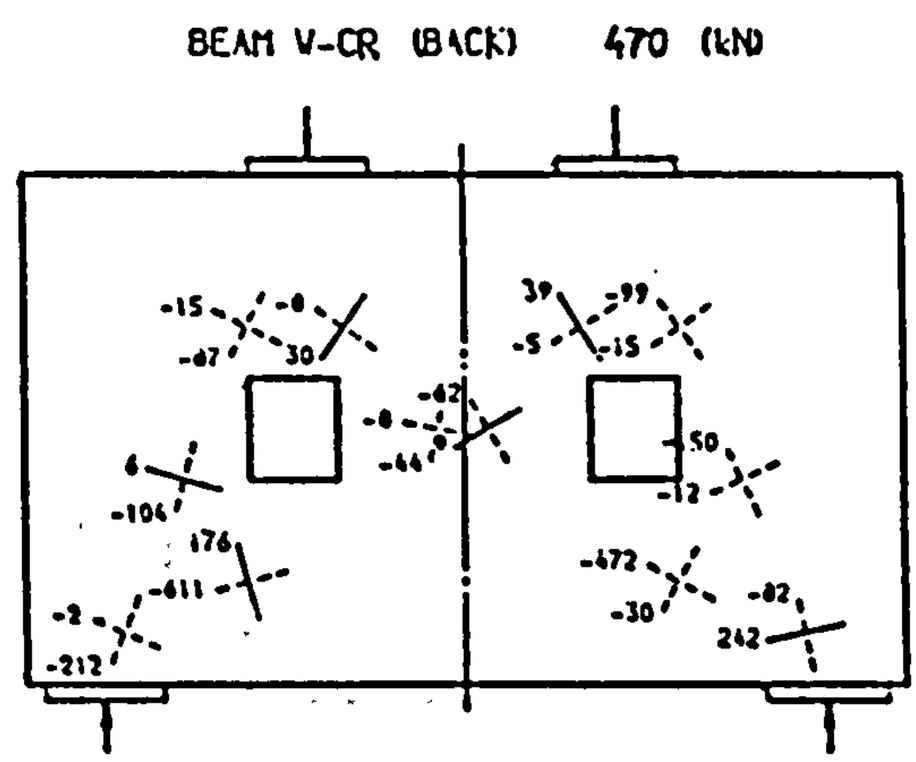

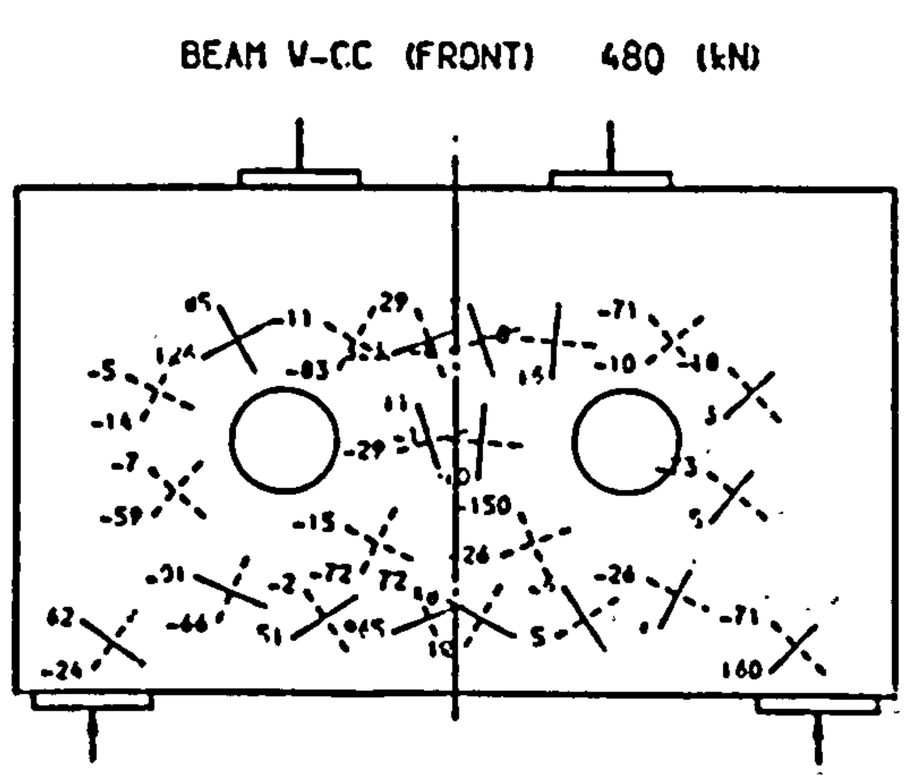

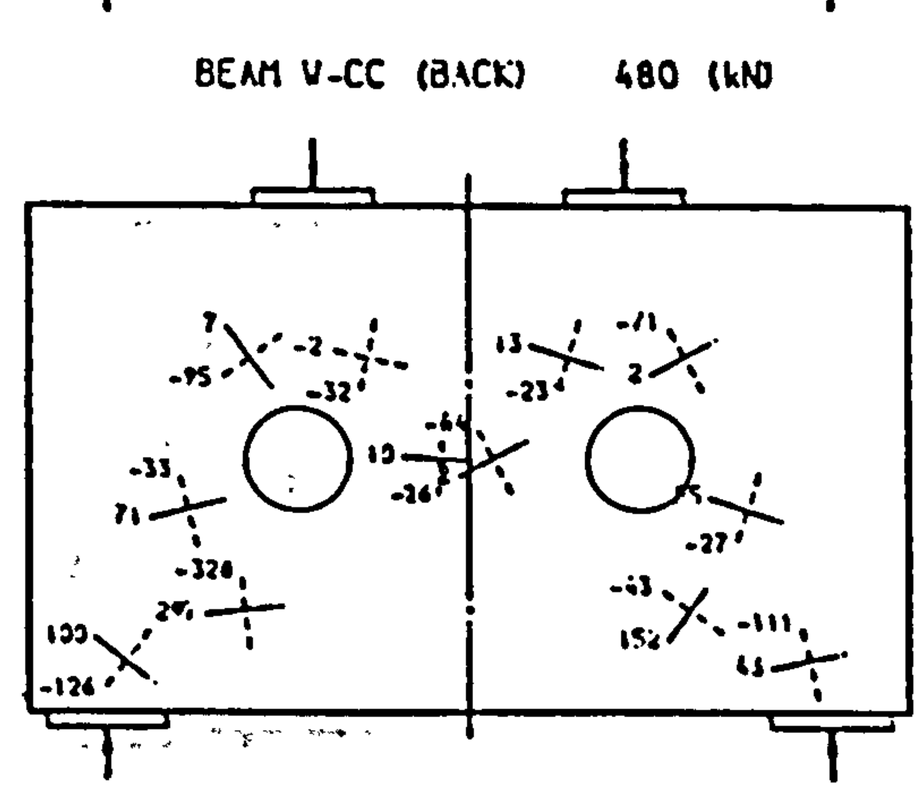

—— Tension Positive
---- Compression Negative

(All figures are in (N/mm^2)

Figure 6.37 : Principal stresses after the last load increments (W-Series beams, theory of elasticity) [cont'd]

BEAM V-DR (FRONT) 300 (kN)

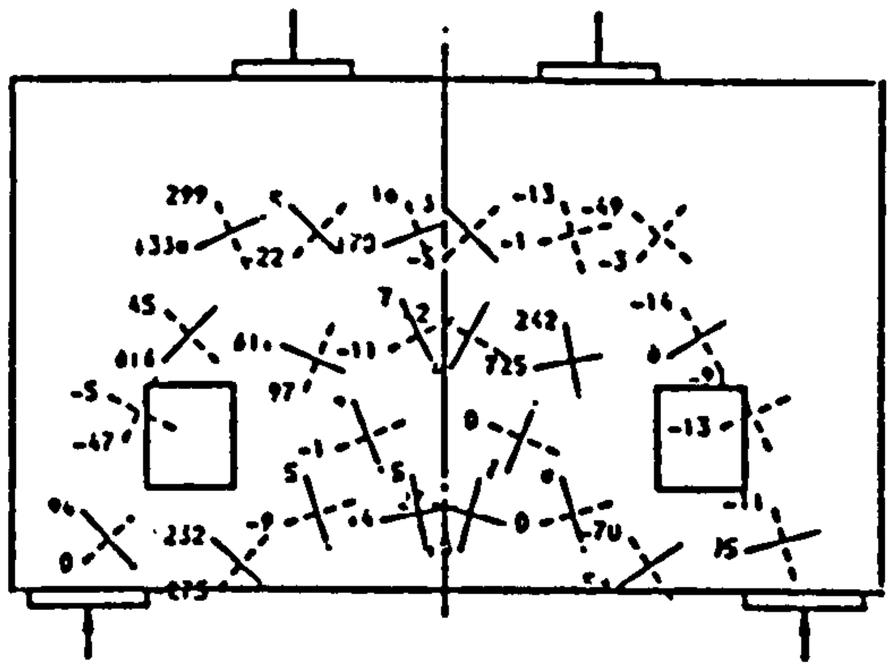

BEAM V-DR (BACK) 300 (kN)

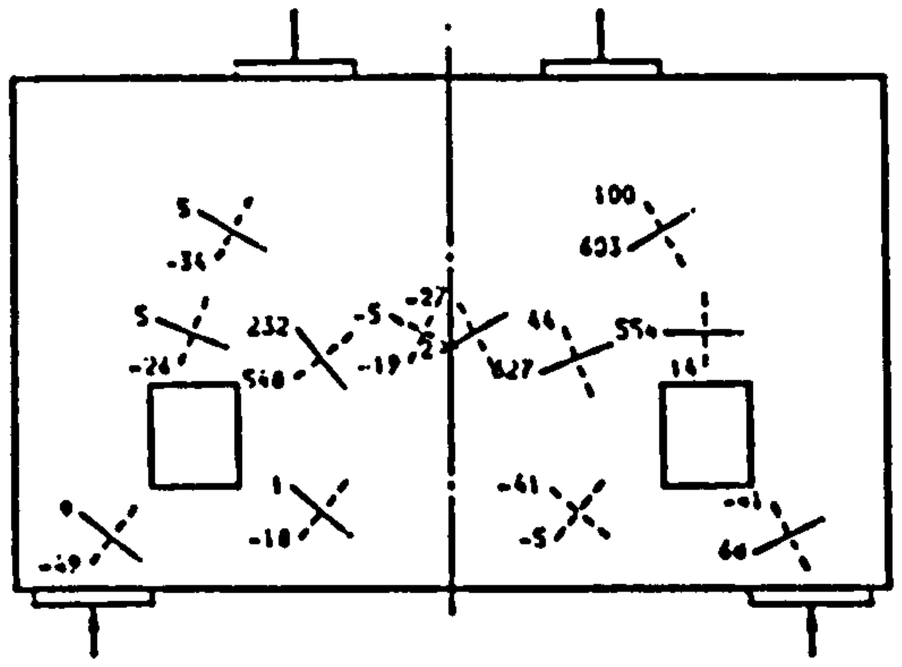

BEAM V-DC (FRONT) 350 (kN)

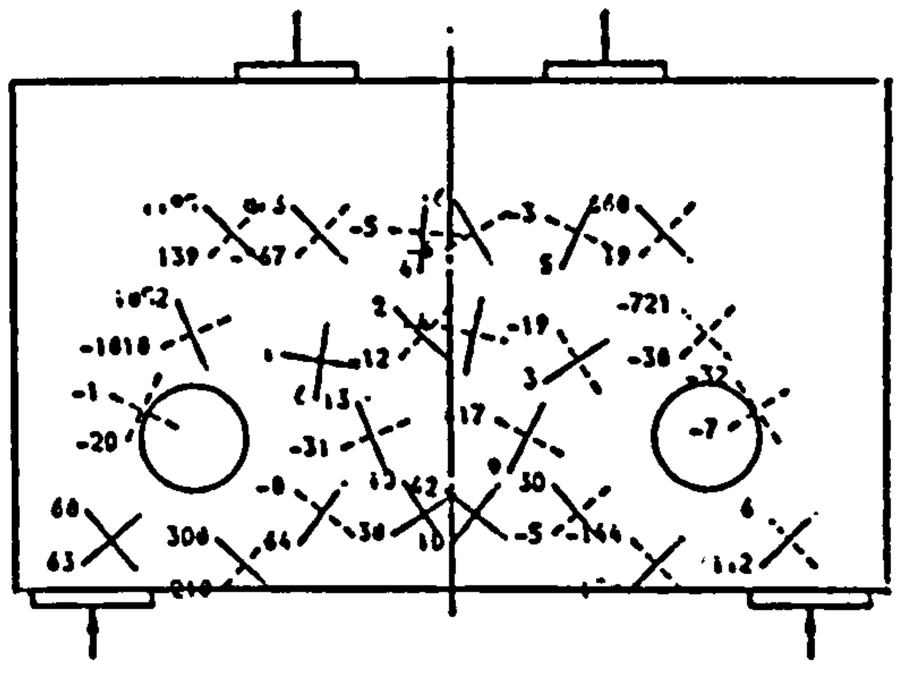

BEAM V-DC (BACK) 350 (kN)

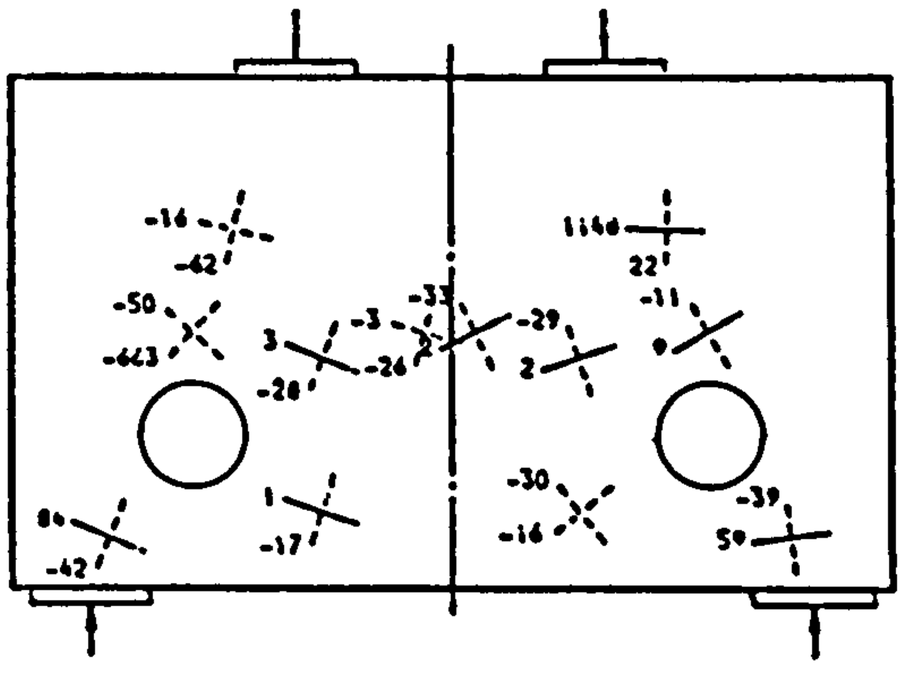

BEAM V-ER (FRONT) 300 (kN)

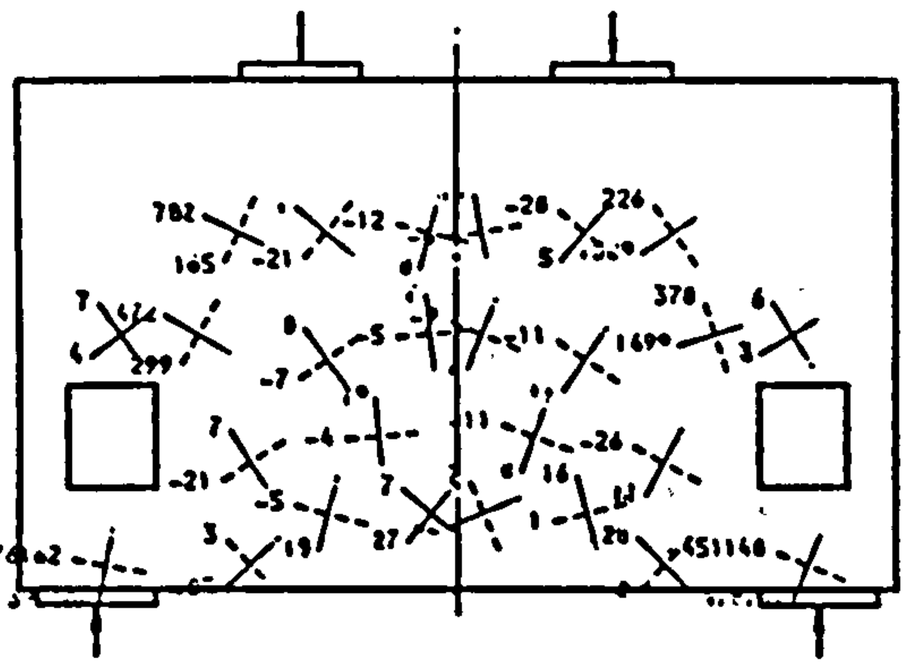

BEAM V-ER (BACK) 300 (kN)

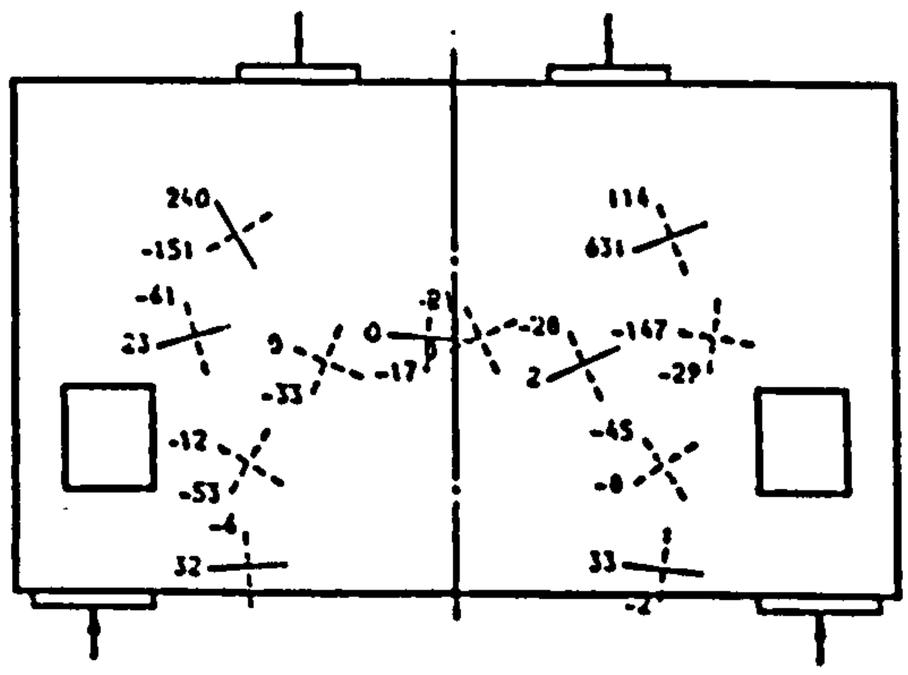

BEAM V-EC (FRONT) 350 (kN)

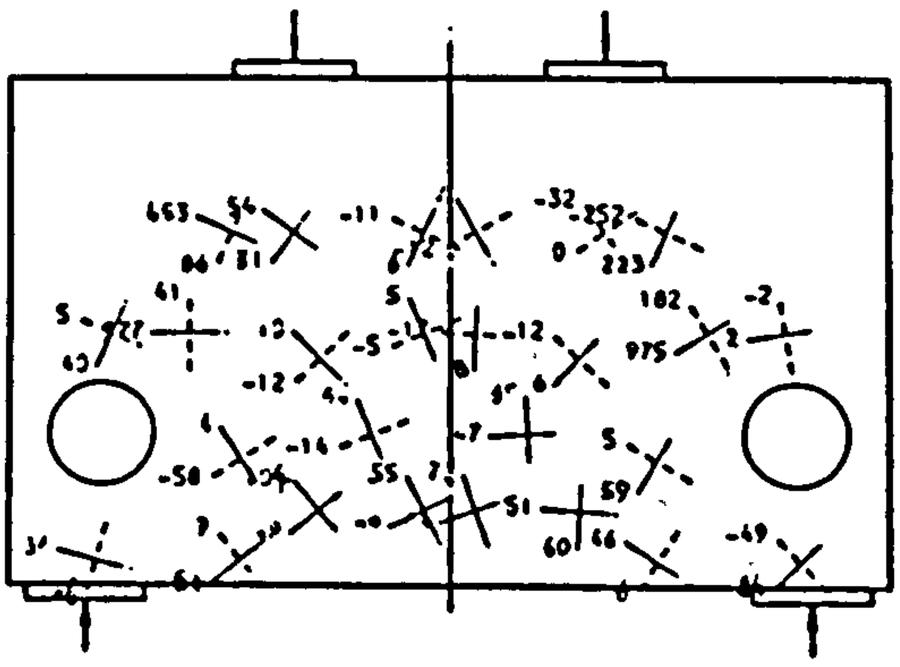

BEAM V-EC (BACK) 350 (kN)

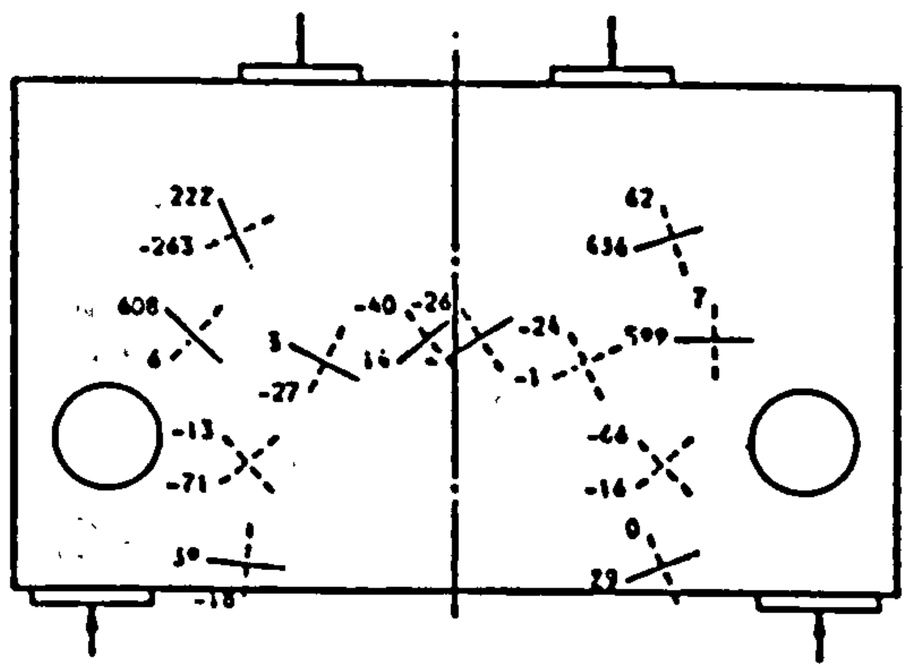

—— Tension Positive

---- Compression Negative

(All figures are in N/mm^2)

Figure 6.37 : Principal stresses after the last load increments (W-Series beams; theory of elasticity) [cont'd]

BEAM W-AR-S (FRONT) 320 (kN)

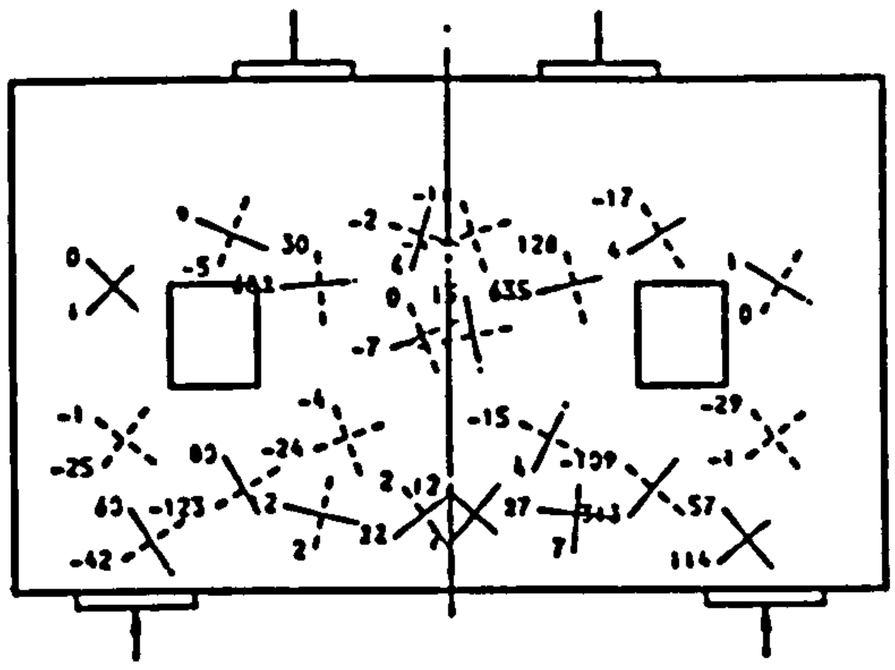

BEAM W-AR-S (BACK) 320 (kN)

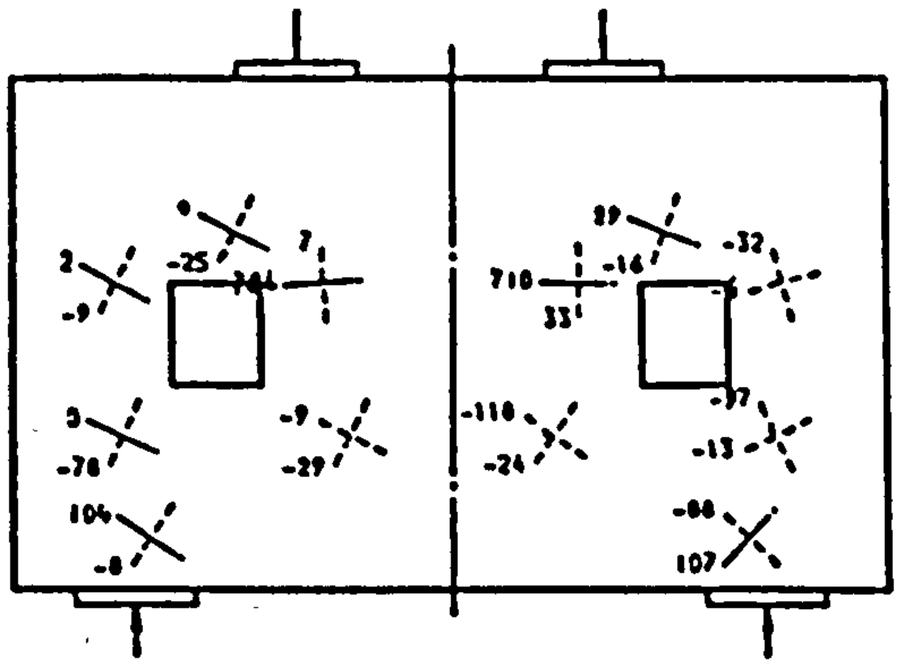

BEAM W-AC-S (FRONT) 460 (kN)

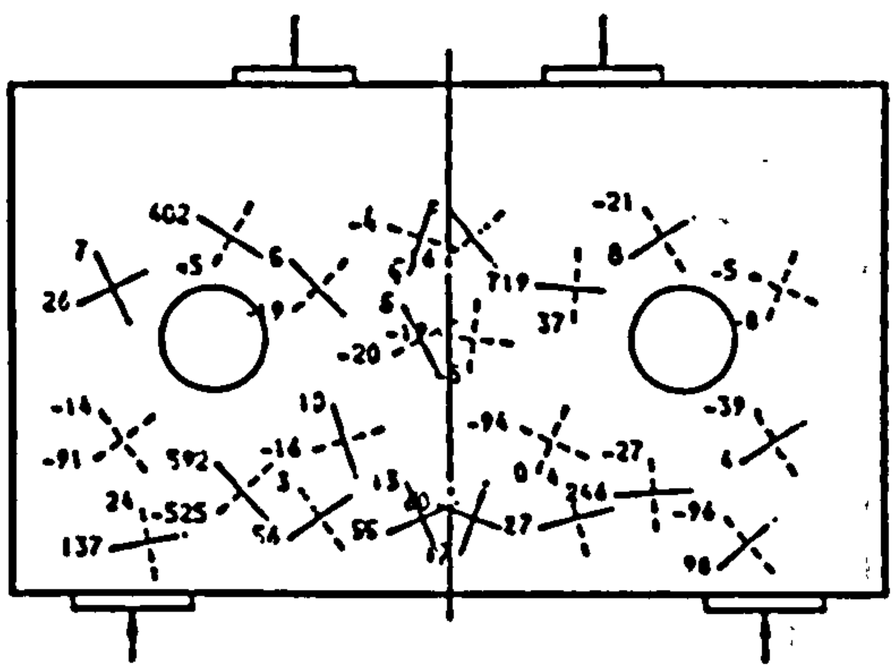

BEAM W-AC-S (BACK) 460 (kN)

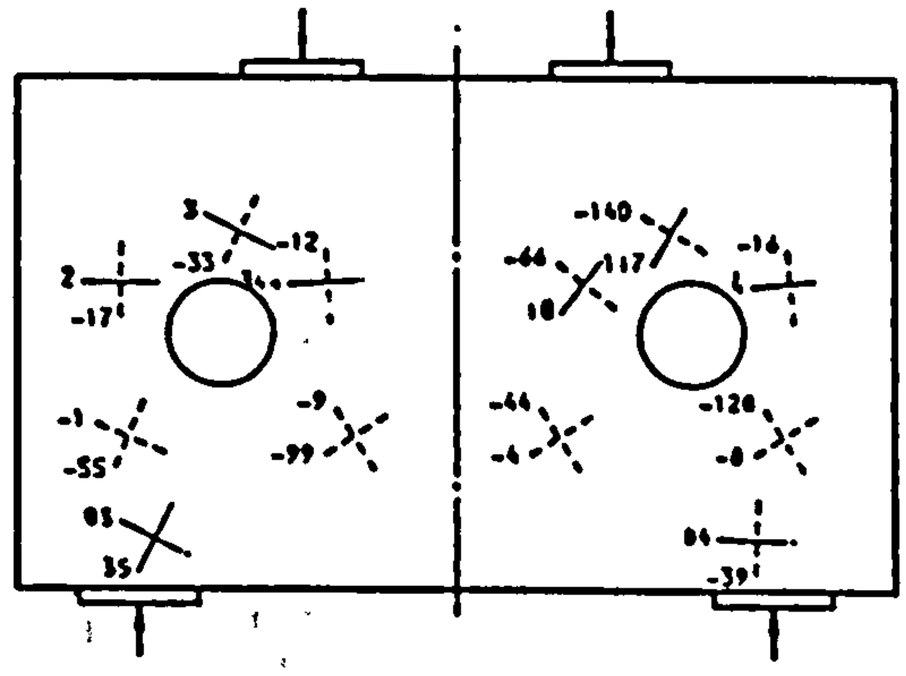

BEAM W-29-0.1-R1 (FRONT) 520 (kN)

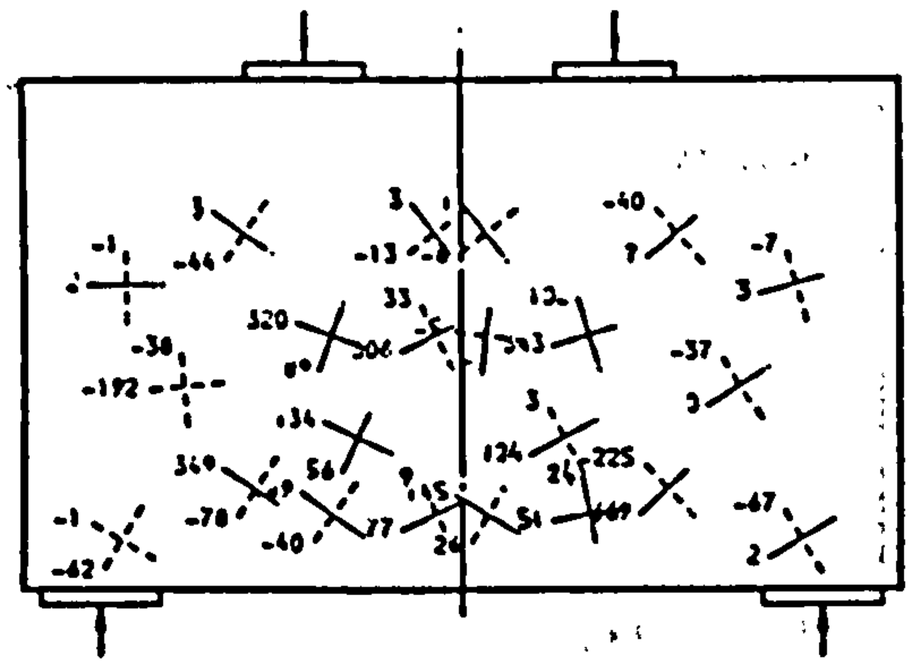

BEAM W-29-0.1-R1 (BACK) 660 (kN)

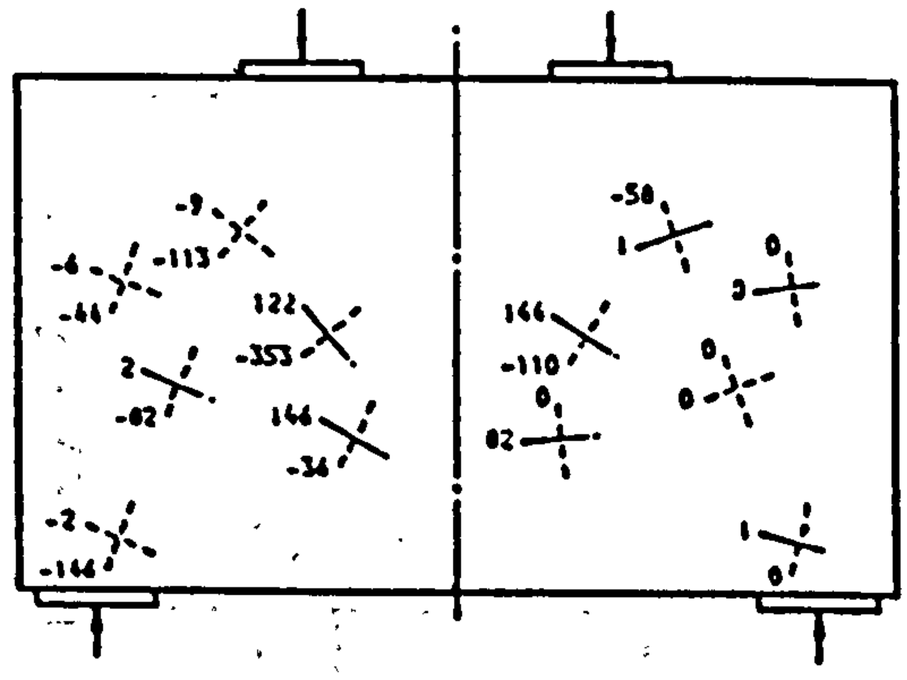

BEAM W-29-0.1-R2 (FRONT) 650 (kN)

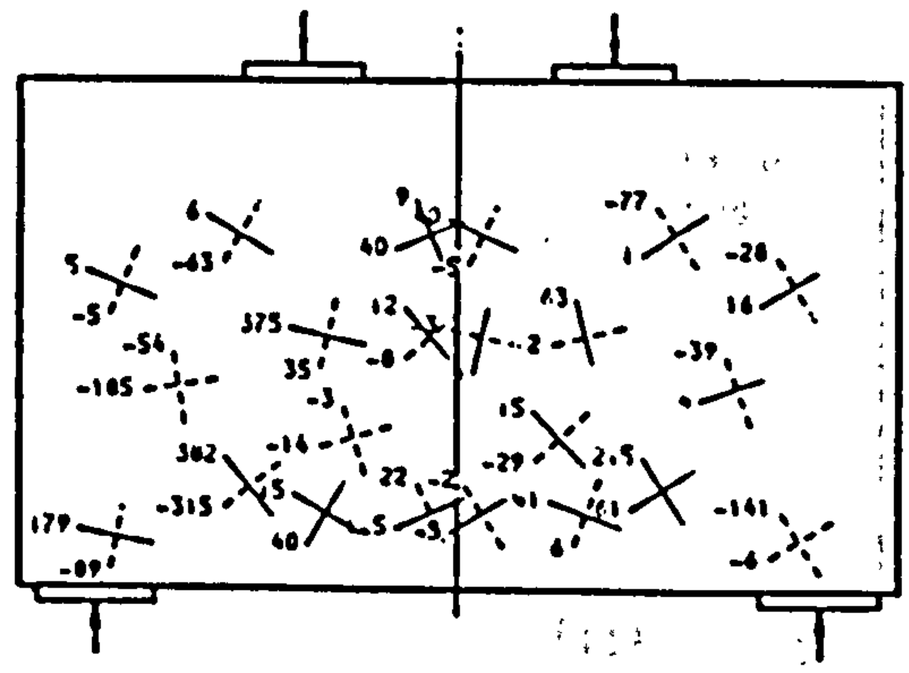

BEAM W-29-0.1-R2 (BACK) 900 (kN)

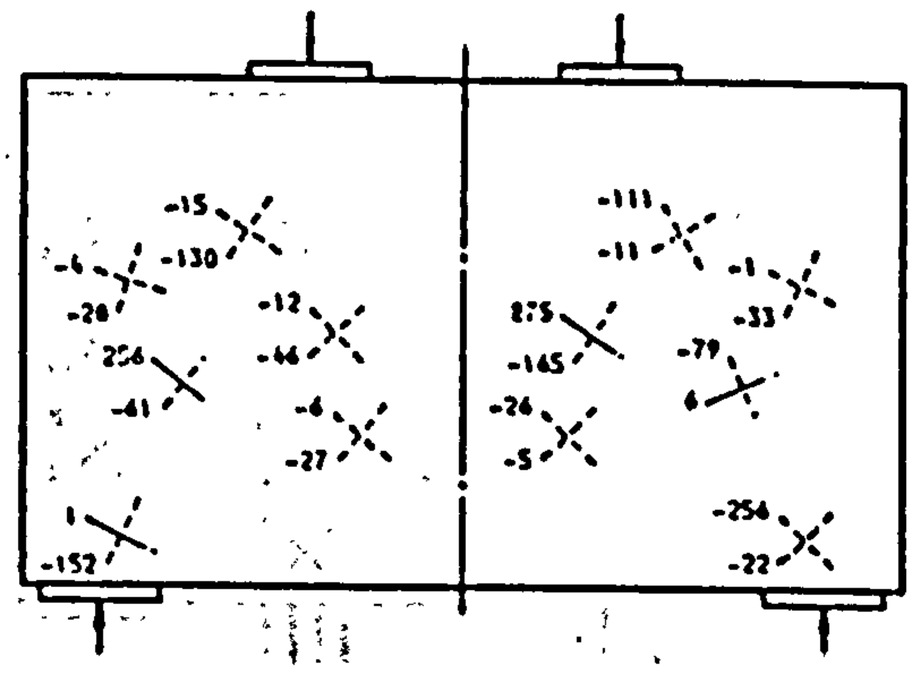

—— Tension Positive

---- Compression Negative

(All figures are in (N/mm^2)

Figure 6.37 : Principal stresses after the last load increments (W-Series beams, theory of elasticity) [cont'd]

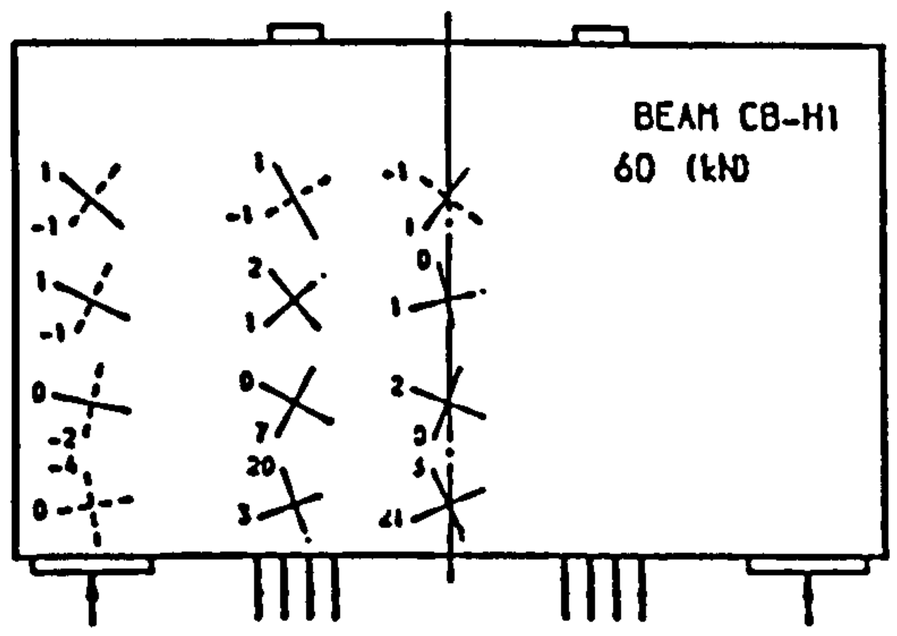

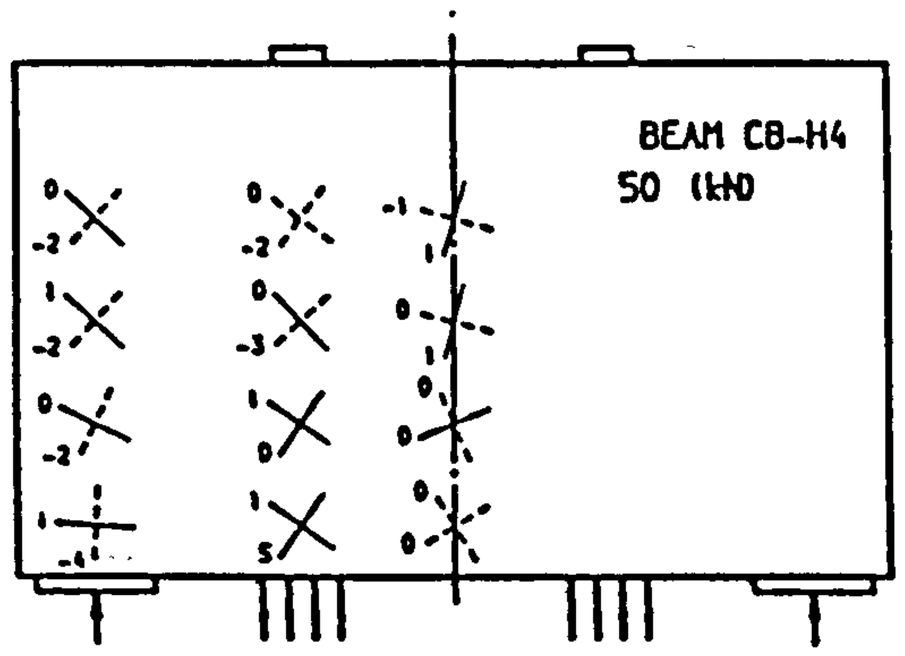

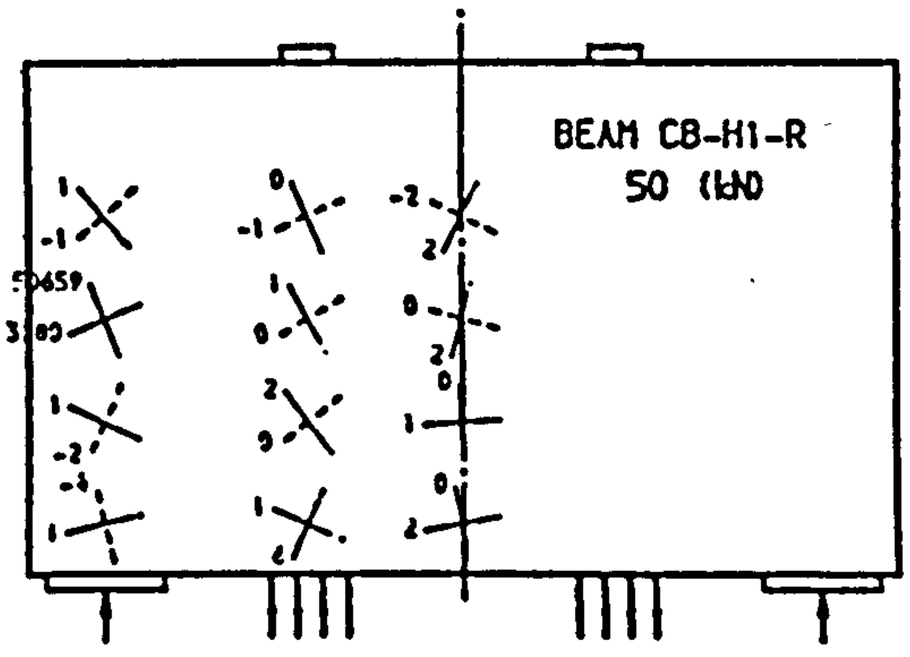

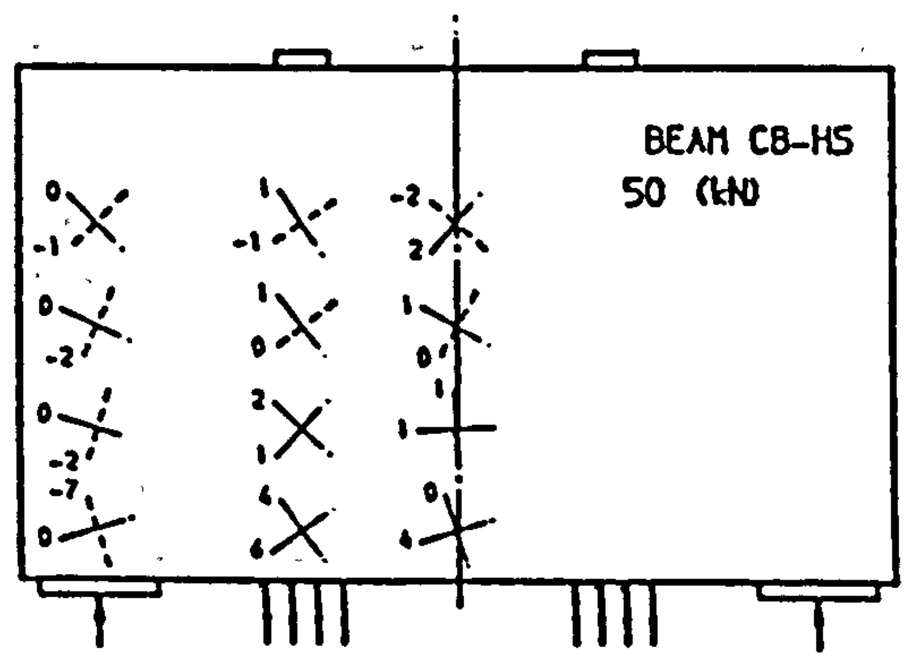

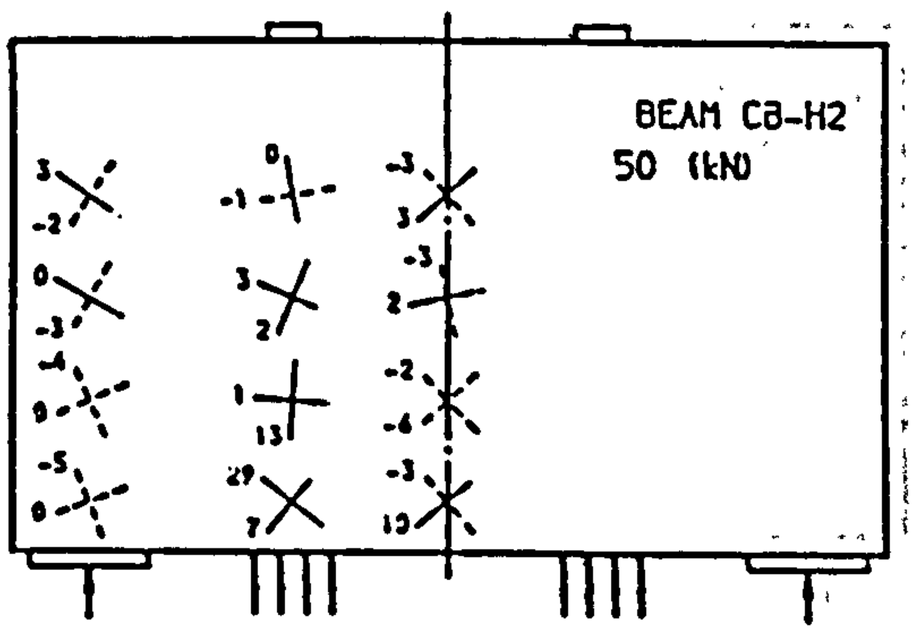

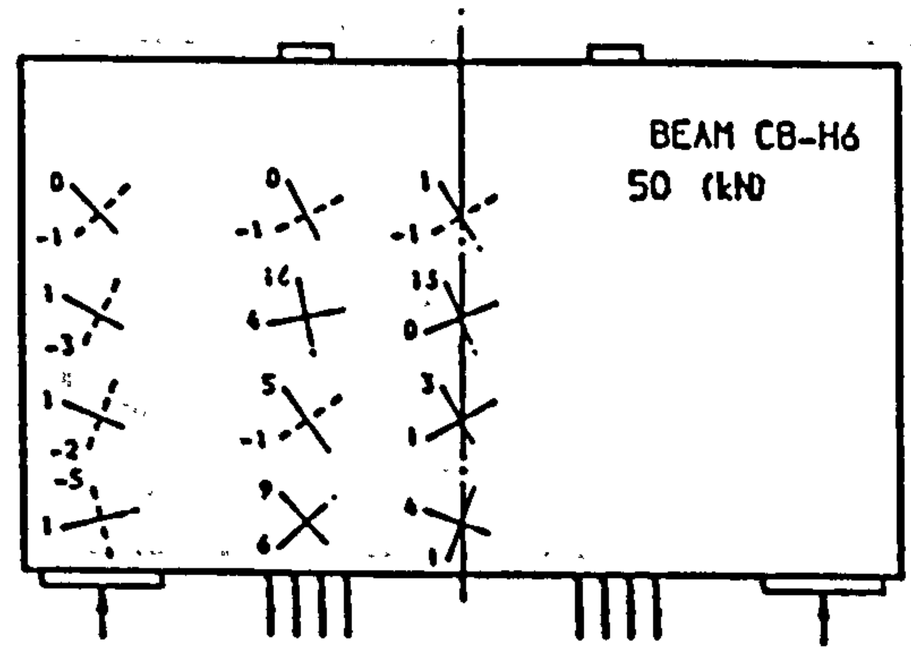

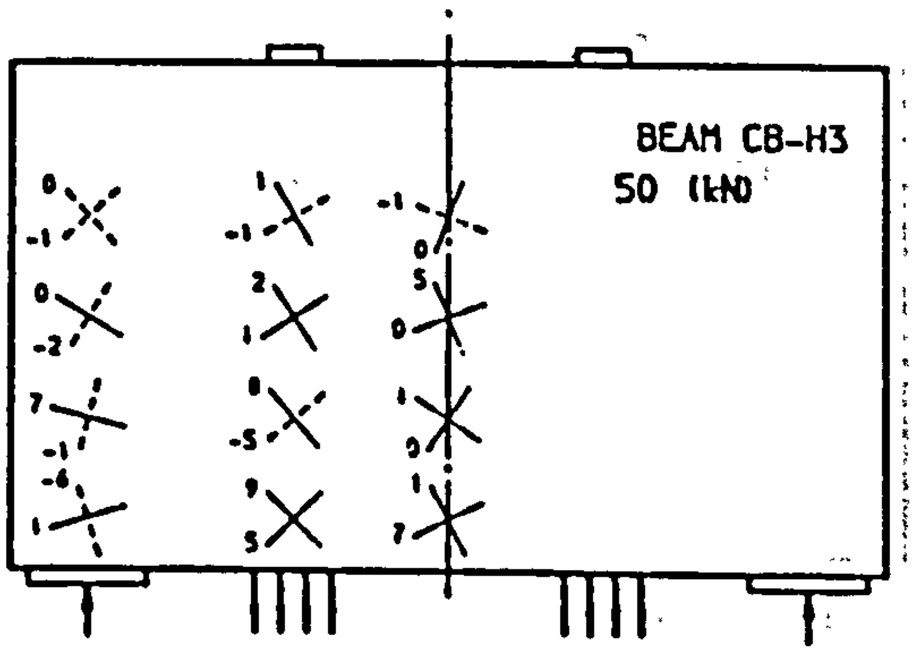

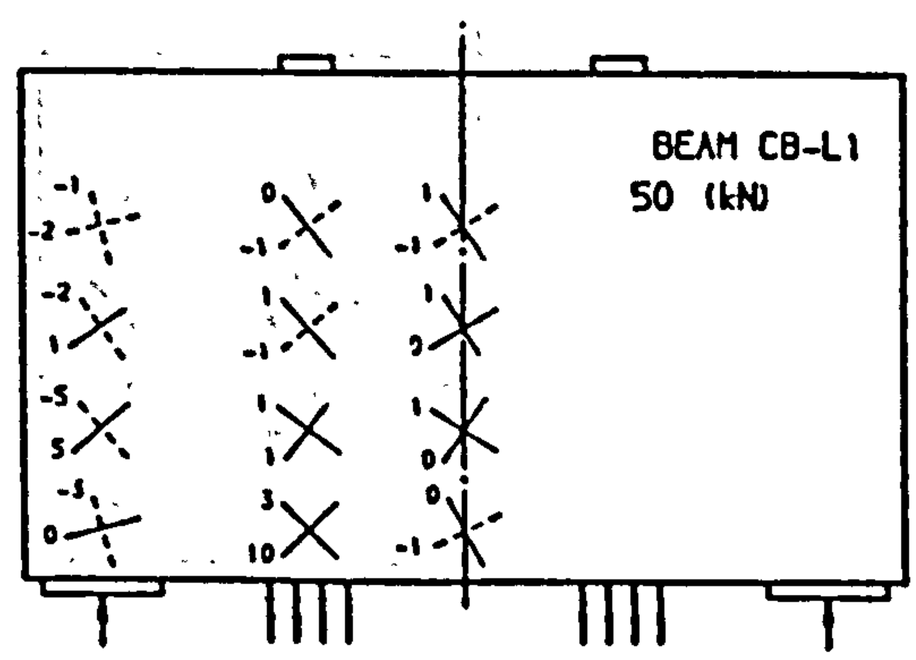

—— Tension Positive
---- Compression Negative

(All figures are in (N/mm^2)

Figure 6.38 : Principal stresses after the first load increments (CB-Series beams, theory of elasticity)

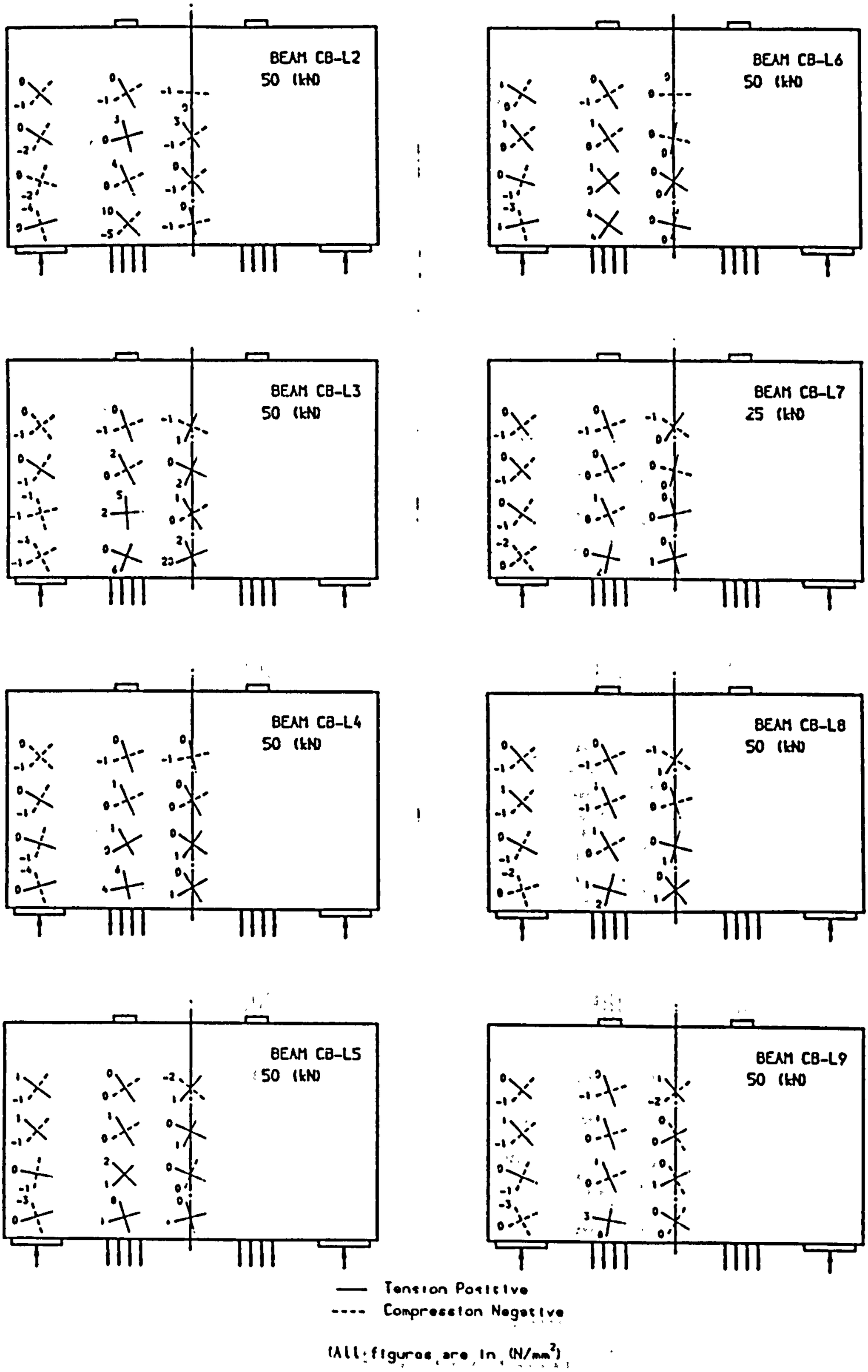

Figure 6.38 : Principal stresses after the first load increments (CB-Series beams, theory of elasticity) [cont'd]

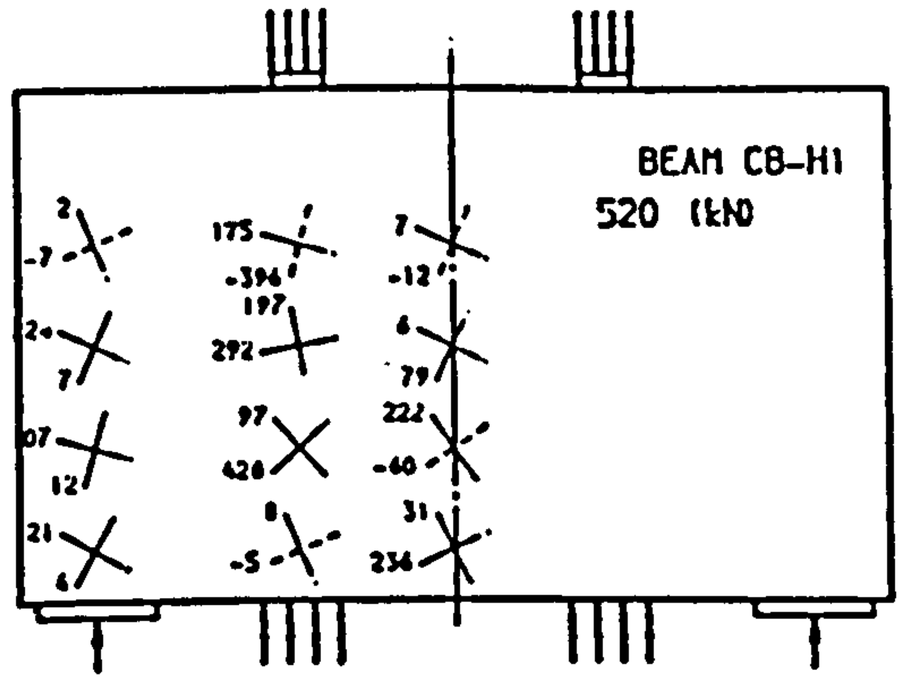

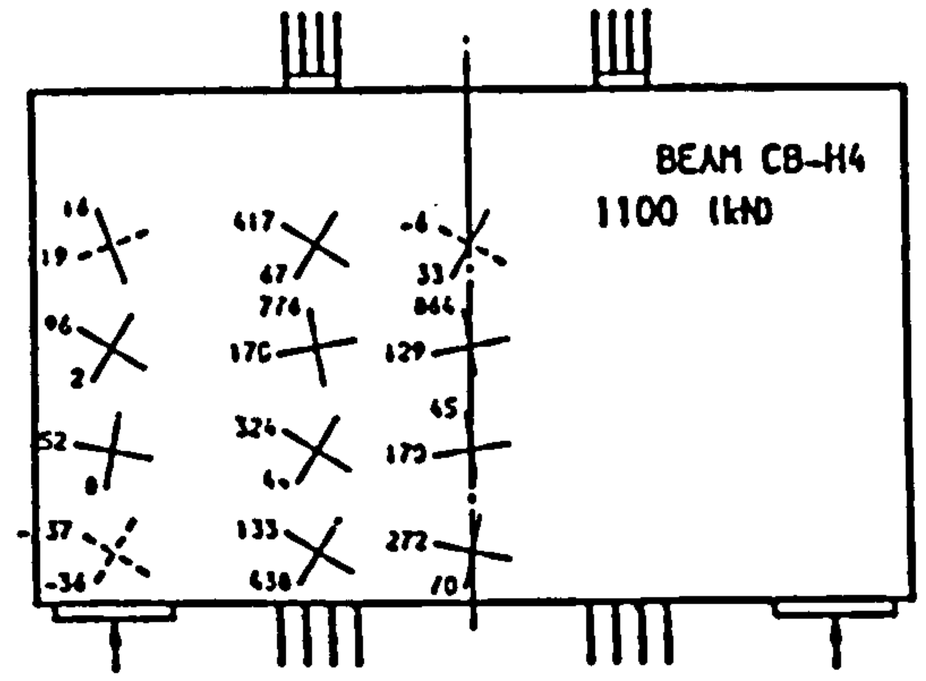

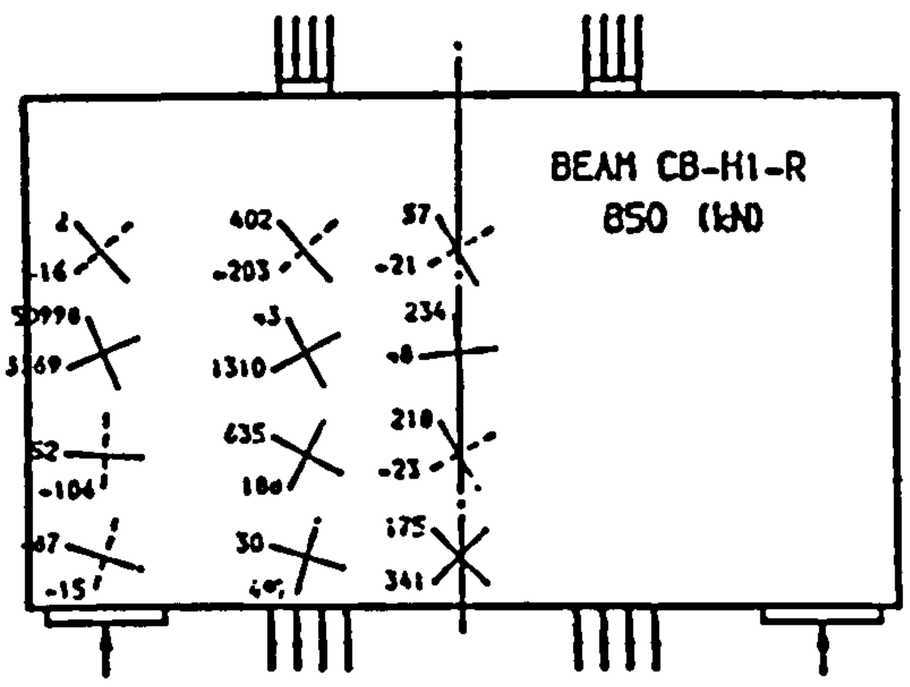

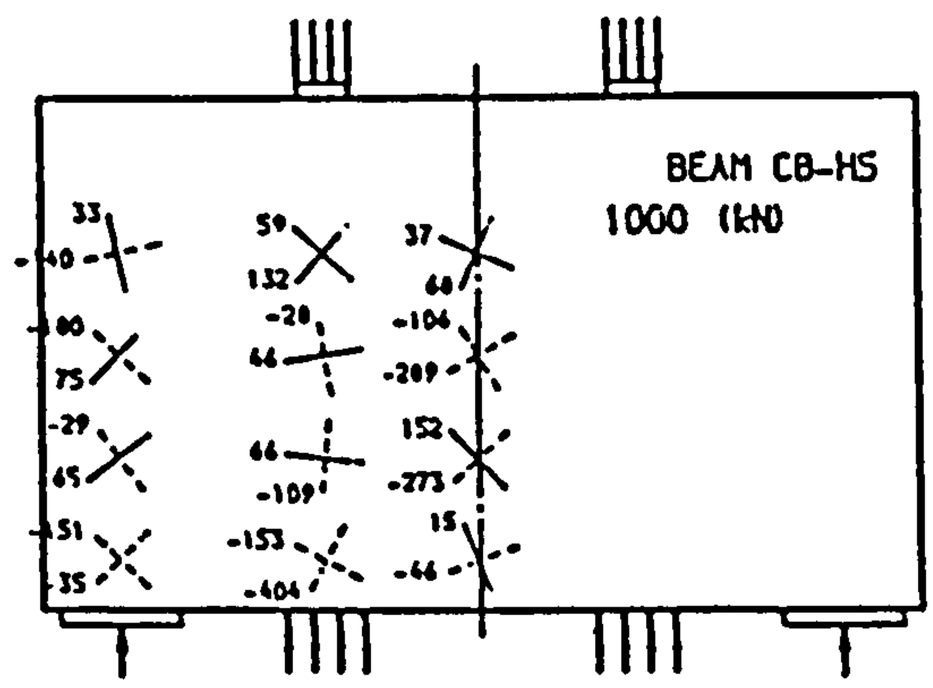

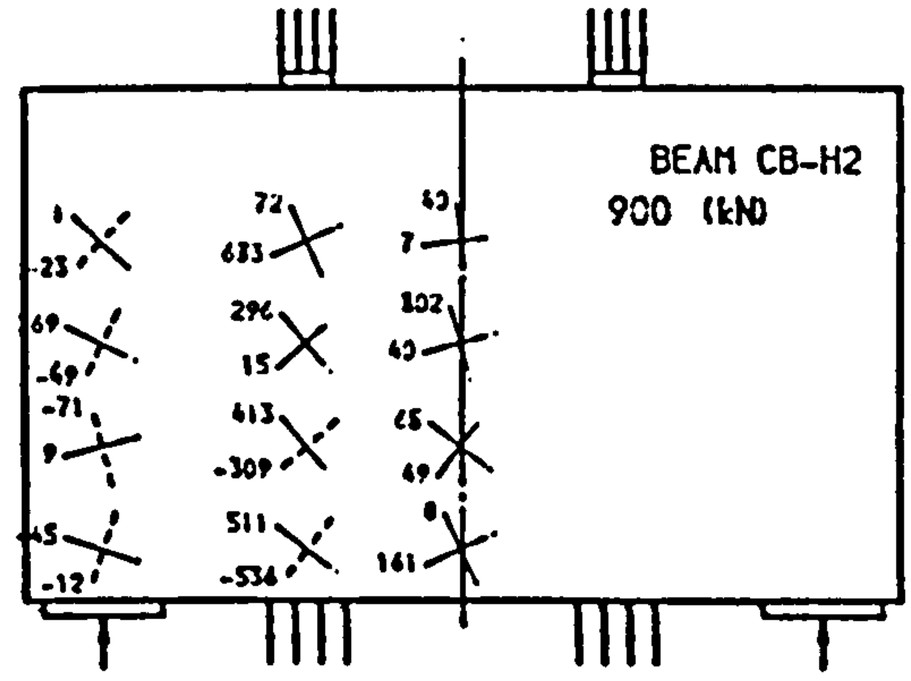

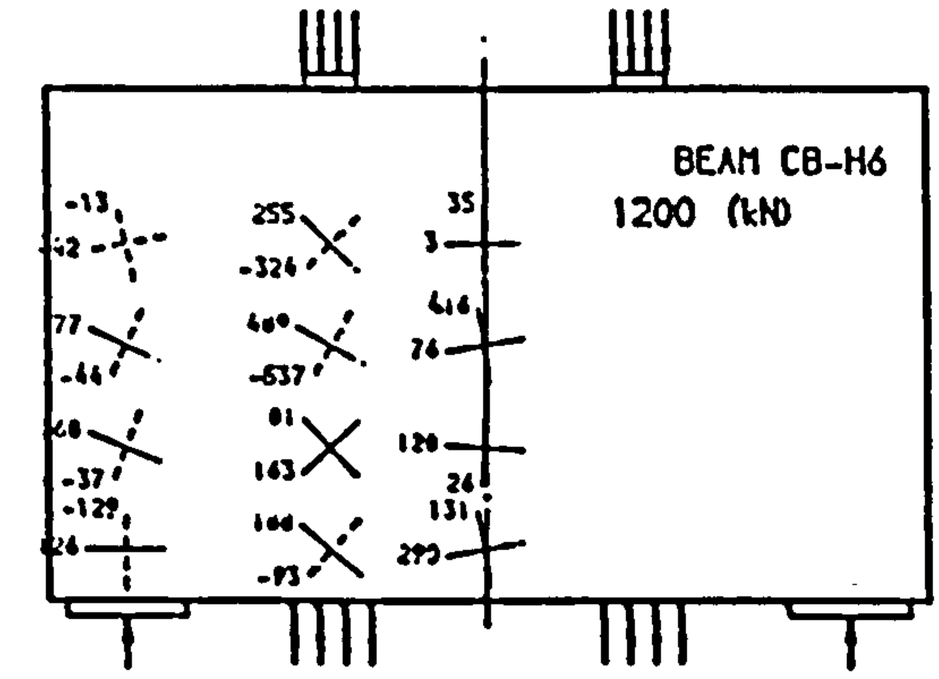

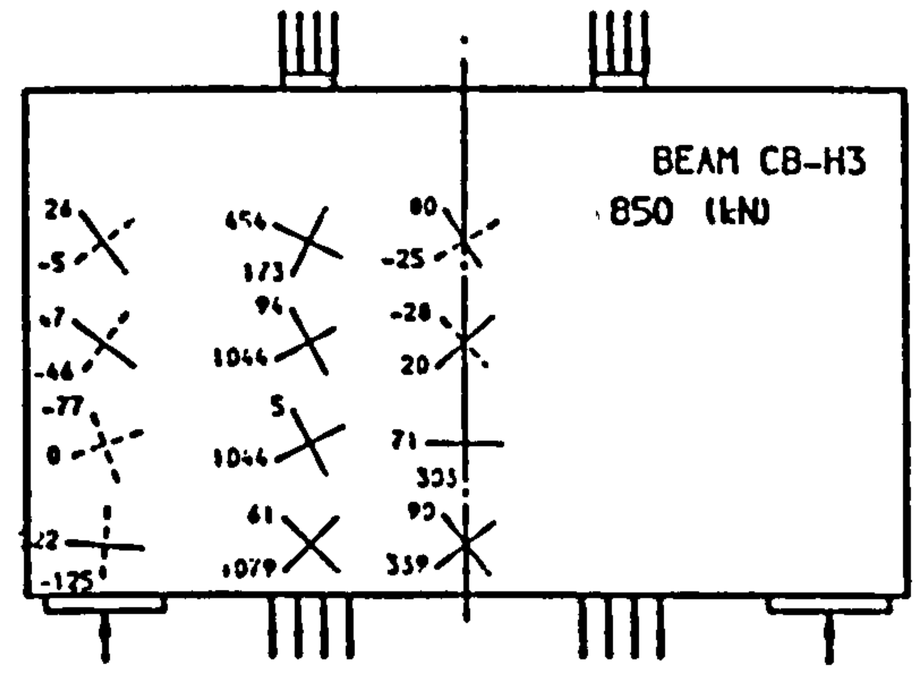

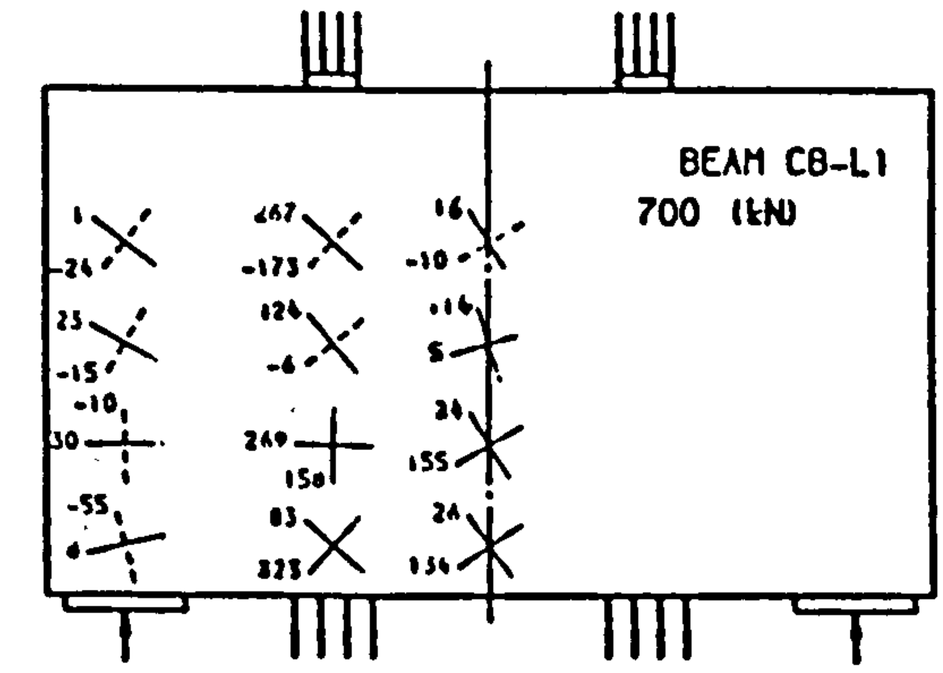

—— Tension Positive

---- Compression Negative

(All figures are in (N/mm^2)

Figure 6.39 : Principal stresses after the last load increments (CB-Series beams, theory of elasticity)

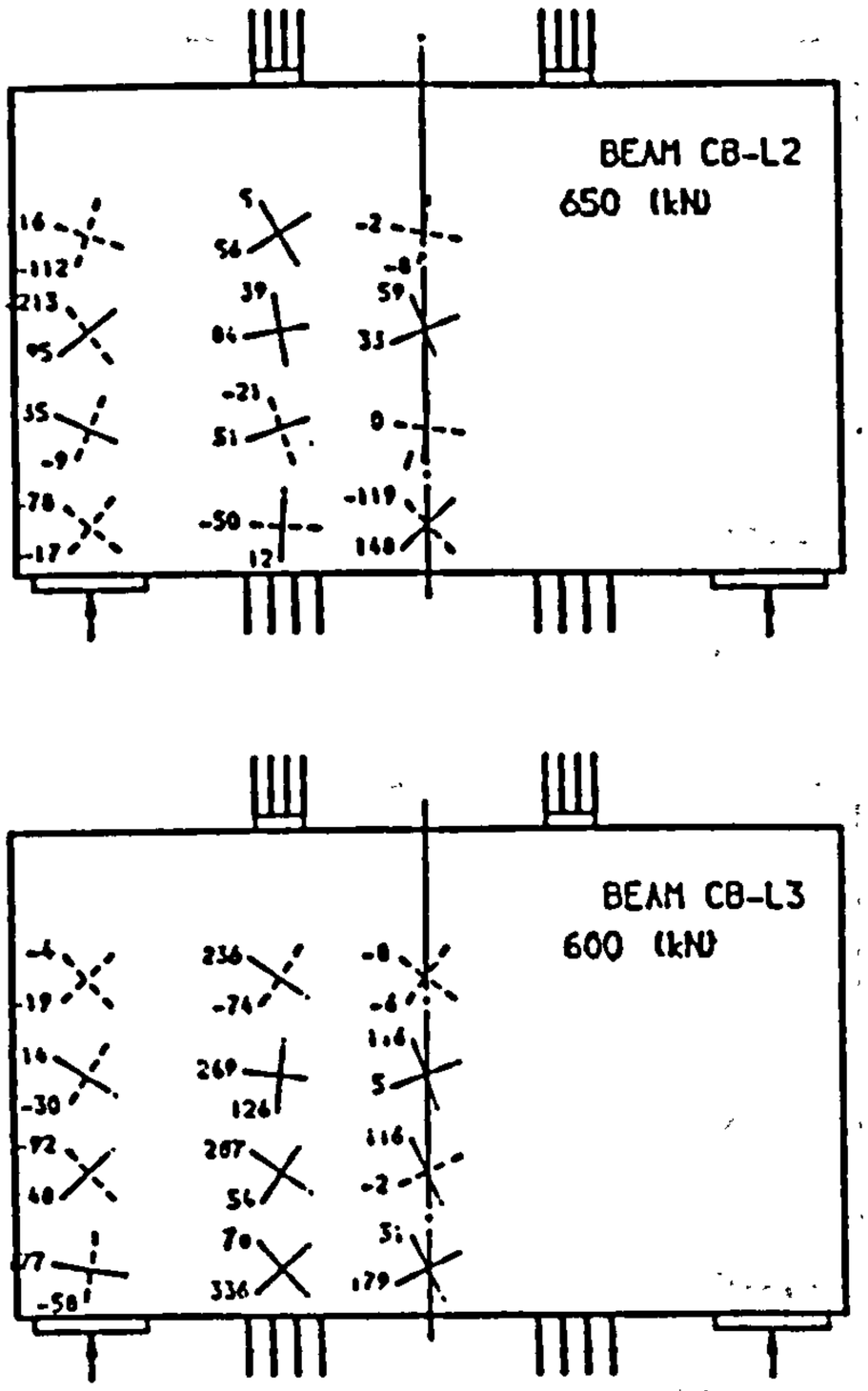

Figure 6.39 : Principal stresses after the last load increments (CB-Series beams, theory of elasticity) [cont'd]

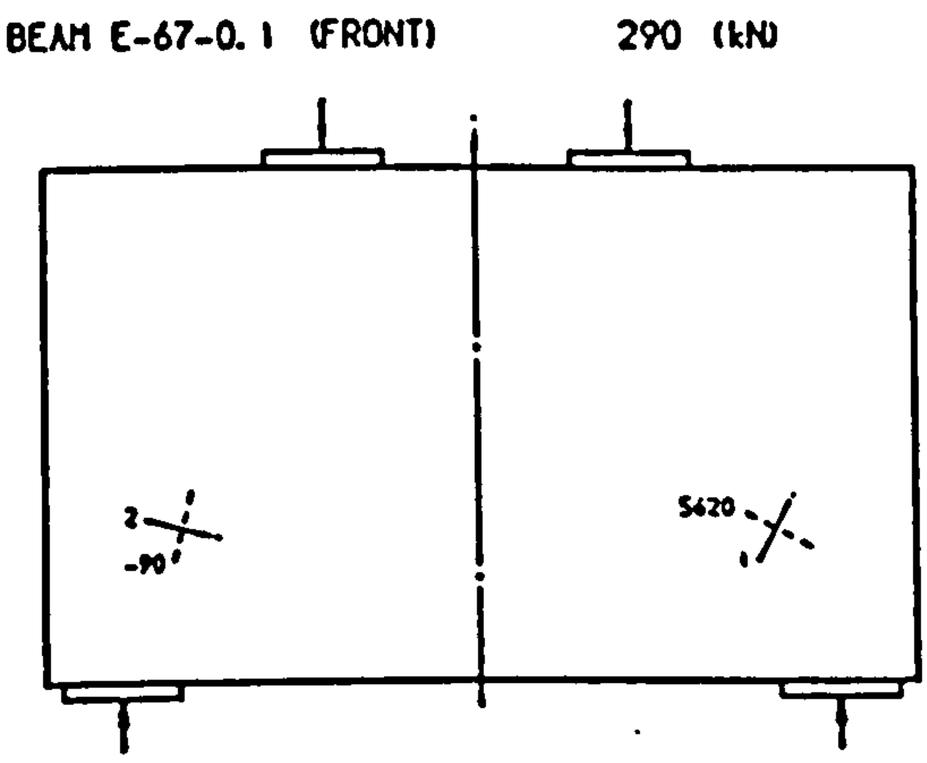

Figure 6.40 : Principal stresses after the last load increments (E-Series beams, compression field theory)

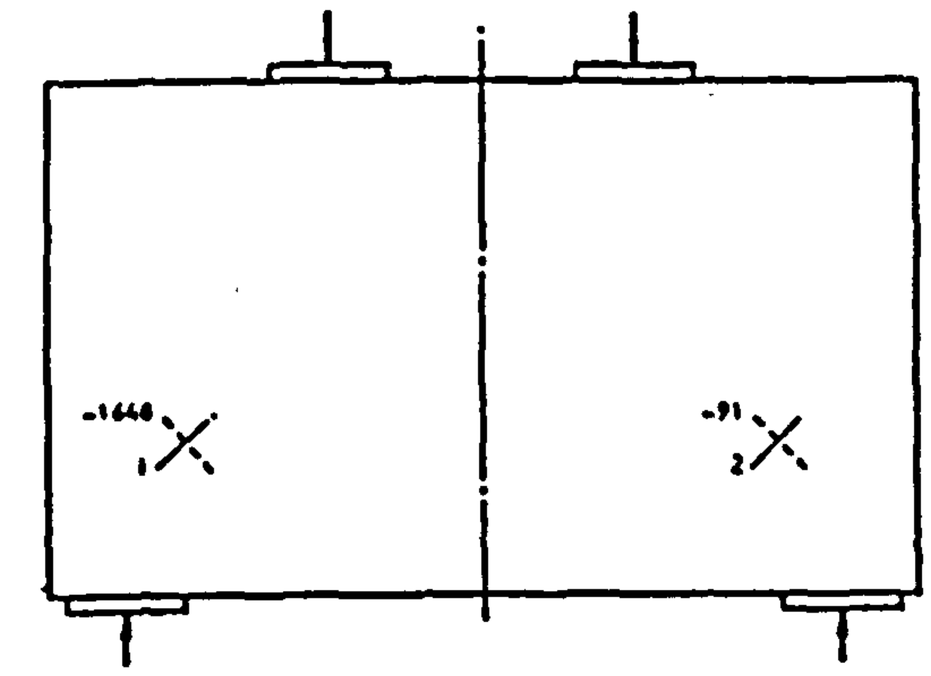

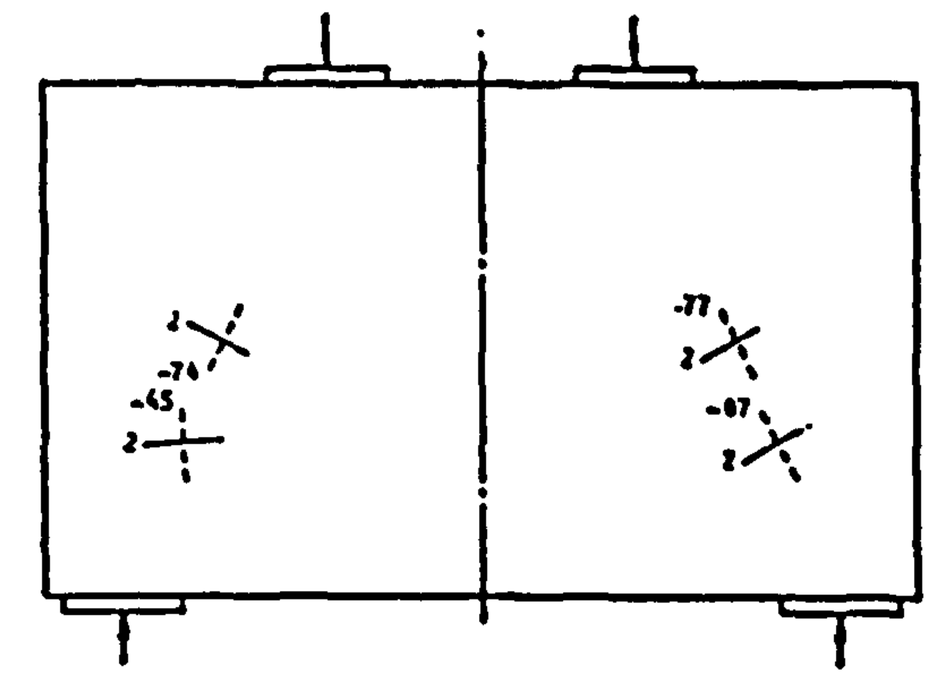

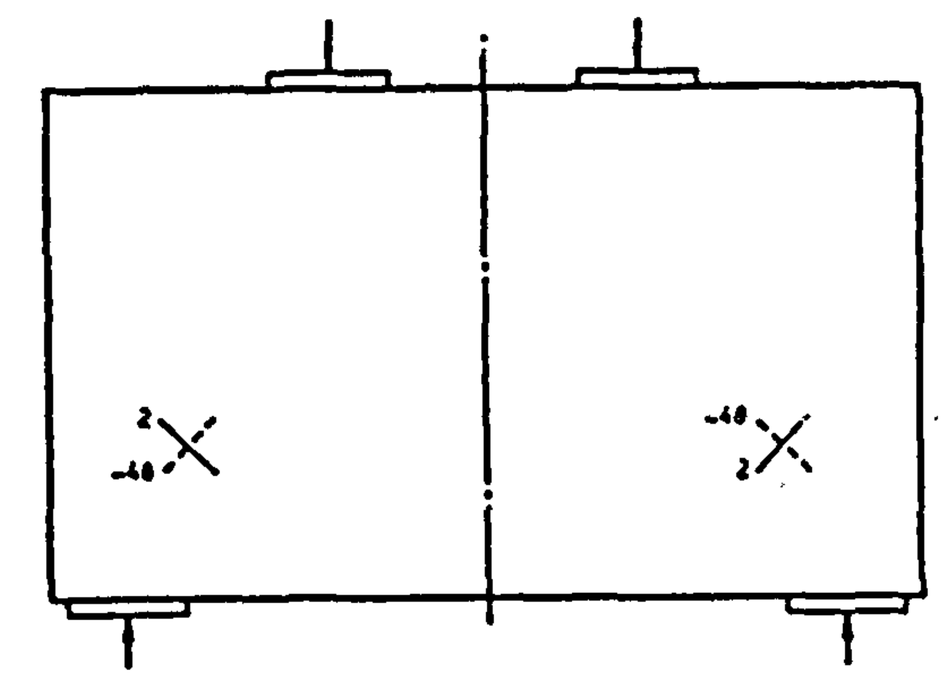

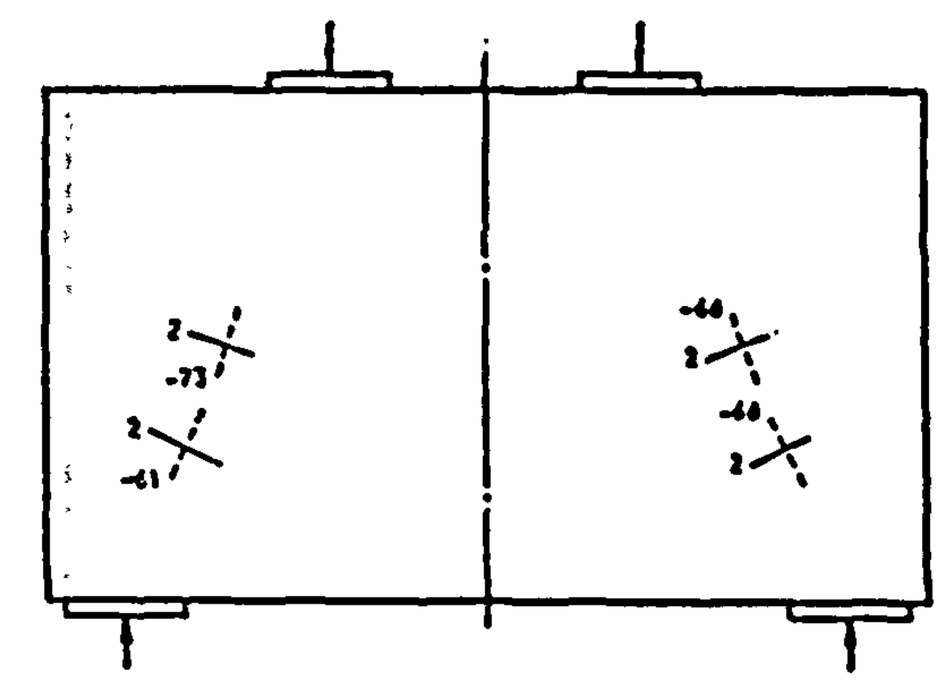

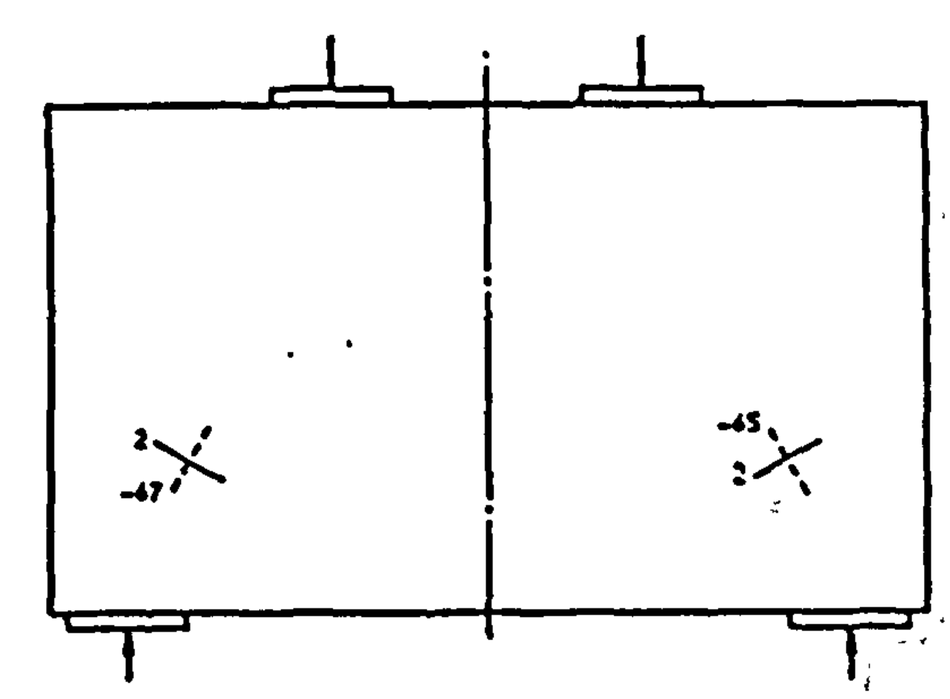

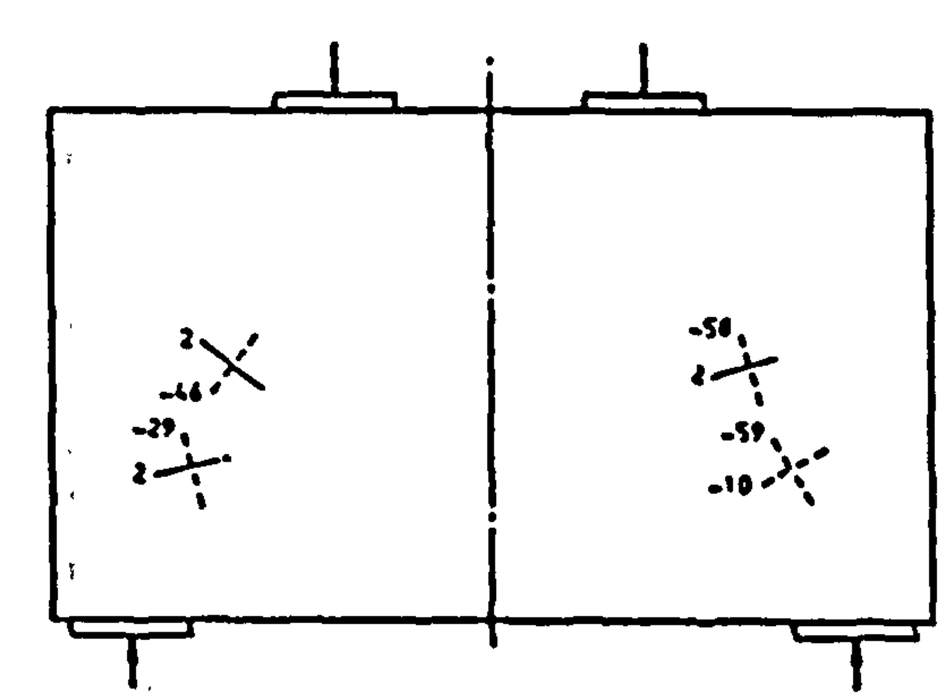

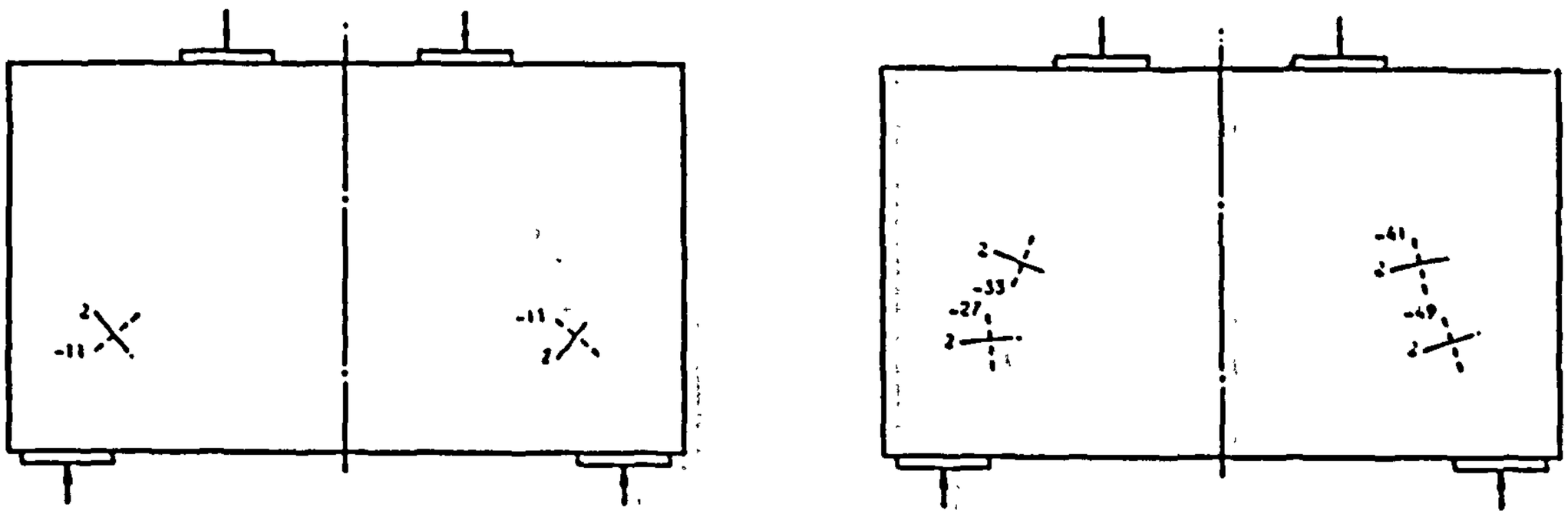

Figure 6.40 : Principal stresses after the last load increments (E-Series beams, compression field theory) [cont'd]

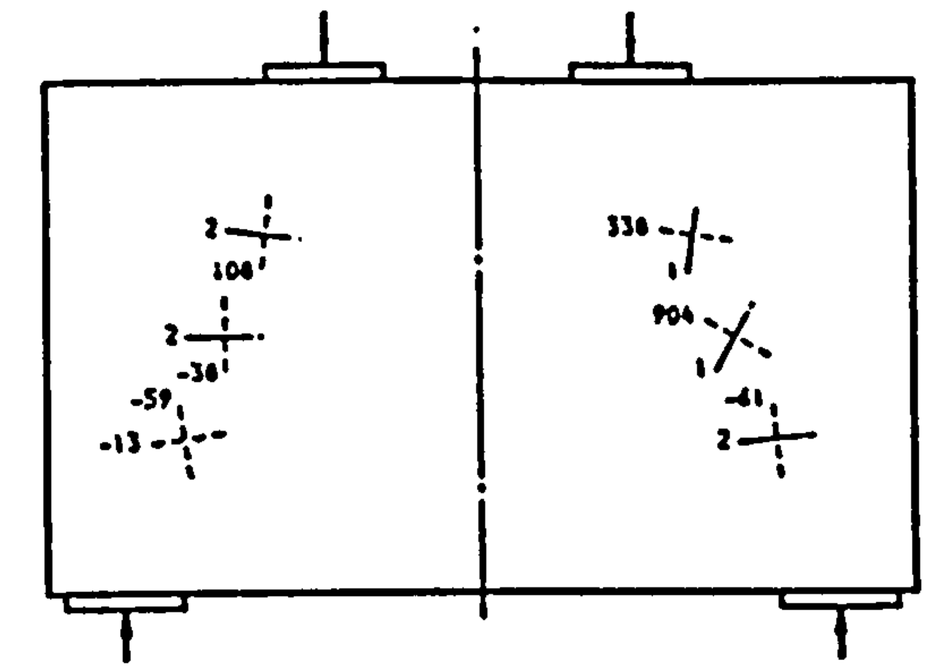

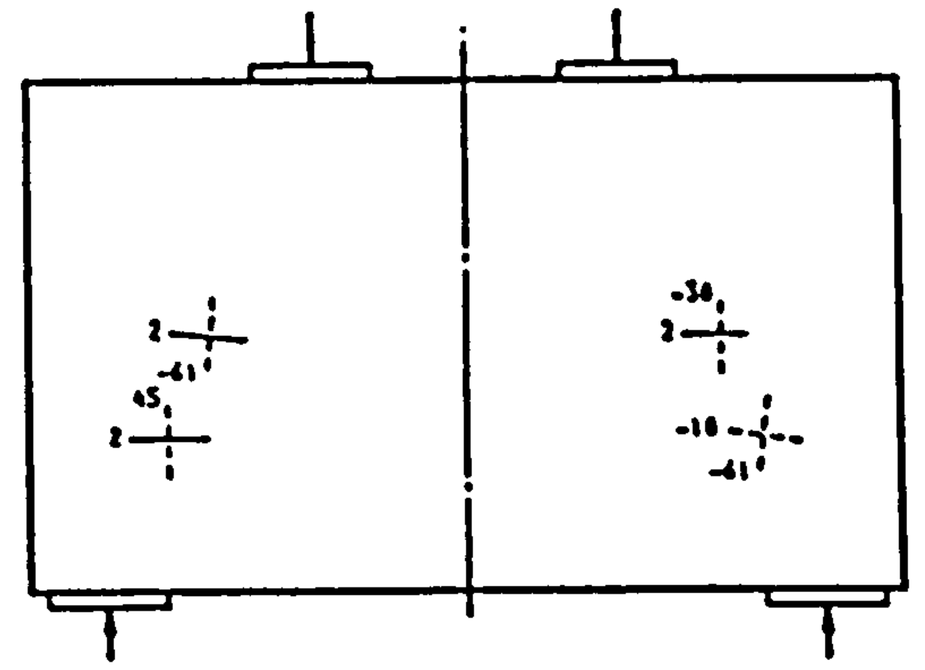

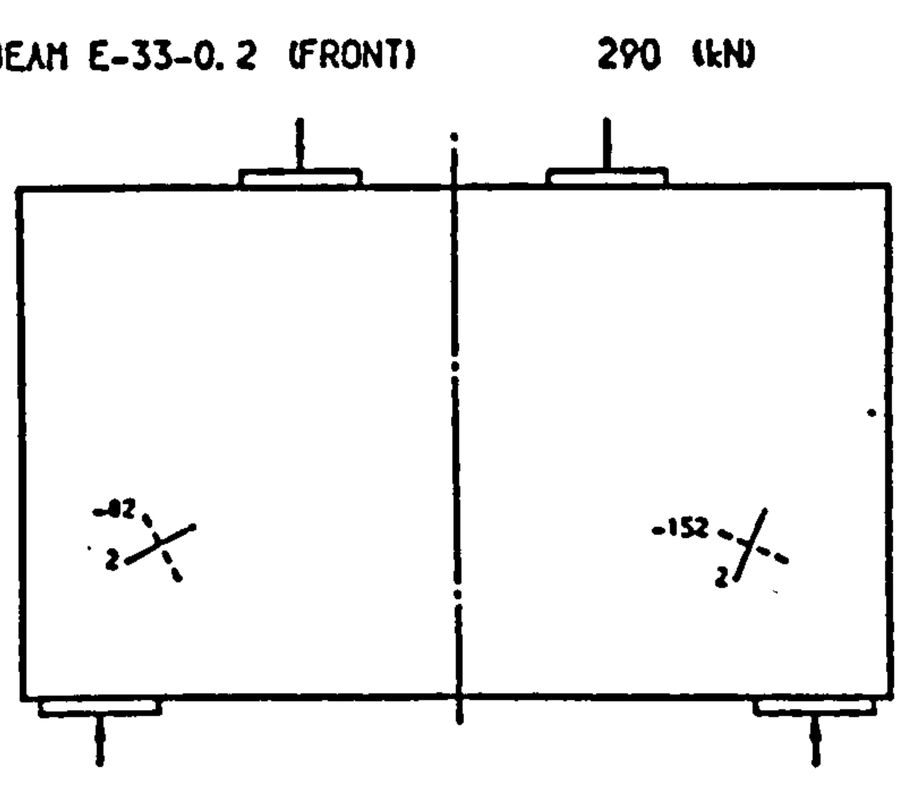

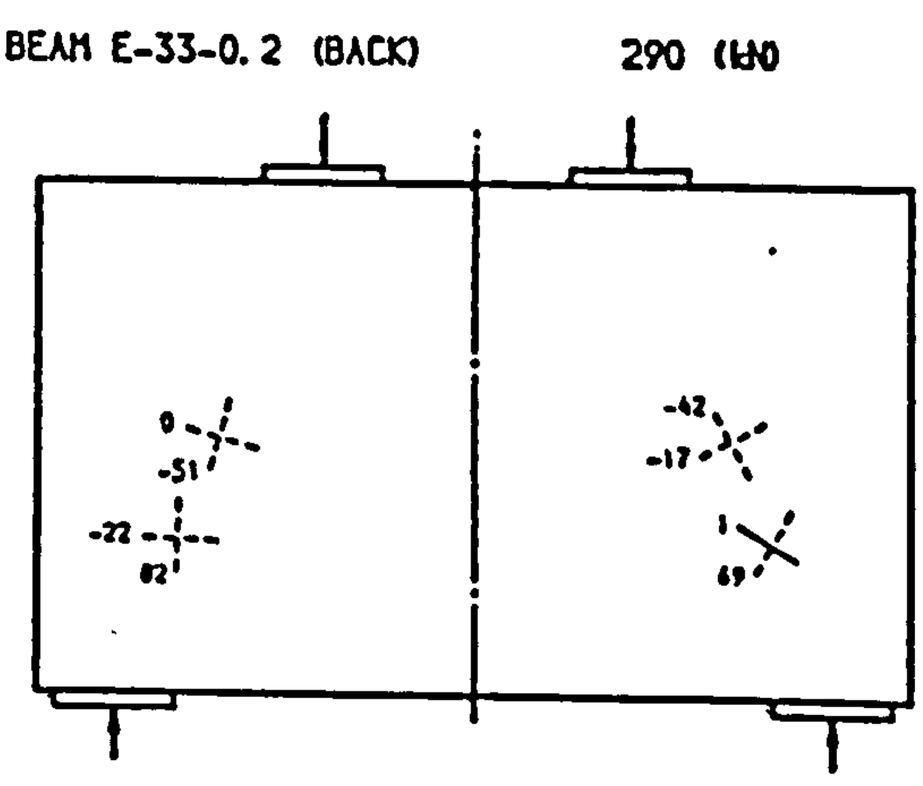

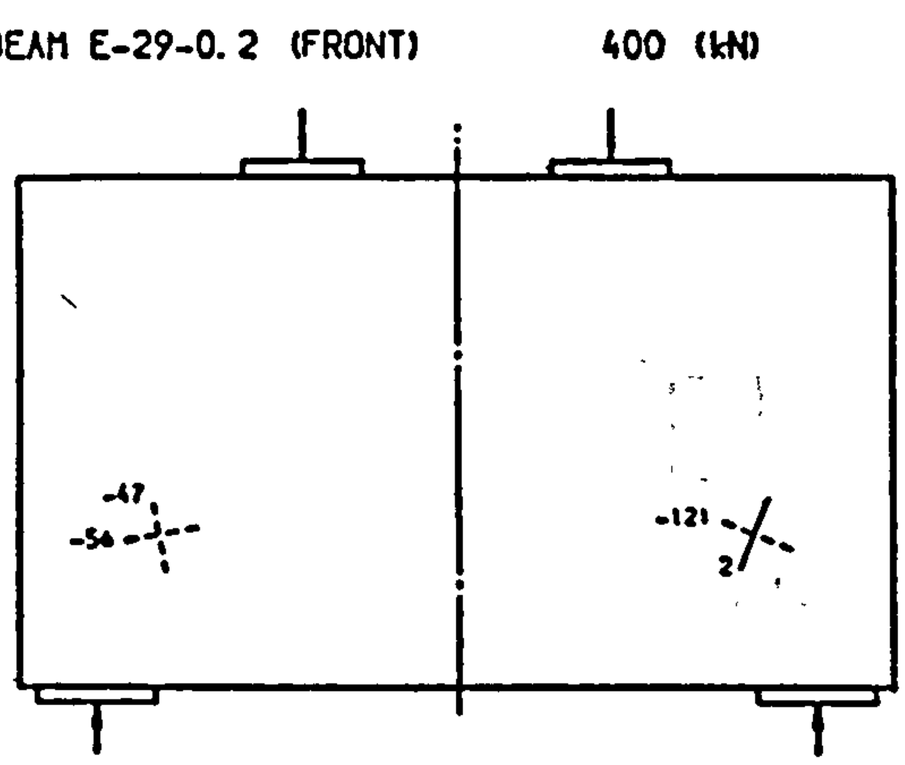

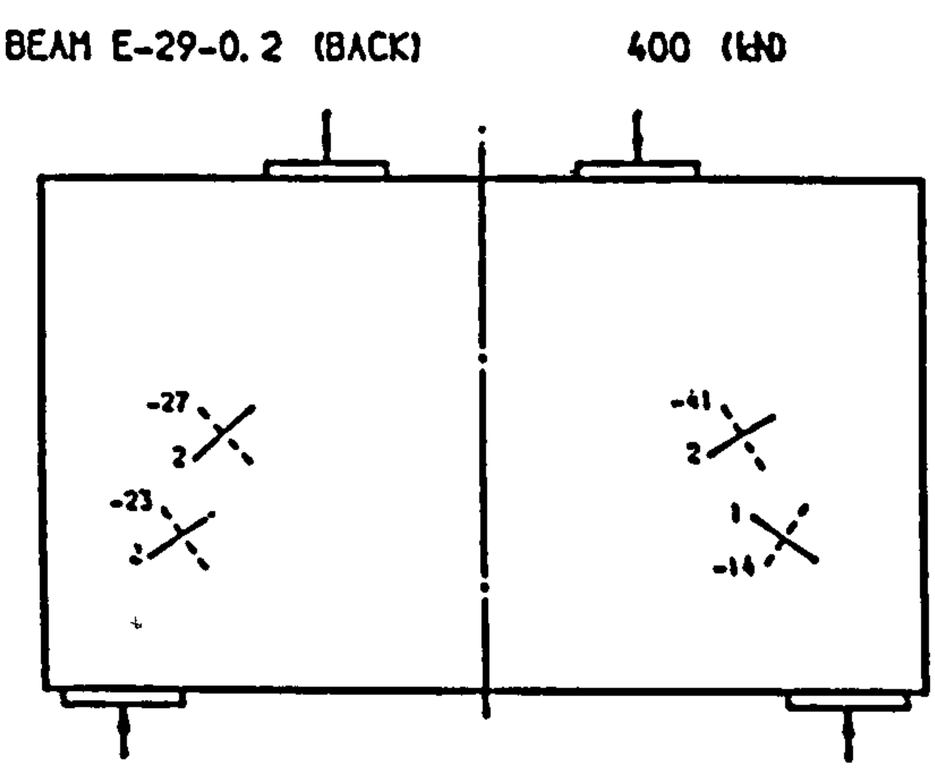

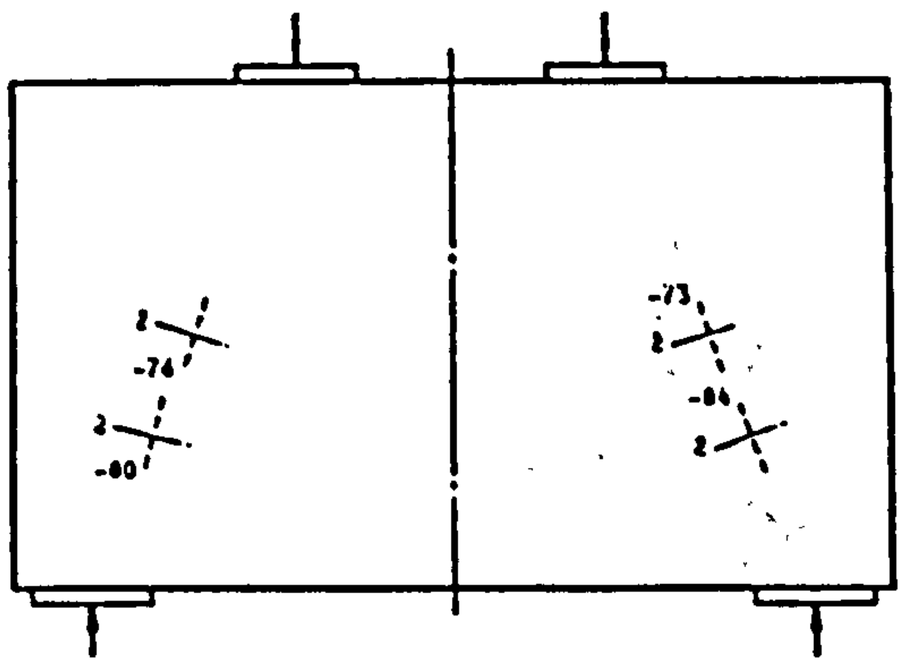

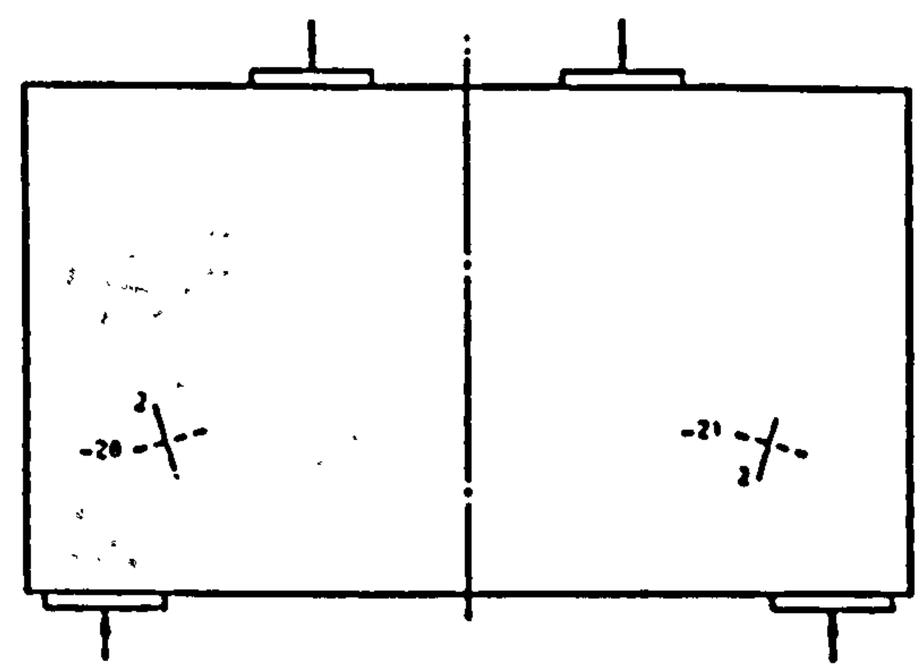

—— Tension Positive
---- Compression Negative

(All figures are in N/mm^2)

Figure 6.40 : Principal stresses after the last load increments (E-Series beams, compression field theory) [cont'd]

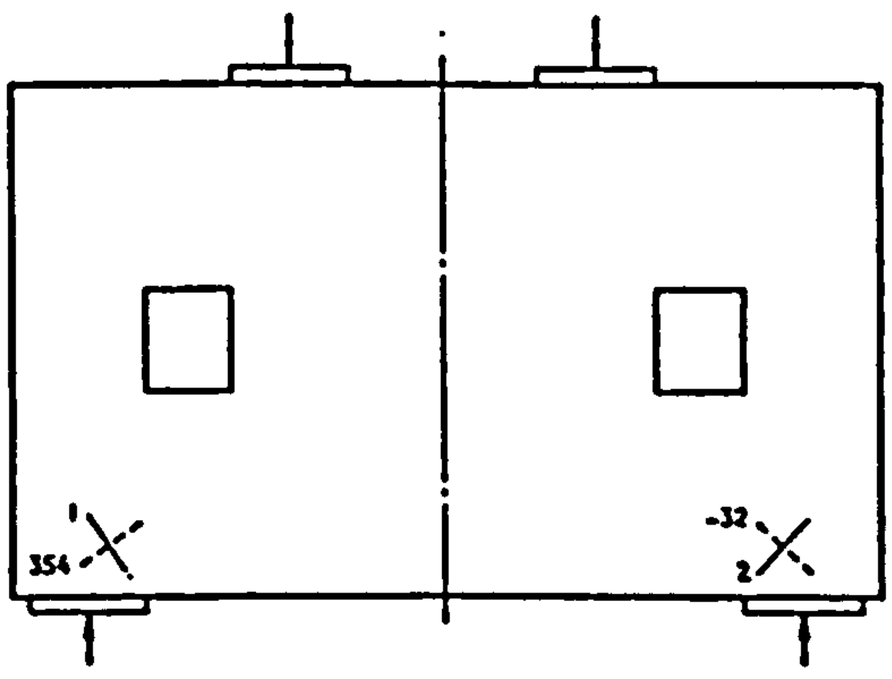

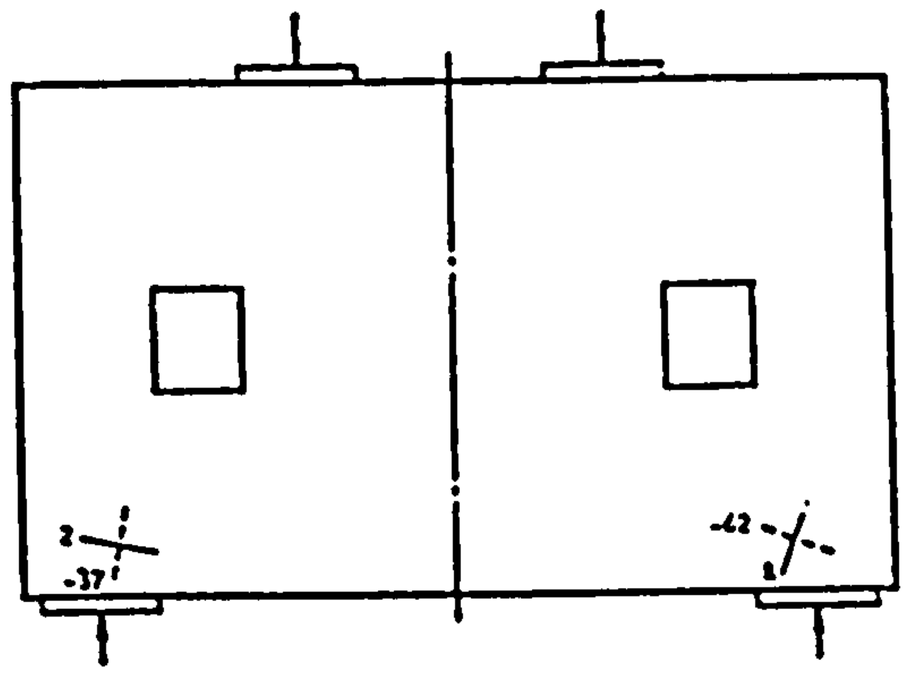

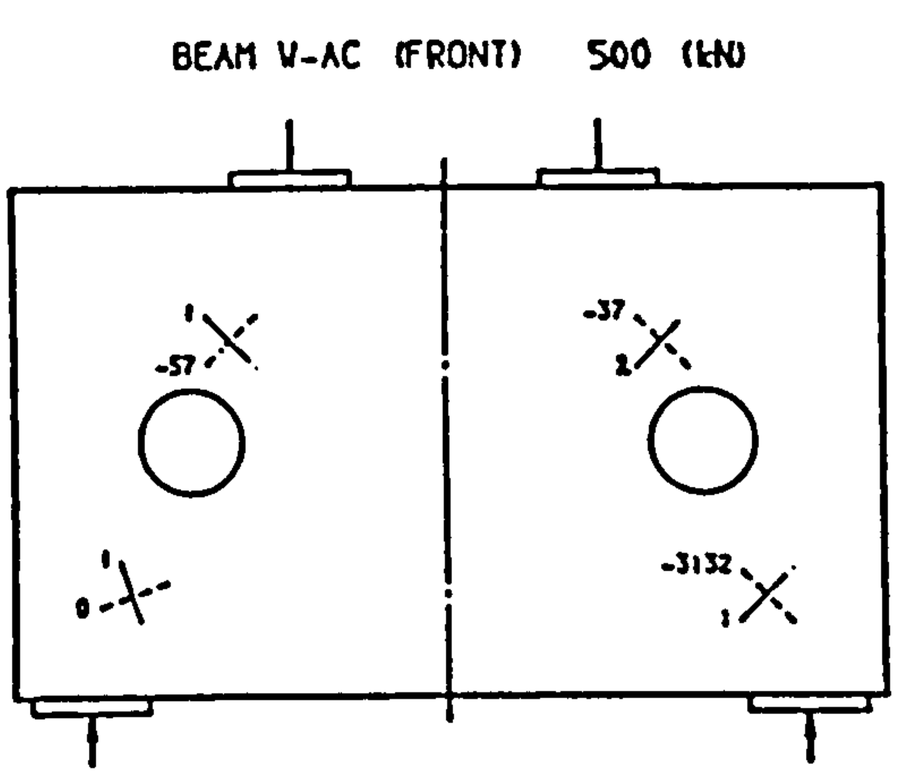

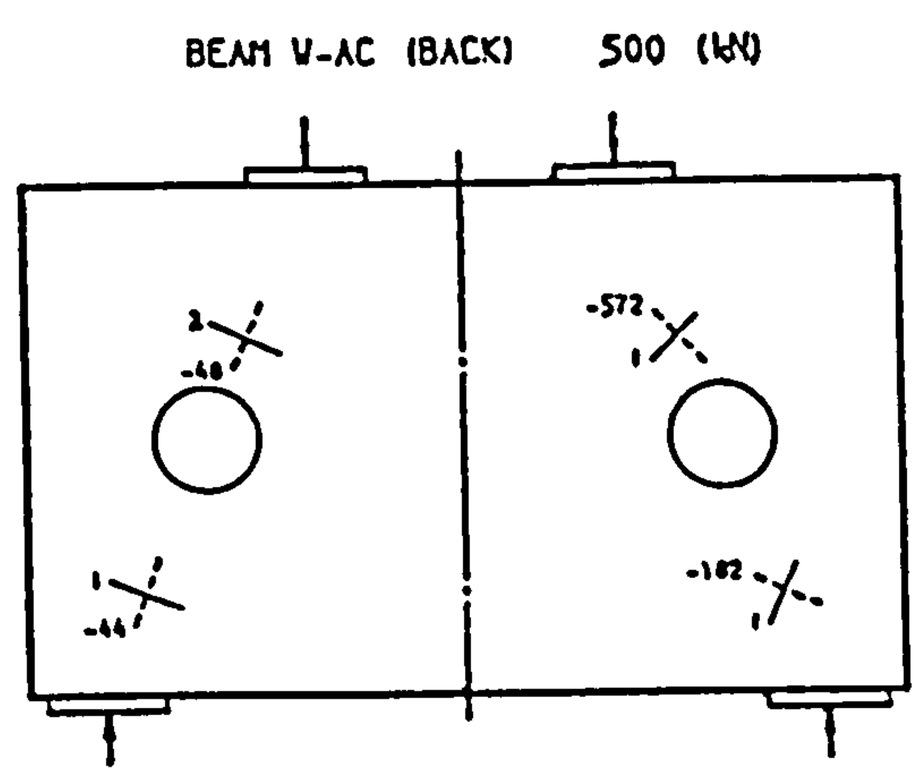

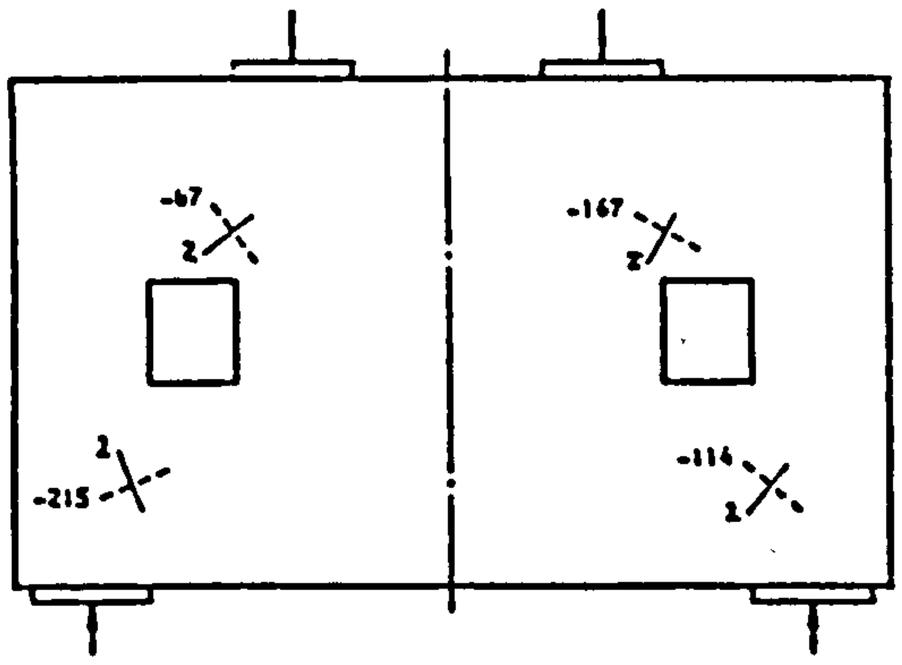

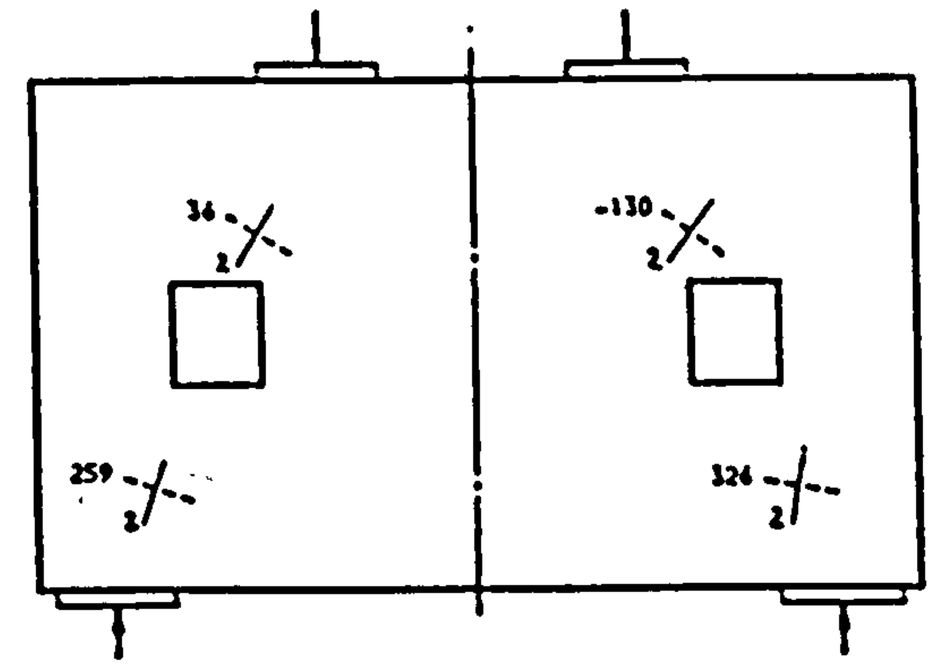

BEAM V-AC-R (FRONT) 480 (kN)

BEAM V-AC-R (BACK) 480 (kN)

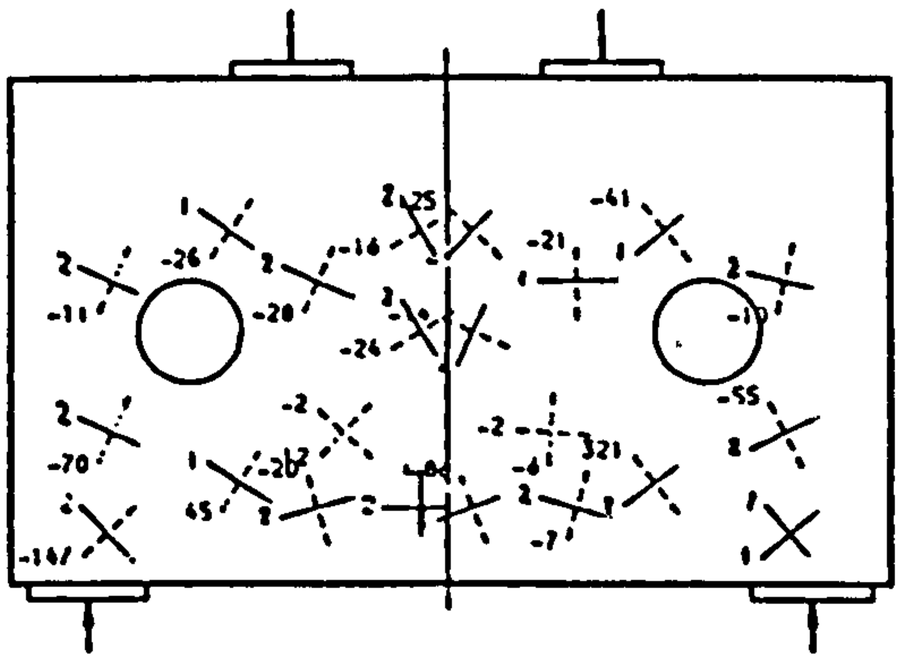

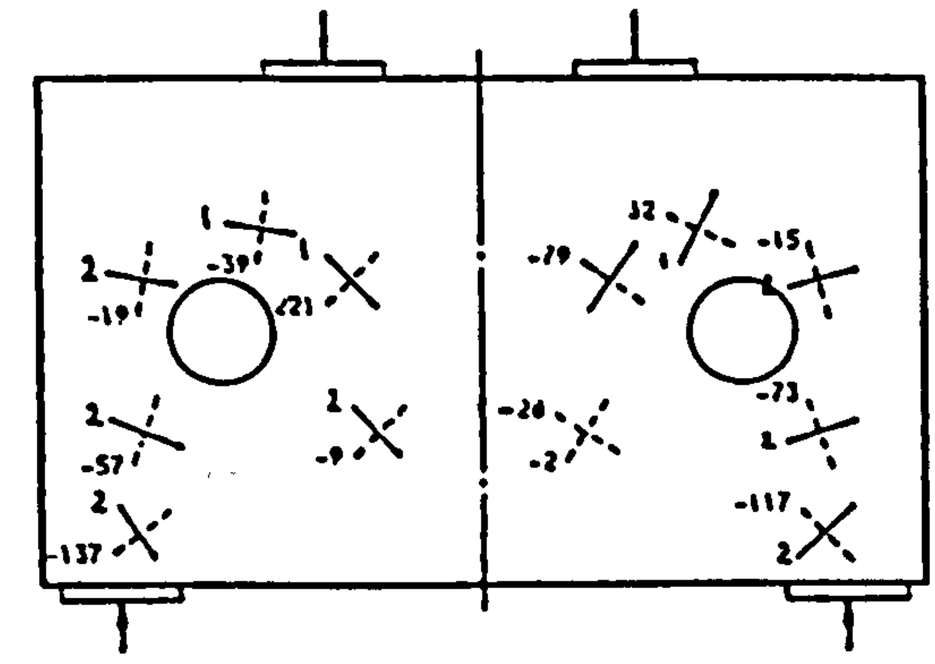

—— Tension Positive

---- Compression Negative

(All figures are in (N/mm^2))

Figure 6.41 : Principal stresses after the last load increments (W-Series beams, compression field theory)

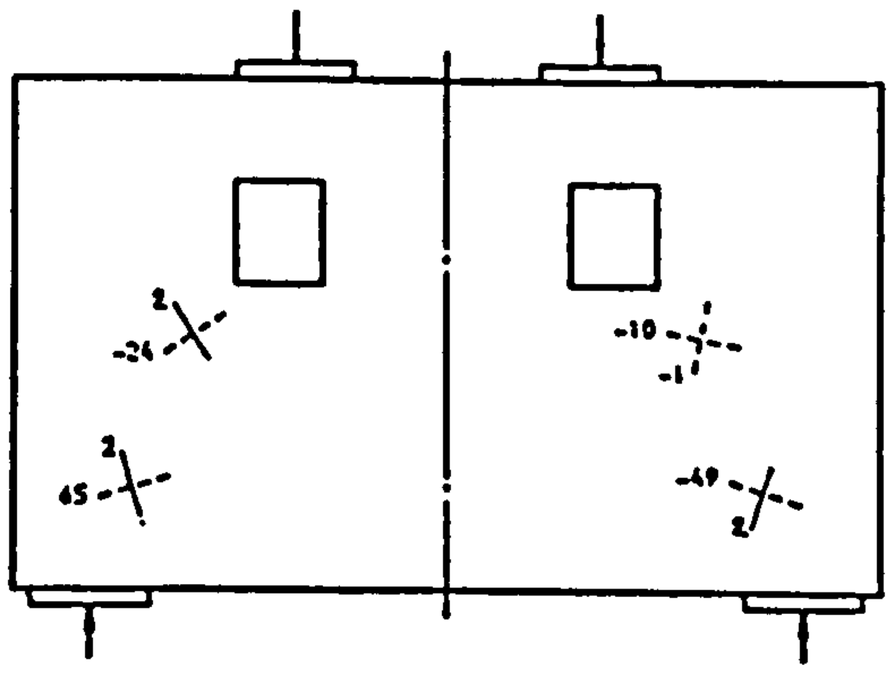

Figure 6.41 : Principal stresses after the last load increments (W-Series beams, compression field theory) [cont'd]

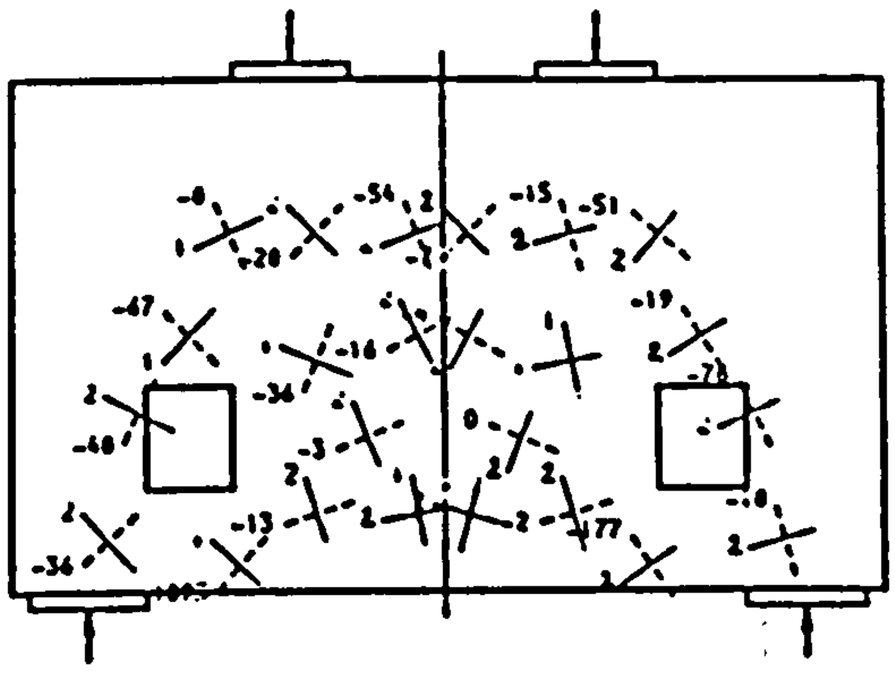

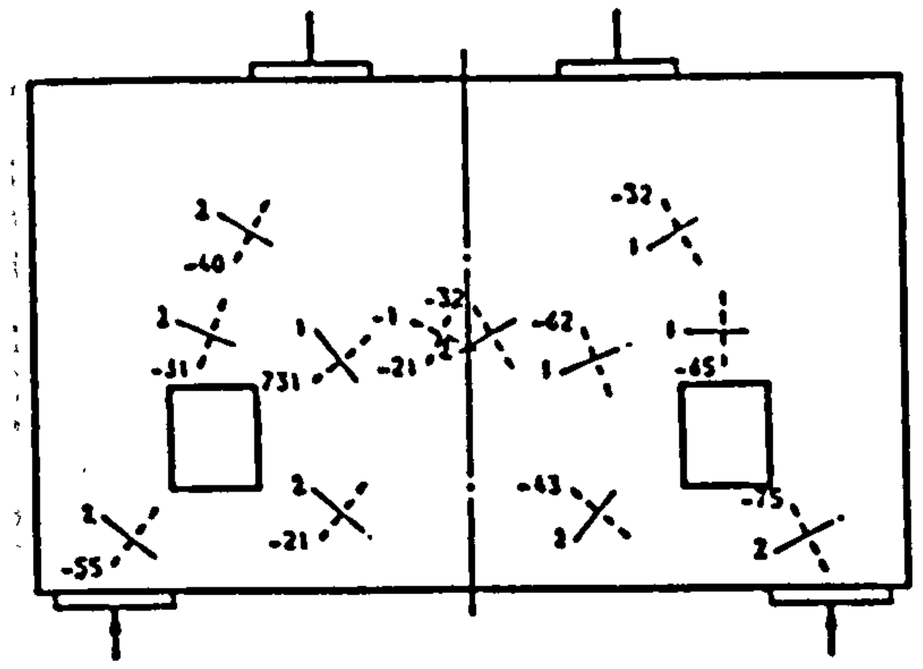

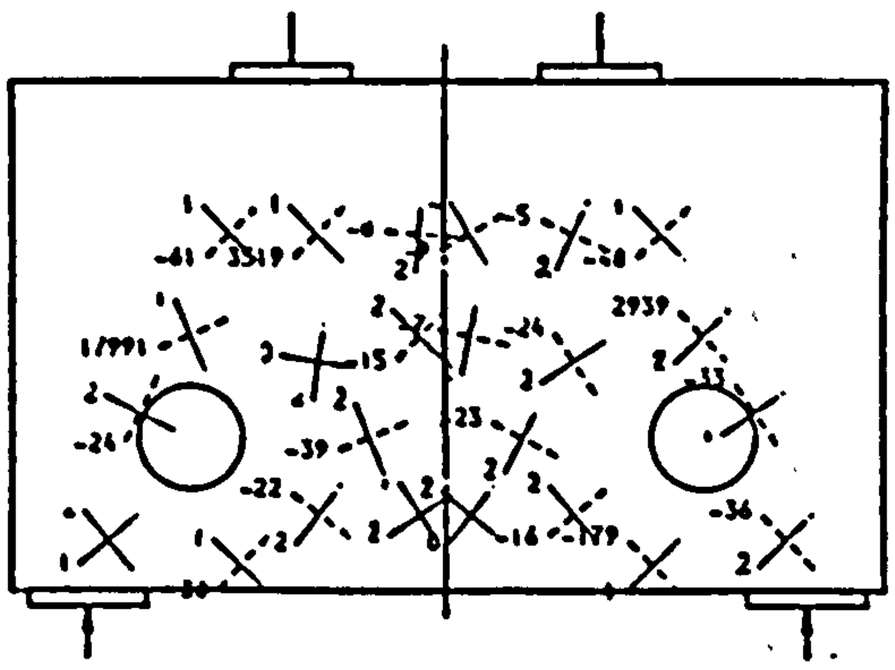

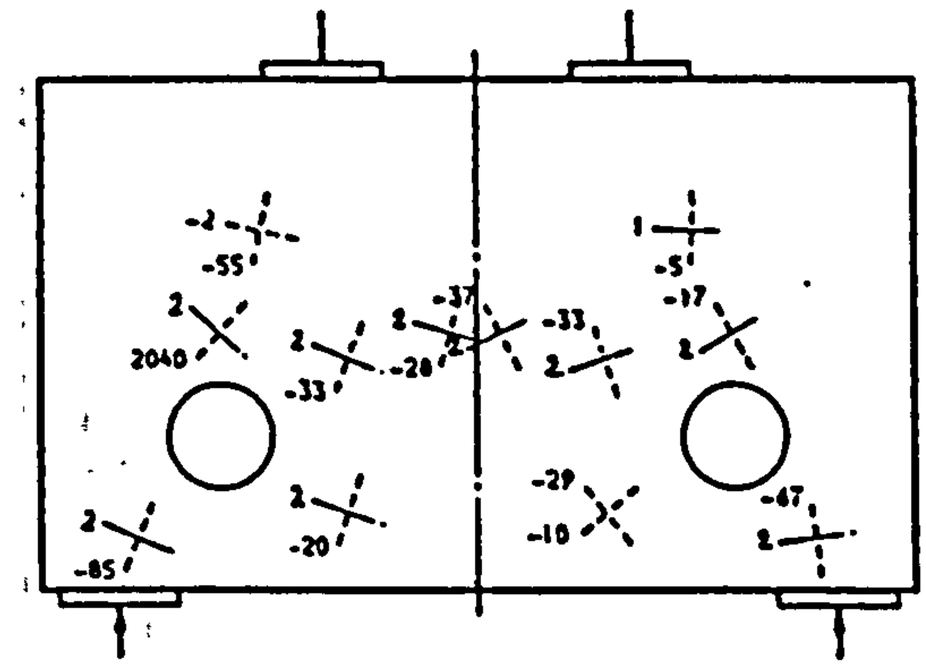

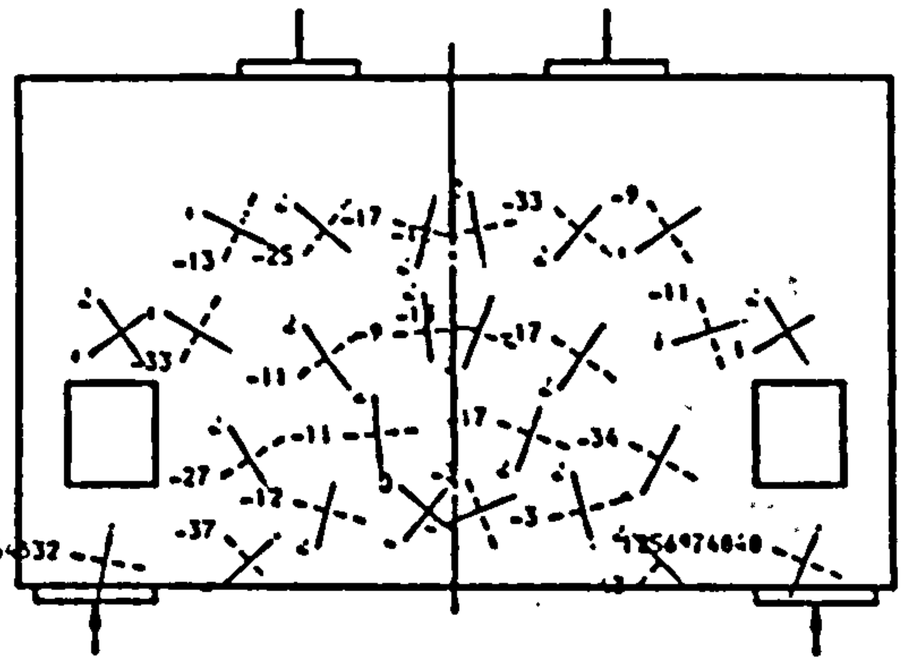

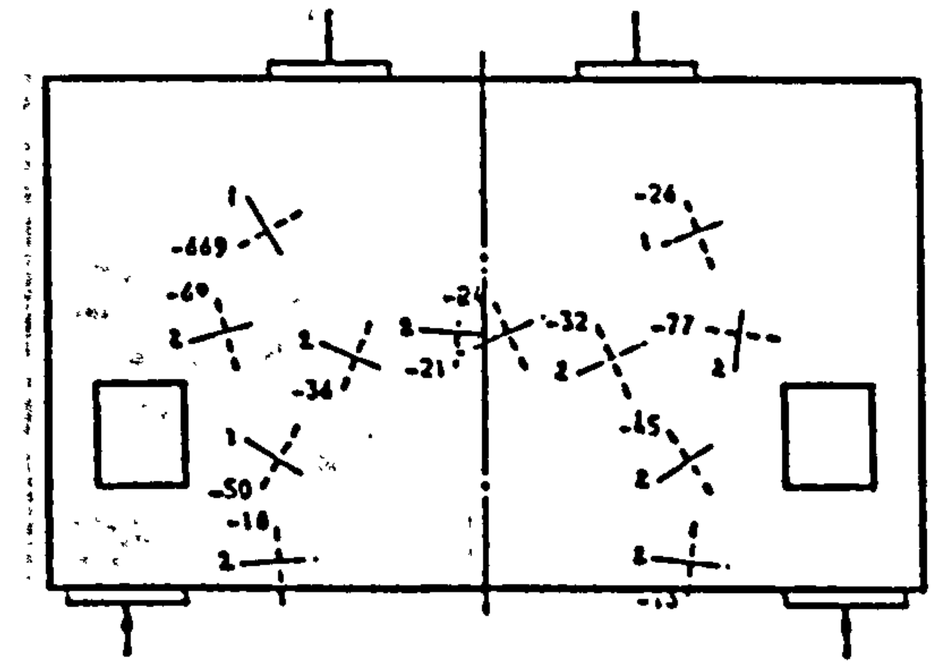

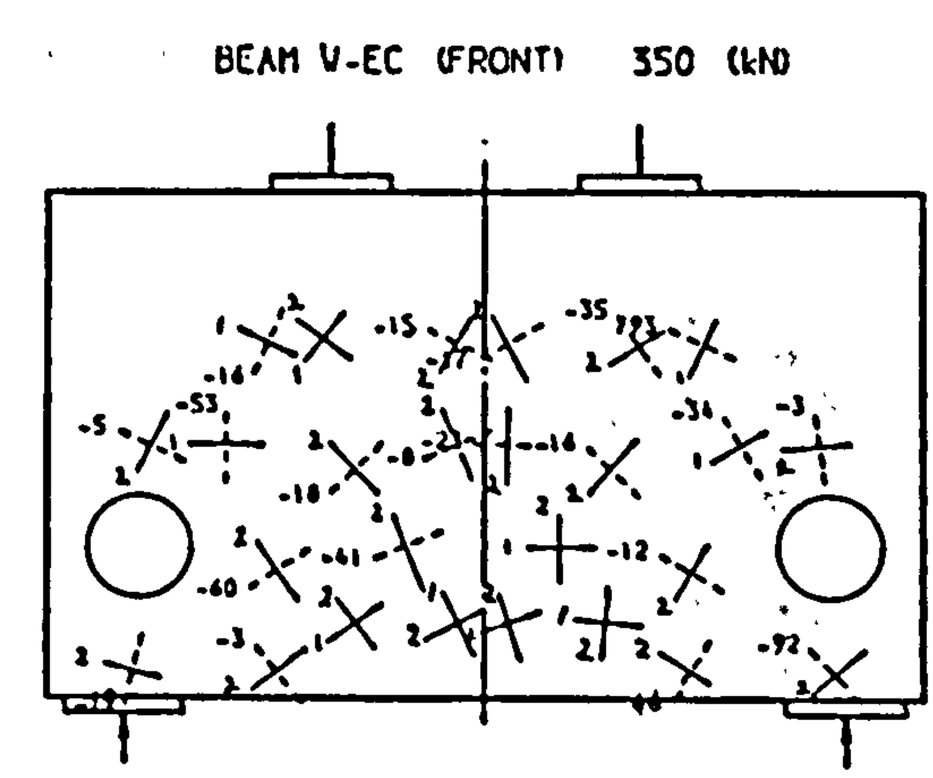

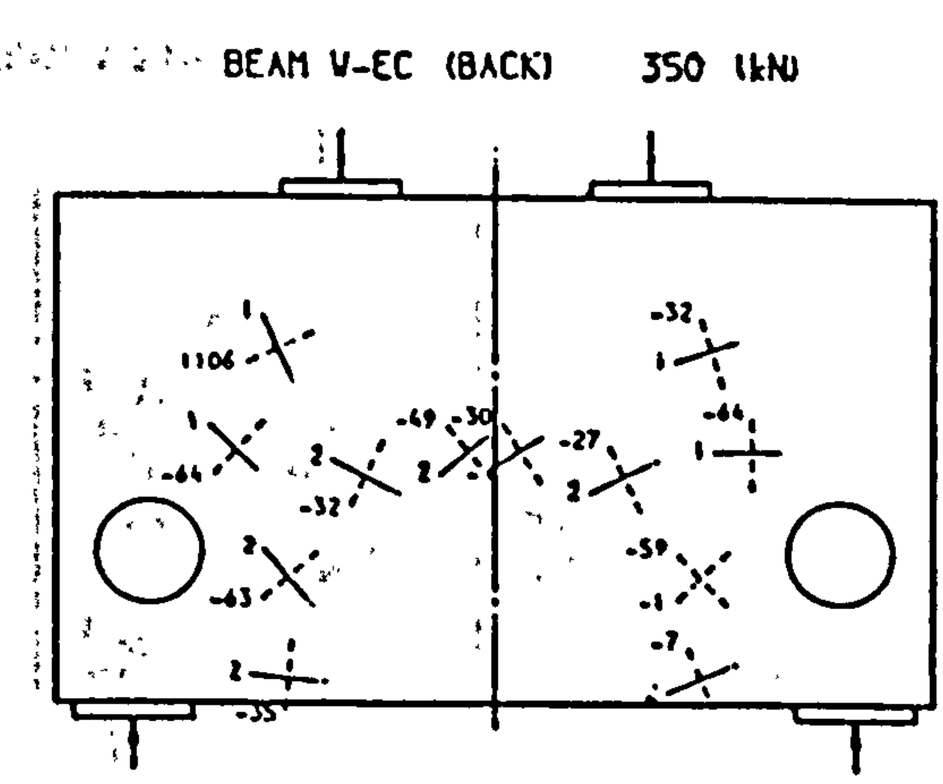

Figure 6.41 : Principal stresses after the last load increments (W-Series beams, compression field theory) [cont'd]

BEAM V-AR-S (FRONT) 320 (kN)

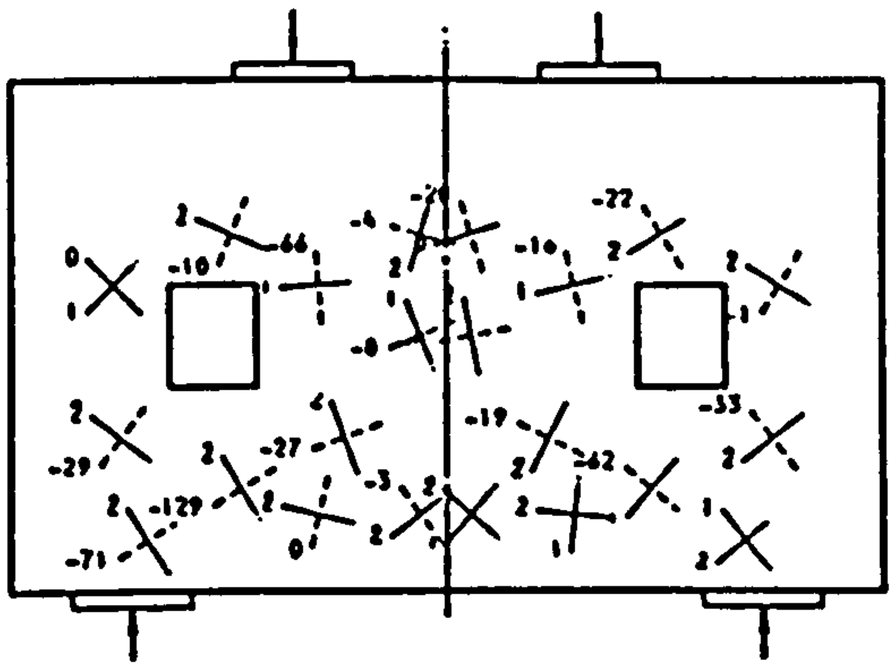

BEAM V-AR-S (BACK) 320 (kN)

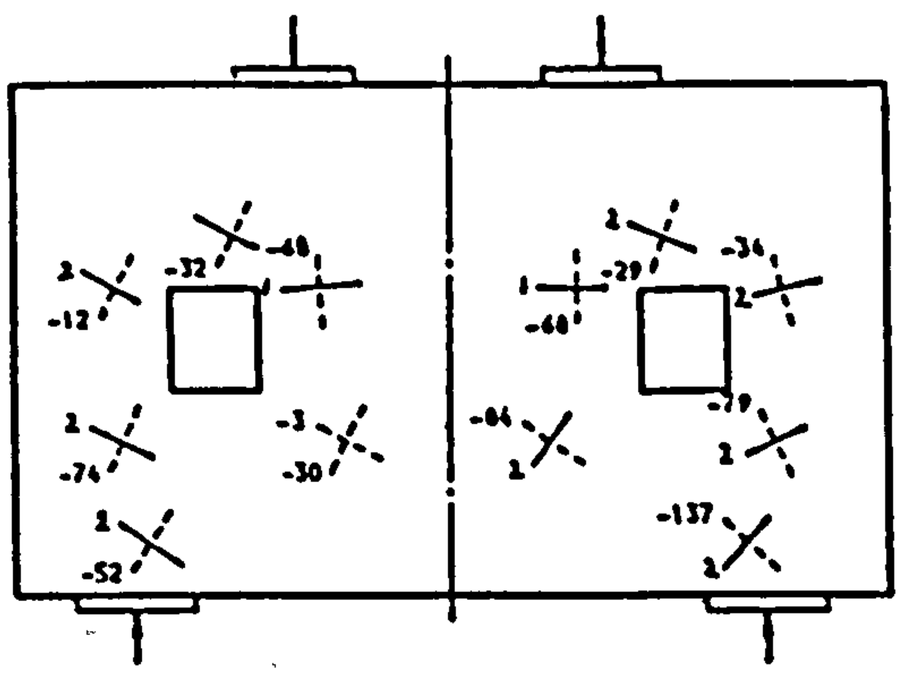

BEAM V-AC-S (FRONT) 460 (kN)

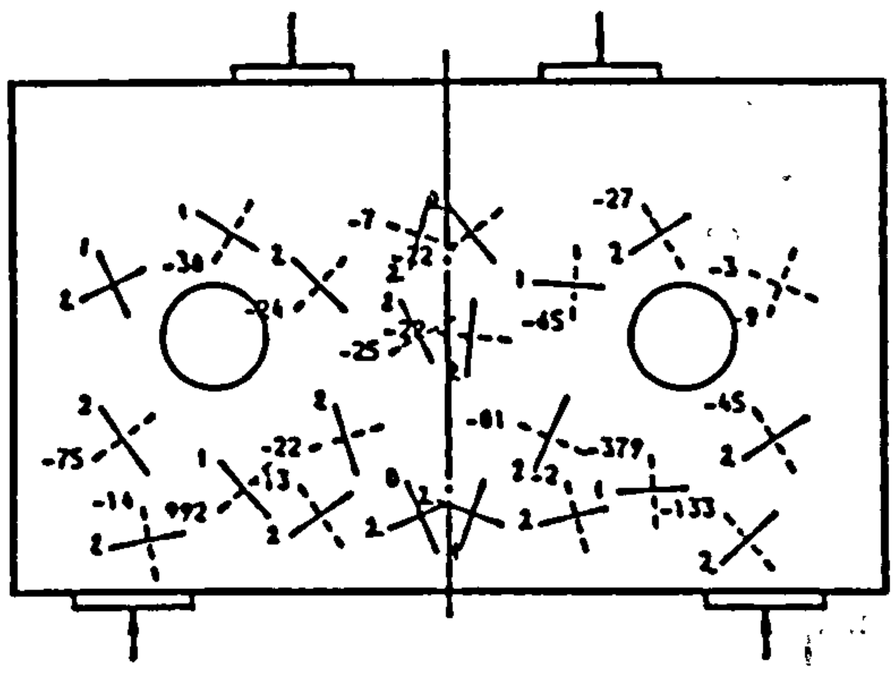

BEAM V-AC-S (BACK) 460 (kN)

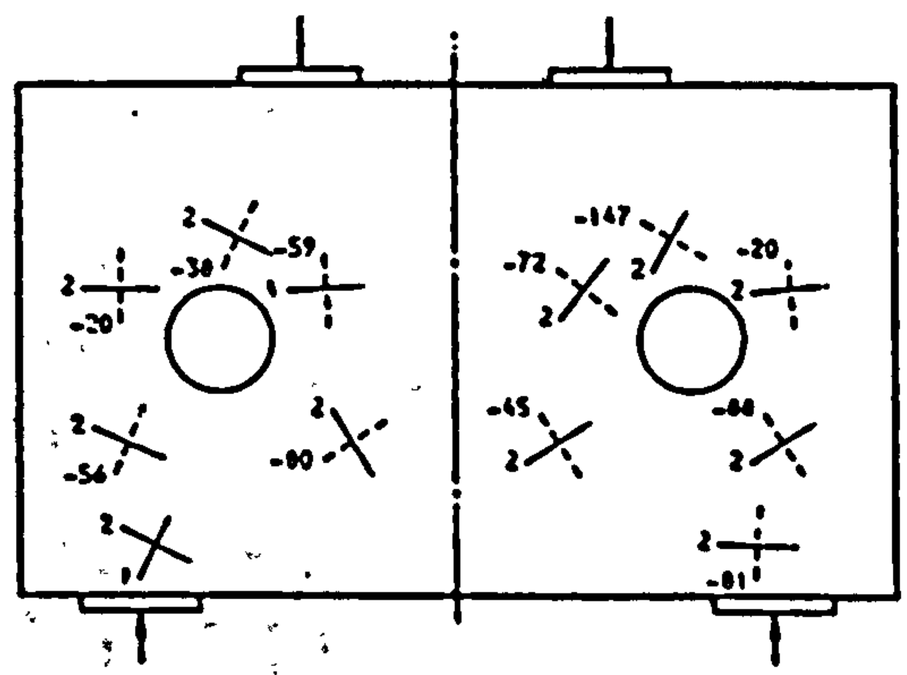

BEAM V-29-0.1-R1 (FRONT) 520 (kN)

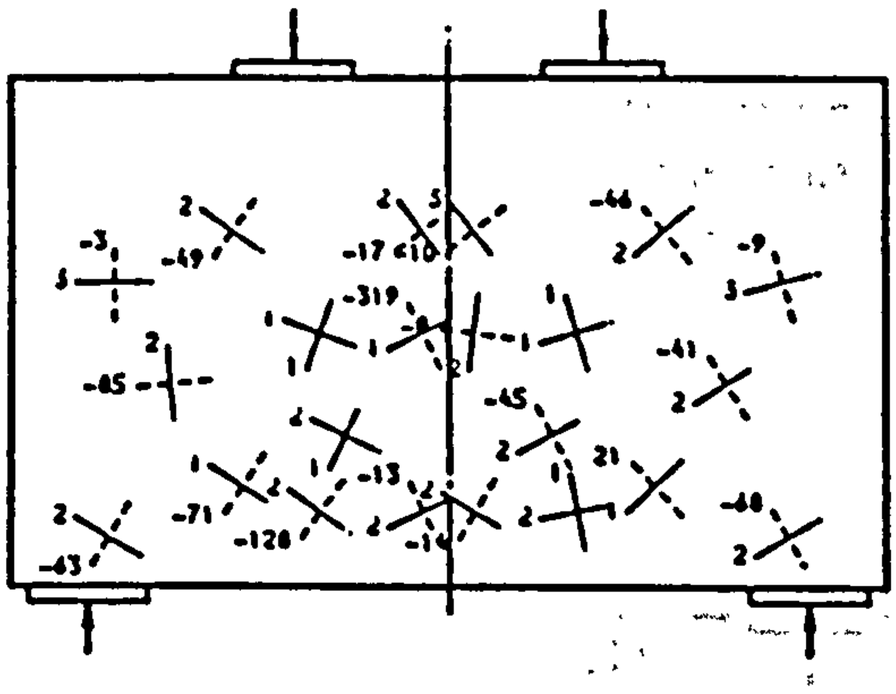

BEAM V-29-0.1-R1 (BACK) 660 (kN)

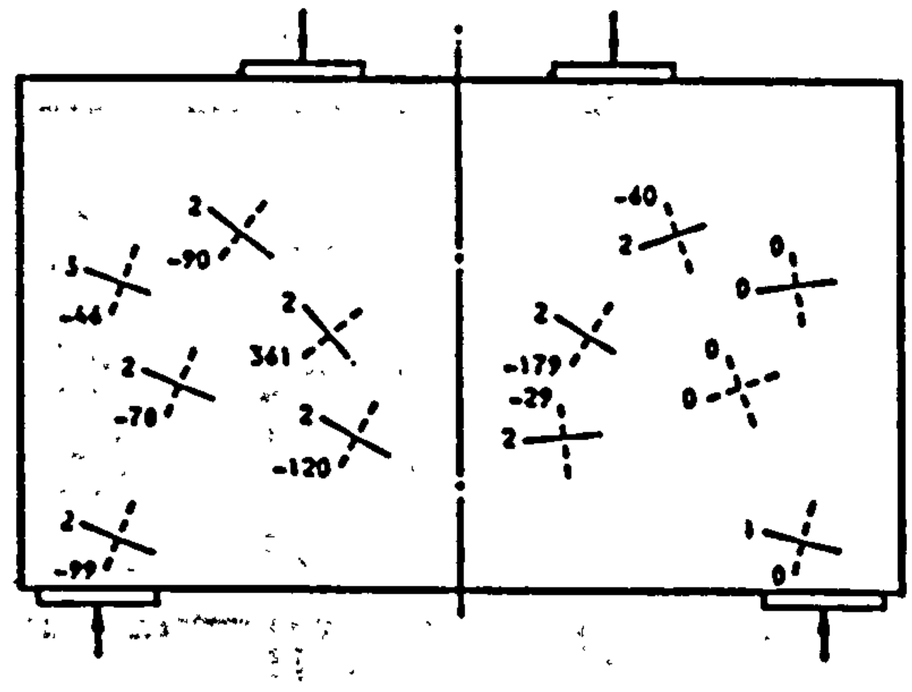

BEAM V-29-0.1-R2 (FRONT) 650 (kN)

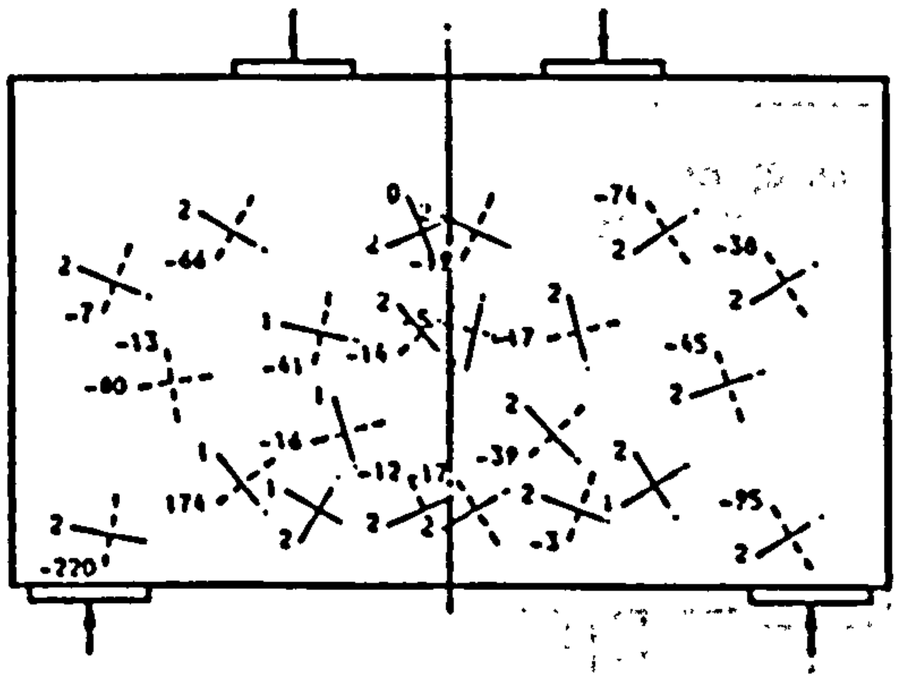

BEAM V-29-0.1-R2 (BACK) 900 (kN)

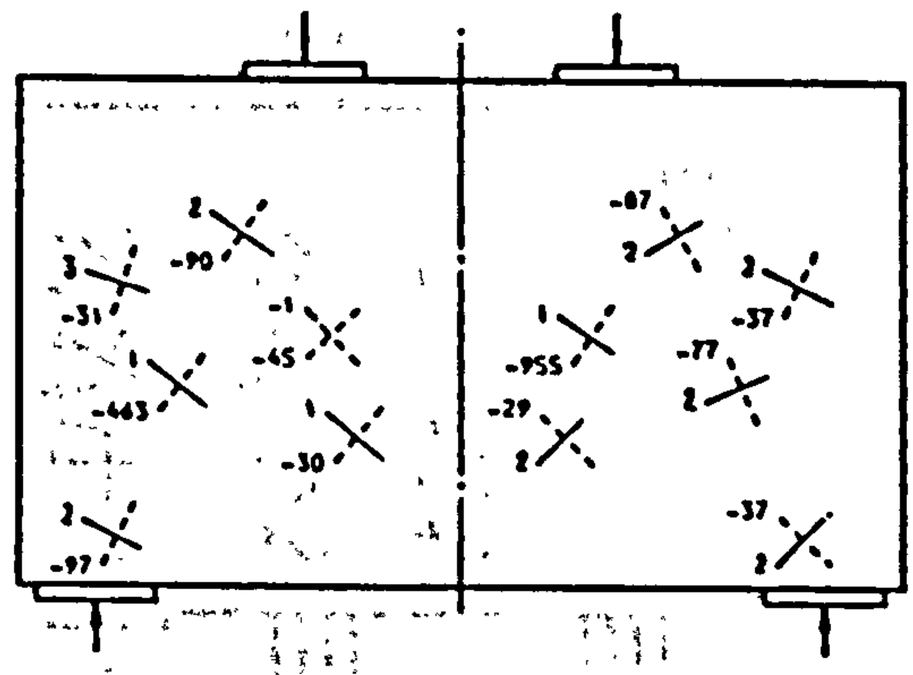

— Tension Positive
---- Compression Negative

(All figures are in (N/mm^2)

Figure 6.41 : Principal stresses after the last load increments (W-Series beams, compression field theory) [cont'd]

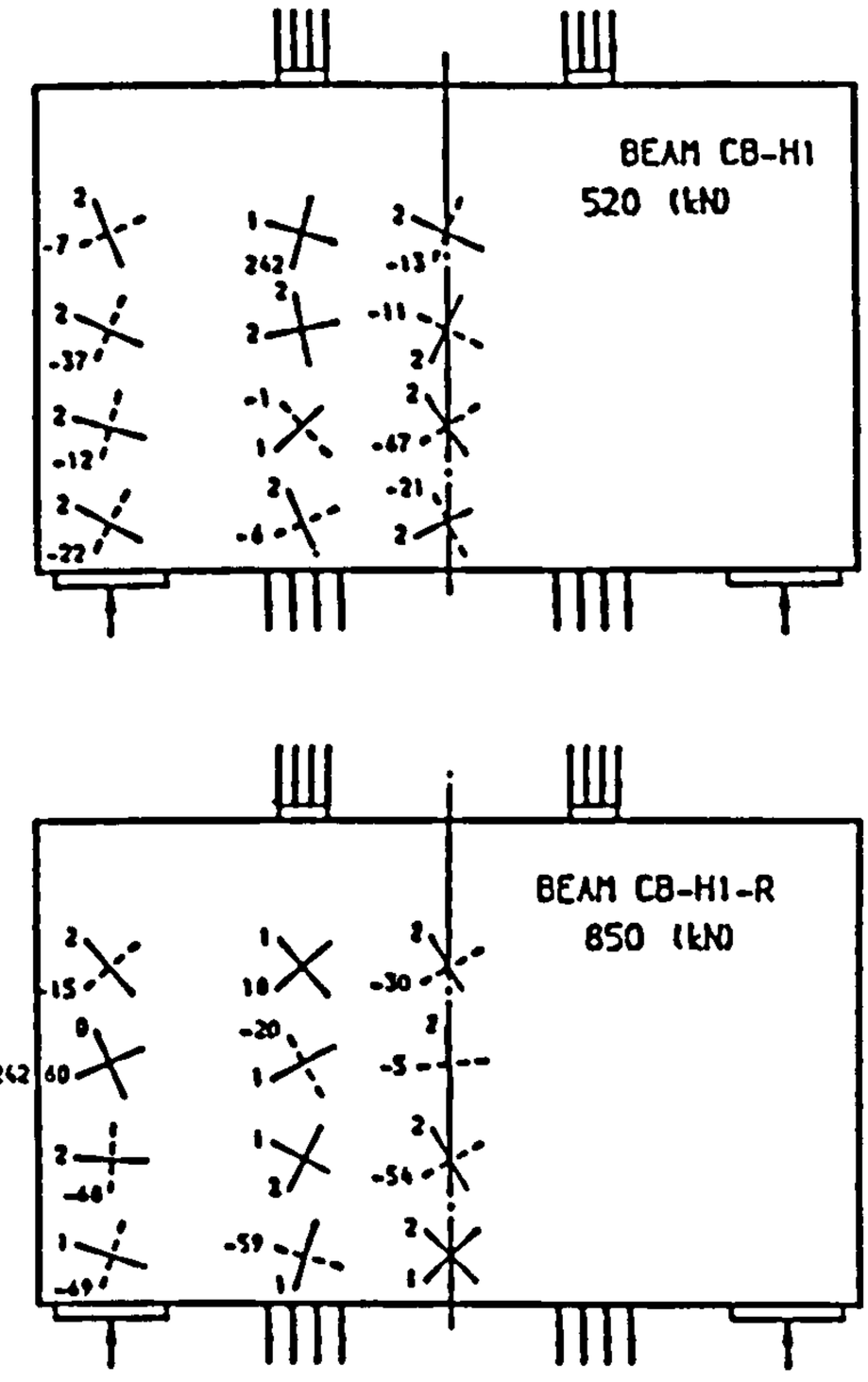

Figure 6.42 : Principal stresses after the last load increments (CB-Series beams, compression field theory)

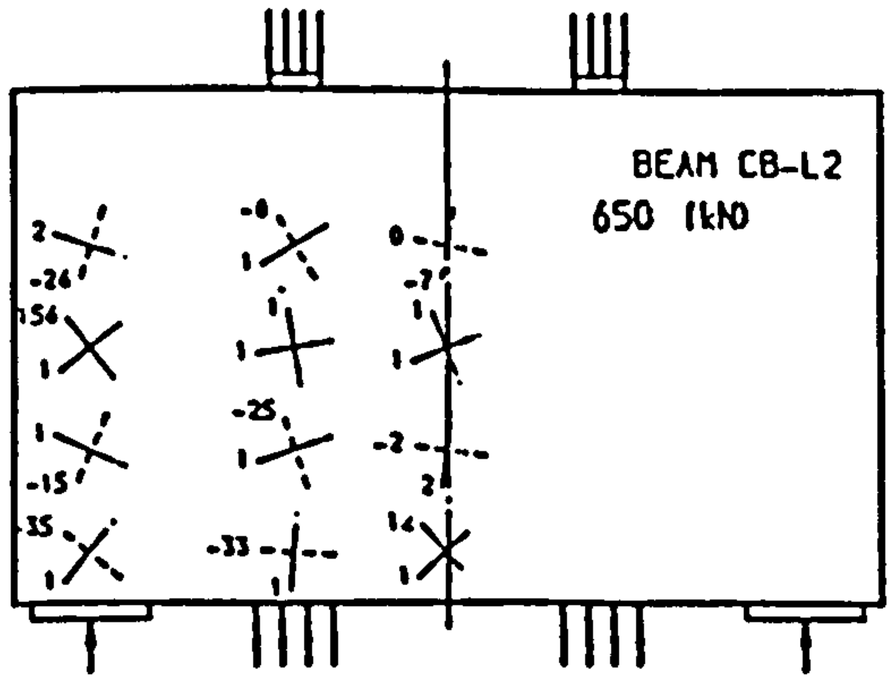

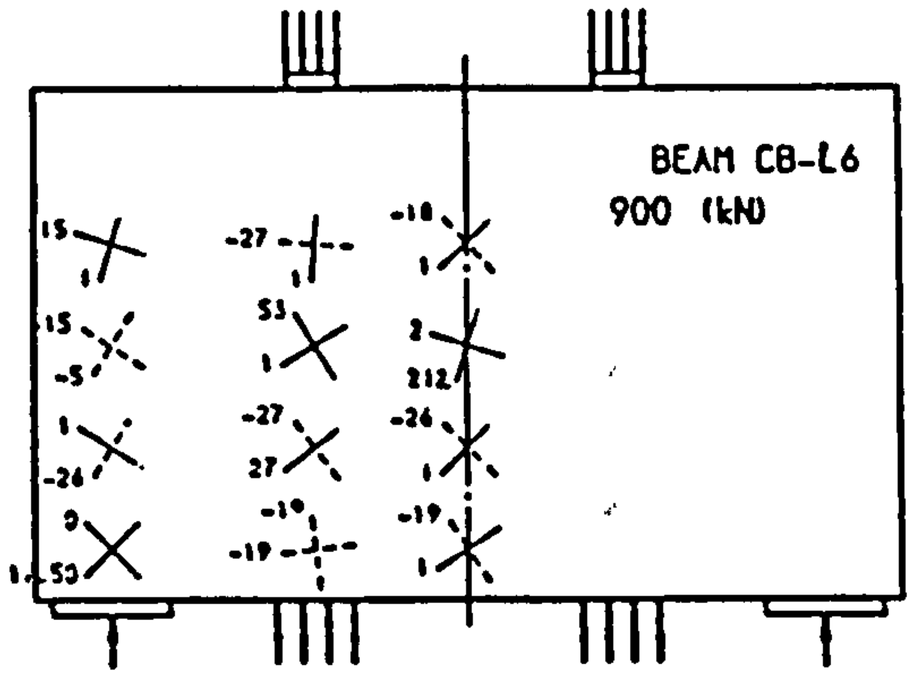

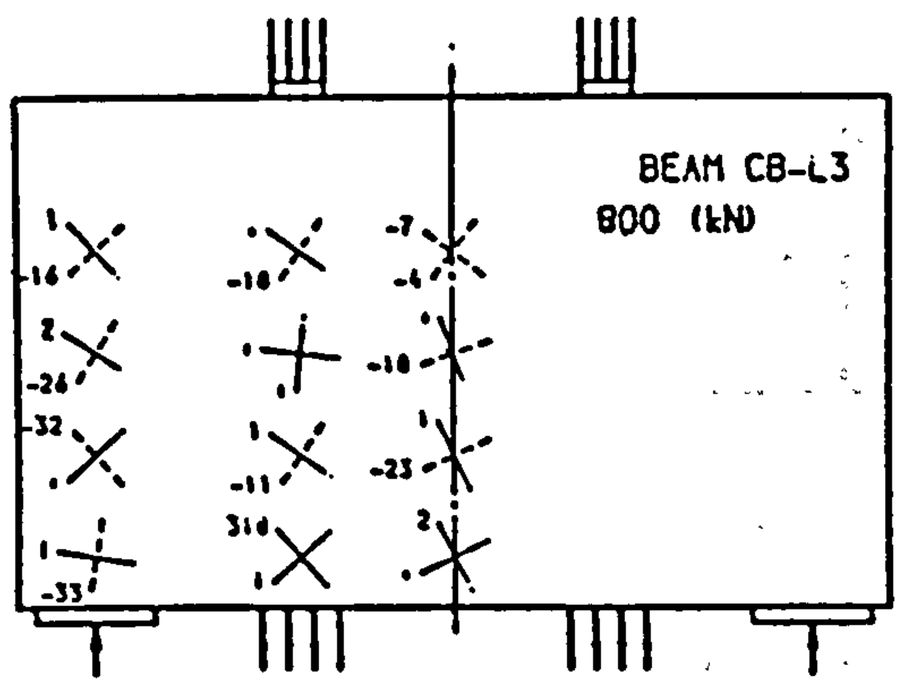

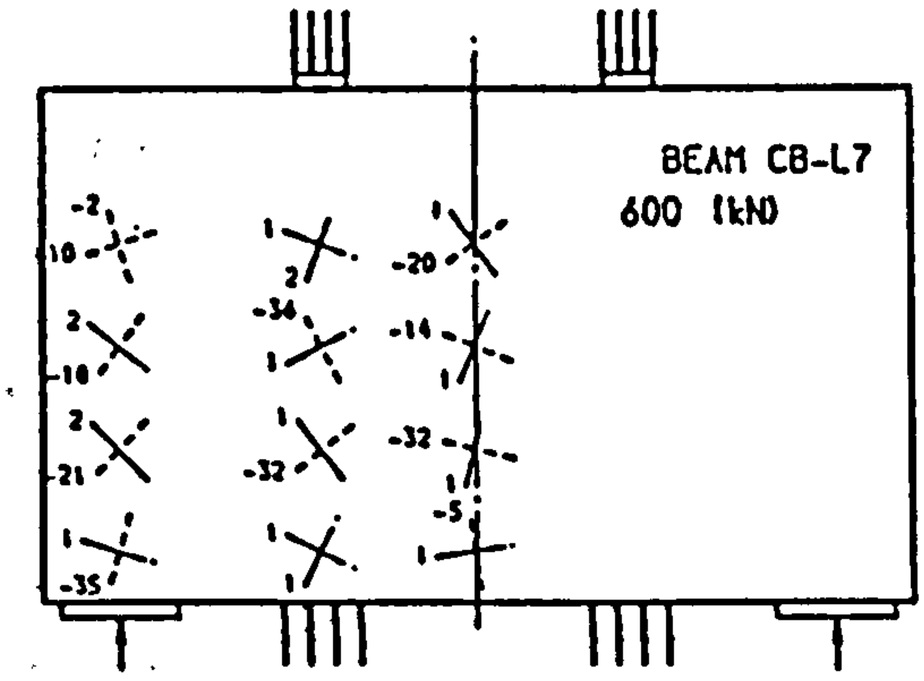

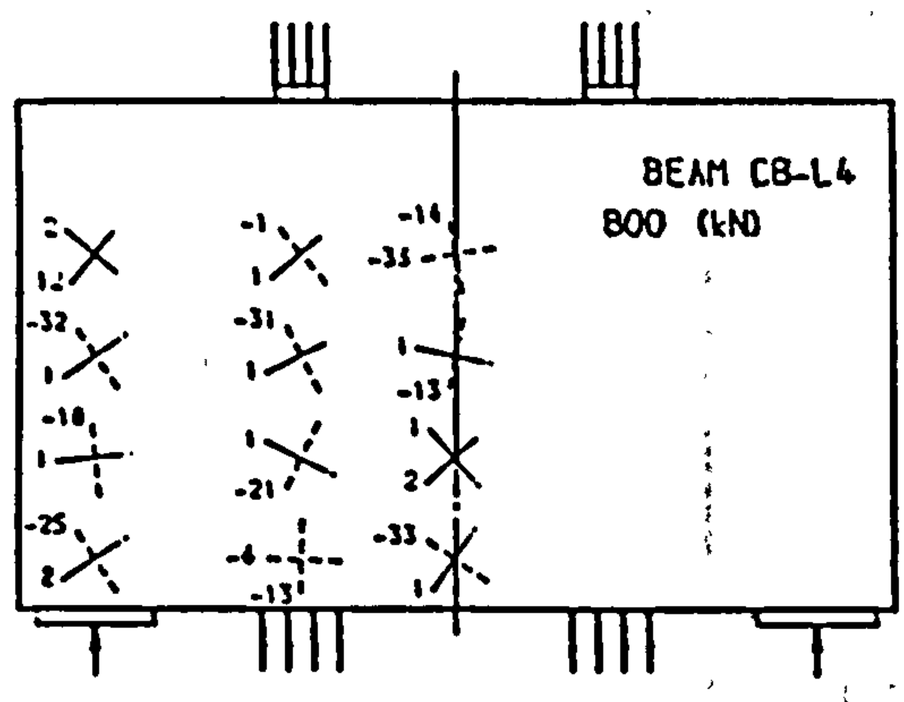

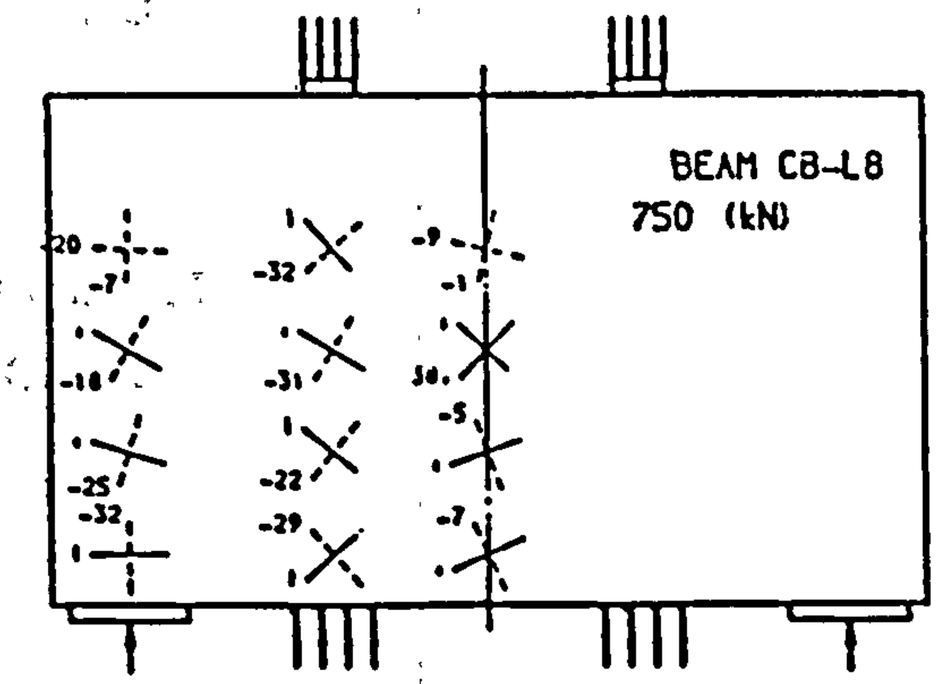

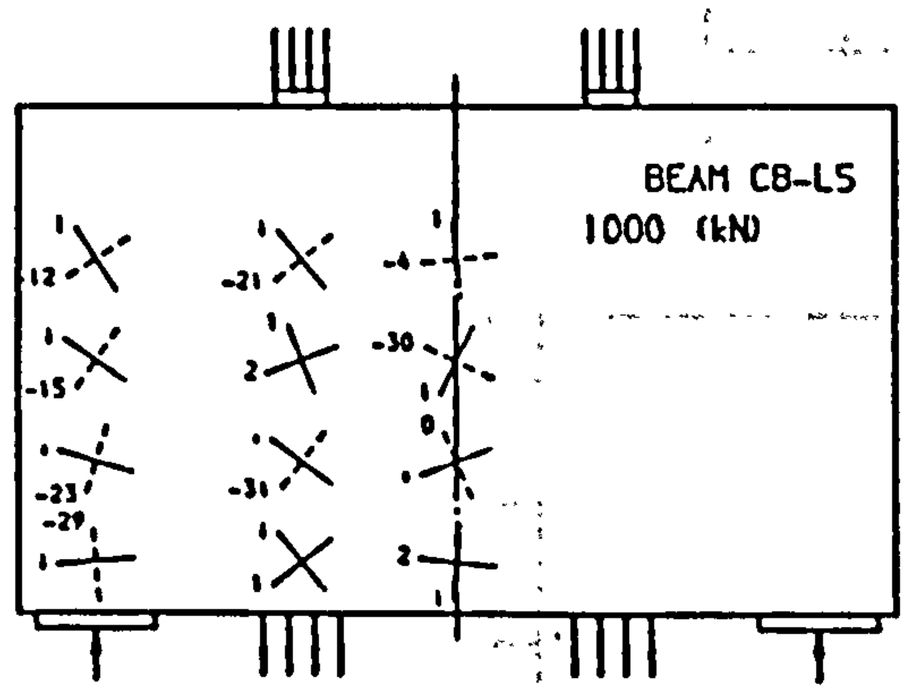

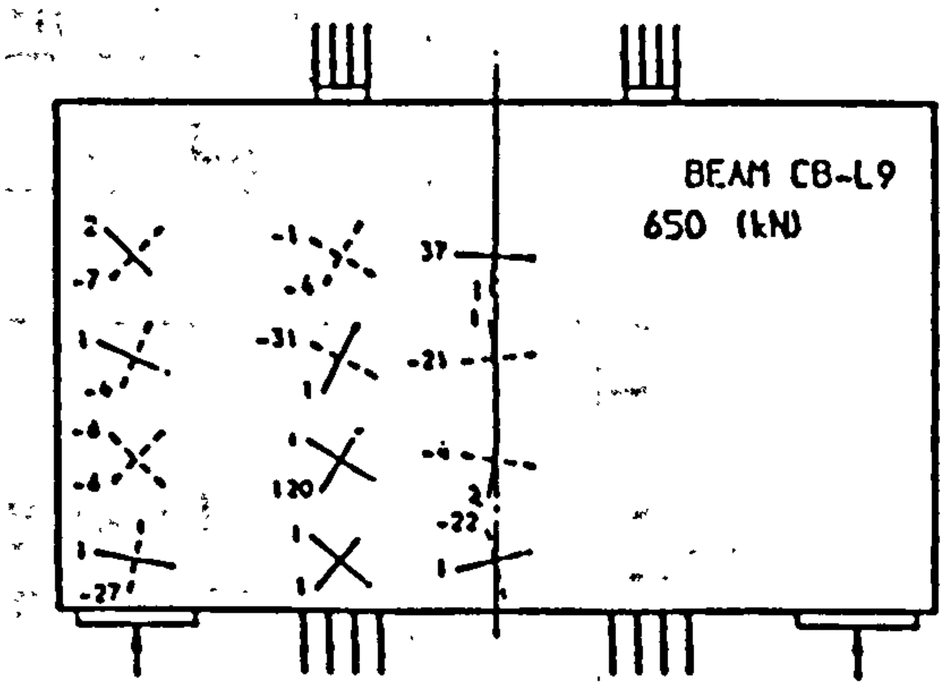

—— Tension Positive

---- Compression Negative

(All figures are in N/mm^2)

Figure 6.42 : Principal stresses after the last load increments (CB-Series beams, compression field theory) [cont'd]

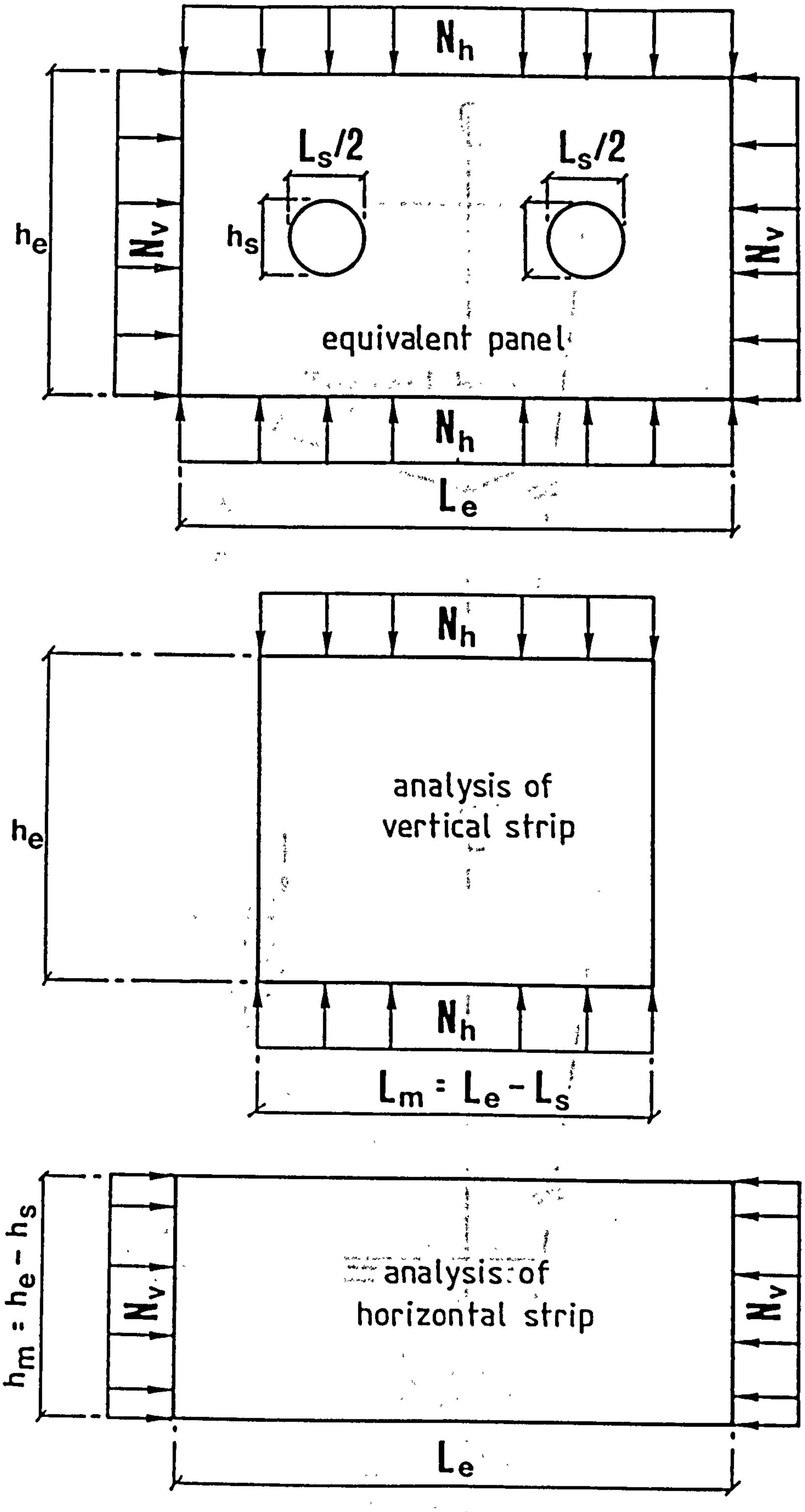

Figure 7.1 : Analysis of equivalent panel with web-openings

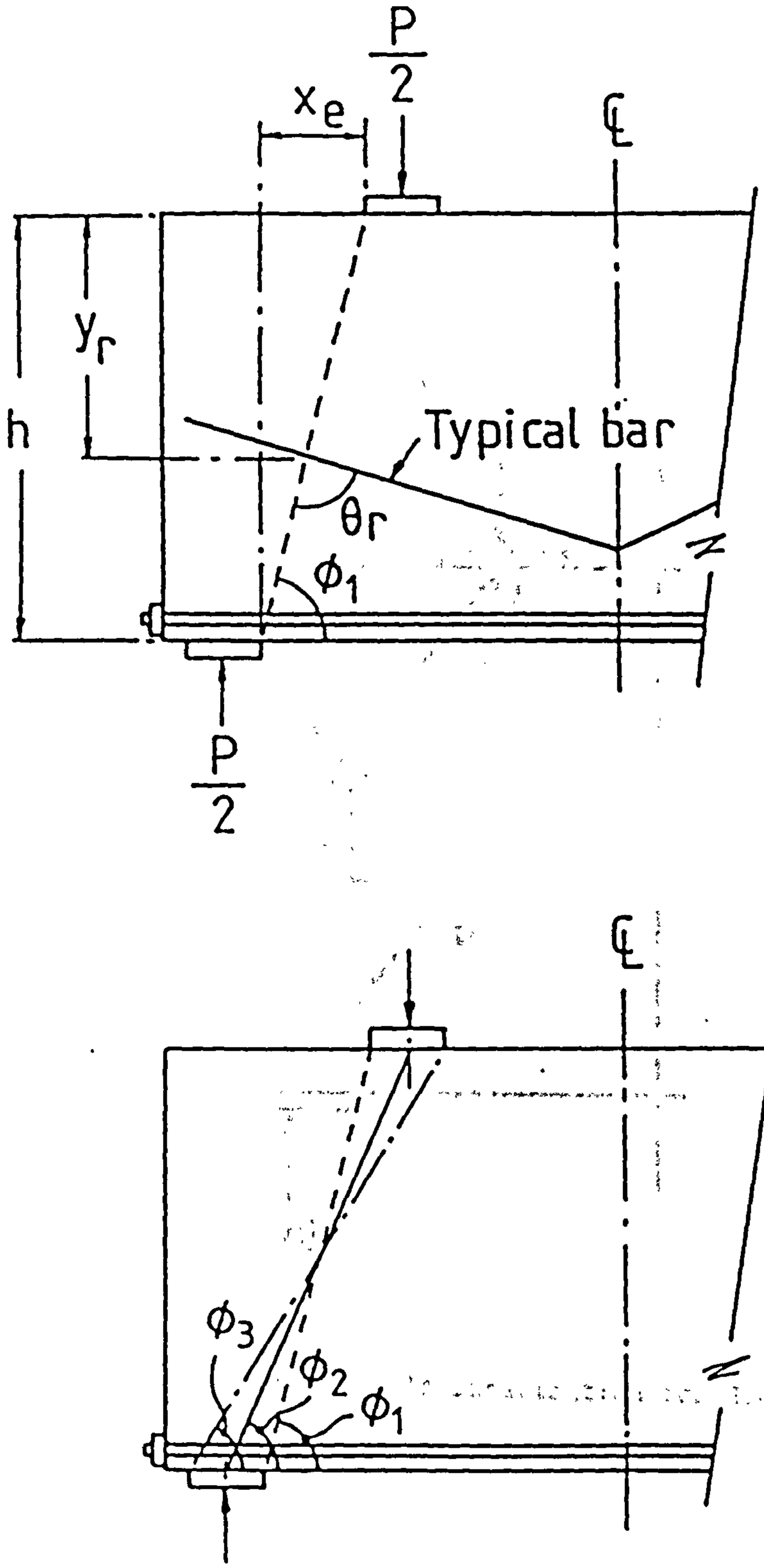

Figure 7.2 : Meanings of symbols in the CIRIA's shear equation

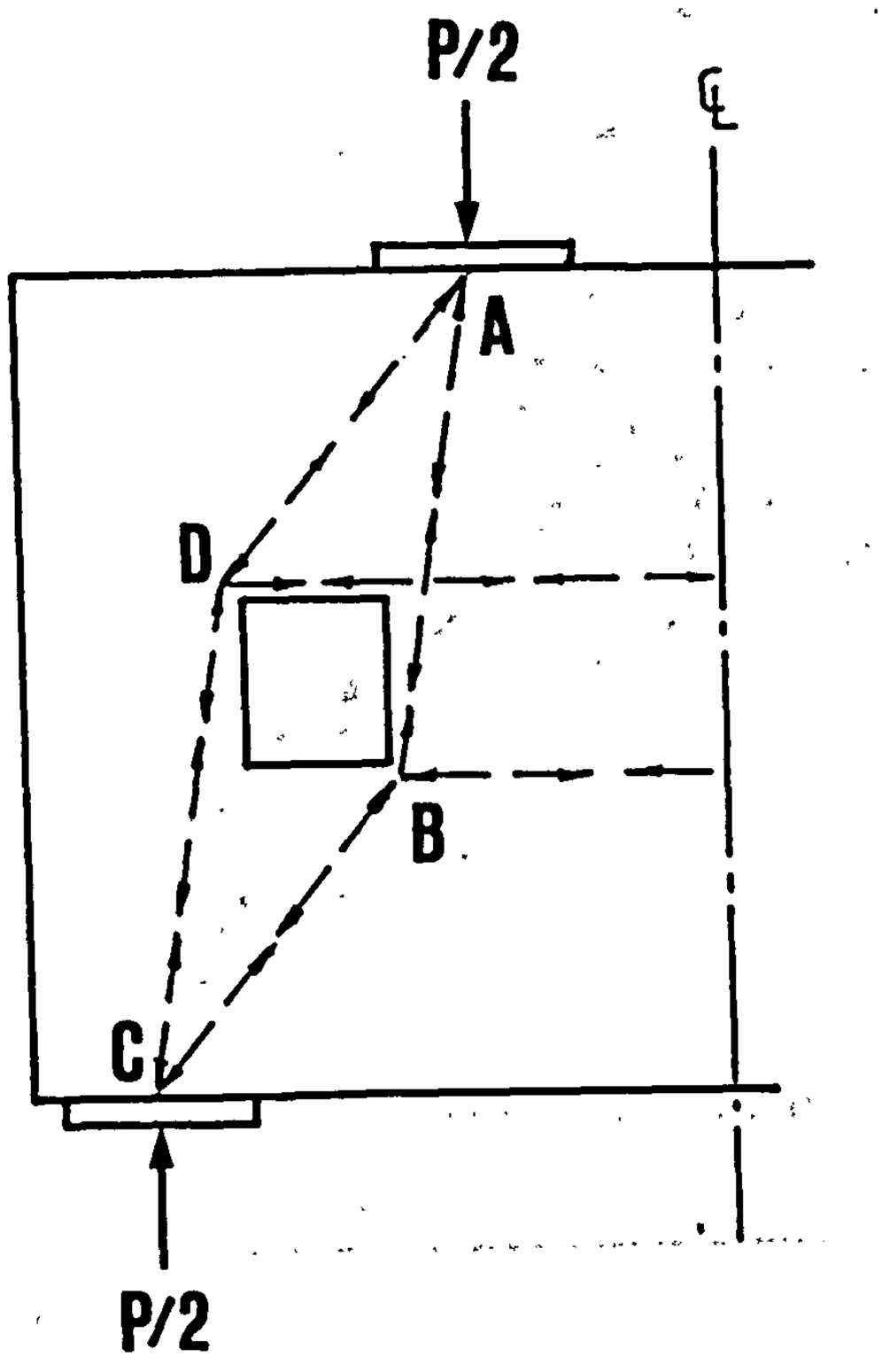

Figure 7.3 : Kong et al's idealization for deep beams with web-openings

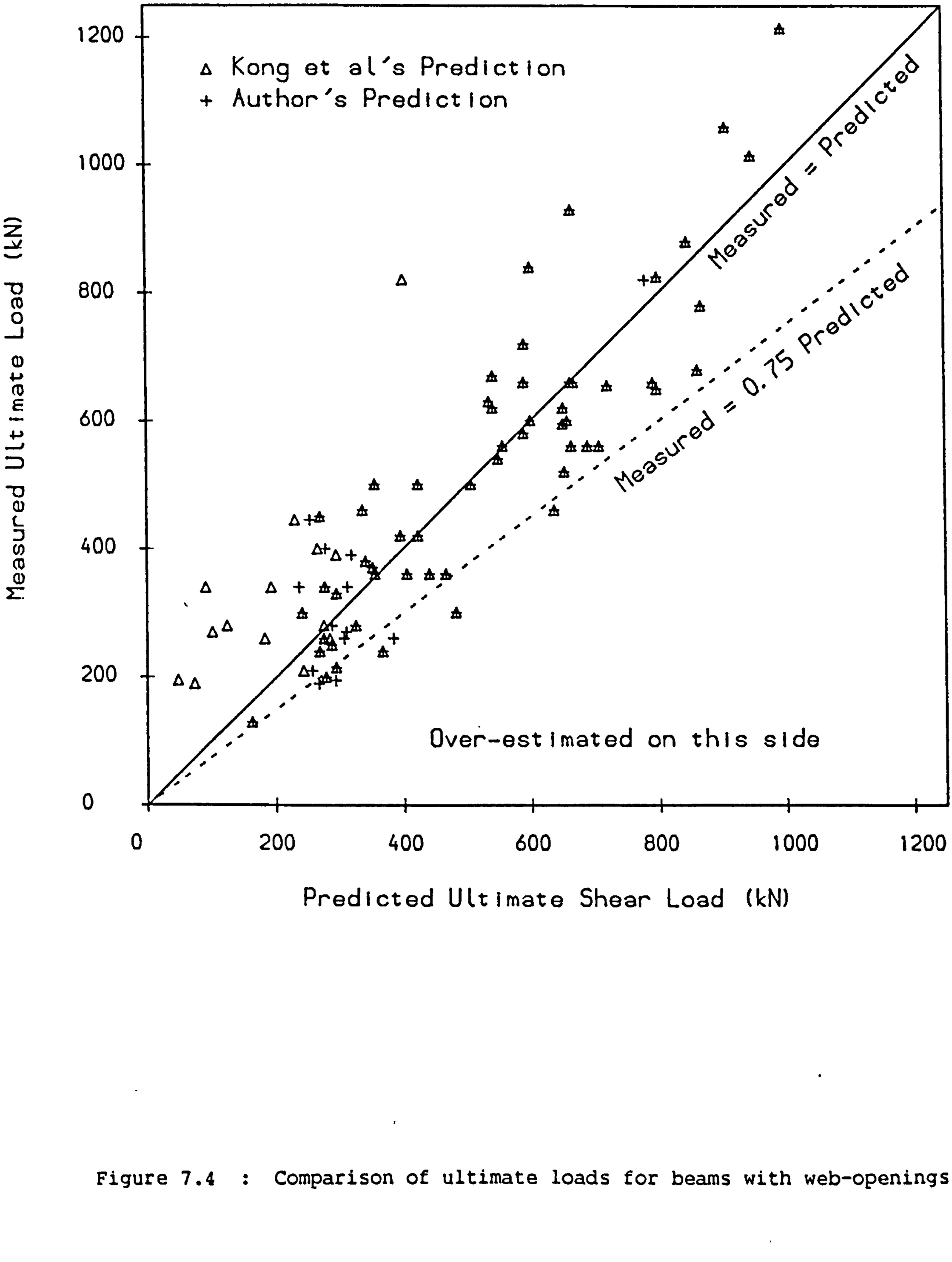

Figure 7.4 : Comparison of ultimate loads for beams with web-openings

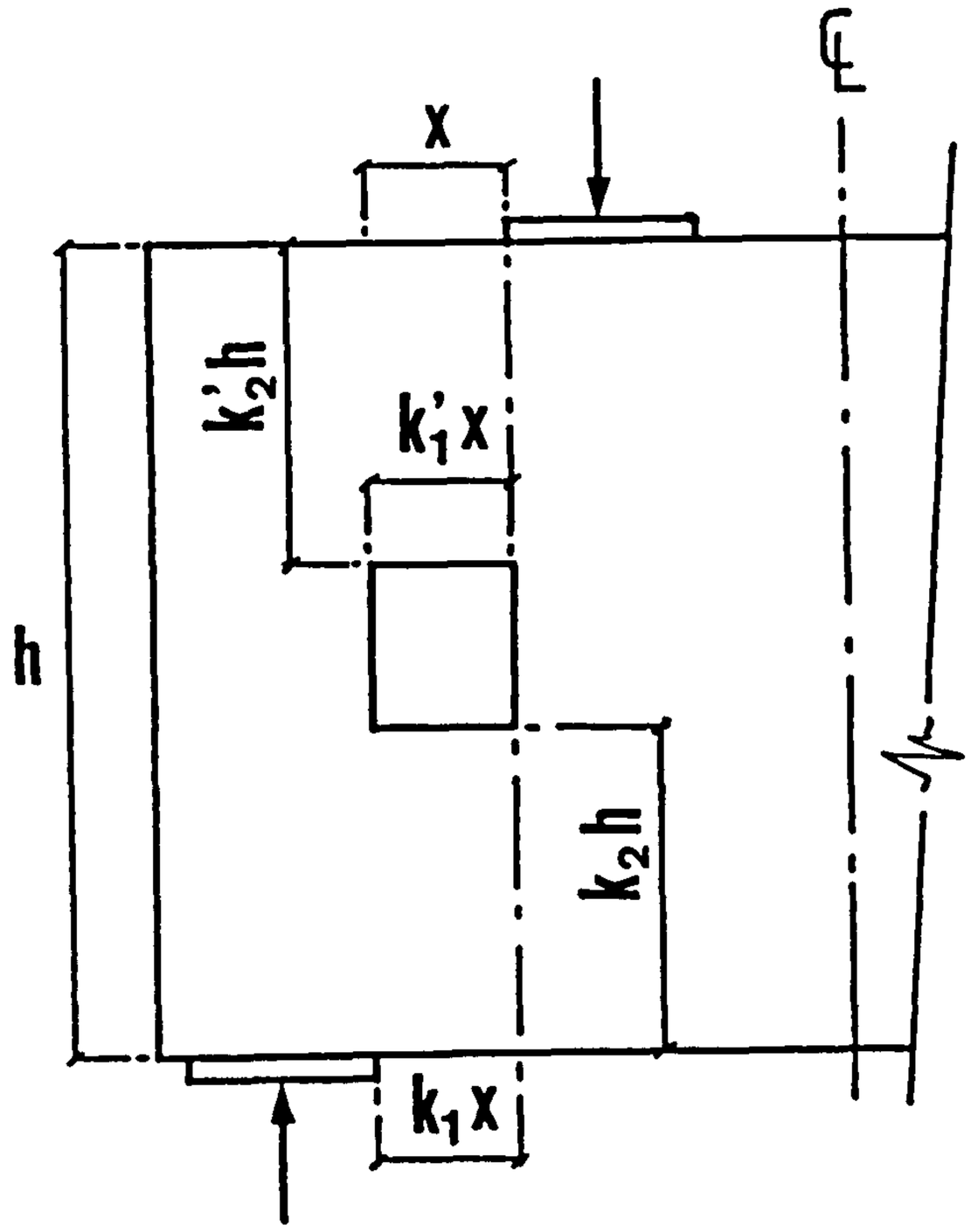

Rectangular

Web-opening

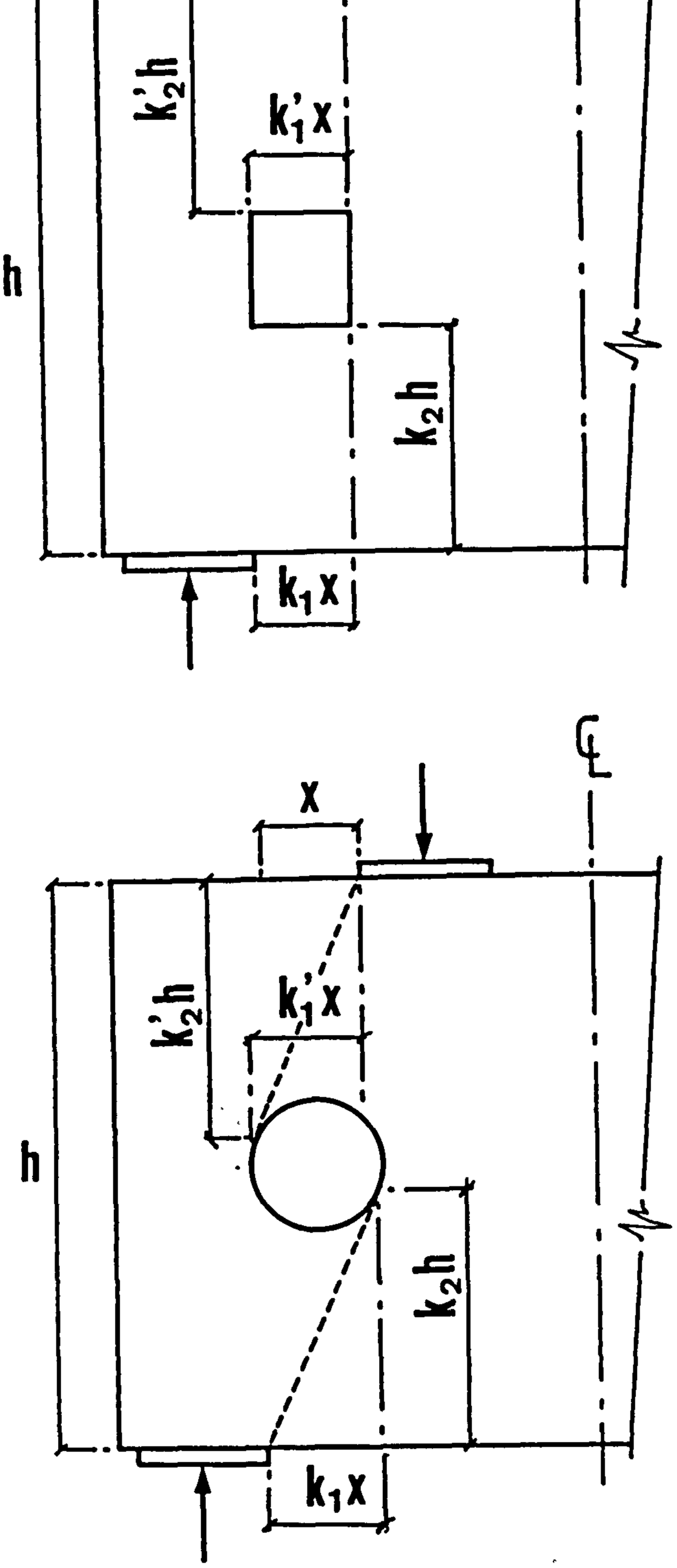

Circular

Web-opening

Figure 7.5 : Generalized notations for deep beams with web-openings

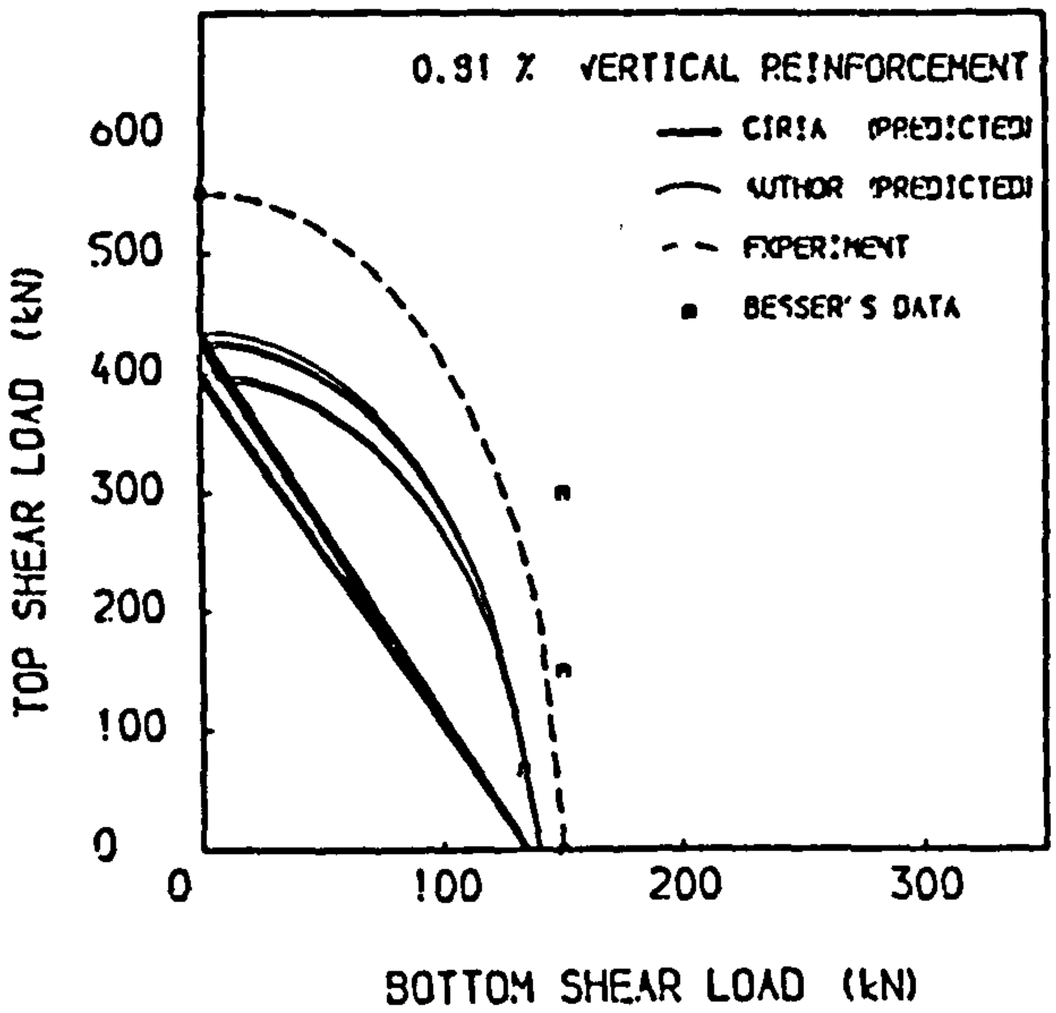

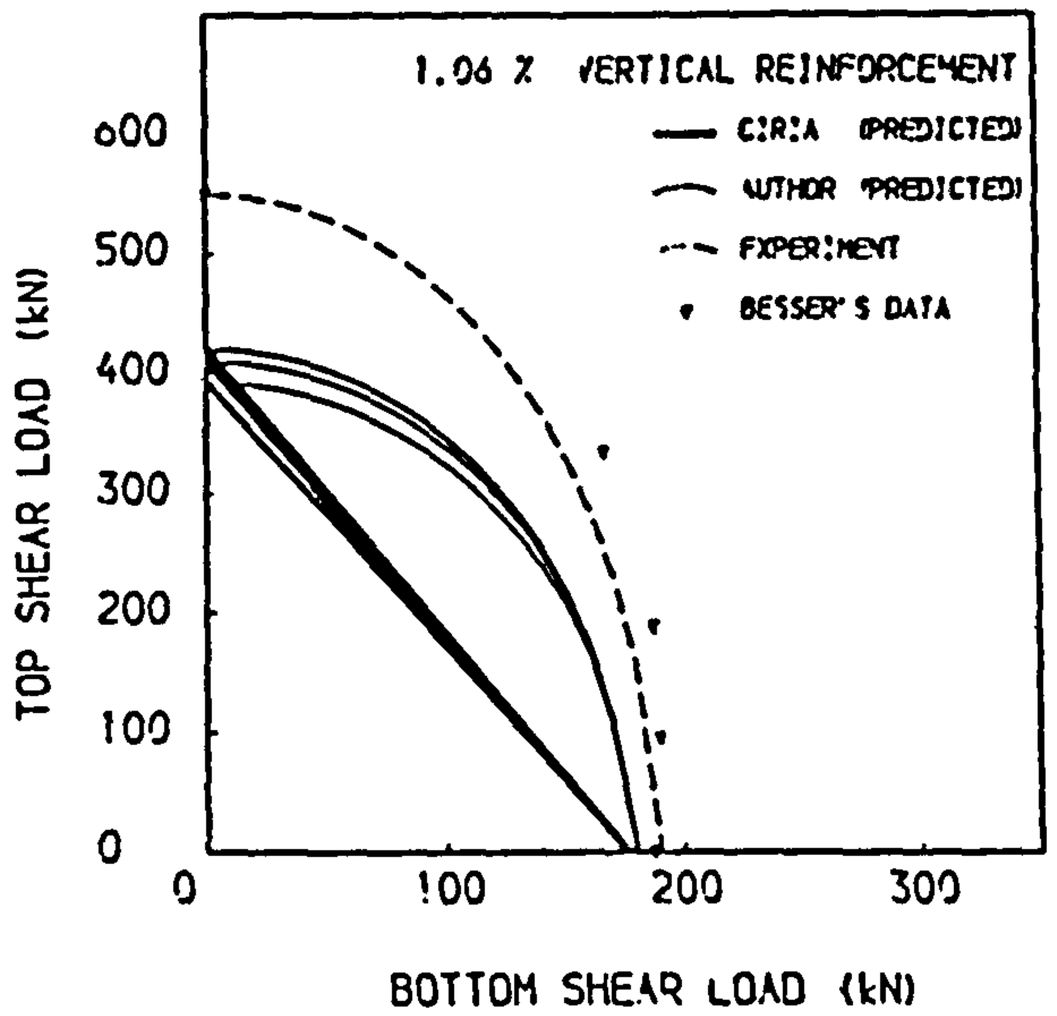

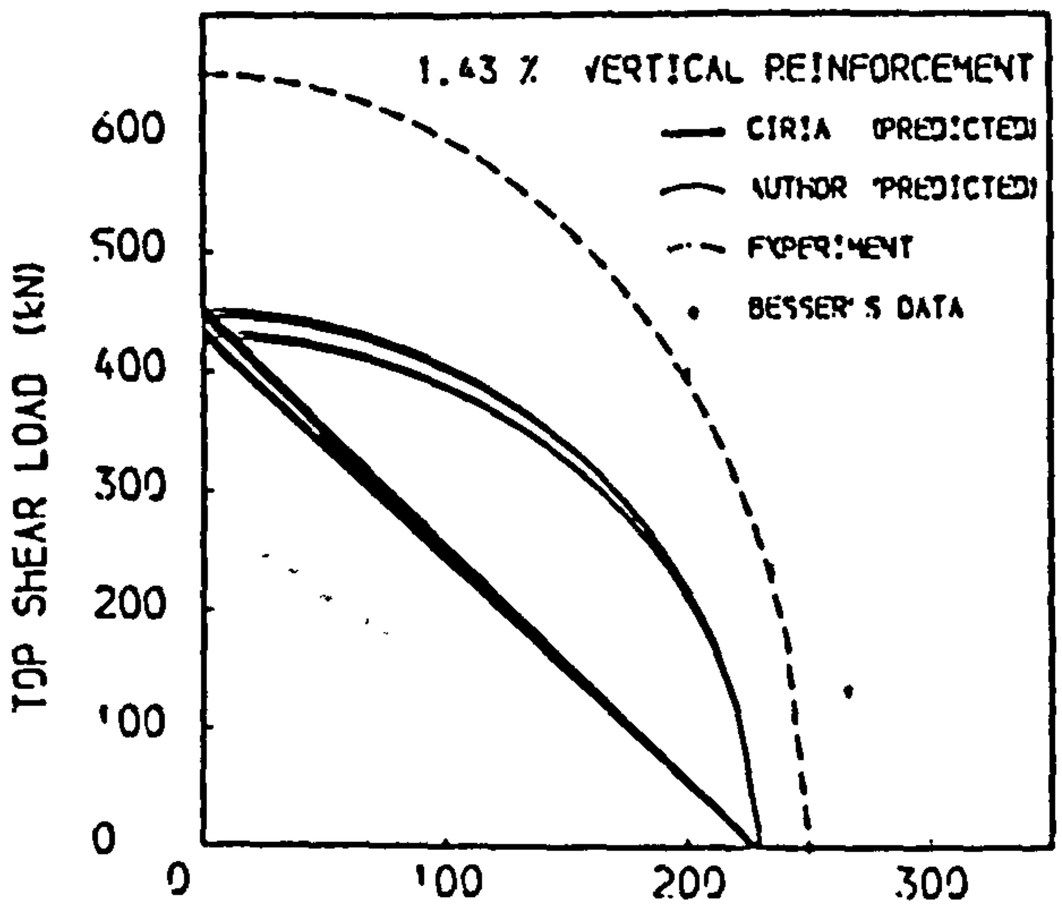

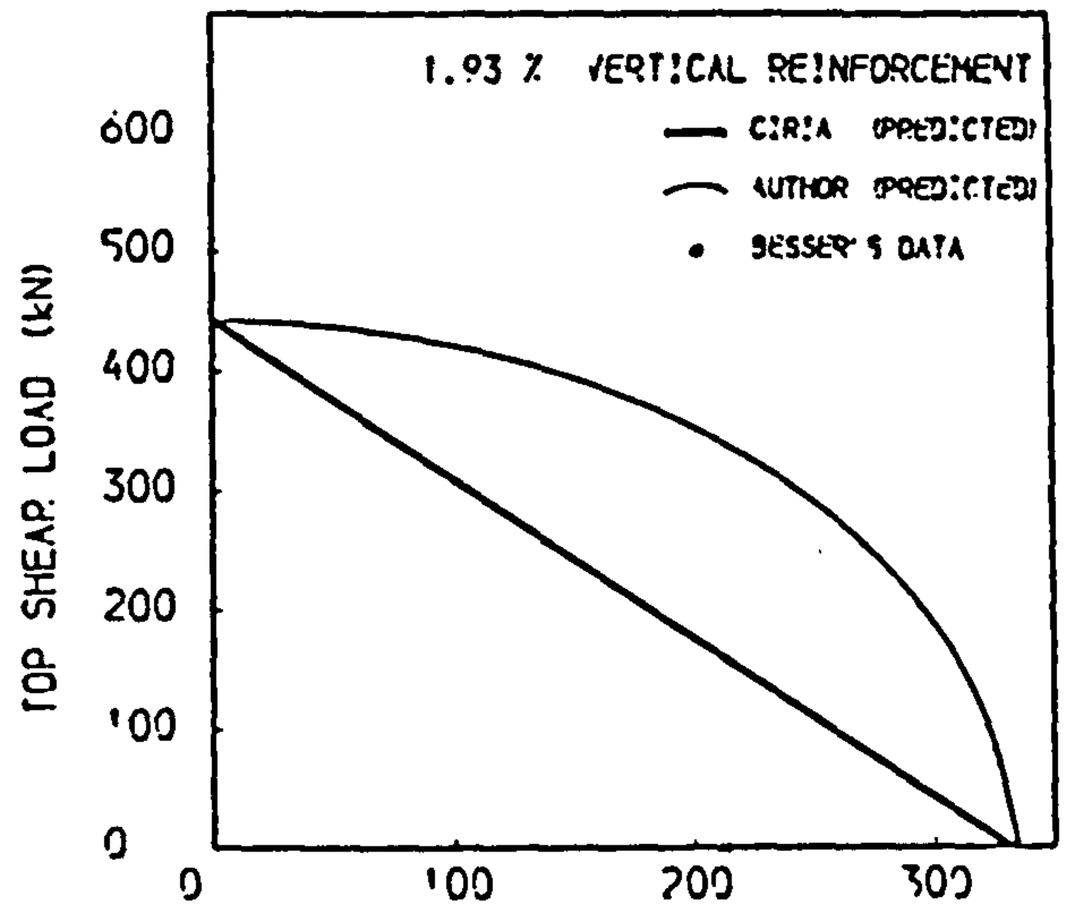

Figure 7.6 : Top and bottom loads interaction diagrams (predicted)

Figure 7.7 : Top and bottom loads interaction diagrams (computed)

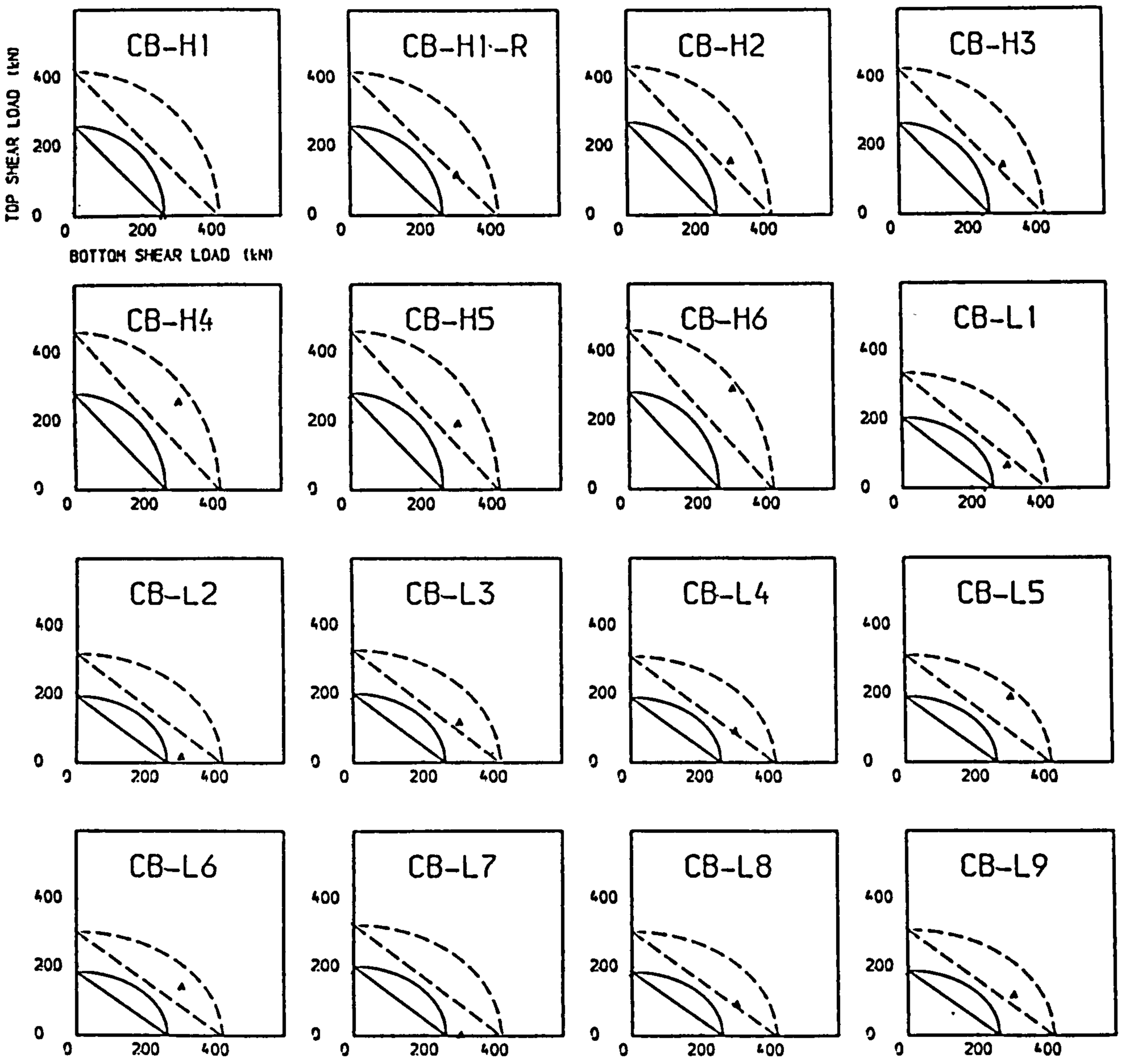

Figure 7.8 : Top and bottom loads interaction diagrams (CB-Series)

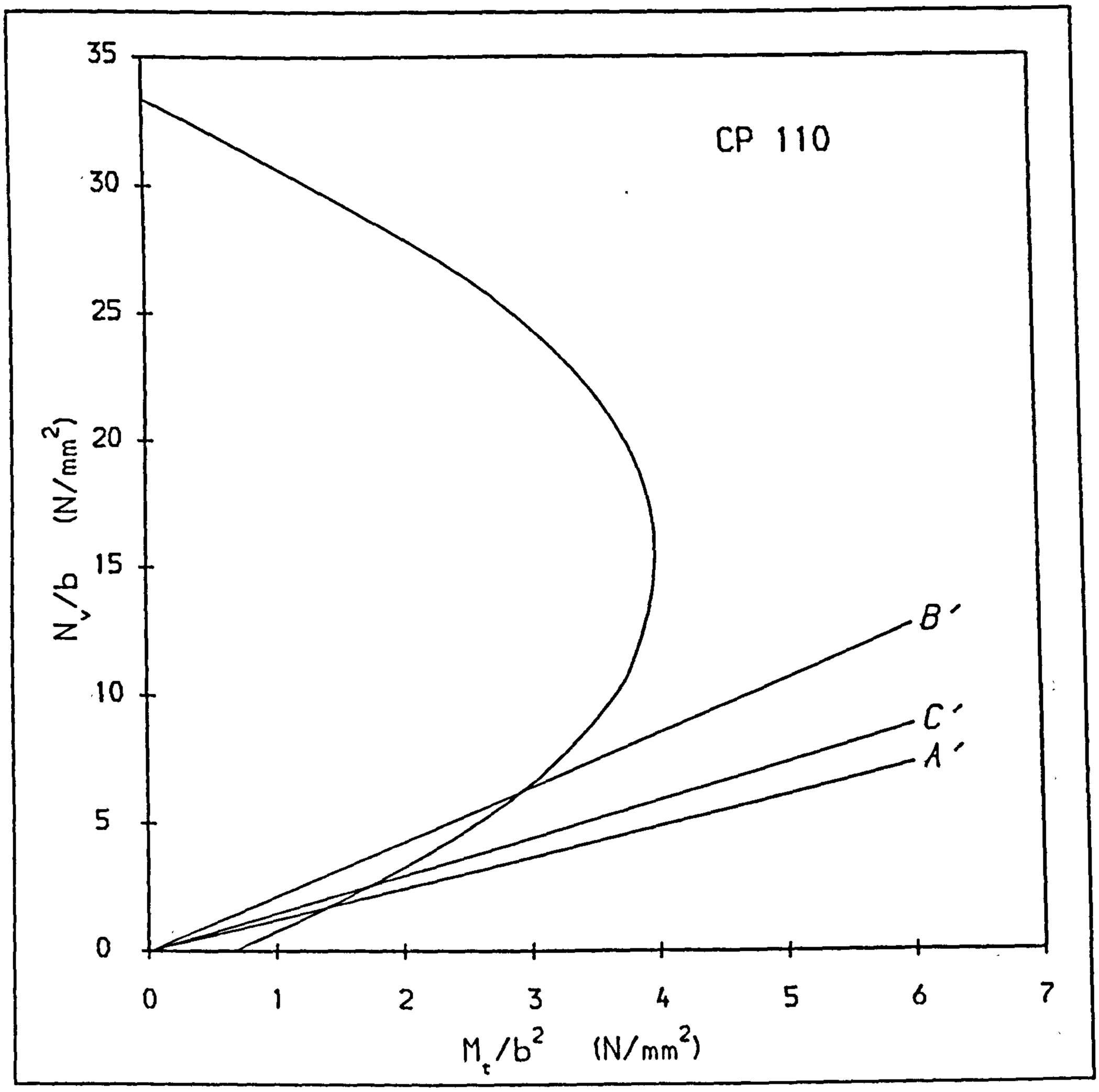

Figure A.1 : Load-moment interaction diagram (CP 110, Beam A-25-0.2)

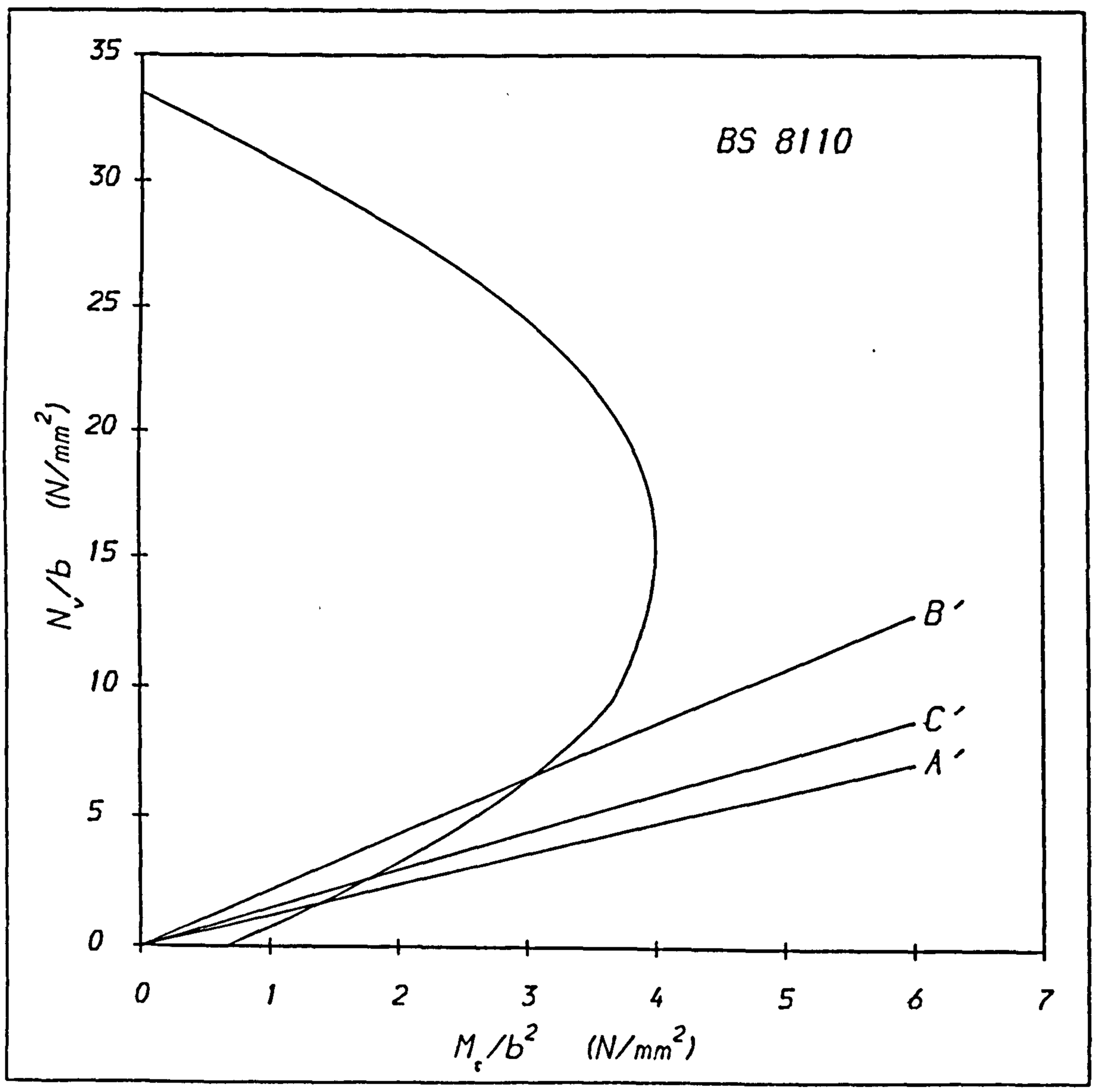

Figure A.2 : Load-moment interaction diagram (BS 8110, Beam A-25-0.2)

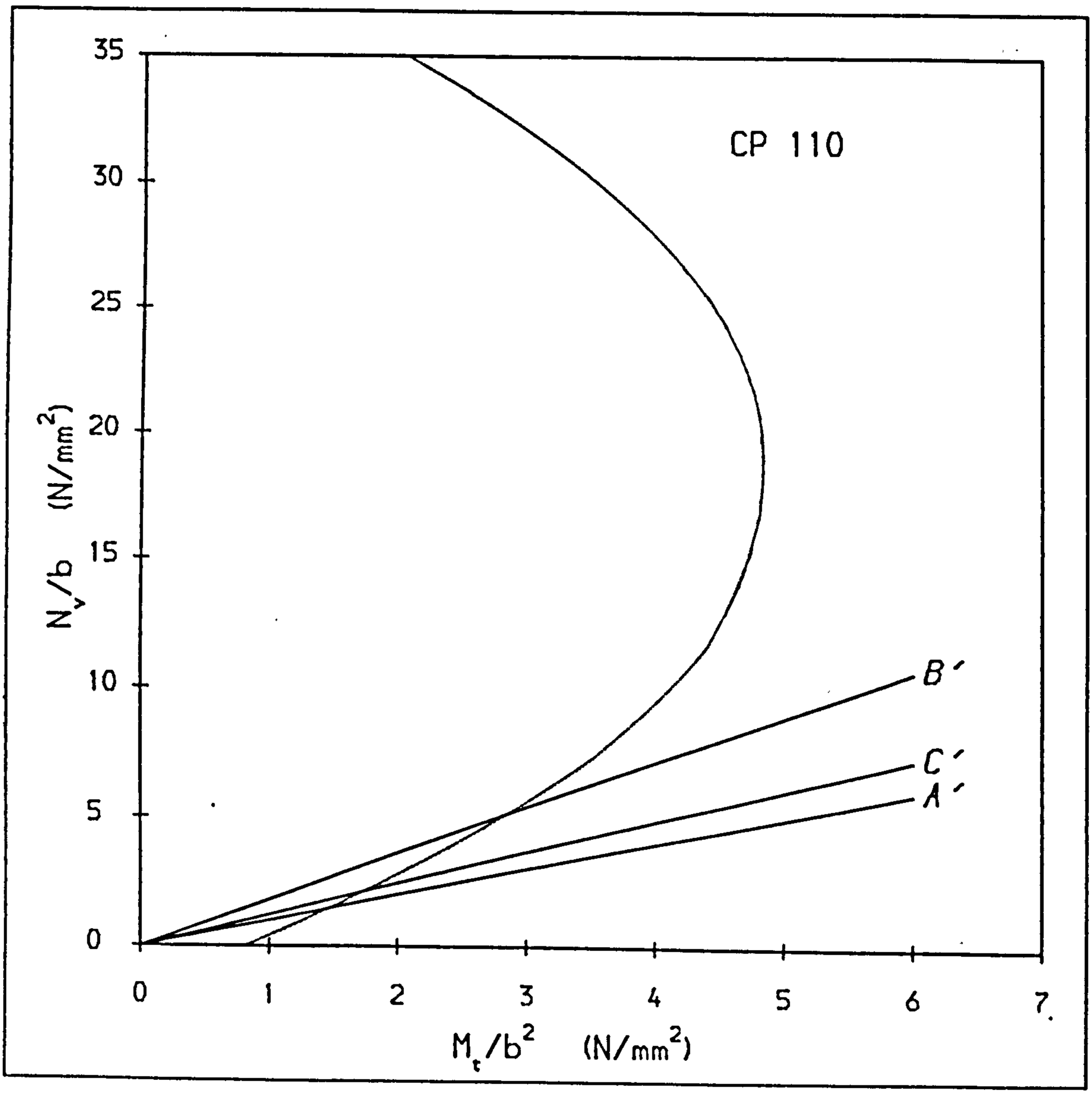

Figure B.1 : Load-moment interaction diagram (CP 110, Beam W-AC)

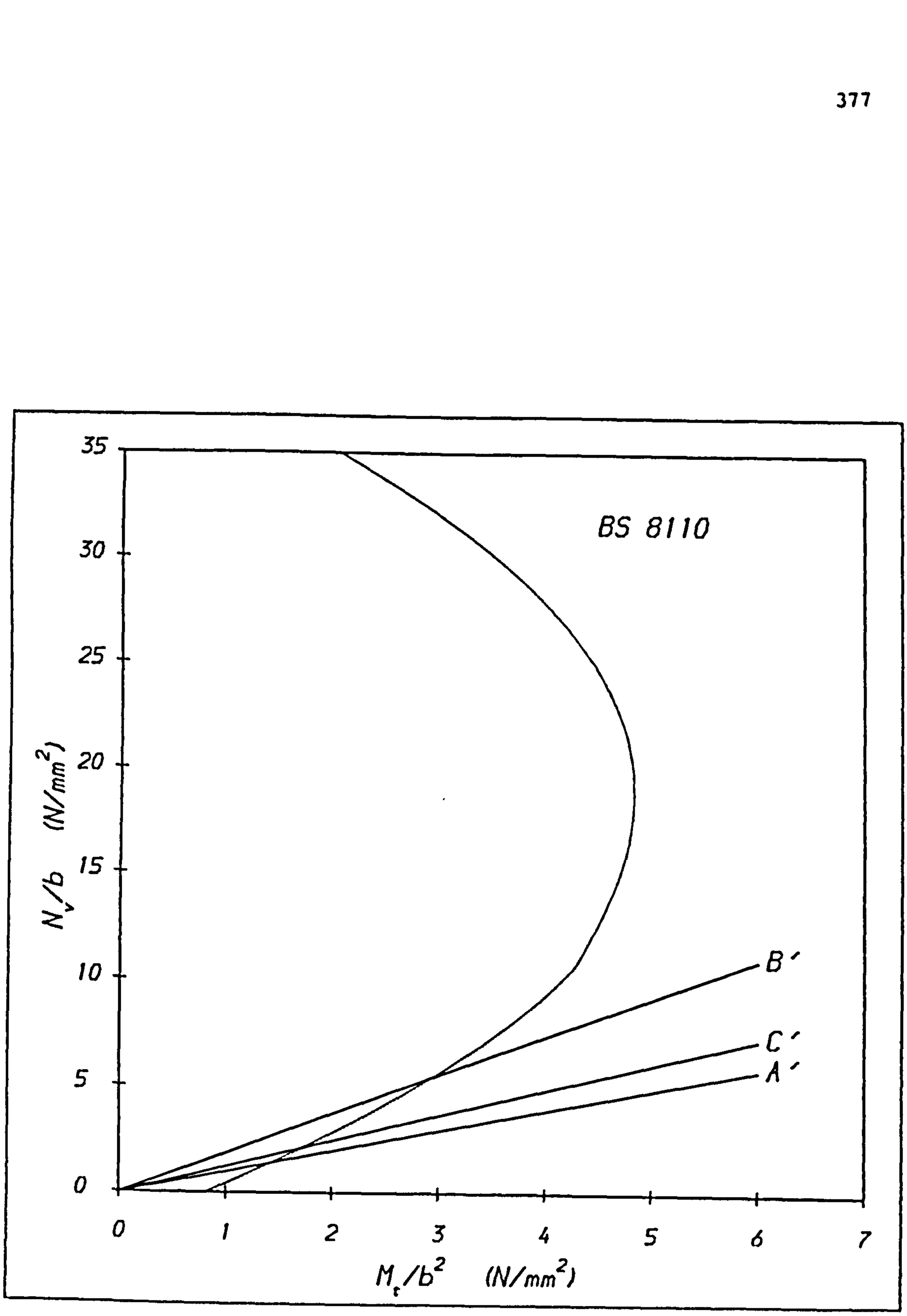

Figure B.2 : Load-moment interaction diagram (BS 8110, Beam W-AC)